Metabolic and Bioprocess Engineering – a Fruitful Symbiosis

Ralf Takors

Metabolic and Bioprocess Engineering – a Fruitful Symbiosis

Ralf Takors

Metabolic and Bioprocess Engineering

-

a Fruitful Symbiosis

Dr.-Ing. R. Takors

reprinted at 18.09.2005

ii

ABSTRACT This report has been written as a German 'Habilitations-schrift' summarizing some of the research results which were acquired in the working group 'Fermentation technology' at the Institute of Biotechnology, Forschungszentrum Jülich GmbH. After finishing the Ph.D.thesis (1997) the author became the assistant group leader and subsequently gained official full-group leadership at the beginning of 2000. This 'Habilitationsschrift' only considers results mainly dating from 2000 until January 2004. The author has been responsible for the co-supervision of the Ph.D. and master students which considers the primary topic identification, preparation and funding, the scientific instruction and superivision of the students and the common publication / patenting of the obtained results. Each chapter contains a detailed description about the origin of the presented results.

Contents

2   Contents

1

From Pools and Fluxes to Titers and Rates

We have gone from the era of 'who' to that of 'how' and are now entering the era of 'how much.' With this statement Koshland [Kos98] illustrated the on-going development in understanding cellular metabolism starting from the Era of Pathway Identification (1890 - 1950), passing through the period of Pathway Regulation (1950 - 1980) and stepping into the Era of Pathway Quantification (1980 - ?). Almost recently, the latter term has been replaced by the so-called Post-Genomic Era [WKss] thus stressing the current need to elucidate the basic questions of functional genomics for understanding how the genome influences physiology ([Bai98], [Bai01b], [NO02]). Without doubt, metabolism modeling plays an important role in this context [GN00].

However, the pertinent question arises how this qualitative and quantitative understanding can be achieved. During the past years, manifold experimental indications have revealed that the problem's solution is not trivial because of the robustness, redundancy and homeostasis observed in cellular systems leading to multigene / multitranscript / multiprotein responses after any perturbations [Bai99b]. According to Bailey [Bai01b] 'blind' computer simulators incorporating tens of hundreds of components just because they 're in a database, are not useful for this purpose. Despite the cellular complexity, indications are given that basics in cellular physiology can also be understood without the comprehensive, quantitative knowledge of the whole cellular system [Bai01a].

Besides, current activities in system biology ([CSF$^+$01], [Kit02]) aim at understanding the whole cell using a systemic modeling approach. In the case of absent detailed information, typically cellular constraints were considered thus allowing the analysis of the global cell instead of the reduced system [Pal00]. These approaches are also intended to incorporate expression-profiling data as well as selected metabolomic data in upcoming model generations [Pal02].

Metabolic engineering provides the notional framework for all these research activities. Since its foundation (and definition) in 1991 [Bai91], defining it as *the directed improvement of cellular properties through the modification of specific biochemical reactions or introduction of new ones using recombinant DNA technology,* it has emerged as a very interdisciplinary field, possessing a strong relationship to bioinformatics [Ste00]. Comprehensive reviews regarding successful *metabolic engineering* examples are given by Nielsen [Nie01] and Rohlin *et al.* [ROL01].

While the first years of *metabolic engineering* considered strain improvement by pathway engineering, future (and current) works will increasingly consider techniques such as DNA microarrays, directed evolution (gene shuffling) and tracer-based flux measurements [SS01]. Today's *metabolic engineering* focuses on the four categories of cellular variables, namely the small metabolites (metabolome), the fluxes (fluxome), the mRNA (transcriptome) and the proteins (proteome) [SS02]. This appeared to be necessary because a restrictive sight on transcriptome and proteome alone does not suffice to assess biological function [KW01].

The expanded scope of *metabolic engineering* even resulted in definition updates, such as the one of Westerhoff [Wes01] who introduced a modern *metabolic engineering* aiming at the (ambitious) calculation of the functioning of the living cell on the basis of the known gene expression levels taking into account kinetic and thermodynamic properties of all macromolecules in the cell. However, *the combination of analytical methods to quantify fluxes and their control ... to implement genetic modifications is* (still) *the essence of metabolic engineering* ([Ste99], [CBC00], [CBC02]).

Being aware of these promising *metabolic engineering* topics and perspectives, one might wonder about the remaining role of the classical *biochemical engineering* whose birth is dated as of 1947, when the first recognizable *biochemical engineering* process emerged for the large-scale streptomycin production at Merck [Cha97]. According to an American saying 'The job of an engineer is modeling and scale-up'. Hence, one should ask: Is that all? - Certainly not.

According to a 'classical' definition given by Weuster-Botz [WB03] *biochemical engineering science represents the fundamental research into all*

aspects of the interactions between engineering and other disciplines necessary to underpin the development of industrial-scale biologically based processes. Hence *metabolic* and *biochemical engineering* are not excluding themselves, on the contrary they support each other [Ste02]. The traditional scale-up role of *biochemical engineering* remains an important activity in practice as well as in research [Bai99a]. However, the scope of chemical engineering has broadened from the steel tank to the individual cells and their metabolic pathways ([Bai99a], [Ste03]) thus being directly related to *metabolic engineering.*

The pace of development for large-scale bioprocesses can be accelerated by increasingly applying basic principles of chemical engineering together with front line concepts of molecular biology [LPV01]. This is particularly important if high-volume, lower-value products such as commodities (and also fine chemicals) are considered. In contrast to high-value processes such as the roller-bottle based erythropoietin production at Amgen (USA), the high-volume processes are usually developed under the pertinent constraint to be only commercially viable at low costs. Hence the concerted approach of *metabolic engineering* and 'classical' *biochemical engineering* is necessary to achieve this aim, thus preventing a 'biotechnology without technology' [Wan01].

The role of biochemical engineering sciences is to provide a sound scientific basis for the engineering activities, i.e., a sound basis of know-why ... to provide tools for rational, rapid and efficient development of processes, products and services [SVM$^+$03].

In this sense, this 'Habilitationsschrift' is a typical *biochemical engineering* thesis.

Novels methods and apparatus will be presented that focus on intracellular pools and fluxes, maybe the most typical *biochemical engineering* variables [SVM$^+$03], to gain a quantitative understanding of the living cell thus enabling an efficient bioprocess development. After that examples of 'classical' bioprocess development will be given. Figure 1.1 roughly depicts the structure of this 'Habilitationsschrift'.

The subsequent chapters 2 and 3 focus on the development of novel *metabolic engineering* tools, intended to accelerate and optimize the bioprocess development by gaining quantitative information about intracellular pools and fluxes in recombinant microbial production strains. Especially the development of the Sensor reactor for metabolic flux analysis was predominantly motivated by its application under production-like process conditions. *Biochemical engineering* studies for 'classical' bioprocess development are given in the subsequent chapters 4 and 5 focusing on the process parameters titers and rates.
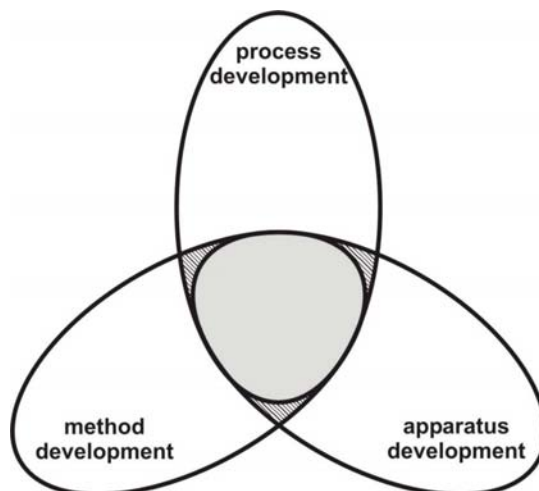
FIGURE 1.1. *Biochemical engineering* topics as mirrored in this 'Habilitationsschrift'. Method and apparatus development including typical *metabolic engineering* activities are considered as well as the process development (together with scale-up). Intersections of all topics are possible as shown.

Regarding the 2002-report of Ernst & Young [EY02] it seems to be remarkable that only 6% of all biotechnological activities in German companies can be attributed to the 'grey biotechnology', a maybe unskillful term describing biotechnological production processes as well as biotechnological applications for environmental protection This might contrast the situation in the United States where Cargill Dow (Blair, Nebraska, USA) has recently started its polylactide production at 140.000 tons-per-year scale and is even suspected to use an *ISPR* approach for the on-line removal of lactate by overpressured CO_2 [SS03]. Nearby, the amino acid lysine is successfully produced using *Corynebacterium glutamicum* in the company Midwest Lysine (up to 70.000 tons per year) thus representing a product with an expected annual market increase of ∼10% [Her03]. Furthermore, the company DuPont (Willmington, USA) has announced to start the 1,3 propanediol production (about 70.000 tons per year) using recombinant *E. coli* strains [WB03]. These high-volume, lower-value processes are only a few examples of actual large-scale processes thus indicating the need to consider *biochemical engineering* know-how to develop and to run large-scale applications.

Besides the bulk products, also the production of fine chemicals represents an interesting *biochemical engineering* target. As outlined by Frost and Lievense [FL94] and Schmid *et al.* [SDH⁺01], the production of aromatics benefits from its access using renewable resources instead of fossil feedstocks. Therefore chapter 4 focuses on the production of the aromatic

amino acid L-phenylalanine using recombinant *E. coli* strains. Finally an *E. coli* based approach for pyruvate production is presented in chapter 5, again motivated by the idea to replace existing, energy-intensive processes by those with low environmental burden.

2

In vivo Metabolic Dynamics after Pulse Stimulation: Tools and Results

Parts of the following sections were subjects of the Ph.D. thesis of A. Buchholz [Buc01a], M. Oldiges [Old03], J. Hurlebaus [Hur01] and D. Degenring [Deg03] who were (and still are) co-supervised by the author. Review-like publications were given by Buchholz *et al.* [BHWT02] or submitted for publication by Oldiges and Takors [OT03].

2.1   Motivation

Today, we are witnesses to current, novel technology developments intended to elucidate the gene/phenotype relationship in 'simple' prokaryotic cells as well as in complex eukaryotic mammalian cells. Usually, these essential studies [Bai01b] are bringing together bioinformatics and *metabolic engineering* [Ste00] while analyzing gene sequences (genomics), gene transcription (transcriptomics) and gene translation (proteomics) thus trying to find answers on questions such as (i) How many genes with what kind of distinct functions can be identified in a genome? (ii) How (and why) is gene expression controlled with respect to external culture conditions? (iii) Which proteins (enzymes) are encoded by the genes and how are their characterized? etc.

Despite the invaluable results obtained so far, the metabolome analysis seemed to be somewhat neglected within this concerted 'omics' approach. This might be surprising because the metabolome is downstream

of genome, transcriptome and proteome [ADB$^+$03], thus mirroring the upstream 'genotype-control' of several thousand genes in a (relatively) condensed biochemical pool of several hundred metabolites. For instance, less than 600 estimated metabolites ([TBWO98], [RTB$^+$01]) represent the biochemical analogues to 6000 genes in *S. cerevisiae* [GBB$^+$96]. In the case of *E. coli*, about 4800 genes are identified, coding for approximately 2500 proteins [LS99] while only about 627 metabolites are actually listed in the Eco-Cyc data base ([KRS$^+$00], [MB01b], http://ecocyc.panbio.com/ecocyc). Both examples give rise to the assumption that the reduced number of metabolites should enable a simplified gene/phenotype analysis.

Hence, the metabolome study should keep abreast of the 'up-to-now dominating' functional genomics technologies [Fie01]. The knowledge of intracellular metabolite concentrations certainly offers a promising basis to quantitatively understand biochemical interactions (e.g. the *in vivo* enzyme kinetics) in the metabolic network [BHWT02]. Metabolomics even allow functional genomic studies by combining metabolome analysis with *in silico* pathway analysis [FGN02]. Consequently, microbial metabolome analysis is currently attracting interest [KW01]. While 'early' taxonomic classification studies of 132 *Penicillium* strains [LF95] and 169 yeast strains [Wes98] already applied intensive, qualitative metabolome research, pioneering quantitative metabolome studies did not focus on microbial systems but on plants such as *Arabidopsis thaliana* ([FKD$^+$00], [Fie01], [Fie02]). These *metabolic fingerprinting* approaches considered more than 300 intracellular metabolites at the same time and were supplemented later on by *metabolic footprinting* [ADB$^+$03], analyzing the culture supernatant of *S. cerevisiae* strains.

Regarding the popular, classical definition of *metabolic engineering* defining it as 'the directed improvement of product formation or cellular properties through the modification of specific biochemical reactions or introduction of new ones with the use of recombinant DNA technology' [Ste99], a *modern metabolic engineering* has been introduced almost recently [Wes01]. Accordingly, the new definition aims at 'the calculation of the functioning of the living cell on the basis of the known expression levels of all enzymes taking into account kinetic and thermodynamic properties of all macromolecules in the cell'.

To achieve this - without doubt - ambitious aim homologous data sets of *in vivo* enzyme kinetics are necessary. However, most of the enzyme kinetic data available from databases such as EMP [EMP], MEDLINE [NCB], ENZYME [Bai00], BRENDA [Bre] and LIGAND [Lig] are heterogeneous in origin and are often based on *in vitro* experiments. Because of differences in liquid viscosity (protein content) and reactant/effector concentrations under *in vitro* experimental conditions compared to *in vivo* conditions,

enzyme kinetic parameters derived from *in vitro* experiments should be used with care to describe *in vivo* enzyme activities. Nevertheless, research studies are currently performed which aim at modeling complex microbial cells solely based on the enzyme kinetic information derived from databases [dJ02]. As an alternative, experimental and modeling approaches will be presented in the following that strive for studying enzyme kinetics *in vivo*, in the presence of all interactions inside cellular metabolism. These studies were intended to offer the opportunity of investigating not only one single enzyme (as the classical approach) but a whole set of interacting ones, in the sense of 'classical' *metabolic engineering* [Ste99].

To model enzyme kinetics, the knowledge of enzyme activities as a function of reactant and effector concentrations is necessary [CB95]. If steady-state experiments are used, one should consider the comparably small experimental data set that can limit the identifiability of complex enzyme kinetics [WT03] and that can make additional measurements necessary, for instance using ^{13}C metabolic flux analysis [PMdG$^+$01]. As an alternative, the knowledge of time-variant intracellular metabolite courses can offer a sufficient database [WT03], even for the identification of complex kinetic equations.

Stimulus-response experiments, for instance by pulsing the sole carbon source glucose to a glucose-limited culture, have already been developed as an appropriate method for the generation of (intracellular) transient metabolite concentration data[1]. These data sets can be a most valuable basis for the estimation of dynamic flux control coefficients and concentration control coefficients [MAR97] which represent the key values of the metabolic control theory. Pioneering examples have been published using *S. cerevisiae* ([TMB$^+$97], [RBTR97]) by Vaseghi *et al.* ([VBRR99], [VMZR01]), Buziol *et al.* [BBB$^+$02], Ostergaard *et al.* [OON01] and *Visser* [Vis02], studying *E. coli* ([SBTWB99], [CNRS$^+$02], [SKB$^+$02a]) and investigating *Z. mobilis* ([WBdG96], [WB97]). Pulse experiments are usually started in a glucose-limited steady-state by pulsing a significant amount of glucose to the culture to ensure a saturated glucose consumption afterwards. Cells are then rapidly taken out of the culture, while at the same time metabolism is inactivated. Further analysis of intracellular metabolite concentrations finally provides the data for subsequent modeling taking into account the stoichiometry of the metabolic network as well as kinetic expressions for the enzymatic reactions in focus.

---

[1] These stimulus-response experiments are related to the rather slow shift-up, shift-down experiments, such as the one of Melchiorsen *et al.* [MJC$^+$01], which aim at studying metabolism shifts under transient conditions usually lasting for several hours.
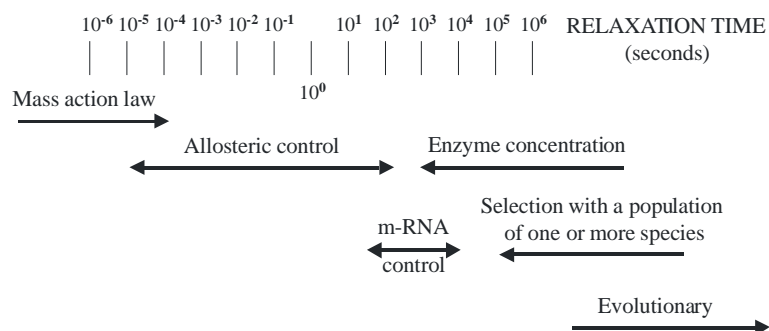
FIGURE 2.1. Adaptional mechanisms in organisms and order of magnitude of their relaxation timespan - taken from [Roe83].

It is noteworthy that only relatively small observation windows up to several minutes (in the case of *S. cerevisiae* experiments) are usually realized. This timespan represents a consequence of the need to get sufficient experimental data for enzyme kinetic identification and to prevent unwanted enzyme activity changes by superimposing gene regulations as a result of the initial glucose pulse. Figure 2.1, which is derived from Roels [Roe83], indicates that mass action law and allosteric control relaxation times are much shorter than for instance messenger (m)-RNA control or the changes of active enzyme concentrations. Considering a typical observation window of 40 seconds (see below) no changes of active enzyme pools should thus be assumed.

In general, stimulus-response experiments for identifying *in vivo* enzyme kinetics typically consist of different, sequential steps as follows:

- stimulus-response experiment with rapid sampling (to generate the samples after metabolism stimulation)

- cell quenching (to rapidly inactivate metabolism thus 'freezing' the current metabolic state after stimulation)

- metabolite extraction (to extract metabolites, nucleotides etc. out of the samples for further analysis)

- *in vivo* pool analysis (to quantify metabolite, nucleotide concentrations)

- metabolism modeling (to identify quantitative, mechanistic models based on the experimental data)

Each of these topics will be treated in the following and the results obtained will be presented and contrasted to already published findings.

2.2   Rapid Sampling and Sample Preparation

Depending on the microorganisms used, the constraints for the sampling frequency can change. For *Saccharomyces cerevisiae*, intracellular concentration changes on second-scale after the pulse were reported ([TMB$^+$97], [RBTR97], [VBRR99], [Vis02]), while, for instance, an intracellular increase of glucose 6-phophate (G6P) after external glucose addition took place on the sub-second scale in *E. coli* ([SBTWB99], [CNRS$^+$02],[SKB$^+$02a]). Hence, rapid sampling approaches must consider these characteristic time constants of the biological systems under investigation.

To successfully perform stimulus-response experiments, the microbial stimulation (for instance by glucose pulsing) must be chosen with care. On the one hand, the stimulus should be strong enough to call forth curves of detectable, time-variant intracellular pool sizes. On the other hand, the stimulus (together with the preceding experimental period) must not cause any damage of the cell function which could falsify the experimental observations. Studying (industrial) production strains the additional constraint should be followed to choose the experimental conditions as similar as possible to the production process in order to allow the transfer of the experimental results.

As a consequence, microbial systems such as *E. coli*, *Z. mobilis* or *S. cerevisiae* are often stimulated by a rapid, step-wise increase of the sole carbon source (for instance glucose). Usually this carbon source is limiting before and is added by a rapid glucose pulse[2]. Before the pulse, the metabolism should be at (pseudo-) steady-state which is shifted-away due to the stimulus. To prevent any time-lags of the external stimulation, the one-step increase of the extracellular carbon source should be transmitted into the cell as fast as possible. In general, this can be achieved by profiting of highly affine carbon uptake systems such as the carbohydrate phosphoenolpyruvate:phosphotransferase system (PTS) [RMR$^+$00] or (fast) facilitated diffusion mechanisms which are often the basis for substrate uptake in bacteria. It is noteworthy that other substrates which are not consumed as quickly are consequently less suited to stimulate the biological system. This limitation should be considered if the pulsing of co-substrates or auxotrophic substances is discussed. So far, glucose is most commonly used as the pulse substrate although alternatives - for instance using glycerol to stimulate *E. coli* [BHWT02] - are also described.

---

[2]It is noteworthy that the the term 'glucose pulse' might be misleading because it basically describes the technical procedure to add the (limiting) carbon source into the bioreactor. However, the cells observe a step-wise increase of the previously limiting substrate, because no significant decline of the extracellular substrate concentrations can usually be detected during the post-pulse observation period.

While performing stimulus-response experiments, the 'rapid sampling' step takes over the functions of

- rapidly taking samples out of the culture (immediately after the pulse) with sufficient sampling frequency and sample volume

- inactivating the cell metabolism during sampling by quenching.

Both items will be treated separately in the following subsections.

2.2.1   Rapid Sampling Devices

As long ago as 1993, Theobald *et al.* [TMRR93] developed a manual sampling device, consisting of a sampling valve and a pre-cooled (e.g. -20°C) quenching fluid (for instance methanol) to monitor intracellular changes of the nucleotide pools in *S. cerevisiae* after glucose pulsing into a bioreactor. This device was also used for studying yeast metabolism dynamics ([TMB$^+$97], [RBTR97]) allowing a maximum manual sampling frequency of about 6 to 12 samples per minute. Later on, an improved, similar sampling strategy using a pre-cooled quenching solution (-40°C) prepared in a vacuum tube was presented [LEZ$^+$01], again to monitor *S. cerevisiae* intracellular metabolite dynamics after vacuum drying of the cell extracts. Recently, this sampling device was again modified in a comparative study by filling the syringe with pre-cooled stainless steel beads ($\varnothing$ 4 *mm*) and quickly withdrawing the solution via a 0.45 μm filter [MGVH03]. It was found that this approach was superior to the alternative method of quick sample freezing in liquid nitrogen.

Further developments of the technology led to a stopped-flow method ([MVR00], [BBB$^+$02]). This approach was characterized by a turbulent mixing chamber which was connected to a sampling tube consisting of a series of valves. The biosuspension leaving the reactor was brought into contact with glucose in the turbulent mixing chamber before it streamed into the valve cascade and from there into different sampling tubes with pre-cooled quenching fluid. By controlling the valve opening at different positions in the valve cascade, the glucose/biosuspension contact time was controlled, too, thus allowing first samples to be taken within milliseconds after glucose addition. However, a long-term (multiple seconds) sampling window could not be realized owing to e.g. dissolved oxygen gradients that must be prevented in too long valve cascades.

Parallel to this approach, a similar system called BioScope ([Vis02], [VZD$^+$02]) has been developed, aiming at long-term sampling times of up to 100 s using a sampling tube device of several meters length. In contrast to the previously described valve cascade, BioScope is characterized by

comparatively low flow rates through an oxygen permeable silicon tube[3]. The perturbing agent (for instance glucose) is added at the inlet of the silicon tube. Hence, different glucose/biosuspension contact times are realized by analogy to the valve cascade system of Buziol *et al.* [BBB$^+$02].

As an alternative approach, experiments with the anaerobic strain *Z. mobilis* were carried out ([WBdG96], [WB97]) using a rubber sampling tube system [WBW96]. After pulsing glucose into the bioreactor, cell suspension was rapidly drained off into a flexible sampling tube that was directly brought into contact with 35% perchloric acid at $-25°C$ and later frozen *in situ*. Following this procedure, the time-dependent cellular responses on the glucose pulse were located in frozen volume elements inside the tube while the distance to the tube inlet was inversely correlated to the glucose contact time. Further sampling analysis was enabled by piecewise thawing of tube parts.

The stimulus-response experiments presented in the following sections made use of an automatic sampling system that was already developed in 1998 by Paschold *et al.* [PWBSB98]. The perturbing agent (for instance glucose) was pulsed directly into the 20 L bioreactor (working volume: 7.5 L) allowing the monitoring of metabolic dynamics under realistic cultivation conditions. Usually 70 to 100 mL pulsing volume were automatically injected causing a glucose concentration shift from apparently zero $g \cdot L^{-1}$ (during the glucose limited steady-state) to three $g \cdot L^{-1}$.

Later, the pulsing technique was optimized (see Figure 2.2) to prevent any other perturbation apart from the substrate injection and to reduce the resulting mixing times [BWT01]. For instance, sudden shifts of dissolved oxygen concentration or reactor pressure could successfully be prevented during pulsing, indicating that overpressured air was not co-pulsed into the bioreactor. The amount of pulsing volume added to the reactor was automatically controlled via the opening time of the two membrane valves used. The injection valves possessed nozzles at the reactor inlet, which targeted the injection stream directly to the Rushton turbines used for mixing the cell suspension. A θ_{90} mixing time of 640 ms was achieved [Buc01a], which is lower than the usually estimated values of 2 to 3 seconds [MVR00]. Samples taken during this time are subject to the superimposing effects of mixing and intracellular metabolic kinetics. However, one should consider the glucose uptake characteristics of e.g. *E. coli* strains used for the experiments. Very low K$_S$-values of $3 - 10$ μMol (0.6 - 1.8 $mg \cdot L^{-1}$)

---

[3]Currently, the original BioScope apporach is extended by installing an additional aeration system along the sampling tube to increase the oxygen transfer rates (unpublished results).
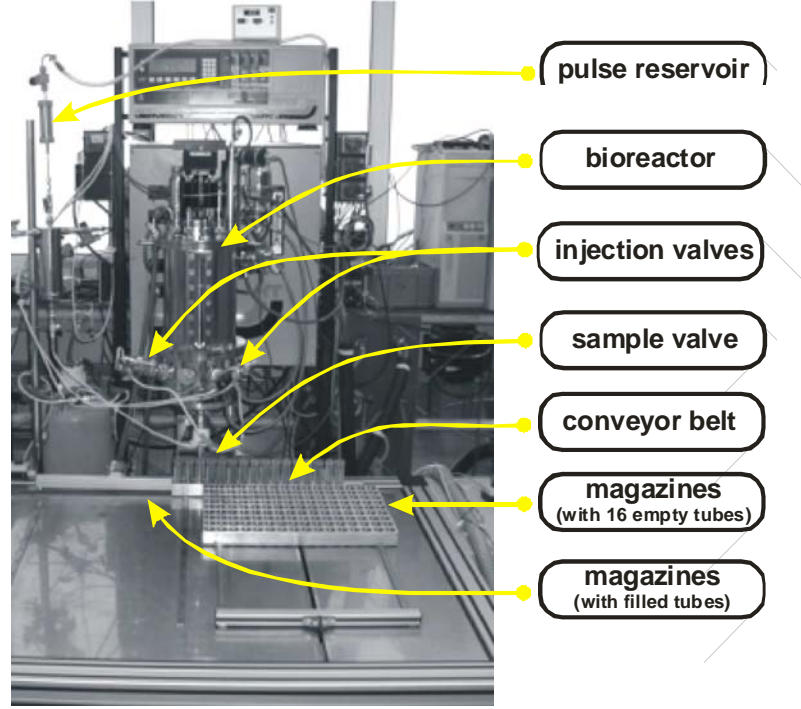
FIGURE 2.2. Experimental set-up of the pulse system used for stimulus-response experiments. As indicated, a 20 L bioreactor was equipped with a glucose pulse unit (left hand-side), corresponding injection valves, a sample valve and a conveyor belt that transported the precooled (60% v/v methanol at $-50^\circ C$) sampling tubes beyond the sample valve. A sampling frequency of 4 to 5 Hz was achieved.

were reported for the glucose-specific PTS [4], which is responsible for the prevailing amount of glucose consumption. These low K_S values are more than 1600-fold smaller than the typical, final pulse concentration of 3 $g \cdot L^{-1}$. Thus it can be assumed that saturating glucose uptake conditions are achieved very much faster than within 640 ms mixing time.

Immediately after the pulse, a sampling valve is opened at the bottom of the bioreactor and cell suspension is continuously drained off at a flow rate of 33.3 $mL \cdot s^{-1}$. Below the sampling valve, pre-cooled (-50°C) sam-

---

[4]Glucose uptake in *E. coli* is enabled by different systems depending on the extracellular glucose levels. At micromolar external levels, half-saturated glucose uptake via Mgl at 0.2 μM (0.036 mg/L) and via glucose specific PtsG at 3 to 10 μM or 0.6 to 1.8 $mg \cdot L^{-1}$ takes place, while at millimolar external levels glucose uptake via PtsG and mannose specific PtsM (half-saturated at 1.3 mM or 230 $mg \cdot L^{-1}$) should be considered ([Fer96], [Fer99], [LS99], [PLJ93], [HK79]).

pling tubes are positioned automatically via a conveyor belt. Usually, a sampling volume of 5 ± 0.08 mL [SBTWB99] cell suspension is quenched into 15 mL 60 % v/v aqueous methanol causing an immediate cessation of metabolic activity[5]. Further research led to an optimized composition of the quenching fluid by addition of 70 mM Hepes (2-[4-(2-hydroxyethyl)-1-piperazinyl]ethanesulfonic acid) [BTW01]. With Hepes, a quenching fluid at $-50°C$ can be used instead of the formerly $-40°C$ as previously applied. Using the automated conveyor belt, a maximum sampling frequency of 4 to 5 Hz can be achieved, which leads to an observation time window of approximately 40 seconds for the 160 samples available. However, longer observation time windows are possible by lowering the automatically controlled sampling frequency. Figure 2.2 gives an overview of the automated rapid sampling machine. A movie of the rapid sampling apparatus in action is provided on the internet at http://www.fz-juelich.de/ibt/ferm.

2.2.2 Cell Quenching Approaches

As outlined in the preceding subsection, the major task of cell quenching is to halt metabolism activity by sudden cell cooling thus to prevent any further metabolite conversions owing to enzymatic reactions. Because of the immediate metabolism responses observed after stimulation ([SBTWB99], [CNRS$^+$02],[SKB$^+$02a]), quenching should be realized within a subsecond time-scale after pulse.

Early approaches of Theobald et $al.$ [TMB$^+$97] followed the strategy to disrupt the cells immediately after sampling (via extraction) at the same time denaturing all cellular enzymes using extreme pH conditions. Although this method was successfully applied, it possesses the inherent disadvantage that intracellular metabolites are diluted in the fermentation supernatant of the sample and that the fermentation medium cannot be separated from the cells. Hence, such a procedure should only be preferred to study metabolites which are likely to occur only inside the cells.

Compared with this, the separation of the quenching and the cell extraction step offers the advantage of subsequent cell concentration by sample centrifugation or filtration at low temperature, thereby removing the fermentation medium. Saez and Lagunas [SL76] suggested the washing of the sampled cells after filtration with 50% methanol at $-40°C$ and de Koning and van Dam [dKD92] optimized this strategy for yeasts by spraying the sample into the pre-cooled methanol solution. They demonstrated that the cellular methanol quenching succeeded to halt metabolic activity and that $S.$ $cerevisiae$ was resistant to metabolite leakage when suspended in the

---

[5]Weuster-Botz [WB99] already estimated the necassarry time to cool an (hypothetical) sample drop of 100 μm from $37°C$ to $-20°C$ at about 50 ms.

cold methanol quenching solution. These results were experimentally re-confirmed by Hans *et al.* ([HHW01], [HHW03]) using HPLC-based amino acid analysis. As an alternative, liquid nitrogen quenching of *S. cerevisiae* cells was studied, which was found to be inferior to the cold methanol quenching based on a pre-cooled syringe filled with stainless steel beads [MGVH03][6].

It is noteworthy that the leaking resistance is not a general cellular property because it strongly depends on the cell membrane composition. For instance, metabolite leaking was reported for glycolytic intermediates of *Lactococcus lactis* [JJV99]. Own studies using gram-positive *C. glutamicum* strains for amino acid production (L-valin, L-lysine etc.) also revealed significant leaking of glycolytic intermediates during the methanol quenching procedure (data not shown). In a comprehensive study, Maharjan and Ferenci [MF03] studied the metabolite extraction of gram-negative *E. coli* applying six, commonly-used methods including acid or alkaline [HBGF98] treatment, permeabilization by freezing with methanol, high-temperature extraction in the presence of ethanol [TNMF98] or methanol [SRB86] and by lysis with chloroform-methanol [dKD92]. Analyzing the detected ^{14}C-labeled compounds after methanol quenching of *E. coli,* the authors outlined the significant influence of the extraction procedure on the results of metabolome analysis. Although the cold methanol procedure was favored, no phosphorylated glycolytic compounds, metabolites of the pentose-phosphate pathway or cofactors (such as the adenosinphosphates (ATP, ADP, AMP) were identified in their study. Own investigations of Buchholz [Buc01a] supported this finding by measuring a constant - and not increasing - NAD content in the extract during methanol extraction lasting for 7 h[7]. Similar observations were reported by Oldiges [Old03] regarding ATP, ADP, AMP, PEP and the lumped pentose-phosphate pool P5P.

Hence, our own studies followed the protocol as already presented in the foregoing subsection: 50 mL sample tubes containing 15 mL of 70 mM Hepes (2-[4-(2-hydroxyethyl)-1-piperazinyl]ethanesulfonic acid) and 60 % methanol were pre-cooled at -50°C and subsequently filled with 5 mL samples taken from the fermentation experiment at 37°C. Because of liquid mixing, the sample temperature rose to ≤-20°C before the samples were stored at -28°C for subsequent preparation and analysis. These steps were always realized within the next 8 hours after storage.

---

[6]In addition to the aforementioned approaches Chassagnole *et al.* [CNRS$^+$02] used liquid nitrogen (-196°C) for cell quenching, which was subsequently removed by evaporation and the sample was further subjected to extraction. If and how the culture supernatant was removed before cell disruption is not known.

[7]Additionally, measurements of protein content in the cell extract revealed a cell lysis of less than 5% under methanol extraction conditions.

2.2.3 Metabolite Extraction

As shown in the preceding subsection, cell quenching and cell extraction/ disruption were separated to analyze *E. coli* samples after stimulus-response experiments. Therefore a subsequent cell extraction/disruption step was needed that

- allows a fast and quantitative cell disruption to provide analytical access to the released intracellular components

- ensures metabolism inactivation during the extraction/disruption procedure

- prevents the (chemical) degradation of the interesting intracellular metabolites, nucleotides etc.

- denatures enzymes to prevent subsequent metabolite conversions, also after the extraction/disruption procedure is finished

- does not hamper the subsequent analytical procedures

- should be as simple as possible to allow the preparation of the 160 samples of a typical stimulus-response within usual working practice.

Considering these constraints typical approaches such as mechanical/ physical or enzymatic cell disruption as well as lyophilization were not preferred. Instead chemical methods were favored as shown in the following.

So far, a variety of extraction methods has already been described for different cells [Kar80]. For instance, *S. cerevisiae* was treated with chloroform [dKD92], perchloric acid and alkaline ethanol solution [TMB$^+$97] and buffered hot ethanol ([GFR97], [HHW01], [HHW03]). Additional freeze/ thaw cycles were applied to complete the cell disruption [TMRR93]. In analogy, *E. coli* extraction/disruption was subjected to perchloric acid treatment ([SBTWB99], [BTW01], [CNRS$^+$02]), potassium hydroxide solution [CNRS$^+$02] or a hot Tris-H$_2$SO$_4$/EDTA solution [CNRS$^+$02]. In contrast to *S. cerevisiae* additional freeze/thaw cycles showed no effect on the extraction of adenosine phosphates using *E. coli* [MNRRN99].

As already emphasized in the comparative study of Maharjan and Ferenci [MF03], the choice of the appropriate extraction method strongly depends on the metabolites of interest and - additionally - on the biological system that should be investigated. Reduced nucleotides such as NADH or NADPH are instable during acid extractions, but stable under alkaline conditions. On the other hand, the oxidized nucleotides NAD and NADP are rapidly degraded under alkaline conditions, requiring acid extraction
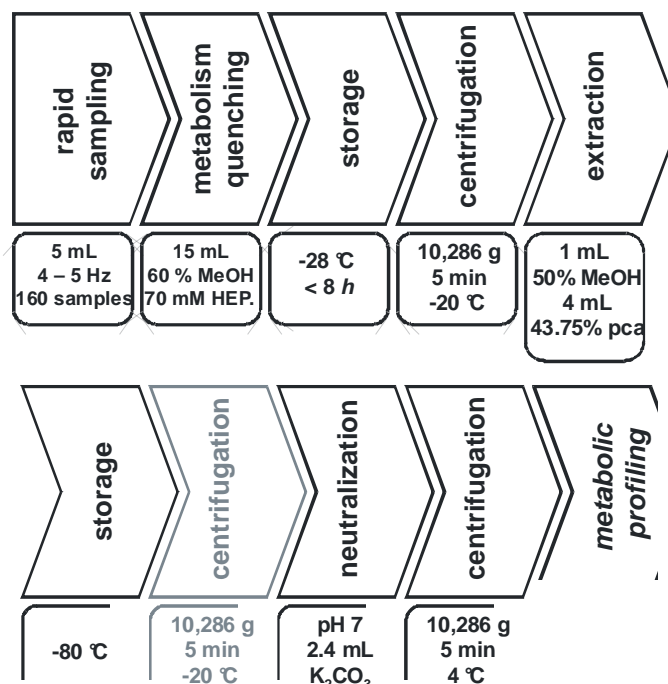
FIGURE 2.3. Scheme of the current protocol for sample preparation. The 'gray' indicated centrifugation step is a matter of current optimization. After the last centrifugation step, the clear solution can be sujected to *metabolic profiling* analysis. Abbreviations used: pca - perchloric acid; MeOH - methanol.

[SSS89]. This representative example clarifies that it is essential to study the stability of the interesting metabolites under extraction conditions. Hence, care must be taken to find the optimal extraction conditions concerning metabolite stability and extraction efficiency. Furthermore, the characteristics of the biological system should be considered as well. In a comparative study of Schmid *et al.* [SSS89] adenosinetriphosphate (ATP) was chosen as an indicator for the extraction efficiency during acid and alkaline extraction ([BF72], [MNRRN99]). For *Thermoanaerobacter finii* both methods resulted in quite similar levels, whereas perchloric acid extraction yielded a higher ATP content for *E. coli* compared to the alkaline procedure. Again, this result underlines the necessity to identify optimal extraction conditions with respect to the biological system and the pools that should be analyzed.

Several preliminary studies were carried out by Buchholz [Buc01a] and Oldiges [Old03] to identify optimal extraction conditions for *E. coli*. Extraction protocols using perchloric acid, alkaline ethanol (with KOH) and

hot ethanol were considered. As a result, the following procedure was identified which currently serves as a standard protocol: The samples which were stored at -28°C (see preceding section) are centrifuged at 10,286 g (5 $min,$ -20°C). The methanol-containing supernatant is subsequently removed. Then, the cell pellet is resuspended in 1 mL 50% methanol solution (at -28°C) to ensure a declustering of the cells. 4 mL of 43.75% (w/v) perchloric acid solution is added and well mixed with the cell suspension. After this, the samples are stored again at -80°C. In the following, the thawed samples were centrifuged (and ultrafiltrated concomitantly) to separate cell debris and proteins and neutralized at pH 7 by addition of 2.4 mL potassium-carbonate solution. Because of strong foaming, samples are cooled (with liquid nitrogen) during neutralization. Finally, the samples are 'heated' to 0°C in an ice-batch, the precipitate is removed via centrifugation (10,286 g at 4°C) and the samples are stored at -28°C for subsequent *metabolic profiling* analysis. A summarizing overview of the total sample preparation procedure is given in Figure 2.3.

2.3   *In vivo* Pool Analysis - *Metabolic Profiling*

2.3.1   *Reviewing Metabolic Profiling Approaches*

The term *metabolic profiling* represents a rather new definition for an equally novel research field [HG03]. According to Fiehn [Fie02], *metabolic profiling* belongs to metabolome analysis, which is multifunctional, making use of different analytical approaches depending on the topic of the study. Metabolome analysis can thus be subdivided into

- *target analysis*, aiming at the measuring of distinct substrates or products, for instance to qualify genetic modification

- *metabolic profiling*, focusing on a complete pathway or linked pathways with the aim to quantify the intracellular metabolites and

- *metabolomics*, striving for an unbiased, semi-quantitative overview of the whole-cell metabolic patterns.

Metabolic fingerprinting [Fie01] was presented as a tool for geno- (and phenotype) classification with the aid of rapid metabolome pattern analysis only focusing on those metabolites with biochemical relevance. Almost recently, another variant of high-throughput classification was presented, called *metabolic footprinting* [ADB+03], which differs from the aforementioned methods by analyzing extracellular metabolites instead of intracellular pools.

Hence, *target analysis* allows to optimize the analytical approach with respect to the distinct metabolites of interest, at the same time ignoring the metabolic information of other compounds. *Metabolomics* aims at a full uncovering of all metabolome information. However, the different chemical properties of the cytoplasm components restrict this approach to be semi-quantitative but - more or less - unbiased. *Metabolic profiling* thus represents a combination of both focusing on a group of metabolites which represents a characteristic segment of the metabolism (for instance all pathway intermediates together with the precursors). On the one hand, only a limited number of metabolites is considered which simplifies the approach. On the other hand, this group needs to be analyzed quantitatively, i.e. the intracellular concentration of each component should be measured as accurately as possible.

The measuring of intracellular concentrations is an ambitious task because the following experimental constraints should be considered:

- Typically, a 5 *mL* sample (see Figure 2.3) contains only 2 to 3 v/v% of *E. coli* cells before methanol quenching. Intracellular concentrations are reported to be at best in *mM* range ([BCKF93], [RC95],

[BFI95], [TGB97]). Hence the metabolite concentrations in the final assay should be expected at low μM or nM levels because of the necessary dilution steps during the sample preparation procedure.

- Cell matrix effects should be carefully considered while developing protocols for intracellular metabolite analysis. First, effects of the extracellular matrix (fermentation supernatant) should be ruled out (see preceding section). Second, appropriate separation steps should be applied to identify and to quantify the metabolites of interest in the complex cytoplasm solution also containing substances with similar chemical property.

- Regarding the 160 samples which were typically taken during a stimulus-response experiment, the analytical procedure should be as simple and as 'universally valid' as possible to minimize the analytical effort.

.

Motivated by the high substrate specificity, enzymatic test systems are used as a prevalent, state-of-the-art approach for intracellular metabolite analysis of the neutralized cell extracts. Examples are given for *S. cerevisiae* ([TMRR93], [RBTR97], [TMB$^+$97], [VBRR99], [LEZ$^+$01], [Vis02]), *Z. mobilis* ([WBdG96], [WB97]) and *E. coli* ([SBTWB99], [CNRS$^+$02]). These methods are usually based on standard approaches published in [Ber85]. In general, metabolites such as G6P, F6P, FBP, G3P, DHAP, GAP, PGA, PEP, PYR, AcCoA, CIT, OXO, SUC, MAL, OAA and FUM can be quantified to detection limits of about 10 - 100 μM (for abbreviations see tables B.1 and B.3 in Appendix) which corresponds to about 0.1 to 1 mM inside the cells ([Sch99a], [Buc01a]).

However, despite the invaluable results obtained by enzymatic analysis so far, some drawbacks must be considered.

- **Relatively large sampling volume**: Enzymatic tests usually need a relatively large sample volume of approximately 100-300 μL/assay. Considering the sample volume that is harvested by rapid sampling, only a limited number of enzymatic tests can be carried out. As a consequence, the final monitoring frequency of measured intracellular metabolites is limited too.

- **Error-prone procedure**: Enzymatic tests always need a final NAD-(P)H- dependent reaction step that can be detected photometrically (UV) at 340 nm. Therefore, reaction cascades are sometimes used that are more error-prone than single reaction steps. Additionally, enzyme instabilities can cause erroneous measurements.

- **Specialized analysis**: In general, each metabolite requires a different enzymatic test system (assay). Hence enzymatic measurements are not universally applicable but very specific for each metabolite, which makes the approach time-consuming.

- **Limited enzyme availability**: Although a lot of enzymatic tests are already known [Ber85] not all intracellular metabolites can be measured following this approach due to the limited availability of the enzymes needed. This especially holds true for the analysis of anabolic pathways where already established enzymatic tests are almost entirely missing.

- **Effect of the cytoplasmic matrix:** The selectivity of the enzymatic assays can be strongly influenced by the sample matrix (the cytoplasmic composition), as found by our own studies. As an example, Figure 2.4 is given showing the 'fictive' course of the enzymatically measured, intracellular glucose-6-phophate (G6P) concentration as a function of the assay incubation time considering a cell extract of *E. coli* K12 which was treated according to the sample preparation protocol given in the preceding section. Taking into account the strong acidic extraction conditions, one would assume that no measurable enzyme activity is left after cell disruption. However, Figure 2.4 reveals that enzymatic measurements obviously strongly interfered with the sample matrix resulting in a steady increase of the measured 'fictive' G6P concentration - and not in a final steady-state. It is noteworthy that enzymatic tests are usually expected to be finished within a couple of minutes and not after hours of incubation. It is also remarkable that this effect - although reproducible - was found to be specific for the samples used. Considering an additional sample ultrafiltration step (molecular cut-off: 5 kDa) before enzymatic testing successfully prevented this unwanted, superimposing matrix effect. In Oldiges and Takors [OT03], examples are given to demonstrate the severe influence of the sample 'rest activity' after perchloric acid treatment. Hence, sample preparation for enzymatic measurements must consider an additional ultrafiltration step although the overall protocol becomes even more complex and time consuming.

As an alternative to the enzymatic approaches, different methods were already studied. Examples are: GC-MS ([HH73], [KSMP99], [VBDAN03]), NMR ([OGMH82], [TRTP99], [dGSW$^+$99]), HPLC-UV [MNRRN99], HP-AE-PAD [BFI95], HPLC-MS ([Str99], [BTW01], [PCED00]), HPAE-MS [DEF$^+$02], CE-MS ([SUN$^+$02], [SOU$^+$03]) and MALDI-TOF-MS [TWK$^+$02].

If NMR approaches are compared - for instance - with enzymatic approaches, the NMR differs in relatively low sensitivity thus requiring a
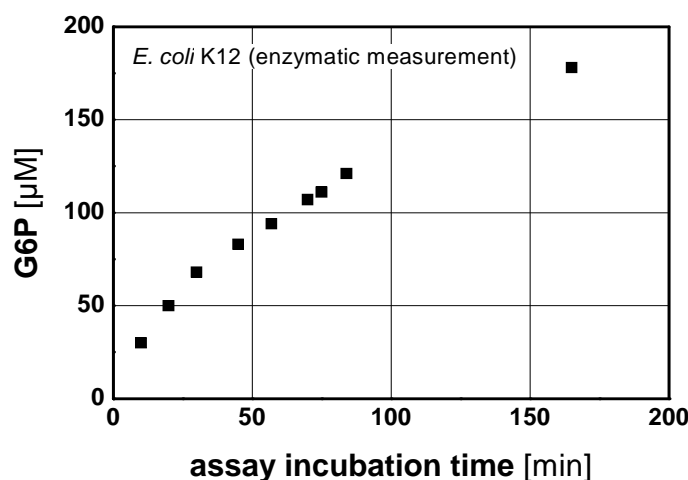
FIGURE 2.4. Measurement artefacts owing to the enzymatic measurement of intracellular glucose 6-phosphate (G6P) concentrations in *E. coli* K12. The dependency of the 'fictive' result with respect to the assay incubation time is given.

biomass content of several grams cell-dry weight for a quantitative cell content analysis [DMW⁺03]. Regarding the aforementioned *metabolic profiling* demands, this NMR property obviously limits its applicability.

The application of alternative HPLC based methods with UV detection is also limited, because only nucleotides are well detectable (e.g. via HPLC-UV) while central metabolism intermediates, such as sugar phosphates from glycolysis and pentose phosphate pathway, only show poor UV activity. Even in the case of nucleotide analysis, the cytoplasmic sample composition (matrix) can still cause detection problems because of the presence of other substances with similar HPLC column affinity (similar steric and chemical properties).

To overcome the detection problems of compounds with low UV activity, pulsed amperometric detection (PAD) coupled to high-performance anion exchange (HPAE) chromatography was used instead [BFI95]. Because most of the metabolites can be deprotonated and thus negatively charged, anion exchange chromatography is a suitable separation method. However the salt and buffer content of the matrix can also hamper PAD. Additionally, the HPAE-PAD approach is limited to metabolites which are stable under extremely high pH-values, because of the sodium hydroxide gradient used for column elution. Smits *et al.* [SCB⁺98] improved the HPAE-PAD method

by applying solid-phase extraction (SPE) to clean up the sugar phosphates in extracts of *Saccharomyces cerevisiae* prior to injection.

In the recent years, the application of mass spectrometry gained more and more interest for the analysis of biological samples [Cos99]. Hence, the coupling of chromatographic separation with mass spectrometric identification seemed to be the logical consequence of the analytical problems described in the preceding paragraphs. First, GC-MS approaches were published focusing on the isotopomer analysis of proteinogenic amino acids in biomass hydrolysates ([CN99], [DS00]). Later on, the GC/MS approach was improved by Wittmann *et al.* [WHH02] even allowing the identification of intracellular amino acid labeling patterns in *S. cerevisiae* cells. Recently, Villas-Boas *et al.* presented a new protocol based on alkyl chloroformates derivatives for derivatization of amino acids simultaneously with di- and tricarboxylic acids [VBDAN03]. However, the common characteristic of all GC/MS methods is that they need an additional sample preparation step for metabolite derivatization to increase their volatility. Thus thermolabile or large molecules are difficult to detect apart from the problems that might occur during the derivatization procedure.

Using MALDI-TOF-MS (matrix-assisted laser desorption/ ionization time-of-flight mass spectrometry) an appropriate derivatization procedure is essential as well. Additionally, the analysis of biological samples with complex solutions can be hampered by the high volatility of the analytes used and the possible interference with sample matrix signals. However, an appropriate derivatization protocol for MALDI-TOF-MS applications was recently presented [TWK$^+$02] allowing the labeling of alcohols, aldehydes, ketones carboxylic acids α-keto carboxylic acids and amines.

CE (capillary electrophoresis) -MS approaches, such as the one of Soga *et al.* ([SUN$^+$02], [SOU$^+$03]), are currently followed too, allowing the determination of more than 350 metabolite and nucleotide standards in parallel. However, own studies [Buc01a] focusing on CE with UV-absorption revealed a very high sensitivity of CE applicability with respect to the salt content in the sample, which of course, is a consequence of the electrophoresis principle used for analyte separation. Because our samples typically contained high salt fractions (due to perchloric acid treatment), the application of CE was no longer followed.

The application of liquid chromatography combined with mass spectrometry offers the opportunity to benefit from the (typically) high MS sensitivity considering an additional chromatographic separation step, at the same time avoiding necessary sample preparation procedures such as derivatization. Therefore, the LC-MS approaches seemed to be superior to the alternatives presented in the preceding paragraphs thus encouraging their use

for *metabolic profiling*. After reliable sources with electrospray ionization were commercially available, it could be shown that the LC-MS technique can be successfully applied to analyze cell extracts of *E. coli* [BTW01] using a Finnigan LCQ iontrap mass spectrometer. In total, 15 glycolytic metabolites, nucleotides and cofactors could be identified and quantified in parallel only using a minimal amount of sample volume. Two different chromatographic approaches were presented - one based on cyclodextrin-bonded phases, the other making use of a porous graphitic carbon column to separate isobaric substances with respect to analyte polarity and steric differentiation.

TABLE 2.1. Compound specific parameters for MS/MS fragment detection using the triple stage quadrupole ESI-MS (TSQ Quantum, ThermoFinnigan)

compound	ParI (m/z)	ProdI (m/z)	CE (-)
3-Deoxy-ara.-hept. 7-phos. (DAHP)	287.1	79.0	45
3-Deoxy-ara.-hept. (DAH)	207.2	87.0	12
3-Dehydroquinate (3-DHQ)	189.1	170.8	12
3-Dehydroshikimate (3-DHS)	171.1	127.0	12
Shikimate (SHI)	173.1	93.0	17
Shikimate 3-phosphate (S3P)	253.1	97.0	17
Phenylpyruvate (PP)	163.2	91.0	10
L-Phenylalanine (L-Phe)	163.2	147.0	12
L-Tryptophane (L-Trp)	203.2	116.0	17
L-Tyrosine (L-Tyr)	180.2	162.9	15
Phosphoenolpyruvate (PEP)	167.0	79.0	13
Dihydroxyacetonphosphate (DHAP) / Glyceraldehyde 3-phosphate (GAP)[a]	259.1	97.0	10
2-Phospho-D-glycerate (2PG) / 3-Phospho-D-glycerate (3PG)[a]	185.1	79.0	35
Pentose-5-phosphates (P5P)[a]	229.1	97.0	15
Glucose-6-phosphate (G6P) / Fructose-6-phosphate (F6P)[a]	259.1	97.0	17
6-Phosphogluconate (6PG)	275.1	97.0	17
Fructose 1,6-bisphosphate (FBP)	339.1	97.0	20
Adenosine 5-monophosphate (AMP)	346.2	79.0	35
Adenosine 5-diphosphate (ADP)	426.2	134.0	25
Adenosine 5-triphosphate (ATP)	506.2	158.9	33
Nic. amide ad. dinucl. (NAD)	662.4	540.1	17
Nic. amide ad. dinucl. phos. (NADP)	742.4	620.0	17

[a]lumped pools of isobaric compounds with identical frag. patterns; Abbreviations: ParI - parent ion; ProdI - product ion; CE - collision energy

Later on, a novel approach was presented analyzing cell extracts of *S. cerevisiae* with the aid of HPAE-MS [DEF$^+$02] making use of a triple-quadrupole devise. Compared to the LC-MS approach previously developed [BTW01], much lower detection limits (of up to two orders of magnitude) were achieved applying the HPAE-MS technique, most presumably due to the 'delicate' ion trap used in the LC-MS approach whose performance was influenced by the sample composition and the spray process [SKD03]. However, as already outlined in the preceding paragraphs, the applicability of HPAE may be limited due to the sodium hydroxide gradient necessary for elution which is usually not encountered using HPLC-MS.

2.3.2   The Current LC-MS/MS Approach

Based on the results of Buchholz *et al.* [BTW01], an improved LC-MS method was developed by Oldiges [Old03], which is currently used for *metabolic profiling*. Instead of the previously used iontrap MS, a triple stage quadrupole mass spectrometer with an electrospray ionization source (ESI) for detection (TSQ Quantum, ThermoFinnigan) was applied. This replacement was also motivated by the results of Oldiges [Old03], indicating that no further improvement of the metabolite detection limit could be achieved with the iontrap device because of the high sensitivity of the MS performance owing to increasing salt contents. However, the latter was a consequence of the sample concentration thus hampering the iontrap based approach to become as sensitive as the HPAE-MS protocol, described elsewhere [DEF$^+$02].

Today, the novel LC-MS approach enables the parallel measurement of metabolites of the catabolic central metabolism as well as of the anabolic aromatic amino acid pathway[8]. The optimized MS specific and compound specific MS/MS parameters are shown in the Tables 2.1 and 2.2, respectively. The LC separation is performed using the previously described cyclodextrin method 1 [BTW01] except for the LC split flow of $100\ \mu L\cdot\min^{-1}$ pumped into the MS detector (see Table 2.2). Method 2 was developed to separate isobaric substances and was only applied for the 'old' iontrap MS device:

Method 1 was developed primary for the analysis of nucleotides such as GTP, GDP, ATP, ADP, AMP, NADP, NAD, cGMP, FAD and also for metabolites such as 6PG, FBP, PEP, PYR, G3P and AcCoA. A reversed-phase system consisting of two Nucleodex β-OH columns (250 x 4 mm,

---

[8]It is noteworthy that the measurement of aromatic amino acids compounds requires purified standards which were not commercially available. Their preparation was part of the Ph.D. thesis of Oldiges [Old03] and will be presented in the subsequent sections.

TABLE 2.2. Parameters used to specify mass spectrometry with a triple stage quadrupole and an electrospray ionization source (TSQ Quantum, ThermoFinnigan)

MS parameter	Value
LC split flow	100 $\mu L \cdot \min^{-1}$
ionization	electrospray (ESI)
sheath gas	50 units (nitrogen)
auxiliary gas	15 units (nitrogen)
capillary voltage	4.0 kV
capillary temperature	375 $^\circ C$
MS scan modus	multiple reaction monitoring (MRM)
polarity	negative (-)
data type	centroid
Q2 collision gas	argon (1.5 $mTorr$)
isolation width	1.5 amu
scan time	150 ms per SRM
Q1 + Q3 peak width	0.7 amu

5μm, Machery-Nagel, Düren, Germany) connected in series was used. It was protected by a guard column of the same material which was installed upstream. A binary gradient at a flow rate of 0.5 $mL \cdot \min^{-1}$, consisting of solvent A with 12 mM aqueous ammonium acetate and solvent B with 80% v/v methanol and 20 % v/v solvent A, was applied using a Gynkotek M 480 HPLC pump. The gradient was kept at 2% B for the first 15 min and then increased to 100% B in the following 15 min. After 10 min, the gradient was reduced to the starting conditions (2% B) within 10 min. 20 μL (Gynkotek Gina 50 Autosampler) was used for injection. 100 $\mu L \cdot min^{-1}$ was pumped into the mass spectrometer via a postcolumn T-splitter. To ensure good ionization conditions, a sheath flow of 25 $\mu L \cdot min^{-1}$ methanol was injected into ESI (Jasco PU 1585).

Method 2 was primarily developed to allow isobaric substances such as G6P/F6P or 3PG/2PG to be separated as retention times in chromatography were too similar. Therefore chromatographic separation was realized via steric differentiation using a single porous graphite carbon Hypercarb column (2500 x 4 mm, 5 μm, Thermo-Hypersil, Kleinostheim, Germany) which was protected by an upstream guard column of the same material. Buffer A was used isocratically at a flow rate of 0.5 $mL \cdot \min^{-1}$ during the entire run time of 30 min. After 10 sample injections, a cleaning step with 30 % 2-propanol and 70 % buffer was applied for 300 min, which made this protocol rather lengthy. Other injection conditions for ESI were the same as described in method.

Based on the LC-MS approach, intracellular metabolite concentrations were determined with the aid of the standard addition method [Bad80] to

compensate matrix effects of the sample, which for instance could cause ion suppression during the ionization process [Zim03]. Peak detection and integration was based on the signal-to-noise ratio in the compound specific MS/MS traces. Intracellular concentrations were estimated using the measured concentrations of the sample, taking into account all sample dilution steps and considering cell volumes according to amperometric measurements with the CASY counter (Schärfe System GmbH, Germany) as well as preliminary findings of Buchholz *et al.* [BTW01].

2.4 Developing MMT - the Metabolic Modeling Tool

Parts of the following section were published in Hurlebaus *et al.* [HBA$^+$02] and they were also subjects of the Ph.D. thesis of J. Hurlebaus [Hur01] who was co-supervised by the author.

With the aid of LC-MS and enzymatic analysis, a total amount of approximately 20 to 40 intracellular metabolites and nucleotides of the central metabolism and of the aromatic amino acid pathway can be quantified per sample to date (applying the analytical approaches of the preceding section). Considering that 160 samples are taken during each rapid sampling experiment (see section 2.2), a huge amount of data points representing the metabolic dynamics is produced. Usually the amount of data is in the range of $2000 - 3000$ per experiment. Obviously, this data needs to be stored and handled adequately to ensure its correct use later on. Furthermore, one can assume that its information content is too complex to be analyzed 'intuitively'. To identify *in vivo* enzyme kinetics, the measured metabolite and nucleotide concentrations must be transferred into enzyme kinetic rates and enzyme kinetic parameters, respectively. This can only be done by the application of detailed, structured metabolic models, which have to consider reaction stoichiometry as well as enzyme kinetic rate equations. Mechanistically motivated enzyme kinetic models should preferably be used to identify parameters such as v_{max} (maximum reaction rate), K_S (half-saturation constant) or K_I (inhibition constant), which are typically considered for enzyme characterization.

Motivated by these experimental and modeling constraints, the following demands were formulated for a software tool suitable for the quantitative data analysis:

- **Data management**: All data derived from rapid sampling experiments must be adequately stored and handled to enable its easy use for detailed modeling. Smoothing approaches for raw data should also be included to ensure consistent data sets.

- **Model construction**: The construction of new complex metabolic models must be facilitated to enable fast testing of new modeling ideas. Variations of model structure (topology) as well as kinetic approaches should be readily achievable, thus enabling the formulation of a set of competing metabolic models.

- **Numerical calculations**: Owing to the complexity of the metabolic models, numerical methods used have to be optimally adaptable to

the calculation tasks. Hence special settings for solving ordinary differential equation systems (e.g. especially for stiff systems) and subsequent parameter regression (in a highly dimensional parameter space) must be available. This also includes the necessity to perform sensitivity calculations.

- **Saving modeling results**: For an efficient modeling process, modeling results together with their underlying assumptions (models, constraints etc.) must also be stored.

- **Visualization**: Modeling results have to be adequately visualized to qualify the result.

- **Interface**: The software used should facilitate data transfer to other commercially available software such as *MAPLE* to offer the possibility of additional calculations for e.g. numerical algorithm testing.

- **Open source code:** The source code should be open to allow further software developments driven by current necessities.

2.4.1   Software Overview

When modeling activities were started in 1999, commercial and public-domain software was studied. With respect to the above-mentioned criteria, neither the general modeling tools for dynamic systems such as MODELICA [Ott97], MATLAB/SIMULINK [Inc], MAPLE [Map], gPROMS [Ltd] nor the specialized metabolic modeling tools such as METAMODEL [CBH91], METATOOL [PSVN$^+$99], MIST [EZ95], METASIM [SSB$^+$92], KINSIM/FITSIM [DF97], E-CELL [THT$^+$99] , JARNAC-SCAMP [Sau], DYNAFIT [Kuz96], DBSOLVE [GHS99] and GEPASI ([Men93], [MK96], [Men97], [MK98]) fulfilled our special demands to apply them for rapid sampling data analysis.

This valuation was especially motivated by our ambition to allow the formulation of a set of competing metabolic models, each intended to mirror the experimental data as well as possible. According to our understanding, the formulation of a competing model set was necessary to cope with

- the lacking information of the biological system under investigation,

- the lack of experimental information

- the noise of experimental data and

- the need to simplify the metabolic models as much as possible to uncover the most important underlying reaction mechanisms.
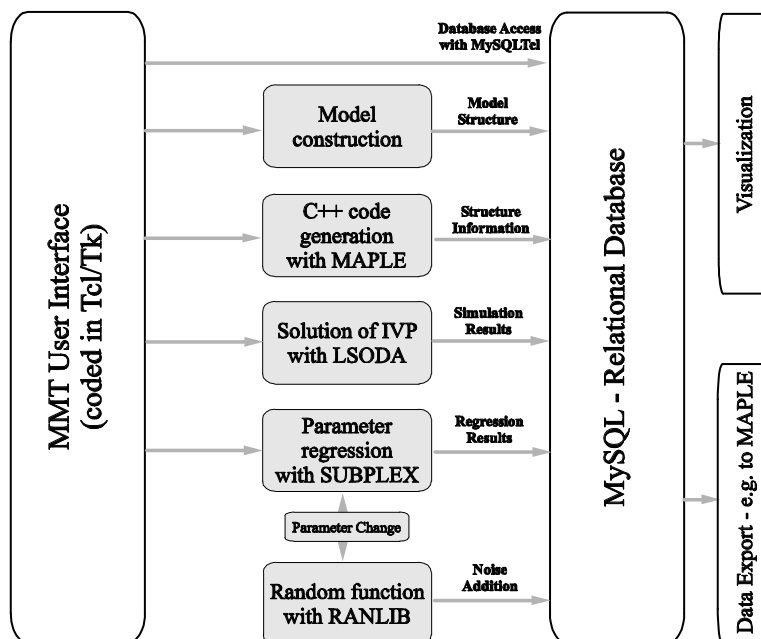
FIGURE 2.5. Global MMT Structure. As indicated, a relational database represents the core element of MMT storing the information for model construction, simulation and optimization. Data for external calculations (e.g. in MAPLE) can also be extracted and visualized. Additionally, complex metabolism models can be constructed via MMT user interface, which are automatically transfered into C++ code via integrated MAPLE routines. Based on LSODA, the stiff ordinary differential equation system is solved and parameter identification is realized using the SUBPLEX algorithm. The RANLIB function allows the randomized start of new parameter identification problems.

Hence the development of a new software product – namely the Metabolic Modeling Tool (MMT) - was started for LINUX systems [HBA$^+$02]. As it will be shown in section 2.7, MMT 1 has been the basis for the development of MMT 2, which is currently performed by our cooperating partners (Haunschild *et al.* [HFWT02]).

2.4.2   The Metabolic Modeling Tool (MMT)

As indicated in Figure 2.5, one of the core elements of MMT is its database that is implemented in the relational database system MySQL [Sys] and coded for Tcl/Tk. Metabolic pathways are regarded as mathematical graphs, only considering relations between reactants (and effectors) and reaction rates. MMT stores these pathways on three levels, which are: (i) modeling group, (ii) model and (iii) simulation and parameter identification.

While the modeling group level contains information about the metabolic network, general kinetic rate equations and experimental data, the model level contains all the models of one metabolic network. A model is defined by relations between the kinetic rate equations and the reactants (stoichiometry). Alternative models can thus be easily defined by changing relations between reactions and kinetics within one modeling group. The third database level 'simulation and parameter identification' stores all parameters of different models.

In general, the metabolic model has the following structure

$$\dot{\mathbf{c}} = \mathbf{N} \cdot \mathbf{v}\left(\mathbf{c}, \mathbf{e}, \mathbf{p}\right) \tag{2.1}$$

where $\mathbf{c}$ denotes the vector of all metabolite concentrations (and $\dot{\mathbf{c}}$ the time derivative), $\mathbf{N}$ represented the stoichiometric matrix of the reactions used and $\mathbf{v}$ codes for the reaction rates. The latter considers mechanistic enzyme kinetic models and depends on the metabolite (reactant) concentrations (also including additional effectors such as cofactors, nucleotides etc.), the vector of (active) enzyme concentrations $\mathbf{e}$ and the kinetic parameters of each enzymatic step, which are lumped in the parameter vector $\mathbf{p}$. It is noteworthy that experimental measurements of active enzyme concentrations were not available thus simplifying the general model structure to

$$\dot{\mathbf{c}} = \mathbf{N} \cdot \mathbf{v}\left(\mathbf{c}, \mathbf{p}\right) \tag{2.2}$$

As a consequence, a model-based maximum reaction rate, which is typically described by v_{max}, basically represents the product of the enzyme specific maximum reactions rate with the unknown amount of active enzyme.

The stoichiometric matrix $\mathbf{N}$ only includes the stoichiometry of the metabolic pathways. Therefore, for each of the reaction rates used an equation has to be assigned that includes kinetic phenomena as well as effectors of reaction rates. Databases such as EMP [EMP], MEDLINE [NCB], ENZYME [Bai00], BRENDA [Bre] and LIGAND [Lig] offer enzyme kinetic data including suggestions for mechanistic models. However, these data are heterogeneous in origin and almost entirely based on *in vitro* experiments, which obviously do not well reflect the intracellular *in vivo* situation. Additionally, the *in vitro* enzyme kinetic data are not infrequently inaccurate, contradicting and incomplete, thus creating significant problems to formulate the 'unequivocal' kinetic model of a distinct reaction step. As a consequence, the strategy was followed to formulate a set of 'competing' mechanistic approaches for such type of reactions instead of considering only one enzyme kinetic model. As outlined in the preceding paragraph,
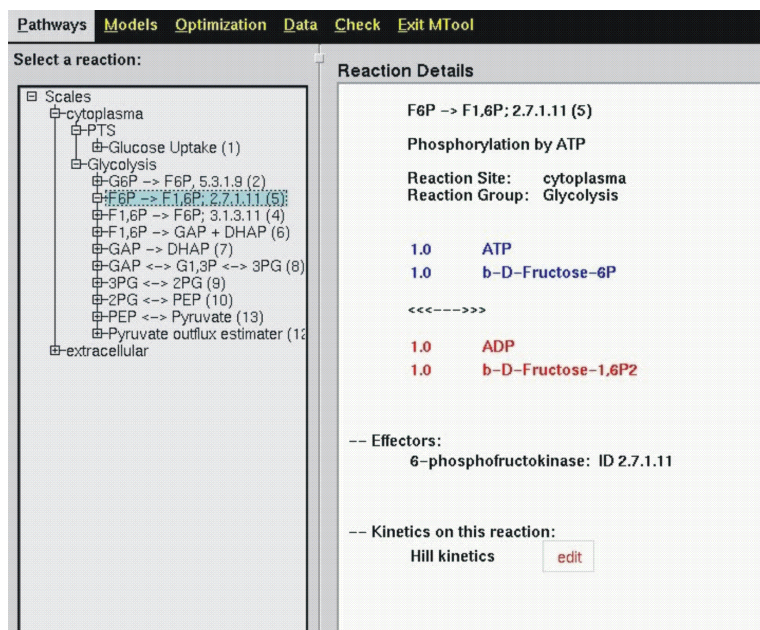
FIGURE 2.6. The main window of the MMT software tool used to configure distinct enzyme kinetic rates as part of metabolic models (see right hand-side). On the left hand-side, different modeling groups (cytoplasma, extracellular) as well as different reaction groups (PTS, glycolysis) are shown.

this strategy necessitated the consideration of a complex data base to handle the resulting, different models[9].

After models have been defined (see also Figure 2.6), an automated model generation starts by setting up a system of ordinary differential equations (ODEs) and the initial value problem (IVP). A text file in MAPLE notation is created, which is used by MAPLE to produce the corresponding C-code. This code is then linked into a simulator and optimizer which are both integrated in MMT. Owing to large differences in metabolic reaction rate velocities, the resulting ODE system is known to be stiff. This is why the freely available ODE solver LSODA [PH] was implemented in MMT, which was optimized for the solution of stiff systems. As parameter values of the metabolic models must be estimated, a parameter regression procedure must be carried out after ODE solution. Optimizers that use gradient information for the calculation of new optimization steps showed

---

[9]It is noteworthy that the number of competing metabolic models can rapidly increase, if different enzyme reactions are queried, even if the overall stoichiometry of the metabolic model (namely the model topology) remains unchanged.

poor performance in preliminary test runs, which is probably caused by the complexity of the parameter space in focus. So, the gradient-free algorithm SUBPLEX [Row90] was used. The optimizer is an extension of the well-known Nelder-Mead approach, using only subspaces of the complete parameter space. In general, model identification was realized by using weighted least-square fitting.

As pointed out elsewhere [HBA$^+$02], MMT is also intended to calculate output sensitivities of the ODE modeling system. Considering the fact that the metabolite vector $\mathbf{c}$ depends on the initial conditions $\mathbf{c_o}$, the parameter vector $\mathbf{p}$ and the time t, it is necessary to make use of the total differential operators

$$\mathbf{D_P c}\left(\mathbf{c_o}, \mathbf{p}, t\right) \tag{2.3}$$

$$\mathbf{D_{c_o} c}\left(\mathbf{c_o}, \mathbf{p}, t\right) \tag{2.4}$$

according to the introductory notes given in the Appendix (see A.6.1). Because the function vector $\mathbf{c}\left(\mathbf{c_o}, \mathbf{p}, t\right)$ is not explicitly known at the beginning of the calculations, the differential equation system has to be solved following the Schwarz' rule according to

$$\frac{d}{dt}\mathbf{D_P c}\left(\mathbf{c_o}, \mathbf{p}, t\right) = \mathbf{D_P}\left[\frac{d}{dt}\mathbf{c}\left(\mathbf{c_o}, \mathbf{p}, t\right)\right] = \mathbf{D_P}\left[\mathbf{N} \cdot \mathbf{v}\left(\mathbf{c}, \mathbf{p}\right)\right]$$

$$= \mathbf{N} \cdot \left(\frac{\partial \mathbf{v}}{\partial \mathbf{c}}\frac{\partial \mathbf{c}}{\partial \mathbf{p}} + \frac{\partial \mathbf{v}}{\partial \mathbf{p}}\right) \tag{2.5}$$

$$\frac{d}{dt}\mathbf{D_{c_o} c}\left(\mathbf{c_o}, \mathbf{p}, t\right) = \mathbf{D_{c_o}}\left[\frac{d}{dt}\mathbf{c}\left(\mathbf{c_o}, \mathbf{p}, t\right)\right] = \mathbf{D_{c_o}}\left[\mathbf{N} \cdot \mathbf{v}\left(\mathbf{c}, \mathbf{p}\right)\right]$$

$$= \mathbf{N} \cdot \left(\frac{\partial \mathbf{v}}{\partial \mathbf{c}}\frac{\partial \mathbf{c}}{\partial \mathbf{c_o}}\right) \tag{2.6}$$

For details see Hurlebaus [Hur01]. Please notice that a much more complex ODE system of $n^2 + n \cdot m$ equations at maximum (with n being the number of ODEs in the original system and m the total number of parameters) is then to be solved using LSODA. Owing to the complexity of the resulting ODE system, this represents an ambitious computing problem. However, knowledge of the time-dependent derivatives of all ODEs with respect to the parameters (output sensitivity matrix) is a prerequisite for qualifying the identified models, as pointed out in Wiechert and Takors [WT03]. MMT is capable to provide this information via an interface to commercial programs like MAPLE, which offers the possibility of easily testing different model discrimination approaches without too much programming effort[10].

---

[10] As an alternative to the explicit solution given in the preceding paragraph, the strategy can be followed to derive the output sensitivities by infinitissimal changes of

As shown in Hurlebaus *et al.* [HBA+02], MMT can cope with the complexity of metabolic models consisting of 26 dynamic variables and 302 parameters, allowing a model parameter identification and an efficient handling of model information in the integrated data base. Hence, the software tool was subsequently used for further metabolism modeling.

---

model parameters used for simulation. Differences of the resulting model predictions can thus be calculated and used for output sensitivity calculation. This robust approach has successfully been applied by Degenring [Deg03], as will be shown in the next section as well as in the Appendix A.6.3.

2.5   Modeling Metabolism Dynamics: Aims and Pitfalls

2.5.1   Modeling Constraints and Simplifying Assumptions

The data sets derived from stimulus-response experiments (for instance by applying a glucose pulse) possess some characteristics which should be carefully considered before the modeling procedure is started. As it will be shown, model structure, model identifiability and validity are significantly determined by the experimental data set.

- **Pulse stimulation:** Typically, stimulus-response experiments are conducted by pulsing glucose to a glucose-limited culture (see section 2.1). While it can be assumed that the cellular PTS allows a rapid pulse transmission into the cell, the direct, experimental evidence cannot be readily achieved, solely applying the protocols of the preceding sections[11]. During the observation window of 20 to 40 seconds, the extracellular glucose concentration typically remains (almost) constant thus providing no experimental basis to estimate the time-variant glucose uptake rate immediately after the pulse. Therefore, glucose uptake rates are usually estimated based on the total metabolism model and not - as it may be preferred - with the aid of additional measurements.

- **Analysis of a single operation condition**: Stimulus-response experiments are typically performed at suitable operation conditions - namely during the glucose-limited growth phase. Although this operating point is beneficial for these experiments, it might not be representative for other culture conditions. For instance, the cellular composition of active enzymes can (and will) be significantly different during the exponential growth phase. Hence, modeling results should be treated with care if they are intended to be extrapolated to other culture conditions.

- **Constant enzyme composition:** As outlined above, it is expected that the intracellular active enzyme content remains constant during the observation window of 20 to 40 seconds, thus allowing the estimation of enzyme specific $v_{\max}$ values. However, it is noteworthy that these values are still dependent on the intracellular enzyme content because no experimental measurements of the real active enzyme

---

[11]Obviously, the use of additional on-line signals such as the dissolved oxygen concentration or the exhaust gas analysis would be helpful to offer an independent basis for the estimation of the glucose uptake flux. While own studies have not yet been performed, strategies for rapid OUR and CER estimation during pulse experiments based on a 'black-box' fermentor model have already been published ([BWG$^+$03], [WLGH03]).

concentration have been performed so far. As a consequence, these metabolic models cannot easily be applied to predict the metabolism behavior under different culture conditions.

- **Average cell composition:** Owing to the rapid sampling protocol used so far, only one representative, mean metabolite concentration is measured in the sample which averages potential inhomogenities caused by cell segregation, cellular compartments (in eucaryotes), spatial gradients, metabolite channeling, macromolecular crowding etc.[12]. Hence, models considering cellular inhomogenities, should not be readily used.

- **Limited insight into the cellular metabolism:** Besides the invaluable results of *metabolomics* obtained so far, they still provide only a limited insight into the cellular metabolism. Only a relatively small fraction of the overall metabolome is quantitatively accessible. Additionally, regarding the aforementioned protocols used so far, for instance any experimental information about *in vivo* enzyme activities is still missing. Hence metabolism models must be aware of these experimental limitations.

- **Identifiability of enzyme kinetics:** Apart from the fact that the information about *in vivo* enzyme mechanisms may be incomplete, contradicting or missing, one should take into consideration that enzyme kinetics are not necessarily identifiable from dynamic data sets. Measurement noise, non-optimal data distribution or insufficient metabolite stimulation are dominant factors that can significantly influence the identifiability of enzyme kinetics [WT03].

Summarizing the aforementioned experimental restrictions, it is obvious that metabolic models derived from stimulus-response data sets can only provide a limited insight into the cellular metabolism. Nevertheless, the approach is still valuable to get a quantitative 'idea' of the *in vivo* biochemical mechanisms in a small part of the total metabolism. For this purpose, structured, non-segregated models should be preferred to mirror the metabolism dynamics observed after glucose pulse experiments (see Figure 2.7).

---

[12] The potential existence of metabolite channeling effects was (and still is) often a matter of controversial discussion. While, for instance, clear evidences are found for channeling in the urea cycle, this is not the case for fatty acid oxydation. However, based on experimental indications ([Hof91], [Mat93], [AS97]) the assumption can be formulated that channeling effects are more likely to occur in eukaryotes (such as yeasts) than in prokaryotes.
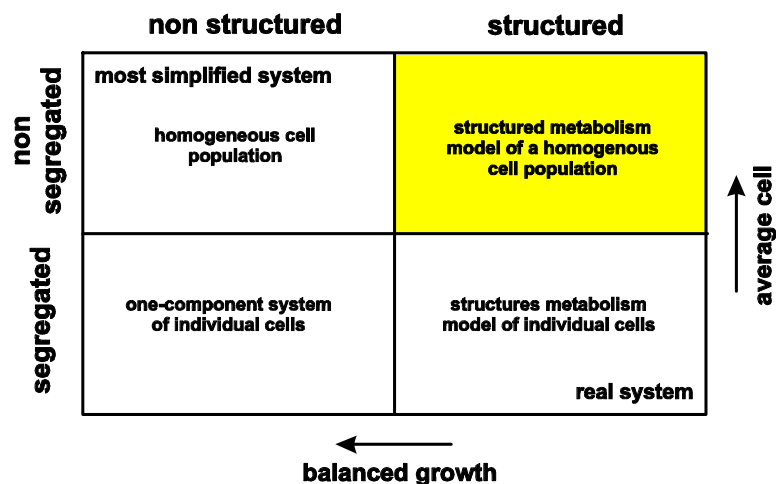
FIGURE 2.7. Model classification with respect to their complexity (according to [Chm91]). While non-segregated, one-component models (macrokinetic approaches) represent the simplest case, segregated, structured models aim to mirror reality. Models used to mirror stimulus-response experiments are usually structured but non-segregated according to the experimental constraints presented in the text.

2.5.2 Stimulus-Response Models

Even the 'simple' bacterium *Escherichia coli* possesses about 4800 genes coding for 2500 proteins and enzymes, uses 50 to 70 sensors surveying changes in the environment and converts substrates via hundreds of metabolic pathways into intermediary products and cellular structures [LS99]. To cope with this complexity, the cell contains functional units that are structured in an hierarchical way [Len00] - namely the modulon, the regulon and, most downstream, the operon. As a consequence, whole cell metabolic models that aim at describing the cellular behavior under varying culture conditions should 'somehow' represent this structure and complexity by a similar modular concept [GBK95].

Following this modular concept, models have been presented that describe distinct functional units, for instance to model *E. coli*'s substrate uptake during diauxic growth on glucose and lactose ([KJLG00], [KG01], [KBL+01]). Apart from these current developments, other 'classical' whole cell models are still well-known. Examples are the pioneering works of Shuler *et al.* [SLD79], Domach, Shuler and co-workers ([DLC+84a], [DS84a], [DS84b]) and Laffend and Shuler [LS94], the latter considering the *lac* operon as well. Alternative methods for whole-cell modeling have been presented by Varner and Ramkrishna ([VR99a], [VR99b]) putting forward the idea of cybernetic metabolic networks which was subsequently supple-

mented by a large-scale modeling concept that aims at marrying stoichiometry and kinetics with metabolic regulation and control [Var00].

Although this list of *E. coli* models is by far not completed, the limited applicability of such type of models to the typical stimulus-response data sets should be clear. As outlined in the preceding subsection, only nonsegregated, structured models solely describing the biochemical metabolism dynamics and ignoring any genetic regulation can be identified with the aid of the experimental data.

In the pioneering work of the Reuss' group ([RBTR97], [TMB$^+$97]), Rizzi and coworkers managed to identify a structured model of glycolysis and tricarboxylic acid cycle of *S. cerevisiae* consisting of 22 dynamic variables (mass balances), 23 reaction rates and about 90 parameters. Later, this model was extended by Vaseghi *et al.* [VBRR99] considering *in vivo* dynamics in the pentose-phosphate pathway. Because pentose-phosphate pools could not be measured *in vivo*, these metabolites were estimated according to a near-equilibrium estimation [SHR81]. It was shown, that the overall metabolism dynamics could - in general - be well mirrored by the structured model. However, the most significant differences between model prediction and experimental observation was found for the intracellular pyruvate concentrations. As shown by Rizzi *et al.* [RBTR97], the model-predicted pyruvate rise after the pulse could not keep pace with the experimental observations and was still increasing when intracellular concentrations were already declining. Additionally, the authors outlined the problem of model uniqueness by stating that '...*the set of equations used for simulation is not exclusive and other kinetic expressions may also lead to reasonable results...*'. However, following works of Mauch *et al.* [MVR00] stressed the general importance of this model identification approach by revealing clear differences of the kinetic structure and parameters of phosphofructokinase I in *S. cerevisiae* between modeling results and *in vitro* enzyme kinetic findings.

In 2002, Chassagnole *et al.* [CNRS$^+$02] presented a structured model of *E. coli*'s central metabolism, which again was identified by glucose pulse experiments. The authors also announced the use of the model for the optimized production of aromatic compounds[13], in analogy to the preceding works of Mauch *et al.* [MBSR01] which lead to an increased ethanol flux in *S. cerevisiae*. Again, the model managed to reflect the measured intracellular metabolism dynamics. However, in the case of pyruvate, this metabolite was repeatedly identified as the one with the most significant difference between measured and predicted values. Anew, the fast pyruvate ascent immediately after the pulse (within 100 *ms*) was not mirrored by

---

[13]Presumably, the L-tryptophane production is meant.

the model which could also not predict the subsequent decline followed by a slow rise during the post-pulse period (30 seconds).

The modeling problems with respect to the pyruvate pool dynamics seem to be remarkable because of the dominating role of pyruvate in the cellular metabolism. For instance, pyruvate serves as a phosphate acceptor for the PTS based glucose uptake; it is an important precursor for the synthesis of several amino acids; it is an glycolytic intermediate and thus involved into glucose overflow metabolism, anaplerosis etc. Recently, pyruvate has been identified as one of the mostly used metabolites/reactants (apart from cofactors and nucleotides) in *E. coli's* metabolism [FW00]. Regarding the general model identification problems outlined in the preceding paragraphs, one might thus conclude that also other, 'competing' modeling approaches would have been successful which would have tried to compensate the (obviously) lacking pyruvate modeling information by alternative models. Hence, instead of one unique model, a family of competing models could have been identified that allows to predict metabolism dynamics equally well, although the model structures and the kinetic equations used may differ.

The problem of model identifiability has also been addressed by Wiechert and Takors [WT03], who stressed the general challenge of model identification based on noisy data sets and also analyzed the possibility of using classical model discrimination approaches together with corresponding experimental design strategies. Visser *et al.* [VdHM$^+$00] proposed the idea of *tendency modeling*, achieving a significant *S. cerevisiae* model reduction by means of time scale analysis. Additionally, the approach of *linlog* kinetics was presented later on [VH03], which aims at combining metabolic control analysis with kinetic modeling. Although it has not yet been applied for measured data of stimulus-response experiments, the approach seems to be a promising tool to model metabolism kinetics with the aid of 'pseudo'-mechanistic, enzyme kinetic models.

2.5.3   Model Identification Problems

Significant parts of the following subsection are already in press (Degenring *et al.* [DFDT03]). They are also subject of the Ph.D. thesis of D. Degenring [Deg03] and were treated in the master thesis of C. Froemel [Fro03] who have been both co-supervised by the author.

Motivated by the published results and based on own experimental findings [Buc01a] as well as on the previously developed MMT software, the aim was followed to identify *E. coli* central metabolism models with the aid

of structured, non-segregated modeling approaches. Because of the modeling problems previously encountered, the paramount goal was to develop a suitable model reduction procedure to eliminate redundant parameters and to uncover the most important control mechanisms of the metabolism models.

For this purpose, the following subsection deals with the presentation of two classical model reduction procedures which were applied to analyze complex metabolism models. For the testing of the model reduction strategies,a set of 13 metabolic models, which originated form approximately 200 different modeling approaches, has been chosen. These 13 models were primary selected because they offered the best, similar model prediction quality taking into account the minimal sum of least squares achieved during the model identification process shown elsewhere [DT02]. This zoo of models was formulated as a consequence of

- missing measurement information, for instance because not all necessary metabolic effectors, reactants etc. can be measured,

- simplifying assumptions, for instance because not-all enzymatic reactions can be formulated in detail and thus must be simplified or even lumped with other reactions,

- model topology variations, for instance because distinct pools of the pentose-phosphate pathway, which are not accessible via measurements, are neglected, lumped or simulated.

For the sake of brevity, not all models are presented in detail, however models 11 and 13 are exemplarily presented (in the sections A.7.3 and A.7.5 in the Appendix) to give an impression of model complexity. Additional information will be given in [Deg03].

Parameter sensitivity analysis will be based on two different criteria - namely **tuning importance** and **principal component analysis** (PCA). Exemplarily using model 11, it will be shown that both approaches lead to comparable results which means that model predictions are still very similar to the original, non-reduced model and the model itself is mechanistically correct. Hence, using the PCA approach, the opportunity for an automatic model reduction is given.

As outlined in the preceding sections, the dynamic model consists of a system of ordinary differential equations (ODE), each equation thus representing a mass balance of the ith metabolite according to

$$\frac{dc^i}{dt} = \sum_{j=1}^{m} \nu_j^i v_j \qquad c^i(t_0) = c^{i,0} \qquad (2.7)$$
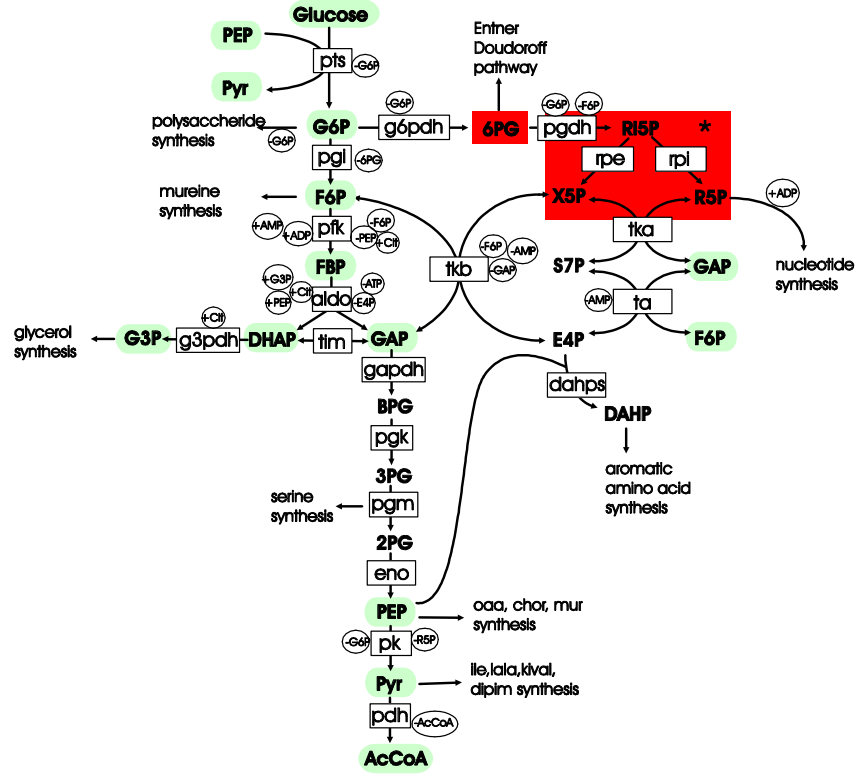
FIGURE 2.8. Reaction network used in model 11 to describe glycolysis in Escherichia coli K12. Squares denote enzyme reactions, cirlces code for regulatory effectors. Blue and red backgrounds indicate the enzymatic or LC-MS/MS based analytical approach used for metabolite quantification. In the pentose-phosphate pathway only the lumped pentose pool was measured. The following abbreviations were used for the enzymatic reactions: aldolase (aldo), dahps (DAHP synthase), enolase (eno), GAP dehydrogenase (gapdh), G3P dehydrogenase (g3pdh), G6P dehydrogenase (g6pdh), PYR dehydrogenase (pdh), phosphofructokinase (pfk), 6PG dehydrogenase (pgdh), G6P isomerase (pgi), phosphoglyceratekinase (pgk), phosphoglyceratemutase (pgm), PYR kinase (pk), Ru5P epimerase (rpe), Ri5P isomerase (rpi), transaldolase (ta), triose-phosphate isomerase (tim), transketolase a (tka), transketolase b (tkb).

where t is the time, c^i denotes the concentration of metabolite i, ν^i_j means the stoichiometric coefficient of this species in reaction j and v^i_j is the rate of reaction j. A detailed description of the mass balance equations together with the enzyme kinetic models is given in the Appendix (see A.7.3). Additionally, Figure 2.8 is shown, representing a rough visualization of the topology of model 11. It is noteworthy that model 11 basically depicts a simplification of Figure 2.8 because some metabolites could not be measured with sufficient analytical accuracy. As already emphasized, this is a typical problem. Therefore, subsection A.7.1 (Appendix) lists some of the most often used, simplifying assumptions which were the consequence of the experimental limitations. As already pointed out, the MMT software was applied for simulation, model identification and analysis. Details of the model identification process are given in the Appendix (see subsection A.7.2).

As outlined in the preceding paragraphs, it was a major aim of this study to identify an appropriate model reduction procedure for complex metabolic models. For this purpose, the normalized sensitivity matrices $\mathbf{S}^i$, which are specific for each metabolite i and are composed of the normalized local sensitivity coefficients $s^i_{j,k}$ at $j = 1 \ldots n$ time intervals considering the kth parameter, were calculated as shown in the Appendix (see subsection A.6.2). In principle, two different approaches for sensitivity calculation could be performed - namely the direct, explicit calculation, which necessitates the solution of a complex ODE system, or the finite difference approximation (see subsection A.6.2).

Figure 2.9 (top diagram) shows the comparison of the sensitivity function curves resulting from both calculation approaches regarding one of the 'most important' parameters in the original model 11 (see below), namely the partial derivatives with respect to $p_g = K_{i,PEP,pfk}$ (see Equation A.17). Based on the high similarity of the corresponding curves the conclusion was drawn that the finite difference approximation using $\Delta p_g = 10^{-5}$ can be chosen to estimate the concentration sensitivities accurately. Therefore this approach was followed in all subsequent studies, since the calculation of the sensitivity functions based on the direct method is very intensive owing to the necessary consideration of all cross-dependencies in the complex metabolism model. The parameter tuning importance, described in subsection A.6.4, and the PCA approach, described in subsection A.6.3, were used to reduce model 11 which originally consisted of 122 parameters in 22 reactions. Both model reduction procedures made intensive use of the normalized sensitivity matrices $\mathbf{S}^i$. In general, the strategy was followed to reduce the model such that no significant discrepancies in the prediction of the metabolite courses or resulting reaction rates (fluxes) occurred [Tur90].
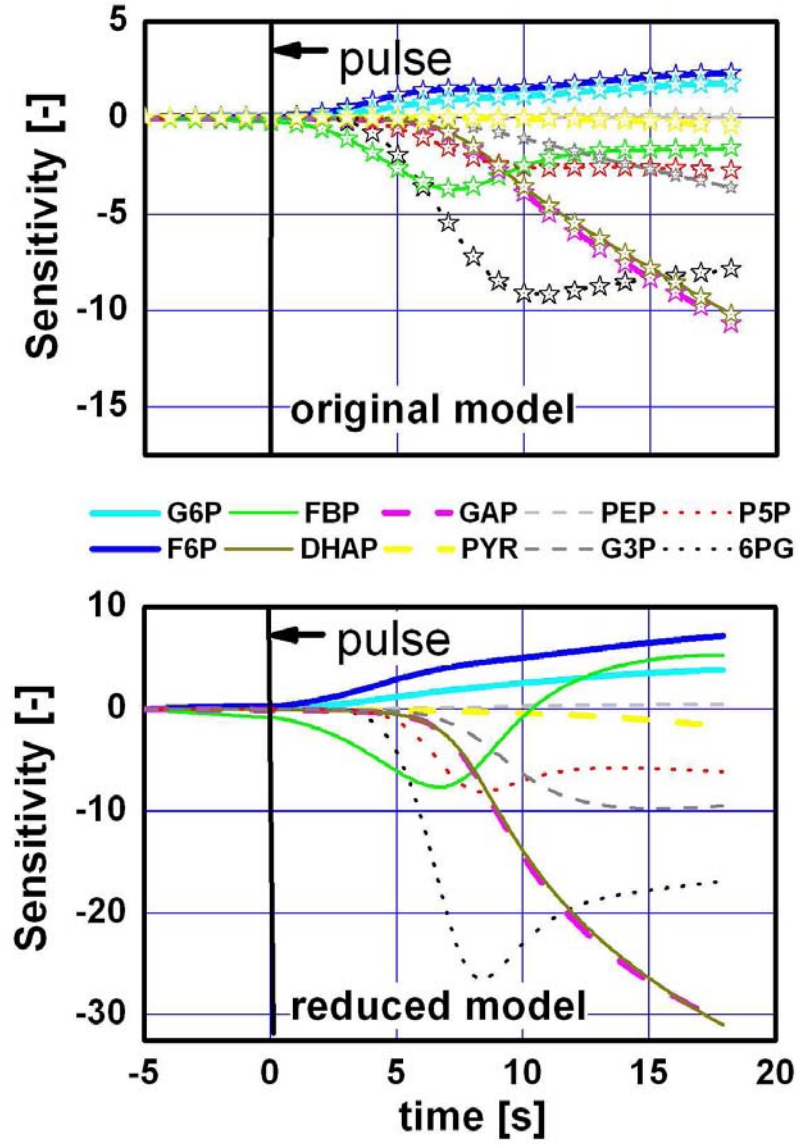
FIGURE 2.9. Overview of the sensitivity functions of the original model (top diagram) and the reduced model (down diagram) which were obtained with respect to $K_{i,PEP,pfk}$ using model 11. Sensitivities were calculated by the finite difference approach (lines, top diagram) or using the explicit calculation (stars, top diagram). Only the explicit sensitivity calculation was used for the reduced model.
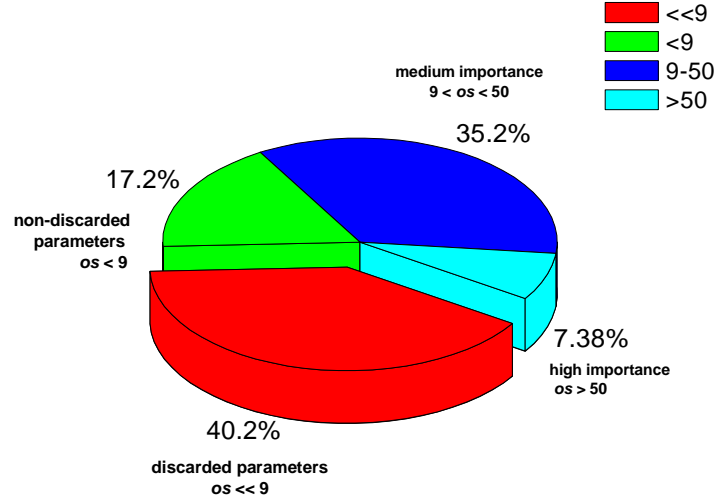
FIGURE 2.10. Distribution of the total overall sensitivities os_p of the 122 parameters used in the original model 11. 49 parameters were discarded because of the low $os_p \ll 9$, which - strictly speaking - represents a heuristic threshold.

Model Reduction Using the Parameter Tuning Importance

As described in Section A.6.4, the 'classical' way of model reduction was primary performed and the parameter ranking was identified considering the corresponding overall sensitivity, os. Starting at the bottom of the list, parameter values were sequentially set to 0 (or to 1, depending on the respective mathematical expression) and the model simulations were restarted. Parameters, which revealed to possess significant influence on the system behavior, although their computed overall sensitivity was low, were not discarded and the reduction procedure was continued with the next parameter.

Figure 2.10 indicates that, although approximately 35 % of all parameters possess a 'medium' importance, only 7.4 % of the parameters revealed to be highly important. Among them, mainly parameters of the glycolysis and the phosphotransferase system were found. The inhibition of the phosphofructokinase by PEP turned out to be a dominating effect in glycolysis. Considering $K_{i,PEP,pfk}$, very high overall sensitivities (up to 600) were calculated, which are one order of magnitude higher than most of the other parameters.
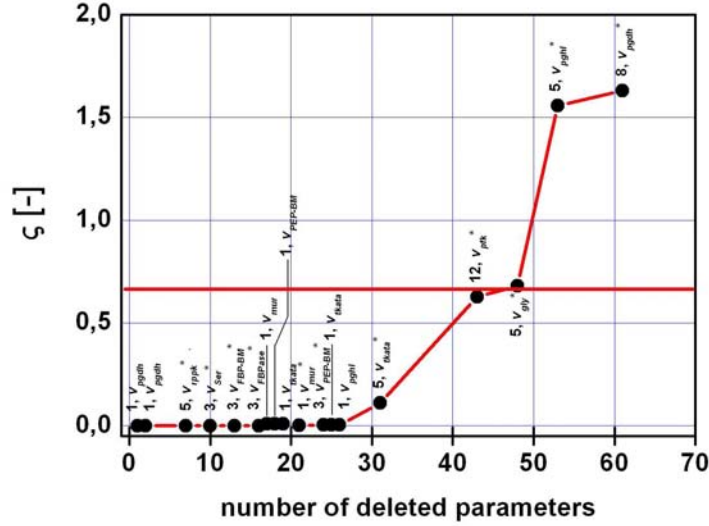
FIGURE 2.11. Error functional ς depending on the number of discarded model parameters in the original model 11. Additionally, the number of PCA-based discarded parameters and their original reaction rate are indicated by labeling. The star (*) denotes the complete elimination of the reaction rate caused by sequential parameter reduction. The ς threshold was fixed heuristically such that significant discrepancies of model predictions caused by on-going model reduction were avoided.

Based on the ranking list, 49 parameters with an overall sensitivity up to 8.88 could be eliminated from the model without significant changes on the systems behavior (see bold written terms in subsection A.7.3, Appendix). However, 21 (17.2 %) parameters of the pentose phosphate pathway and the pyruvate metabolism which possessed low tuning importance smaller than 9.00, could not be discarded from the model because their influence on the model prediction turned out to be too significant. This striking fact was already described elsewhere [VVT85] and was considered to be disadvantageous for the model reduction, because no distinct upper limit for the overall sensitivity values could be given in order to discard all parameters with a smaller value from the model.

Model Reduction Using PCA

As already pointed out, the model reduction with PCA only discarded these parameters which were commonly identified by all three methods. In analogy to the procedure based on parameter's tuning importance, the model prediction after reduction were compared with the original model

prediction in order to qualify whether both models are still similar. For this, the error functional ζ (see subsection A.7.2) with respect to the concentrations of the original model, $c^i(t_j, \mathbf{p})$, and the concentrations of the reduced model, $\tilde{c}^i(t_j, \tilde{\mathbf{p}})$, was used.

Figure 2.11 indicates that approximately 31 parameters were eliminated without any effect on the model predictions. Then, a set of 12 parameters was discarded at one single reduction step because a complete reaction was identified as non-significant. This caused an $\zeta-$increase to about 0.6. Subsequent model reduction lead to even more increasing values. Therefore, the PCA based model reduction was stopped after the elimination of 43 parameters of model 11.

Only minor differences between the PCA approach and the reduction technique via the overall sensitivities os were detected. The reaction catalyzed by the phosphofructokinase was only partially reduced by os-based approach, since an additional constraint, namely the maintenance of the flux distribution, was considered here besides the error functional ζ. Further on only 6 parameters coding for a simple model of the oxidative pentose phosphate branch were not yet detected by the PCA reduction. Thus we concluded, that the reduction results using the PCA approach, as shown in figure 2.11, are basically the same compared with those of the os-based reduction approach.

General Remarks

The parameters discarded from model 11 are shown in subsection A.7.4, Appendix. It was found that parameter elimination usually coincided with the loss of complete mathematical terms, when original *in vitro* kinetic approaches were primary employed without simplification. From this we concluded that it may even be favorable to start model building with already simplified kinetic expressions. For instance, the models can consider mass action kinetics or alternative terms, such as proposed in subsection A.7.1. This holds also true for biomass building reactions, which turned out to be usually a target of model simplification or even complete neglecting (see Table A.7.4), most presumably owing to the significant lack of corresponding information.

Although the model structure was strongly simplified by the model reduction process, the systems behavior did not change significantly. Representative examples are depicted in the Figures 2.12 and 2.13 with respect to the simulated metabolite trajectories of G6P, F6P, PYR, 6PG and the fluxes catalyzed by the PTS, the G6P dehydrogenase (g6pdh), the G6P isomerase (pgi) and the phosphofructokinase (pfk), respectively. Because the flux into the pentose phosphate was lower than 0.01 mM s^{-1} before the reduction and all parameters of the g6pdh-catalyzed reaction revealed to be
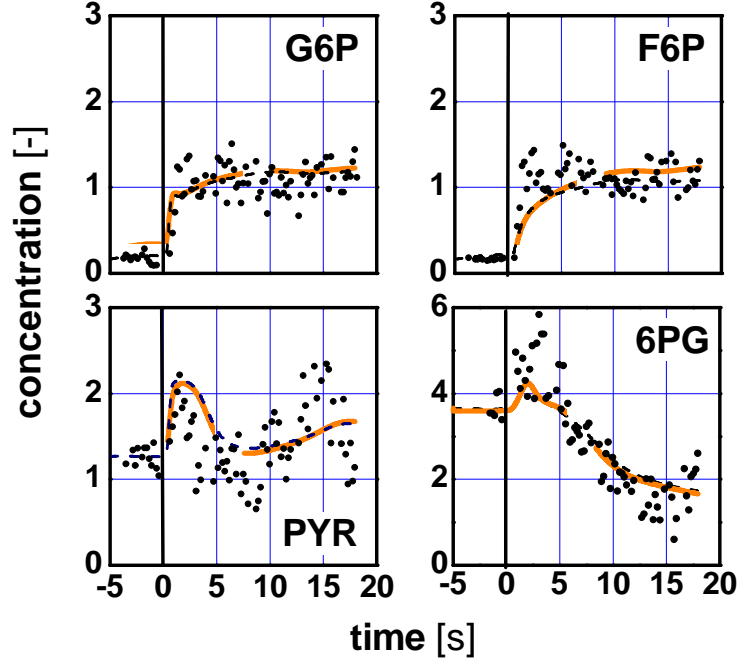
FIGURE 2.12. Curves of some selected, measured (dots) and simulated (lines) metabolites. The light, orange line represents model predictions after reduction, while the dark, black (dotted) line denotes the original model.

insignificant, the reaction was omitted. For the same reason the combined transketolase and transaldolase reactions were eliminated. Thus, the original model was subdivided into one part describing the pentose phosphate pathway and another one modeling the glycolysis.

While modeling the pentose phosphate pathway it turned out that the high steady-state 6PG concentrations of 3.7 mM (see subsection A.7.2, Appendix) could only be maintained by low exchange fluxes between 6PG and P5P. During the subsequent pulse experiment, the intracellular 6PG and P5P levels even sharply decreased, as shown in Figure 2.12. That drop was achieved in the model by the simulation of an enlarged drain off flux for the biomass synthesis, which was qualified as biologically meaningless. However, the remaining model part for the glycolysis remains realistic and allows predictions comparable to those published by Chassagnole *et al.* [CNRS+02].
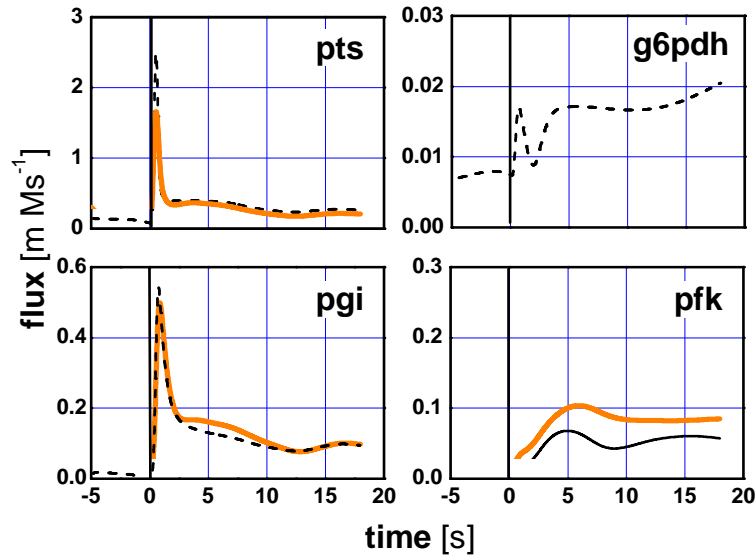
FIGURE 2.13. Curves of some selected, simulated fluxes according to model 11. The light, orange line represents model predictions after reduction, while the dark, black (dotted) line denotes the original model. In the case glucose 6-phosphate dehydrogenase (g6pdh), this flux was eliminated in the reduced model.

To study the general applicability of the model reduction approach, the other twelve models of the preliminary model identification that was mentioned in the introductory section, were reduced as well (see Table 2.3). After the reduction the models were re-optimized. Thereby it was observed that the least square sum of the re-optimized, reduced models was (sometimes) smaller than the least square sum of the original parameter fit. Most presumably, this was due to the improved initial situation for parameter fitting especially if a gradient-free, Nelder-Mead Simplex [NM65] derivative was used, as implemented via the subplex routine [Row90] in MMT.

It was found that all structures could be simplified significantly. For instance the same final structure was uncovered for the models 3, 4 and 5 in Table 2.3. Additionally, model reduction revealed that the models 1-8, and 12 all suffered from the same structural problem, namely an interruption of glycolysis by neglecting the aldolase reaction and transaldolase/transketolase reactions after model reduction. Obviously, these models are not meaningful in a biological sense.

TABLE 2.3. Results of the model reduction process taking into account all 'competing' 13 metabolic models. The models differ by the number of differential equations (DE), the number of model parameters and the achieved least-square sum. Additionally, the least-square sum before and after subsequent optimization is given.

| Model | | before red. | | after reduction. | | |
No.	DEs	Para.	ς	Para	ς before opt.	ς after opt.
1	8	101	1.749	44	2.045	1.523
2	9	105	1.482	35	1.307	1.080
3	9	102	1.189	26	1.264	1.034
4	9	102	1.189	26	1.264	1.026
5	9	102	1.248	26	1.275	0.980
6	9	102	0.951	34	0.944	0.944
7	9	99	1.696	29	1.577	1.302
8	10	122	1.461	73	1.740	1.550
9	10	134	1.087	64	1.508	0.862
10	10	80	1.370	72	1.924	1.372
11	10	122	1.515	73	1.501	1.098
12	9	92	1.151	64	1.151	1.151
13	9	96	0.669	75	1.469	0.814

Models 9 and 10 had the same model structure problem as model 11 and could adequately mirror the glycolysis dynamics. Summarizing, all models revealed some difficulties to simulate the metabolite trajectories in the pentose phosphate pathway, which was most presumably caused by the non-physiological, high 6PG level (3.7 mM, which is more than 22-fold higher than the G6P level). The level is also in disagreement compared to the results of Chassagnole *et al.* [CNRS+02]. This is why it was assumed, that the experimentally determined metabolite curves for 6PG (and maybe P5P) are inconsistent and additional experiments have to be carried out for the reproduction of these trajectories.

Model 13 seems to be most meaningful in a biological sense, because the originally chosen model structure was conserved (see subsection A.7.5, Appendix). However, the low value of the least square sum in Table 2.3 indicates that only highly concentrated metabolites such as FBP, DHAP and GAP could be adequately described, while the model failed to predict the steady-state concentrations and the dynamics of other metabolites.

Interim-Summary

The analysis of the two different model reduction approaches showed that both procedures basically discard the same parameters. However, the PCA approach offers the opportunity to be used as a self-controlled routine, meaning that this procedure can automatically be repeated until a prede-

fined upper-limit of the error-functional ζ is achieved. Using the parameter tuning importance, no unique criterion could be identified because even parameters with small parameter tuning importance caused significant model prediction discrepancies. Therefore, this procedure must be performed step-by-step critically studying each model reduction result.

2.6   Broaden the Scope: From Central Metabolism to Anabolic Pathways

Motivated by the basic problems that were encountered during the glucose-pulse modeling studies of the central metabolism, the (ambitious) aim was formulated to broad the scope of stimulus-response experiments by analyzing anabolic pathways instead of the usually sighted catabolic routes.

Reviewing the comprehensive previous works using *Saccharomyces cerevisiae* ([TMB+97], [RBTR97], [VBRR99], [MVR00] [LEZ+01] [MBSR01], [Vis02]), *Escherichia coli* ([SBTWB99], [BTW01], [BHWT02], [CNRS+02], [SKB+02a]) and *Zymomonas mobilis* ([WBdG96], [WB97]), one might be surprised to recognize that all studies solely focused on the central metabolism, namely the glucose uptake, the glycolysis, the pentose-phosphate pathway and the tricarboxylic acid cycle.

This focus might be unexpected because especially pathway products like amino acids, vitamins, antibiotics etc. are of outstanding commercial interest and are thus at the forefront of *metabolic engineering*. However, when the focus changes from catabolic to anabolic reactions two inherent drawbacks must be taken into account that significantly hamper the 'state-of-the-art' glucose pulse approach.

- **Analytical access**: While almost all metabolites of the central metabolism can be measured enzymatically [Ber85] or, most promisingly, with the aid of LC-MS/MS technology ([BTW01], [DEF+02], [OT03]), similar analytical approaches for other pathway intermediates are usually lacking. Although tools like LC-MS/MS offer great promise for quantifying intracellular metabolite concentrations in general, nevertheless at least purified standards of the intermediates are necessary, which are usually not available commercially. Hence, time-consuming chemical synthesis or the isolation (and purification) of the substance from fermentation supernatant using special 'knock-out' mutants is the consequence.

- **Signal dilution**: The analysis of metabolite concentration profiles of the central metabolism benefits from the relatively short reaction sequence from the signal input (glucose pulse) to its output (metabolite of interest). However, the signal cascade to intermediates of anabolic pathways is significantly longer meaning that concentration dynamics may be strongly 'diluted' in the metabolic network before they reach the desired target metabolite. Hence, the analysis of anabolic pathways dynamics not only necessitates a sufficient stimulation of substrate uptake but also a fortification of the carbon flux into the anabolic pathway of interest.

Despite these potential drawbacks, the results presented in this section will show that the analysis of pathway dynamics by *metabolic profiling* [Fie01] is possible and it provides valuable information about the pathway structure and enzyme kinetics even allowing the identification of potential *metabolic engineering* targets. As an example the aromatic amino acid pathway in *E. coli* for the production of L-phenylalanine was chosen because of the extensive knowledge about this route [Pit96] combined with its commercial importance ([FL93], [SDH+01], [BKM+01]) at the same time embracing the typical drawbacks as mentioned above[14].

Before details of *in vivo* pathway oscillations will be presented, the next subsection compiles some essentials about the aromatic amino acid (AAA) pathway in *E. coli*. Then preliminary experiments are described studying the signal dilution caused by glucose pulse experiments. Finally, details of the AAA pathway dynamics will be given together with novel analytical approaches.

2.6.1   Basics of the Aromatic Amino Acid Pathway in E. coli Focusing on L-Phe Synthesis

In the following, a short, condensed picture of the aromatic amino acid pathway in *E. coli* will be given. For the sake of brevity, this overview cannot be complete and must necessarily ignore all aspects which are not directly involved in the biosynthesis of L-phenylalanine in *E. coli*. Most of the information given in this subsection is taken from the comprehensive review of Pittard [Pit96]. Additionally the review of Bongaerts *et al.* [BKM+01] and detailed publications such as the one of Dell and Frost [DF93] can be recommended for further information.

The Reaction Scheme

A scheme of the aromatic amino acid (AAA) pathway in *E. coli* is presented in Figure 2.14. Additionally, Tables 2.4 and 2.5 provide an overview of the AAA metabolites used to synthesize L-Phe. A selection of some basic chemical properties is given as well. Furthermore, the following section will contain a list of some selected enzyme kinetic properties in Table 2.10.

It is noteworthy that the aromatic amino acid pathway not only leads to the final pathway products L-tyrosine, L-tryptophane and L-phenylalanine but also to folate, menachinone, ubiquinone and enterochelin. Figure 2.14

---

[14]Please notice that the L-phenylalanine bioprocess development represents an additional research focus of this group, which will be presented in chapter 4. Therefore, general motivations to focus on L-Phe production will be given later.
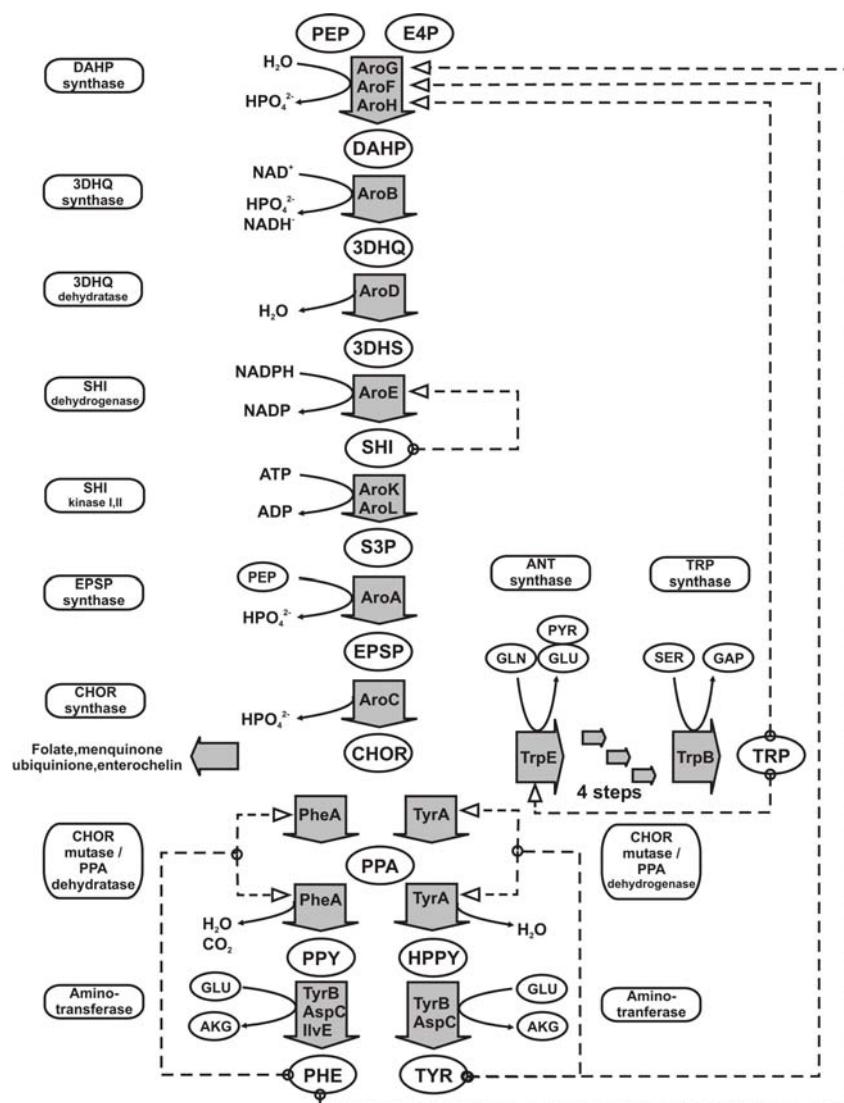
FIGURE 2.14. Principle reaction scheme of the aromatic amino acid pathway (AAA) with special focus on L-phenylalanine production. Arrows indicate enzymatic reactions, ellipses code for metabolite pools and enzyme names are given in the fields. Dotted arrows symbolize feedback inhibition (allosteric control) of the respective enzymes. Transcriptional control is not included. For abbreviations see text and Appendix.

shows that chorismate (CHOR) represents the branch point for these different biosynthetic routes. The route to chorismate is the common pathway for all aforementioned products and has sometimes been referred to as shikimate pathway. All enzymes of this part - except for shikimate kinase (AroL) - appear to be synthesized constitutively [TCP76].
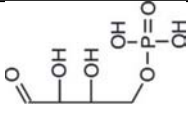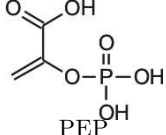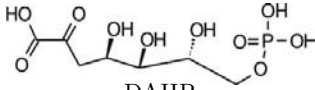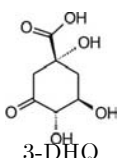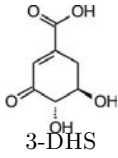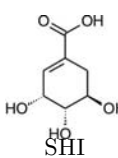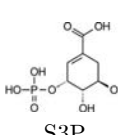
The following presentation of AAA pathway characteristics, focusing on L-Phe production, will show that 'AAA pathway' activity is subject to various controls at different levels thus enabling *E. coli* to adapt the AAA product synthesis tightly to its demands. Feedback inhibition of various key enzymes and gene expression control affecting gene transcription rather than mRNA translation will be in the foreground of the complex, hierarchical control system that hampers the 'simple' construction of - for instance - an L-Phe producing strain.

As depicted in Figure 2.14, the AAA pathway is closely connected to the central metabolism of *E. coli* by converting phosphoenolpyruvate (PEP) from glycolysis and D-erythrose-4-phosphate (E4P) from the pentose- phosphate pathway via **DAHP synthase** into 3-desoxy-arabino-heptulosonate 7-phosphate (DAHP). At the same time a dephosphorylation takes place. This entrance reaction of the AAA pathway is catalyzed by three isoenzymes namely AroF, AroG and AroH. Each of them is feedback inhibited by at least one final pathway product, i.e. L-tyrosine, L-tryptophane and L-phenylalanine. It was found that AroF is subject to tyrosine (TYR) inhibition and AroG is inhibited in the presence of phenylalanine (L-Phe). In both cases a significant inhibition of 95% is observed while only 60% AroH inhibition occurs in the presence of tryptophan ([PG70], [Pit96]). It was found that enzyme kinetics are likely to follow an ordered, sequential reaction mechanism with PEP as the first substrate to be bound [DDS73]. All three DAHP synthases have been shown to be metalloenzymes needing iron (Fe^{2+}) for high activities.

Studying growing *E. coli* cells using LB medium, the phenylalanine sensitive AroG was found to be responsible for more than 80% of the total DAHP synthase activity. However, if no tyrosine inhibition of AroF occurs, this enzyme dominates the total DAHP activity.

It is noteworthy that also the synthesis of all three isoenzymes can be inhibited by the respected aromatic amino acids. In analogy to the feedback inhibition, *aroF* expression is repressed by tyrosine or very high levels of phenylalanine. The AroG synthesis is repressed by phenylalanine and tryptophane as well and AroH synthesis is equally repressed by tryptophane [Pit96]. These controls are partially results of the *tyrR*-regulon which is activated in the presence of tyrosine ($> 36 \ mg \cdot L^{-1}$ [FH88]) thus reducing the expression of *aroF*. The *tyrR* regulon plays a key role in AAA gene

TABLE 2.4. Precursors and metabolites of the aromatic amino acid pathway in E. coli including some selected chemical properties. Part I

Compound	Properties	
E4P		$C_4H_8O_7P$
	M_r	199
	comment	commercially available
		unstable, tends to dimerize
PEP		$C_3H_5O_6P$
	M_r	168
	comment	commercially available
DAHP		$C_7H_{13}O_{10}P$
	M_r	288
	comment	not commercially available
3-DHQ		$C_7H_{10}O_6$
	M_r	190.15
	comment	not commercially available
3-DHS		$C_7H_8O_5$
	M_r	172.15
	comment	not commercially available
SHI		$C_7H_{10}O_5$
	M_r	174.15
	comment	commercially available
S3P		$C_7H_{11}O_8P$
	M_r	254.13
	comment	not commercially available

transcription control by modulating eight unlinked operons via the binding of the corresponding TyrR protein.

3-dehydroquinate (3-DHQ) is synthesized via **3-DHQ synthase (AroB)** taking DAHP as substrate. Cofactors are NAD^+ which is subsequently reduced and Co^{2+}. As shown in Figure 2.14, DAHP is dephosphorylated too. Early studies of Ogino *et al.* [OGMH82] gave rise to the assumption that wildtype AroB activitiy might be insufficient because DAHP accumulation was observed in *aroF* overexpressed strains.

The dehydroquinate dehydratase (**3-DHQ dehydratase, AroD**) catalyzes the conversion of 3-DHQ to 3-dehydroshikimate (3-DHS) by separating H_2O at the same time introducing the first double bond of the aromatic ring. The reaction was found to be reversible.
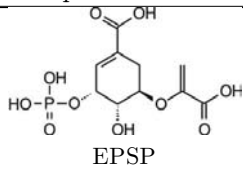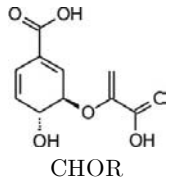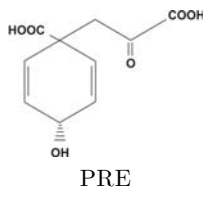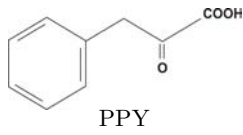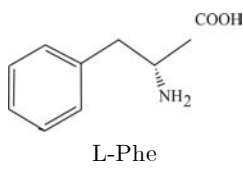
Shikimate (SHI) is synthesized from 3-DHS via **shikimate dehydrogenase (AroE)** taking the protons of $NADPH + H^+$ to reduce the substrate. AroE was found to be feedback inhibited by shikimate, which is characterized by an inhibition constant of $K_{I,SHI} = 0.16\ mM$ [DF93].

Via **shikimate kinase**, shikimate, (SHI) is phosphorylated to shikimate 3-phosphate (S3P) using ATP as P_i donor. *E. coli* possesses two isoenzymes - namely shikimate kinase I (coded for by *aroK*) and shikimate kinase II (coded for by *aroL*)[15]. It was found that both isoenzymes have very different affinities to the substrate shikimate. While the K_M of AroL was identified at 200 μM, the respective value of AroK is about 5 mM. Hence, a dominant role of AroL for AAA flux catalysis can be deduced for typical *E. coli* cultivation conditions. AroL requires Mg^{2+} as cofactor. Although no feedback control on the biochemical level was found for the shikimate kinases, the *aroL* expression revealed to be repressed by the TyrR protein, which is part of the *tyrR* regulon mechanism (see preceding paragraph). Additionally, *aroL* was found to be under the control of a second repressor - called TrpR. In analogy to *tyrR*, the *trpR* regulon controls the expression of genes involved in the tryptophane synthesis. Hence, the regulatory control of both regulons makes it likely that AroL can significantly control the flux through the 'shikimate' pathway.

An additional molecule of phosphoenolpyruvate (PEP) is needed to synthesize 5-enolpyruvoylshikimate-3-phosphate (EPSP) from S3P at the same time dephosphorylating PEP. This reaction is catalyzed by **EPSP synthase (AroA)**. In accordance with the other enzymes of the 'shikimate' pathway (except for *aroL*) the coding gene is constitutively expressed.

---

[15] The kinase numbering corresponds to the sequence the enzymes are eluted from DEAE-Sephadex column.

TABLE 2.5. Precursors and metabolites of the aromatic amino acid pathway in E. coli including some selected chemical properties. Part II

Compound	Properties.	
EPSP		$C_{10}H_{13}O_{10}P$
	M_r	324.18
	comment	not commercially available
CHOR		$C_{10}H_{10}O_6$
	M_r	226.18
	comment	unstable at room temperature
		commercially available
PRE		$C_{10}H_{10}O_6$
	M_r	226.18
	comment	unstable at acid pH
		converts to PPY
		commercially available
PPY		$C_9H_8O_3$
	M_r	164
	comment	unstable
		tends to dimerize
		commercially available
L-Phe		$C_9H_{10}NO_2$
	M_r	165.19
	solubility	~30 g/L ($25°C$)
		equally low in methanol, ethanol
	stability	stable
	pK_1	1.83
	pK_2	9.13
	comment	optically active
		melting point at 283 - $284°C$
		decomposition at 310 - $312°C$
		essential, proteinogenic amino acid
		human daily demand: 2.2 g
		L-Phe: bitter taste
		D-Phe, racemic mixture: sweet taste

The chorismate synthase reaction, which is catalyzed by **CHOR synthase** (**AroC**), introduces the second double bond into the aromatic ring system while P_i is cleaved. The enzyme is known to be oxygen sensitive and it was found to be inhibited in the presence of high Fe^{2+}, although iron is known to be a cofactor for chorismate synthase. Because several authors (Gollub *et al.* [GZS67], Tribe *et al.* [TCP76]) observed that the specific activity of chorismate synthase in cell extract is only 10 to 20% of that of the prior enzyme - namely EPSP synthase - AroC can also be regarded as a potential *metabolic engineering* target.

As illustrated in Figure 2.14, **chorismate** (**CHOR**) represents the most important **branch point** in the aromatic amino acid pathway. CHOR serves as a substrate for ubiquinone, menaquinone, folate and enterochelin synthesis and it is also the substrate for L-tyrosine, L-tryptophane and L-phenylalanine formation. Three enzymes are responsible for the conversion of CHOR into the AAA pathway intermediates phenylpyruvate (PPY), 4-hydroxy phenylpyruvate (HPPY) and anthranilate (ANT) The bifunctional enzyme **chorismate mutase / prephenate dehydrogenase** (**TyrA**) uses chorismate as substrate ($K_{M,CHOR}^{TyrA} = 92\ \mu M$) to synthesize 4-hydroxy phenylpyruvate in a two step reaction via prephenate for L-tyrosine formation. The bifunctional enzyme **chorismate mutase / prephenate dehydratase** (**PheA**) serves for L-Phe synthesis and converts chorismate into prephenate and subsequently into phenylpyruvate (PPY) possessing a chorismate affinity of $K_{M,CHOR}^{PheA} = 45\ \mu M$. The **anthranilate synthase** (**TrpE**) is involved in the tryptophane synthesis and converts glutamine (GLN) together with chorismate (CHOR) into anthranilate, glutamate (GLU) and pyruvate. Because this enzyme revealed the lowest $K_{M,CHOR}^{TrpE} = 1.2\ \mu M$ the tryptophane synthesis seems to be favored by the cells[16].

It is noteworthy that the enzymes TyrA, PheA and TrpE are all significantly feedback inhibited by the final pathway products. In the case of the bifunctional enzymes TyrA and PheA the second reaction is mostly affected. Tyrosine can cause up to 95% inhibition of TyrA catalyzed prephenate dehydrogenase activity. Phenylalanine can reduce the prephenate dehydratase activity of PheA up to 90% and TrpE is inhibited by tryptophane as well. Furthermore it was observed that the PheA synthesis can be repressed in the presence of tyrosine. Hence, to achieve an increased L-Phe production, the overexpression of *pheA* and/or the use of feedback resistant mutants should be favored.

---

[16] For the sake of brevity tyrosine and tryptophane pathway details will not further discussed. The same holds true for the ubiquinone, menaquinone, folate and enterochelin biosynthesis. However, these pathways play an increasing role in current research as indicated in section 4.6.

The final step of both tyrosine and phenylalanine formation is the **trans-amination** of phenylpyruvate (PPY) and 4-hydroxy phenylpyruvate (HPPY) with the amino donor glutamate to tyrosine and phenylalanine and α-ketoglutarate (AKG). It was found that at least three amino transferases can catalyze this reaction: the **branched-chain amino acid aminotransferase** coded for by *ilvE,* the so-called **aromatic aminotransferase** encoded by tyrB and the **aspartate aminotransferase** coded for by *aspC*. Under physiological conditions, the aromatic aminotransferase TyrB is assumed to play the dominant role ($K_{M,PPY}^{TyrB} = 56 \ \mu M$, $K_{M,HPPY}^{TyrB} = 32 \ \mu M$, $K_{M,GLU}^{TyrB} = 280 \ \mu M$) while the aspartate aminotransferase AspC only contributes at high phenylpyruvate and 4-hydroxy phenylpyruvate levels ($K_{M,PPY}^{AspC} = 650 \ \mu M$, $K_{M,HPPY}^{AspC} = 400 \ \mu M$, $K_{M,GLU}^{AspC} = 900 \ \mu M$). The synthesis of the aromatic aminotransferase TyrB can be repressed by tyrosine.

Transport Systems

In analogy to independent studies focusing on the L-lysine export in *C. glutamicum* ([BEK93], [VSE96], [KLB$^+$96]) it would be fortunate whether an active transport system in L-Phe producing *E. coli* could be identified and designed such that no intracellular product accumulation occurs. However, studies of Jacobi and Krämer [JK96] indicate that diffusion-driven L-Phe exports is more likely than active export of the aromatic amino acid. Besides, indications of an active transport system given by Grinter [Gri98] were not supported by others ([SWG$^+$91], [PP96], [CP97]) who studied the L-Phe specific permease in *E. coli*. Hence it must be assumed that L-Phe leaves the cell mediated by an L-Phe specific permease following a diffusion driven transport.

2.6.2   *Preliminary Glucose Pulse Experiments*

> Significant parts of the following subsection were already published by Schmitz *et al.* [SHBT02]. They are also subjects of the Ph.D. thesis of M. Oldiges [Old03] and were treated in the master thesis of E. Hirsch [Hir01] who have been both co-supervised by the author.

In the introductory part of this section, the statement has already been emphasized that the successful application of glucose-pulses can significantly be hampered by (i) the limited analytical access to the pathway intermediates and (ii) by signal dilution.

When these preliminary experiments were planned and performed, the first drawback was still existing. The LC-MS/MS based analytical access to measure intracellular pools of the AAA pathway was not yet developed. This is why an extracellular pool analysis was applied using three

knock-out mutants[17]. Because the strains contained catalytically inactive 3-dehydroquinate synthase (AroB), shikimate dehydrogenase (AroE) or 5-enolpyruvoylshikimate 3-phosphate synthase (AroA), these *E. coli* strains produced 3-deoxy-D-arabino-heptulosonate 7-phosphate (DAHP), 3-dehydroshikimate (DHS) or shikimate 3-phosphate (S3P), respectively. For simplicity, the strains are thus called *E. coli* DAHP, *E. coli* DHS and *E. coli* S3P (for details see subsection A.1.1, Appendix). Presumably based on (facilitated) diffusion, the pathway intermediates were secreted into the fermentation supernatant and thus accumulated. Because their accumulation could be detected applying different analytical techniques (A.3.4, Appendix), this approach offers the possibility to detect production rate changes after a glucose pulse.

Hence it was the aim of this study to investigate whether and how glucose pulse experiments affect the accumulation rates of DAHP, DHS or S3P. The results obtained should give rise to the conclusion whether a significant signal dilution exists and how it could be prevented or overcome to enable the successful application of intracellular AAA pathway dynamic studies later on.

Experimental Procedure

The fed-batch fermentations (with the manual glucose pulse using a syringe with a 0.22 μm filter) were performed in a 2 L Labfors bioreactor (Infors, Switzerland) at 37°C and pH 6.5 (titrated with 25% NH$_4$OH) using the medium 'GPM' for glucose pulse experiments as indicated in the Table A.2. Please notice the extra addition of the auxotrophic substances which was essential for growth of the knock-out mutants. The glucose feed was realized with a Dosimat 665 (Metrohm AG, Switzerland). IPTG induction was achieved with a final concentration of 100 μM. To monitor adequately the fermentation process, 4 to 6 samples of cell suspension (4 mL) per hour were taken during the phases II and III of the experiment (see below). Standard analytical approaches were applied (see subsection A.3.3, Appendix) identifying the correlation $CDW = 0.43 \ gL^{-1} \cdot OD_{650}$. The analysis of DAH(P), DHS and S3P accumulation in the culture supernatant was performed following a concerted enzymatic, HPLC- and ^{1}H-NMR-based approach (see subsection A.3.4, Appendix).

Fermentation Strategy

In order to identify the effects of glucose pulses on the *E. coli* strains used, an experimental protocol had to be developed allowing different glucose

---

[17] These mutants were kindly provided by U. Degner, M. Kremer, J.Bongaerts and G. Sprenger as indicated in the Appendix.
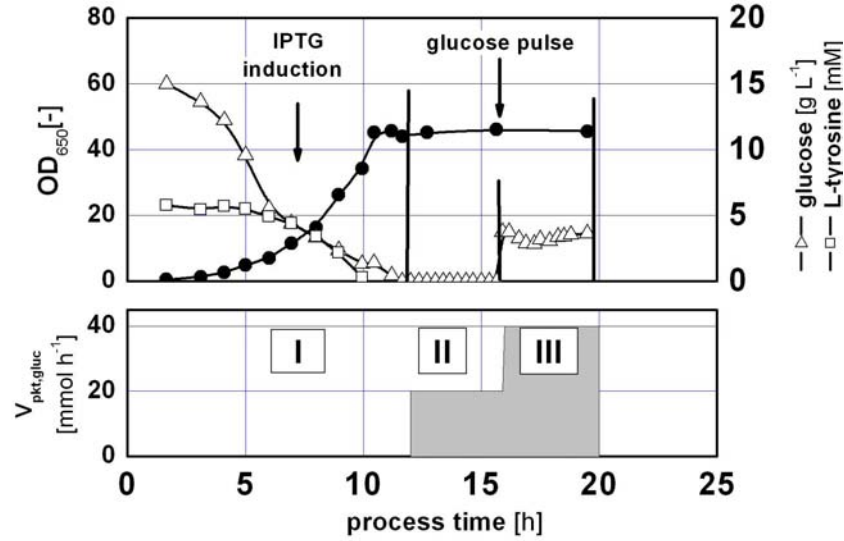
FIGURE 2.15. Example of the fermentation strategy used to study the effects of glucose pulses to a glucose-limited *E. coli* DAHP culture. During phase I cell growth takes place, while no biomass is produced during the following periods. A glucose pulse together with a sudden increase of the glucose feed $V_{pkt,gluc}$ is installed to finish phase II and to begin phase III.

limitation levels to be controlled and their impact on the strain physiology after glucose pulses to be qualified. Using the DAH(P) producing *E. coli* strain as an example, the following fermentation strategy was applied:

The fermentation process consisted of three phases (see Figure 2.15). During the first phase (I) biomass was produced until the aromatic amino acids PHE, TYR and TRP were depleted[18]. IPTG was added to overexpress plasmid-encoded genes thus causing an increased carbon flux into the aromatic amino acid pathway. In the second phase (II), the glucose feed was reduced to a limiting value, followed by an increase in phase (III). The latter was installed such that a saturated glucose supply was ensured. In phases II and III no biomass was produced. During all phases aerobic conditions with DO setpoints as 30, 60 an 40% during the phases I, II and III, respectively, were chosen.

To investigate the effects of the glucose pulse on different glucose limitation levels, the maximum, strain-specific glucose consumption rate realized

---

[18]Please notice that ample amounts of the other auxotrophic substances were supplied.

in phase III was estimated in a previous experiment. For *E. coli* DAHP, *E. coli* DHS and *E. coli* S3P the glucose consumption rates were determined as 37.9, 78.8 and 30.3 $mmol \cdot h^{-1}$, respectively. All three strains achieved biomass concentrations at about 19.7 $g \cdot L^{-1}$. For instance, taking the observed glucose consumption rate of *E. coli* DAHP (37.9 $mmol \cdot h^{-1}$) as a reference, 0%, 25%, 50% and 75% glucose limiting feeds were calculated according to 37.9, 28.4, 19.0, 9.5 $mmol \cdot h^{-1}$. These glucose feed rates were installed during phase II. Then, after about 4 h, 25 mL of a glucose solution was rapidly added to finish the limitation period (II) and to immediately shift the glucose concentration up to 5 $g \cdot L^{-1}$ (27,6 mM). At the same time, the glucose feed was enhanced to ensure saturated glucose consumption rates, which resembled the determined 0% limitation value. As already pointed out, the accumulating pathway intermediates were frequently measured during the periods II and III to detect changes of the resulting production rates caused by the glucose pulse.

Experiments with *E. coli* DAHP

Using *E. coli* DAHP, pulse experiments with 25, 50 and 75% limitation were performed (and each repeated) as described in the preceding paragraphs (see Figure 2.16). As depicted in the figure, a clear dependency of the rate of the DAH(P) synthesis on the degree of glucose limitation can be recognized. This is also shown in Table 2.6, generally indicating that the weaker the glucose limitation in phase II, the higher the rate of DAH(P) production. In accordance with the saturated glucose supply in phase III, the highest production rate was observed in this phase.

Based on the observed variations of DAH(P) formation it was concluded that the glucose pulse experiments changed significantly the carbon fluxes into the aromatic amino acid pathway revealing a strong correlation of DAH(P) formation and glucose supply. The stronger the glucose limitation before the glucose pulse was, the larger the observed flux changes were. Phase III after the glucose pulse was characterized in all experiments by

TABLE 2.6. Results of a series of experiments studying *E. coli* DAHP strains under different glucose limited conditions as indicated. To qualify the experimental accuracy the standard deviation sd is given.

rate.	limitation degree [%]			
$mmol \cdot g^{-1} h^{-1}$	**75**	**50**	**25**	**0**
$\pi_{DAH(P)}^{a}$	0.118	0.224	0.299	0.531
$\pi_{DAH(P)}^{b}$	0.122	0.221	0.348	-
$\overline{\pi}_{DAH(P)} \pm sd$	0.120±0.003	0.223±0.002	0.324±0.035	0.531±0.01^{c}

[a,b]independent experiments

[c]result from all six experiments
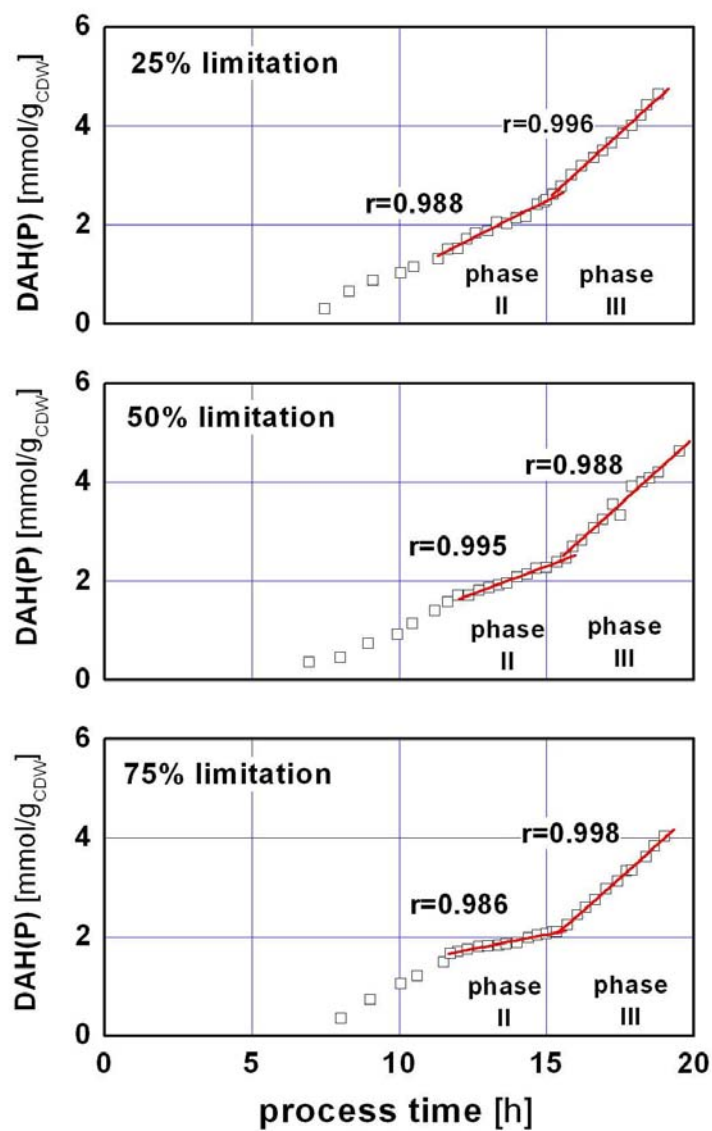
FIGURE 2.16. DAH(P) production rates related to the cell-dry weight of *E. coli* DAHP as a function of process time and installed glucose limitation are given. During phase II glucose limitations ranging from 25 to 75 % of the maximum glucose uptake rate were applied. Additionally, the regression coefficient r is given to qualify the almost constant DAHP production rates.
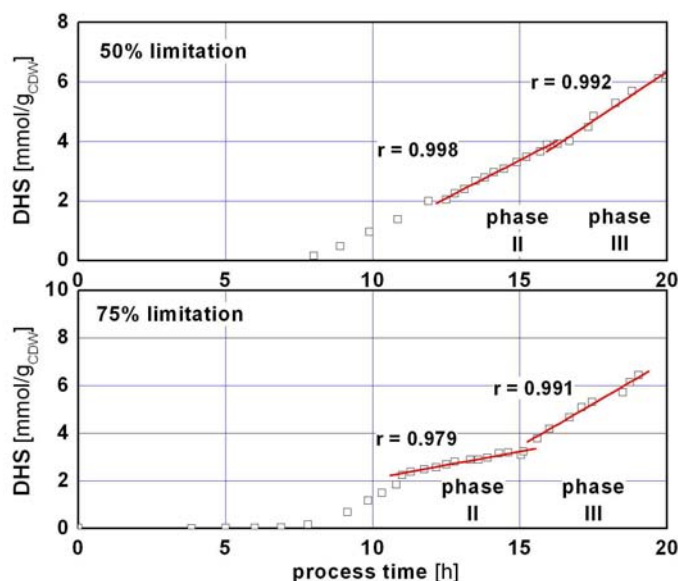
FIGURE 2.17. DHS production rates related to the cell-dry weight of *E. coli* DHS as a function of process time and installed glucose limitation are given. During phase II glucose limitations ranging from 50 to 75 % of the maximum glucose uptake rate were applied. Additionally, the regression coefficient r is given to qualify the almost constant DHS production rates.

a highly reproducible biomass-specific DAH(P) productivity (see the low standard deviation in Table 2.6), irrespective of the extent of the previous limitation. Obviously, cell metabolism was not irreversibly affected by the strong glucose limitation in period II, leading to very similar, final DAH(P) formation rates of $0.531 \pm 0.014 \ mmol_{DAH(P)} \cdot g_{CDW}^{-1} \cdot h^{-1}$. Hence it was concluded that this experimental strategy can be applied to study the effect of glucose pulses on the AAA pathway.

Experiments with *E. coli* DHS

The effects of glucose pulses were also studied using *E. coli* DHS, following the same protocol as before, performing pulse experiments with 50 and 75% limitation and repeating them once. As it can be seen from Figure 2.17 and Table 2.7 the same correlation between glucose pulse intensity and DHS formation was observed: the stronger the glucose limitation, the larger the difference in productivity after glucose pulse during the third period. However, if product formation rates of *E. coli* DHS and *E. coli* DAH(P) at 50% glucose limitation are compared, a relatively high DHS production (∼74% of the maximum value) is found. For comparison: DAH(P) production only achieved 40% of its maximum. Therefore, it was assumed that a further de-

TABLE 2.7. Results of a series of experiments studying *E. coli* DHS strains under different glucose limited conditions as indicated. To qualify the experimental accuracy the standard deviation sd is given.

rate.	limitation degree [%]			
$mmol \cdot g^{-1}h^{-1}$	**75**	**50**	**25**	**0**
π_{DHS}^{a}	0.183	0.488	n.d.	0.647
π_{DHS}^{b}	0.107	0.516	n.d.	-
$\overline{\pi}_{DHS} \pm sd$	0.145±0.054	0.502±0.020	n.d.	0.647±0.01^{c}

[a,b]independent experiments

[c]result from all four experiments

n.d.: not determined

cline of glucose limitation to 25% would not reveal any differences in DHS formation compared to the maximum value. The 25% glucose limitation experiment for *E. coli* DHS was thus omitted. In analogy to the previous findings using *E. coli* DAH(P), a high reproducibility of the maximum DHS formation rates was found again (see Table 2.7; $\overline{\pi}_{DHS} = 0.0647 \pm 0.017$ $mmol_{DHS} \cdot g^{-1}h^{-1}$).

Experiments with *E. coli* S3P

Further studies with *E. coli* S3P were carried out to investigate the glucose pulse transmission via DAH(P) and DHS downstream to S3P. Experiments with 50 and 75% glucose limitation were performed. While the strains *E. coli* DAH(P) and *E. coli* DHS accumulated only the intermediate, which is prior to the catalytically inactive enzyme, *E. coli* S3P exhibited a different behavior. Apart from S3P, shikimate and DHS were also detected in the fermentation supernatant. While the shikimate accumulation could be a consequence of an unspecific phosphatase activity taking S3P as a substrate, the DHS appearance could give a hint to an insufficient shikimate dehydrogenase (AroE) activity. The latter is likely to occur as a result of feedback inhibition by shikimate [DF93].

In the experiment with 75% limitation, the production rates of S3P, shikimate and DHS increased after the glucose pulse (see Figure 2.18 and Table 2.8). However, it is noteworthy that the significance of rate changes strongly depended on the relative intermediate position in the aromatic amino acid pathway. Intermediates further downstream of the pathway were less affected than those upstream. For instance, π_{DHS} increased significantly more strongly than π_{SHI} shikimate, which could be a consequence of the increasing feedback inhibition at rising shikimate concentrations. Additionally, much stronger changes of π_{DHS} were observed than those of π_{S3P}. Studying the 75% limitation experiment, the most dominant change of the production rate is observed for DHS, showing a more than 11.8-fold increase of the production rate after the pulse. In case of S3P a 5.6-fold
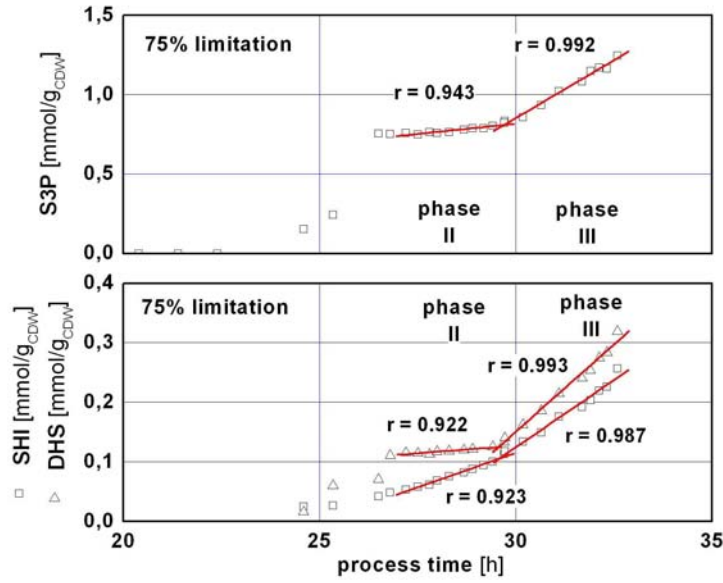
FIGURE 2.18. S3P production rates related to the cell-dry weight of *E. coli* S3P as a function of process time and installed glucose limitation are given. During phase II a glucose limitation of 75 % of the maximum glucose uptake rate was applied. Additionally, the regression coefficient r is given to qualify the almost constant S3P production rates. As shown, significant by-product formation of SHI and DHS took place during the same experiment.

increase could be observed, while the shikimate production rate only doubled.

Analyzing the experiment with 50% glucose limitation, the same scenario was found. (Figure 2.19, Table 2.8). In analogy to the 75% limitation experiment the most significant change was observed for DHS. The production rate of DHS showed a 3.4-fold increase after the glucose pulse, while the production rates of S3P and shikimate remained almost constant. In both experiments the most significant shift of production rates was ob-

TABLE 2.8. S3P and by-product formation using *E. coli* S3P under different glucose limited conditions. To qualify the experimental accuracy the standard deviation sd is given.

| rate.	limitation degree [%]			
$mmol \cdot g^{-1}h^{-1}$	**75**	**0**	**50**	**0**
π_{DHS}	0.005	0.059	0.018	0.062
π_{SHI}	0.023	0.045	0.005	0.005
π_{S3P}	0.026	0.146	0.099	0.105
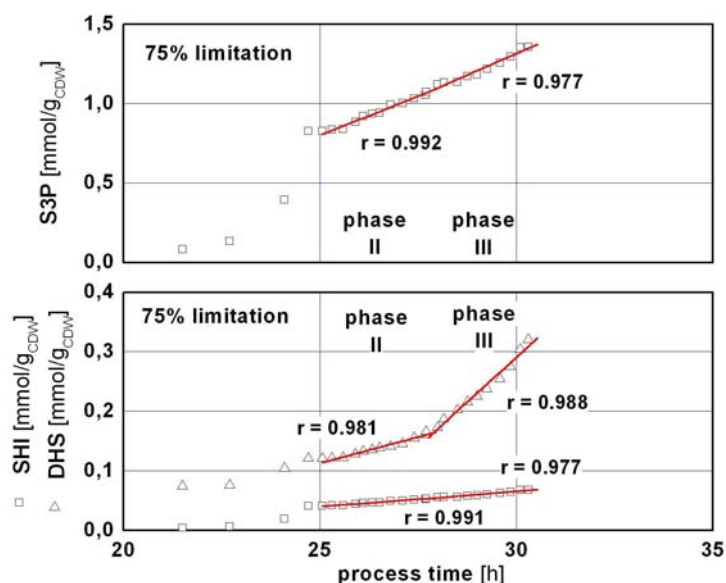
FIGURE 2.19. S3P production rates related to the cell-dry weight of *E. coli* S3P as a function of process time and installed glucose limitation are given. During phase II a glucose limitation of 50 % of the maximum glucose uptake rate was applied. Additionally, the regression coefficient r is given to qualify the almost constant S3P production rates. As shown, significant by-product formation of SHI and DHS took place during the same experiment.

served for DHS, which is the most upstream intermediate. Significantly smaller changes of the production rates were observed in both experiments for the more downstream intermediates S3P and shikimate. The observed quantitative differences between the shikimate production rates in both experiments is a surprising result and which is not yet understood.

Interim Conclusion

Summarizing it can be stated that significant flux changes can be observed in the aromatic amino acid pathway as a consequence of extracellular glucose pulses. Interestingly, these changes strongly depend on the pulse intensity and on the relative position of the pathway intermediate in focus. The more downstream an intermediate is, the higher the stimulus must be to detect significant carbon flux shifts. While relatively small changes of 25% glucose supply could still be detected for DAH(P), a 75% increase was necessary to influence S3P production. Figure 2.20 illustrates this general finding considering the metabolites E4P and PEP as (secondary) stimulators of the primary glucose pulse with respect to the AAA pathway. It
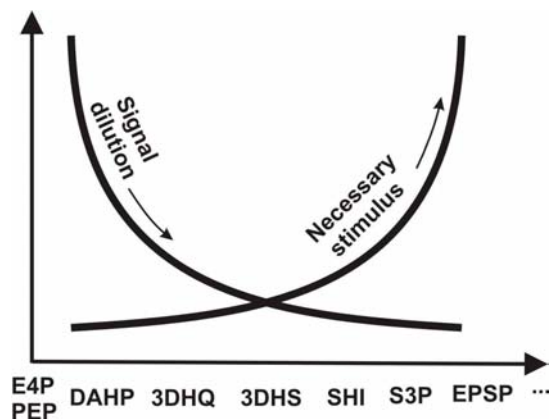
FIGURE 2.20. Principle scheme of the signal dilution observed in the aromatic amino acid pathway as a consequence of extracellular glucose stimulation. The intracellular stimulators are thus represented by E4P and PEP which transmit the glucose pulse signal into the AAA pathway. Because intermediates such as EPSP only 'see' a very diluted signal, high extracellular stimulations are necessary to cause identifiable effects.

seems to be noteworthy that glucose pulses did affect S3P, provided that their intensity was strong enough. Indeed, this observation is remarkable because of the fact that the following reaction, namely EPSP synthase, condenses S3P with PEP thus being again stimulated by the glucose pulse via PEP addition.

2.6.3   In vivo Analysis of the Aromatic Amino Acid Pathway

Significant parts of the following subsection were submitted for publication (Oldiges *et al.* [OKDT03]). They are also subjects of the Ph.D. thesis of M. Oldiges [Old03] and were treated in the master thesis of M. Kunze [Kun03] who have been both co-supervised by the author.

The experimental results presented in the preceding subsection were qualified such promising that further activities focused on the identification of post-pulse intracellular metabolite dynamics in the AAA pathway. As already indicated, the lack of purified standards of the pathway intermediates was regarded as a major problem before the LC-MS/MS-based analysis approach could be developed and used for the investigation of *in vivo* metabolite concentrations. Table 2.9 shows that almost all intermediates upstream of the branch point chorismate were not commercially available (except for SHI). This is remarkable because it is exactly this part of the

TABLE 2.9. List of the AAA pathway intermediates for L-PHE synthesis with respect to their commercial availability.

metabolite	commercial availability	
	yes	**no**
E4P	•	
PEP	•	
DAHP		•
DAH		•
3DHQ		•
3DHS		•
SHI	•	
S3P		•
EPSP		•
CHOR	•	
PRE	•	
PPY	•	
L-Phe	•	

aromatic amino acid pathway which is highly feedback regulated by the final pathway products and by pathway intermediates (see section 2.6.1). Hence, the primary studies focused on the preparation of these standards, which were not commercially available

Standards of AAA Pathway Intermediates

For the production of **DAHP** and **DAH** the *aroB*-negative *E. coli* mutant *E. coli* DAHP (see section A.1.1), which was already introduced in the preceding subsection, was cultivated. Following the procedure of Mehdi *et al.* [MFK87], the samples were centrifuged and further processed via several chromatographic ion exchange steps followed by vacuum drying and product extraction until approximately 1.6 g Li-DAH (purity ∼75%) was achieved. In contrary to the previous findings, DAHP was not found as a significant fraction of 17 to 34 %. Instead, only very low DAHP amounts could be isolated to serve as a qualitative standard for subsequent analytical developments. According to the current hypothesis DAHP is subject of intracellular dephosphorylation which hampered its isolation from the culture supernatant.

3-DHQ was chemically synthesized following the procedure of [GJ56], based on the oxidation of shikimate with concentrated nitric acid.

For the production of **3-DHS** the *aroE* -negative *E. coli* mutant *E. coli* DHS (see section A.1.1), which was already introduced in the preceding subsection, was cultivated in analogy to *E. coli* DAHP. 3-DHS was isolated from the supernatant following the procedure of Dell and Frost [DF93],

which consisted of ethyl acetate-based extraction followed by sample concentration and subsequent anion exchange chromatography.

In analogy to DAH(P) and 3-DHS, the production of **S3P** based on the *aroA*-negative strain *E. coli* S3P (see section A.1.1) which was presented in the preceding section. The S3P isolation from the culture supernatant included the steps cell separation, cation/anion exchange, sample concentration and extraction following the previously published protocol of Coggins *et al.* [CBC+87].

Finally, DAH, 3-DHQ, 3-DHS and S3P were quantitatively available for the analytical development based on LC-MS/MS, while the small amount of DAHP only allowed its use as a standard for peak identification and not for metabolite quantification. E4P, PEP and SHI were commercially available. Hence the LC-MS/MS method (presented in section 2.3) was developed by Oldiges [Old03] to quantify the intracellular concentrations of the first five AAA pathway intermediates. That means, an access was achieved to monitor *in vivo* the first five steps of L-Phe synthesis, which are the most feedback regulated reactions.

Experimental Expectations and Limits

Glucose pulse experiments were planned following the previously described procedures. Accordingly, cells were stimulated by a sudden rise of glucose uptake changing the intracellular levels of glucose 6-phosphate (G6P), phosphoenolpyruvate (PEP) and pyruvate (PYR) immediately because of the underlying PTS in *E. coli*. As a consequence, a negative signal transduction to PEP (expressed by dropping PEP concentrations) originating from the positive glucose stimulation can be expected.

Within this study, the decision was made to focus the interest on the linear, upstream part of the aromatic amino acid pathway, namely the conversion of the precursors PEP and erythrose 4-phosphate (E4P) via five subsequent reactions to shikimate 3-phosphate (S3P). This was motivated by the fact that the subsequent reaction from S3P to 5-enolpyruvoylshikimate 3-phosphate (EPSP) again needs PEP for condensation thus leading to an 'unusual' second stimulation of the pathway. Additionally, the following, commercially available metabolites chorismate and prephenate are chemically instable, which would significantly hamper their use for *metabolic profiling* analysis.[19]

Anticipating it can be stated that no E4P was detectable in any experiment, which is in agreement with previous observations of Williams *et al.*

---

[19] For the sake of brevity, the resulting metabolism dynamics of the glycolysis are not shown here, although they were measured. Details can be found in [Old03].

[WBDM80]. These authors critically reviewed *in vivo* measured E4P levels concluding that only very low E4P pools should be expected *in vivo* (if at all), because of E4P's tendency to react into dimeric forms. Also Ruijter and Visser [RV99] outlined that no E4P could be detected in *Aspergillus niger* strains although the respective detection limit was about 25 $pmol$[20]. Considering that even $aroF^{fbr}$ fortified strains were used in this study, no significant E4P pools could be expected. Therefore the lumped pentose-phosphate pool P5P was used as a reference instead, allowing at least some speculations about the E4P supply via transketolase (*tktA*) reaction.

In the case of DAHP, the small amount of isolated standard showed some impurities making it difficult to apply it for quantification and thus motivating the use of the dephosphorylated derivative DAH instead. This decision was justified by the experimental finding that the ratio of DAH concentrations versus DAHP peak area was constant at 3.3 ± 0.308 $nM \cdot peakArea^{-1}$ in all LC-MS/MS measurements. Thus, a common DAH(P) pool is considered in the following discussion.

Experimental Procedure

For experiments, the L-Phe producing strains *E. coli* 4pF20 and *E. coli* 4pF78 were used[21]. As indicated in subsection A.1.1, Appendix, both strains were tyrosine auxotrophic and contained the tyrosine feedback resistant gene $aroF^{fbr}$ to ensure a sufficient carbon flux into the aromatic amino acid pathway via DAHP synthase. Additionally, the plasmid contained the L-Phe feedback resistant gene $pheA^{fbr}$ to avoid an feedback inhibition of the L-Phe sensitive chorismate mutase / prephenate dehydratase, downstream of the branch point chorismate. However, the strains differed with the overexpression of *aroB* (coding for 3-DHQ synthase, converting DAHP into 3-DHQ) which was only considered in *E. coli* 4pF78 to study to what extend the total carbon flux into AAA pathway is effected by AroB.

Fed-batch fermentations (7 L) were carried out in a 20-L bioreactor (ATGU503, Infors AG, CH), using the defined medium and culture conditions as indicated in the Appendix (subsection A.2.1) and applying the 'standard' fermentation techniques for on-line analysis and data acquisition as listed in subsection A.4.2, Appendix. The L-tyrosine feed was realized with a Dosimat 665 (Metrohm AG, Switzerland) ensuring L-tyrosine excess (0.20 to 0.30 $g \cdot L^{-1}$) during the whole fermentation. The supply of the sole carbon source glucose was used to control cell growth. This resulted

---

[20] Additionally the authors wondered whether the presence of E4P in the cells makes sense at all because the phosphoglucose isomerase (PGI) was found to be strongly inhibited by E4P with $K_{I,E4P} = 1$ μM !

[21] Both strains were kindly provided by co-operating partners as indicated in the subsection A.1.1.

in a non-limited batch and fed-batch phase (permanent glucose level 3 to 5 $g \cdot L^{-1}$) and a growth-limited glucose supply (50 $g \cdot h^{-1}$) after optical density OD_{600} ∼50 was achieved. The glucose-limited, tyrosine-rich period lasted for 20 (*E. coli* 4pF20) and 45 (*E. coli* 4pF78) minutes, respectively, before the glucose pulse (50 mL, 420 $g \cdot L^{-1}$) was added automatically to the bioreactor, thus shifting the concentration to 3 $g \cdot L^{-1}$, while rapid sampling was started at the same time.

The rapid sampling and sample preparation procedure followed the same protocols as already presented in the preceding sections. However, technical problems of the experimental set-up reduced the pre-pulse observation window from –4.5 to –2.5 seconds for *E. coli* 4pF78 and shortened the post-pulse observation window of *E. coli* 4pF20 to 18 seconds. The quantification of intracellular metabolite levels (of the cell extract) was realized using an Agilent1100 HPLC with a HTC Pal autosampler (CTC Analytics) coupled to a TSQ Quantum mass spectrometer (ThermoFinnigan) and following the aforementioned analytical protocol (see section 2.3).

Glucose Pulses Monitored in *E. coli* 4pF20

As shown in Figure 2.21 (dark columns), the intracellular pre-pulse pools found in the *E. coli* 4pF20 were most at physiological levels of several 100 μM – apart from DAH(P), which showed a very large pool of about 10 mM. From this the conclusion was drawn that the huge DAH(P) pool was a consequence of the sole overexpression of $aroF^{fbr}$ caused by a high flux into this pool which could not be compensated by a corresponding downstream reaction. The considerable inequality of pool sizes between DAH(P) and the subsequent 3-DHQ of almost three orders of magnitude should be noted as well.

Figure 2.22 (left column) presents the results of the glucose pulse experiment using strain *E. coli* 4pF20. Before the pulse, the PEP and the P5P pool were in steady-state. After the pulse, both pool sizes changed significantly as was indicated by a strong increase followed by oscillating behavior of P5P and PEP. Both pools served as precursors for the DAHP-synthase. Table 2.10 indicates, that none of the three DAHP-synthase isoenzymes is supposed to be limited by PEP supply, because the measured intracellular levels of 70 - 140 μM were well above the reported K_M values.

In the case of E4P, no pools were measured thus suspecting an almost entire limitation of DAHP synthase activity ($K_{M,E4P}$ ∼35 – 900 μM) at first glance. However, it should be queried whether dissolved E4P really exists in cell cytoplasm [RV99] because of its high affinity for dimerization thus supporting the hypothesis of E4P channeling via DAHP-synthase [WBDM80].
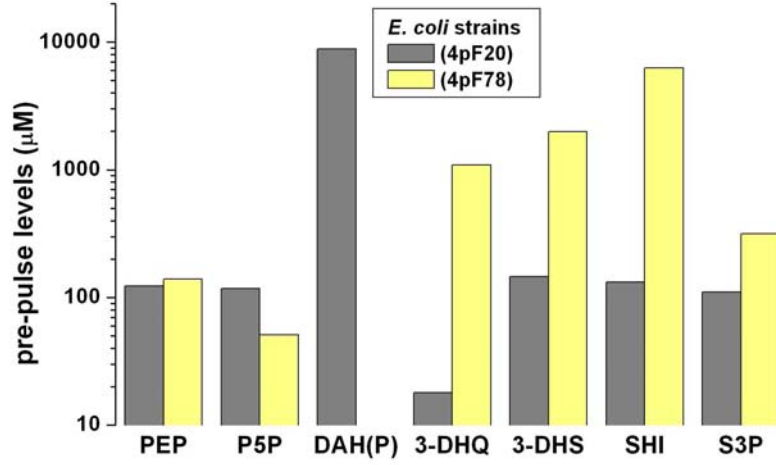
FIGURE 2.21. Comparison of the different intracellular pool levels analyzed during the last 2.5 to 5 seconds before the glucose pulse. Two different L-Phe producers were used - namely *E. coli* 4pF20 and *E.coli* 4pF78, the latter possessing plasmid-encoded, additional *aroB* overexpression. The precursors PEP, the lumped pentose-phosphate pool P5P, DAH(P), 3-DHQ, 3-DHS, SHI and S3P are shown.

Hence, we concluded that pulse signal transduction into the aromatic amino acid pathway in *E. coli* 4pF20 was not limited by PEP or E4P, but it was buffered by the subsequent, huge DAH(P) pool. Most presumably, the buffering occurred as a consequence of the significant AroB inhibition in the presence of 8 to 12 mM DAH taking into account previous findings of Maitra and Sprinson [MS87] who observed that already 5 mM DAH caused 72% AroB inhibition. As a consequence, glucose pulse signaling to the subsequent pools was hampered.

The pure analysis of the concentration courses can only provide a limited insight into the underlying reaction mechanisms. This is why the standardized pool velocity v^* $[s^{-1}]$ was introduced, taking into account the pre-pulse concentration $\bar{c}_i$ and the current concentration c of pool i as follows

$$v_i^* = \frac{1}{\bar{c}_i} \frac{dc_i(t)}{dt} \qquad (2.8)$$

The standardized pool velocity thus resembles the definition of an ordinary mass balance of the pool species i. High positive values indicate a fast pool size increase while high negative values represent a rapid decrease,
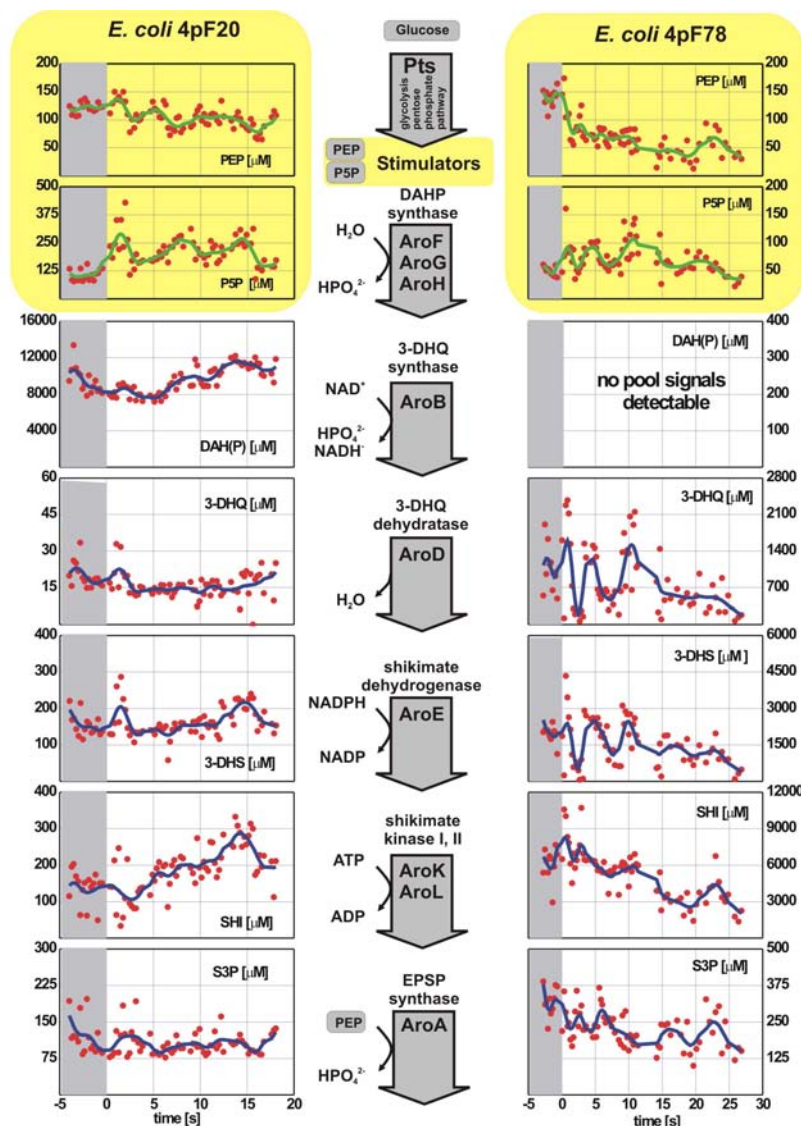
FIGURE 2.22. Metabolism dynamics observed in the first five reactions of the AAA pathway forced by the independent stimulators PEP and P5P (coding for the lumped pentose-phosphate pool) immediately after the glucose pulse. Left: *E. coli* 4pF20; Right: *E. coli* 4pF78. Reaction steps are given according to subsection 2.6.1. Smoothed curves were achieved by fast Fourier transformation (FFT) using Origin (OriginLab Corporation, USA) applying a smoothing window of 5 points. Preliminary test with 3 to 7 points smoothing window revealed similar results. Experimental errors identified after multiple LC-MS/MS measurements in each sample with cytoplasm matrix were $\preceq 15\%$.

TABLE 2.10. Overview of some characteristic kinetic values of the enzymes in the AAA pathway leading to EPSP.

Enzyme	Substrate	$\mathbf{K}_M$ $[\mu M]$ $\mathbf{S}^*_{0.5}$ $[\mu M]$	Reference
DAHP synthase (4.1.2.15)			
AroF (TYR sensitive)	E4P	80 - 90	[RE97], [SH76]
	PEP	5.8 - 13	
AroG (L-Phe sensitive)	E4P	˜80; 900	[Sim50], [SD76]
	PEP	˜5; 80	
AroH (TRP-sensitive)	E4P	35^*	[MFLA80], [AB97]
	PEP	5.3^*	
DHQ synthase (4.2.3.4)			
AroB	DAHP	4; 30 - 50	[MFK87], [CPH78], [MS87], [WBK89]
DHQ dehydratase (4.2.1.10)			
AroD	3-DHQ	10 - 18	[CLMC86], [CDC87], [KDK$^+$92]
SHI dehydrogenase			
AroE	3-DHS	n.d.	
SHI kinase (2.7.1.71)			
AroK (SK I)	SHI	˜5000	[FP86]
	ATP	˜160	
AroL (SK II)	SHI	200	[Fey87]
	ATP	160	
EPSP synthase (2.5.1.19)			
AroA	S3P	2.5 - 3.6	[DLC84b], [GWS92], [LC87]
	PEP	10 - 20	

both related to the pre-pulse concentration. Using this criterion, concentration courses were transferred to velocity series as indicated in Figure 2.23. It is shown that the precursor P5P obviously represented the most perturbed pool, which was still oscillating at the end of the observations after 18 seconds. This held also true for shikimate. However, no common behavior such as in-phase oscillations can be observed in the pools, neither before nor after the pulse. The most striking effect is the inertia of the DAH(P) pool, which is also detected by pool velocity analysis, showing almost unchanged values about zero.

Motivated by this finding, the observed amplitudes were ranked with respect to the minimum standardized pool velocity ($\min(v_i^*)$), i.e. the highest (negative) standardized pool velocity of each species was selected. The guiding idea was to define a simple criterion called 'pool efflux capacity (PEC)' that aims at identifying the slowest pool decline of the reaction sequence considering the corresponding enzyme as the one that exerts the
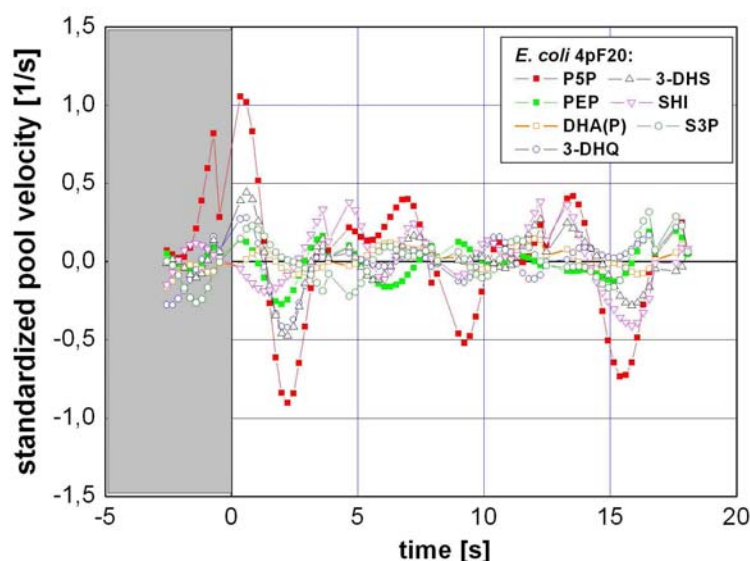
FIGURE 2.23. Standardized pool velocity curves before and after the glucose pulse in *E. coli* 4pF20.

main flux control in this pathway[22]. This criterion is standardized by the pool size thus eliminating this effect from the analysis. Following the procedure, absolute pool efflux capacities $[s^{-1}]$ of 0.09, 0.42, 0.48, 0.41 and 0.22 were calculated for DAH(P), 3-DHQ, 3-DHS, SHI and S3P (see Figure 2.24). According to the working hypothesis that the lowest 'pool efflux capacity' (here: DAH(P)) indicates the slowest, subsequent enzymatic reaction, the 3-dehydroquinate synthase, encoded by *aroB*, was identified as a promising target, which is in agreement with previous studies ([SDF96], [Pit96], [YLDF02]). Hence, strain *E. coli* 4pF78 was constructed.

It is noteworthy that the PEC criterion cannot readily be compared with the classical definitions given by the metabolic control analysis (MCA). Here, highly dynamic data were analyzed while classical MCA typically uses small deviations of steady-state fluxes to identify flux control coefficients, elasticity coefficients etc. MCA has rejected the idea of a single rate-limiting step (bottleneck) in a (linear) pathway and introduced the shared flux control by all enzymatic reactions instead ([WK96], [Bai99b]). In general,

---

[22] The introduction and application of the PEC criterion should be understood in the sense of the MCA 'dogma' that flux control is shared among the enzymes of a pathway thus rejecting the idea of a single reaction-limiting step. In this sense, the different PEC values given in Figure 2.24 mirror the distributed flux control in the pathway.
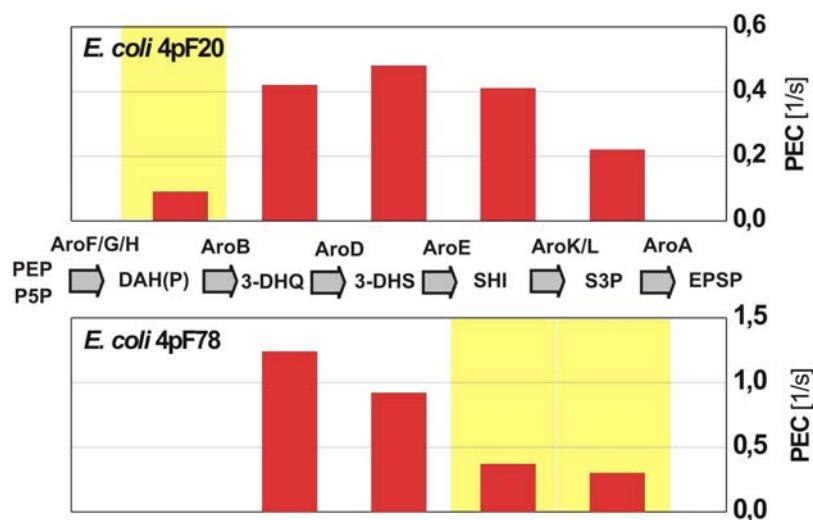
FIGURE 2.24. Pool efflux capacity criterion (PEC) of strains *E. coli* 4pF20 and *E. coli* 4pF78 identified after glucose pulse experiments with respect to the pools DAH(P), 3-DHQ, 3-DHS, SHI and S3P. Furthermore, the independent stimulators PEP and P5P as well as EPSP, the subsequent pool of the reaction sequence, are given in the reaction scheme also considering the enzymes involved. The yellow background highlightes the pool which assigns the subsequent reaction bottleneck.

this holds also true for the PEC values of the aromatic amino acid pathway given in Figure 2.24. In analogy to the MCA findings, the distributed PEC values can be regarded as the consequence of shared flux control for each enzymatic step. In this sense, the PEC criterion is in agreement with the lessons of the classical MCA.[23]

Glucose Pulses Monitored in *E. coli* 4pF78

Figure 2.21 (light columns) gives an overview of the pre-pulse concentrations in *E. coli* 4pF78 possessing an overexpression of $aroF^{fbr}$ and $aroB$. Most strikingly, no intracellular DAH(P) could be measured, although the intracellular levels of PEP and P5P remained almost constant compared to the results of *E. coli* 4pF20. This allows the conclusion that the previously existing AroB limitation had been alleviated. However, the finding

---

[23]Recently Visser and Heijnen [VH03] presented a novel approach to combine kinetic modeling (linlog-approaches) with MCA. This framework represents an interesting tool to be additionally applied for the analysis of these stimulus-response data.
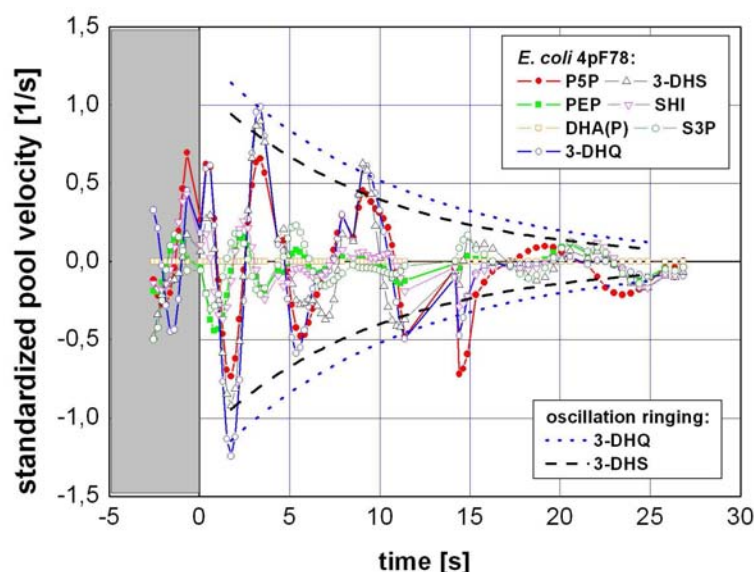
FIGURE 2.25. Standardized pool velocity curves before and after the glucose pulse in *E. coli* 4pF78. In-phase oscillation ringing is observed for the standardized pool oscillations of 3-DHQ and 3-DHS. The dotted lines symbolize the corresponding coating curves.

coincided with a strong increase of the pool sizes downstream of DAH(P) in *E. coli* 4pF78, indicating an additional flux limitation further down[24].

Significant differences were also observed following the intracellular metabolite dynamics (Figure 2.22). The precursors PEP and P5P showed different pool courses in *E. coli* 4pF78 compared to *E. coli* 4pF20, which held especially true for the decreasing PEP pool. Very strong oscillations were found in the pools of 3-DHQ and 3-DHS, but also in SHI and S3P. The high DAHP affinity of AroB, the increased AroB concentration and the missing DAH inhibitor, were most presumably the reasons for the fast DAHP-to-3-DHQ conversion without an intermediary accumulation of DAH(P). It is noteworthy that the initial jump of the 3-DHQ and 3-DHS pool size is not fully covered by the fast Fourier transformation (FFT)-smoothing approach.

To further investigate the underlying reaction mechanisms, the standardized pool velocities were calculated again and presented in Figure 2.25. In

---

[24] This finding is in agreement with the MCA theory because no single rate-limiting step exists and flux control is distributed on several enzymatic steps, as observed.

comparison to the results of *E. coli* 4pF20, pool velocities of *E. coli* 4pF78 show significant differences expressed by damped, in-phase vibrations of the intermediates. Owing to the removed DAH(P)-buffer in *E. coli* 4pF78, precursor stimulations are now signaled down via DAHP leading to in-phase oscillations of the (subsequent) pool velocities 3-DHQ and 3-DHS during the observation period of 27 seconds. Both oscillations appear to be in-phase with P5P. On the other hand, P5P and PEP are counteroscillating most of the time. With respect to S3P, a strong correlation with the PEP pool velocity can be assumed, which originates most presumably from stoichiometric conversion of S3P and PEP into EPSP via EPSP-synthase.

Correlation Analysis

Based on the standardized pool velocities shown in Figure 2.25, a correlation analysis was performed analyzing the covariance matrix of all post-pulse data of *E. coli* 4pF78 with the aid of MATLAB (The Mathworks Inc., USA). This approach was motivated by the previously published results of Arkin *et al.* [ASR97] (see also [Ros03]). However, it is noteworthy that not the original approach was applied to achieve the results of Figure 2.26. Instead, only a 'simple' correlation analysis regarding the standardized pool velocities was used. Most strikingly, the correlation analysis reveals declining reliance on the precursor P5P with advancing reaction sequence. In analogy, the dependency on PEP grows from 3-DHQ via 3-DHS, SHI to S3P. While P5P was correlated with 3-DHQ and 3-DHS with 0.92 and 0.77, respectively, the inverse was found for S3P, which was negatively correlated (-0.6) with P5P and positively correlated (0.71) with PEP.

As indicated in Figure 2.25, a high positive correlation (0.91) was found between 3-DHQ and 3-DHS, allowing the conclusion that the AroD catalyzed H_2O separation from 3-DHQ to 3-DHS was very fast. This corresponds to the *in vitro* measured, low K_M value for 3-DHQ (10 to 18 μM, see Table 2.10), which was far below the intracellular substrate level. Hence, a constant 3-DHS production rate must have occurred giving rise to the conclusion, that reaction rates of the subsequent shikimate dehydrogenase (AroE) must have been variable to cause 3-DHS pool oscillations as observed. As a consequence, high K_M values for 3-DHS or NADPH of AroE could be assumed.

Significantly changing shikimate kinase reaction rates can also be deduced from the data. In the case of *E. coli* 4pF78 extraordinary high shikimate levels of several mM were found, which gave rise to the assumption that not only AroL but also the isoenzyme AroK was active (see Table 2.10). The latter is characterized by a very high K_M value which significantly limits AroK activity in wild-type strains [Pit96] and also in *E. coli*
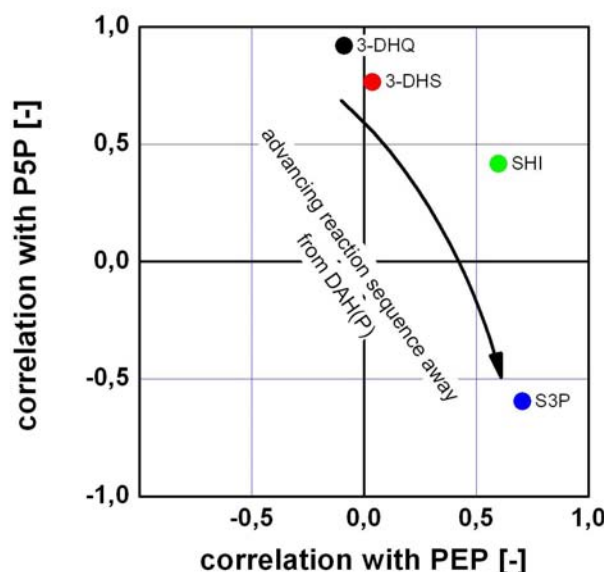
FIGURE 2.26. Correlation analysis of the aromatic amino acid pathway intermediates 3-DHQ, 3-DHS, SHI and S3P with respect to the stimulating precursors P5P and PEP measured in *E. coli* 4pF78 after glucose pulse.

4pF20 where such high shikimate levels were not found. However, in the presence of high intracellular shikimate levels in *E. coli* 4pF78 the total shikimate conversion reflects a superposition of both enzyme activities, meaning a saturated (constant) AroL activity together with a strongly varying AroK catalyzed conversion (see Table 2.10)

The correlation analysis supports the qualitative impression derived from Figure 2.25 that the intermediates 3-DHS and 3-DHQ were strongly correlated with the precursor P5P while S3P (and also SHI) showed higher correlations with the PEP supply. The latter can be explained by the subsequent EPSP-synthase reaction, taking S3P and PEP for (reversible) EPSP synthesis. Corresponding K_M values of 10 to 20 μM for PEP and 2.5 – 3.6 μM for S3P were measured by *in vitro* experiments (see Table 2.10) giving rise to the assumption that the decreasing PEP levels could hamper EPSP-synthase activity *in vivo*.

To explain the high 3-DHS, 3-DHQ dependence on P5P, consideration should be given to their proximity to the P5P stimulation, the missing DAH(P) buffer and the close connection between the 3-DHQ and 3-DHS pools. However, the question arises why the PEP reliance of the DAHP synthase, the 3-DHQ 'supplier', led to only surprisingly small correlation values. In wild-type *E. coli* cells, almost 80% of the total DAHP synthase
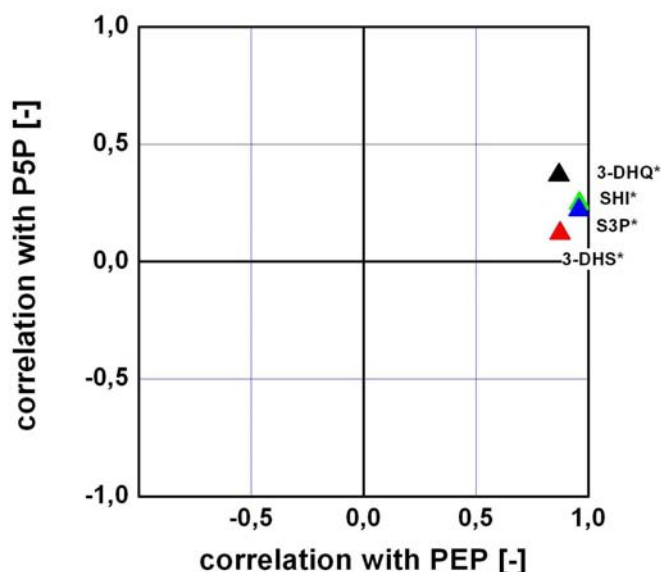
FIGURE 2.27. Correlation analysis of the aromatic amino acid pathway intermediates 3-DHQ, 3-DHS, SHI and S3P with respect to the stimulating precursors P5P and PEP measured in *E. coli* 4pF78 after glucose pulse. Only the data from 17.5 seconds until the end of observation (27 seconds) were used for analysis.

activity is realized via AroG and to a less extent by AroF. The tryptophan sensitive AroH is only of minor importance [Pit96]. Because *E. coli* 4pF78 possessed a plasmid-encoded $aroF^{fbr}$ overexpression, it can be expected, that $AroF^{fbr}$ and AroG were responsible for the prevailing amount of carbon flux into the aromatic amino acid pathway. As indicated in Table 2.10, a high PEP affinity of the native AroF ($K_M \sim 13 \ \mu M$) and some conflicting results with respect to AroG ($K_M \sim 5 - 80 \ \mu M$) were found by *in vitro* studies. Provided that the feedback-resistant $AroF^{fbr}$ mutant possessed similar PEP affinity compared to AroF (Jossek *et al.* [JBS01]), PEP-limited $AroF^{fbr}$ or AroG activities should not necessarily occur during the first phase of experimental observations when intracellular PEP levels were sufficiently high. However, they were likely to occur during the later phase, when intracellular PEP levels decreased. Hence, a first indication was found that the intracellular PEP levels significantly controlled the activity of enzymes in the aromatic amino acid pathway

With respect to Figure 2.25, the remarkable observation is made, that all precursors and intermediates show a zero-crossing at about 17.5 seconds, indicating the start of a common in-phase oscillation after a short pool inertia. At this time, intracellular PEP levels had already diminished

to about 35 μM. This finding was the motivation for a separate correlation analysis, now using all pool velocity data from 17.5 seconds onwards. Interestingly, it was found (see Figure 2.27) that all intermediates showed very high correlations to PEP (3-DHQ (0.87), 3-DHS (0.87), SHI (0.96), S3P (0.96)) and only low correlations to P5P (up to 0.37 in the case of 3-DHQ). All intermediates were now closely intercorrelated, showing values of not less than 0.74 in subsequent reactions. From this we concluded that DAHP-synthase activity (meaning AroF^{fbr}, AroG and to a minor extent AroH) obviously became PEP limited, thus switching the previous dependence on P5P now to PEP, which coincides with the corresponding correlation change of 3-DHQ and 3-DHS. Pool velocity oscillations of these compounds were now in-phase with SHI and S3P – which is in contrast to the previous situation before 17.5 seconds. As a consequence, oscillation ringing occurred, because the pool velocities of 3-DHQ and 3-DHS became limited by the PEP supply during the course of the experiment.

The finding that limited PEP supply dominated pool velocity oscillations in the aromatic amino acid pathway - and especially those of S3P, the substrate of EPSP-synthase - can also be understood as an indication for further production-strain optimization. Previous studies of Draths *et al.* [DPC$^+$92], Patnaik and Liao [PL94], Patnaik *et al.* [PSL95], Berry [Ber96], Flores *et al.* [FXB$^+$96] and Li *et al.* [LMD$^+$99] already addressed the problem of well-balanced PEP and E4P availability to achieve a maximum carbon flux into the aromatic amino acid pathway. It has also been shown by Sprenger *et al.* [SSS$^+$98b] that an optimized precursor supply can be achieved by a combination of transketolase (*tktA*) over-expression together with a phosphoenolpyruvate synthase (*pps*) amplification or by implementing an alternative, non-PTS based glucose uptake. In general, the results of this study support the findings. However, with respect to the correlation analysis of the L-Phe producing *E. coli* 4pF78, PEP availability is assigned to be even of higher importance than E4P supply, represented by P5P in this study.

Finally, the 'pool efflux capacity' criterion (PEC) was applied again (Figure 2.24), based on the pool velocities presented in Figure 2.25. Absolute minima like 1.24 (3-DHQ), 0.92 (3-DHS), 0.37 (SHI) and 0.3 (S3P) were calculated. As a consequence, AroB, AroD and AroE, using DAH(P), 3-DHQ and 3-DHS as substrates, could be excluded as potential candidates for *metabolic engineering*. Because the observed criterion differences for SHI and S3P were relatively small, AroL/AroK (shikimate kinase), catalyzing SHI to S3P, as well as AroA (EPSP synthase), catalyzing S3P with PEP to EPSP, were regarded as promising candidates with enhanced flux control. In the case of AroK/AroL, *aroL* should be preferred owing to its higher shikimate affinity (see Table 2.10). Again, this target identification is in agreement with previous observations of Dell and Frost [DF93] and

Snell *et al.* [SDF96]. The criterion even succeeded to avoid the misleading identification of AroE (shikimate dehydrogenase) as a target for gene over-expression, which could occur if pure concentration analysis would have been performed ([DF93], [SDF96]). Nevertheless, the simple 'pool efflux capacity' criterion should be used with care, as its applicability is limited to linear pathways and superimposing effects like additional substrate limitations of bimolecular enzyme kinetics are not thoroughly considered.

Summarizing Remarks

The experimental and analytical approach of *metabolic profiling* focusing on anabolic pathways is not exclusive to the analysis of the aromatic amino acid pathway. In contrast, considering the fact that a positive signal stimulation (rising precursor concentration) should be favored to ensure measurable pool changes in the pathway, the example of negative PEP signaling into the aromatic amino acid pathway anticipates even higher signals in positively stimulated routes. This includes, for instance, amino acids, vitamins or antibiotics originating from precursors such as pyruvate, intermediates of the pentose-phosphate pathway or even TCA-metabolites such as oxaloacetate, for which positive glucose pulse responses were already found (data not shown).

The analysis of pathway dynamics offers new insights because of the high data density gained after step-function or Dirac-like system stimulation. Because short-term observation windows were chosen, gene regulatory effects can be excluded thus focusing the analysis on pure enzyme kinetics. Therefore, corresponding dynamic data represent a valuable basis for model-based *in vivo* enzyme kinetic identification or thorough oscillation analysis, as it is currently performed. It can be assumed that model identification of the linear pathway will be simplified compared to complex network analysis because cross-interactions usually encountered should not be expected.

Indeed, no detailed model analysis was necessary to obtain the presented results. Pathway mechanisms were elucidated by simple correlation and oscillation analysis and even the pathway reconstruction is enabled by correlation analysis too. Hence, the analysis of pathway dynamics stimulated by glucose pulses should no longer be restricted to central metabolism but it should be extended to anabolic pathways. This enables the use of simple criteria such as the 'pool efflux capacity' criterion to identify the distributed flux control in linear pathways thus revealing potential *metabolic engineering* targets.

2.7   Pulse Stimulation: Conclusions and Outlook

- **Rapid Sampling and Sample Preparation:** Based on the previously developed rapid sampling device ([PWBSB98], [SBTWB99]) some technical improvements were realized ([BWT01], [Buc01a]) preventing unwanted side-effects of glucose pulsing such as pressure and/ or dissolved oxygen rise at the same time enabling low θ_{90} mixing times of about $640\ ms$. The methanol based cell quenching protocol was optimized such that low quenching temperatures of -50$°C$ could be used for *E. coli,* which accelerated cell cooling and metabolism inactivation. Still, the perchloric acid extraction method is applied for cell disruption and metabolite extraction because its applicability has been shown for the analysis of *E. coli* samples in large numbers of 160 samples per experiment. However, alternative methods, optimized for other biological systems and metabolites, are currently investigated as well.

- **Metabolic Profiling:** While the first stimulus-response experiments were analyzed using enzymatic assays ([SBTWB99], [Buc01a]) to monitor the metabolism dynamics of glycolysis, pentose-phosphate pathway and tricarboxylic acid cycle, subsequent studies focused on the alternative LC-MS/MS technology to achieve higher measurement accuracy, lower detection limits and an increased monitoring frequency because of significantly reduced sample volumes needed for analysis. For the first time, Buchholz *et al.* [BTW01] managed to develop an LC-MS based analytical approach for central metabolism metabolites and nucleotides using an ESI iontrap mass spectrometer. A significant improvement of measurement accuracy and detection limit was further achieved by applying a triple-stage quadrupole MS instead ([OT03], [Old03]). The latter was intensively used for stimulus-response studies which also included the intermediates of the aromatic amino acid pathway. After the access to purified standards of the aromatic amino acid pathway has been achieved, this LC-MS/MS approach was successfully applied to measure intracellular concentrations of pathway intermediates. This opened the door to perform - for the first time - *metabolic profiling* for the analysis of an anabolic pathway after glucose pulse experiments.

- **Metabolic Modeling Tool (MMT)**: Because the analysis of rapid sampling data demanded for a specialized software, which was not available, the metabolic modeling tool MMT was developed ([Hur01], [HBA^{+}02]). Some basic software characteristics are (i) the relational data base, which allows the management of complex experimental data sets, models and modeling results, (ii) the implemented mathematical routines, which allow the solution of stiff ordinary differential equation systems, the parameter identification and the calculation of

output sensitivity matrices and (iii) the interface to commercial programs such as MAPLE to allow the rapid test of new mathematical algorithms which could be programmed later in the open source code. MMT has been shown to cope with the complexity of metabolic models consisting of 27 dynamic variables and 302 parameters.

- **Modeling Metabolism Dynamics:** Using MMT, a comparative study was performed to identify an appropriate model reduction approach for simplifying complex metabolic models thus uncovering the most important underlying mechanisms. Considering a set of 13 primary identified models, two different model reduction approaches were tested, which both used the normalized sensitivity matrices, calculated by MMT. It was shown that the PCA-based model reduction is superior to the 'classical' parameter sensitivity analysis, because an upper-limit of the error-functional ζ can (heuristically) be achieved which consequently allows to use the approach as an automatic routine. Hence, compared to previous results of Visser *et al.* [VdHM$^+$00], an alternative approach is presented, which is solely based on mathematical constraints and which is intended to be used in MMT as a standard routine.

- **Broaden the Scope to Anabolic Pathways:** Motivated by the fact that the analysis of glucose pulse experiments was limited to the central metabolism so far, metabolism dynamics of the aromatic amino acid pathway, as a typical example of a commercially interesting biosynthesis, were monitored. It was shown that the basic drawbacks, namely signal dilution and limited analytical access can be overcome by the appropriate experimental procedure and the preparation of purified standards for LC-MS/MS analysis using knock-out mutants and chemical synthesis in a concerted approach. For the first time, *metabolic profiling* has thus been applied to monitor anabolic pathway dynamics (AAA pathway) after glucose pulse. Based on the dynamic pool curves measured the standardized pool velocities were introduced. Thereof, the maximum (negative) values of each species were identified and ranked, thus defining the data-driven criterion 'pool efflux capacity (PEC)'. As a consequence, the need to overexpress *aroB* (coding for 3-DHQ-synthase) was experimentally reconfirmed studying *E. coli* 4pF20. While analyzing the resulting strain *E. coli* 4pF78, damped oscillations of the pathway intermediates were found. The repeated application of PEC permitted the conclusion that *aroD* and *aroE* are not necessarily *metabolic engineering* targets but *aroL* and *aroA*. In addition, the correlation analysis of the oscillating standardized pool velocity curves allowed the reconstruction of the aromatic amino acid reaction sequence. Beyond it, it was found that PEP supply should preferably be optimized for e.g. L-Phe production.
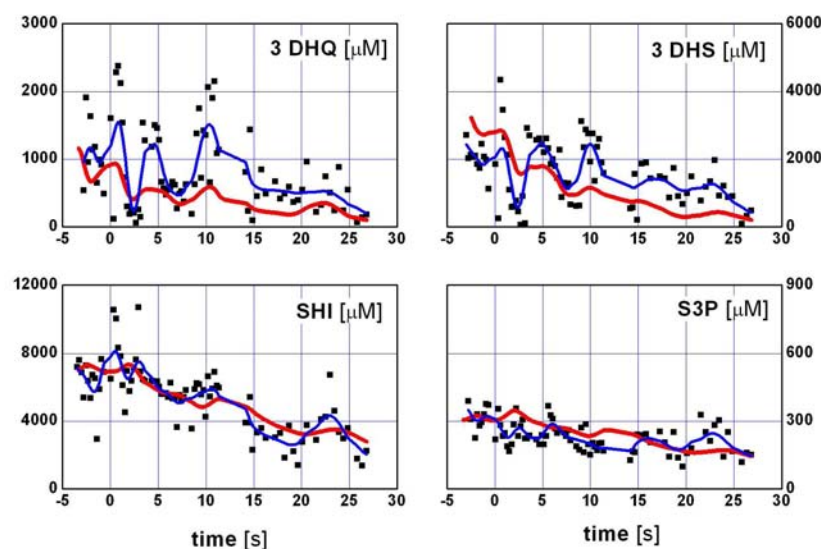
FIGURE 2.28. Current simulation results modeling the metabolism dynamics in the aromatic amino acid pathway in *E. coli* 4pF78 with respect to 3-DHQ, 3-DHS, SHI and S3P. Model predictions are indicated by (red) lines while FFT smoothed concentration courses are given by small (blue) lines.

Based on the aforementioned results, the current and future activities of stimulus-response studies focus on three major parts.

- **MMT 2:** As already pointed out, the primary software MMT (1) has currently been replaced by a novel software MMT 2, which is actually developed by the project partners at University of Siegen [HFWT02]. Some basic features of this novel MMT tool are: XML-based model configuration and automatic model generation for different model topologies and reaction mechanisms, model discrimination including system analysis considering for instance elementary flux modes, distributed computing using a PC-cluster (currently 128 computers connected in the 'Rubens'-cluster) for simulation and model identification, detailed graphical visualization of the modeling results etc. Although this tool development is competing with likewise specialized software alternatives such as GEPASI 3.30 (http:/gepasi.dbs.aber.ac. uk/softw/gepasi.html), E-CELL and Insilico discovery 1.0 (Insilico biotechnology, Stuttgart, http://www.insilico-biotechnology.com) and it also competes with comprehensive modeling approaches using general simulation tools such as ProMoT/DIVA ([MHBG87], [TGZG97], [KJLG00], [KG01], [KBL+01], [MG03]) and ModelMaker (Cherwell Scientific, Oxford, http://www.modelmanager.com/), the current MMT

2 development is still motivated by the special modeling demands outlined in subsection 2.4. As a result, the identification of the 'correct' model out of the set of competing approaches will be facilitated by the distributed modeling and system analysis approach implemented in MMT 2, as it will be shown by future studies.

- **Modeling pathway dynamics:** As indicated in the preceding section, the analysis of the AAA pathway dynamics so far was only performed by applying 'simple' statistical tools such as correlation analysis. However, detailed modeling approaches are currently studied by Degenring [Deg03]. As an example of the actual, unpublished results, Figure 2.28 is given. For the sake of brevity, only the model predictions compared to the experimental data are shown. 3-DHQ, 3-DHS, SHI and S3P were used as dependent variables while PEP, P5P and cofactors were taken as measured (smoothed) input values. It can be observed that general experimental tendencies are well reflected by the model, which holds especially true for SHI and S3P. However, the strong vibrations observed in 3-DHQ and 3-DHS (see also Figure 2.22) are not yet mirrored by the model predictions which obviously demands for model refinement, for example by taking into account central metabolism dynamics or feedback inhibitions by L-Phe, which were both ignored so far.

- **Studying alternative systems:** The analysis of anabolic pathway dynamics after glucose pulses is currently extended taking into account alternative biological systems. As already outlined, a positive pathway stimulation for instance by increasing stimulator concentrations would be fortunate. Because of the PTS-based glucose uptake in *E. coli* - which also exists in *C. glutamicum* - pyruvate (PYR) would thus be an appropriate stimulator for pathway dynamics. This is why current studies already focus on L-valin biosynthesis in *C. glutamicum* L-valin producers (together with an industrial partner). Two molecules of pyruvate are needed to synthesize one L-valin molecule in the cells, which gives rise to the assumption that the stimulating signal into the pathway should even be fortified by factor 2. It is noteworthy that L-valin synthesis in *C. glutamicum* is closely connected to L-isoleucine and L-Leucine formation as well as to the production of pantothenic acid. All pathway products are of commercial interest.

3

Serial ^{13}C Flux Analysis Using the Sensor Reactor

3.1 Motivation

Without doubt, metabolic flux analysis (MFA) has become an important tool in *metabolic engineering* during the last decade ([Wie01], [Ste02]). Since the foundations for MFA were laid in the 1990s, this tool increasingly gained attraction because of the intracellular carbon flux distributions, which were derived as a result of analysis. The knowledge of intracellular flux maps obviously allows a quantitative valuation of the physiological cell state, the estimation of maximum product formation yields making use of linear programming ([VS93], [JNVM95]), the identification of promising *metabolic engineering* targets, and the retrospective assessment of previous genetic manipulations [Nie98]. These MFA applications are thus in agreement with the *metabolic engineering* demands formulated in various definitions ([Bai91], [CT93], [Ste99], [Wes01]).

Furthermore, MFA also plays an important role when control coefficients or theorems of the metabolic control analysis (MCA) should be applied [KA93]. For instance, the most often-used flux control coefficients (FCCs, [Nie97], [Nie98]) (usually) make use of the fractional changes of steady-state fluxes caused by infinitesimal activity variations of the respected enzymes. Hence, the MFA-based knowledge of the intracellular fluxes is most valu-

able to apply classical MCA approaches, reviewed in [Fel92] and [VH02][1]. MFA is still valuable for the application of the more recently published, new MCA approaches which proposed a facilitated MCA access by getting rid off restrictive experimental constraints such as an infinitessimal system perturbation ([HB96], [KCH$^+$98], [Hat99],[VH02]). In general, these approaches make use of simplified enzyme kinetics, such as lin(log)-approaches, to reach this aim.

Early MFA approaches used stoichiometric metabolism models together with measured substrate consumption and product secretion rates in order to identify intracellular fluxes. Following this strategy the first flux map for a complete central metabolism was published by Vallino and Stephanopoulos ([VS93]) studying L-Lysine production in *C. glutamicum*. However, the application of this concept for complex metabolism networks necessitated sensitive balancing assumptions such as a constant P/O ratio (about 2.5) and/or closed balances for energy (ATP) or reducing equivalents, which were both, highly speculative and not well justified [Wie02b]. Additionally, experimental observations of subsequent studies outlined the speculative character of these assumptions ([MdGW$^+$96], [SB99]). Moreover, bidirectional fluxes and cyclic pathways (not coupled to measurable fluxes) could not be resolved by pure metabolite balancing [BST97]. Hence, a more detailed MFA – also allowing the identification of bidirectional fluxes – was required.

As a consequence, ^{13}C labeling experiments were performed providing additional measurement information about ^{13}C-^{13}C correlations or fractional ^{13}C enrichments by NMR or (later on) by MS analysis ([Szy98], [Wit02]). In general, these methods focused on the analysis of labeling patterns found in the amino acids of the protein hydrolysate or in the metabolites of the supernatant [Wie02a]. While Zupke and Stephanopoulos [ZS94] published the first MFA results studying hybridoma cells with the aid of ^{1}H NMR, Marx *et al.* [MdGW$^+$96] investigated the central metabolism of *C. glutamicum* in detail based on ^{13}C analysis and metabolite balancing. Later on, 2-dimensional (namely ^{1}H and ^{13}C) NMR was intensively used by [SHB$^+$97] to study the riboflavin production in *Bacillus subtilis*. Concomitantly, mathematical tools were developed to keep abreast of the increasing metabolic model complexity and the rising amount of labeling information. Examples were the introduction of the isotopomer mapping matrix ([SCNV97], [SNV99]), the thorough statistical and mathemat-

---

[1]Flux control coefficients (FCCs) have also been shown to support MFA in underdetermined modeling systems [LD98]. It is noteworthy that the estimation of FCCs can also be achieved if a kinetic metabolism model is already know, as shown by Prathumpai *et al.* [PGW$^+$03]. Besides, current MCA approaches (such as the one of Visser *et al.* [VH03]) intend to derive FCCs from non-steady state data by applying linlog-kinetics.

ical analysis of the model identification problem ([WdG97], [WSdGM97], [WMI$^+$99]), the introduction of bondomers [Win02] and the detailed analysis of metabolic network structure (i.e. null-space analysis, elementary flux modes, extreme pathways etc. [HS98], [SSPH99], [SFD00], [SKB$^+$02b], [SKW$^+$02], [SVC02], [KS03]). Hence, numerous MFA studies were subsequently performed considering these tools. For example, applications are found for *E. coli* ([SNV99], [EDP$^+$02]), *Z. mobilis* [dG00b], *C. glutamicum* [dG00a], *P. chrysogenum* [WGS$^+$03] and *S. cerevisiae* ([GSCN01], [CGN02]).

At the same time, GC-MS based analysis of the labeled amino acids in the protein hydolyzate was developed ([CN99], [DS00], and recently [KAS03a]) and successfully applied in subsequent studies. Using the GC-MS labeling data, for instance *Penicillium chrysogenum* strains were studied to qualify the penicillin production [CTN00] of high- and low-yielding strains, to analyze the metabolic network [CN00], to elucidate the adipate degradation in 7-ADCA-producing strains [TCN02] and to estimate the flux split between oxidative pentose phosphate pathway and glycolysis, not only in *P. chrysogenum* but also in *B. clausii* and *S. cerevisiae* [CCG$^+$01]. Additional studies were performed analyzing the carbon flux distribution in serine protease (Savinase) producing *Bacillus clausii*.[CN02]. *Streptomyces nursei* was studied during nystatin (an antibiotic polyketide) production [JCN01] and co-substrate metabolism was elucidated by a novel approach called '*reciprocal* ^{13}C *labelling*' [CN02]. In addition, MALDI-TOF MS increasingly gained interest to measure label patterns of preferably amino acids in the culture supernatant [WH00]. Following this approach, MFA was applied for L-Lysine production with *C. glutamicum* strains ([WH01a], [WH01b]).

Although ^{13}C-based MFA appears to be the method-of-choice to determine intracellular flux distributions, the classical approach of metabolite balancing was still successfully followed in numerous studies. Maybe the possible pitfalls of ^{13}C based MFA with respect to metabolite channeling and model incompleteness [WVH01] also motivated the use of the classical approach. For instance *S. cerevisiae*, was investigated by Nissen *et al.* [NSNV97] and Vanrolleghem *et al.* [VJGG$^+$96], the latter pointing out that the P/O ratio in *S. cerevisiae* can be accurately estimated thus allowing its use for stoichiometric models. Also, penicillin production in *Penicillium chrysogenum* strains was intensively studied ([JNVM95], [GdLVH00]), providing changing flux maps of the growth phase and the product formation period. Beyond it, the flux balance approach (FBA, [VP94a], [VP94b], [EP98]) should be noted which overcomes the problem of under-determined stoichiometric systems using optimization objectives (such as growth maximum) in combination with flux restrictions. With the aid of FBA, for instance phenotype phase planes were identified to predict the substrate-

specific maximum growth of *E. coli* cells [ERP02], to allow the prediction of evolutive strain development with respect to optimal growth [IEP02] and to analyze the effects of gene additions and deletions systematically [BM01]. Nevertheless, ^{13}C-based MFA seems to be favored by most of the experimentalists nowadays, presumably because there is no alternative if detailed flux analysis should elucidate bidirectional steps or cycles and sensitive balancing assumptions should be avoided.

However, despite the invaluable results which were obtained by ^{13}C-based MFA, some drawback hampered its use as a standard technology, especially with respect to cell monitoring under industry-like production conditions.

- First, the state-of-the art analysis of ^{13}C labeling experiments assumed labeling equilibrium, e.g. in the amino acids of the protein hydrolyzate, which forced the experimentalist to use the technology either in steady-state experiments or under pseudo-stationary labeling conditions, i.e. during the exponential growth phase in batch experiments ([Wie01], [Wie02a])

- Second, labeling can usually be performed only once per experiment. Otherwise residual background ^{13}C labeling, resulting from prior labeling, could interfere with the analysis, thus hampering the MFA accuracy.

- Third, experimentalists always had to consider the significant labeling costs (approx. € 250 /g fully labeled glucose) that made small-scale experiments more attractive than large industrial-scale applications.

As a consequence, MFA based on labeling experiments was usually restricted to small-scale *in vitro* conditions that were only partially comparable to the large-scale industrial cultivations which - however - would be an interesting target for the technology. Besides, MFA results only represented 'snapshots' of the intracellular flux distributions of these *in vitro* conditions whereas experimentalists would prefer information about time-variant flux maps of realistic cultivation conditions in order to qualify the strain performance.

Motivated by this discrepancy, the goal was defined to develop the so-called '**Sensor reactor**' that enables the use of ^{13}**C-based MFA under large-scale semi-industrial cultivation conditions**. The technology aims at the calculation of a **series of flux maps**, each map consisting of 'integrated fluxes', **documenting the changes of intracellular flux distributions during a typical fed-batch process**. Hence, the 'Sensor Reactor' represents a tool allowing the time-resolved analysis of realistic production processes comparable to 'classical' studies - but with more extensive use of ^{13}C labeling information.

It is noteworthy that the Sensor reactor concept is not restricted to a certain mode of labeling or labeling analysis. Different labeling sources such as [U-^{13}C] or [1-^{13}C] glucose (or others) should be applicable under glucose-limited and/or glucose-saturated cultivation conditions with different growing or non-growing cells. This also includes the possibility to analyze the labeling pattern in the most meaningful way. Hence the state–of-the-art labeling analysis regarding the hydrolyzed pool of proteogenic amino acids, which is mostly preferred for growing cells, the analysis of labeling patterns found in the metabolites/amino acids of the culture supernatant and the not-yet fully established methodology to analyze the labeling pattern in the metabolome should be supported by the Sensor reactor[2]. As a consequence, techniques for cell labeling and rapid sampling have to be developed.

---

[2] Recently, van Winden published the first MFA approach based on metabolome labeling patterns using HPAE-MS for analysis [Win02].

3.2   The Sensor Reactor Concept
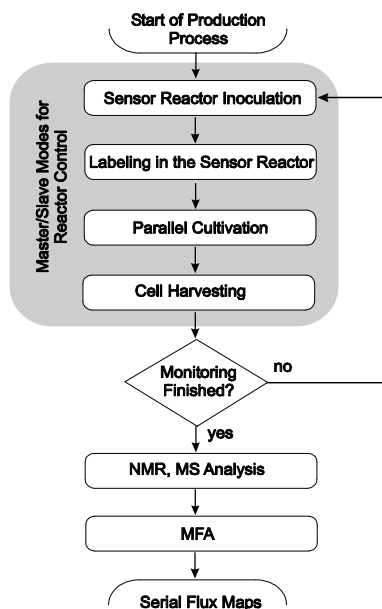
FIGURE 3.1. Flow scheme of labeling experiments using the Sensor reactor. After inoculation from the production process, the biomass is labeled, cultivated in parallel to the production process (via Master/Slave control), harvested and later analyzed to perform 13C based MFA. This process can be repeated several times while the production process is running.

As a basic idea of the 'Sensor Reactor' concept, a small-scale bioreactor of 1 L working volume is run in parallel to a large-scale production reactor. Labeling experiments are carried out in the Sensor Reactor after it has been inoculated with cells automatically taken from the production process at freely chosen process time. The two reactors run in parallel, which is ensured by a master/slave control mode, until cell labeling is sufficient. This can be achieved either by long-term labeling aiming at completely equilibrated labeling patterns (for instance in the proteinogenic amino acids) or by 'mid-term' labeling making use of a subsequent mathematical 'wash-out' correction of non-equilibrated labeling patterns [Win02]. During the labeling procedure, samples were taken frequently from both reactors in order to verify process similarities. Labelled cells from the Sensor Reactor are harvested and used for further ^{13}C analysis providing the data for detailed MFA. Thus an integral, time-averaged flux analysis of the labeling period is enabled. After the Sensor Reactor had been emptied, it could be used for

additional labeling experiments in analogy to the described procedure monitoring the on-going production process (see.Figure 3.1). Provided that the Sensor Reactor and production process show a similar performance, the MFA results of the Sensor Reactor mirror the intracellular fluxes of the production process.

3.3   Technical Development

> Significant parts of the following section were published in [MSD$^+$03].
> Results were acquired during the Ph.D. thesis of M. El Massaoudi
> and during the master thesis of Spelthahn [Spe02] who were co-
> supervised by the author. The Sensor reactor system was applied for
> patent [MFdGT01].

3.3.1   Settling on Corynebacterium glutamicum

Without doubt, the gram-positive, nonpathogenic, soil bacterium *Coryne-bacterium glutamicum* represents one of the most interesting bacterial strains for industrial purposes. Since its isolation in 1957 [KUS57] and the subsequent finding that L-glutamate was secreted under biotin limitation [SOT62], the strain was subjected to mutagenesis numerous times, thus achieving a 'dynasty' of excellent L-glutamate producers reaching product titers up to 150 $g \cdot L^{-1}$ ([ES99], [DHK$^+$02]). These strains were used in large-scale production processes (up to 500 m^3) to serve an increasing glutamate market. Beyond it, mutagenesis also enabled the construction of lysine, threonine, isoleucine, tyrosine and phenylalanine producing strains [Leu96]. In 1999, worldwide market of the 'big three' amino acids L-glutamate, L-Lysine and D,L-methionine (including their salts) counted more than 700 to 840, 370 to 430 and 380 to 450 kilotons per year, respectively ([Mül01], [DHK$^+$02]), representing approximately 95% of the total amino acid volume. Today, the worldwide consumption of amino acids is estimated to be over 2 million tons [Her03], of which 1.5 million tons of L-glutamate are produced using coryneform bacteria. In 2001, 550 kilotons L-lysine were produced worldwide to serve a market with 7% growth rate per year [Her03]. The majority of mono-sodium glutamate (MSG) is still used as a taste enhancer, while D,L-methionine and L-lysine·HCl are most preferably added to animal feed to enhance the nutritive value [DHK$^+$02][3]. In the case of L-glutamate and L-Lysine, these amino acids were exclusively made by *C. glutamicum* which stresses the importance of the strain.

However, *C. glutamicum* strain development obviously kept not restricted to classical mutagenesis. *Metabolic engineering* tools were increasingly applied in subsequent studies focusing for instance on the construction of L-lysine producers. Comprehensive reviews covering these works are written ([EES93], [SLEEK95], [Krä96], [ES99], [dGES01], [PMBM03]). For instance, L-lysine production was increased by over-expression of genes coding for aspartate kinase and dihydrodipicollinate synthase ([CES91], [EOS98]),

---

[3] The addition of 0.5% L-lysine increases feed quality as much as the addition of 20% soybean meal [Her03].

lysine export was studied and thus improved ([BEK93], [VSE96]), the beneficial effect of glucose co-substrates (such as acetate) was discussed [PR03], the need for a well balanced NADPH regeneration was outlined [WH02] and addressed [MHM$^+$03], acetate overflow mechanism were studied in detail [GWS$^+$03] etc.

Apart from these approaches, the availability of precursors such as aspartate but also pyruvate, NADPH and ATP was investigated. Aspartate, the product of the transamination reaction with oxaloacetate, was found to be highly essential for an optimum L-lysine formation [MTES89] and pyruvate, NADPH and ATP were discussed as candidates that could potentially limit lysine production ([VS94], [MSdG$^+$97]), [WH02], [PMBM03]).
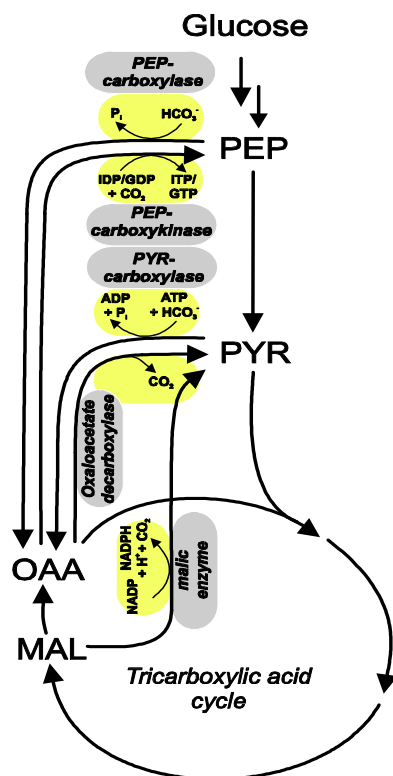
FIGURE 3.2. Scheme of the five anaplerotic reactions found in *C.glutamicum* - namely: PEP-carboxykinase, oxalacetate decarboxylase, malic enzyme, PEP-carboxylase and pyruvate carboxylase. The corresponding pools are: phosphoenolpyruvate (PEP), pyruvate (PYR), oxaloacetate (OAA) and malate (MAL).

Because of the dependency of L-lysine formation on the precursor supply, the refilling of the oxaloacetate pool via the anaplerotic reactions was one of the most interesting targets of the on-going *metabolic engineering* research. Considering the results of Peters-Wendisch *et al.*, ([PWWdG$^+$96], [PWWP$^+$97]), who identified the pyruvate carboxylase as an additional anaplerotic enzyme in *C. glutamicum* (which is, by the way, in contrast to the anaplerotic reactions found in *E. coli*), altogether five enzymatic reactions had to be considered to cover *C. glutamicum*'s anaplerosis completely. These are: (i) GTP/ITP dependent decarboxylation of oxaloacetate via PEP-carboxykinase [JS93], (ii) oxaloacetate decarboxylase leading to pyruvate [JS95], (iii) NADP dependent malic enzyme (leading to pyruvate) [EES93] and the refilling reactions (iv) PEP carboxylase ([EFGS89], [PWWdG$^+$96]) and (v) ATP dependent pyruvate carboxylase [PWWP$^+$97] (see Figure 3.2). It is noteworthy that *C. glutamicum* does not possess transhydrogenase activity [KT72], thus giving the reaction cycle of pyruvate carboxylase and malate dehydrogenase the potential task to deliver sufficient NADPH in the case of a limiting oxidative pentose-phosphate activity. Recently, Koffas *et al.* [KJAS02] outlined the necessity to properly adjust pyruvate carboxylase with aspartate kinase activity because of aspartate inhibition and lactate and acetyl CoA activation of this enzyme.

Motivated by previous findings ([SSdG$^+$95], [MdGW$^+$96], [MSdG$^+$97], [MES$^+$99]) revealing that both, carboxylation and decarboxylation, occurred simultaneously *in vivo*, Petersen *et al.* [PdGE$^+$00] succeeded to quantify the individual anaplerotic fluxes and showed that PEP carboxykinase is responsible for recycling two-thirds of the anaplerotically synthesized oxaloacetate to PEP. Very recently, this results was critically discussed by Klapa *et al.*, [KAS03b] estimating a very low PEP carboxykinase flux in another L-lysine producing *C. glutamicum* strain.

Despite these invaluable results presented above, it might be surprising that all ^{13}C based flux analysis accomplished so far was limited to small-scale experiments, preferring glucose limited chemostat cultures or shaking flasks. Obviously, these experimental conditions did not reflect realistic production conditions of a several 100 m^3 bioreactor which represents the usual industrial reaction system of today's L-lysine production. Hence, the L-lysine producing *C. glutamicum* strain MH20-22B [SES92] was found to be an excellent biological system to develop and to test the Sensor reactor technology under industry-like production conditions.

3.3.2   Sensor Reactor Set-up

As indicated in Figure 3.3, the Sensor reactor was installed close to the production process. While the production reactor had a total volume of 300 L, the volume of the Sensor reactor was two orders of magnitude smaller (2
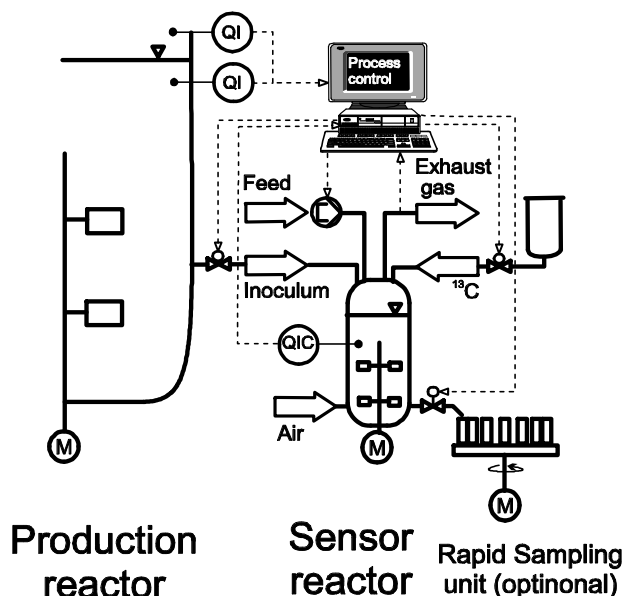
FIGURE 3.3. Experimental set-up of the production reactor/Sensor reactor unit. Characteristic on-line measurements from the 'master' production reactor (such as pH, pressure, aeration) were taken as setpoints to control the Sensor reactor. Labeled glucose is added via a special apparatus. The possibility of rapid sampling is optionally considered, which is basically motivated by the (not yet realized idea) that rapidly changing labeling patterns in the metabolome should be analyzed. The Sensor reactor is automatically inocculated from the production process.

L). There was a similar ratio for the working volumes of the two reactors (approximately 180 L/1.0 L).

3.3.3   Inoculation

An important aspect of the Sensor reactor approach is that similar process performances should be obtained in both reactors during the labeling process. Hence, cells drained off from the production reactor must not experience any differences in cultivation conditions and – even more important – the cell metabolism must not be affected during the inoculation procedure to ensure the same cell activity in the Sensor reactor. As a consequence, the inoculation of the Sensor reactor should be a fast process that does not cause any significant gradients in fermentation parameters such as pH, pressure (p), temperature (T), dissolved oxygen concentration (DO), substrate concentrations etc.

To estimated the required maximum inoculation time, the following assessment is given: The oxygen uptake rate (OUR) for a typical fermenta-

tion with *Corynebacterium glutamicum* is 140 $mmol \cdot (L \cdot h)^{-1}$ (exponential growth, $OD = 70$), which is equivalent to 0.039 $mmol \cdot (L \cdot s)^{-1}$. The oxygen solubility at 30 % DO (1.5 bar, 37 °C) is equivalent to approximately 0.22 $mmol \cdot L^{-1}$ (6.9 $mg \cdot L^{-1}$), which means that the DO will drop to zero after 6 seconds. Hence a fast inoculation process is needed (< 2 seconds) to prevent potential oxygen limitation. In addition, the inoculation procedure should not cause cell damage for instance owing to increased shear stress.

Finally, from the point of view of an experimentalist working in large-scale semi-industrial processes, the Sensor reactor technology should be readily adaptable to conventional production reactors and it should not cause any negative impact on the production process. As a consequence, the authors decided to dispense with additional apparatus that had to be installed inside the production reactor. Instead, the inoculation of the Sensor reactor was performed by simply using the (hydrostatic) overpressure of the production reactor, which was assumed to be present in the large-scale bioreactors of interest.
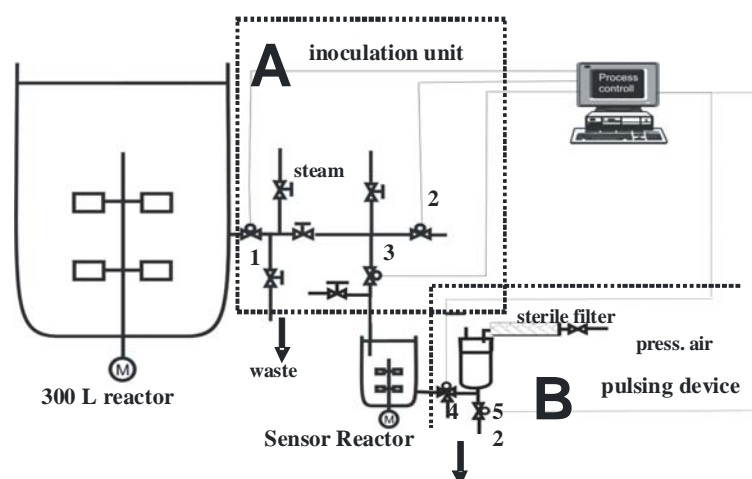
FIGURE 3.4. Experimental setup of the inoculation (A) and the pulsing device (B). Both are automatically controlled. They can be cleaned roughly by air and sterilized by steam switching the solenoid valves 1-3 and 4,5, respectively.

As indicated in Figure 3.4(A) the Sensor reactor was connected to the production reactor via the inoculation unit consisting of stainless steel tubing (inner diameter 21 mm) between valves 1, 2 and 3 and a flexible tube together with a 'quick-connect' unit installed behind valve 3. At the production reactor, a standard port with diameter 25 mm was used. The di-

aphragm valves 1-3 (type 2031, EPDM diaphragm, Bürkert, Germany) were pneumatically controlled (7 bar air pressure) allowing

- the drain-off of potential 'dead zone' inoculation volume (located directly in front of valve 3) into the waste before Sensor reactor inoculation (valves 1 and 2 were open, 3 was closed)

- the inoculation of the Sensor reactor (valves 1 and 3 were open, 2 was closed)

All valves were automatically controlled via the process control system run on the PC. Additionally, manually controlled valves were integrated to clean the tubing by air flow and to sterilize the unit with steam. Using this system, an experimental series was carried out which identified a total inoculation volume accuracy of $1.025 \pm 0.021 L$ considering production process overpressures from 0.4 to 0.7 *bar* and *simulating* fed-batch volume changes by studying 140 L and 180 L reaction volume. Table 3.1 indicates that the inoculation took between 1.20 and 1.56 s. Hence, if, for instance, a typical glucose consumption rate of 0.5 $g_{glu\cos e} \cdot (g_{CDW} \cdot h)^{-1}$ were assumed and a high biomass concentration of 50 $g_{CDW} \cdot L^{-1}$ were considered, then 0.007 $g_{glu\cos e} \cdot L^{-1}$ would be consumed by the cells during a 'slow' inoculation procedure of 1.56 s, which we did consider to be not critical with respect to unwanted cell-limitations.

TABLE 3.1. Inoculation volume accuracy using setpoint 1.02 L, considering variations of overpressure and liquid volume of the production process (PR)

		Reactor overpressures (bar)		
		0.4	**0.5**	**0.7**
PR volume (L)				
140	Mean inoculation vol. (L)	1.014	1.018	1.026
	Standard deviation (L)	0.0276	0.01257	0.022
	Filling time (s)	1.56	1.40	1.20
	Num. of experiments	10	10	9
180	Mean inoculation vol. (L)	1.034	1.032	1.026
	Standard deviation (L)	0.0244	0.0133	0.026
	Filling time (s)	1.47	1.30	1.29
	Num. of experiments	10	10	10

Total mean inoculation volume: 1.025 L; weighted standard deviation: 0.021 L

3.3.4   Master/Slave Mode

As mentioned above, the Sensor reactor was run in the 'slave' mode compared to the 'master' production reactor to ensure pH, temperature, pressure and dissolved oxygen concentration were similar in the two reactors. Figure 3.5 gives an example of the master/slave controlling results considering the courses of dissolved oxygen concentration (DO) after a series of drastic set-point shifts including the sudden addition of antifoam to the production process. As indicated, owing to the relatively small working volume of the Sensor reactor, it is possible to follow the dynamic changes of the production process very accurately and quickly.

3.3.5   Pulsing

Figure 3.4(B) represents a scheme of the automated pulsing device that was also controlled by the process control software. As shown, the pulsing liquid (maximum volume 60 mL) was pumped into the storage tank via a sterile filter (1) (20 μm, Schleicher & Schüll, Dassel, Germany) or directly via port (2). At the outlet of the tank, a system of 2 valves was installed to admit the labeling solution into the Sensor Reactor when the 3/2 diaphragm valve (1) was open and the 2/2 valve (2) was closed. Otherwise, for instance the liquid from the storage tank could be released. The pulsing system was sterilized by using 1 M NAOH for the solenoid valves and tubings and by autoclaving of the storage tank and the connected sterile filter

Using an overpressure of 4 bar at the storage tank, the labeling substance was pulsed into the Sensor Reactor by controlling the pulsing amount via the opening time of valve (1). A nozzle pipe was installed inside the Sensor Reactor so that the pulsing stream was directed at one rotating 4-blade Rushton turbine thus dispersing the labeling substance most efficiently. Figure 3.6 shows two examples of conductivity measurements with KCl as an indicator of the mixing of 5 $g \cdot L^{-1}$ glucose from which mixing times were determined. This amount was chosen because 'real' labeling pulse experiments were expected to need an ^{13}C glucose enrichment of 10 % in the bioreactor. From Figure 3.6 mixing times of 0.72 s (for a glucose pulse concentration of 250 $g \cdot L^{-1}$) and 0.51 s (for 500 $g \cdot L^{-1}$) were identified. Hence, the technology could certainly be used for 'slow' labeling processes (like the labeling of the amino acids in the proteins), but also to monitor quick, 'short-term' labeling effects, for instance in the metabolome. The latter has not been studied yet. However, current research activities aim at identifying rapidly changing ^{13}C labeling patterns in the intracellular metabolome, which necessitates a rapid sampling technology to enable a highly frequent metabolic flux analysis (see section 3.6).
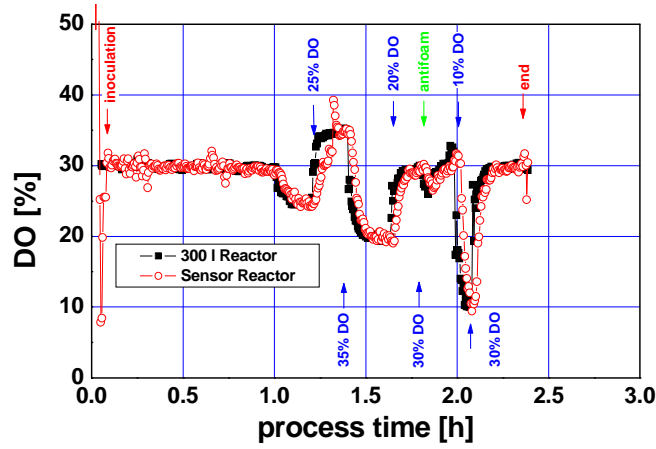
FIGURE 3.5. Example of master/slave controlling mode: Dynamic dissolved oxygen setpoint shifts (DO) in the production reactor were performed (see arrows). The measured DO concentrations in the production (filled rectangles) and in the Sensor reactor (open circles) are shown.
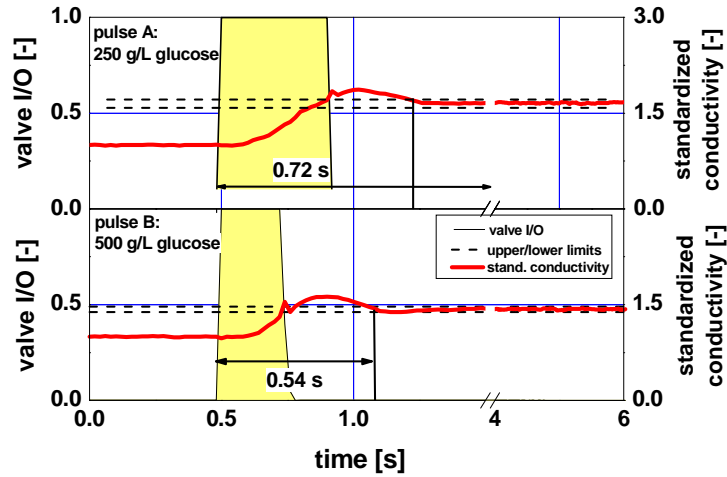
FIGURE 3.6. Estimated θ_{90} mixing times of glucose pulses (indicated as arrow labels) of two experiments with 250 $g \cdot L^{-1}$ (A) and 500 $g \cdot L^{-1}$ glucose-containing pulsing liquid are shown. Both pulses caused a sudden increase of 5 $g \cdot L^{-1}$. For standardized conductivity measurements KCl was added to the glucose solution. Accordingly, 10 % upper/lower limits and pulsing valve I/O are given.

3.3.6   Cultivation Experiments
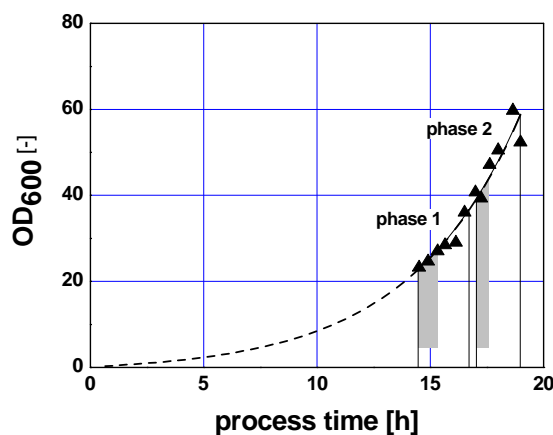
FIGURE 3.7. Sensor reactor test during a batch fermentation with *C. glutamicum* MH20-22B. At the beginning of phases 1 and 2 the Sensor reactor was inoculated and ran in parallel for approximately 2.5 hours, (see shaded areas). The filled down triangle indicates OD measurements in the production process. Exponential growth is shown by the line.

Using the Sensor reactor, batch experiments were carried out with *C. glutamicum* MH20-22B for L-lysine production. The reaction volume of the production process was 180 L and 1 L was chosen for the inoculation into the Sensor reactor. As indicated in Figure 3.7, the Sensor Reactor was filled twice at a process time of 14.5 h and 17 h for parallel fermentations, thus allowing studies of the exponential phase of the fermentation process. This phase is of particular interest for qualifying the technology because medium limitations are excluded (*per se*) and potential differences in process performance (measurable via discrepancies for growth, (co-) substrate consumption and (by-) product formation) can only be caused by different process conditions or originate from (partial) cell damage during inoculation.

Figure 3.8 gives an overview of the experimental results using phase diagrams instead of usually presented time-resolved plots to illustrate the similarity of the fermentations in the Sensor reactor and in the production process. As indicated, optical density (OD_{600}) together with the curves of the main carbon (glucose) and nitrogen source (ammonium), the auxotrophic compound L-leucine, the main product L-lysine and typical (intermediary) by-products like isoleucine, alanine, glycine, acetate, pyruvate
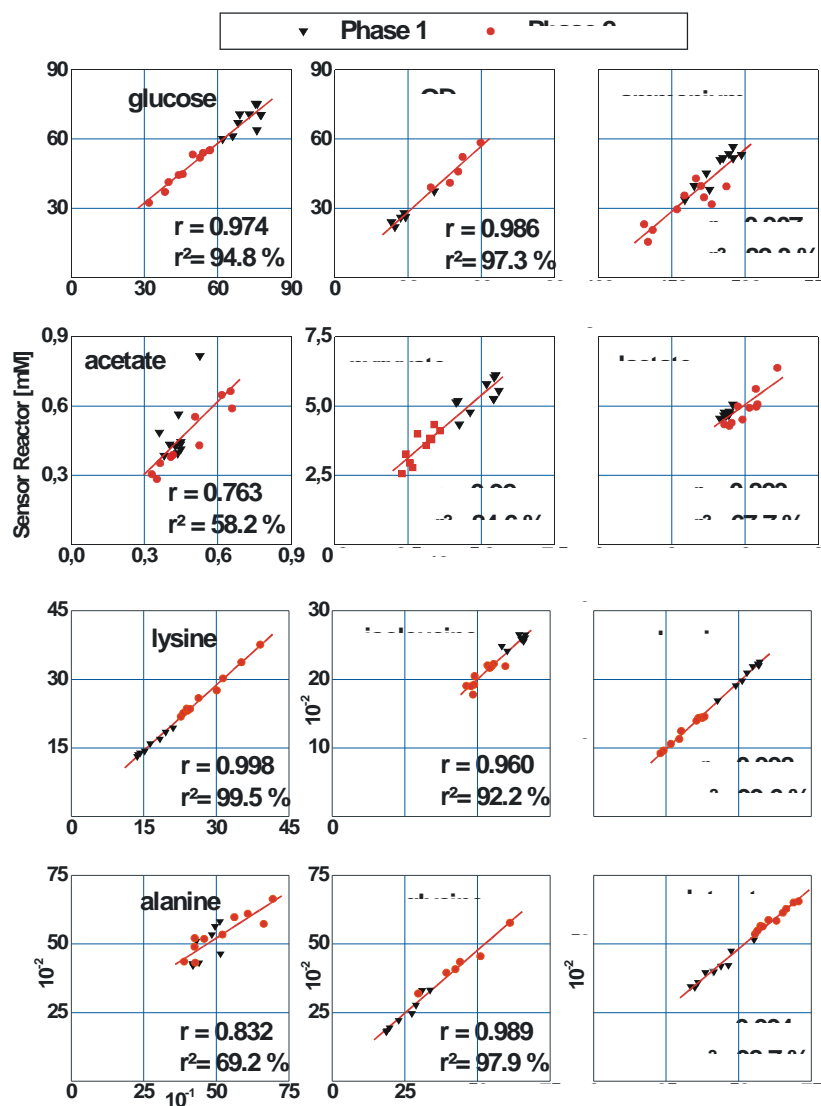
FIGURE 3.8. Overview, representing the concentrations of glucose, optical density (OD_{600}), ammonium, acetate, pyruvate, lactate, lysine, isoleucine, leucine, alanine, glycine and oxoglutarate in the two parallel runs of phase 1 (down triangle) and phase 2 (circle) in the Sensor reactor and in the production process. To qualify the similarity of Sensor reactor and production reactor fermentations, linear fits are given (line), together with regression coefficients (r) and the coefficients of determination (r^2).

and lactate were analyzed in the samples taken simultaneously, approximately every 20 min, during the parallel operation of the two reactors. As Sensor reactor concentrations were plotted versus the corresponding concentrations in the production process, a good similarity of the two reactor runs is shown by linear correlation with the 45° slope and an intercept close to zero. The regression coefficient r is given as a quality criterion of the linear fit. Additionally the coefficient of determination r^2 [%] is calculated to indicate how much of the original variability of the Sensor reactor results is explained by the regression line regarding the corresponding values of the production process.

If the criteria of 45° slope, (estimated) intercept close to zero, high regression coefficient and high coefficient of determination are taken into account, most of the curves of phases 1 and 2 show good similarity between the production process and the Sensor reactor fermentations. Concentrations in the two reactors were very similar at corresponding process times. This holds true for the main carbon and nitrogen sources glucose and ammonium, the biomass (indicated by the optical density OD_{600}), the auxotrophic compound leucine, the targeted product L-lysine and the (intermediary) by-products isoleucine, glycine and oxoglutarate. In the case of isoleucine, it should be stressed that this amino acid was produced in an earlier fermentation phase (not indicated here) and consumed later. The metabolites acetate and lactate also showed acceptable 45° linear slopes. However, the regression coefficients r and r^2 for lactate and acetate were significantly lower than the corresponding values of the other metabolites, indicating a noisier linear fit. For acetate, this was mainly due to the last measurements in phase 1 carried out more than 2.5 h after inoculation. Here, a technical problem with oxygen control occurred in the Sensor reactor.

A good similarity between the two reactors was not only shown by the concentrations in the Sensor Reactor and the production rector, but also by the appropriate rates e.g. lysine production rate $[mmol_{ly\sin e} \cdot (OD \cdot h)^{-1}]$ $(0.115 \pm 0.018$ production reactor, 0.0963 ± 0.013 Sensor reactor), leucine consumption rate $[mmol_{leucine} \cdot (OD \cdot h)^{-1}]$ $(0.0239 \pm 0.0023$ production reactor, 0.0239 ± 0.0026 Sensor reactor), glycine production rate $[mmol_{glycine} \cdot (OD \cdot h)^{-1}]$ $(0.00237 \pm 0.00038$ production reactor, 0.00250 ± 0.00033 Sensor reactor) and glucose consumption rates $[g_{glu\cos e} \cdot (OD \cdot h)^{-1}]$ $(0.197 \pm 0.036$ production reactor, 0.233 ± 0.033 Sensor reactor). Hence we concluded that rates for biomass production, glucose consumption, lysine production etc. were sufficiently similar thus fulfilling the necessary *similarity criterion* for a successful interpretation of a Sensor reactor MFA as a mirror of the production process.

However, when ^{13}C labeling experiments were carried out, a ^{13}C-containing glucose pulse had to be added to the culture in order to label, for
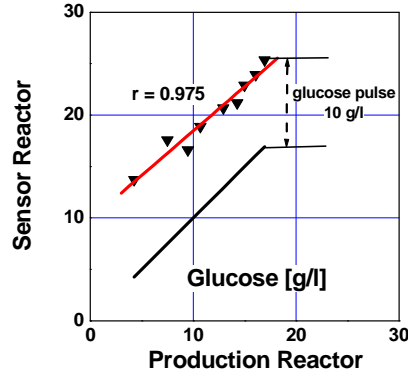
FIGURE 3.9. Effect of a 10 $g \cdot L^{-1}$ glucose pulse on the concentration curves in the Sensor reactor compared to the production reactor. To illustrate the quality of fit the regression coefficient r is given.

instance, the amino acids inside the cells. Hence the question arises, if cellular metabolism is affected by the sudden glucose addition. In analogy to *E. coli*, *C. glutamicum* also has a phosphotransferase system (PTS) for an active glucose uptake. Assuming that K_S values for the glucose specific uptake were in the same order of magnitude as those of *E.coli* [Fer99], we expected the glucose uptake to be fully saturated in the presence of relatively high extracellular concentrations $\gg 0.01 \ mM$ (a criterion which is usually fulfilled during batch processes). Hence, an additional glucose labeling pulse should not affect glucose uptake and should create a constant mixture of labeled/unlabeled glucose in the Sensor reactor.

To study this hypothesis, glucose pulse experiments were carried out following the same experimental procedure as described above except for the addition of a significant 10 $g \cdot L^{-1}$ glucose pulse into the Sensor reactor. In Figure 3.9, measured glucose concentrations in the Sensor reactor are plotted versus their counterparts in the production process. Again, a good linear correlation ($r = 0.975$) showing a 45° slope was identified. The vertical gap between the identity of the linear course and the measured values clearly indicated the glucose pulse, which could also be identified by the interception at 0 $g \cdot L^{-1}$ in the production reactor. Using these data, glucose consumption rates $[g_{glu\cos e} \cdot (OD \cdot h)^{-1}]$ of 0.122 ± 0.0025 for the production reactor and 0.11 ± 0.0105 for the Sensor reactor were calculated (assuming a mean OD during the 'labeling' procedure), which were identified as statistically equal. This also holds true for the lysine production rate $[mmol_{ly\sin e} \cdot (OD \cdot h)^{-1}]$ (0.00912 ± 0.00075 production reactor, 0.00964 ± 0.00084 Sensor reactor), leucine consumption rate $[mmol_{leucine} \cdot (OD \cdot h)^{-1}]$ (0.00544 ± 0.00065 pro-

duction reactor, 0.00642 ± 0.00077 Sensor reactor) and glycine production rate $[mmol_{glycine} \cdot (OD \cdot h)^{-1}]$ (0.000479 ± 0.000043 production reactor, 0.000532 ± 0.000048 Sensor reactor). Hence cell metabolism was obviously was not affected by the glucose pulse.

3.3.7   Interim Summary: Sensor Reactor Development

The experimental results showed that a fast inoculation of the Sensor reactor, simply based on the existing overpressure of the production process, was possible within 1.20 to 1.56 s without using additional technical devices of the production reactor. A negative impact of the Sensor reactor on the production process could be ruled out. In the later fermentation process, the master/slave modes ensured parallel operation of the Sensor and the production reactor. Pulses with labeled glucose were shown to be added quickly to the culture within 0.51 to 0.72 s mixing time, thus also allowing fast labeling experiments (for instance by analyzing labeling patterns of the metabolome) to be performed in future studies. Fermentation experiments with *C. glutamicum* showed very good similarities between the Sensor reactor and production reactor, even when significant pulses of 10 $g \cdot L^{-1}$ glucose were added to the Sensor reactor.

In summary it can be stated that the Sensor reactor (shown in Figures 3.10 and 3.11) represents a promising tool for serial ^{13}C labeling experiments. Hence the tool was applied as shown in the following sections.

FIGURE 3.10. Experimental setup of the 1-L Sensor reactor together with the standard equipement for fermentation control and the 300-L bioreactor.
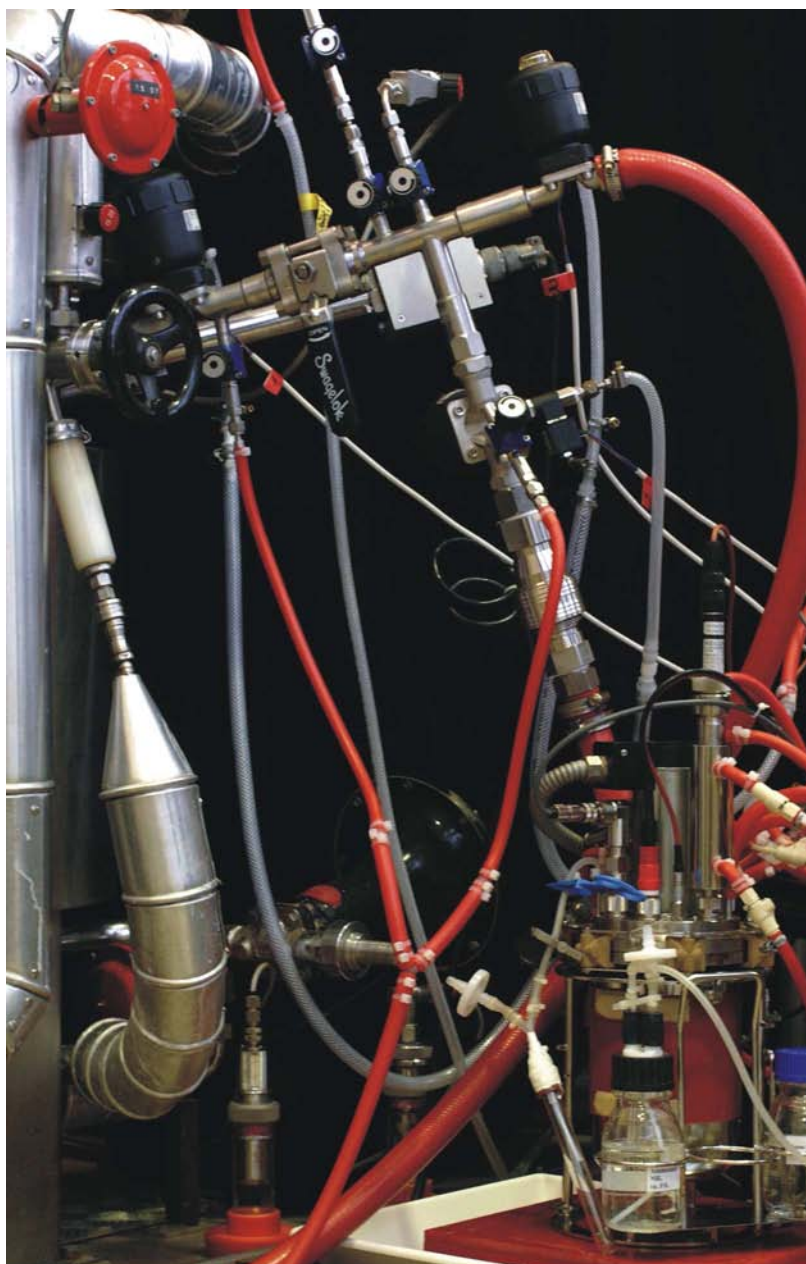
FIGURE 3.11. Details of the Sensor reactor setup used. The 300-L bioreactor is connected to the 1-L Sensor reactor via an inoculation unit (including PC controlled valves for inoculation and cleaning).

3.4   MFA for L-Lysine Producing *C. glutamicum*

3.4.1   Analysis of the Growth Phase

Significant parts of the following subsection were published by Drysch *et al.* [DMM$^+$03] Results were acquired during the Ph.D. thesis of M. El Massaoudi and A. Drysch which were co-supervised by the author.

Using the Sensor reactor technology, a batch experiment with lysine-producing *C. glutamicum* MH20-22B was carried out to study the alterations of the *in vivo* metabolic flux distribution during lysine production. Therefore, a series of three parallel fermentations was performed representing three subsequent periods during exponential growth with a growth rate of $0.20\pm0.01\ h^{-1}$. As indicated in Figure 3.12, experiments were performed from 8.5 to 10.5, 11 to 13.5 and 14 to 16.25 hours process time. For the estimation of the concentration courses of the main carbon source glucose, the auxotrophic compound leucine, the target product lysine and the by-products trehalose, valine and lactate, supernatants from the production and Sensor reactor were analyzed by ^{1}H-NMR (see A.3.5). Comparing the three Sensor reactor fermentations with each other, a gradual significant increase of lysine production was identified, even though the auxotrophic substrate L-leucine was not limiting at all times 3.13.
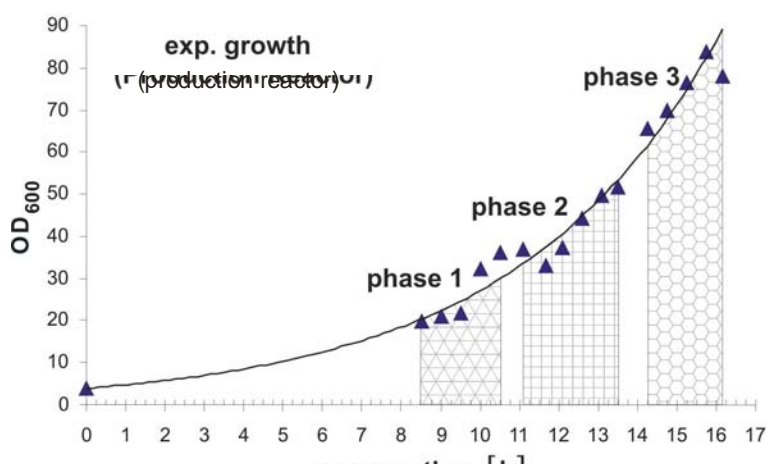
FIGURE 3.12. Growth curve of L-lysine producing *C. glutamicum* MH20-22B in the 300-*L* bioreactor. 3 subsequent Sensor reactor experiments were run as indicated by the shaded phases 1 to 3.
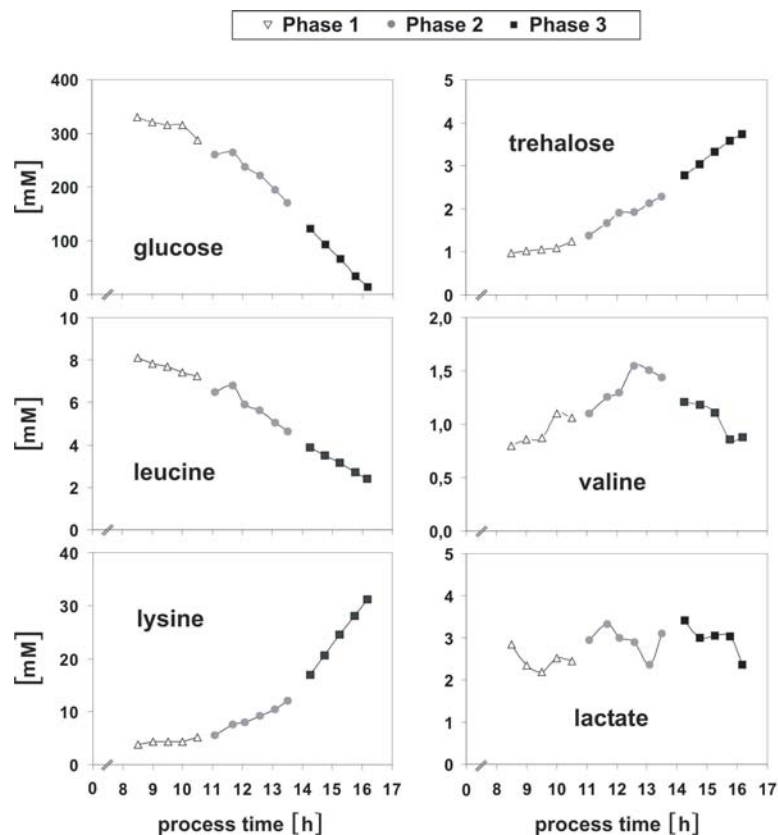
FIGURE 3.13. Overview of the concentration courses in the fermentation supernatant of the sole carbon source glucose, the principal product lysine, the auxotrophic substrate leucine and the by-products trehalose, valine and lactate during the phases 1 to 3 in the Sensor reactor.

According to the previously described procedure, a ^{13}C-containing glucose pulse was added to the culture at the beginning of each parallel fermentation (see Appendix A.5.1) in order to label the proteinogenic amino acids. The glucose pulse was limited to max. 10 % of the total glucose amount of the Sensor reactor to prevent, for instance, unwanted osmotic stress. Because of the similarity between the phosphotransferase system in *E. coli* and *C. glutamicum*, and the fact that the K_M-value of the glucose-specific PTS in *E. coli* is known to be in the range of 3 to 10 μM [Fer99], no significant changes of glucose uptake before and after the pulse are to be expected (under these conditions), as already shown in the previous section.
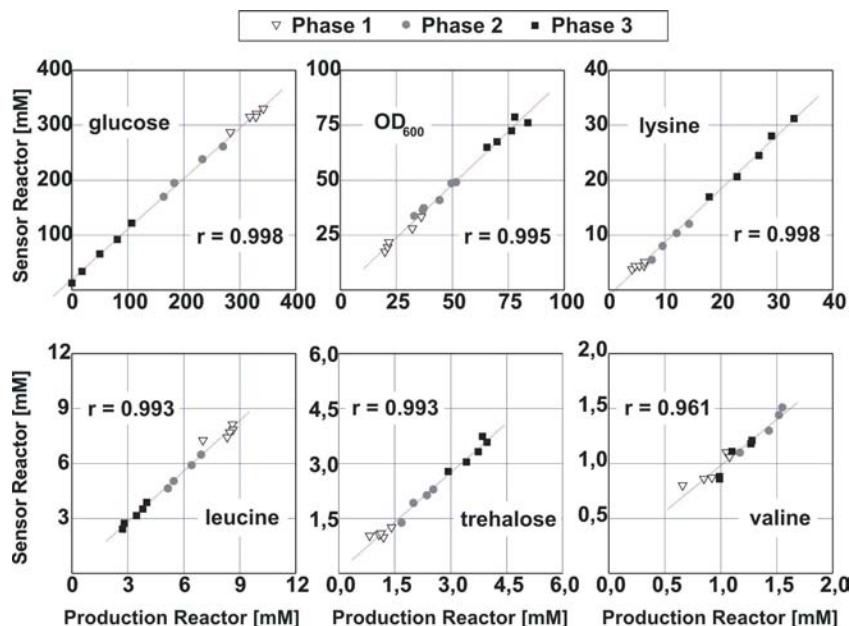
FIGURE 3.14. Concentrations measured in the supernatant of the Sensor reactor versus their analogues measured in the production reactor. Glucose, biomass (OD_{600}), lysine, leucine and the by-products trehalose, and valine are shown. Additionally, the correlation coefficient r is given.

To study the similarity of the fermentations, the concentrations of metabolites in the Sensor reactor were plotted versus their analogues measured in the production reactor. The correlation courses show satisfactory slopes of about $45°$, high regression coefficients approaching 1 and an (estimated) intercept at the origin of the diagram 3.14. This holds true especially for the most important physiological values such as biomass (indicated by the optical density OD_{600}), the main carbon source glucose, leucine, and the product lysine. From that we concluded that in all three fermentation phases a very good similarity of the metabolic states of the cells in the production and Sensor reactor existed thus allowing to transfer the results of the subsequent MFA from the Sensor reactor to the $300\ L$ production process.

For the flux analysis, rates of glucose consumption, lysine production etc. of all three Sensor reactor fermentations were calculated from the concentration measurements at different time points (see Table 3.2) and used in an integrated metabolic balancing and isotopomer labeling analysis as described in section A.7.7. The model presented in section A.7.8 was used.

Isotopomer labeling data were derived from the hydrolyzate of the proteinogenic amino acids as described in sections A.3.7, and A.3.8. The fine

TABLE 3.2. Important extracellular fluxes for *C. glutamicum* MH20-22B during exponential growth in the three Sensor reactor fermentations used for metabolic flux analysis

Specific rates $[mmol \cdot g_{CDW}^{-1} \cdot h^{-1}]$	Phase 1	Phase 2	Phase 3
glucose consumption	3.7 ± 0.34	3.8 ± 0.37	3.2 ± 0.20
leucine consumption	0.074 ± 0.007	0.076 ± 0.006	0.042 ± 0.002
lysine production	0.113 ± 0.024	0.260 ± 0.015	0.414 ± 0.024
trehalose production	0.013 ± 0.009	0.037 ± 0.005	0.029 ± 0.002

Standard deviations were derived from regression analysis indicating measurement errors and corresponding flux variations. The cell-dry weight (CDW) concentration used as a reference for the production and consumption rates was obtained by optical density as $CDW \left[g \cdot L^{-1} \right] = 0.25 \left[g \cdot L^{-1} \right] \cdot OD_{600}$.

structures of ^{13}C multiplet signals (intensities) from different carbon atoms in eleven amino acids were evaluated from the 2D NMR spectra of the cell hydrolysates obtained from all three Sensor reactor fermentations (see in Appendix A.3.9 Tables A.5, A.6 and A.7). The spectra showed clear and well-resolved multiplet patterns indicating that the labeling grade of 7 - 10 % used was sufficient for the flux analysis even after the short incubation times of only 2 - 2.5 hours.

During a batch culture, the metabolism is not fully at steady state. Up to now, no adequate mathematical tools for the treatment of such non-steady state labeling experiments have been published, although corresponding research is currently performed and will without doubt lead to a thorough understanding of the underlying non-linear, dynamic mechanisms (see 3.6). Therefore, the fluxes in each phase were calculated as if the labeling patterns were the result of a constant metabolism and can be termed as "integrated or summarized fluxes" [JCN01]. As a consequence, these fluxes simply reflect "summarized tendencies" in the metabolism of each phase and should not be interpreted as actual *in vivo* fluxes at the end of each parallel fermentation.

It is noteworthy that the 2 to 3 hours labeling applied during the exponential growth phase were presumably not sufficient to achieve a stationary labeling pattern in the proteinogenic amino acids. Therefore, only a fraction of labeled glucose was used as input value for the model identification process with the ^{13}C-flux software package. Details are given in the appendix A.7.7 and A.5.2.

Using the mathematical framework, fluxes in the central metabolism were identified by the best fit of simulated labeling data to the NMR measurements. The weighted sums of squared residuals were 167 (phase 1), 136

TABLE 3.3. Selected calculated intra- and extracellular fluxes and their standard deviation in *C. glutamicum* MH20 -22B during the phases 1 to 3 of the batch culture in the Sensor reactor

Reactions	Flux estimates $\left[mmol\ g_{CDW}^{-1}h^{-1}\right]$		
glucose consumption[a]	3.13 ± 0.07	3.23 ± 0.07	3.29 ± 0.07
G6P→P5P[b]	1.18 ± 0.20	0.98 ± 0.24	1.12 ± 0.46
G6P→F6P	1.88 ± 0.20	2.13 ± 0.23	2.06 ± 0.44
GAP→PEP/PYR[c]	4.98 ± 0.15	5.15 ± 0.14	5.25 ± 0.17
PEP/PYR→AcCoA	3.69 ± 0.13	3.59 ± 0.12	3.43 ± 0.15
AcCoA→TCA cycle	3.16 ± 0.15	3.05 ± 0.14	2.90 ± 0.17
SUCC→OAA/MAL	2.88 ± 0.10	2.77 ± 0.10	2.62 ± 0.10
PEP/PYR→OAA/MAL[d]	1.70 ± 0.08	1.58 ± 0.07	1.32 ± 0.07
OAA/MAL→PEP/PYR[e]	0.98 ± 0.02	0.72 ± 0.03	0.32 ± 0.05
OAA/MAL→Asp	0.32 ± 0.01	0.47 ± 0.01	0.61 ± 0.01
lysine formation[f]	0.13 ± 0.01	0.27 ± 0.01	0.41 ± 0.01

[a]calculated glucose consumption rate from flux analysis; [b]P5P codes for the lumped pools of ribose-5-phosphate (R5P), ribulose-5-phosphate (Ri5P) and xylulose-5-phosphate (X5P); [c]Net flux; [d]lumped anaplerotic reactions - namely PEP carboxylase, PYR carboxylase; [e]lumped reverse anaplerotic reactions - namely PEP carboxykinase, OAA decarboxylase, malic enzyme; [f]calculates lysine production from flux analysis

(phase 2) and 213 (phase 3), respectively, for 100 measurement values of labeling patterns and extracellular rates. Thus, the average residual was max. 1.5 standard deviations indicating a good model consistency.

The resulting metabolic flux maps are shown in Figures 3.15, 3.16 and 3.17. Table 3.3 summarizes some key fluxes together with the statistical error estimates. According to the flux maps, the flux entering the pentose phosphate pathway (G6P → P5P) was calculated at 38, 30 and 35 % of the molar glucose consumption in the three Sensor Reactor experiments, respectively, with estimated relative standard deviations ranging from about 20 to 40 %. These values differ from the 47 % also found in exponentially growing *C. glutamicum* MH20-22B [SSdG+95] (i.e. to be compared with phase 1) and from the 66.4 % found for this strain in chemostat culture during lysine production [MdGW+96] (more or less comparable to phase 3). However, the differences are hardly significant because of the relatively large imprecision in the flux estimates which are most presumably a consequence of the $\left[U-^{13}C\right]$ glucose used. This labeling substrate was previously found to be non-suited for the determination of the flux split ratio of glycolysis versus pentose phosphate pathway [MWKdG99].

As indicated by Table 3.3, the absolute flux through the glycolysis (from F6P to PEP/PYR) was identical within the error margins in all three par-

allel fermentations, which also holds true for the normalized fluxes (molar percentage). If the glucose uptake is compared to the flux of C3 units at the triose phosphate level (GAP), a drain off from central metabolism to biomass production and CO_2 formation of about 20 mol% can be derived. The flux through isocitrate lyase and malate synthase (glyoxylate shunt) was found to be nearly 0 in all three Sensor reactor experiments indicating that no significant activity of the glyoxylate pathway was present *in vivo,* which is in agreement with previous findings ([SSdG$^+$95], [MdGW$^+$96]) supporting the hypothesis that the glyoxylate cycle is significantly reduced in *C. glutamicum* during growth on glucose as compared to acetate as the sole carbon source [WdGSE00].

As already mentioned in subsection 3.3.1 (see also Figure 3.2), lysine production in *C. glutamicum* is strongly influenced by the precursor availability and thus depends on the anaplerotic C3-carboxylation and the reverse C4-decarboxylation reactions. As indicated in Table 3.3, these fluxes showed only low calculation errors, which allows their detailed discussion. Interestingly, the most noticeable flux difference in all three parallel fermentations was observed at the anaplerotic node. The *in vivo* C4-decarboxylating flux significantly decreased in the course of the three fermentation phases (see Figures 3.15, 3.16 and 3.17). This decrease, of 30 % in the second phase and as much as 70 % in the last phase, strongly correlated with the lysine production that doubled and tripled in the 2*nd* and 3*rd* phase, respectively, compared to the 1*st* phase.

Using ^{13}C labeling-based MFA, Petersen *et al.* ([PdGE$^+$00], [PMdG$^+$01]) already showed that the decarboxylating flux via the enzymes oxaloacetate (OAA) decarboxylase and malic enzyme is almost negligible in cells growing in chemostate cultures. Therefore, it was presumed that the decarboxylating flux at the anaplerotic node during exponential growth was mainly catalyzed by the PEP carboxykinase. However it is noteworthy that very recent findings of Klapa *et al.* [KAS03b] partially contradict the results of Petersen *et al.* [PMdG$^+$01] by identifying a low PEP carboxykinase flux and a high OAA decarboxylating flux in (another) lysine producing *C. glutamicum* strain, which was identified by MS-based $\left[1 - ^{13}C\right]$ analysis[4]. Yet, this Sensor reactor study cannot distinguish between the different decarboxylating fluxes in *C. glutamicum.* Nevertheless, because the same strain compared to Petersen *et al.* ([PdGE$^+$00], [PMdG$^+$01]) was used, the as-

---

[4]As a potential reason for these conflicting results, the authors outline the benefits of their own, improved ^{13}C-GC-MS-analysis of biomass hydolyzate compared to the previoulsy used NMR approach. They also postulate triggering effects of the lactate addition used in the Petersen experiments [PMdG$^+$01] with respect to an increased gluconeogenesis activity.
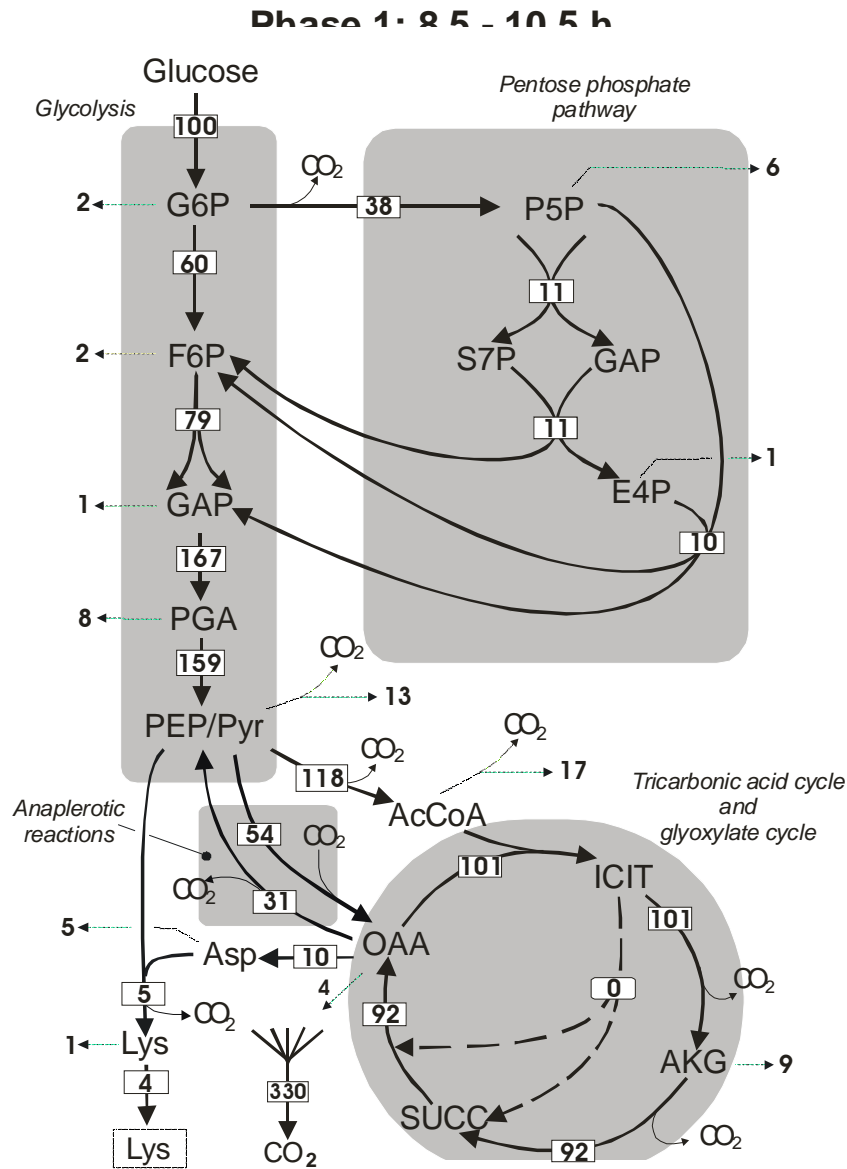
FIGURE 3.15. Map 1 of a series of three subsequent flux distributions representing the integrated fluxes of lysine producing *C. glutamicum* MH20-22B during batch culture monitored by ^{13}C labeling form 8 to 10.5 *h* process time using the Sensor reactor approach. All fluxes are given as molar precentage of the glucose uptake. Thick and thin lines indicate central metabolism reactions or fluxes into anabolic pathways and by-products, respectively. For abbreviations see Appendix.
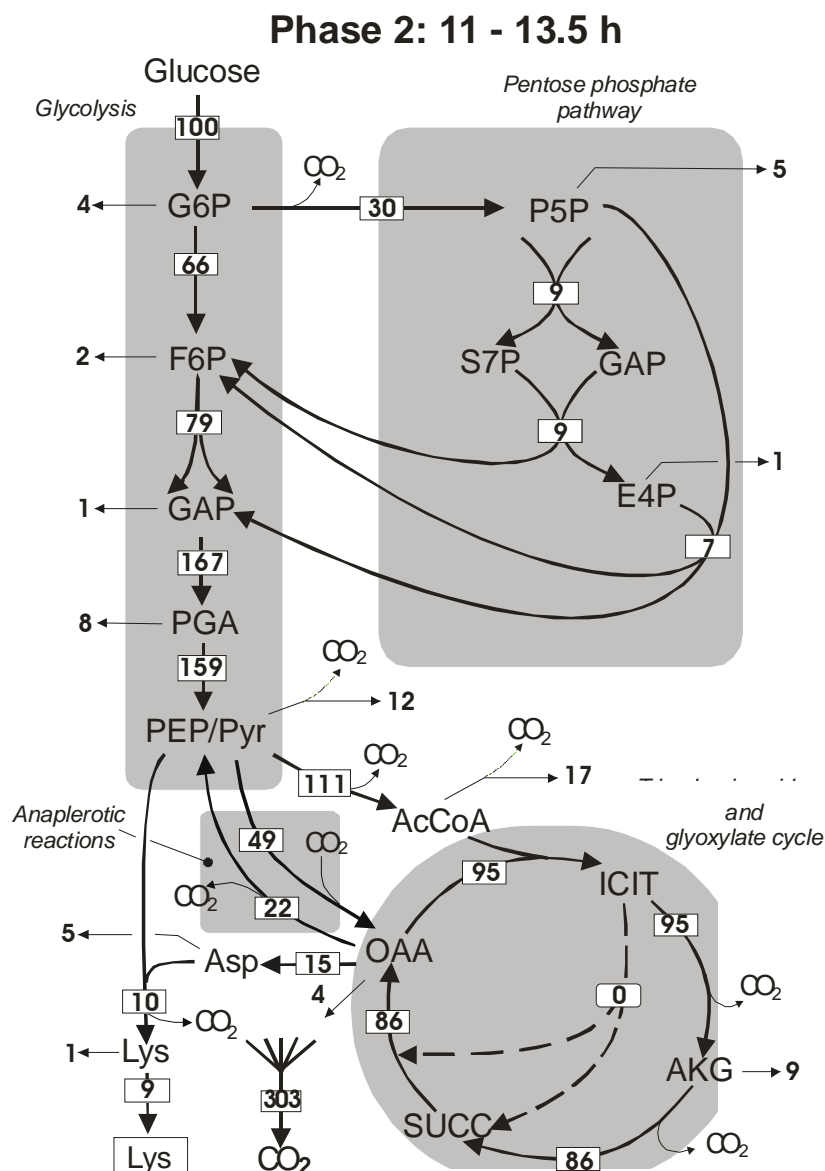
FIGURE 3.16. Map 2 of a series of three subsequent flux distributions representing the integrated fluxes of lysine producing *C. glutamicum* MH20-22B during batch culture monitored by ^{13}C labeling form 11 to 13.5 *h* process time using the Sensor reactor approach. All fluxes are given as molar precentage of the glucose uptake. Thick and thin lines indicate central metabolism reactions or fluxes into anabolic pathways and by-products, respectively. For abbreviations see Appendix.

Phase 3: 14 - 16.5 h
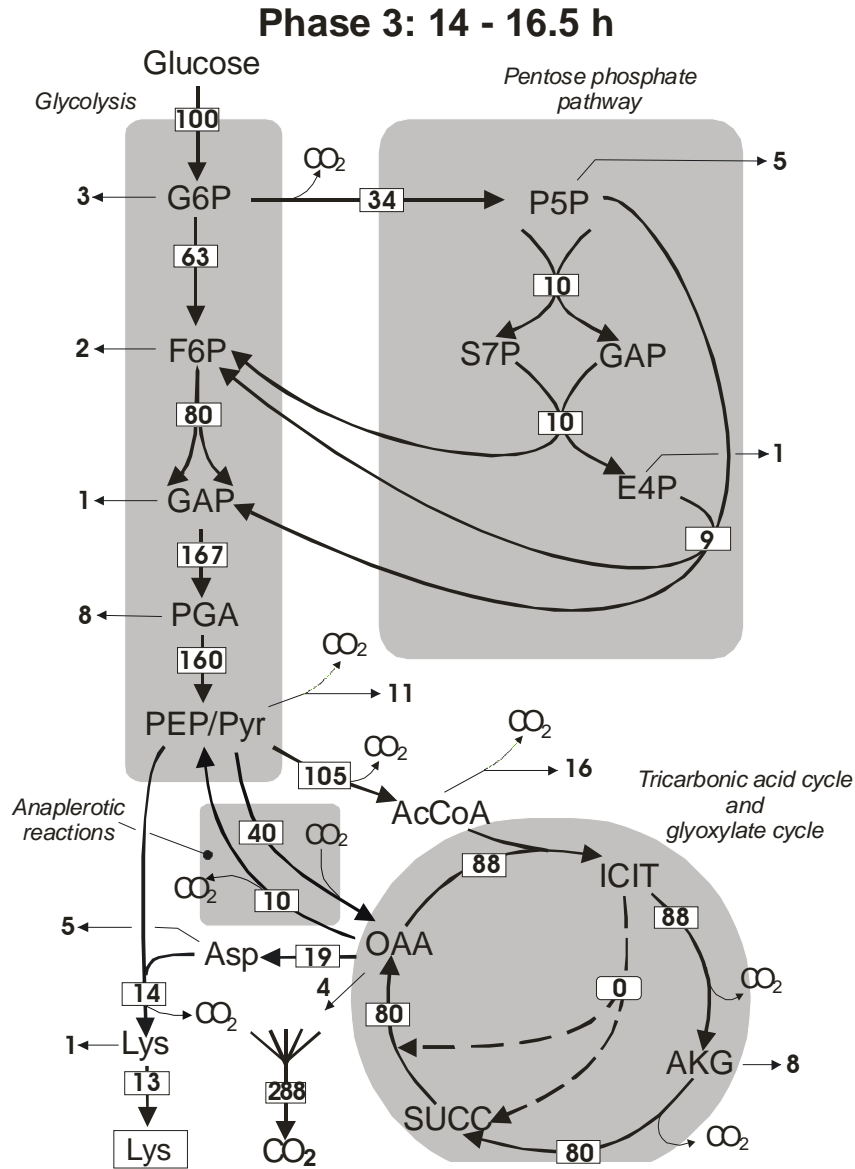
FIGURE 3.17. Map 3 of a series of three subsequent flux distributions represent-
ing the integrated fluxes of lysine producing *C. glutamicum* MH20-22B during
batch culture monitored by ^{13}C labeling form 14 to 16.5 *h* process time using
the Sensor reactor approach. All fluxes are given as molar precentage of the glu-
cose uptake. Thick and thin lines indicate central metabolism reactions or fluxes
into anabolic pathways and by-products, respectively. For abbreviations see Ap-
pendix.

sumption was made that (still) PEP carboxykinase is mainly responsible for the decarboxylating flux in lysine producing *C. glutamicum* MH20-22B.

Riedel *et al.* [RRD$^+$01] showed that the presence of PEP carboxykinase activity is counteractive to the production of lysine, probably because rising enzyme activity reduces the intracellular concentration of the lysine precursor oxaloacetate (OAA). In accordance with this finding, the elimination of the PEP carboxykinase activity in *pck* mutants led to a 60 % increase of lysine formation concomitantly with increasing pool sizes of pyruvate, α-ketoglutarate, aspartate and oxaloacetate in *C. glutamicum* MH20-22B growing in chemostate cultures [PMdG$^+$01]. Therefore, the present scenario of a decreasing PEP carboxykinase flux coupled to an increasing lysine formation, well confirms previous findings. It also outlines the quality of the Sensor reactor system, because previous findings were independently reconfirmed moreover offering the possibility to discuss temporary changing flux patterns thus deriving working hypothesis for further *metabolic engineering.*

Up to now, little information is available on the regulation of PEP carboxykinase activity in *C. glutamicum.* Jetten and Sinskey [JS93] found out that the enzyme is strongly inhibited by ATP for oxaloacetate (OAA) synthesis making it very unlikely that PEP carboxykinase catalyzes OAA formation *in vivo.* To further elucidate the *in vivo* PEP carboxykinase regulation, enzyme activity measurements were additionally performed using cell-free extracts of all three Sensor reactor experiments (see protocol given in section A.3.11). It was observed that the specific activities $\left[U \cdot mg_{proteine}^{-1} \right]$ were almost identical (phase 1: 0.072 ± 0.002, phase 2: 0.067 ± 0.020 and phase 3: 0.072 ± 0.006, respectively). Again, this finding is in agreement with previous results of Riedel *et al.* [RRD$^+$01], who found that the enzyme is not regulated by cell-growth but weakly regulated by the carbon source.

Studying the anaplerotic net fluxes given in the Figures 3.15, 3.16 and 3.17, an increase from 23 % (phase 1) to 30 % (phase 3) is identifiable which coincides with rising lysine formation rates from 4 % (phase 1) to 13 % (phase 3). Obviously, the improved oxaloacetate and aspartate availability enabled increasing lysine production, in accordance with previous findings [MTES89]. However, it is noteworthy that increasing anaplerotic net fluxes were not the consequence of rising carboxylation rates. On the contrary, the carboxylating flux diminished from 54 % (phase 1) to 40 % (phase 3). Increasing net anaplerotic rates were thus caused by concomitantly declining decarboxylation rates from 31 % (phase 1) to 10 % (phase 3) - a fact that might not have been expected before the experimental observations were made.

This (maybe surprising) finding also outlines the benefit of the Sensor reactor approach. Only the analysis of a series of subsequent flux maps reveals temporary changes of intracellular fluxes and it thus allows the formulation of further working hypothesis. In the current study, growing enzyme inhibition by increasing, inhibitory pool sizes could be assumed to explain - for instance - the declining carboxylation rates. In *C. glutamicum* both anaplerotic enzymes PEP carboxylase and pyruvate carboxylase are known to be feedback inhibited by aspartate ([OS69], [MS85],[PWWP$^+$97]) while α-ketoglutarate and oxaloacetate have been suggested as possible inhibitors of pyruvate carboxylase ([PWWP$^+$97], [PMdG$^+$01]). Hence, to further elucidate the regulation of the anaplerotic node reactions with respect to lysine formation, it would be most meaningful to measure the intracellular concentrations of potential effectors such as aspartate, α-ketoglutarate and oxaloacetate during Sensor reactor experiments. Following this concerted approach using pool and flux analysis, the current underlying inhibitory mechanism could be revealed and promising targets for production strain optimization identified.

3.4.2 Analysis of the L-Lysine Production Phase

> Significant parts of the following subsection were already accepted for publication [DMW$^+$03]. Results were acquired during the Ph.D. thesis of M. El Massaoudi and A. Drysch who were co-supervised by the author.

As a continuation of the previous work, the Sensor reactor technology was subsequently applied to study the lysine production with non-growing *C. glutamicum* MH20-22B in an industry-like fed-batch process. The analysis of the fed-batch production phase with non-growing cells was chosen because this process mode represents a typical industrial application. Industrial fermentation processes usually consist of a phase of cell growth followed by a long lasting production phase during which negligible cell growth takes place and which is characterized by a highly selective substrate/product conversion. While the growth phase has already been studied (see preceding subsection) the current investigation focused on the production phase.

It is noteworthy that the serial flux analysis of the production phase necessitated some significant changes of the experimental procedure used so far:

- **Sensor reactor operation:** It must be secured that the (substrate) feeding profiles of the production reactor and the Sensor reactor are identical so as to be able to install the same culture conditions in both reactors.

- **Labeling:** While labeling with ^{13}C-glucose was performed by a single addition of the labeled substrate at the beginning of the labeling process to analyze the growth phase, the fed-batch process additionally requires the appropriate continuous feeding of the labeled substrate.

- **Labeling analysis:** Because non-growing cells are studied, the labeling information cannot be derived from the labeling patterns of the proteinogenic amino acids in the biomass, as it was performed during the serial flux analysis of the growth phase. Instead, the labeling information must be taken from free metabolite pools either in the supernatant or inside the cells. Intracellular pools are preferred because of their supposedly short turnover times and an absence of memory effects with respect to the ^{13}C labeling. Memory effects would be expected with respect to the native amount of ^{13}C labeling found in the accumulated products in the supernatant that superimpose the added ^{13}C labeling aimed at.

- **Modeling:** Compared to the stoichiometric model used for cell growth analysis, the current study allows the simplification of the model structure because fluxes into amino acid biosynthesis, representing cell growth, can be neglected.

In analogy to the foregoing study, the anaplerotic node was again in the focus of the detailed flux analysis because of its importance for the production of amino acids of the aspartate family. The total experimental set-up was similar to the preceding experiments. Again, the 300-L bioreactor was used as the production process which was coupled to the 1-L Sensor reactor in master/slave controlling mode and which was inoculated, labeled and harvested twice according to the previously presented procedure (Figure 3.1).

At the beginning, the production process was started in batch mode (for start medium, see A.2.2). 24.5 h process time after the inoculation of the production reactor, the first Sensor reactor experiment was started (phase 1) coinciding with the beginning of the L-leucine limited L-lysine production phase. An inoculation volume of 1 L was automatically taken out of the 300 L production process and injected into the Sensor reactor. Immediately after inoculation, the glucose pulse for labeling was added and the ^{13}C containing feed started such that a constant level of 15 % ^{13}C labeled glucose was maintained in the Sensor reactor for the next 3 hours (for details see A.5.3). Then, cells were sampled according to the protocol given in the Appendix (A.3.1). Finally the Sensor reactor was emptied and cleaned by aeration. After 0.5 hour the device was prepared for the
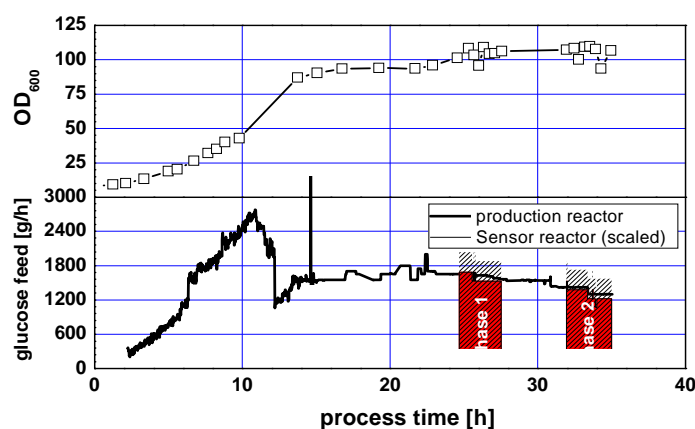
FIGURE 3.18. Comparison of the feed rates installed in the Sensor reactor (thin lines with filled area) and in the 300-*L* scale production process (thick line) together with the courses of the biomass production (given by OD_{600}). Please notice that the feed rate of the Sensor reactor is scaled-down to the production process by taking into account the current ratio of the reaction volumes of the two reactors.

next experiment which was performed after 32 *h* process time (phase 2)[5]. Hence, the beginning of the L-leucine limited production phase as well as a subsequent phase 6 hours later could be monitored (and compared) making use of the Sensor reactor.

As indicated in Fig. 3.18 differently scaled but otherwise identical feeding profiles of the sole carbon source glucose during the L-Leucine limited production phase (no cell-growth) were established in the production process and in the Sensor reactor. The scaled-down feeding profile of the Sensor reactor was calculated based on the relationship of the current reaction volumes in the two bioreactors. A typical scale factor was 1:153. A small amount of L-Leucine was also included in the feed medium (see A.2.2) to fulfill the maintenance demands of *C. glutamicum*.

Figure 3.19 illustrates the similarity of the two fermentation runs in the different bioreactors. Metabolite measurements were performed using standard analytical approaches (see A.3.2) as well as ^{1}H-NMR measurements (see A.3.5). The metabolites glucose, lysine, lactate, trehalose, isopropyl

---

[5] Please notice that the numbering of process phases should not be mixed up with the corresponding numbering of the preceding batch experiments.
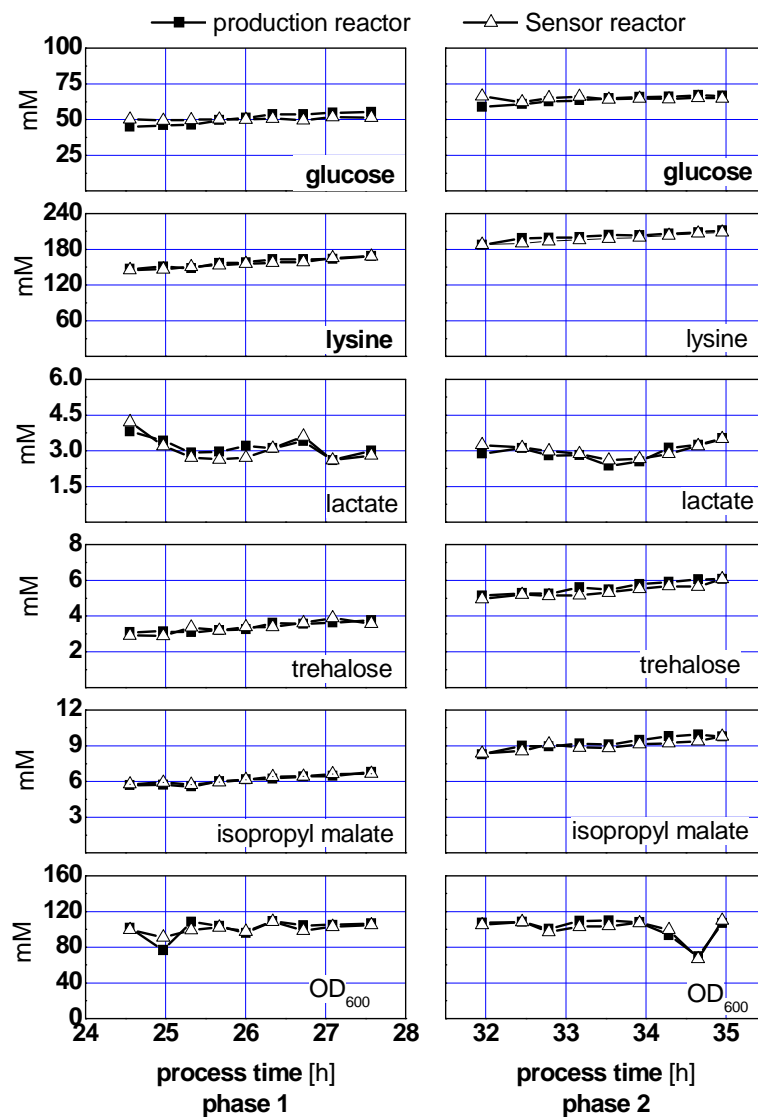
FIGURE 3.19. Overview of representative metabolite courses observed during the labeling periods 1 and 2 of the L-lysine production phase with non-growing *C. glutamicum* MH20-22B cells. Filled square symbols indicate the production process while open (up) triangles represent measurements of the Sensor reactor.

malate and the optical density OD_{600} were chosen to represent the major carbon source, the most important product and the formation of important by-products. Courses of the auxotrophic substance L-leucine are not shown, because the concentration was zero during the production phase with non-growing cells. As indicated, high similarities were found for each course, allowing the conclusion that similar cultivation conditions were achieved in each bioreactor, which obviously is the basis to transfer metabolic flux analysis (MFA) results of the Sensor reactor to the production process.

Following the modeling procedure presented in A.7.7 (which was already applied in the preceding subsection), MFA considers measured rates such as substrate consumption and production formation (so-called extracellular fluxes) together with the labeling information in a least-square model identification process. Therefore extracellular fluxes represented by glucose consumption and lysine, trehalose, isopropyl malate production rates ($mmol \cdot g_{CDW}^{-1} \cdot h$) were determined for phase 1 (1.16 ± 0.09; 0.31 ± 0.01; 0.012 ± 0.002; 0.014 ± 0.001) and phase 2 (0.86 ± 0.11; 0.27 ± 0.01; 0.012 ± 0.002; 0.015 ± 0.001) of the Sensor reactor fermentations.

Results of the 2D-NMR measurements of isotopomer distributions are given in the Appendix (see tables A.8, A.9) as well as the analytical protocol used (see subsection A.3.13). It should be pointed out that these measurements were made on an extract prepared from approximately 5 *g* dry weight of quenched cells and thus represents the labeling state of the important intracellular pools of free metabolites *in vivo*. These include trehalose, citrate, alanine, aspartate, threonine, valine, isoleucine, glutamate and lysine (as indicated in the tables). Since these pools rapidly turn over also in non-growing cells, (example: see below), their labeling state accurately reflects the pseudo-stationary metabolic state during the labeling period. This is in contrast to extracellular compounds present in the culture broth, that to a large extent may have been synthesized in the 300 L bioreactor before being transferred to the Sensor reactor and as a consequence are largely unlabeled and therefore less suited to take as a basis for flux analysis. Indeed, the NMR analyses evidenced that the labeling degree of valine and isoleucine, two uncharged amino acids that may strongly exchange with the extracellular compartment via diffusion over the cell wall, was considerably lower than that of the precursor alanine.

For modeling, the combined metabolic balancing/isotopomer analysis approach already applied in the preceding subsection and also presented in subsection A.7.7 was chosen. Basically, the model of Marx *et al.* [MdGW+96] was used as shown in the Appendix A.7.9. However, the model was simplified because the cells were observed under non-growing conditions. Strictly spoken no fluxes from precursor metabolites into the amino acid pools for biomass protein synthesis should be considered. Since this, however, would

Production Phase 1: 24.5 - 27.5 h
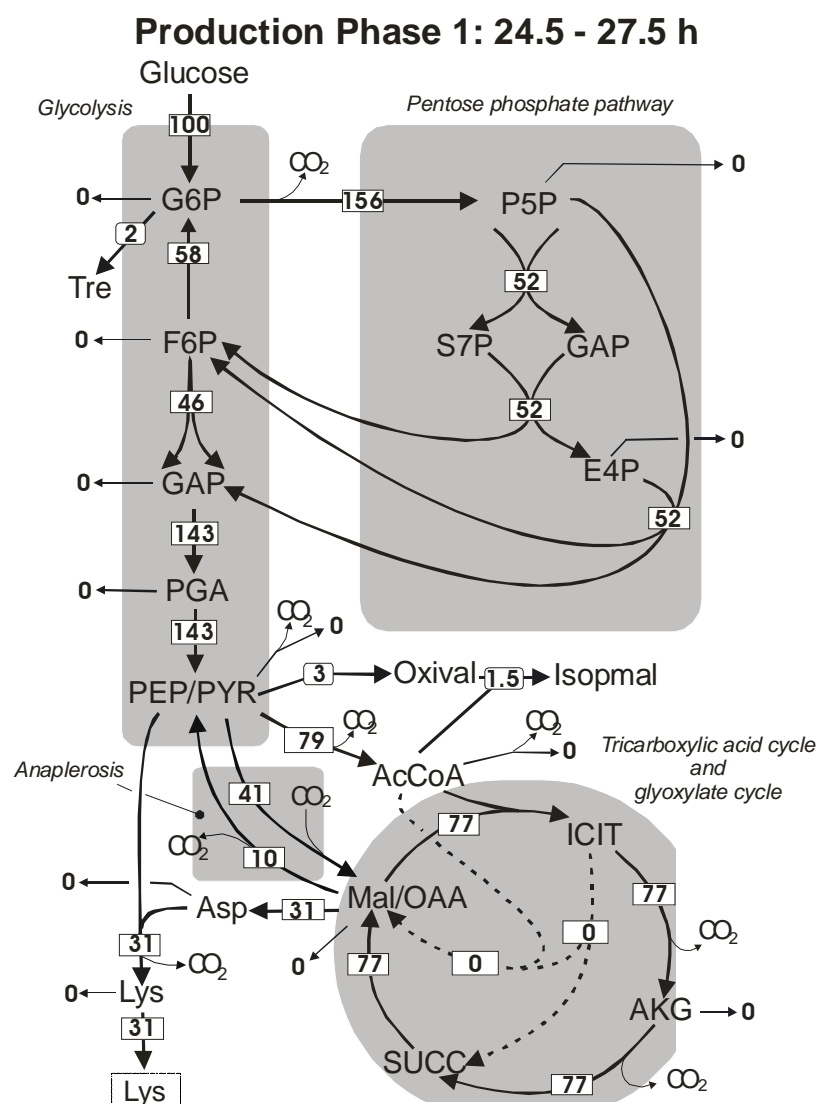
FIGURE 3.20. Carbon flux distribution in non-growing L-lysine producing *C. glutamicum* MH20-22B during phase 1 (24.5 to 27.5 *h* process time) in the Sensor reactor. Fluxes are given as molar percentage of the glucose consumption. Thick lines indicate estimated fluxes of central metabolism while thin lines show reactions to by-products, anabolic pathways etc. For abbreviatons see Table B.1 in the Appendix.
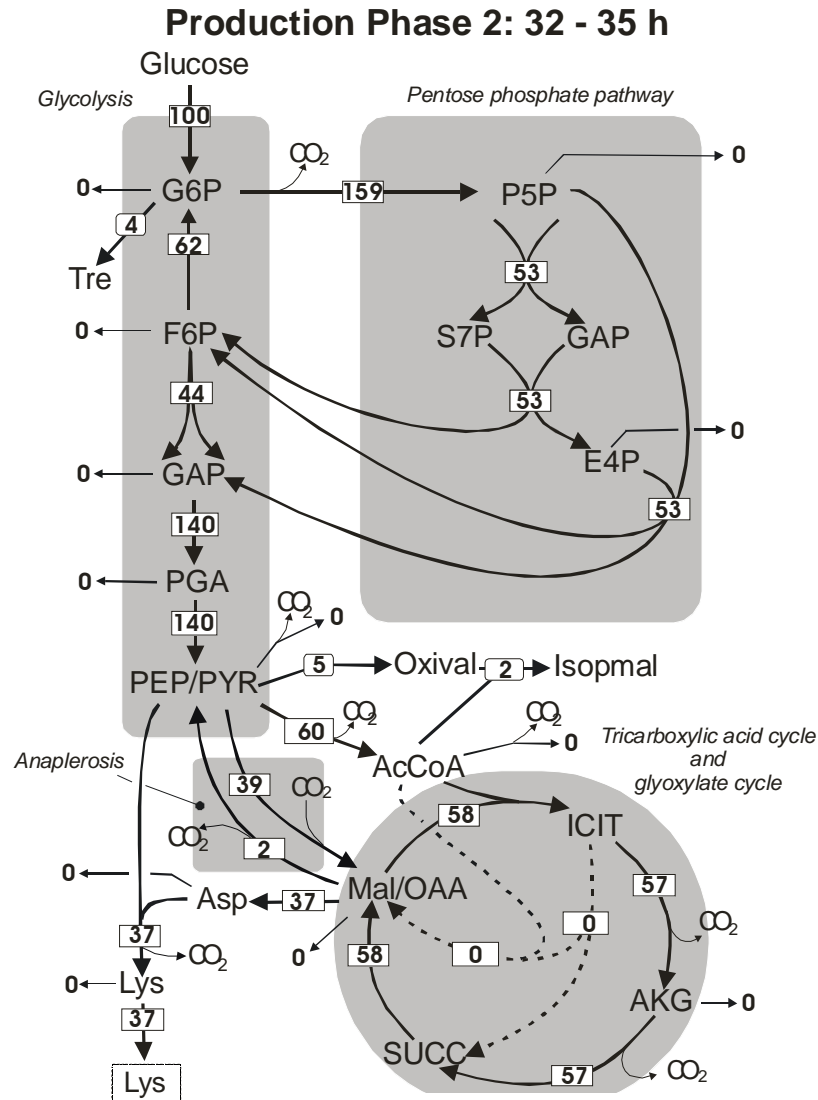
FIGURE 3.21. Carbon flux distribution in non-growing L-lysine producing *C. glutamicum* MH20-22B during phase 2 (32 to 35 *h* process time) in the Sensor reactor. Fluxes are given as molar percentage of the glucose consumption. Thick lines indicate estimated fluxes of central metabolism while thin lines show reactions to by-products, anabolic pathways etc. For abbreviatons see Table B.1 in the Appendix.

lead to unrealistic unlabeled amino acid pools in the model, all the effluxes of the amino acid pools for protein/biomass synthesis were set to a negligibly small non-zero value ($0.0001\ mmol \cdot (gh)^{-1}$) to prevent numerical problems. In addition to the directly measured cellular effluxes (such as lysine formation), very small synthesis rates (non-measurable by standard ^{1}H-NMR) of $0.0008\ mmol{\cdot}g_{CDW}^{-1}{\cdot}h^{-1}$ of valine and $0.0003\ mmol{\cdot}g_{CDW}^{-1}{\cdot}h^{-1}$ of isoleucine, as well as a transmembrane exchange of these amino acids had to be considered in the model to account for the labeling observed in the intracellular pools of these amino acids. Results of the flux calculations are given in the figures 3.20 and 3.21 and in Table 3.4.

As indicated by the values given in Table 3.4, most of the intracellular reactions were estimated sufficiently accurate to allow the discussion of the overall flux distribution. This especially holds true for the fluxes of the anaplerotic reactions, which are in the focus of this study due to their importance for L-lysine synthesis. A striking feature is that for both fermentation phases, a net reverse glycolytic flux of F6P→G6P was calculated together with a very high inaccuracy of the glucose-6-phosphate isomerase reaction qualifying this result as not statistically significant. It should be noticed that previous studies of Drysch *et al.* [DMM$^+$03] achieved a higher accuracy for the same isomerase reaction - namely 10% error margins. However, the previous study focused on the exponential growth phase and thus could make use of labeling information in the aromatic amino acids tyrosine and phenylalanine as well as of labeling patterns in nucleosides like cytidine and uridine that were also found in the biomass hydrolyzate. As can be seen in the isotopomer data given in the Appendix (see tables A.8, A.9), this information was not available in this study. Therefore, the high error margins for the glycolytic flux encountered in the present study are caused by limited labeling information detected by NMR. Future studies employing mass spectroscopy for analysis of isotopic enrichments should alleviate this problem.

As pointed out above, these flux analysis results can only be trusted if the ^{13}C labeling of the detected large intracellular pools truly reflects the steady state value. This is the case if the pools have a sufficiently rapid turnover meaning that at least 95% of the pools are exchanged during the labeling period. Making use of the well-known 'classical' chemical engineering theory, this constraint realistically corresponds to a 3 fold pool exchange considering the mean pool-residence time of a constant pool size with a constant pool in- and efflux.

Historically, *C. glutamicum* is well-known as an L-glutamate producer ([KUS57], [SOT62]), thus recommending the intracellular glutamate pool as an appropriate example to test the hypothesis. The representative metabolite L-glutamate was analyzed and found to be 50 (phase 1) and 40 mM

TABLE 3.4. Selected calculated intra- and extracellular fluxes and their standard deviation in *C. glutamicum* MH20-22B during the phases 1 and 2 of the L-lysine production in the fed-batch processin the Sensor reactor

Reactions	Flux estimates $\left[mmol \cdot g_{CDW}^{-1} \cdot h^{-1}\right]$	
glucose consumption[a]	1.05 ± 0.05	0.75 ± 0.05
G6P→P5P[b]	1.63 ± 0.59	1.19 ± 0.41
G6P→F6P	0.61 ± 0.73	0.47 ± 0.63
GAP→PEP/PYR[c]	1.50 ± 0.17	1.05 ± 0.08
PEP/PYR→AcCoA	0.82 ± 0.15	0.45 ± 0.07
AcCoA→TCA cycle	0.81 ± 0.16	0.43 ± 0.09
SUCC→OAA/MAL	0.81 ± 0.14	0.43 ± 0.09
PEP/PYR→OAA/MAL[d]	0.43 ± 0.03	0.29 ± 0.02
OAA/MAL→PEP/PYR[e]	0.11 ± 0.07	0.02 ± 0.04
OAA/MAL→Asp	0.32 ± 0.01	0.28 ± 0.01
lysine formation[f]	0.31 ± 0.01	0.28 ± 0.01

[a]calculated glucose consumption rate from flux analysis; [b]P5P codes for the lumped pools of ribose-5-phosphate (R5P), ribulose-5-phosphate (Ri5P) and xylulose-5-phosphate (X5P); [c]Net flux; [d]lumped anaplerotic reactions - namely PEP carboxylase, PYR carboxylase; [e]lumped reverse anaplerotic reactions - namely PEP carboxykinase, OAA decarboxylase, malic enzyme; [f]calculates lysine production from flux analysis

(phase 2), which is equivalent to 0.025 and 0.02 $mmol \cdot g_{CDW}^{-1}$. The guiding idea for the estimation of the L-glutamate turnover was to use its biochemical function as an ammonium donor for L-lysine synthesis together with the following assumptions:

- The turnover rate of the intracellular glutamate pool can be estimated from the nitrogen flux considering that under conditions of ample extracellular ammonium availability, the glutamine 2-oxoglutarate-aminotransferase system (GOGAT) in *Corynebacterium glutamicum* is inactive and all nitrogen not used for the synthesis of glutamine-derived compounds is assimilated by the glutamate dehydrogenase reaction [TdGS99]. This means that a lower boundary for the turnover of the glutamate pool is set by the nitrogen assimilation necessary for transamination and aminotransferase reactions involved in the synthesis of lysine and its precursor aspartate.

- For lysine production, the following ammonium demands were assumed: 1 mol aspartate is transaminated per mol of lysine (entrance reaction of the lysine pathway) and 1 mol glutamate is needed for the succinyl-diaminopimelate aminotransferase reaction per mol of lysine unless the ammonium-dependent diaminopimelate dehydrogenase pathway is used. Obviously, the latter does not require gluta-

mate but ammonium instead. According to the findings of Sonntag *et al.* [SEdGS93], approximately 70% of lysine formation is expected to proceed via the succinyl-diaminopimelate aminotransferase route at the extracellular ammonium concentrations of 300 mM (phase 1) and 275 mM (phase 2). Thus, the flux via the glutamate pool comes up to 1.7 fold of the L-lysine production.

As a consequence a glutamate flux of 0.527 $mmol \cdot g_{CDW}^{-1} \cdot h^{-1}$ was estimated for phase 1 and 0.476 $mmol \cdot g_{CDW}^{-1} \cdot h^{-1}$ for phase 2 (see also Table 3.4). From this, glutamate turnover rates of 26.35 per hour (phase 1) and 19.04 per hour (phase 2) were calculated, which represent 2.28 min and 3.15 min mean pool-residence times (turnover times). 95% pool exchange was thus achieved after 6.84 min ($= 3 \cdot 2.28$ min) and 9.45 min respectively. Hence, 3 h of labeling were obviously enough to achieve an equilibrated labeling pattern even in a high concentrated pool like L-glutamate.

Inspection of the flux analysis results for the anaplerotic reactions, the main MFA target in this study, reveals some interesting effects. Despite an increase in lysine selectivity going from phase 1 (31 mol%) to phase 2 (37 mol%), the anaplerotic carboxylating flux (i.e. PEP/PYR → MAL/OAA) remained almost constant at 39 – 41 % of the molar glucose uptake rate. During the same period, a surprisingly strong decrease of the reverse decarboxylating flux MAL/OAA→ PEP/PYR (10 mol% during phase 1, reduced to 2 mol% during the 2*nd* phase 6 hours later) was found that inversely correlated with the increased lysine selectivity.

This finding is in remarkable agreement with previous studies of Petersen *et al.*, ([PdGE$^+$00], [PMdG$^+$01]) and Riedel *et al.* [RRD$^+$01], which were already discussed in the preceding subsection. According to their findings, the presence of PEP carboxykinase activity is counteractive for lysine formation, most presumably owing to a reduced supply of the precursor oxaloacetate. While strictly speaking the present study - once again - cannot discriminate between the enzymes PEP carboxykinase and malic enzyme or oxaloacetate decarboxylase, Petersen *et al.*, ([PdGE$^+$00], [PMdG$^+$01]) showed that malic enzyme and oxaloacetate decarboxylase are almost negligible inactive in cells growing in glucose chemostat cultures[6]. So the working hypothesis can be concluded that the decarboxylating fluxes found in the present study are mainly catalyzed by PEP carboxykinase and that their decline is closely correlated to the rising lysine formation. So far, the results of the serial MFA in the production phase are similar to those findings considering L-lysine production during the growth phase.

---

[6] Again, the author wants to indicate that instead of PEP carboxykinase, oxaloacetate decarboxylase was identified by Klapa *et al.* [KAS03b] to be mainly responsible for the decarboxylating fluxes.
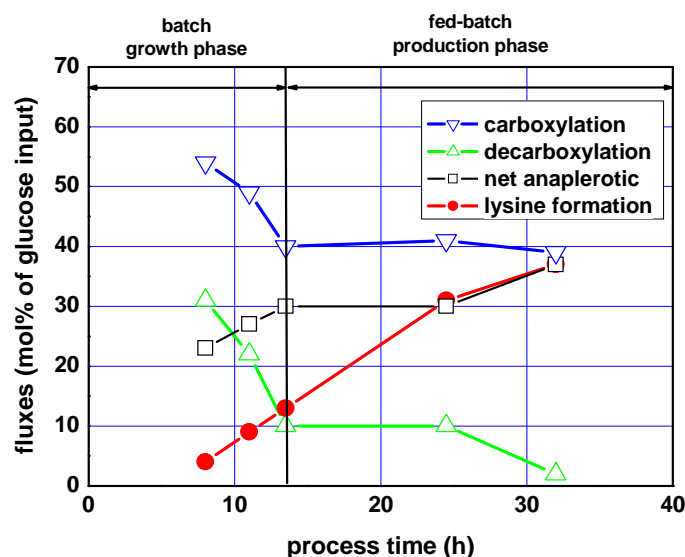
FIGURE 3.22. Serial flux distributions in anaplerosis considering growing and non-growing lysine producing cells of *C. glutamicum* MH20-22B. Carboxylating (down triangle, open) decarboxylating (up triangle, open) net anaplerotic (square, open) and lysine formation rates (circles, filled) are shown.

3.4.3 Flux Map Comparison - Growth vs. Production Phase

Up to now, the serial MFA results of the growth phase and the L-lysine production phase were separately discussed leading to the similar finding that - presumably - PEP carboxykinase activity declined and thus L-lysine formation rates increased. From this one could conclude that PEP carboxykinase activity should be (fully) suppressed in an optimum L-lysine producing strain to achieve maximum product formation rates. Whether and how this was realized in the L-lysine production strain investigated remains unclear. Either gene regulation or feedback inhibition by intracellular pools can be assumed as potential reasons for the PEP carboxykinase activity decline observed during the course of L-lysine production. However, more detailed serial studies, in combination with transcriptome and metabolic profiling analysis are necessary to elucidate the underlying mechanism.

Unfortunately, little is known about PEP carboxykinase activity regulation *in vivo* (as already mentioned) apart from an inhibition of the reverse catalyzing potential at physiological ATP levels [JS93]. Therefore, the

discussion of flux analysis results must remain limited to phenomenological explanations based on comparative studies. For that, the summarizing anaplerosis flux distributions given in Figure 3.22 offer the opportunity to identify phenomenological differences between the growth and the L-lysine production phase with non-growing cells.

The combined presentation of the preceding findings considering the separate batch and fed-batch experimental results is motivated by the fact that both fermentation experiments were performed using a similar medium (see A.2.2). During both fermentations, almost identical maximum growth rates of $0.2 \pm 0.01 \ h^{-1}$ were achieved thus excluding any medium effects (including glucose and leucine) during the growth phase.

As shown, in growing cells decreasing fluxes via the decarboxylating and the carboxylating anaplerotic reactions were observed. Because the carboxylating rates were higher than the reverse rates, an increasing net anaplerotic flux was found that led to an increase of growth-associated lysine formation during the course of the batch phase, however at low lysine selectivities not exceeding 15%. During the high-selective lysine formation phase the scenario is different. For the first 10 h the carboxylating fluxes and decarboxylating fluxes remain apparently at the values pertinent to the final stage of the growth phase, thus leading to high lysine formation rates because growth is halted. After 25 h lysine production even increases because the decarboxylating fluxes (via PEP carboxykinase) reduce to almost negligible rates while carboxylation rates remain almost constant. The high lysine/glucose yield of 37 $mol\%$ indicates an optimum of lysine selectivity for this strain.

Motivated by these findings, one can conclude that in order to achieve improved lysine selectivities during the fed-batch production phase, on-going production strain development should aim at improving the carboxylating reactions – namely PEP carboxylase and pyruvate carboxylase. PEP carboxykinase and oxaloacetate decarboxylase are almost inactive at optimum lysine production, thus only the carboxylating reaction can further increase the flux into the product.

It is noteworthy that this conclusion, which is essentially based on the results of the serial flux analysis using the Sensor reactor, exceeds the further finding that decreasing PEP carboxykinase activity enabled increased L-lysine formation rates. Now, two *metabolic engineering* targets are identified -namely the reduction of PEP carboxykinase activity and the fortification of PEP carboxylase and/or pyruvate carboxylase activity - to further improve the selectivity of L-lysine production with *C. glutamicum*.

3.5 MFA for L-Phenylalanine Producing *E. coli*

Significant parts of the following section were submitted for publi-
cation [WMS$^+$03]. Results were acquired during the Ph.D. thesis of
A. Wahl and M. El Massaoudi which are/were co-supervised by the
author.

The preceding sections have shown that the Sensor reactor approach
enables serial flux mapping during batch and fed-batch periods exemplar-
ily studying the L-lysine formation in *C. glutamicum* MH20-22B under
industry-like production conditions. In order to demonstrate that the Sen-
sor reactor technology is not limited to *C. glutamicum*, an alternative strain
- namely the recombinant L-phenylalanine (L-Phe) producing *E. coli* 4pF81
(for genotype details see Table A.1) - was chosen, which has played an im-
portant role during the L-Phe process development as presented in the
subsequent chapter 4. Hence the results obtained during serial flux anal-
ysis of L-Phe production were intended to be used for further *metabolic
engineering* of L-Phe producing strains. Additionally, these results are also
relevant with respect to the current research topics presented in section 4.6.

3.5.1 Settling on L-Phenylalanine Producing E. coli

Although a detailed motivation for choosing 'L-phenylalanine' as a tar-
get for microbial process development will be given in section 4.1, some
introductory notes, elucidating the necessity to study intracellular flux dis-
tributions in an L-Phe producing strain will be presented in the following.

The production of aromatic amino acids, corresponding pathway inter-
mediates or derivatives thereof is without doubt of great commercial impor-
tance ([FL94], [BKM$^+$01], [SDH$^+$01], [DHK$^+$02]). Several approaches were
published in the past using for instance recombinant *E. coli* strains. Exam-
ples are the production of pathway intermediates such as 3-dehydroshikimic
acid [LMD$^+$99], shikimic acid ([CYD$^+$03], [KBR$^+$03]), chorismate deriva-
tives such as 2,3 cyclohexane *trans* diole [FLE$^+$03] or 3,4 cyclohexane *trans*
diole [FSM03] and the final pathway products L-tryptophane, L-tyrosine
and L-phenylalanine ([BKM$^+$01], [DHK$^+$02], [GMK$^+$02]). Among these
products, L-Phe currently represents the largest economical market with
11,000 to 12,000 tons per year and a product price of 20 to 40 US$ per *kg*
depending on the product purity [BKM$^+$01]. In the case of L-Phe, the ma-
jority is used for the production of the artificial sweetener aspartame, for
instance in the 'Thermolysine' process at DSM, The Netherlands [SDH$^+$01].

Motivated by these promising commercial perspectives, several studies
were previously performed investigating the optimum supply for the path-
way precursors D-erythrose-4-phosphate (E4P) and phosphoenolpyruvate

(PEP). To ensure a sufficient E4P availability, transaldolase (*tal*) [JLLL97] and/or transketolase (*tktA*) over-expression was studied [DPC$^+$92] and subsequently combined with phosphoenolpyruvate synthase (*pps*) over-expression ([PL94], [PSL95], [Ber96], [GYXB96], [YLDF02], [CYD$^+$03]) or alternative glucose uptake systems in phosphotransferase system (PTS) negative strains ([Ber96], [GYXB96], [FXB$^+$96], [CYPB97]). In addition, Csr (carbon storage regulator) disrupted strains were used to ensure a sufficient PEP supply [TR01].

Despite the invaluable importance of these results for the optimization of the aromatic amino acid precursor supply, detailed (^{13}C-based) flux analysis was not (yet) used to elucidate intracellular flux redistributions in strains producing AAA pathway intermediates (or final products) such as L-Phe. So far, flux analysis was applied to estimate (theoretical) optimum flux distributions in DAHP (3-desoxy-arabino-heptulosonate-7-phosphate) producers ([PL94], [PSL95]), which even achieved a glucose-to-DAHP conversion with theoretical yield [LHC96]. Also the effect of inactivated PTS for DAHP production was studied by MFA [FGF$^+$02]. Furthermore, aromatic amino acid precursors such as PEP were investigated for instance in pyruvate kinase (Pyk) knockout *E. coli* strains [EDP$^+$02]. However, one should consider that MFA for L-Phe producing strains significantly differs from the DAHP-studies because of the second PEP molecule needed for L-Phe production. It is also noteworthy that all studies were limited to shake flasks or small, lab-scale bioreactors which obviously did not represent industry-like production conditions in large-scale bioreactors.

Hence it was planned to apply the Sensor reactor technology to an L-Phe producing *E. coli* strain - namely *E. coli* 4pF81 - under realistic production conditions. Following the optimized L-Phe process strategy described elsewhere ([GMK$^+$02], [RHK$^+$03]) a serial ^{13}C based metabolic flux analysis should be enabled aiming at

- identifying changing intracellular flux distributions during the L-Phe production phase,

- comparing the identified fluxes with the theoretical, optimum flux distribution,

- qualifying discrepancies between real an optimum flux distribution by flux sensitivity analysis and

- finally deriving a working hypothesis for further production strain optimization.

3.5.2 Fermentation Experiments

Fermentations with *E. coli* 4pF81 were started in four shaking flasks (250 *mL*) to inoculate the 30-*L* and subsequently the 300-*L* bioreactor (using 11 *L* biomass suspension) after OD_{620} ~3 was achieved. Fermentations were performed under aerobic conditions at *pH* 6.5 and 37°*C* (for details see Appendix A.2.1).

As shown in subsection A.1.1, *E. coli* 4pF81 is tyrosine auxotrophic and additionally very sensitive to tyrosine accumulation owing to the plasmid-encoded, tyrosine feed-back inhibited, native *aroF* gene used to fortify L-Phe production. An optimized tyrosine feeding was thus necessary which was realized as follows: The tyrosine containing feed (20 $mL \cdot min^{-1}$ including 25 $g \cdot L^{-1}$ tyrosine dissolved in 5% NH_3) was started at the beginning of the exponential growth phase (OD_{620} ~8) and lasted until OD_{620} ~80 was achieved. Then the feed was drastically reduced to 1 $mL \cdot min^{-1}$ until the end of the fermentation to fulfill only maintenance demands of the cells. The glucose profile (containing 600 $g \cdot L^{-1}$ glucose H_2O) was based on the results of fermentation process development (see following chapter 4) and was manually controlled such that no significant glucose accumulation occurred in the production process. All feed profiles of the Sensor reactor were similar to the production process but automatically scaled down (with the aid of LabView^{TM} process control) with respect to the current working volume ratio of the two processes. As indicated in subsection A.2.1, a diluted tyrosine feed concentration was used for the Sensor reactor to ease accurate feeding. After OD_{620} 10 ~15 was achieved, 100 μM IPTG was added for induction. As already described in the preceding section, the Sensor reactor was coupled to the 300-*L* production process in master/slave controlling mode thus allowing the monitoring of three subsequent phases during L-Phe production with non-growing *E. coli*.

Because previous experiments [RHK$^+$03] revealed maximum product formation rates shortly after the beginning of the tyrosine limited production phase (followed by a significant product formation decline), this period was chosen to study changing intracellular flux maps and to derive thereupon working hypothesis trying to identify promising *metabolic engineering* targets for further production strain improvement.

Figure 3.23 shows a selection of characteristic state variables representing the phenomenological state of the cells in the production process and in the Sensor reactor. Details of the analytical protocols used are given in subsection A.3.3. The figure illustrates that labeling periods from 14 to 16.8 *h*, 17.2 to 20 *h* and 20.5 to 23.3 *h* process time were applied thus exemplarily representing the L-Phe production phase with non-growing *E. coli* 4pF81. Before, biomass production halted after 11 *h* at OD_{620} ~80 as a result of the significantly reduced tyrosine feed as described above.
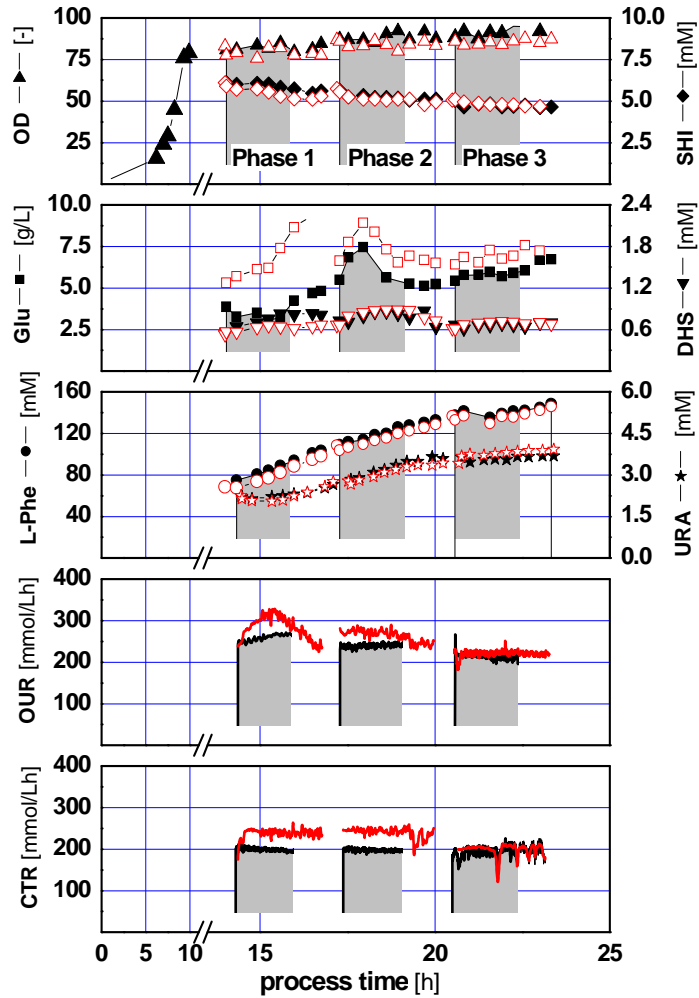
FIGURE 3.23. Comparison of some phenomenological state variables such as optical density (OD_{620}), glucose concentration (Glu), L-phenylalanine concentration (L-Phe), by-products like shikimate (SHI), 3-dehydroshikimate (DHS), uracil (URA) and the oxygen uptake rate (OUR) as well as the carbon dioxide tranfer rate (CTR). All variables are shown for the production process (filled, black symboles/lines) and for the Sensor reactor (open red symbols/lines). Labeling experiments were started 14, 17.2 and 20.5 h process time, lasting for about 2.5 hours.

For ^{13}C labeling $\left[1 - ^{13}C\right]$ glucose was added to the Sensor reactor immediately after inoculation such that a 25 % ^{13}C glucose enrichment was achieved in the culture supernatant which was maintained during the subsequent feeding phases (following the procedure described in subsection A.5.4). As a consequence, the total glucose level in the Sensor reactor was accordingly higher compared to the production process nevertheless following the same course, especially during phase 2 and phase 3. Differences between the glucose curves occurred during phase 1, because of some technical feeding problems in the Sensor reactor. However, different cultivation conditions were not the consequence because glucose levels of both reactors ensured well-saturated glucose uptake[7].

With respect to the measured metabolite concentration courses in the supernatant, a high similarity was found. The L-Phe accumulation was almost identical in both reactors (regression coefficient $r = 0.999$). This also holds true for the uracil (URA) synthesis ($r = 0.971$) following the β-alanine route via aspartate and oxaloacetate, respectively. Obviously, the two intermediates of the aromatic amino acid pathway, 3-dehydroshikimate (DHS) and shikimate (SHI), were produced before Sensor reactor monitoring was started. Their production stopped during the labeling periods, which was indicated by an almost constant level.

In the case of the oxygen uptake rate (OUR), high similarities were found regarding the Sensor and the production reactor. The dissolved oxygen concentration (DO) was always above 30 % in both processes (data not shown) thus ensuring a non-limited oxygen supply. On the other hand, carbon dioxide transfer rates (CTR) in the Sensor reactor were observed to be 15 to 20 % higher than in the production process during the phases 1 and 2. However, this is an 'artificial' offset that occurred because the maximum CO_2 detection limit was exceeded in the exhaust gas analysis device used to monitor the production process.

Summarizing it can be concluded, that the phenomenology of both processes was sufficiently consistent thus allowing to perform ^{13}C based flux analysis of the three labeling phases and to transfer the results from the 1-L Sensor reactor to the 300-L scale production process.

---

[7] *E. coli* 4 pF81 possesses an active phosphoenolpyruvate:carbohydrate phosphotransferase system (PTS). According to the results of Ferenci ([Fer96], [Fer99]) and others ([LS99], [PLJ93], [HK79]) half-saturated glucose uptake via Mgl at 0.2 μM (0.036 $mg \cdot L^{-1}$) and via glucose specific PtsG at 3 to 10 μM or 0.6 to 1.8 $mg \cdot L^{-1}$ at micromolar external levels can be assumed while at millimolar external levels glucose uptake via PtsG and mannose specific PtsM (half-saturated at 1.3 mM or 230 $mg \cdot L^{-1}$) should be considered.

TABLE 3.5. Important extracellular fluxes for *E. coli* 4pF81 during L-Phe production phase with non-growing cells. The measured rates for non-labeled glucose uptake (upt1), labeled glucose uptake (upt2), L-Phe formation, CO2 production and uracil formation are given

Rates $[mmol \cdot L^{-1} \cdot h^{-1}]$	Phase 1	Phase 2	Phase 3
upt1	52.9	42.32	39.52
upt2	17.53	14.13	13.48
L-Phe formation	14.12	10.69	5.96
CO_2 production	253.6	238.1	199.5
uracil formation	0.26	0.33	0.20

3.5.3 MFA Results

In analogy to the procedure described in the preceding sections, MFA was (again) based on the combined approach of metabolite balancing and isotopomer analysis (see A.7.7) using the software 13CFlux. The Table 3.5 provides an overview of the measured rates which were used as input values for the intracellular flux analysis.

Furthermore, labeling information of the L-Phe fraction which was solely produced during each labeling period, was needed for MFA. Because natively ^{13}C labeled L-Phe (1.1 %) could already exist in the culture supernatant before each labeling experiment was started, the measured labeling patterns (see protocol A.3.6) were corrected following the procedure described in the Appendix A.5.5. The corrected NMR data together with the measured rates (Table 3.5) were used for MFA considering the stoichiometric and C-transition model presented in subsection A.7.10. The resulting flux maps are given in Figures 3.24, 3.25 and 3.26 as well as the absolute values of the calculated fluxes in Table 3.6.

As shown, most of the fluxes were estimated sufficiently accurate within error margins of 5 to 15%. This especially holds true for the flux estimations of the production phases 1 and 2. Sole exceptions were the closely correlated reactions emp1, ppp1 and ppp2 coding for the glucose 6-phosphate isomerase, the oxidative pentose phosphate pathway and the ribulose-5-phosphate epimerase, respectively. Flux errors higher than 25% were found. Most presumably, these errors were caused by lacking nucleoside labeling information (from e.g. cytidine or uridine) considering ribulose-5-phosphate (Ru5P) as the precursor which was not accessible using strains under non-growing L-Phe production conditions. Analyzing the fluxes of emp1, ppp1 and ppp2 in phase 3, the consequences of information lacks become even more apparent, because the fluxes of the pentose-phosphate pathway were

Production Phase 1: 14 - 16.8 h
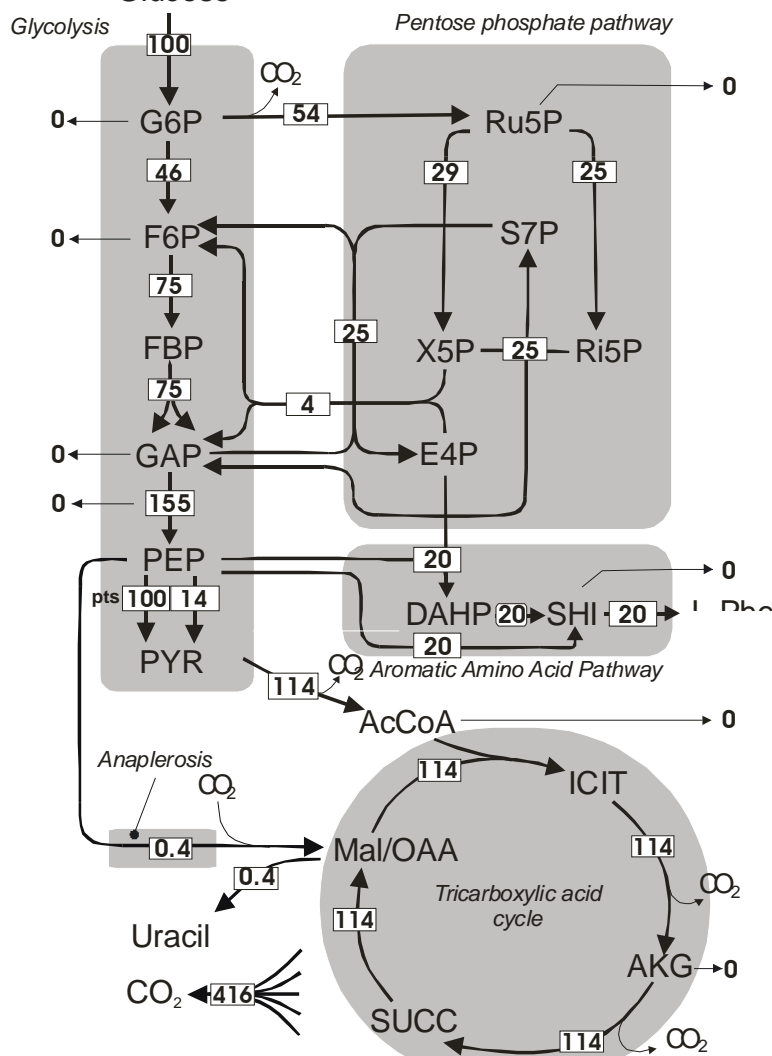
FIGURE 3.24. Estimated intracellular carbon flux distribution based on the ^{13}C labeling experiment in the Sensor reactor during the L-Phe production phase from 14 to 16.8 *h* process time studying non-growing (tyrosine limited) *E. coli* 4pF81. All fluxes are standardized by the corresponding glucose uptake rate thus representing *mol*%. Counter-current fluxes are indicated by minus signs. Because ^{13}C flux analysis considered a lumped PEP/PYR pool, the PEP→PYR flux was reconstructed by stoichiometric constraints including a flux portion for PTS (left box) and the resulting net flux catalyzed by PEP synthase and/or PYR kinase.
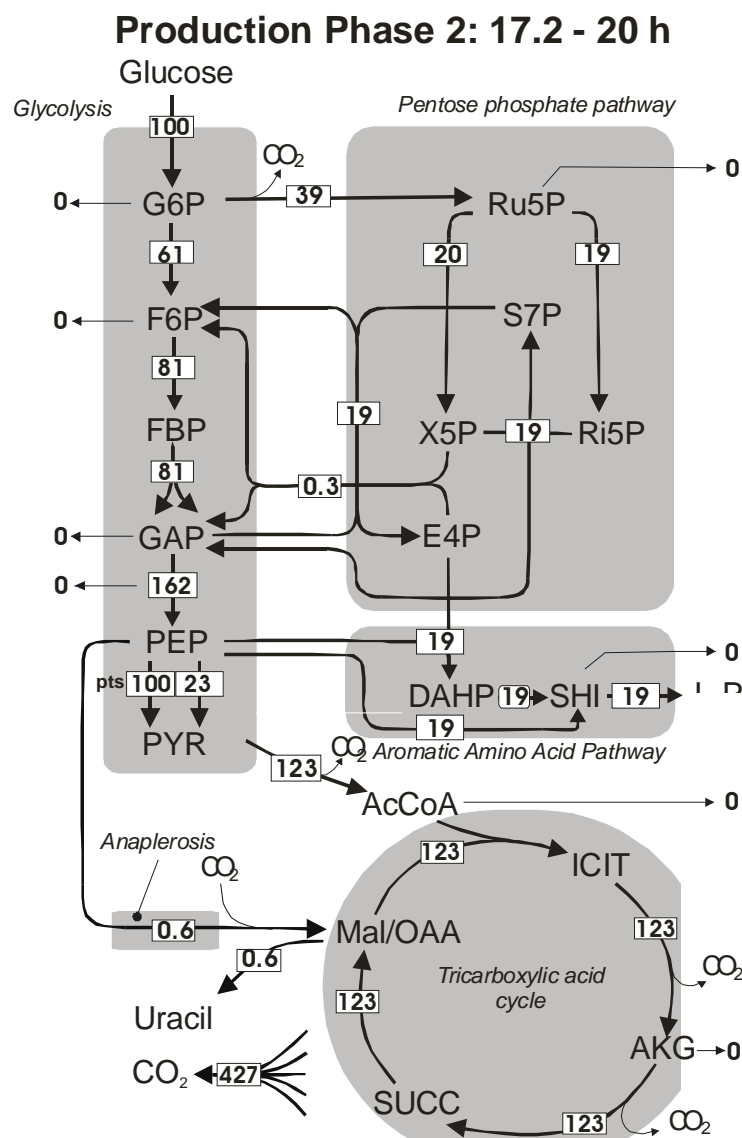
FIGURE 3.25. Estimated intracellular carbon flux distribution based on the ^{13}C labeling experiment in the Sensor reactor during the L-Phe production phase from 17.2 to 20 h process time studying non-growing (tyrosine limited) *E. coli* 4pF81. All fluxes are standardized by the corresponding glucose uptake rate thus representing $mol\%$. Counter-current fluxes are indicated by minus signs. Because ^{13}C flux analysis considered a lumped PEP/PYR pool, the PEP→PYR flux was reconstructed by stoichiometric constraints including a flux portion for PTS (left box) and the resulting net flux catalyzed by PEP synthase and/or PYR kinase.

Production Phase 3: 20.5 - 23.3 h
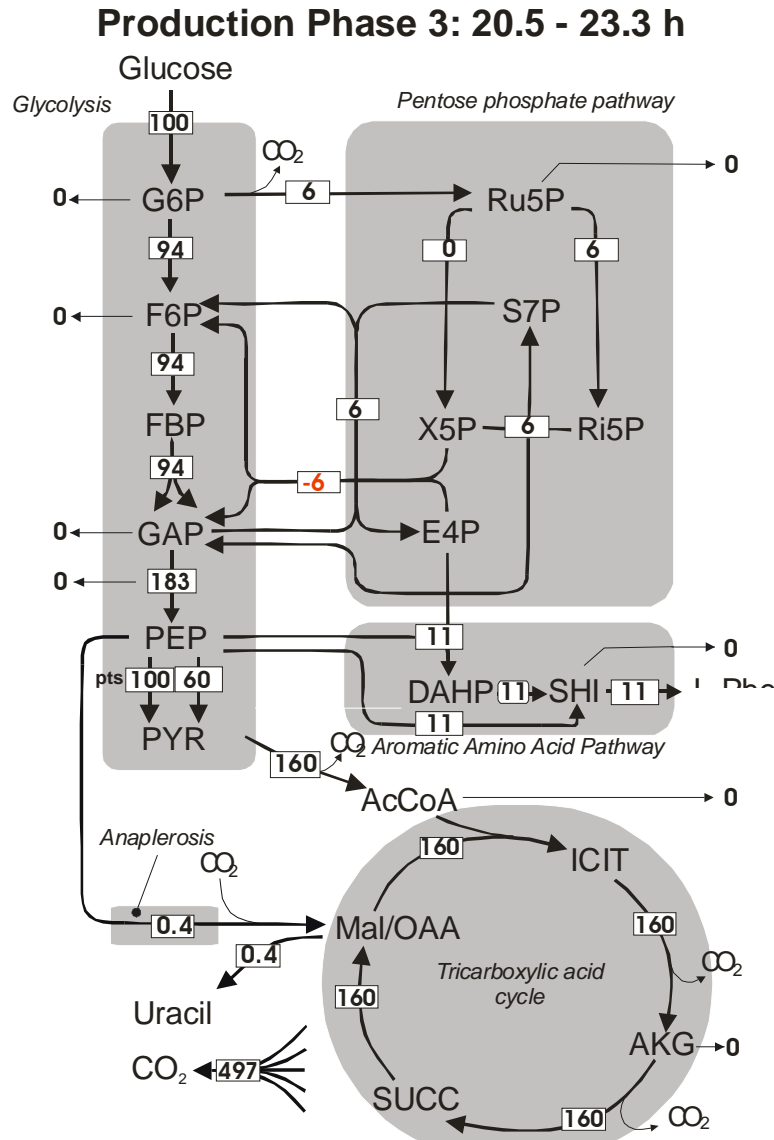
FIGURE 3.26. Estimated intracellular carbon flux distribution based on the ^{13}C labeling experiment in the Sensor reactor during the L-Phe production phase from 20.5 to 23.3 *h* process time studying non-growing (tyrosine limited) *E. coli* 4pF81. All fluxes are standardized by the corresponding glucose uptake rate thus representing *mol*%. Counter-current fluxes are indicated by minus signs. Because ^{13}C flux analysis considered a lumped PEP/PYR pool, the PEP→PYR flux was reconstructed by stoichiometric constraints including a flux portion for PTS (left box) and the resulting net flux catalyzed by PEP synthase and/or PYR kinase.

TABLE 3.6. Estimated fluxes resulting from metabolic flux analysis studying non-growing *E. coli* 4pF81 during L-Phe production. Flux naming corresponds to the model given in Appendix.

Flux	Phase 1 $[mmol \cdot L^{-1} \cdot h^{-1}]$	Phase 2 $[mmol \cdot L^{-1} \cdot h^{-1}]$	Phase 3 $[mmol \cdot L^{-1} \cdot h^{-1}]$
upt1	17.52 ±0.30	14.13 ±0.30	13.43 ±0.30
upt2	52.08 ±0.30	42.31 ±0.30	39.47 ±0.30
emp1	31.79 ±8.50	34.62 ±8.98	49.90 ±26.27
emp2	52.29 ±2.85	45.60 ±3.01	49.90 ±8.76
emp3	52.29 ±2.85	45.60 ±3.01	49.90 ±8.76
emp4	197.77 ±2.94	91.36 ±3.09	96.81 ±8.79
ppp1	37.81 ±8.51	21.82 ±8.99	3.00 ±26.27
ppp2	20.50 ±5.67	10.99 ±5.99	0.00 ±17.51
ppp3	17.31 ±2.84	10.84±3.00	3.00 ±8.76
ppp4	3.19 ±2.84	0.15±3.00	-3.00 ±8.76
ppp5	17.31 ±2.84	10.84±3.00	3.00 ±8.76
ppp6	17.31 ±2.84	10.84±3.00	3.00 ±8.76
tcc1	79.27 ±3.00	69.65±3.15	84.63 ±8.81
tcc2	79.27 ±3.00	69.65±3.15	84.63 ±8.81
tcc3	79.27 ±3.00	69.65±3.15	84.63 ±8.81
tcc4	79.27 ±3.00	69.65±3.15	84.63 ±8.81
tcc5	79.27 ±3.00	69.65±3.15	84.63 ±8.81
ana1	0.26 ±0.26	0.33±0.02	0.2 ±0.02
bsUracil	0.26 ±0.26	0.33±0.02	0.2 ±0.02
bsDAHP	14.12 ±0.20	10.69±0.20	5.99 ±0.20
bsSHI	14.12 ±0.20	10.69±0.20	5.99 ±0.20
bsPhe	14.12 ±0.20	10.69±0.20	5.99 ±0.20
CO2aux	289.50 ±3.11	241.14±3.09	262.67 ±3.09

no longer statistically identified. This observation needs to be stressed because it illustrates the potential drawback of a single metabolic flux analysis which, by retrospective analysis, could reveal the insufficiency of the experimental data measured during the pre-chosen observation window. If a serial flux analysis is carried out – as it will be presented in the following – potential data limitations could be overcome additionally uncovering systematic flux changes, which were not accessible with a single snapshot study.

Studying the current results from 14 to 23.3 h process time, the series of flux maps allows the conclusion that a continuously increasing fraction of carbon was metabolized via glycolysis (emp1) compared to the branching off into the oxidative pentose phosphate pathway (ppp1). As a consequence, transketolase (ppp4, ppp5) and transaldolase (ppp6) catalyzed fluxes of the

pentose-phosphate pathway declined significantly giving rise to the assumption that the E4P precursor supply for the aromatic amino acid pathway reduced concomitantly.

As illustrated in the Figures 3.24, 3.25 and 3.26, the lumped PEP/PYR pool of ^{13}C analysis was decomposed by stoichiometric analysis, allowing the estimation of a net flux via pyruvate kinase and the inversely directed phosphoenolpyruvate synthase (Pps) reaction. The serial flux analysis indicates that the *pykA* and *pykF* encoded kinase reaction obviously increasingly dominated the net flux and consequently amplified the flux into the tricarboxylic acid cyclic from 114 to 160 *mol* %. As a result, CO_2 formation steadily increased from 416 to 497 *mol* % while at the same time L-Phe formation rates reduced from initially 20 to 11 *mol* %. It is noteworthy, that cultivation conditions like *pH*, temperature etc. did not change during this period (see Figure 3.23). Also, the availability of the sole carbon source glucose as well as the tyrosine supply and oxygen availability were unchanged during the whole observation period.

3.5.4   Linear Programming

To qualify the experimental MFA results, a theoretical carbon flux distribution was estimated representing an optimal flux map with respect to maximum L-Phe formation ($mol\%$). Following the linear programming approach it was assumed that maximum L-Phe formation occurred during the tyrosine-limited production phase thus allowing to neglect all biomass refilling fluxes. The stoichiometric model included metabolites of the glycolysis (G6P, FBP, PEP, PYR), the pentose-phosphate (Ru5P, RiP, S7P, E4P) and the aromatic amino acid (DAHP, SHI) pathway while reactions of the tricarboxylic acid were lumped in one reaction step (tca). Co-Metabolites such as NADH, NADPH and ATP were included with "open" balances; for instance futile cycling (fut) was allowed as a free flux to consume ample ATP. It was assumed that the L-Phe producing strain possessed an active PEP synthase (Pps, represented by reaction emp5) and a transhydrogenase (thy) reaction enabling the proton transfer from NADH to NADPH. In total, the model consisted of 16 balanced metabolites and 19 reactions signifying three degrees of freedom. To cover the three degrees, the input flux (pts) was set to one, which reduced the degree of freedom to two. With the aid of two additional optimization criteria - namely maximization of L-Phe formation and minimization of futile cycling (fut, i.e. ATP consumption) - the linear equation system was solved. Further details are given in subsection A.7.11.

As a result, an intracellular, optimal carbon flux distribution according to Figure 3.27 was calculated. Most strikingly, an optimum L-Phe formation of 59.7 $mol\%$ was estimated provided that the tricarboxylic acid cycle

Optimum L-Phe Production
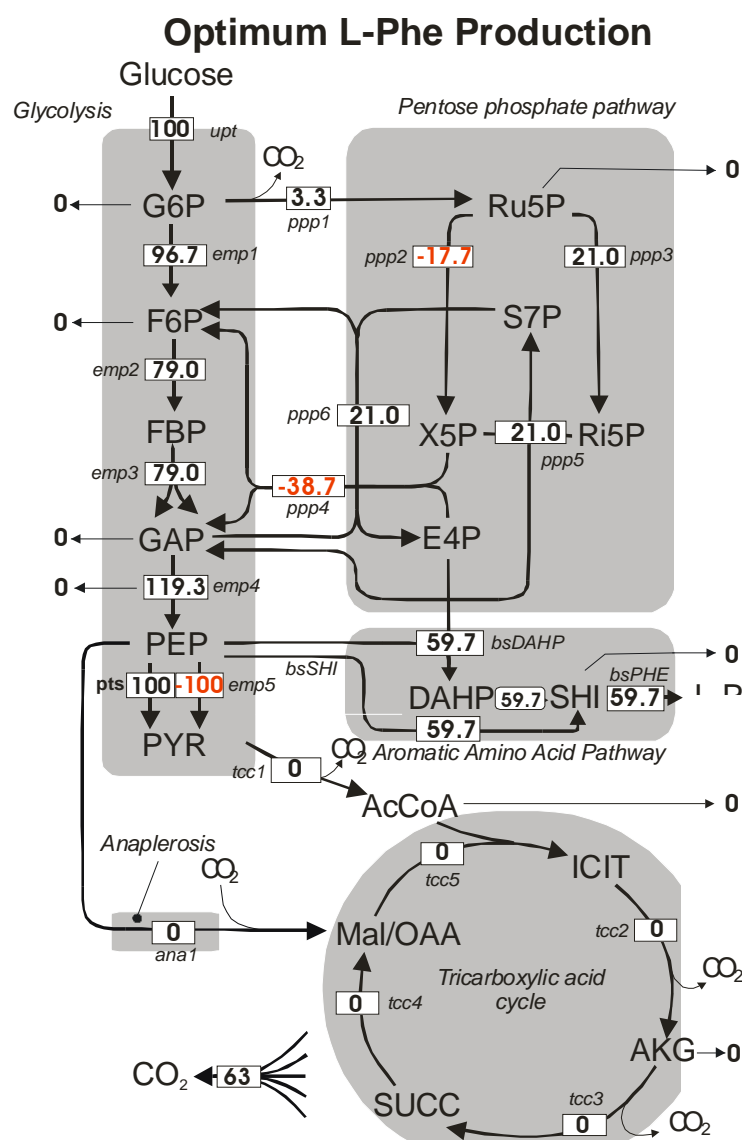
FIGURE 3.27. Linear programming result for an optimal intracellular carbon flux distribution considering the maximum L-Phe formation in non-growing *E. coli*. Counter-current fluxes are indicated by a minus sign. PEP → PYR net fluxes are decomposed with respect to the underlying PTS-based glucose uptake and the PEP synthase and/or PYR kinase reaction. For modeling details see Appendix A.7.11.

was inactive in non-growing cells[8]. As a consequence, the PTS caused PYR formation is redirected into PEP via PEP synthase (Pps, -100 $mol\%$). Interestingly, only a small flux of 3.3 $mol\%$ via the oxidative pentose-phosphate route was favored compared to a significant transketolase activity (ppp4) providing a high flux of – 38.7 $mol\%$ into the E4P pool. Together with the in-coming transaldolase reaction (ppp6) 59.7 $mol\%$ of E4P were thus delivered into the aromatic amino acid pathway. It is noteworthy that, under optimum L-Phe production conditions, a reaction cycle was build up taking GAP and F6P from glycolysis, transferring them into E4P and X5P, the latter subsequently converted into Ru5P and further metabolized via ppp3 into Ri5P and then back into GAP. This demonstrates that all pentose-phosphate reactions must be well equilibrated to enable an optimum E4P supply – including transketolase and transaldolase as well as the phosphoribose isomerase (ppp3) and the ribulose 5-phosphate 3-epimerase (ppp2).

3.5.5   Theoretical Fluxes vs. MFA Results

To compare the linear programming results with those of MFA, some characteristic fluxes - namely ppp1 (coding for the oxidative pentose-phosphate branch), ppp4 (coding for transketolase), ppp6 (coding for transaldolase), emp5 (coding for the net flux of PEP synthase and PYR kinase) and the L-Phe formation (phe) - were studied.

Figure 3.28 provides an overview of the differences between measured and theoretical fluxes. The comparison reveals that even at the beginning of the production phase, which was previously identified as the best production period, the flux distribution was far away from the optimum. The flux via oxidative pentose phosphate pathway (ppp1) was about 50 $mol\%$ too high. Similar observations were made for the transketolase reaction ppp4 and an even worse situation was found for the net flux via PykA/PykF and Pps (emp5). Against it, the transaldolase reaction ppp6 showed an almost optimum flux and kept this level although the measured L-Phe/glucose yield achieved only 20 %, compared to the theoretical value of 59.7 %. From this, we concluded that transaldolase is probably not the most interesting *metabolic engineering* target. This statement partly contradicts previous findings of Lu and Liao [JLLL97] who identified a positive effect of *tal* overexpression for DAHP production. However, no amplified DAHP synthase was used in their study and DAHP production was investigated with partly growing cells in shaking flask cultures, which significantly differed from the experimental conditions of Sensor reactor experiments used here.

---

[8]It should be outlined that 59.7 $mol\%$ resembles 89.55 % of the total carbon input, because a C9 molecule (L-Phe) is produced from a C6 source (glucose).
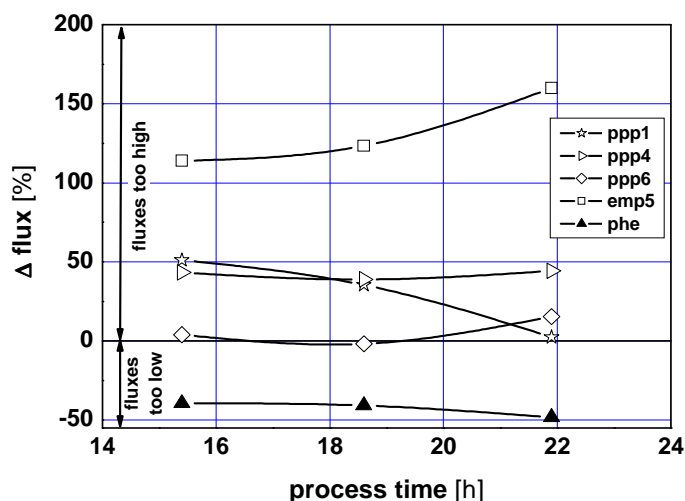
FIGURE 3.28. Selection of characteristic carbon fluxes differences in L-Phe producing, non-growing *E. coli* 4pF81 monitored during three subsequent labeling periods from 14 to 22 *h* process time. Flux difference refer to the optimum carbon flux distribution obtained by linear programming. All flux differences are given as *mol*% of glucose uptake. For abbreviations see the text.

As already pointed out, large differences occurred between (theoretical) optimal and measured fluxes for transketolase (ppp4) and the net reaction of PykA/PykF and Pps (emp5). The flux differences coincided with low (insufficient) L-Phe/glucose yields, which even deteriorated during the course of observation. The findings are in agreement with previous studies of Draths *et al.* [DPC$^+$92], and Li *et al.* [LMD$^+$99] thus emphasizing the necessity of *tktA* over-expression. The observations also support the results of Patnaik and Liao [PL94], Patnaik *et al.* [PSL95], Berry [Ber96], Gosset [GYXB96], Yi *et al.* [YLDF02] and Chandram *et al.* [CYD$^+$03], who stressed the need for a common over-expression of *tktA* and *pps* to achieve an increased flux into aromatic amino acid synthesis.

3.5.6   Flux Sensitivity Analysis

So far, the combined approach of MFA and linear programming allowed to identify discrepancies between measured fluxes and the optimal flux distribution for L-Phe production. However, these differences are difficult to qualify because information about flux sensitivities is missing. Therefore, measured fluxes of the MFA were subsequently used as input values for an additional linear programming approach. The basic idea was to derive
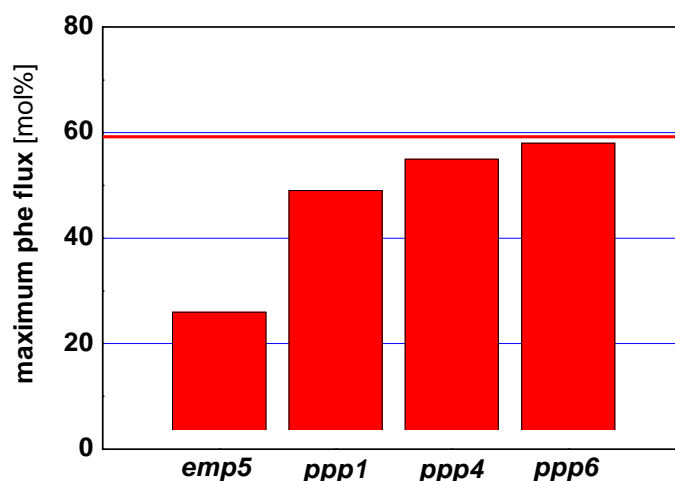
FIGURE 3.29. Ranked list of maximum achievable L-Phe formation rates ($mol\%$) based on the assumption that the measured fluxes of emp5, ppp1, ppp4 or ppp6 (of phase 1) could not be exceeded, glucose uptake kept constant and the rest of the metabolic network could reroute carbon fluxes such that a maximum L-Phe formation is achieved. The upper maximum L-Phe formation (59.7 $mol\%$) is given by a straight line and was calculated by linear programming as illustrated in the text.

flux sensitivity data which were not as dependent on the choice of fixed fluxes as in the classical approach of Delgado and Liao [DL97]. Based on the experimentally determined metabolic fluxes the glucose uptake was set constant together with one of the interesting fluxes such as emp5, ppp1, ppp4 or ppp6. Using the constraint of L-Phe flux maximization the rest of the metabolic network was free to rearrange. Basically, the resulting flux patterns thus represent optimum L-Phe formation rates under the constraint that each of the fixed flux emp5, ppp1, ppp4 or ppp6 could not be amplified because of biochemical limitations or gene regulations. High L-Phe formation rates (close to the theoretical optimum of 59.7 $mol\%$) thus indicate that the corresponding fixed flux does not significantly hamper the reachable, optimal L-Phe yield. On the other hand, the lowest achievable L-Phe yield obviously corresponds to the limiting affect of the fixed flux thus revealing it as a promising *metabolic engineering* target.

Figure 3.29 presents the results of the flux sensitivity analysis using the MFA fluxes of phase 1 (the 'best' production phase) as a reference. It is clearly identifiable that emp5, coding for the net reaction of PykA/PykF and Pps, represents the reaction that mostly limited the maximum achiev-

able L-Phe formation. In the case of transaldolase (ppp6), its low limiting impact on the L-Phe formation becomes obvious, because the theoretical optimum of 59.7 mol % is almost achievable with a fixed ppp6 flux. Fixing the transketolase reaction, encoded by ppp4, still 49 mol % L-Phe flux are possible. Hence, emp5 should be the preferred *metabolic engineering* target to improve the existing L-Phe production strain.

3.5.7   Working Hypothesis

However, the identification of emp5 as a promising *metabolic engineering* target as such is not sufficiently unequivocal, because emp5 codes for the net flux of PykA/PykF and the conversely directed Pps reaction. Furthermore, the question should be addressed, why emp5 even deteriorated showing increasing net fluxes during the observed phases (see Figures 3.24, 3.25 and 3.26). Therefore, a working hypothesis is derived taking into account that increasing net fluxes indicate rising PykA/PykF rates together with decreasing Pps rates.

In the case of PykA/PykF, FBP (and to a minor extent G6P, Ri5P) activate the pyruvate kinase activity [VMP$^+$96]. Provided that increasing glycolytic fluxes (see absolute flux values in Table 3.6) also entailed increasing FBP pool sizes because of underlying Michaelis-Menten type reaction kinetics, rising pyruvate kinase activity would be the consequence. Furthermore, it is known that PEP synthase activity can be inhibited by TCA metabolites such as 2-oxoglutarate (AKG) and oxaloacetate (OAA; [CK74], [CA73]), both important precursors for amino acid synthesis which - most noticeable - was not active in the non-growing *E. coli* cells of this study. Regarding the increased, absolute TCA fluxes and following the same argumentation as above, a diminished Pps activity owing to accumulating AKG and OAA pools could be assumed.

Hence, deteriorating L-Phe/glucose levels could be caused by decreasing Pps activity together with increasing PykA/PykF activity, both regulated on a biochemical level by enzyme inhibition and/or activation respectively. *pps* over-expression could thus be an appropriate means to compensate a potential Pps inhibition and to redirect the PykA/PykF flux. However, total flux redirection from PYR to PEP (as proposed by linear optimization) could only be achieved if *pykA* and *pykF* would be completely inactivated in resting cells. So, the serial MFA using the Sensor reactor enabled the identification of two *metabolic engineering* targets which are promising targets for further strain optimization to maximize L-Phe production.

3.6   Sensor Reactor: Conclusions and Outlook

- **Sensor reactor development:** A 1-*L* Sensor reactor was developed
  to monitor temporary changing intracellular carbon flux distributions
  in industry-like production processes by serial ^{13}C based metabolic
  flux analysis (MFA). The apparatus consisted of automatic devices for
  inoculation, ^{13}C pulsing and (optionally) rapid sampling. Realizing
  master/slave controlling mode, i.e. on-line measured state variables
  of the production process such as *pH*, temperature, dissolved oxy-
  gen concentration etc. were used as setpoints for the Sensor reactor,
  very similar fermentations could be performed in the Sensor reactor
  compared to the (300-*L*) production process. Exemplarily studying
  lysine production with *C. glutamicum* MH20-22B revealed high re-
  gression coefficients and high coefficients of determinations in a set
  of three subsequent fermentations (each lasting for 2 to 3 hours) thus
  recommending the Sensor reactor for further ^{13}C labeling studies.

- **Serial ^{13}C based flux analysis of lysine producing *C. glutam-
  icum* MH20-22B:** ^{13}C labeling experiments with lysine producing
  C. glutamicum MH20-22B illustrated that the Sensor reactor can suc-
  cessfully be applied to monitor the exponential growth phase as well
  as the (leucine) limited lysine production period with non-growing
  cells. Because of the essential importance of the anaplerosis for lysine
  production in *C. glutamicum*, in total five flux carbon maps based
  on $\left[U -^{13}C\right]$ glucose labeling were calculated which - for the first
  time - give overview of the temporary changing intracellular flux
  patterns during industry-like production conditions. As a result, the
  correlation between decreasing decarboxylating (PEP carboxykinase)
  fluxes and increasing lysine production rates as well as the need to
  fortify PEP carboxylase and/or pyruvate carboxylase activity were
  identified as promising *metabolic engineering* targets in *C. glutam-
  icum* MH20-22B.

- **Serial ^{13}C based flux analysis of L-Phe producing *E. coli*
  4pF81:** The application of the Sensor reactor approach for the analy-
  sis of L-phenylalanine production with non-growing (tyrosine limited)
  E. coli 4pF81 allowed the serial flux mapping of three subsequent
  phases. As a major result, the need to overexpress *pps* (coding for
  PEP synthase) was found owing to comparative studies with respect
  to linear programming results together with flux sensitivity estima-
  tions. Based on the observed changes in the series of three subsequent
  flux maps the working hypothesis was derived that intracellular pool
  accumulations of oxaloacetate (OAA) and 2-oxoglutarate (AKG) are
  presumably the reasons for the deteriorating L-Phe formation rates.

Summarizing, the aforementioned results show that the novel Sensor reactor can be successfully applied for the serial flux mapping of industry-like production processes thus providing the experimental data for detailed MFA to identify promising *metabolic engineering* targets for further strain improvement. Different biological systems such as *C. glutamicum* and *E. coli* were studied in batch and fed-batch mode focusing on growing and non-growing cells at the same time applying different labeling analysis methods (biomass hydrolyzate, metabolome labeling patterns and labeling information of the culture supernatant) for different products (lysine and phenylalanine). Consequently, the Sensor reactor should be usable for a broad range of different applications as it is currently planned in cooperation with different industrial partners.

However, the Sensor reactor results obtained so far make also evident that the technology is not yet finally developed and that there are still promising challenges left to be fulfilled:

- **Combination of pool and flux information:** The analysis of lysine producing *C. glutamicum* and the study of L-Phe production in *E. coli* revealed significant temporary changes of intracellular carbon flux distributions although the external culture conditions remained unchanged during the observation period. Regarding the working hypothesis already presented in the preceding section, one could assume that intracellular pool accumulations may be the major reason for increasing or decreasing fluxes. Hence, the knowledge of these potentially existing biochemical effects is without doubt of outstanding importance for further *metabolic engineering*. Therefore, future Sensor reactor studies should aim at combining MFA with e.g. *metabolic profiling* to elucidate the underlying mechanisms.

- **Exploiting ^{13}C labeling information of the metabolome:** Own studies (data not shown) as well as published results of other groups [Win02] have already shown that low concentrated ^{13}C labeling information in the metabolome originating from ^{13}C labeled glucose is accessible for instance with the aid of novel, sophisticated LC-MS/MS (or HPAE-MS/MS) approaches or with the aid of GC/MS analysis [WHH02]. The quality of today's commercial LC-MS/MS devices offers a new access not only to the quantification of intracellular metabolite concentrations but also to the identification of ^{13}C labeling patterns in the metabolome! This is especially remarkable with respect to the significant benefits that follow for serial metabolic flux analysis - for instance using the Sensor reactor:

  1. **Focusing on ^{13}C labels in the metabolome significantly reduces the necessary labeling period**. As shown in section 3.4.2, typical labeling equilibration timespans of about 10

minutes can be assumed for metabolism intermediates, which is significantly shorter than the several hours of labeling needed for instance to equilibrate the labeling patterns in the proteinogenic amino acids. Besides, Christensen *et al.* [CGN02] already argued that the relatively slow protein synthesis significantly buffers the amino acid pool exchange, thus causing equilibration delays which are consequently mirrored by metabolic flux analysis and not the carbon metabolism, which is the original target. Furthermore, the focus on ^{13}C labels of the metabolome would simplify further labeling data handling because a data correction - as performed in section 3.5 - is no longer necessary. Hence, using ^{13}C labeling information of the metabolome instead of the 'classical' sources used so far, would drastically reduce the labeling period thus allowing the Sensor reactor to be inoculated, labeled and analyzed more frequently.

2. **The analysis of ^{13}C labels in the metabolome demands for rapid sampling.** If ^{13}C labeling patterns in the metabolome can be identified by new analytical approaches, the sampling out of the Sensor reactor must be adapted as well. In analogy to the results of the preceding chapter, samples must be taken rapidly out of the Sensor reactor while the metabolism should be inactivated immediately to prevent any unwanted metabolic conversion, i.e. changes of the metabolic labeling pattern. The necessity of rapid sampling also demands for a fast mixing of the ^{13}C labeled substrate, which was already subjected during the past studies. Currently, an appropriate rapid sampling device is developed.

3. **^{13}C metabolome information demands for novel MFA software tools.** Obviously, the ^{13}C labeling information originating from mass spectrometry measurements, differs from the labeling results obtained for example from 'classical' NMR measurements. Instead of measuring labels at distinct carbon-atom positions applying NMR, MS methods can only give 'integral' answers with respect to the increased molecular mass in molecules or fractions thereof due to labeling. Hence, the existing software tools must be adapted to be able to use this information. More strikingly, another, fundamental aspect demands for the development of novel mathematical approaches - namely the use of temporary changing ^{13}C labeling patterns for MFA. Basically, a new mathematical approach must be developed enabling the instationary MFA instead of the state-of-the-art (pseudo-) steady state MFA: The analysis of temporary changing labeling patterns is much more ambitious than the 'classical' MFA approach assuming pseudo-steady state conditions. Prospective ^{13}C la-

beling data sets will include temporary changes of the labeling patterns in each pool. As a consequence a set of instationary differential equations has to be solved instead of the (pseudo-) stationary analysis accomplished so far. Hence, novel mathematical tools must be developed, which is already in progress [WN03], in cooperation with the author's research group.

Hence, future Sensor reactor technology will (most presumably) aim at monitoring processes with increased flux map frequency benefitting from ^{13}C labeling information which originates from the metabolome and which is provided by LC-MS/MS measurements and used by novel mathematical tools for serial MFA.

4

L-Phenylalanine Bioprocess Development

4.1 Market Driven Motivation for L-Phenylalanine Production

Currently, the overall annual consumption of amino acids is estimated to be over 2 million tons [Her03]. The 'big three' amino acids L-glutamate, L-lysine·HCL and D,L-methionine which count for approximately 95% of the total market ([Mül01], [DHK$^+$02]) are almost entirely produced using coryneform bacteria in bioreactors up to 500 m^3 scale. These amino acids are commonly used as flavour enhancers (such as MSG: mono-sodium glutamate) or feed additives to increase the nutritive value [DHK$^+$02].

Compared to this huge market which is dominated by companies such as Ajinomoto, ADM (Archer Daniels Midland), BASF AG, Cheil-Jedang, Degussa AG (via Midwest Lysine), Kyowa-Hakko and Miwon, the production of other amino acids with a significantly smaller market segment seems to be not as attractive - at first sight. However, actual market analysis show that almost all amino acid markets are expected to grow 10% per year and more [Her03] thus offering promising perspectives in general.

This holds especially true for the production of aromatic amino acids as fine chemicals. Already in 1994, Frost and Lievense [FL94] emphasized the possibility to produce aromatics for industrial purposes not by exploiting fossil feedstocks for the preparation of precursors such as benzene, toluene and xylene but by making intensive use of biological (microbial) systems

instead. This route, converting D-glucose via the microbial aromatic amino acid pathway into the desired aromatic products or synthesis precursors thereof, offers environmental benefits at the same time liberating the chemical industry from imported petroleum.

Schmid *et al.* [SDH$^+$01] encouraged this general idea by presenting a couple of successful biocatalytic examples which were already realized in research laboratories as well as in industrial companies such as BASF AG, DSM and Lonza. Examples are the production of enantiopure alcohols, (non-proteinogenic) amino acids, penicillins and heterocyclic compounds which were produced by whole cells or isolated enzymes. Without doubt, also the aromatic amino acids L-tyrosine, L-tryptophane and L-phenylalanine belong to this 'promising' fine chemical group As pointed out by Bongaerts *et al.* [BKM$^+$01], the 1997-worldwide market for tyrosine, tryptophane and phenylalanine was about 150, 500 - 600 and 11,000 - 12,000 tons per year, respectively. The corresponding prices for chemical/pharma product quality were about 51/124.5, 22/35 and 19/34.5 US\$/kg for the aforementioned aromatic amino acids.

It is noteworthy that not only the final products of the aromatic amino acid (AAA) pathway are of (commercial) interest because of their importance as feed/food additives, precursors for drug synthesis or drugs itself. Also the AAA pathway intermediates were chosen as promising targets for bioprocess developments. Examples are published by the 'Frost' group for the production of pathway intermediates such as 3-dehydroshikimic acid [LMD$^+$99] and shikimic acid [CYD$^+$03] but also from others [KBR$^+$03] focusing on chorismate derivatives such as 2,3 cyclohexane trans diole [FLE$^+$03] or 3,4 cyclohexane trans diole [FSM03]. The latter will be presented in section 4.6.

As already shown, L-phenylalanine represents the largest economical market of the three aromatic amino acids. Today, worldwide L-Phe production is estimated to be 14,000 tons per year [Bud01] and is expected to increase to sales of US\$ 850 million in 2004 [Mül01]. This high demand is not caused by L-Phe's importance for parenteral nutrition [DHK$^+$02]. The majority of phenylalanine is used to produce a substance that goes back to the 'accidental' discovery of the chemist J.M. Schlatter in 1965 - namely the identification of N-L-α-aspartyl-L-phenylalanine 1-methyl ester better known as aspartame [Gri98]. The low calorie sweetener aspartame is the condensation product of L-phenylalanine with L-aspartic acid and is about 200 times sweeter than sucrose (glucose-α-1,2-fructose) [Cou02]. In 1981 aspartame became the first low-calorie sweetener approved by the American Food and Drug Administration (FDA) and it is produced worldwide by companies such as Ajinomoto, The NutraSweet$^®$ Company and The Holland Sweetener Company (HSC, a joint venture of DSM with Tosoh).

It is noteworthy that for each molecule of aspartame one molecule of L-phenylalanine is needed.

The kiloton-scale process of HSC uses a proteolytic enzyme, called thermolysin, to catalyze the dipeptide formation from N-protected L-aspartic acid and the racemic mixture of D/L-phenylalanine methyl ester.[SDH$^+$01]. Thanks to the high selectivity of thermolysin, the enzyme predominantly couples L-phenylalanine methyl ester to the α-carboxyl group of Z-Asp for Z-aspartame production and ignores the other three possible side-products. While the Z-group is removed by catalytic hydrogenation, the remaining D-phenylalanine methyl ester has to be racemized and recycled to get access to an new L-enantiomer fraction.

Hence, motivated by the idea to simplify the existing HSC process by preparing only the L-enantiomer of phenylalanine for the thermolysin process, the cooperation with the DSM company was started in mid 1997 to study to what extend purified L-phenylalanine can be produced with appropriate *E. coli* strains for further large-scale aspartame production.

4.2   Access to L-Phenylalanine

4.2.1   L-Phenylalanine Production

The access to phenylalanine (for chemical properties see Table 2.5 in subsection 2.6.1) which was first discovered in 1881 in plants by Schulze and Barbieri, is manifold. As almost all amino acids, L-Phe could be extracted from natural raw materials after the containing proteins were hydrolyzed and further processed via technical chromatography steps (as for instance performed by the AMINO GmbH, Frellstedt, Germany). Another, classical approach, which could generally be applied for the production of α-amino acids, is the well-known Strecker-synthesis. Accordingly, aldehydes are converted to α-amino nitrils in the presence of sodium cyanide (NACN) and ammonium chloride (NH_4Cl) and further hydrolyzed to the racemic mixture of the respective amino acids. Other possibilities for phenylalanine synthesis are the carboxylation of benzyl chloride leading to N-acetyl D,L-phenylalanine or the condensation of benzaldehyde with hydantoin to D,L-phenylalanine.

However, most of these routes lead to a racemic mixture of D,L-phenylalanine which is disadvantageous with respect to the aforementioned aim (see preceding section). Hence biotechnological approaches should be favored which can deliver the pure L-entantiomer.

One biotechnological route to L-phenylalanine considers the use of **isolated (purified) enzymes**. A large-scale production example is the resolution of N-acetyl-D,L-phenylalanine by carrier-fixed microbial amino acylase (N-Acyl-L-amino acid-amino hydrolase, EC 3.5.1.14) ([DHK+02], [Roe03]). Although pharmaceutical-grade L-Phe was produced via the enzymatic cleaving of the N-acetyl group form the L-enatiomer, the process was hampered by the necessary racemization and recycling of the remaining D-enantiomer [1]. Alternative approaches were presented by Ziehr *et al.* [ZKS+87] considering the continuous L-Phe production by transamination based on *Pseudomonas putida* enzymes and by Hummel *et al.* ([HSWK86], [HSS+87]) using enzymes from *Brevibacterium sp.* and *Rhodococcus sp.* for reductive amination of the substrate phenylpyruvate. The phenylalanine dehydrogenase from *Spoosarcina ureae* for L-Phe production was applied by Asano *et al.* [AN87]. Rozzel presented an approach based on the transaminase reaction using α-keto acid and aspartic acid as substrates for L-amino acid production with oxaloacetate (OAA) as by-product [Roz85], also in a coupled multi-step approach [Roz89].

---

[1] The separation of the L-amino acids from the mixture was achieved by making use of its low solubility compared to the N-acetyl-D,L-substrate. The industrial production of L-amino acids belongs to the first applications of carrier-fixed enzymes ([Roe03], [LSW00]).

Additionally, **whole cells** were used as 'enzyme bags' for **biotransformation** approaches. Typically these cells were immobilized and/or permeabilized to ensure a sufficient catalyst availability [BD90b]. An industrial process example, which was realized during the first aspartame production campaign [DHK$^+$02], is the stereo- and enantioselective addition of ammonia to *trans*-cinnamic acid, which was catalyzed by L-Phe ammonia lyase (PAL, EC 4.3.1.5) containing *Rhodotorula rubra* strains [McG86]. Up to 50 $g \cdot L^{-1}$ were achieved in an continuous process [ECPM87]. Alternative approaches were published by Nakamichi *et al.* [NNNT89] focusing on the (trans-) amination of phenylpyruvate with *Paracoccus denitrificans,* with *E. coli* cells ([CWO$^+$86], [TDN$^+$87], [WC88], [BD90b]) or with (partially growing) *C. glutamicum* cells ([BC85],[EBG$^+$87]). Recently Xu *et al.* [XWZ$^+$03] presented an approach, which is similar to the previous findings of Chao *et al.*([CLaJC99], [CLL00]), using a coupled two-strain *E. coli* system consisting of a transaminase and an aspartase overproducing strain. By addition of ammonium fumarate and phenylpyruvic acid L-Phe was produced. [2]

However, Drauz *et al.* [DHK$^+$02] emphasized that the '*fermentation processes based on glucose-consuming L-phenylalanine overproducing mutants of E. coli and coryneform strains turned out to be more economical*' (compared to the alteratives routes of L-Phe production). Therefore, a number of different processes have been presented, which mainly focused on *E. coli, C. glutamicum* and *Brevibacterium strains* [BD90b]. However, early process approaches using *Bacillus subtilis* [MJ74] were known as well.

For instance, *Brevibacterium species* such as *B. flavum* [SSK88] and *B. lactofermentum* [TKM$^+$87] were applied for L-Phe production after their selection succeeded based on classical screening methods looking for feedback deregulated key enzymes. For instance, Goto *et al.* [GIS$^+$81] achieved about 25 $g \cdot L^{-1}$ with a tyrosine and methionine requiring mutant of *Brevibacterium lactofermentum.*

In a similar way, the first coryneform L-Phe production strains were selected. Additionally, *metabolic engineering* methods were applied to *C. glutamicum* strains by overexpressing plasmid-encoded (heterologous) chorismate mutase / prephenate dehydratase and/or feedback resistant DAHP synthase variants ([OKOF85], [IK92], [IOK93]) thus achieving about 26 $g \cdot L^{-1}$ L-Phe titers. In the following, appropriate process engineering methods were studied for L-Phe producing *C. glutamicum* by applying an oxys-

---

[2] Additionally, the L-amino acid production from hydantoins should be mentioned. For instance, three enzymes, namely L-hydantoinase, L-N–carbamoylase and the hydantoin racemase, were overexpressed in *E. coli* for L-tryptophane production [WWS$^+$01].

tat fed–batch process [WYSL94]. Shu and Liao [SL02] achieved 23.2 $g \cdot L^{-1}$ with a space-time yield of 0.37 $g_{L-Phe} \cdot (Lh)^{-1}$.

So far, L-Phe process development has been dominated by the application of different, metabolically engineered *E. coli* strains, which is also documented by the patent list ([LWPL91],[KRL$^+$94], [KRL$^+$95], [SSS$^+$98a], [SSS$^+$98b]) For the sake of brevity, only a selection of the different approaches will be presented in the following:

While early process engineering studies for L-Phe production were already performed in 1979 by Akashi *et al.* [ASH79] and in 1982 by Choi and Tribe [CT82], this topic gained increasing interest in the late 80s and onwards. Based on the *E. coli* K12 mutant of Choi and Tribe[3], Park and Rogers ([PR86], [PR]) achieved L-Phe titers of 22.4 $g \cdot L^{-1}$, revealing a space-time yield of 0.72 $g_{L-Phe} \cdot (Lh)^{-1}$. Hwang *et al.* [HGC$^+$85] presented their approach using an auxotrophic *E. coli* strain. Förberg *et al.* ([FH87], [FH88], [FEH88]) studied the L-Phe production with recombinant *E. coli* possessing a (plasmid encoded) feedback-resistant chorismate mutase / prephenate dehydrogenase ($pheA^{fbr}$) together with the wild-type $aroF^{wt}$ in aromatic amino acid auxotrophic strains. Tyrosine and glucose feeding was empirically adjusted (not-controlled) leading to inhibiting Tyr levels during the growth phase which consequently repressed L-Phe production. L-Phe production was thus achieved only with non-growing cells leading to the maximum product/substrate yield of 0.2 $mol \cdot mol^{-1}$ and low titers at about 3 - 4 $g \cdot L^{-1}$.

A temperature-controllable expression vector (optimal temperature 38.5 $°C$) was used by Sugimoto *et al.* [SYK$^+$87] carrying the genes for feedback resistant $aroF^{fbr}$ (coding for DAHP synthase, formerly TYR sensitive) and $pheA^{fbr}$ (coding for L-Phe feedback-resistant chorismate mutase / prephenate dehydratase). By optimizing the temperature profile and by employing a temperature-distributed dual bioreactor system 28.5 $g_{L-Phe} \cdot L^{-1}$ with a space-time yield of 0.52 $g_{L-Phe} \cdot (Lh)^{-1}$ could be achieved [SKK$^+$90]. Based on this strain, further process developments were presented by Konstantinov *et al.* ([KNY90],[KY90],[KKSY90], [KYNS91]) introducing an OUR (oxygen uptake rate)-based glucose-limiting feeding strategy to prevent unwanted acetic acid formation. In total 46 $g_{L-Phe} \cdot L^{-1}$ could be produced in 48 hours. The integral space-time yield was about 0.85 $g_{L-Phe} \cdot (Lh)^{-1}$. Later on, Takagi *et al.* [TNOY96] presented a further approach with the same strain taking into account the previously published results of Konstantinov *et al.* An improved on-line estimation method was applied for the maximum glucose uptake rate (so-called MGUR) to keep the glucose

---

[3]This mutant possessed feedback resistant AroF, AroG and PheA and was $aroH^-$.

level below 0.1 $g \cdot L^{-1}$. Additionally, tyrosine was fed to fulfill maintenance demands[4].

Independently, Weikert *et al.* [WSB98] selected the strain *E. coli* CWML2 which exhibited shorter lag phases, decreased acetate production and higher specific growth rates (compared to the wild-type strain) and introduced $pheA^{fbr}$ and $aroF^{fbr}$ into this strain. Maximum L-Phe/glucose yields of 0.057 $g \cdot g^{-1}$ and titers up to 10 $g \cdot L^{-1}$ were achieved.

In 1998, Grinter [Gri98] presented some of the achievements of the NutraSweet Company with respect to their 15-years lasting (successful) efforts to establish an L-Phe production process. He listed a number of *metabolic engineering* targets which were realized in the current *E. coli* L-Phe producer. Without giving details, for instance the use of $pheA^{fbr}$, the partial inactivation of pyruvate kinase activity, the modification of glucose uptake and hints for the existence of an active L-Phe export system were given. However, the latter is not supported by other findings (see subsection 2.6.1). Titers > 30 $g \cdot L^{-1}$ are achieved in this process. Further details are also given by Fotheringham *et al.* ([FTH94], [Fot98]).

Hitherto, the highest L-Phe titers of about 50 $g \cdot L^{-1}$ measured after 36 hours process time were published by Backman *et al.* [BOM+90] concomitantly achieving an L-Phe/glucose yield of 0.23 $g \cdot g^{-1}$ with 23 $g \cdot L^{-1}$ cell-dry weight concentration. The authors engineered an *E. coli* strain possessing $pheA^{fbr}$ and $aroF^{fbr}$ and outlined that '...*contrary to conventional wisdom, the tyrosine-specific DAHP synthase determined by aroF is in fact inhibited by phenylalanine...*'. Therefore the authors '...*adopted an historically proven approach and isolated feedback-inhibition-insensitive mutations in the gene(s) for DAHP synthase by means of resistance to toxic amino acid analogues...*' and thus selected an appropriate *E. coli* L-Phe producer. Presumably, because of this strategy, such high L-Phe titers were achieved [5].

4.2.2   Metabolic Engineering Targets

If the aim is followed to construct the optimal L-Phe producing *E. coli* strain, the following *metabolic engineering* targets should be focused according to Berry [Ber96], Grinter [Gri98] and Bongaerts *et al.* [BKM+01]:

---

[4]Unfortunately no absolute product titers were given in this publication.

[5]This statement is supported by previous findings of other groups such as Gil *et al.* [GKBL85], Park and Rogers [PR89] and Konstantinov *et al.* [KYNS91], who also assumed a product inhibition hampering the L-Phe synthesis.

Optimization of E4P supply

As shown in subsection 2.6.1, erythrose-4-phosphate (E4P) represents one of the two precursors of the AAA pathway, which obviously necessitates its optimal supply in L-Phe producing strains. Because E4P is synthesized via transaldolase and transketolase reactions in the penthose-phosphate pathway, Draths and Frost [DF90] and Draths *et al.* [DPC+92] identified the beneficial effect of transketolase overexpression for DAHP production. Later on, this was reconfirmed by *tktA* overexpression in *E. coli* possessing a non-PTS uptake systems [FXB+96] and by a comparative study of Gosset *et al.* [GYXB96] considering pyruvate kinase and/or PTS mutants with/without overexpressed *tktA*. It was also found in L-tryptophane producing *E. coli* [KTHN+00]. However, using xylose as substrate, this positive effect was not observed [PSL95]. Regarding transaldolase (encoded by *talB*), similar results were uncovered because *talB* overexpression resulted in increasing DAH(P) [JLLL97] and L-Phe [SSS+98a] formation. Additionally, Lu and Liao [JLLL97] emphasized that *talB* overexpression showed no effect in strains already possessing overexpressed *tktA*, thus giving the latter a higher priority for *metabolic engineering*. Also Frost [Fro92] disclosed the necessary expression of transketolase to increase the flux into the AAA pathway.

Optimization of PEP supply

To produce one molecule of L-Phe, two molecules of PEP are needed (see subsection 2.6.1). This is remarkable, because only 3.3% of the flux via the phosphoenolpyruvate node is directed into the AAA pathway in wildtype *E. coli* ([Hol86], [VMP+96]). Hence, the PEP availability should be optimized to prevent a PEP-limited L-Phe formation. This can be achieved by either reducing the PEP consuming reactions - (i) phosphoenolpyruvate carboxylase (encoded by *ppc*), (ii) pyruvate kinase (encoded by *pykA* and *pykF*) and (iii) the PTS demand for glucose uptake - or by enhancing the refilling reactions (iv) phosphoenolpyruvate synthase (encoded by *pps*) and (v) phosphoenolpyruvate carboxykinase (encoded by *pck*) [6].

ad (i): Miller *et al.* [MBOH87] studied the effects in phosphoenolpyruvate carboxylase deficient mutants observing an increased L-Phe production which coincided with unwanted by-product formation of pyruvate and acetic acid. These results are in accordance with the findings of Gokarn et al. [GEA00] who observed an increased succinate production in *ppc*- mutants under anaerobic conditions. Interestingly, these authors inserted a

---

[6]For visualisation the reader may consider Figure 3.2 depicting the anaplerosis of *Corynebacterium glutamicum*. However it is noteworthy that anaplerotic fluxes in *E. coli* are limited to the PEP $\leftrightharpoons$ OAA conversion thus lacking of the PYR $\leftrightharpoons$ OAA interactions as existing in *C. glutamicum*.

pyruvate carboxylase of *Rhizobium etli* in *ppc-* mutants thus revealing its promising potential to compensate the missing anaplerotic flux.

ad (ii): Gosset *et al.* [GYXB96] showed that the total inactivation of *pykA* and *pykF,* which resulted in the complete loss of *E. coli's* ability to directly convert PEP into pyruvate, increased the carbon flux into AAA synthesis by the factor 3.4. However, this beneficial effect was not found in strains that already possess an *tktA* overexpression thus stressing the need to fortify TktA activity in the production strains. Additionally, Emmerling *et al.* [EDP$^+$02] investigated the flux redistribution in pyruvate kinase knockout strains, which were not optimized for L-Phe production. They identified a general local flux rerouting via the combined reactions of phosphoenolpyruvate (PEP) carboxylase and malic enzyme.

ad iii): Flores *et al.* [FXB$^+$96] succeeded in selecting a PTS$^-$ *E. coli* strain whose ability to grow on glucose was attributed to an amplified galactose permease activity realized with the aid of classical mutagenesis. The flux into the AAA pathway was found to be increased in the non-PTS strain and it could even be fortified by the overexpression of *aroG^{fbr}* and *tktA*. Based on this strain, an *aroB$^-$* mutant was constructed which accumulated DAH(P) in the culture supernatant [BBG01]. From the excretion rates it was concluded that carbon flux redirection was such successful that 83% of the theoretical optimum of 0.855 $mol \cdot mol^{-1}$ was achieved. Subsequent metabolic flux analysis [FGF$^+$02] revealed that also the glycolytic fluxes were increased in these strains compared to the wild-type *E. coli* and that an additional glucose kinase (*glk*) gene is required in the chromosome to ensure rapid glucose uptake. While no flux was observed via phosphoenolpyruvate carboxykinase in the non-PTS strains, the malic enzyme was active instead, both in contrast to the findings regarding the wild-type *E. coli*. The PTS$^-$ mutant selected by Flores *et al.* [FXB$^+$96] was also applied in the comparative study of Gosset *et al.* [GYXB96] showing that a 19.9-fold increase of carbon flux into DAH(P) synthesis could be achieved using the PTS$^-$ strain with overexpressed *tktA* and inactivated *pykA* and *pykF*.

Rather conflicting observations were made by Chen *et al.* [CHY$^+$97] who found that a non-PTS strain - which managed to consume glucose via the proton-galactose symport system - revealed less phenylalanine production, attained lower biomass concentration and consumed more O$_2$. These surprising results coincided with significantly changed metabolic patterns in aerobic and anaerobic cultivations [CYPB97]. Lower levels of total sugar phosphates, NAD(H), nucleoside triphosphates and PEP were observed, while nucleoside diphosphate levels were increased.

Frost and Draths [FD95] also addressed the possibility to replace the wild-type PTS by an heterologous glucose uptake system. The combina-

tion glucose facilitator (encoded by *glf*) and glucokinase (*glk*) - both originating from *Zymomonas mobilis* - was successfully applied by Snoep *et al.* [SAY$^+$94] and Weisser *et al.* [WKSS95]. The same genes were amplified in PTS-negative *E. coli* strains leading to increased DAH(P) secretion [Krä00] in *aroB$^-$* mutants and elevated L-Phe production [SSS$^+$98b]. Additionally, *gdh* (coding for glucose dehydrogenase from *Bacillus megaterium*) together with *gntk* (coding for gluconate kinase) were overexpressed in such strains to co-increase the E4P availability thus leading to an enhanced L-Phe production as well [KKSS99]. Recently Chandram *et al.*[CYD$^+$03] presented the results of an *E. coli* shikimic acid producer achieving a maximum product titer of 87 $g \cdot L^{-1}$ with a PTS$^-$ mutant which expressed *Z. mobilis glf* and *glk* together with *aroF^{fbr}* and *tktA*. Currently Yi *et al.* [YDLF03] have studied the effect of different glucose uptake systems, namely native PTS, the *glf/glk* encoded approach using the *Zymomonas mobilis* genes and the recruitment of native *E. coli galP*-encoded galactose permease. In general, the PTS- mutants are favored for AAA intermediate production, however '...*the impact of a given strategy for increasing phosphoenolpyruvate availability differs as a function whether 3-dehydroshikimic acid or shikimic acid is targeted for synthesis'*.

ad iv) Regarding the PEP refilling reactions, the overexpression of *pps* (coding for phosphoenolpyruvate synthase) was usually the preferred target to achieve an increased PEP supply. Patnaik *et al.* [PSL95], estimated that the theoretical DAH(P)/glucose yield of 43 % $mol \cdot mol^{-1}$ could be increased to 86 % $mol \cdot mol^{-1}$ in the case of a complete pyruvate recycling - for instance by overexpressing *pps*. In a series of experiments the authors overexpressed *aroG*, *tktA* and *pps* in *aroB$^-$ E. coli* mutants [PL94]. Based on the DAH(P) accumulation they concluded that *pps* overexpression must be accompanied by *tktA* overexpression thus suggesting that E4P supply is the dominant problem in the *E. coli* strain investigated[7].

Later on, Yi et al. [YLDF02] emphasized the need to overexpress *pps* properly meaning that '... *an optimal expression level of phosphoenolpyruvate synthase was identified which did not correspond to the highest expression levels of this enzyme, where the total yield of 3-dehydoshikimic acid...synthesized from glucose was 51 % $mol \cdot mol$'*. According to the authors this is attributed to the necessarily increased glucose consumption that causes increased and unwanted by-product formation thus reducing the optimum expression level of *pps*.

ad v) The overexpression of *pck* (coding for phosphoenolpyruvate carboxykinase) was studied in 3-dehydroshikimate producing *E. coli* which

---

[7]It is noteworthy that our metabolic flux analysis results presented in section 3.5 clearly stress the necessity to overexpress *pps* in our L-Phe production strains.

were supplied with succinate in addition to the main carbon source glucose [LF99]. It was shown that 57 $g \cdot L^{-1}$ of DHS could be produced when glucose and succinate were used. In the case of glucose as the sole carbon source only 44 $g \cdot L^{-1}$ were achieved.

Alleviating Flux Control in the Aromatic Amino Acid Pathway

As already mentioned in the subsection 2.6.1 the AAA pathway is subject to transcriptional and allosteric control. While transcriptional control can be circumvented by gene insertion behind promoters that are not regulated by TrpR and TyrR or by the deletion/inactivation of the respective regulators [Ber96], allosteric control must be addressed specifically for each feedback inhibited enzyme. Examples for the structure of feedback resistant enzymes such as AroF^{fbr}, AroG^{fbr} and PheA^{fbr} are given by Bongaerts *et al.* [BKM$^+$01].

Additionally, the results of the 'Frost' group exemplarily demonstrate that flux control in the AAA pathway can be alleviated step-by-step in order to achieve an 'unlimited' carbon flux from DAH(P) to the AAA intermediate of interest. After the limiting role of transketolase (encoded by *tktA*) was shown by DAH(P) accumulation experiments using *aroB$^-$* mutants of *E. coli* with *tktA* and *aroG^{fbr}* overexpression [DPC$^+$92], the role of *aroB* (coding for 3-dehydroquinate synthase), *aroL* (coding for shikimate kinase II) and *aroA* (coding for EPSP synthase) was analyzed. Using ^{1}H-NMR analysis of the culture supernatant these enzymes were identified as potential *metabolic engineering* targets of the AAA pathway [DF93][8]. In the following [SDF96], an *E. coli* producer was presented that possessed a mutation in the *tyrR* locus thus preventing a potential trancriptional repression of *aroL*. Additionally *aroA* (coding for EPSP synthase), *aroC* (coding for chorismate synthase) and *aroB* (coding for 3-dehydroquinate synthase) were inserted in the chromosome using a multigene cassette. As a result, the L-Phe/glucose yield was doubled. Later on, 69 $g \cdot L^{-1}$ of 3-dehydoshikimic acid were achieved [LMD$^+$99] using *E. coli* with *aroB* and *aroG^{fbr}* overexpressed genes and 57 $g \cdot L^{-1}$ were the result of a fed-batch fermentation with *E. coli* possessing *aroF^{fbr}*, *tktA* and *pck* overexpression using succinate as an adjunct to glucose [LF99]. Current studies of this

---

[8] It is noteworthy that the identification of AroL was not straightforward. The authors mention that '...*The discovery that the rate-limiting nature of both shikimate dehydrogenase and shikimate kinase could be removed upon amplified expression of aroL came as a surprise...The impact of amplified expression of aroL also indicated that an enzyme's apparent rate-limiting character may not result from inadequate expression levels or catalytic sluggishness but rather could be the consequence of feedback inhibition by the substrate of a distal, rate-limiting enzyme in the pathway.*' This statement seems to be remarkable because the PEC criterion presented in the preceding section allowed the unequivocal identification of AroL thus preventing misleading interpretations with respect to AroE (shikimate dehydrogenase).

group focus on the PEP availability as already mentioned in the preceding paragraphs.

Global Regulatory Gene Disruption

Tatarko and Romeo [TR01] showed that the disruption of *csrA* (coding for the carbon storage regulator) resulted in a twofold increase of L-Phe production. This result is attributed to the now-inactivated Csr-functions which are: repression of PEP carboxykinase, PEP synthase, gluconeogenesis etc. and amplification of pyruvate kinase, glycolysis etc.

4.3 Preliminary Studies

4.3.1 Small-Scale Production Strain Characterization

Since the beginning of the 'L-Phe project' in mid 1997, a large amount of different *E. coli* strains has been constructed and tested by small- and large-scale fermentations. As already indicated in Table A.1 (section A.1.1, Appendix) none of these strains was constructed in the author's group but they were kindly provided by our cooperating partners. Therefore and for the sake of brevity, the following subsection does not aim at giving an overview of the *E. coli* constructs used. Instead, the fermentation procedure will be presented which was usually applied to characterize novel *E. coli* strains in parallel experiments.
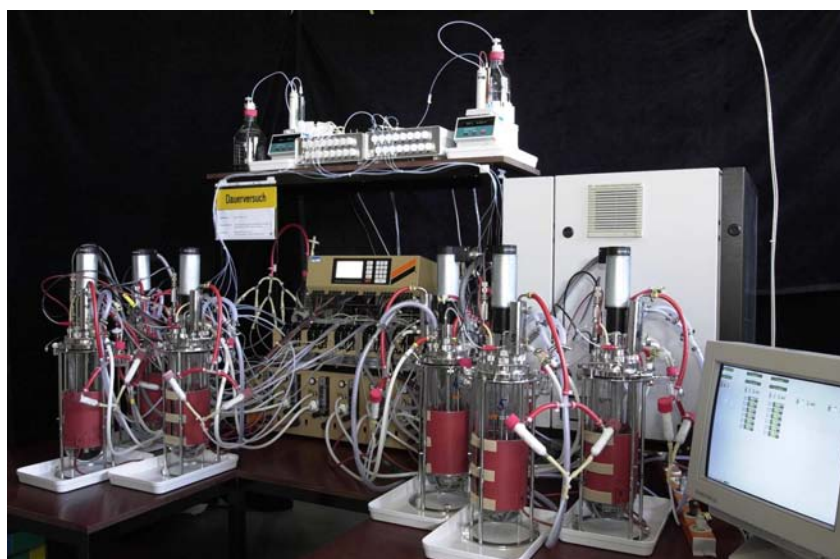
FIGURE 4.1. The Sixfors Vario system (Infors AG, CH) consisting of 6 3.5-*L* bioreactors was additionally equipped with a Dosimat 665 system (Methrom AG, CH) for the accurate feeding of two independent feeds and a multiplexed, 6-channel exhaust gas analyzer (Fisher-Rosemount, Germany).

For this purpose the Sixfors Vario system (Infors, Basel, CH, Figure 4.1) was installed. The system consists of 6 3.5-*L* stirred tank bioreactors, each equipped with 6-bladded Rushton turbines to ensure sufficient oxygen transfer[9]. Usually a working volume of 0.5 to 2 *L* was used in each biore-

---

[9] During typical fermentation conditions dissolved oxygen levels $\succeq 20\%$ were installed for growing and non-growing cells.

actor. The central controlling unit supervised the automatic control of pH, temperature, dissolved oxygen and antifoam addition.
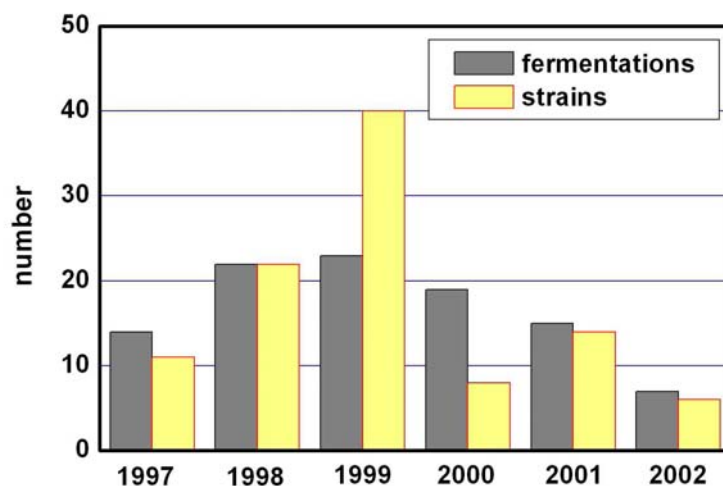
FIGURE 4.2. Number of newly constructed strains and number of (parallel) fermentations carried out per year to qualify the strains in preliminary, parallel experiments.

Additionally, the total system was equipped with a two-feed Dosimat 665 system (Metrohm AG, Switzerland) The feed control was achieved using the process control software of DASGIP (Jülich, Germany). With this feed system, accurate glucose and tyrosine feeding within error margins $< 1\%$ and $<1.5\%$ for glucose and tyrosine were realized. Because exhaust gas analysis was enabled by a multiplex O_2/CO_2 device (Fisher-Rosemount, Germany) carbon balances could be formulated while analyzing the fermentation results. This turned out to be highly beneficial because potential carbon gaps could be identified at an early step of process development. The fermentation apparatus was also capable to apply the tyrosine feed profile according to the findings of Gerigk $et\ al.$ [GMK$^+$02], to be shown further down.

Usually, preliminary shaking flask experiments were performed to achieve a rough estimation of the maximum growth rates and glucose and tyrosine
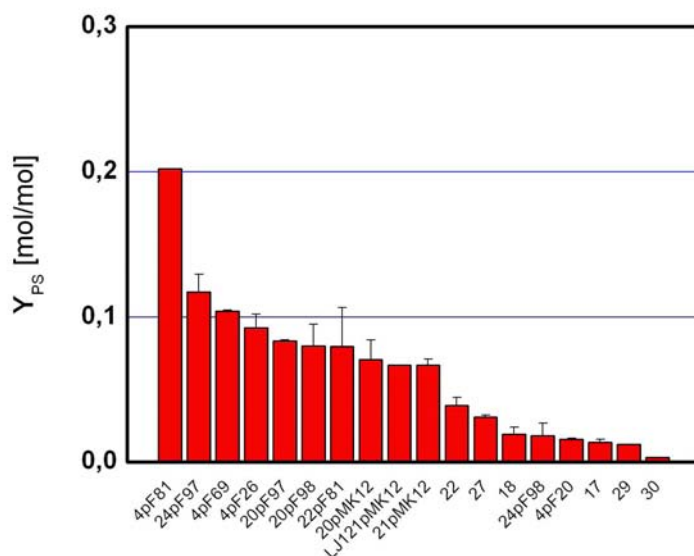
FIGURE 4.3. Ranking of some selected strains with respect to the final product/glucose yield Y_{PS} achieved in parallel experiments. Error bars indicate the result of parallel fermentations.

consumption rates of the novel *E. coli* strain [10]. If multi-auxotrophic strains were used, corresponding consumptions rates had to be estimated as well. These data were the basis for the glucose and tyrosine feeding applied in the Sixfors Vario apparatus. As a guideline, glucose feeds were adjusted such that glucose levels between 5 to 10 $g \cdot L^{-1}$ were realized during the experiments thus preventing a carbon-limited L-Phe production. Usually, tyrosine limitation was realized during the L-Phe production phase to enable selective L-Phe formation with non-growing cells. IPTG was manually added during the growth phase.

---

[10] These preliminary experiments were typically performed following 'classical' protocols, i.e. $\sim$ 100 mL biosuspension in 500 or 1000 mL shaking flasks with a shaking frequency of about 100 - 200 rpm. Occasionally, on-line pH control combined with small-scale substrate feeding [WBARA01] was applied depending on the purpose of the experimental study. Baffled as well as unbaffled flasks were used for the experiments. Unbaffled flasks were preferred because of the out-of-phase hydrodynamic phenomena occuring in baffled systems [BLM01] which can finally reduce the oxygen transfer rate [MB01a]. Summarizing, shaking flask conditions might have been non-optimal with respect to the maximum achievable oxygen transfer rate ([AB01], [Büc01b]), however, one should consider the preliminary character of these experiments delivering only some rough estimates of basic strain characteristics. As indicated, the final strain evaluation was performed in the Sixfors Vario system.

To give an overview of the fermentation activities Figure 4.2 is given. As depicted in the figure, up to 40 different *E. coli* strains were constructed per year by the cooperating partners and qualified in parallel fermentation experiments. In general, the same *metabolic engineering* topics as already presented in the preceding sections were studied such as PEP and E4P availability and the alleviation of the AAA pathway flux control. To qualify the performance of these strains, usually the product/glucose yield $[mol \cdot mol^{-1}]$ was applied as a criterion, together with additional characteristics such as product titer and the general performance of this strain. Figure 4.3 provides an overview of the product/glucose yields achieved comparing some selected strains. For the sake of brevity, no detailed strain description is given. However, these strains which were selected for further process development up to 300-L fermentations will be presented in the following sections. Please notice that the strain *E. coli* 4pF81 (see also Table A.1, section A.1.1, Appendix) revealed to be best suited already in the small-scale bioreactor fermentations.

4.3.2   Statistical Analysis Based on PCA

> Significant parts of the following subsection were already published in Takors *et al.* [TGPW01].

Introduction

The identification of fermentation key parameters seems to be attractive because fermentation process development can be facilitated by simply considering the key parameters at the same time ignoring the less important fermentation variables. Hence, trajectories of fermentation key values can provide a promising data basis for the development of optimized fed-batch processes. Moreover, the on-line analysis of these parameters can allow the implementation of on-line control strategy to optimize the process.

Despite these advantages, the identification of key parameters is hampered because of the complexity and heterogeneity of fermentation data sets. Thus a data-handling procedure is needed that reduces the dimensionality of fermentation data sets with respect to the key effects. A statistical tool for this purpose is the principal component analysis (PCA). So far, a lot of PCA applications have been published covering the field of chemical, economical or medical studies [Jol86]. Beyond it, PCA is also used to analyze fermentation experiments. For instance, applications were shown for on-line sensor signal analysis ([LMG$^+$98], [MHD$^+$98], [ME97]), fermentation pattern recognition ([SS92], [KSG94]), identification of fermentation key variables [Pat97], and fermentation fault diagnosis ([SYUS97], [Lia89]). However the number of PCA applications for fermentation data analysis is still rather small although this tool holds great promise [Ree97].
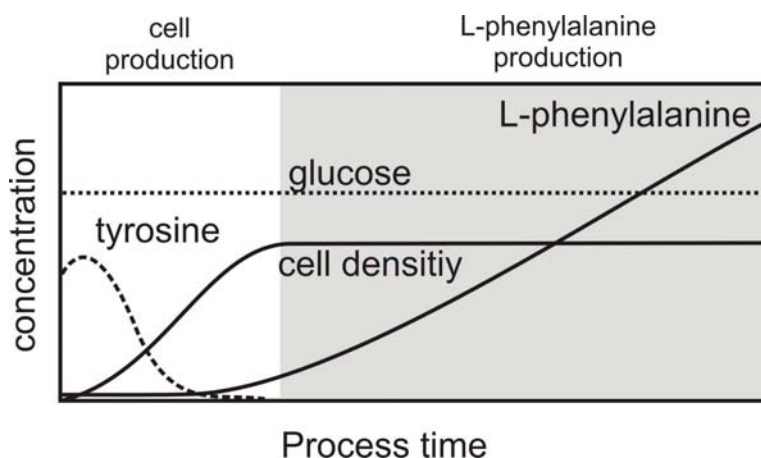
FIGURE 4.4. Rough scheme of a typical fed-batch fermentation for L-Phe production using the strain *E. coli* DSM as indicated in the text.

Therefore, as a matter of preliminary studies, the aim was followed to investigate whether and how PCA can be applied for fermentation data analysis. Using eight fed-batch fermentations with a recombinant L-phenylalanine producing *E. coli* strain as a test system it was studied (i) if PCA is principally applicable for heterogeneous fermentation data sets and (ii) if it allows the identification of key parameters even considering typically noisy measurement data. The latter also included the detailed analysis of PCA score values.

Experimental Conditions

The strain *E. coli* DSM (see also Table A.1, section A.1.1, Appendix) was used for all eight fermentations. As indicated, the strain was tyrosine auxotrophic and possessed the feedback resistant genes $aroF^{fbr}$ together with $pheA^{fbr}$. Fermentations were carried out using the 'DSM' medium given in Table A.2 (see Appendix) at constant pressure (1 bar), temperature (33 °C) and pH (6.8).

Typical fermentation courses using the strain *E. coli* DSM can be divided into two parts (see Figure 4.4). At the beginning all medium components including tyrosine and glucose were provided in the bioreactor. Additionally, a pre-defined feed consisting of glucose and tyrosine was installed. During this fermentation phase cell growth occurred and tyrosine concentrations in the bioreactor slowly decreased. When tyrosine was depleted, the end of the growth phase was observed. Then, under tyrosine limited conditions, a constant glucose feed was installed. During this production phase glucose was converted to L-phenylalanine with high L-phenylalanine/glucose-

selectivity. Relatively high glucose concentrations occurred temporarily in the bioreactor as the feeding profile was manually controlled. Glucose levels were not close-loop controlled but measured off-line by enzymatic analysis.

TABLE 4.1. Basic characteristics of the eigth fed-batch fermentations for L-Phe production with E. coli DSM used for PCA.

name	fermentation characteristic
F1	inoculum treatment changed
F2	highest L-Phe concentration achieved
F3	tyrosine feed concentration doubled during the cell growth
F4	L-Phe added at the beginning of fermentation
F5	standard fed-batch fermentation
F6	reduced glucose feed leading to glucose limitation
F7	increased glucose feed leading to glucose concentrations $> 20\ g \cdot L^{-1}$
F8	empirical 'new' glucose feed trajectory

For PCA the experimental data of eight fed-batch fermentations have been used. These fermentations were carried out according to the fermentation procedure described above. However, some modifications have been realized to investigate their effect on fermentation results. Differences in fermentation characteristics are listed in Table 4.1. As indicated, fermentation F5 represents the standard fed-batch procedure. In comparison to F5 fermentation F3 for instance was carried out using relatively high tyrosine feed concentrations during the first fermentation phase; a significant amount of L-phenylalanine was added to the bioreactor at the beginning of F4 and so on. Courses of the fermentations F1-F8 with respect to certain fermentation variables are given in Figure 4.5. Details of the PCA application as well as of the error estimation are given in the Appendix (see sections A.6.5 and A.6.6, respectively)

PCA Results

Figure 4.6 shows the PCA results based on the experimental data of eight fed-batch fermentations with the L-Phe producing strain *E. coli* DSM. Approximately 90% of total variance can be described using only the first three loading vectors. Even when loading vectors 1 and 2 are studied alone, 79% of total variance is covered. Thus it is statistically sufficient to consider only the first three loading vectors for further analysis. Subsequently, the n-dimensional problem of fermentation course discussion can now be reduced to three dimensions consisting of the loading vectors 1, 2 and 3.

To identify fermentation key parameters a detailed study of these loading vectors is necessary. As shown in Figure 4.6 the respiration quotient rq and the dissolved oxygen concentration DO possess small values in all loading vectors. This indicates, that the eigenvectors' direction is hardly
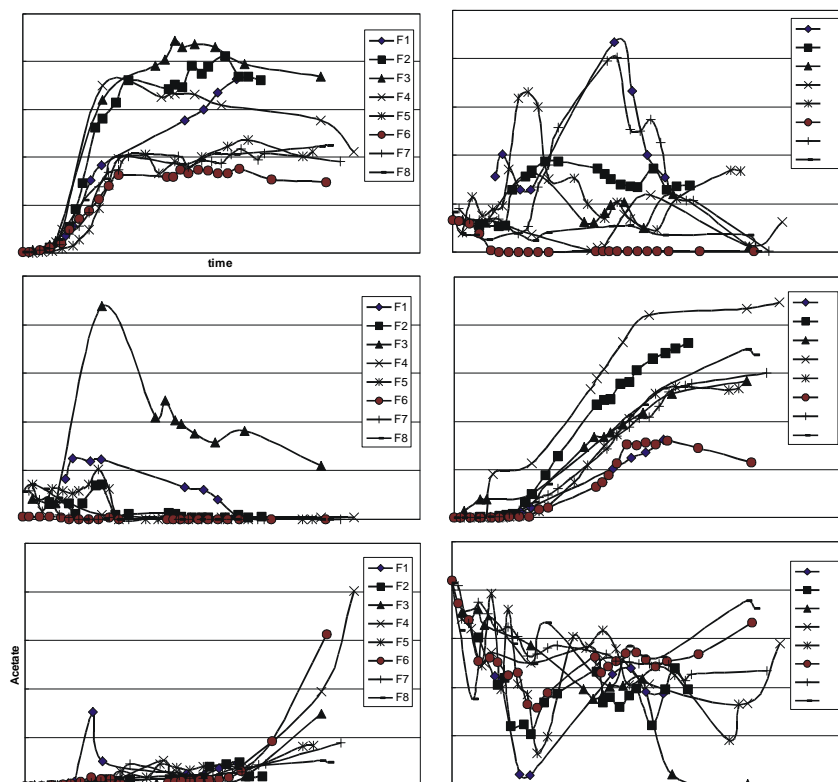
FIGURE 4.5. Courses of Optical density (OD) dissolved oxygen (DO), glucose, acetate, tyrosine and L-phenylalanine concentrations of eigth fed-batch fermentations using arbitrary units. PCA was performed with the absolute values, which - however - cannot be shown following the requests of the industrial partner DSM Biotech.

influenced by these observations. Thus, rq and DO are not key parameters. The minor importance of DO could be explained by high dissolved oxygen levels ($>>10\%$) that were maintained during all fermentations and that prevented any limitation of growth or product formation. In the case of rq the conclusion can be drawn that this (easy obtainable) signal would not be suited as an on-line fermentation control variable (e.g. for indirect substrate control).

However, when tyrosine and acetate concentrations were studied, these observations can be identified as key fermentation parameters. Both dominate loading vectors 1 and 2 strongly influenced 79% of the total variance. With respect to tyrosine, this result was expected since a tyrosine auxotrophic *E. coli* strain was used for fermentations. Thus tyrosine limi-
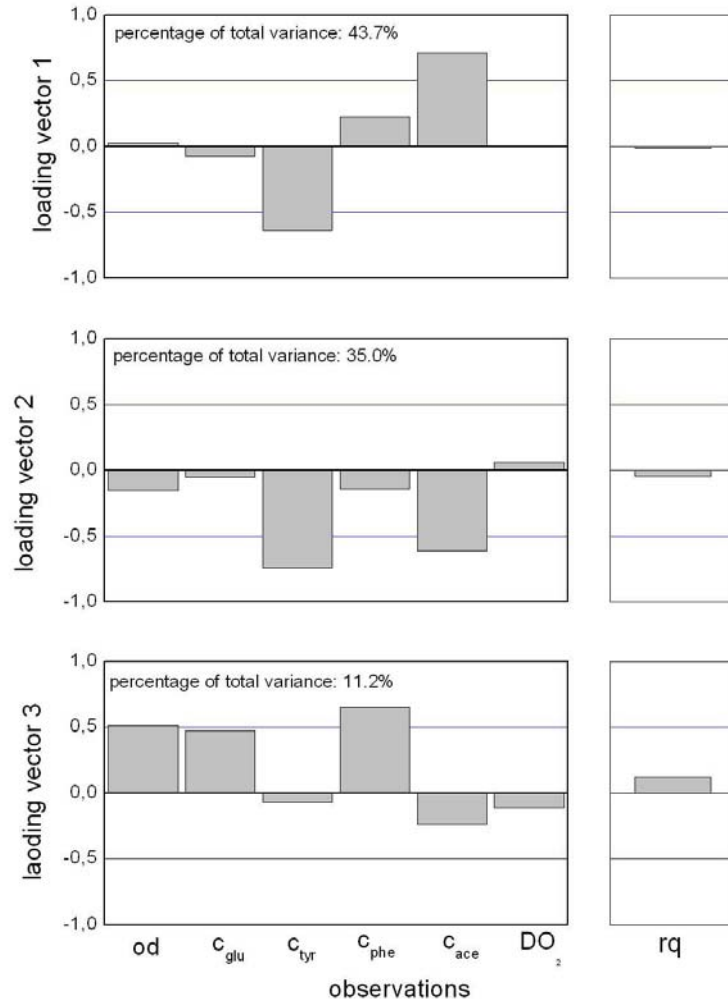
FIGURE 4.6. PCA results considering the data set of eight fed-batch fermentations including the observations optical density (od), concentrations of glucose (c_{glu}), tyrosine (c_{tyr}), L-phenylalanine (c_{phe}), acetate (c_{ace}), dissolved oxygen (DO) and the respiration quotient (rq) (Remark: rq was only measured during 4 fermentations.)
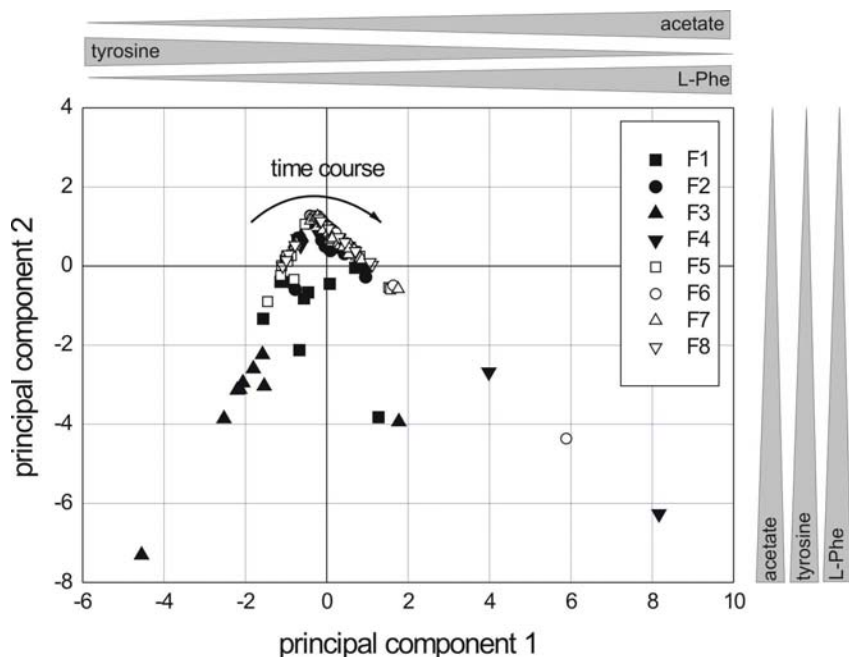
FIGURE 4.7. Phase diagram with courses of principal components scores pc1 and pc2 representing eight fed-batch fermentations (F1 – F8) for L-Phe production using the tyrosine auxotrophic strain *E. coli* DSM. For explanation of grey arrows see text

tations not only strongly reduced the microbial growth rate but also controlled the selectivity of L-Phe production. In the case of acetate it should be mentioned that, due to the pre-defined glucose feed rates, glucose accumulations (>10 $g \cdot L^{-1}$) temporarily appeared during fermentations. These led to temporarily high acetate production rates (see also Konstantinov *et al.* [KNY90], [KYNS91]). As a result, a high acetate significance was calculated.

Other observations like *od*, c_{glu} and c_{phe} are only significant within the third loading vector. According to the minor importance of this loading vector with respect to the total percentage of variance, these variables are also of minor importance for fermentation characterization.

When values of c_{tyr} and c_{ace} in loading vectors 1 and 2 were compared, different effects on the loading vector orientation can be identified. While both observations possess similarly directed influence on the orientation of loading vector 2 (both values have negative signs), an inverse effect was found for loading vector 1 (see Figure 4.6). Figure 4.7 indicates that this prospective contradiction can be explained when time courses of the scores

are studied. The score phase diagram includes all observations with respect to the loading vectors 1 and 2.

As shown in Figure 4.7 the time courses of pc_1 and pc_2 of all fermentations are similar. All fermentations started with pc_1-scores smaller than 0 and this value increased until the end of the experiment. Moreover all pc_2 courses posses a maximum that coincides with the beginning of tyrosine limitation which obviously is a dominant fermentation characteristic.

For the explanation of score trajectories the grey arrows at the top and at the right of the diagram are given. The arrows elucidate effects of acetate, tyrosine and L-phenylalanine concentrations on pc_1 and pc_2 scores. These observations have been chosen because they have the strongest influence on score values according to Figure 4.6. Regarding equation A.29 (see section A.6.5, Appendix) scores are calculated as a product of the loading vector and the standardized measurement variables. As a consequence of standardization, concentrations that are higher than average receive a positive sign. In the case of acetate these values are multiplied with a positive value of loading vector 1 or a negative value of loading vector 2 (see Figure 4.6). Thus high acetate concentrations lead to high pc_1 or low pc_2 scores - as indicated by the grey arrows. Analogously, the effects of tyrosine and L-phenylalanine can be discussed.

Using these relations, pc_1 courses of the phase diagram could generally be explained as an increase of acetate and L-phenylalanine concentrations in combination with a decrease of tyrosine concentrations. Moreover, the maximum of pc_2 courses could be discussed as a decrease of tyrosine content during the first fermentation period and an increase of L-phenylalanine and acetate concentration during the following production period. This general explanation also fits to the experimental observations of fermentations F3 and F4. The doubled tyrosine feed concentrations during the first period of fermentation F3 caused low pc_1 and pc_2 scores. Moreover high pc_1 and low pc_2 scores are calculated for F4, after L-phenylalanine was added to the fermentation.

Error Analysis

Results of the Monte-Carlo error estimation based on the measurements of $\mathbf{X}$ are presented in Figure 4.8. Errors for the loading vectors 1 – 3 assuming measurement errors from $\pm$ 1 to 10% are shown. As expected, relative loading vector errors are increasing with increasing measurement errors. However the error distribution with respect to the observations is different for each loading vector. Especially those observations that are not identified as key parameters according to Figure 4.6 possess high relative error values. For example, α_{od} and α_{DO} in loading vector 1 achieve errors
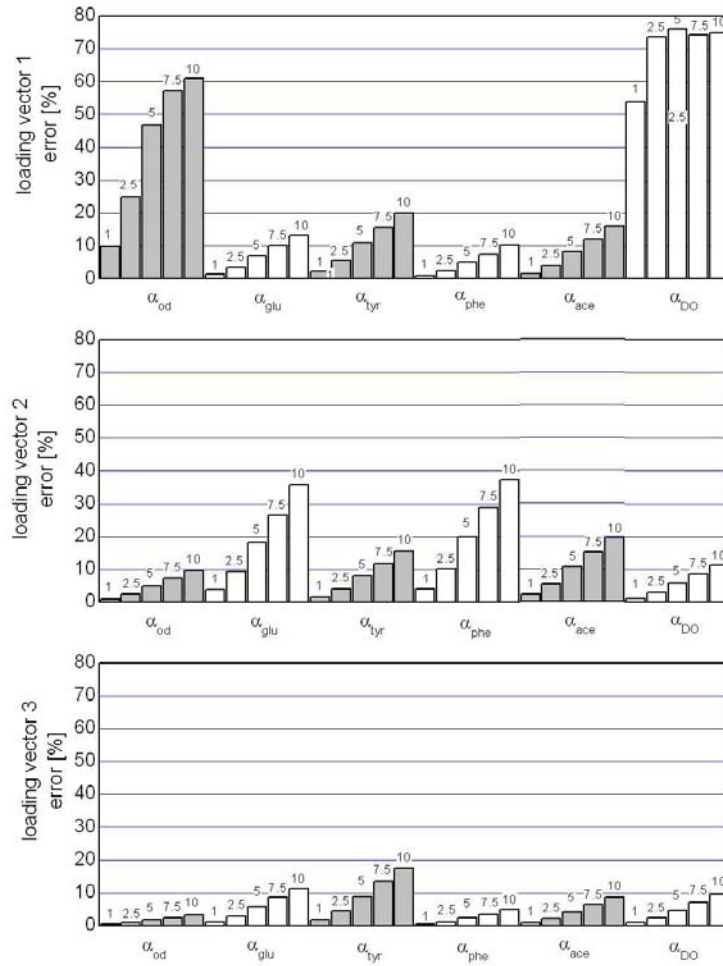
FIGURE 4.8. Estimated errors of loading vectors 1 - 3 with respect to the observations optical density (od), concentrations of glucose (c_{glu}), tyrosine (c_{tyr}), L-Phe (c_{phe}), acetate (c_{ace}), and dissolved oxygen (DO). Measurement errors of 1, 2.5, 5, 7.5 and 10% are assumed for calculations (see colums).
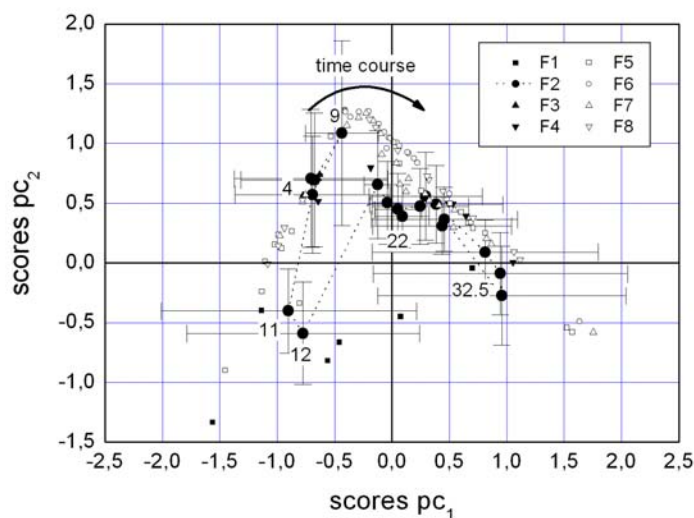
FIGURE 4.9. Phase diagram of pc_1 and pc_2 score courses considering eight fermentations (F1-F8) with the L-Phe producing strain *E. coli* DSM. Estimated errors are indicated for the most successful fermentation F2. Some selected sampling times (indicating the fermentation course) of F2 are given as well.

up to 75% if measurement errors of 10% are assumed. Similar tendencies are indicated for α_{glu} and α_{Phe} in loading vector 2. However, estimated errors of the key parameters tyrosine and acetate show relatively small values in loading vector 1 and loading vector 2. Thus it can be concluded that the identification of the key parameters tyrosine and acetate is not influenced by measurement errors.

In analogy to the discussion of score courses based on the phase diagram of Figure 4.7, the effects of measurement errors on these trajectories was studied as well. The aim was to investigate whether scores can be used for fermentation discussion taking into account obviously existing measurement errors. Score courses and the corresponding error bars are presented in Figure 4.9. Special focus is laid on the origin of the diagram to enable detailed discussion of fermentation F2, which has been identified as the most successful experiment because of the high L-Phe titers achieved.

As indicated in Figure 4.9 some score error bars were calculated as larger than 100%. This circumstance obviously hampers a detailed discussion of the score courses. However, scores of fermentation F2 at 11 and 12 hours appear to be significantly lower than scores of other fermentations. This pc_2 difference can be caused by relatively high tyrosine concentrations that

were detected at this time. During this phase tyrosine is needed for the production of *E. coli* cells that should produce L-Phe in the next fermentation period. Thus there might be a hint to a relatively high tyrosine concentration which is needed in this phase to enable high L-Phe production in the next period (as also discussed in [KNY90] and [KY90]). However it must be stressed that this can only be regarded as a vague hypothesis since the large score errors severely limit a detailed score course analysis.

Summarizing Comment

The PCA of eight fed-batch fermentations with the L-Phe producing strain *E. coli* DSM has shown that this statistical tool is generally suited for fermentation data analysis taking into account an unlimited number of standardized data. As a result, tyrosine and acetate concentrations were identified as fermentation key parameters, which will be studied in detail in the following section.

It is noteworthy that the dominant PCA result, the identification of the so-called key parameters tyrosine and acetate, was not affected by measurement errors of 10%, as shown by the Monte-Carlo simulations. This stresses the reliability of the PCA approach, although a detailed score course analysis failed owing to the large error margins of the scores. Furthermore, it would be interesting to study additional effects such as data distributions, different fermentation kinetics or the use of derived variables such as substrate consumption or product formation rates instead of pure concentration courses to further qualify the PCA tool for the analysis of fermentation runs. However, these studies have not yet been performed.

4.4   Fed-Batch Process Development

In the following the results of the fermentation process development for different, L-Phe producing *E. coli* strains will be presented. It is noteworthy that not all strains listed in Table A.1 (see subsection A.1.1, Appendix) were available at the beginning of the project. Instead, they were sequentially constructed during the course of the cooperation project by our collaborating partners (as indicated). Especially the close relation to the molecular biologists and biochemists at the Institute of Biotechnology 1 (IBT1) turned out to be invaluable. Thanks to this close cooperation, obviously existing significant (pathway) flux controls, which were observed by lab-scale fermentations in the author's group, could rapidly be alleviated by overexpression of the respected genes. An example was the identification of AroB by ^{1}H-NMR based analysis of DAH(P) accumulation in the fermentation supernatant and the subsequent plasmid-encoded *aroB* overexpression considered in new strain developments by the cooperating partners. Similar examples could be given for *aroL* and so on.

However, because fermentation process development based on 'given' strains was in the foreground of the research activities, the following sections will solely concentrate on this part.

4.4.1   Tyrosine and Glucose Control

> Significant parts of the following subsection were already published in Gerigk *et al.* ([GMK[+]02], [GBGN[+]02]) and applied for patent [GRST01]. Results were acquired during the Ph.D. thesis of M. Gerigk [Ger01] and the master thesis of R. Bujnicki [Buj01] and E. Ganpo-Nkwenkwa [GN01] which were co-supervised by the author.

At the beginning of the fermentation process development, an experimental setup and strategy was applied that was motivated by preliminary results of the industrial partner and by the general aim to keep the process as simple as possible. Therefore, the primary experimental setup was chosen as depicted in Figure 4.10. It was tested in an experimental series consisting of 10 subsequent fermentations using the tyrosine auxotrophic strain *E coli* 4pF20 (see Table A.1, Appendix). The fed-batch protocol, using the 'DSM' medium as indicated in Table A.2 (subsection A.2.1, Appendix) considered the following steps: The initial batch phase was finished after $5\ g \cdot L^{-1}$ glucose was consumed and the initial amount of $0.3\ g \cdot L^{-1}$ tyrosine was depleted. Then a feed containing glucose ($700\ g \cdot L^{-1}$) and tyrosine ($7.5\ g \cdot L^{-1}$) started lasting until the end of the growth phase, which was indicated by $OD_{620} \sim 80$. During this period, 100 μmol IPTG was added for induction. After this, only glucose ($700\ g \cdot L^{-1}$) was fed.
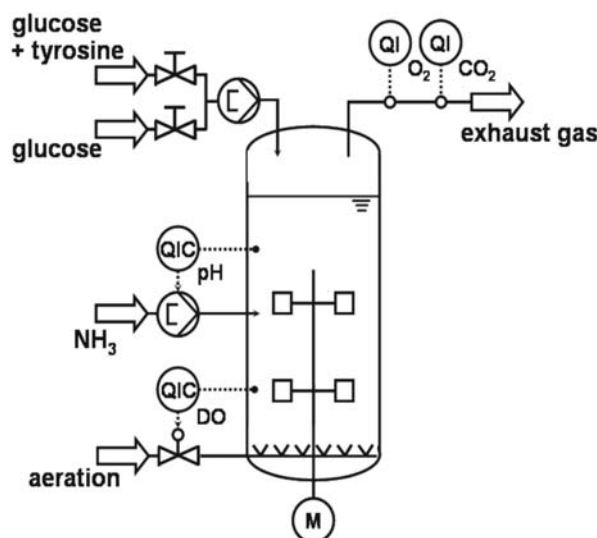
FIGURE 4.10. Experimental setup of the primary fed-batch experiments for L-Phe production with an tyrosine auxotrophic strain of *E. coli* in a 20-*L* bioreactor. Two separate feeds were installed with glucose and tyrosine (during cell growth) and without tyrosine (during the L-Phe production period). NH$_3$ was used for titration. Only *pH* and *DO* (and temperature) were automatically controlled.

It is noteworthy that tyrosine was supplied in a suspension because of its low solubility of about 0.45 $g \cdot L^{-1}$ (at *pH* 7, 25°*C*, in water). The feeds were adjusted manually aiming at realizing almost constant glucose concentration levels at 5 $g \cdot L^{-1}$ by considering the 'current' glucose content which was measured off-line during the process. As a result of this strategy, significantly variant glucose, tyrosine, L-Phe and *OD* curves were achieved. Glucose levels between 25 to 0 $g \cdot L^{-1}$ were measured, together with variant tyrosine concentrations (1 to 0 $g \cdot L^{-1}$) and maximum L-Phe titers of 30.9 to 12.8 $g \cdot L^{-1}$(after 50 h process time). Furthermore, the best results of the latter, namely the L-Phe titer of 30.9 $g \cdot L^{-1}$could not be reproduced. This finding was especially remarkable because the L-Phe titer of 30.9 $g \cdot L^{-1}$ was regarded as promising with respect to the achievements of other groups (see the section 4.2.1).

Taking into consideration that tyrosine was identified as a fermentation key variable (see preceding subsection), all lab-scale experimental results were reconsidered and plotted according to Figure 4.11. This retrospective analysis revealed that maximum L-Phe titers were only achieved if maximum tyrosine levels did not exceed 0.2 $g \cdot L^{-1}$.
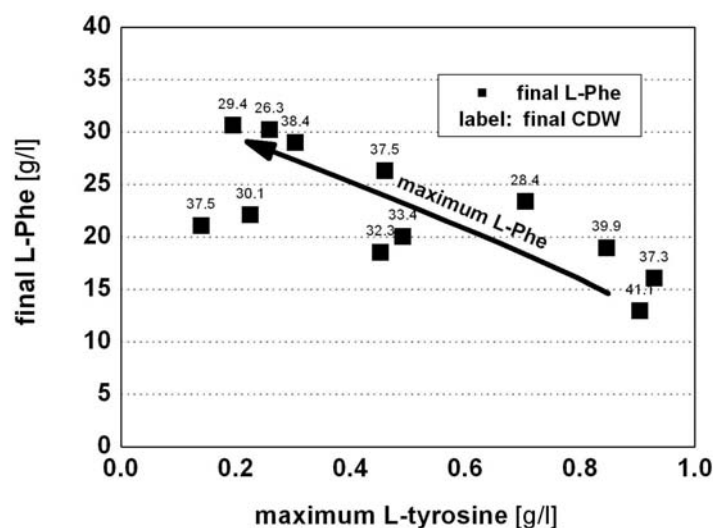
FIGURE 4.11. Final L-Phe titers as a function of the maximum tyrosine concentration achieved during the 20-L fed-batch experiments. The corresponding cell-dry weights $[g \cdot L^{-1}]$ (CDW) are given as labels.

This finding is in agreement with the aromatic amino acid pathway characteristics, which has already been presented in subsection 2.6.1. Accordingly, high tyrosine levels cause allosteric and transcriptional control of the AAA pathway activity. While chorismate mutase / prephenate dehydrogenase (encoded by *tyrA*) and DAHP synthase (encoded by *aroF*) are feedback inhibited by tyrosine, the transcription of *aroB* (coding for shikimate kinase II) is repressed, even in the presence of 36 $mg \cdot L^{-1}$ ([FH88], [FEH88]). Furthermore indications were given that also the synthesis of AroF is repressed by tyrosine (or very high levels of phenylalanine). Additionally it was observed that the PheA synthesis (i.e. the synthesis of chorismate mutase / prephenate dehydratase) can be repressed in the presence of tyrosine as well.

Summarizing, the necessity to optimize the tyrosine supply was clearly identified.

By analogy, the glucose supply should be optimized as well. An optimum glucose feed should aim at an unlimited microbial L-Phe production, while the unwanted by-product formation of acetate should be prevented at the same time. High growth or glucose consumption rates in combination with an insufficient oxygen supply are presumably important reasons for the beginning of acetate overflow metabolism in *E. coli*

([KBW93], [KBW94], [XJE99]). Konstantinov and coworkers ([KNY90], [KY90], [KKSY90], [KYNS91]) developed dynamically adjusted glucose feed strategies to prevent an exceed of oxidative capacities of L-Phe producing *E. coli* cells. As a consequence, glucose concentrations were not detectable during the fed-batch phase ($\prec 0.1\ g \cdot L^{-1}$), which can also be accomplished by using the alternative approach of Takagi *et al.* [TNOY96].

Despite the successful results based on these approaches, their applicability might be hampered if additional genetic changes such as the overexpression of *tktA, tal* and/or *pps* together with alternative glucose uptake systems and additional overexpression of genes coding for AAA pathway enzymes will be considered in future L-Phe production strains. Examples were already presented in the preceding sections.

As a consequence, it seems to be most likely, that the second 'generation' of L-Phe producing strains will possess a combination of genetic changes of central metabolism and of aromatic amino acid pathway. Due to the fundamental character of these genetic alterations, microbial kinetics of growth, substrate consumption and product formation will vary significantly from strain to strain. For instance, the use of an heterologous glucose uptake systems (as proposed by Flores *et al.* [FXB$^+$96] or recently by Chandram *et al.* [CYD$^+$03]) will strongly effect glucose uptake rates and will also affect optimal extracellular glucose levels. Also, tyrosine supply for production strains using the wild-type (tyrosine-feedback sensitive) $aroF^{wt}$ ([FH88], [FEH88]) or the feedback-resistant $aroF^{fbr}$ will be significantly different. A process strategy that aims at identifying the best suited production strain together with its optimal process conditions should be flexible enough to adapt to strain specific microbial kinetics. Hence, a fermentation approach is needed that could be used for different production strains ensuring individually optimal cultivation conditions.

For this purpose the general approach for the control of the two key parameters of L-Phe production, namely glucose and tyrosine, is presented in the following. Experiments were conducted with the two L-Phe producing strains *E. coli* aroF-fbr (4pF26) and *E. coli* aroF-wt (4pF69). As indicated in Table A.1 (see subsection A.1.1, Appendix) both strains differ in the use of $aroF^{wt}$ (in *E. coli* aroF-wt) and $aroF^{fbr}$ (in *E. coli* aroF-fbr). The use of $aroF^{fbr}$ in *E. coli* aroF-fbr should make this strain less sensitive towards high tyrosine concentrations than *E. coli* aroF-wt with $aroF^{wt}$. Note, that *E. coli* aroF-fbr and *E. coli* aroF-wt possessed additional plasmid-encoded *aroL*, which was intended to compensate a reduction of *aroL* transcription in the presence of high tyrosine concentrations. As a consequence, the discussion of tyrosine effects can be focussed on feedback inhibition of DAHP-synthase alone.
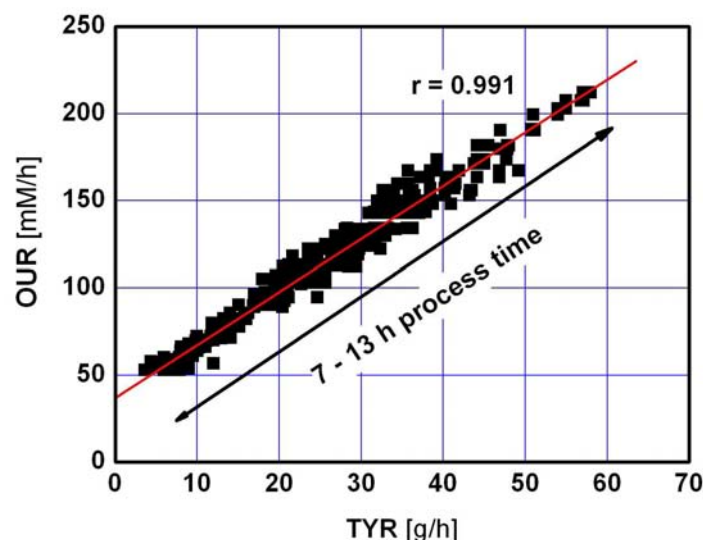
FIGURE 4.12. Correlation of the volumetric oxygen uptake rate (OUR, $mM \cdot h^{-1}$) and the (optimal) tyrosine demand (TYR, $g \cdot h^{-1}$) during the growth phase from 7 to 13 h process time found by empirical lab-scale studies using the L-Phe producing strain *E. coli* 4pF20. Additionally the regression coefficient r is given to indicate the quality of the linear approximation.

Fermentations in the 20-L bioreactor used the sole carbon source glucose in the fed-batch medium as indicated in subsection A.2.1 (Appendix). Standard analysis was applied as shown in subsection A.3.3 (Appendix). pH was controlled by 25 % ammonia water titration. Glucose and L-tyrosine (due to the L-tyrosine auxotrophy of the strain) were added to the bioreactor to ensure cell growth during batch phase. Two separate feeds for tyrosine (25 $g \cdot L^{-1}$ tyrosine dissolved in 5% ammonia water to increase tyrosine solubility) and glucose (700 $g \cdot L^{-1}$) were then started to extend growth phase. The feed rates of both substrates were automatically adapted by the control strategies to be shown in the following. When the feeding phase was started, L-Phe production was induced by addition of IPTG (final concentration 100 μM). Cell growth was stopped by tyrosine limitation (approximately at $OD_{620} \sim 80$) only feeding a limiting tyrosine supply for cell maintenance with a rate of 150 $mg \cdot h^{-1}$ until the end of the fermentation. The process was monitored using the technical setup as described in subsection A.4.2, Appendix.

Tyrosine Control

Motivated by the results of Förberg and Häggström ([FH88], [FEH88]), who identified a maximum tolerable tyrosine concentration of 36 $mg \cdot L^{-1}$, a maximum tyrosine concentration of 20 $mg \cdot L^{-1}$ was regarded as an upper limit for the experiments. Tyrosine control was preferred to be realized as an indirect controlling approach, because on-line HPLC tyrosine measurement was assumed to be not reliable enough[11]. For this, a linear, empirical correlation was identified estimating the volumetric tyrosine consumption rate as a function of the on-line measured oxygen uptake rate (OUR). This simple correlation was motivated by preliminary findings (depicted in Figure 4.12) indicating that the metabolism activity (mirrored by the oxygen uptake rate) can be directly controlled by the tyrosine feeding using growing, tyrosine auxotrophic mutants.

Hence, the tyrosine feed rates were adjusted automatically during the growth phase following the equation

$$\dot{V}_{Tyr}[\frac{g}{Lh}] = \frac{OUR\left[\frac{mmol}{Lh}\right] - 30\left[\frac{mmol}{Lh}\right]}{m\left[\frac{mmol}{g}\right]} \tag{4.1}$$

Here, m represents a controlling parameter that could be used, for instance, to increase tyrosine limitation by increasing m values. To control acetate production, an enzymatic on-line glucose control system was installed (see section A.4.3, Appendix) that used the empirical value of 5 $g \cdot L^{-1}$ as setpoint[12]. To prevent oxygen limitation, DO levels were kept always above 20% saturation (data not shown). The process setup is shown in Figure 4.13.

To study the effect of different tyrosine supply on L-Phe formation rates and final product titers, an experimental series was carried out choosing different set points of the tyrosine controlling parameter m of equation 4.1. m was set to 0.6, 1.0 and 1.5 (and to 2.0 using *E. coli* aroF-wt) thus reducing the tyrosine feeding rates 2.5 fold (3.3 fold) with respect to the maximum feed rate with m as 0.6. In all experiments, the total amount of tyrosine fed to the culture was constant (180 g of tyrosine solution) which finally lead to different lengths of tyrosine controlled periods. Indirect tyrosine control always started approximately after 6 h and lasted until 14 to 20 hours depending on the tyrosine feed rates. After this, tyrosine feed rates were kept constant at 0.15 $g_{TYR} \cdot h^{-1}$ until the end of the fermentation to limit microbial cell growth and to enable an L-Phe production with high L-Phe/glucose selectivity.

---

[11] The HPLC detection limit for tyrosine was found to be about 10 $mg \cdot L^{-1}$.
[12] Details of the glucose control are given in section A.4.3.
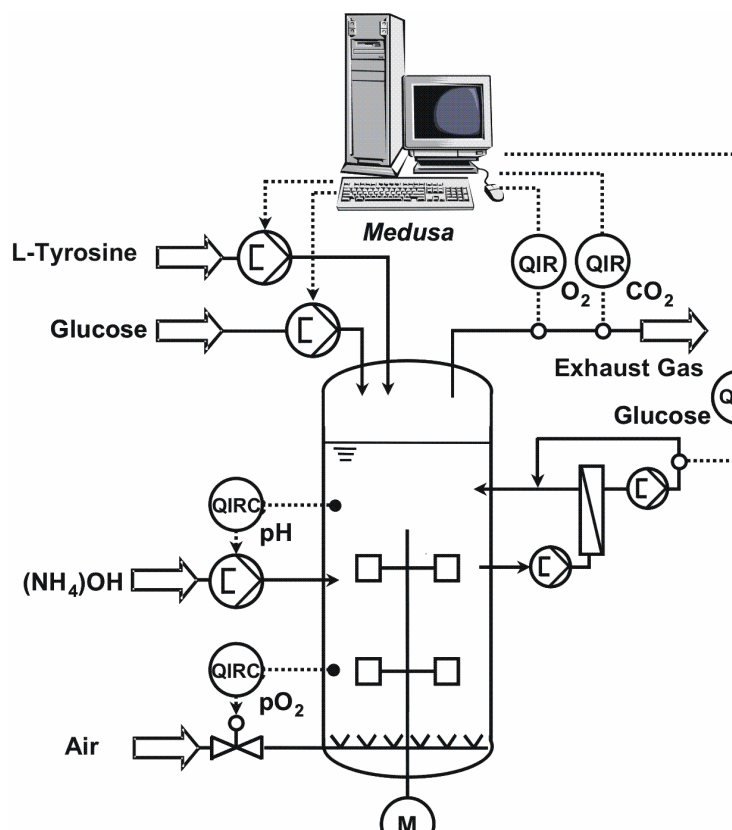
FIGURE 4.13. Experimental setup for lab-scale fermentations using on-line glucose control (measuring glucose levels enzymatically in the cell-free permeate from the bioreactor by-pass) and tyrosine control (using exhaust gas analysis for O_2 measurements for estimating the tyrosine feeding according to equation 4.1).

Figure 4.14 gives an overview of the resulting tyrosine concentrations as a function of process time, controlling parameter m and production strain. In fed-batch fermentations with m as 0.6, an accumulation of tyrosine was observed for *E. coli* aroF-fbr as well as for *E. coli* aroF-wt. Reducing the tyrosine feed rates with increasing m values, tyrosine accumulations were also significantly reduced. In case of *E. coli* aroF-wt, the primary chosen upper limit of 20 $mg \cdot L^{-1}$ tyrosine was only exceeded for m set as 0.6. Higher tyrosine concentrations were temporary measured using *E. coli* aroF-fbr, which should be tolerated by this strain owing to the existing tyrosine resistants in $aroF^{fbr}$. From this we concluded, that the indirect tyrosine control can successfully be used for the tyrosine-sensitive strain *E. coli* aroF-wt, when m values larger than 1 were used.
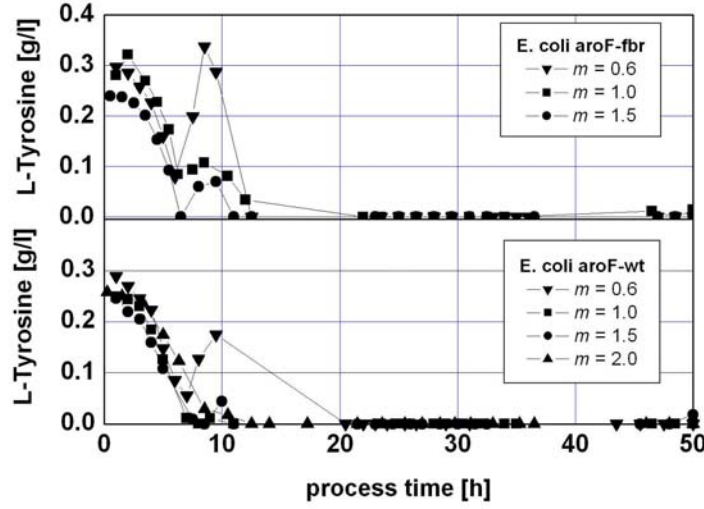
FIGURE 4.14. Tyrosine courses using the strains *E. coli* aroF-fbr and *E. coli* aroF-wt in L-Phe fed-batch production processes with different set points of m ranging from 0.6 to 2.0.

In Figure 4.15, courses of resulting biomass specific L-Phe formation rates π_{Phe} are given. A maximum specific L-Phe formation rate of $0.08\ g \cdot (gh)^{-1}$ was estimated by spline interpolation with the controlling parameter m as 1.0 using the strain *E. coli* aroF-fbr. Using other m values, only 0.04 to $0.06\ g \cdot (gh)^{-1}$ were achieved. Obviously the tyrosine accumulations up to $0.3\ g \cdot L^{-1}$ did not significantly reduce the biomass specific L-Phe formation rate, which was a consequence of the feedback resistant AroF^{fbr}.

Using *E. coli* aroF-wt with the tyrosine feedback regulated gene $aroF^{wt}$ the maximum π_{Phe} values measured in fed-batch processes were $0.06\ g \cdot (gh)^{-1}$. This maximum L-Phe formation rate was the same for all fermentations with a controlling parameter m between 1.0 and 2.0. However, when the tyrosine feed rate was increased (m as 0.6), a significant reduction of the L-Phe formation rate was observed, achieving only a third of the maximum values of the other fermentations. Presumably, the reduction was caused by the external tyrosine accumulation up to $0.18\ g \cdot L^{-1}$, which may have caused intracellular tyrosine concentrations far above the reported inhibiting value of the wild-type AroF of $36\ mg \cdot L^{-1}$. On the contrary, when tyrosine feed was reduced by choosing m as 2.0, a significant extension of high level L-Phe formation with $0.03\ g \cdot (gh)^{-1}$ was observed after $30\ h$ lasting until $45\ h$ process time. Although tyrosine feed rates were all
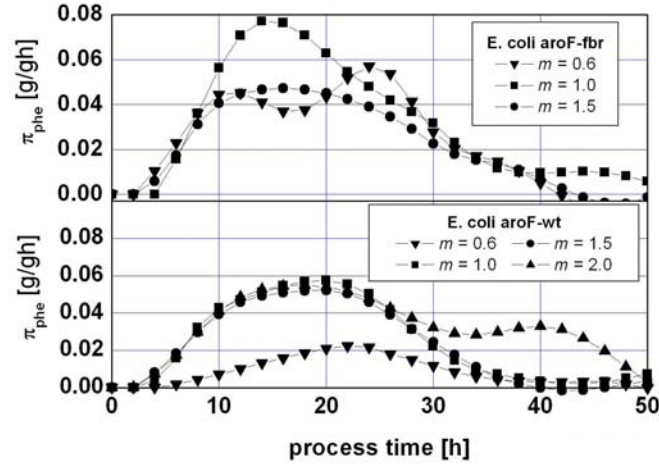
FIGURE 4.15. Comparison of the biomass-specific L-Phe production rates π_{Phe} in fed-batch fermentations with different setpoints of controlling parameter m using the strains *E. coli* aroF-fbr and *E. coli* aroF-wt. Rate curves were derived by spline fitting.
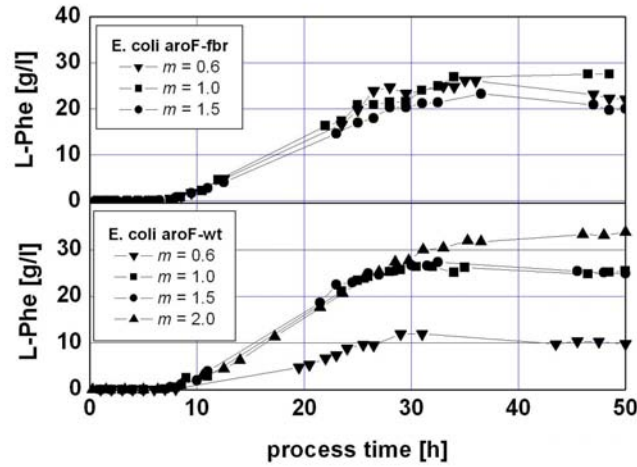
FIGURE 4.16. Courses of L-Phe concentrations of seven fed-batch fermentations with different setpoints of controlling parameter m using the strains *E. coli* aroF-fbr and *E. coli* aroF-wt. HPLC measurement showed error margins less than 5%.
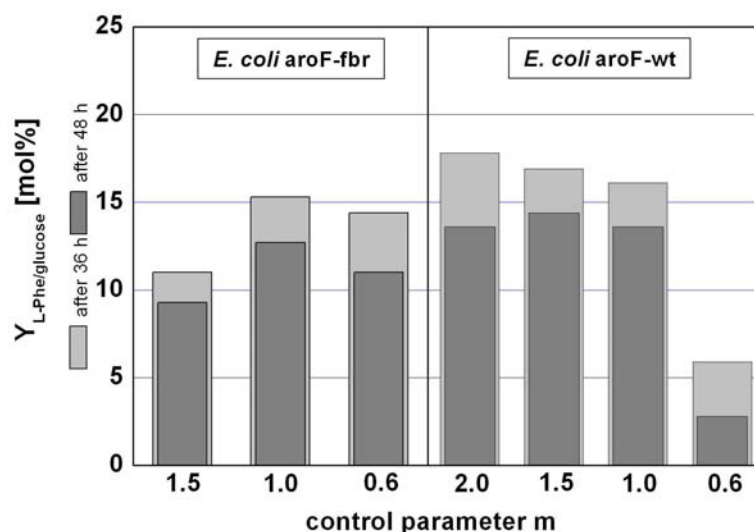
FIGURE 4.17. Comparison of L-Phe/glucose yields after 36 and 48 hours process time using the strains *E. coli* aroF-fbr and *E. coli* aroF-wt under different tyrosine-controlled (parameter m) fed-batch conditions.

similar during this period, the experiment with the lowest tyrosine feeding rate during the earlier cell growth was the one that showed the longest L-Phe production period. Consequently, the highest L-Phe titers ($34 \ g \cdot L^{-1}$, see Figure 4.16) were also measured during this experiment. It should be stressed, that this value is even higher than the maximum titer of $28 \ g \cdot L^{-1}$ achieved for the optimal tyrosine control ($m = 1$) using *E. coli* aroF-fbr.

The effects of different tyrosine feeding strategies on fermentations with *E. coli* aroF-fbr and *E. coli* aroF-wt were also qualified, when L-Phe/glucose yields are compared (see Figure 4.17). In general, yields using *E. coli* aroF-wt were higher than their counterparts of *E. coli* aroF-fbr. An exception was observed for m set to 0.6. Here the tyrosine inhibition on L-Phe production using *E. coli* aroF-wt was such strong, that only a very low selectivity of about 6 % ($mol \cdot mol^{-1}$) was achieved. It should be stressed that the highest glucose/L-Phe yield of about 18 $mol\%$ was reached with the most tyrosine limiting feeding profile with m set to 2.0 using the strain *E. coli* aroF-wt with $aroF^{wt}$. This result is particularly remarkable because it shows, that not necessarily *metabolic engineering* with respect to the cloning of an tyrosine feedback resistant $aroF^{fbr}$ gene for L-Phe production should be preferred. Instead, when an optimum tyrosine feeding is chosen, higher L-

Phe titers and L-Phe/glucose yields are obtained using the wild-type gene $aroF^{wt}$.

Furthermore DAHP-synthase activity measurements (following the protocol presented in subsection A.3.12, Appendix) were carried out for each strain at 10-12 h process time and also after 30 hours. A maximum activity of 0.5 $U \cdot mg_{protein}^{-1}$ was found for *E. coli* aroF-fbr at 13 h using the tyrosine control with m set to 1.0. Other m values lead to reduced activities lower than 0.3 $U \cdot mg_{protein}^{-1}$. After 30 h, no significant DAHP-synthase activity was detected. The measurements were thus in agreement with the above mentioned phenomenological results and they also explained, why L-Phe formation declined after approximately 21 h process time (see figures 4.15 and 4.17). Compared to *E. coli* aroF-fbr DAHP-synthase activities of *E. coli* aroF-wt were significantly higher, for instance achieving a maximum of 2.0 $U \cdot mg_{protein}^{-1}$ after 10 h process time using the tyrosine control with the optimum m set to 2.0. Most notable, DAHP-synthase activities after 30 h process duration were still about 0.6 $U \cdot mg_{protein}^{-1}$ (for m set > 1.0) which was even higher than the maximum value of *E. coli* aroF-fbr. It is noteworthy that AroF^{fbr} did not show significant activity at this time.

From the above results the conclusion can be drawn that *E. coli* aroF-wt should be preferred for L-Phe production, however, only in conjunction with an optimum tyrosine control system. Only in this combination the maximum process selectivity of about 18 % $(mol \cdot mol)$ and the maximum titer of 34 $g \cdot L^{-1}$ was achieved.

Glucose Control

To investigate whether and how different glucose levels effect L-Phe production, an experimental series using *E. coli* aroF-wt was carried out. As the strain possessed an active phosphoenolpyruvate:carbohydrate phosphotransferase system (PTS), the results of Ferenci ([Fer96], [Fer99]) and others (Hunter and Kornberg [HK79], Postma *et al.* [PLJ93],Lengeler *et al.* [LS99]) were considered, assuming a glucose uptake via Mgl (half-saturated at 0.2 μM or 0.036 $mg \cdot L^{-1}$) and PtsG (half-saturated at 3 to 10 μM or 0.6 to 1.8 $mg \cdot L^{-1}$) at micromolar external levels and via PtsG and mannose specific PtsM (half-saturated at 1.3 mM or 230 $mg \cdot L^{-1}$) at millimolar external levels. Thus, glucose control setpoints at 0.1, 5 and 30 $g \cdot L^{-1}$ were chosen that saturate the glucose uptake via PtsG and that also allow a limited glucose uptake via PtsM. In all experiments, tyrosine supply was controlled setting m to 1.

As indicated in Figure 4.18, glucose control started at the end of the batch phase when the setpoint was reached (at approximately 6 to 10 hours after inoculation). The starting glucose concentration was 15 $g \cdot L^{-1}$ in
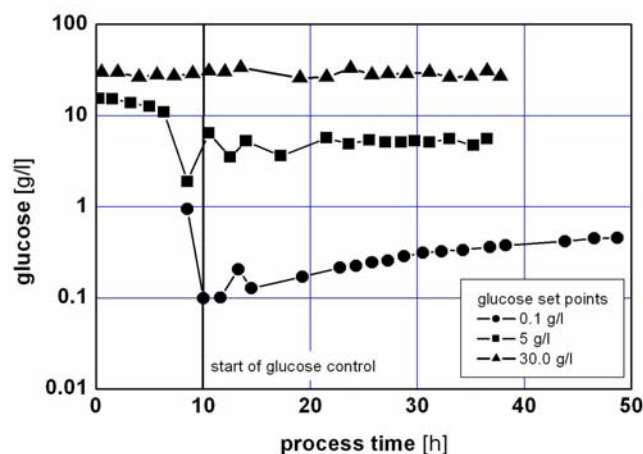
FIGURE 4.18. Three courses of the glucose-controlled fed-batch fermentations at setpoints of 0.1, 5 and 30 $g \cdot L$ are shown. The L-Phe producing strain *E. coli* aroF-wt was used with tyrosine control with m set as 1.0. Enzymatic glucose error margins are within 5%.
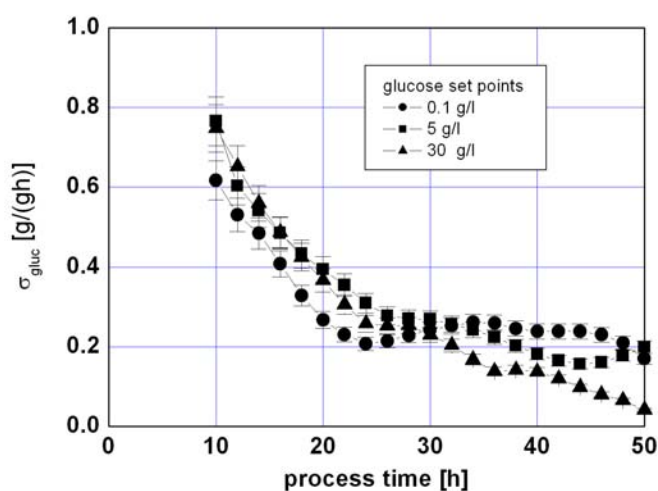
FIGURE 4.19. Biomass-specific glucose consumption rates σ_{Gluc} during the glucose-controlled fed-batch phase of the three experiments with glucose setpoints of 0.1, 5 and 30 $g \cdot L^{-1}$. The tyrosine control with m set to 1.0 was applied for *E. coli* aroF-wt. Rate courses were derived by spline functions.
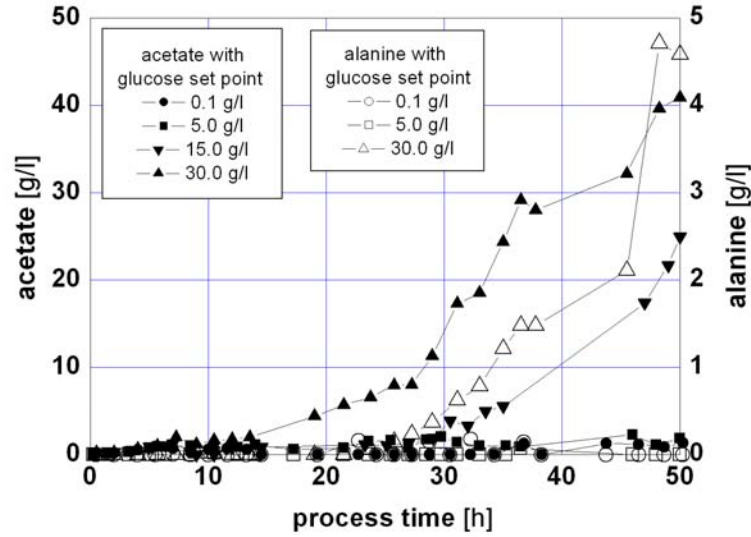
FIGURE 4.20. Alanine and acetate courses in glucose-controlled fed-batch fermentations at 0.1, 5 and 30 $g \cdot L^{-1}$. Tyrosine control was applied using the strain *E. coli* aroF-wt with m set as 1.0. Acetate and alanine error margins from HPLC-measurements were less than 10%.

experiments with setpoints at 0.1 and 5 $g \cdot L^{-1}$ and 30 $g \cdot L^{-1}$ for the last fermentation. As shown, glucose control was well realized for setpoints 5 and 30 $g \cdot L^{-1}$. Using setpoint 0.1 $g \cdot L^{-1}$, a continuous glucose increase during fed batch fermentation was detected. However it should be pointed out, that the on-line measured glucose concentrations did not show this tendency. On-line glucose control always indicated 0.1 $g \cdot L^{-1}$ (data not shown). It was thus concluded that an enzymatic sensor drift, maybe due to partly inactivation of glucose oxidase of the sensor, caused the 'controlled' increase of glucose up to 0.4 $g \cdot L^{-1}$ in the bioreactor.

Figure 4.19 depicts the biomass specific glucose consumption rates σ_{gluc} of the three experiments after the batch phase was finished. Although glucose consumption rates were very similar at the beginning of fed-batch period, a slightly lower glucose consumption rate was observed at 0.1 $g \cdot L^{-1}$ indicating that glucose uptake via PtsM was probably limited. During the later fermentation phase, strongly decreasing σ_{gluc} values (down to 0.05 $g \cdot (gh)^{-1}$) at 30 $g \cdot L^{-1}$ glucose were measured after 30 hours, while glucose consumption rates at 0.1 and 5 $g \cdot L^{-1}$ kept at a stationary level of 0.2 $g \cdot (gh)^{-1}$.

To study the phenomenon, the metabolism overflow indicators acetate ([KBW93], [KBW94]) and alanine were monitored during the fermentations as indicated in Figure 4.20. While acetate is produced (under aerobic conditions) with the aid of pyruvate dehydrogenase, phosphotransacetylase and acetate kinase coproducing one ATP (Majewski and Domach [MD90]), alanine is produced from pyruvate via amino transferase using glutamate as amino donor. Based on further studies of Xu *et al.* [XJE99] and of Luli and Strohl [LS90], acetate is known to be an inhibitor for growth (inhibition constant K_I of 9 $g \cdot L^{-1}$) and also for glucose consumption (inhibition constants between 1 to 5 $g \cdot L^{-1}$ for different *E. coli* wild-type strains).

As shown, glucose levels of 0.1 and 5 $g \cdot L^{-1}$ did not effect the by-product formation of acetate and alanine. Acetate concentrations were lower than 2 $g \cdot L^{-1}$ in both fermentations. By analogy, only very low alanine titers up to 0.1 $g \cdot L^{-1}$ were detected in these fermentations. However, completely different by-product courses were found, when glucose was controlled at 30 $g \cdot L^{-1}$. Significant acetate titers higher than 2 $g \cdot L^{-1}$ were measured at the end of the batch phase. During the glucose controlled production period, acetate titers finally increased up to 41 $g \cdot L^{-1}$ accompanied by high alanine titers up to 4.6 $g \cdot L^{-1}$. These acetate concentrations are (by far) higher than the reported inhibition constants. Hence, the decline of glucose uptake after 30 h process time at 30 $g \cdot L^{-1}$ extracellular glucose concentration can be regarded as a consequence of the acetate inhibition as reported by Luli and Strohl [LS90].

Because an increase of by-product formation can also affect L-Phe production, biomass specific L-Phe formation rates π_{Phe} were given in Figure 4.21. During the first 10 hours, L-Phe formation rates were similar in all experiments. Only a slight reduction could be identified in the presence of 30 $g \cdot L^{-1}$ glucose compared to the fermentations at 5 and 0.1 $g \cdot L^{-1}$. Significant differences occurred during the later L-Phe production phase. While π_{Phe} values between 0.03 and 0.04 $g \cdot (gh)^{-1}$ were maintained in the presence of 0.1 and 5 $g \cdot L^{-1}$ glucose until 43 h process time, L-Phe production strongly reduced after 15 hours and completely broke down after 30 hours at high glucose levels of 30 $g \cdot L^{-1}$. Considering the aforementioned acetate inhibition, we thus concluded, that high acetate titers not only caused a reduction of glucose uptake but also a reduction of L-Phe formation.

These effects are also indicated in Figure 4.22 where L-Phe and tyrosine concentration courses of the three fed-batch experiments are compared. While tyrosine levels were very similar during all fermentations owing to indirect L-Tyr control, L-Phe courses varied significantly in the different experiments. Approximately after 25 hours, no further L-Phe accumulation was detected in the 30 $g \cdot L^{-1}$ glucose experiment, which is in agreement with the calculated L-Phe formation rates of Figure 4.21. On the contrary,
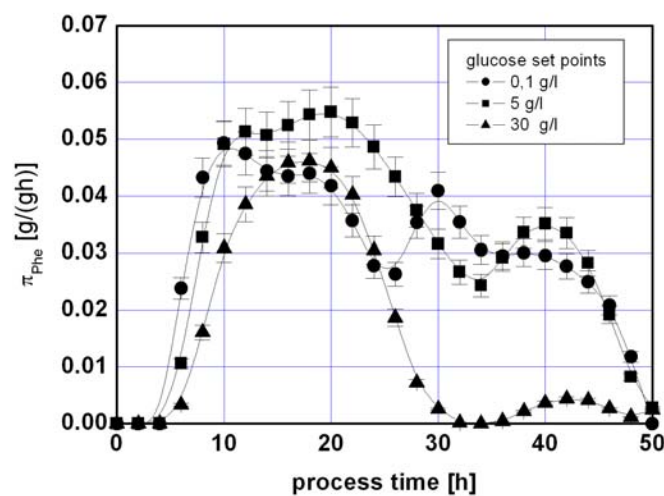
FIGURE 4.21. Biomass specific L-Phe formation rates π_{Phe} at different controlled glucose levels of 0.1, 5 and 30 $g{\cdot}L^{-1}$. Tyrosine control was applied using the strain *E. coli* aroF-wt with m set as 1.0. Rate courses were derived by spline fitting.
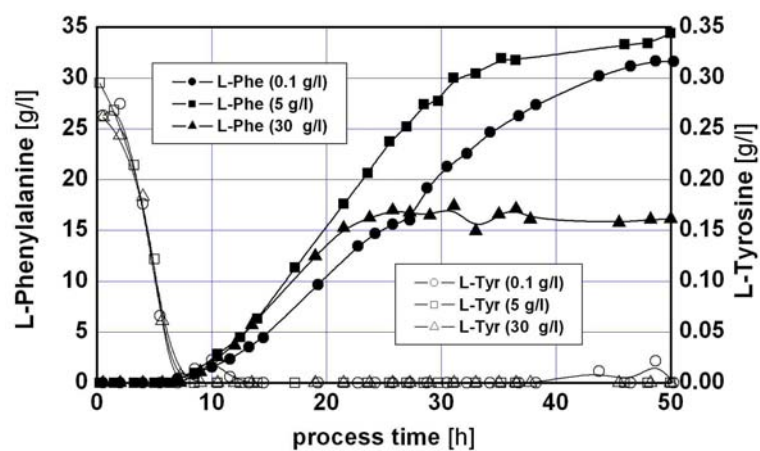
FIGURE 4.22. Courses of L-Phe and L-Tyr titers in glucose-controlled fermentations at 0.1, 5 and 30 $g \cdot L^{-1}$ glucose. Tyrosine control was applied using the strain *E. coli* aroF-wt with m set as 1.0. Error margins for HPLC measurement were less than 10%.

when glucose was controlled at 0.1 or 5 $g \cdot L^{-1}$, an L-Phe accumulation could be observed lasting until 48 h. The highest L-Phe titer was thus achieved in the 5 $g \cdot L^{-1}$ glucose experiment (approximately 35 $g \cdot L^{-1}$). By analogy, the highest total amount of L-Phe (500 g) was also produced in this experiment, followed by 320 g with 0.1 $g \cdot L^{-1}$ glucose and 190 g with 30 $g \cdot L^{-1}$ glucose.

Hence, an optimum for L-Phe production was found with a glucose control setpoint at 5 $g \cdot L^{-1}$ with respect to the three setpoints investigated[13]. This result is remarkable, because former approaches ([KNY90], [KY90], [KKSY90], [KYNS91], [TNOY96]) obviously followed the aim to avoid acetate production by controlling glucose concentrations at a very low level below 0.1 $g \cdot L^{-1}$ at the same time ensuring sufficient oxygen supply. Our experimental results show that the by-product courses as well as the L-Phe production would suggest best process conditions at 5 $g \cdot L^{-1}$ glucose.

This result is advantageous with respect to the upscalability of the total process approach. Following the route of controlling glucose concentrations at a very low concentration level, inhomogeneous mixing and resulting concentration gradients could build up zones of glucose limitation in large production bioreactors. Glucose represents the sole carbon source for microbial L-Phe production in the fermentation medium. Hence, L-Phe formation would be limited subsequently. Controlling glucose levels at 5 $g \cdot L^{-1}$ would at least reduce this phenomenon.

300-L Upscale

The results of the preceding paragraphs have shown that a general fed-batch control approach for L-Phe production with tyrosine auxotrophic strains can be achieved by establishing (i) an indirect tyrosine control and (ii) a direct glucose control. While the first enabled the use of $aroF^{wt}$ which even revealed to be superior to the usually applied $aroF^{fbr}$ genes, the optimal glucose control at 5 $g \cdot L^{-1}$ offers the advantage of a simplified process scale-up by preventing unwanted carbon-source limitation. The latter are likely to occur when the glucose level are controlled at 0.1 $g \cdot L^{-1}$, as proposed by the previous approaches.

To demonstrate the upscaling quality of the current approach, experiments were performed using the strain *E. coli* 4pF20 (for details see Table A.1, Appendix). It is noteworthy that this strain differs from *E. coli* aroF-fbr and *E. coli* aroF-wt by lacking of *aroL* overexpression, thus being

---

[13] In addition to the experiments presented here, similar experiments using 15 $g \cdot L^{-1}$ as glucose setpoint were performed, but not shown here. The results are in agreement with the observations presented in this section.
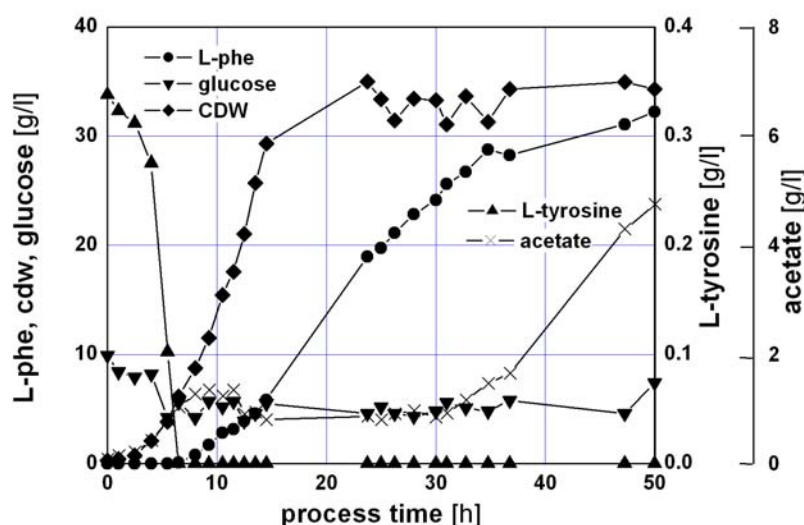
FIGURE 4.23. Courses of L-Phe, glucose, cell dry weight, acetate and tyrosine concentrations in a 20-L fed-batch process using the strain $E.$ $coli$ 4pF20 with glucose control (setpoint: 5 $g \cdot L^{-1}$) and tyrosine control (setpoint: $m = 1.0$). After 14 h process time, a tyrosine-containing feed with 150 $mg \cdot h^{-1}$ was installed to supply sufficient tyrosine for maintenance purposes.

subject to transcriptional control by the $tyrR$ regulon at high tyrosine levels. Besides, the same medium and cultivation conditions were applied as already mentioned.

Figure 4.23 indicates that the glucose/tyrosine control was also applicable for $E.$ $coli$ 4pF20 in 20-L scale fed-batch fermentations. In contrast to previous results cultivating $E.$ $coli$ 4pF20 with the manual fed-batch protocol, highly reproducible L-Phe titers $\succ$ 30 $g \cdot L^{-1}$ were now achieved using the optimum setpoints 5 $g_{glu\cos e} \cdot L^{-1}$ and $m = 1.0$. The slightly variant glucose levels were assumed to be not significant for the microbial glucose uptake owing to the high affinities of the underlying PTS system (as explained in the preceding paragraphs). High by-product formation could not be observed. Similar to reports of Konstantinov et $al.$ ([KNY90], [KY90]) acetate accumulated up to 5 $g \cdot L^{-1}$ only during the final hours of the fermentation. Because of the tyrosine control, tyrosine was only detectable during the feeding phase.

Additional experiments to test the robustness of this approach were carried out on pilot scale. Using the same process parameters and feeding strategies, experiments were performed in a 300-L bioreactor. Figure 4.24
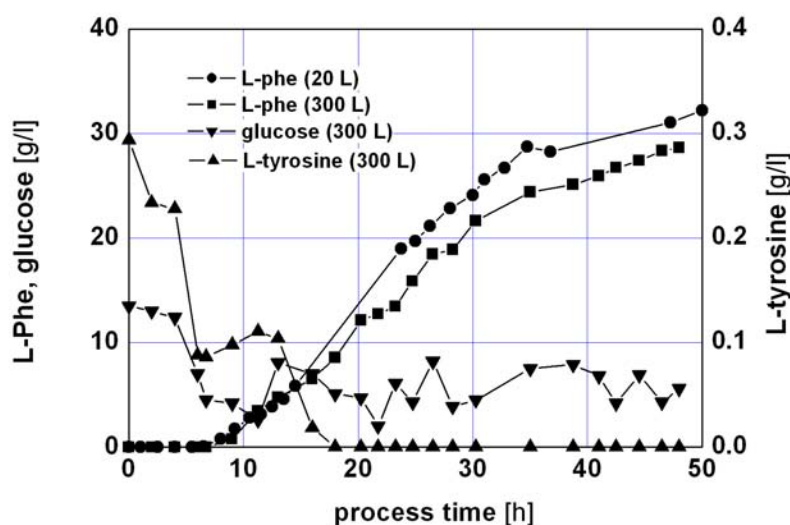
FIGURE 4.24. Concentration courses of L-Phe, glucose and tyrosine in the 20-L approach as well as in the 300-L fed-batch process. Both processes used *E. coli* 4pF20 with glucose control (set point: 5 $g \cdot L^{-1}$) and tyrosine control ($m = 1.0$).

shows the course of glucose, tyrosine and L-Phe in this approach. The comparison with the L-Phe curve of the 20-L bioreactor reveals a high similarity between the 300-L and the 20-L process. Thus it was concluded that an appropriate process (control) strategy was found that is adaptable to different geno- and phenotypes of tyrosine auxotrophic L-Phe producing *E. coli* and that can also be applied in pilot scale experiments.

4.4.2   PTS⁻ L-Phe Producer

> Significant parts of the following subsection represent yet unpublished results and were taken from the current Ph.D. thesis of N. Rüffer [Rüf03] and from the master thesis of R. Bujnicki [Buj01] which have been co-supervised by the author.

As presented in subsection 4.2.2, various authors already outlined the beneficial effects of the native PTS inactivation and its replacement by an alternative, non-PEP consuming glucose uptake system for the production of DAH(P) or other AAA pathway derivatives. In the case of DAH(P), the theoretical DAH(P)/glucose yield of 43 % $mol \cdot mol^{-1}$ could be doubled to 86 % $mol \cdot mol^{-1}$, which was almost achieved by Baez *et al.* [BBG01]. Own studies (see section 3.5) showed that a maximum L-Phe/glucose yield

of 59.7 % $mol \cdot mol^{-1}$ is possible provided that the tricarboxylic acid cycle is inactive thus concluding that either high phosphoenolpyruvate synthase activity (Pps) completely redirects the carbon flux from PYR to PEP or no PEP is produced because a non-PEP consuming glucose uptake system is used[14].

Motivated by these promising perspectives, the strain *E. coli* 20pMK12 was constructed by our cooperating partners, as indicated in Table A.1 (see section A.1.1, Appendix). It is noteworthy that the strain's genotype is similar to *E. coli* 4pF20, which was introduced in the preceding subsection, except for the glucose uptake system used. While *E. coli* 4pF20 realized glucose consumption via the native PTS, *E. coli* 20pMK12 possessed an completely inactivated PTS together with the plasmid-encoded overexpression of *glf* (coding for the glucose facilitator originating from *Zymomonas mobilis*)[15]. Because previous experiments of Krämer [Krä00] revealed a negative impact of the additional *glk* (coding for glucokinase) overexpression in such strains, the incoming glucose had to be phosphorylated by the wild-type, ATP dependent glucokinase in *E. coli*.

In analogy to the experiments presented in the preceding subsection, lab-scale fermentations using a 20-L bioreactor were conducted, following the same protocols, applying the same process controls and using the same media as already presented. However, in contrast to the previous procedure, only 10 μM IPTG were used for induction after OD_{620} ~10 - 12 was achieved. The relatively low IPTG amount turned out to be optimal to induce the membrane based *glf* protein appropriately, although the slightly higher amount of 25 μM IPTG seemed to be favored for the co-expression of plasmid-encoded $aroF^{fbr}$ and $pheA^{fbr}$ [Rüf03].

Based on previous findings of Weisser *et al.* ([WKSS95], [WKS96]), who characterized the glucose facilitator by assigning a glucose-specific K_M value of 4.1 mM, an experimental series was performed studying the L-Phe production at different extracellular glucose levels of 0.5, 5.0 and 30 $g \cdot L^{-1}$, which equals about 3, 30 and 170 mM respectively. Hence, the first glucose setpoint is expected to limit glucose uptake, while the other glucose levels should allow an unlimited glucose consumption.

As illustrated in Figure 4.25, the primary chosen setpoints of 0.5, 5.0 and 30 $g \cdot L^{-1}$ were well realized in the fed-batch experiments using *E. coli* 20pMK12. All fermentations reached similar biomass concentrations

---

[14]It is noteworthy that 59.7% $mol \cdot mol^{-1}$ are equal to 89.6% C-atom yield owing to the formation of the C9-skeleton L-Phe out of the C6-skeleton glucose.

[15]Additionally the feedback resistant genes $aroF^{fbr}$ and $pheA^{fbr}$ were inserted in the chromosome.
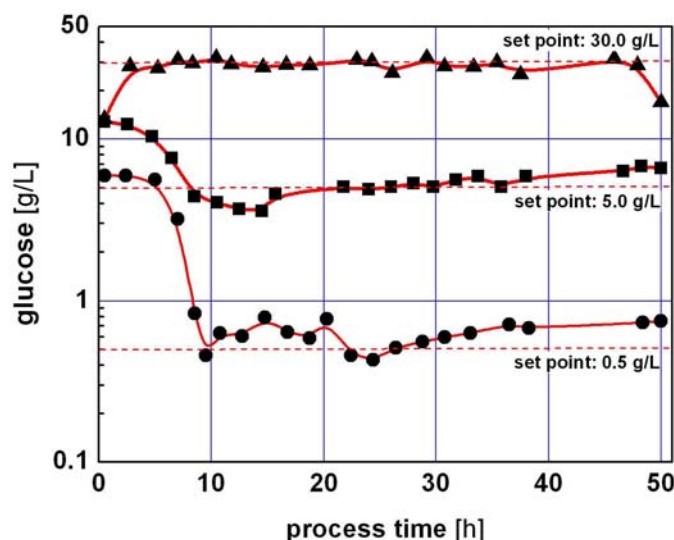
FIGURE 4.25. Off-line measured glucose levels during the three lab-scale experiments using *E. coli* 20pMK12 with the glucose set points 0.5, 5.0 and 30 $g \cdot L^{-1}$ as indicated.

of about 35 $g_{CDW} \cdot L^{-1}$, although the maximum growth rate at external glucose levels of 0.5 $g \cdot L^{-1}$ was the lowest (data not shown).

Figure 4.26 depicts that the extracellular glucose levels severely affected the L-Phe formation of *E. coli* 20pMK12, which is also supported by the findings given in Figure 4.27. As shown, L-Phe formation entirely broke down after 13 hours process time when the extracellular glucose level was controlled at 0.5 $g \cdot L^{-1}$ [16]. In general, L-Phe production at 5.0 and 30.0 $g_{glu\cos e} \cdot L^{-1}$ was very similar. Only slight advantages were observed applying the concentration level of 5.0 $g \cdot L^{-1}$. Here, the initial L-Phe production was higher than at 30.0 $g \cdot L^{-1}$ glucose, which might be the result of an increased lag-phase caused by the non-physiological glucose titer. Also the acetate formation was similar in the experiments with 5.0 and 30.0 $g \cdot L^{-1}$ glucose. Only at the end of the fermentations relatively low amounts of acetate were produced (20 mM at 5.0 $g \cdot L^{-1}$ and 60 mM at 30.0 $g \cdot L^{-1}$).

Because of the diffusion driven glucose transport into *E. coli* 20pMK12 (based on the glucose facilitator used) one could assume that biomass-

---

[16] Figure 4.27 reveals that L-Phe was even consumed as indicated by the decline of the L-Phe levels measured in the biosuspension.
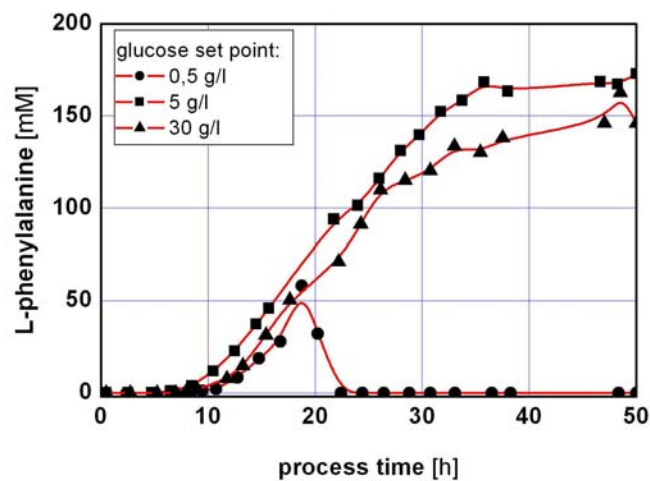
FIGURE 4.26. L-Phe courses of the three lab-scale fed-batch experiments using *E. coli* 20 pMK12 with the different glucose setpoints 0.5, 5.0 and 30 $g \cdot L^{-1}$.
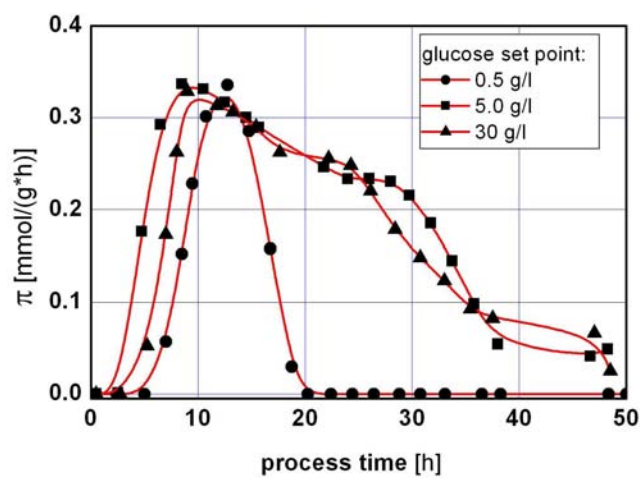
FIGURE 4.27. Biomass-specific L-Phe formation rates π_{Phe} of the strain *E. coli* 20pMK12 at different, controlled external glucose levels of 0.5, 5.0 and 30 $g \cdot L^{-1}$. Rates were derived from splined concentration profiles.
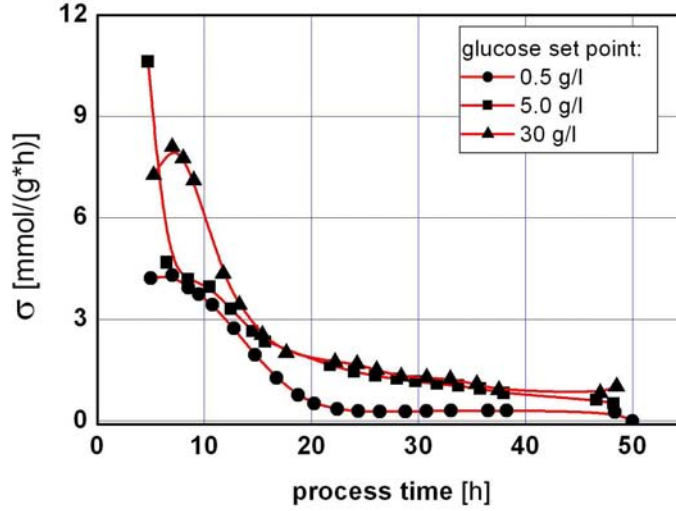
FIGURE 4.28. Biomass-specific glucose consumption rates $\sigma_{glu\cos e}$ of the strain *E. coli* 20pMK12 at different controlled glucose levels of 0.5, 5.0 and 30 $g \cdot L^{-1}$. Rates were derived from splined concentration courses.

specific glucose uptake rates, indicated by $\sigma_{glu\cos e}$, are higher at high extracellular glucose levels of 30 $g \cdot L^{-1}$ than at lower glucose concentrations. Figure 4.28 reveals that this is only partially true. While the glucose uptake at 0.5 $g \cdot L^{-1}$ was obviously limited, almost the same glucose uptake rates were found using 5.0 or 30 $g \cdot L^{-1}$ glucose as setpoints[17]. Hence, the glucose-faciliator based glucose uptake system was either saturated (according to findings of Weisser *et al.* ([WKSS95], [WKS96]) or intracellular carbon flux limitations existed that hampered a further increase of glucose consumption. The latter would (most presumably) make it necessary to co-overexpress *glk* (coding for glucokinase) and *tktA* (coding for transketolase A) as already outlined by Krämer [Krä00] or Frost *et al.* [FD95], Flores *et al.* [FXB+96], and Chandram *et al.* [CYD+03], respectively. However, such strains, which should also include the amplification of some selected genes coding for AAA pathway reactions, were not accessible during this study.

Besides, experiments with *E. coli* 20pMK12 revealed final L-Phe/glucose yields of about 12% $mol \cdot mol^{-1}$ which is lower than the previous results

---

[17]The first $\sigma_{glu\cos e}$ value at 5.0 $g_{glu\cos e} \cdot L^{-1}$ should be treated with care owing to the obviously existing high measurement errors which superimposed the correct $\sigma_{glu\cos e}$ estimation.

based on *E. coli* 4pF20. With this strain L-Phe/glucose yields of about 18 % $mol \cdot mol^{-1}$ (after 36 *h*) and 13.5 % $mol \cdot mol^{-1}$ (after 48 *h*) were observed. Additionally, the amount of DAH(P) detected in the biosuspension was 12 $g \cdot L^{-1}$ using *E. coli* 4pF20 and only 5.6 $g \cdot L^{-1}$ using *E. coli* 20pMK12, thus offering better perspectives for future *E. coli* 4pF20-derivatives provided that the obviously existing *aroB* limitation can be alleviated in future strain constructions.

4.5 *ISPR* Process Development

Backman *et al.* [BOM$^+$90], the authors of one of the most successful L-Phe production process published so far, outlined that '*...contrary to conventional wisdom, the tyrosine-specific DAHP synthase determined by aroF is in fact inhibited by phenylalanine...*'. Own studies (Jossek, unpublished) revealed that 30% of this AroF^{fbr}[18] activity is lost in the presence of only $3\ g \cdot L^{-1}$of L-Phe. This is remarkable because no active L-Phe export system is known so far (apart from the 'vague' indications given by Grinter *et al.* [Gri98]). Hence, L-Phe is supposed to permeate the cellular membrane basically by diffusion [JK96] which necessitates even higher L-Phe levels inside the cell than outside in the supernatant.

Regarding the DAHP isoenzymes in *E. coli,* which are intended to ensure high carbon fluxes into the AAA pathway, the consequences are severe. Of the three potential candidates for DAHP synthesis, namely AroF, AroG and AroH, only AroH can be assumed to convert E4P and PEP to DAHP unaffected by high L-Phe titers. AroG, which is responsible for more than 80% of DAHP synthase activity in wild-type strains, is known to be strongly feedback regulated by L-Phe. As mentioned, AroF activity seems to be strongly inhibited by L-Phe titers as well. Therefore, merely AroH, which has already been qualified to play only a minor role in wild-type strains, is left to catalyze 'high' carbon fluxes into the AAA pathway (for details see also section 2.6.1).

Backman *et al.* [BOM$^+$90] successfully solved this problem because they '*...adopted an historically proven approach and isolated feedback-inhibition-insensitive mutations in the gene(s) for DAHP synthase by means of resistance to toxic amino acid analogues...*' and thus selected an appropriate *E. coli* L-Phe producer. Because such strains were not accessible and a corresponding strategy could not be followed in this project, a different approach was aimed at - namely the on-line, selective separation of the accumulating product L-Phe to prevent or reduce inhibiting, feedback regulating effects.

This strategy was also motivated by the fact that product separation and purification has to be performed anyway and that the downstream processing step, although sometimes overlooked, not infrequently dominates the total production costs. Hence, establishing an *in situ product removal* (*ISPR*) approach offers the possibility to overcome the product inhibition problem concomitantly allowing an overall process optimization which could finally reduce the production costs.

---

[18]Please note that AroF^{fbr} codes for the tyrosine (and not phenylalanine !) feedback resistant mutant of wild-type AroF that was used in previous strain constructions such as *E. coli* 4pF20.
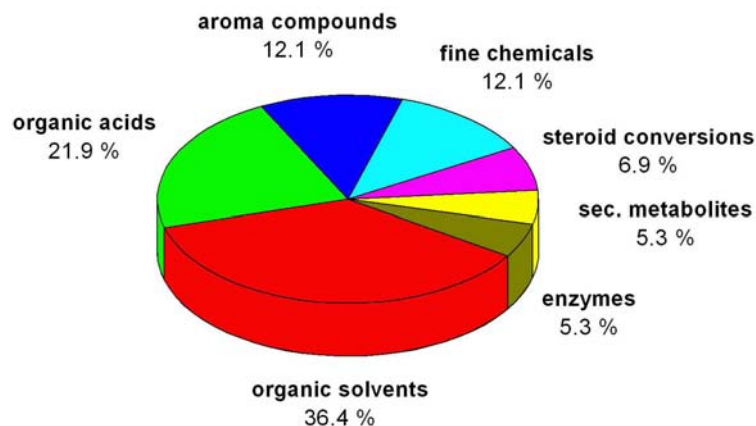
FIGURE 4.29. Percental distribution of the 247 microbial, whole cell *ISPR* projects (of the last 20 years) with respect to the product classes given by Stark and von Stockar [SS03].

Comprehensive examples of *ISPR* reviews covering the last 20-years activities for product removal from whole cell (microbial) bioprocesses are given by Freeman *et al.* [FWL93], Lye and Woodley [LW99], Schügerl [Sch00] and Stark and von Stockar [SS03]. The first defined *ISPR* as '*...the fast removal of product from a producing cell thereby preventing its subsequent interference with cellular or medium components.*' They also pointed out that *ISPR* processes are intended to increase product/substrates yields together with process productivity by aiming at alleviating three different drawbacks:

- to overcome product inhibition

- to minimize product losses

- to reduce the number of subsequent downstream processing steps.

In the case of L-Phe, this primarily holds true for the first and the last item.

Figure 4.29 indicates that *ISPR* process development so far was dominated by approaches focusing on the removal of organic solvents and organic acids. Prominent examples are ethanol and lactic acid separations, which

contributed to each class by 70 % and 55 %, respectively [SS03]. Accordingly, these two substances represent the most successful *ISPR* applications. Separating ethanol (and also butanol) from fermentations resulted in a 20 % reduction of the manufacturing costs, as reported by Roffler *et al.* [RBW87], Daugulis *et al.* [DAM91] and Groot *et al.* [GdLL92]. The yeast-based BIOSTIL process consisting of the continuous ethanol distillation with cell retention by centrifugation [EFD91] succeeded on an industrial scale in Brazil, where sugarcane is excessively available and inexpensive as a renewable raw material [SS03]. Recently, Cargill Dow Polymer LLC (Midland USA) started their 140 kilotons-scale polylactide production based on sugar in Blair (Nebraska, USA). This process is supposed to make use of the patented extractive lactic acid fermentation using pressurized CO_2 (17 bar) together with tertiary amines as organic solvent on industrial scale [SS03].

Despite these successful examples it is noteworthy that industrial or pilot scale *ISPR* processes are still rare. Of the 247 *ISPR* approaches reviewed by Stark and von Stockar [SS03] only a few managed to achieve pilot or even technical scale, which was predominantly caused by the increasing technical complexity (coinciding with increasing investment costs) which was not fully compensated by the *ISPR* benefits achieved. Therefore, it is a common statement of all reviews ([FWL93], [LW99], [Sch00], [SS03]) that future *ISPR* studies should consider (novel) powerful and highly selective *ISPR* techniques preferably to remove high added value products to establish robust and economic processes[19].

Studying the *ISPR* examples published so far, the striking fact is found that no L-Phe based process has been presented up to now[20]. This might be surprising because L-Phe market prices are much higher than those of ethanol or lactic acid thus fulfilling the precedingly mentioned demand to focus on products with higher value. Additionally, selective separation techniques such as reactive extraction/perstraction only play a minor role of about 15 % of all reviewed *ISPR* approaches [SS03]. Again, this might be unexpected because these technologies offer the possibility to selectively remove the product from the biosuspension, as supposed.

Hence, motivated by the biological necessity to separate L-Phe from the fermentation supernatant the aim was followed to develop an *ISPR* process, preferably by applying the selective approach of reactive-extraction,

---

[19]One example of such novel *ISPR* approaches was recently presented by Stark *et al.* [SKM+03] who illustrated the applicability of novel microcapsules for the recovery of alcohols (but also organic acids) inside the bioreactor.

[20]In general, *ISPR* processes for the separation of amino acids are very rare. Only glutamate was reported to be removed by hydrophobic adsorption [SS03].

to enable the on-line separation of the product thus reducing its inhibitory affect on L-Phe formation concomitantly concentrating the aromatic amino acid for further downstream processing.[21]

4.5.1 Basics of Reactive Extraction

To characterize the L-Phe separation, it is meaningful to remember some physicochemical properties of the aromatic amino acid (see also Table 2.5, subsection 3.2): L-Phe is soluble in water up to 30 $g \cdot L^{-1}$ (under typical fermentation conditions: pH 6.7, $T = 36°C$) and possesses an affinity to organic solvents owing to the aromatic ring structure. Depending on pH, L-Phe cations, zwitterions or anions exist that provide a molecule charge useful for L-Phe separation. Own preliminary experiments using the principle of Donnan dialysis ([Miy96a], [Miy96b], own data not shown) had revealed that a purely charge-dependent amino acid separation was not sufficiently L-Phe selective. An additional selectivity barrier - such as an organic phase - needed to be installed which could be realized by reactive extraction. Compared to physical extraction, reactive extraction offers higher efficiencies owing to higher distribution coefficients [ADS89] and it allows the separation of polar agents such as organic and amino acids in contrast to non-carrier-dependent extraction processes [Sch94]. Furthermore, the working temperatures of reactive-extraction and fermentation processes are similar.

The principle of reaction extraction is depicted in Figure 4.30. The scheme considers an external, fully integrated reactive extraction unit in order to avoid any unwanted loss of fermentation medium. L-Phe is separated from a cell-free fermentation solution which can be obtained by biomass retention in a cross-flow ultrafiltration unit. Using for instance hollow fiber modules to install supported liquid membrane (SLM) based L-Phe transfer, the aqueous solution can be brought into contact with an organic phase[22]. An ion exchange takes place at the aqueous/organic interface. If cation-specific carriers are used in the organic phase, a proton is transferred into the aqueous phase while at the same time L-Phe$^+$ is loaded onto the carrier. If anion-specific carriers are used, anions are exchanged

---

[21]It is noteworthy that L-Phe is usually separated and purified from biosuspension following a multi-step procedure consisting of cell separation by ultrafiltration, active carbon-based cleaning of the cell-free permeate, adsorption/ion-exchange and final crystallization ([Leu96], [ASJP97]).

[22]It is noteworthy that hollow fiber modules are not necessarily needed to realize the aqueous/organic interface, as it will be shown in the following sections. However, at the beginning of the project the aim was followed to reduced the potentially negative impact of the organic phase on the fermentation culture as much as possible. Therefore, the hollow fiber system was primary favored beause it offers the advantage of a dispersion-free L-Phe transfer.
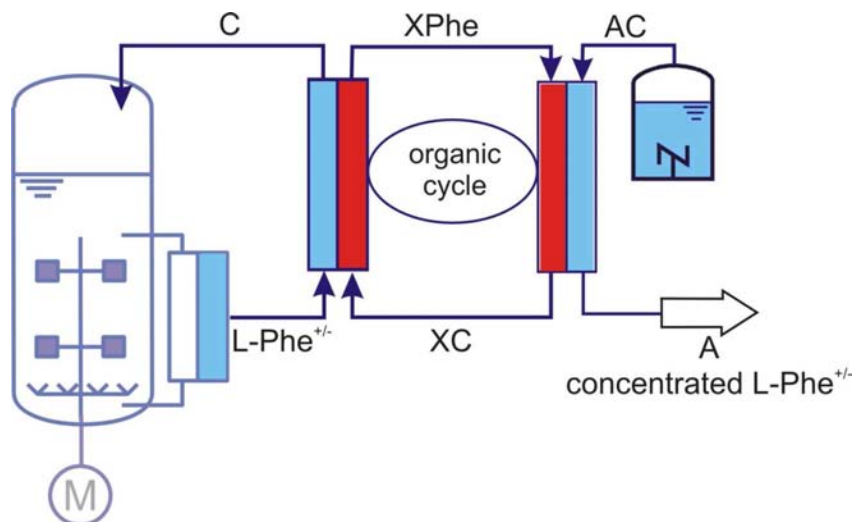
FIGURE 4.30. Principle of reactive extraction shown for L-Phe, which might preferably be charged as anion or cation (or zwitter ion) dependent on the present *pH*. X codes for a carrier, C encodes the counterion and A represents the acceptor phase. For explanation of the mechanistic principle see text.

by analogy. In Figure 4.30 carriers are indicated by X and counter ions (for example: protons) by C. It is assumed that the ion-exchange process occurs dispersion-free, which is mainly caused by the use of the hollow fiber modules that reveal laminar flows inside the fibers (details will be given in the following sections). However, due to the solubility of carriers in aqueous solution, a diffusive carrier and solvent transport into the aqueous phase must be taken into account. After transport of carrier/L-Phe complex to the organic/aqueous interface, L-Phe is released into the stripping phase while the carrier is loaded with the counter ion again and regenerated for the next extraction cycle. As the driving force for the extraction process is not the L-Phe concentration alone, but the stripping phase concentration of counter ions (which could be freely chosen), a concentration of L-Phe against the gradient of the amino acid is possible. Thus, a significant reduction of liquid volumes can be achieved for further product purification, for instance by precipitation[23].

In general, one can think of a variety of possible carriers to be used in the organic phase. However, because it was a major aim to develop an *ISPR*

---

[23] Please notice that the flow scheme of Figure 4.30 can also be changed to countercurrent flow inside the extraction or back-extraction modules. However, own studies revealed that the resulting L-Phe mass transfer differences are small because usually L-Phe mass transfer limits are usually dominated by other effects (see following sections).

TABLE 4.2. Cation- and anion-selctive carriers used for L-Phe removal with the aid of reactive extraction

	D$_2$EHPA[b]	DNNSA[c]	Aliquat 336[d]	Alamine 308[e]
supplier	Bayer	King Ind.	Henkel	Henkel
M [g/mol]	322	495	404	353
density [kg/L]	0.97	0.87	0.88	0.80
flashp. [$^\circ C$]	198	-1.1	110	190
sol. [g/L][a]	<1	<1	<1	<1
affinity	cations	cations	anions	anions

[a]solubility in H$_2$O, 20$^\circ C$

[b]Di-2-ethylhexyl phosphonic acid

[c]Dinonylnapthalene sulfonic acid

[d]Trioctylmethyl ammonium chloride

[e]Tri-isooctylamine

process for pilot or technical scale, only these carriers were considered that have been commercially available. Table 4.2 lists the basic characteristics of the four carriers used for the experiments.

In the past, the application of integrated reactive extraction in fermentation processes was mainly focused on the extraction of organic acids ([Sch00], [SS03]). For instance, lactic acid was separated on-line and off-line from e.g. *Lactobacillus delbrueckii* fermentations with the aid of the anion-specific carrier Alamine 336 in small- and lab-scale approaches ([SHHM91], [YW91], [HTT+95],[YJS96], [TBM01], [WHVP02]). The separation of citric acid during continuous fermentations with *Aspergillus niger* was also described ([WB98a], [WB98b]). Also the separation of lactic acid from a fermentation solution in the presence of citric and acetic acid was studied [FS99]. Using Alamine$^\circledR$ 304-1 (triaurylamine) propionic acid (together with acetic acid) was concentrated from fermentations with *Propionibacterium thoenii* [GRGG99]. Additionally the general applicability of Aliquat 336 for the *in situ* extraction of carboxylic acids from *Pseudomonas putida* cultures was investigated [JQMS99]. Other examples such as the integrated separation and esterification of ethanol using *Saccharomyces cerevisiae* (together with an immobilized lipase) [ORCAB97] were reported as well. Additionally, the antibiotic penicillin V and/or G was subject to numerous *ISPR* approaches using centrifugal extractors [LS87] and hollow fiber modules ([YC00], [LSS02]).

In addition to these applications, the reactive extraction mechanism was also studied for amino acid removal within several projects ([THW86], [YYG86], [DMR90], [TYI+91],[UHLC92], [LKR+96], [ASJP97], [WJM97], [DWJ+99], [COG01], [LD03]). Because of the amino (-NH$_2$) and the carboxyl-group (-COOH), amino acids behave as cations at low pH, as anions at high pH and they are of zwitterionic character at an intermediate pH

[Sch94]. Hence anion-selective carriers such as Aliquat 336 or Alamine 336 or cation-selective carriers such as D_2EHPA or DNNSA can be applied for amino acid removal depending on the *pH*. In general, anion-selective carriers were predominantly used for amino acid treatment, which holds also true for L-Phe[24]. As organic solvents for instance octane, octanol, toluene, n-paraffine or methyl-isobotyl ketone were studied. Corresponding examples are published by Teramoto *et al.* [TYI+91]. Boyadzhiev and Atanassova [BA94], Escalante *et al.* ([EOI96], [EAOI98]), Scarpello and Stuckey [SS00], Liu and Dai [LD03] and Pursell *et al.* [PMTS03] also including modeling aspects of the L-Phe mass transfer.

Despite the promising results which were presented in all these studies, it should be stressed that none of these approaches was applied in an *ISPR* process for L-Phe separation and concentration. Most of the L-Phe reactive extraction studies used 'aqueous model solutions' instead of complex fermentation media and focused their interest only on anion-selective carriers like Aliquat 336. However, this carrier is suspected to be toxic for cells which obviously hampers its use in an *ISPR* approach. Hence it was the aim of the following studies to develop an *ISPR* process using an appropriate reactive extractive system for L-Phe separation.

4.5.2   Identifying the Reactive Extraction System

Significant parts of the following subsection were already published in Maaß *et al.* [MGK+02] and considered in the patent application [MTP+00]. Results were acquired during the Ph.D. thesis of D. Maaß [Maa00] and during the master thesis of K. Silberbach [Sil99] and N. Kaftzik [Kaf99] who were co-supervised by the author.

Experimental Constraints

The aim of developing an *ISPR* process for on-line L-Phe separation (and concentration) represents an ambitious goal, since any inhibitory influence of downstream processing on the fermentation process should obviously be prevented. In order to avoid loss of unseparated product or fermentation components, it was planned to fully integrate the downstream separation step into the fermentation process. Thus, the fermentation medium that was processed should be completely recycled, which represents another challenge since inhibitory effects of L-Phe separation would directly influence *E. coli* cultivation.

---

[24] Additionally, L-Phe separation approaches using charged membranes were reported as well [IFKN97].

With respect to the carrier/solvent composition that had to be identified, the following boundary conditions need to be met:

- Carriers and organic solvents should possess low water solubility.

- The carriers should be readily soluble in the organic phase.

- No tendency for emulsification should occur in the total aqueous/organic system.

- Due to the application of reactive extraction integrated in a bioprocess, sufficient biocompatibility should be achieved.

- The handling of carriers and solvents should not imply unnecessary safety risks.

- Carriers and solvents should be "cheap" in order to limit downstream processing costs.

As a result, the solvents kerosene, butyl stearate, decanol, octanol and xylene were used for preliminary experiments. To consider L-Phe extraction at high pH values (above 9), the liquid cation exchangers tri-octyl-methyl ammonium chloride (Aliquat 336 , Henkel, Germany), which represents a standard liquid anion exchanger for the extraction of heavy metals on an industrial scale, and Tri-isooctylamine (Alamine 308, Henkel, Germany) were considered. Cation-selective reactive extraction should be tested with D_2EHPA or DNNSA. $(NH_4)_2SO_4$, NaOH, KOH, H_2SO_4 and KCl were used as different counter ion candidates.

Carrier Identification

Preliminary experiments were conducted according to the protocol given in subsection A.3.15 (Appendix). Figure 4.31 shows a comparison of extraction degree results using different carriers under appropriate pH conditions and applying equation A.2, Appendix. For cation-specific L-Phe$^+$ extraction with D_2EHPA and DNNSA a pH below 3 was set. Anion-specific L-Phe$^-$ extraction with Aliquat 336 and Alamine 308 was performed at a pH above 9. In this way, L-Phe ions were extracted out of aqueous solution, at the same time leading to the generation of new L-Phe ions after equilibration thanks to dissociation in the aqueous phase. A start concentration of $10 \ g \cdot L^{-1}$ L-Phe in the aqueous phase was chosen in each experiment. In order to prevent carrier-limited L-Phe extraction out of the organic kerosene phase, 10% v/v carrier in kerosene was used. In the case of Aliquat 336 this concentration was reduced to 5% v/v carrier in kerosene.

From Figure 4.31 the conclusion can be drawn that Alamine 308 is not suited for L-Phe separation due to the very low degree of extraction. On the contrary, although only relatively low amounts of Aliquat 336 were
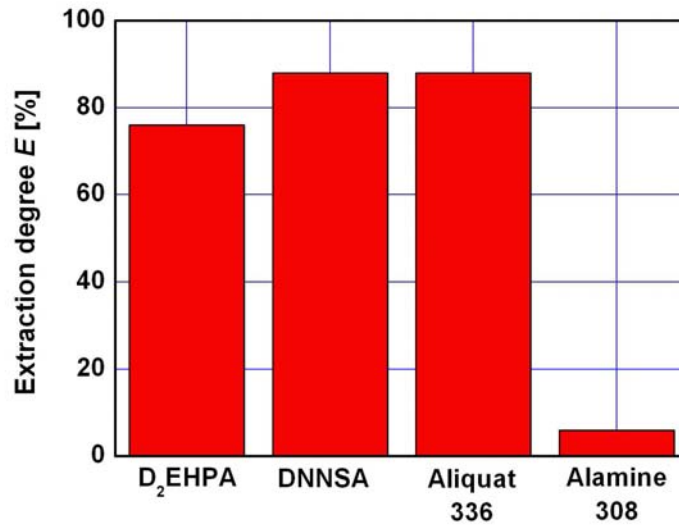
FIGURE 4.31. Comparison of the four carriers used at appropriate *pH* for the separation of L-Phe ions from aqueous solution in separation funnels.

used, a high extraction degree of 88 % was achieved. Extraction results using D$_2$EHPA and DNNSA were similar. Thus, Aliquat 336, DEHPA and DNNSA were favored for subsequent experiments considering the biological compatibility.

Biocompatibility tests were carried out in *pH*-controlled shaking flasks using the FedbatchPro^{TM}-equipment of DASGIP mbH, Jülich, Germany. For batch experiments the precedingly introduced strain *E. coli* 4pF20 was cultivated in the shaking flask medium containing 15 $g \cdot L^{-1}$ glucose (see subsections A.1.1 and A.2.1, Appendix). A number of twelve 1-*L* shaking flasks were used in parallel with the *pH* set point 6.5 at 37°*C* and a working volume of 100 *mL*. Cultures were inoculated at 10 % of the working volume. After 5 hours process time, carriers (15 $\mu L \cdot L^{-1}$) were added to the culture to simulate the effect of carrier toxicity on growth. The amount of carrier addition was chosen such that the maximum solubility was reached. The effects on cell growth were monitored by optical density measurements as depicted in Figure 4.32.

As shown, the addition of the quaternary ammonia salt Aliquat 336 was followed by an immediate growth stop. Compared to the reference fermentation without carrier addition, no significant growth effect could be
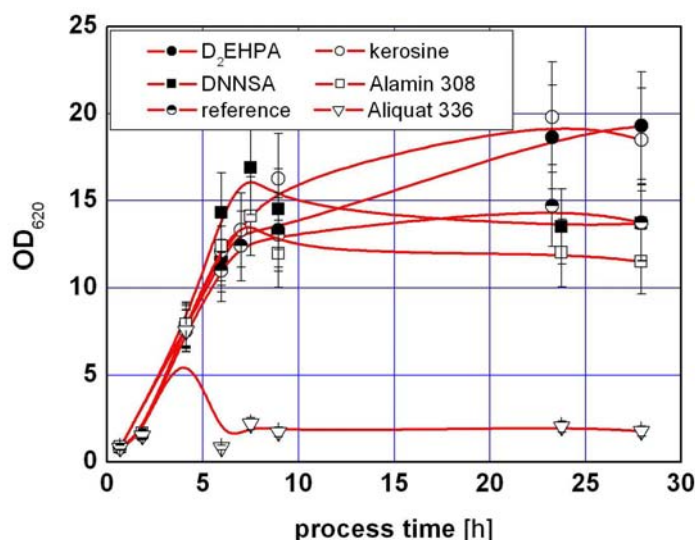
FIGURE 4.32. Comparison of OD_{620} courses in pH-controlled shaking flasks using the strain *E.coli* 4pF20 after addition of the anion-selective carriers Alamin 308, Aliquat 336, the cation-selective carriers D_2EHPA, DNNSA and after addition of kerosine alone. Carrier addition was performed after 5 hours process time such that the maximum solubility was reached.

observed after the addition of D_2EHPA, DNNSA or Alamine 308. These carriers are apparently tolerated by *E. coli*.

As a conclusion from the batch experiments with separation funnels and shaking flasks, the anion-specific carriers Alamine 308 and Aliquat 336 were excluded from further investigations - the first due to insufficient extraction capability, the second due to *E. coli* toxicity. Additional extraction experiments in separation funnels were carried out, now focusing on the back extraction of L-Phe. It was found that back extraction from the DNNSA organic phase was not complete (data not shown). L-Phe was not fully removed from DNNSA, which was indicated by an incomplete L-Phe balance. Furthermore, handling of DNNSA represents a high safety risk compared to D_2EHPA, since the DNNSA flash point is $-1.1°C$. Thus, D_2EHPA was selected for reactive extraction process development.

Solvent Identification

Using 10% v/v D_2EHPA for extraction experiments, different solvents were studied for the extraction of 10 $g \cdot L^{-1}$ L-Phe in separation funnels. As
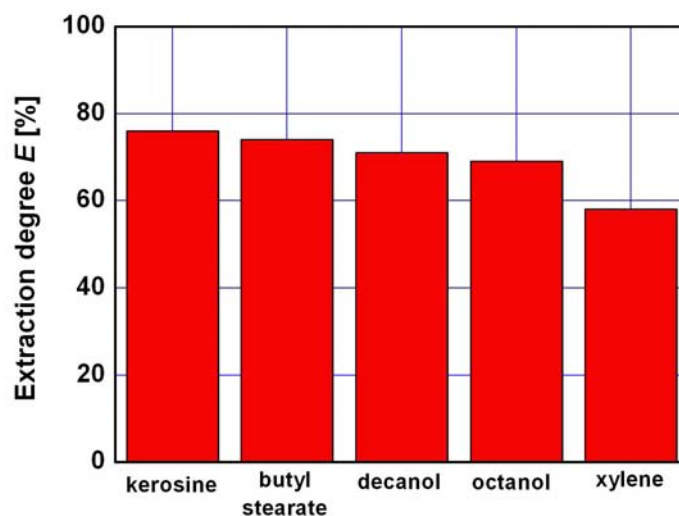
FIGURE 4.33. Comparison of the extraction degree E achieved in separation funnel experiments usind the organic solvents and the cation-selective carrier D_2EHPA for L-Phe separation from aqueous solutions.

indicated in Figure 4.33, kerosene achieved the highest extraction degree E. Kerosene represents a C12 - C16 fraction of mineral oil and it is relatively cheap and readily available on the market. It possesses a low water solubility (5-10 $mg \cdot L^{-1}$). Hence, with respect to the previously mentioned criteria, kerosene was regarded as a promising extraction solvent.

After the solvent identification based on separation funnels was finished, the carrier D_2EHPA together with kerosene was tested in fed-batch fermentations with the L-Phe producing *E. coli* strain 4pF20. Fermentations were performed in a 7.5-L bioreactor that was equipped with an ultrafiltration unit (hollow fiber module, 500 kDa cutoff, 0.042 m^2 membrane area, 1 mm inner fibre diameter; Schleicher & Schuell, Germany) applying the protocols as already presented (see subsections A.1.1, A.2.1, A.3.3, A.4.2, Appendix). A mixture of 10 % v/v D_2EHPA/kerosene (150 $mg \cdot L^{-1}$) was continuously added to the drained-off, cell-free permeate before the total reflux was recycled into the bioreactor. In total, 3.2 mL of D_2EHPA/kerosene mixture was added thus simulating the D_2EHPA/kerosene effect caused by reactive extraction that was not yet installed.

As indicated in figures 4.34 and 4.35, significant changes of microbial L-Phe production were observed after the start of D_2EHPA/kerosene addition
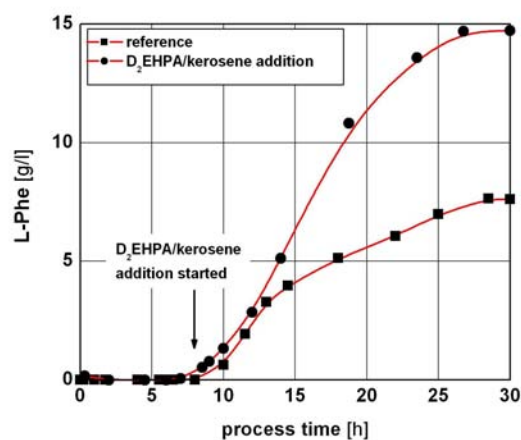
FIGURE 4.34. Effect of D_2EHPA/kerosene addition on the L-Phe production using *E. coli* 4pF20 in a 7.5-*L* bioreactor with an ultrafiltration loop as indicated in the text. The course of L-Phe production with D_2EHPA/kerosene addition is compared to a reference fermentation without addition of the extractive components.
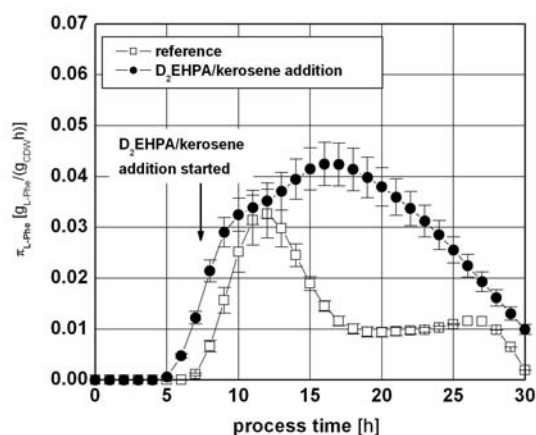
FIGURE 4.35. Effect of D_2EHPA/kerosene addition on the biomass-specific L-Phe formation π_{L-Phe} using *E. coli* 4pF20 in a 7.5-*L* bioreactor with an ultrafiltration loop as indicated in the text. The π_{L-Phe} course with D_2EHPA/kerosene addition is compared to a reference fermentation without addition of the extractive components. Rates were estimated based on splined concentration courses.

at approximately 9 h process time compared to the reference fermentation. In the case of D$_2$EHPA/kerosene addition, considerably higher L-Phe titers were achieved than without carrier/solvent addition. When the reactive-extraction unit was experimentally simulated, L-Phe titers were almost doubled. Because the other process conditions in the two fermentations were comparable, this effect is solely attributed to the addition of the carrier and/or the solvent.

To elucidate the phenomenon, biomass (cell-dry weight) specific L-Phe production rates π_{L-Phe} were compared in Figure 4.35. High L-Phe formation rates $\succ 0.03 \; g_{L-Phe} \cdot (g_{CDW} \cdot h)^{-1}$ were reached when D$_2$EHPA/kerosene was supplied for approximately 15 hours. This high level L-Phe production was only maintained in the reference fermentation for 2 hours. Obviously, the addition of extractive components sustained L-Phe production. Further studies adding the carrier alone revealed that this effect is mainly caused by D$_2$EHPA (data not shown). As a working hypothesis it was assumed that the cell-membrane integrity is changed in the presence of D$_2$EHPA thus facilitating the L-Phe export which coincides with a reduction of its inhibiting impact. In total, this beneficial effect led to a doubling of final L-Phe/glucose yield in the case of D$_2$EHPA/kerosene addition compared to the reference fermentation.

Hence, the interim conclusion can be drawn that the fully integrated reactive extraction unit is not expected to inhibit microbial L-Phe production. On the contrary, an increase of L-Phe/glucose yield due to a prolonged high level L-Phe production phase can be anticipated.

Counter Ion Identification

The most efficient counter ion system was identified by qualifying batch extraction results using separation funnels. The organic phase consisted of 10 % v/v D$_2$EHPA in kerosene which was preloaded by an extraction from 10 $g \cdot L^{-1}$ L-Phe solution. Two counter ion levels (1 and 2 molar) were studied. In the case of KCL, only 1 M was used due to the appearance of emulsions at 2 M. Figure 4.36 gives an overview of the total extraction degrees E that were achieved using different counter ion systems. Overall extraction degrees were calculated referring to the start concentration of L-Phe in the aqueous donor phase.

Back extraction of L-Phe from D$_2$EHPA is based on cation exchange. Thus, cations such as $(NH_4)^+$, Na^+, K^+ and H^+ should be preferred. Experiments with NaOH and KOH showed a clouding of the aqueous phase which was caused by microemulsions produced by the entrainment of carriers into water. Despite the high extraction degrees of NaOH and KOH, these systems were omitted for further investigations because the observed
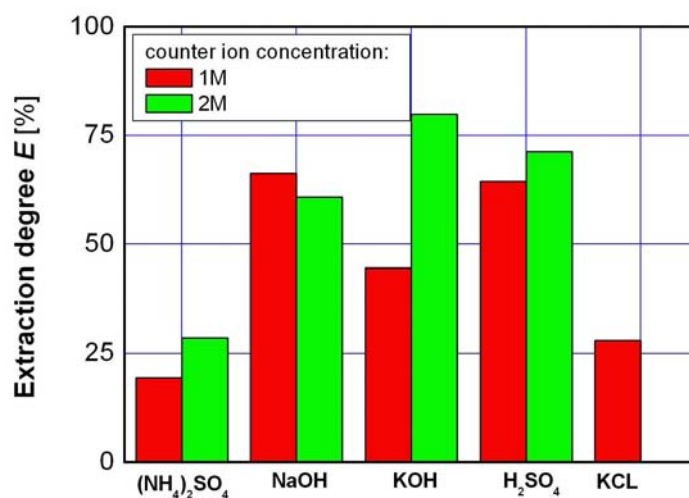
FIGURE 4.36. Overview of the different extraction degrees E achieved after back extraction with the respected counterions at 1 and 2 M using the L-Phe-preloaded D_2EHPA/kerosene organic phase.

unstable aqueous/organic interfaces were expected to cause severe problems in a pilot process scale-up. When 1 molar KCl was used no clouding was found. However the extraction degree was relatively low. Because relatively high extraction degrees without clouding were measured with H_2SO_4, these counterions were used for further experiments.

Extraction Equilibrium

Extraction equilibrium studies were conducted using separation funnels. Different start pHs at 2, 5.9, 7.3, 9.5 and even 12 were chosen in order to investigate the cation-selective L-Phe extraction with 10% v/v D_2EHPA/ kerosene. The start pH was installed by NaOH titration and 10 $g \cdot L^{-1}$ L-Phe was added at the beginning.

As indicated in Figure 4.37, only a negligible amount of L-Phe cations should exist at high pH values such as 12. However, to our surprise, a significant L-Phe extraction was observed nevertheless. To elucidate the effect, 10% v/v D_2EHPA/kerosene was brought into contact with an aqueous phase of pH 12. Hence similar extraction conditions were installed except for the L-Phe addition, which was omitted. After phase mixing and settling a final pH of 4.9 was measured. It was thus assumed that the dissociation
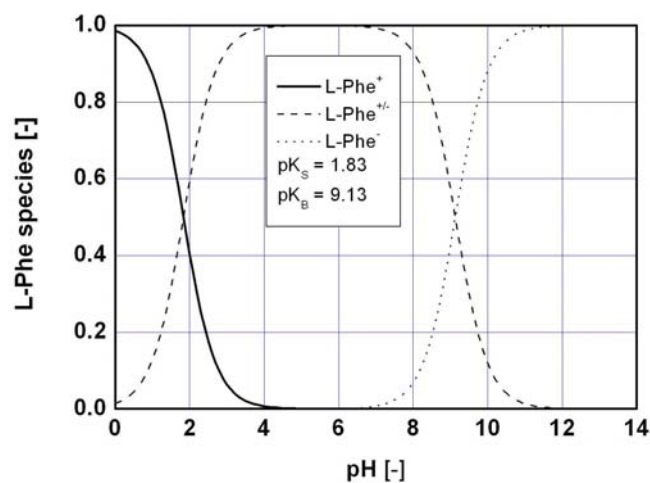
FIGURE 4.37. Illustration of the zwitterionic character of L-Phe (at room temperature) depending on the *pH* installed. At low *pH*, cations predominate, while prevailing concentrations of anions are found at high *pH*. Zwitterions are observed at intermediate *pH* values.
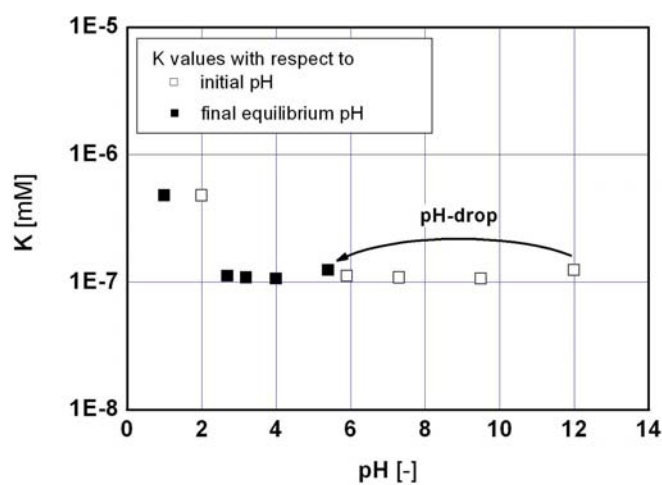
FIGURE 4.38. Estimation of the equilibrium constant K for L-Phe extraction using D_2EHPA/kerosene in the organic phase. The *pH* drop in the aqueous phase owing to the dissociation of phosphoric acid is indicated as well.

TABLE 4.3. Characteristics of the hollow fiber modul Liqui-Cell (Hoechst-Celanese Co., Charlotte, USA) used in pilot scale reactive extraction experiments for L-Phe separation

	4X28 x30 240ID
length [cm]	100
diameter [cm]	10
temperature range [$^\circ C$]	1 - 60
effective are. [m^2]	18.6
specific area [m^2/m^3]	3641
max. transmembrane pressure [bar]	4.14
max. operation pressure [bar]	5
number of fibers	31,800
length of fibres [m]	0.71
membrane	polypropylene
porosity [%]	40
pore size [μm]	0.03
fiber inner diameter [μm]	244
fiber outer diameter [μm]	300
membrane thickness [μm]	28

of phosphoric acid of the D$_2$EHPA was responsible for the pH drop (see Figure 4.38). As a consequence, cationic L-Phe species are now present in the aqueous phase which could be extracted by D$_2$EHPA.

Using the approach given in subsection A.7.12 (Appendix), the estimation of the equilibrium constant K was realized, as shown in Figure 4.38. It should be stressed that the significant pH drop, as introduced in the preceding paragraph, occurred in each experiment thus ensuring the presence of L-Phe cations in the aqueous solution.

Reactive Extraction on Pilot Scale

After the series of preliminary experiments was completed, mass transfer studies were carried out on a pilot scale ensuring that the experimental setup suited to the 300-L fed-batch process, which will be presented in the following subsection. The setup consisted of two pilot-scale hollow fibre modules (see Table 4.3 and Figure 4.39) providing an effective membrane area of 18.6 m^2 for extraction and back extraction of L-Phe. For all experiments, the D$_2$EHPA/kerosene system was used together with sulfuric acid as the proton donor in the stripping phase.

Regarding a general description of the hydrodynamic condition inside the hollow fiber modules (see Figure 4.39), the characteristic Reynolds number
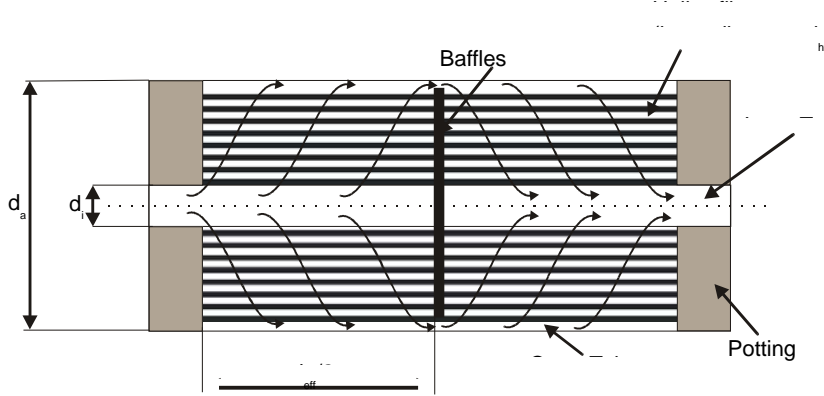
FIGURE 4.39. Scheme of the hollow fiber modules used for L-Phe separation by reactive extraction.

(Re) can be defined according to

$$\mathrm{Re} = \frac{v_{HF} \cdot d_i}{\nu} \qquad (4.2)$$

where v_{HF} denotes the superficial velocity, ν codes for the fluid viscosity and d_i represents a characteristic length (diameter). In the case of Re definition for flux inside the fibres, the inner diameter d_{HF} should be taken. For Re definition of flux outside fibers, the previously published suggestions ([CR86], [SPND98]) can be followed leading to the estimation

$$\mathrm{Re} = \frac{\bar{v} \cdot d_h}{\nu} = \frac{2\dot{V}}{\pi\nu} \cdot \frac{(d_a + d_i) \cdot \ln\left(\frac{d_a}{d_i}\right)}{l_{eff} \cdot N \cdot d_{HF}} \qquad (4.3)$$

where $\dot{V}$ describes the liquid stream, N codes for the number of fibers and d_h denotes the hydraulic diameter. The other parameters are indicated in Figure 4.39.

Using this definition, Re numbers from 11.6-23.3, 2.2-5.7 and 11.6-31.5 which correspond to flow rates from 250-500, 60-156 and 250-680 $L \cdot h^{-1}$ were realized in the aqueous donor, the organic and the aqueous stripping phase in a series of ten mass transfer experiments installing circulating streams as indicated in Figure 4.40 [25]. In addition different levels of D_2EHPA and sulfuric acid concentrations were tested thus leading to five experimental parameters together with different liquid volumes ranging from 5 to 9 L that were used in the ten mass transfer experiments as shown in tables 4.4 and 4.5.

---

[25] Because turbulent flow is expected to begin at Re number $> 2,300$, the hydrodynamic situation inside the hollow fiber modules can be characterized as strictly laminar.
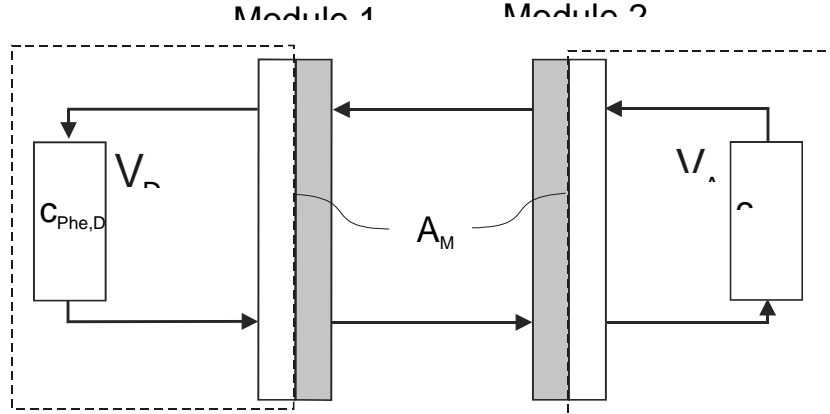
FIGURE 4.40. Setup of circulating donor, organic and acceptor phases used in the series of ten mass transfer experiments. $c_{Phe,D}$ and $c_{Phe,A}$ describe L-Phe concentrations in the donor and acceptor phase, respectively. V_D and V_A are the corresponding liquid volumes and A_M represents the effective membrane area.

Applying the simple modeling approach as shown in subsection A.7.13 (Appendix) good model approximations were achieved as indicated by the regression coefficients near to 1 found for each analysis. As already mentioned (subsection A.7.13, Appendix), the assumption of constant equilibrium concentrations in the aqueous donor and the aqueous stripping phase represents a strong simplification of real conditions where rather time-variant equilibrium concentrations occur. Hence, estimated equilibrium concentration values should be regarded as model parameters which, in case of the aqueous stripping phase, are accurately estimated.

When the resulting mass transfer coefficients are studied, an interesting correlation to experimental conditions can be identified (see Figure 4.41). For instance, the comparison of experiments 2 and 4 (also 9 and 10) indicates that increasing D_2EHPA concentrations caused rising β_D values. If experiments 1 and 3 are compared, a significant improvement of β_A is apparent, while the sulfuric acid concentration was doubled.

Because of technical constraints, Re_D was kept constant for most experiments. However, an increase of β_D and β_A can be observed in experiments 2 and 5 when Re_A was increased. This result was unexpected, but it indicates, that total mass transfer from donor to stripping phase is (obviously) limited by the organic to stripping phase L-Phe transfer. Small changes of β_A coincide with bigger changes of β_D. This statement is supported by the analysis of the Re_O effect. If experiments 3 and 6 or 2 and 7 are compared, an improvement of both mass transfer coefficients is identifiable together with a decline of Re_O. As a possible reason, one can assume that L-Phe

TABLE 4.4. Experimental setup of mass transfer experiments. Reynolds numbers for aqueous donor (ReD), organic (ReO) and aqueous stripping phase (ReA) are given together with DEHPA and H2SO4 (acid) concentrations

Nr	Re_D	Re_O	Re_A	c_{D_2EHPA}	c_{acid}
-	[-]	[-]	[-]	[v/v %]	$[M]$
1	11.6	2.2	11.6	20	1
2	11.6	5.7	23.2	10	1
3	11.6	5.7	11.6	20	2
4	11.6	2.2	11.6	30	1
5	11.6	5.7	31.5	10	1
6	11.6	2.2	11.6	20	2
7	11.6	2.2	23.3	10	1
8	11.6	2.2	11.6	10	1
9	23.2	5.7	11.6	20	2
10	11.6	5.7	11.6	30	2

TABLE 4.5. Absolute errors (delta) for mass transfer coefficients beta D and beta A and standardized equilibrium concentrations cPheD,eq and cPheA,eq are given according to the series of 10 mass transfer experiments in pilot scale. To qualify goodness of fit regression coefficients for donor rPhe,D and stripping phase rPhe,A are presented as well

Nr	$\beta_D \pm \Delta$	$\beta_A \pm \Delta$	$c_{Phe,D}^{eq,s}$	$c_{Phe,A}^{eq,s}$	$r_{Phe,D}$	$r_{Phe,A}$
-	$[\frac{cm}{s}10^{-7}]$	$[\frac{cm}{s}10^{-7}]$	$[10^{-2}]$	[-]	[-]	[-]
1	72±7.5	36±4.7	5.8±1.6	1.1±0.07	0.999	0.991
2	79±3.5	58±4.4	0	1.2±0.04	0.997	0.994
3	80±6.9	54±3.9	0.5±1.1	1±0.03	0.999	0.997
4	96±4.4	50±2.5	2.5±0.6	1±0.02	0.998	0.999
5	117±6.7	67±4.4	8.3±1.6	1.1±0.03	0.997	0.997
6	134±11.7	61±5.3	4.2±1	1.1±0.03	0.993	0.995
7	150±7.1	67±3.6	8.2±0.9	1±0.02	0.992	0.999
8	160±8.1	72±4.4	5.7±1	1.1±0.02	0.999	0.990
9	239±51.1	42±8	9.7±1.3	1.1±0.09	0.925	0.994
10	289±30.6	77±5.3	4.3±0.6	1.1±0.02	0.989	0.998
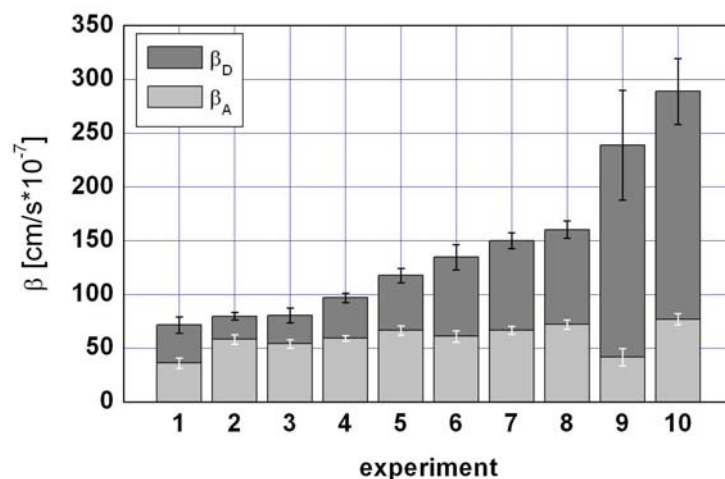
FIGURE 4.41. Overview of the mas transfer coefficients β_D and β_A achieved using the simple balance model as indicated in the text.

back extraction was such slow that still loaded carrier/L-Phe complexes were transported to the extraction module (1) at high organic phase cycling rates. Thus, extractive mass transfer was limited by the availability of 'free' carriers. However, this working hypothesis needs to be critically discussed, as it will be performed in the following subsection.

Summarizing it should be noticed that the mass transfer study identified mass transfer coefficients up to $288 \cdot 10^{-7} cm \cdot s^{-1}$ which are comparable to the results of Escalante et $al.$ [EAOI98] and Cardoso [Car97] who estimated 112 - 116 $\cdot 10^{-7} cm \cdot s^{-1}$ using Aliquat 336 in hollow fibre modules.

L-Phe Separation from Fermentation Solution

The selective separation of L-Phe from cell-free supernatant was studied using the reactive extraction setup on a pilot scale (Figure 4.42). A filtered fermentation solution (42 L) containing 25 $g \cdot L^{-1}$ L-Phe at a fermentation pH 6.5 was connected with the extraction unit. To investigate the concentration potential of reactive extraction, the stripping phase volume was only 1/6 of donor volume and 10% v/v D_2EHPA in kerosene was used. As a result, the total amount of 588 g L-Phe was extracted in 13.5 hours with an averaged permeability of 10 $g_{Phe} \cdot \left(m^2 h \right)$. A four times higher L-Phe concentration was achieved in the stripping phase compared to the donor phase. The elementary analysis of the acceptor phase revealed an

98 % cation portion of L-Phe in the stripping phase. After precipitation of the stripping phase (titration to the isoelectric point with NaOH), the dry product had a purity of more than 99 %.

Hence it was concluded that reactive extraction based on the cation-selective carrier D$_2$EHPA in kerosene using H$_2$SO$_4$ as counter ion donor in the stripping phase represents a promising system for on-line L-Phe separation in a fully integrated *ISPR* approach. Therefore the technique was studied on 300-L bioreactor scale in subsequent experiments.

FIGURE 4.42. Experimental setup used for pilot-scale reactive extraction experiments based on two LiquiCell^{TM} hollow fiber modules for extraction and back extraction, respectively.
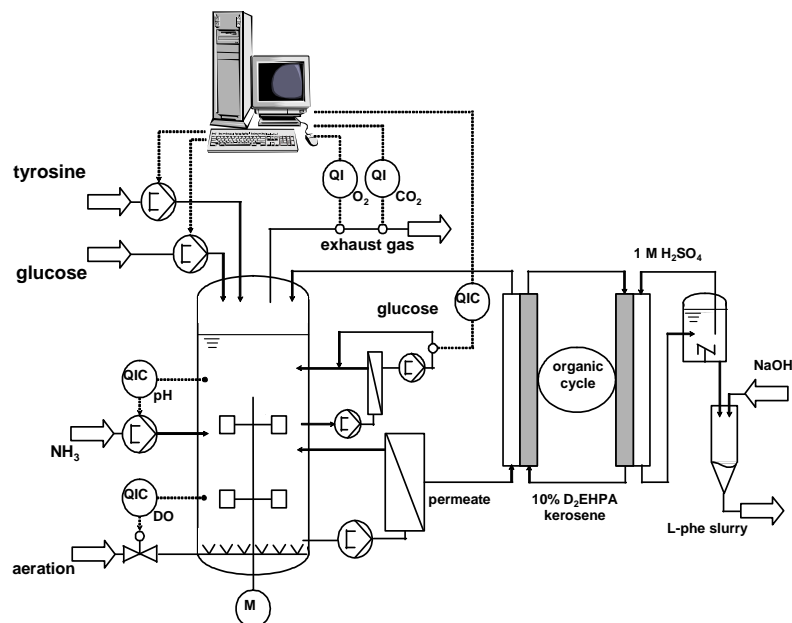
FIGURE 4.43. Setup of the total *ISPR* process using reactive extraction for on-line L-Phe separation on pilot scale. L-Phe was produced in the 300-*L* bioreactor with *E. coli* 4pF20 applying glucose and tyrosine control. Via the ultrafiltration unit, cell-free permeate was drained off to be further processed for reactive extraction. Two hollow fiber modules were installed. Final purification of L-Phe was realized via precipitation after titration to the isoelectrical point in the acceptor phase.

4.5.3   Membrane Based Reactive Extraction on Pilot Scale

> Significant parts of the following subsection were already published in Gerigk *et al.* [GMK⁺02]. Results were acquired during the Ph.D. thesis of D. Maaß [Maa00] and M. Gerigk [Ger01] who were both co-supervised by the author.

Motivated by the promising results of reactive extraction development, pilot-scale *ISPR* experiments were performed using the L-Phe producing strain *E. coli* 4pF20 as precedingly introduced. Figure 4.43, depicts the experimental setup consisting of a 300-*L* bioreactor together with the technical scale reactive extraction unit, as already presented. The experimental approach considered glucose and tyrosine control according to the explanations given in the preceding sections.

At the beginning, fed-batch fermentations were started using the by-pass alone, without integration of the reactive extraction system to study
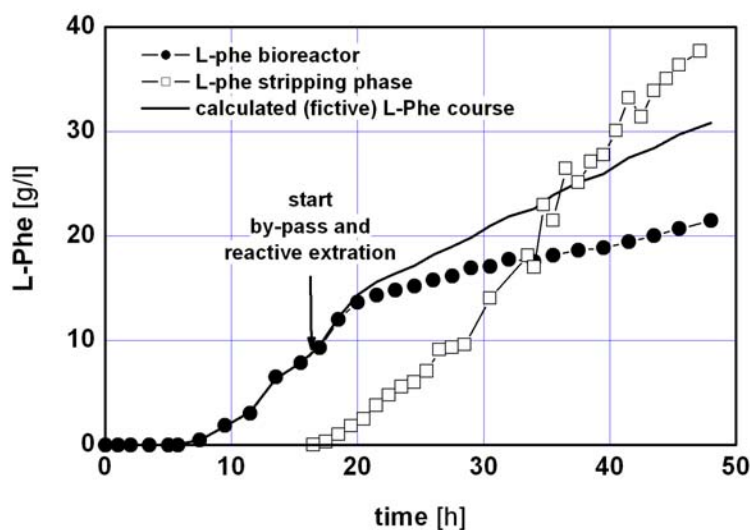
FIGURE 4.44. Courses of L-Phe concentration in the biosuspension (circles) and in the aqueous acceptor phase (rectangles) of the reactive extraction unit during the pilot-scale run of the *ISPR* process. Additionally, the calculated, fictive concentrations of the biosuspension are given.

the influence of the recycling loop on the process performance without superimposing effects of L-Phe extraction. As a result drain-off rates about $30 \ L \cdot h^{-1}$ of cell-free permeate were measured at the beginning of by-pass circulation, which started about 16 hours after inoculation of the 300-L bioreactor. Gradients of dissolved oxygen or pH were not observed.

Subsequent experiments were conducted using the integrated reactive extraction loop. Corresponding results are given in Figure 4.44 focusing on the L-Phe courses[26]. After 48 h process time an L-Phe titer of approximately 22 $g \cdot L^{-1}$ was achieved. Starting after 16 h process time, L-Phe was extracted on-line into the stripping phase reaching the final concentrations in the stripping tank of 37 $g \cdot L^{-1}$. Thus it was possible to extract L-Phe against the concentration gradient existing from the fermentation solution towards the stripping solution. Taking into account the amount of L-Phe that was extracted during the fermentation run, L-Phe concentrations of approximately 32 $g \cdot L^{-1}$ would have been achieved (see calculated, fictive curve in Figure 4.44). Therefore it was possible to achieve an even higher

---

[26]Because courses of glucose, tyrosine, acetate and optical density were similar to previous fermentations, these curves were not shown.
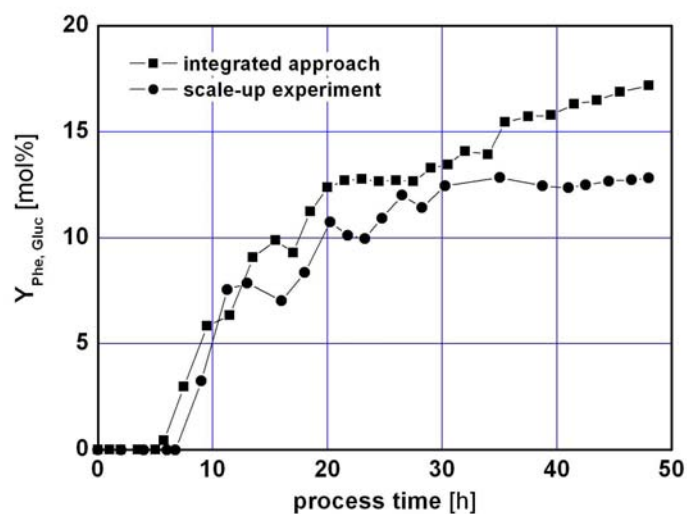
FIGURE 4.45. Courses of the L-Phe/glucose yield $Y_{Phe,Gluc}$ in two similar fed-batch fermentations with (circles) and without (rectangle) reactive extraction.
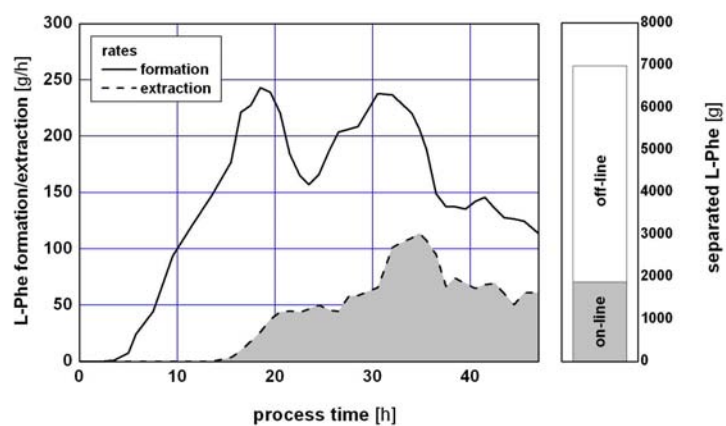
FIGURE 4.46. Comparison of the total L-Phe formation and extraction rates during the pilot-scale *ISPR* process.

(fictive) product titer using the integrated approach than in the scale-up experiment reaching 29 $g \cdot L^{-1}$ L-Phe (Figure 4.23, this section).

FIGURE 4.47. Picture of the total pilot-scale *ISPR* setup used of on-line L-Phe separation using reactive extraction. The 300-L bioreactor is shown together with the by-pass consisting of a peristaltic pump and the ultrafiltration unit. On the bottom, the red tubes are identifiable which connected the bioreactor with the reactive-extraction system (in the background). Also via the red tubes, the L-Phe reduced permeate stream is recycled into the bioreactor. A correponding movie is offered at the internet at www.fz-juelich.de/ibt/ferm.

Obviously the on-line reactive extraction technique did not hamper microbial cell growth and/or product formation. On the contrary, further analysis of the cell-specific product formation and glucose consumption rates revealed an increase of the molar product/substrate ratio, in accordance with the lab-scale results already presented in the preceding subsection. Figure 4.45 illustrates that after 30 h process time the molar yield in

the *ISPR* process was still rising (up to about 17.5 mol%) while the final yield was already achieved in the non-*ISPR* scale-up experiment (about 13 mol%). Thus, the *ISPR* approach offers the advantage to improve the total L-Phe/glucose yield.

Using the *ISPR* approach, a maximum L-Phe formation rate of approximately 250 $g \cdot h^{-1}$ in the 300-L fed-batch fermentation was observed (see Figure 4.46). At the same time, L-Phe was extracted at a maximum extraction rate of 110 $g \cdot h^{-1}$. Hence, L-Phe accumulated in the bioreactor and resulted in the final L-Phe titer of 22 $g \cdot L^{-1}$. In total, about 2 kg L-Phe was separated on-line (indicated by the grey area beneath the extraction course) and about 5 kg L-Phe was left for off-line downstream processing. Further downstream processing by precipitation (titration by NaOH to the isoelectric pH) yielded up to 99% pure product, contaminated with less than 40 $mg \cdot kg^{-1}$ of other organic compounds.

Hence the *ISPR* process was successfully developed thus representing one of the rare examples of fully integrated product removal. It was found that the integration of reactive extraction even allows to improve the whole process performance by increasing the L-Phe/glucose yield and by rising the total process productivity, indicated by the amount of L-Phe produced. However, only 26.7% of the total L-Phe were extracted on-line thus motivating to perform additional studies focusing on potential mass transport limitations.

4.5.4   Total Process Modeling

Significant parts of the following subsection were in press published by Takors [Tak03].

To investigate why only 26.7 % of the total L-Phe amount was separated on-line using the membrane based reactive extraction approach, a simple model of the total *ISPR* pilot scale was formulated thus enabling corresponding simulation studies. These studies were also intended to elucidate how potential L-Phe mass transfer limitations could be overcome experimentally.

The 'black-box' modeling approach introduced in the foregoing subsection can only provide limited insight into the mass transfer of the reactive-extraction unit and is thus not suitable to model and to design the total pilot-scale *ISPR* process. As shown, it turned out that the loading state of the carrier/L-Phe complex in the organic phase plays an important role during L-Phe separation. Unfortunately, concentrations of loaded or unloaded
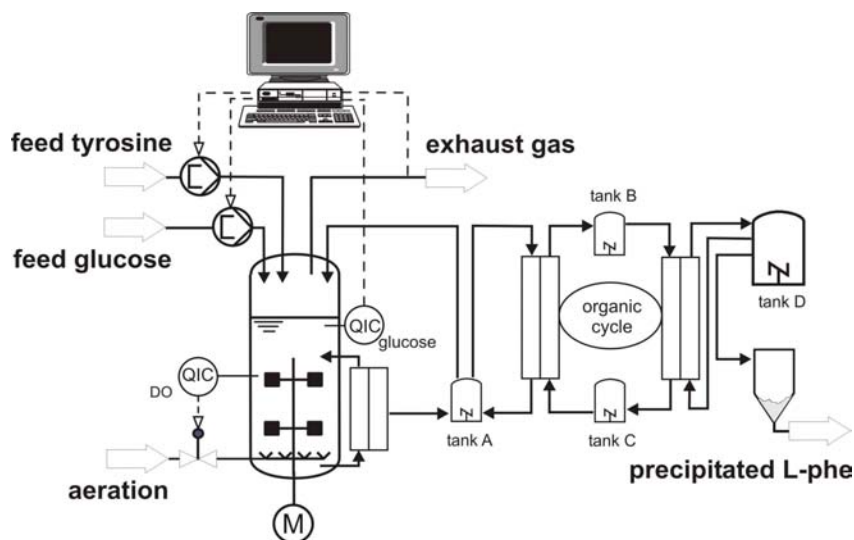
FIGURE 4.48. Extended scheme of the pilot scale *ISPR* process considering all buffer tanks used in the reactive extraction unit.

carriers could not be measured in the organic phase because appropriate analytical approaches were not available. Thus it was an additional aim of the modeling activities to estimate non-measurable carrier/L-Phe complex concentrations to discuss their affect on the total L-Phe mass transfer.

Experimental Basis

As an extension of the setup given in Figure 4.43, Figure 4.48 also depicts buffer tanks of the pilot-scale reactive extraction unit. These are three 5 L tanks B, C and D and the 50 L acceptor tank A. During the fed-batch experiment, the L-Phe containing cell-free fermentation solution was pumped at decreasing rates from (initially) 22 to (later) 8 $L \cdot h^{-1}$ from the ultrafiltration unit (500 kDa cutoff, 4.4 m^2 membrane area, 1 mm inner fiber diameter, Schleicher & Schuell, Germany) into the extraction module and was subsequently recycled into the bioreactor[27]. The aqueous cell-free solution was brought into contact with the organic phase containing kerosene with 10 v/v % of the cation-selective carrier D$_2$EHPA. The proton exchange was assumed to take place in the aqueous phase next to the aqueous/organic interface due to the existing low aqueous carrier solubility ($< 1g \cdot L^{-1}$) and the non-solubility of L-Phe cations in the organic phase.

---

[27] The decreasing pump rates were a consequence of biofouling in the ultrafiltration module.

Loaded carrier/L-Phe complexes were transported to the back-extraction module, where L-Phe$^+$ was replaced by H$^+$ protons of H$_2$SO$_4$ origin.

Mass transfer studies comprised the experiments given in tables 4.4 and 4.5. Time-variant L-Phe concentrations in the donor tank $c_{Phe,D}$ and in the acceptor tank $c_{Phe,A}$ are given in the figures 4.50 and 4.51. Modeling studies considered velocities with respect to the mean flow through the hydrophobic hollow fibers while the velocity of the organic phase was estimated considering the mean flow through the outer space outside the fibers in the modules.

Modeling Assumptions and Simplifications

Modeling was carried out using *gPROMS* 2.1.1 (Process System Enterprise Ltd, London, UK). As pointed out in the introduction, it was a major aim of this study to identify a process model that is able to mirror the experimental results appropriately and that possesses a certain simplicity to encourage its easy use. For these reasons, no *pH* effects were considered in the model because the integrated process under consideration is assumed to be always performed at *pH* 6.5 owing to production strain qualities. Mass transfer modeling followed the idea of studying transfer kinetics in one hollow fiber and transferring the results by analogy to the whole bunch of fibers in the modules. As shown in Maaß [Maa00], only very low concentration changes ($\prec$ 10 %) occurred during a single flow of organic and aqueous solution through the hollow fiber modules, which is in agreement with further observations of Escalante *et al.* [EOI96] even studying opposite and non-opposite aqueous/organic flows. These experimental findings motivated the simplifying modeling assumption that, non-opposite, parallel aqueous and organic streams could be assumed in the model in order to enable a straightforward parameter identification and to avoid complex recursive computing during non-linear parameter identification. Hence, concentration changes along the hollow fibres (dependent on the variable z) are estimated expecting only small changes in accordance with previous experimental observations. For model identification, the total set of concentration courses in acceptor and donor phase was used. Resulting mass transfer coefficients thus represent mean values with respect to process time, module length and different experimental conditions.

Mass Transfer Modeling

Detailed approaches for reactive-extraction modeling have been published, for instance by focusing on fundamentals of counter-transport under steady-state conditions [KS89], by modeling the removal of penicillin G with hollow fiber modules [LSS02] or by studying kinetic effects during L-Phe separation from aqueous solution using Aliquat 336 [EAOI98]. However, the experimental setup used for the *ISPR* L-Phe process (devices, extraction system,
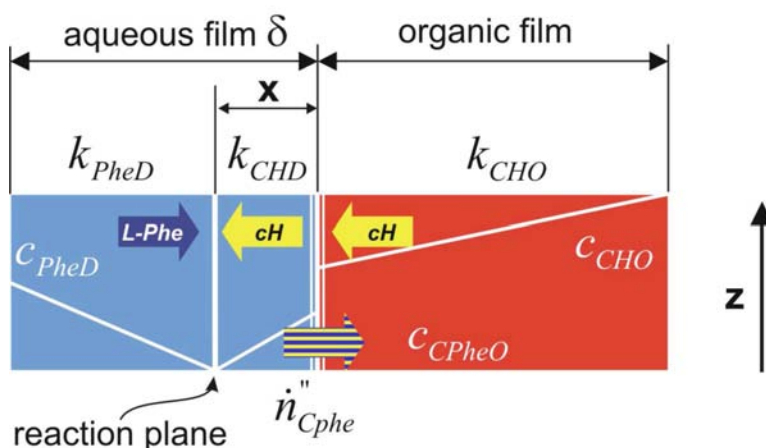
FIGURE 4.49. Modeling approach for the aqueous/organic L-Phe mass transfer. Carrier$^-$/H$^+$ complexes of the organic phase (c_{CHO}) are assumed to be transferred through the organic/aqueous interface to enter the aqueous film (c_{CHD}). By diffusion they are transported to a reaction plane which is assumed to be located next to the interface where L-Phe (c_{PheD}) is taken up and diffusively brought back to the interface resulting in an area-specific carrier$^-$/Phe$^+$ transfer called $\dot{n}_{CPhe}$. All reactions and transport are in steady-state.

process integration etc.) is not covered by these approaches. Moreover, it should be stressed that the following model considers the idea of a 'reaction plane' to identify additional potential mass transfer limitations[28]. This is motivated by the apparently low-solubility of the carrier D$_2$EHPA, which contrasts with the good solubility of the often-used, cell toxic quaternary ammonium salt Aliquat 336.

The modeling approach is based on the well-known 'two-films theory' assuming an aqueous and an organic film which are directly in contact in the hollow fiber modules used. As indicated in Figure 4.49, all mass transfer rates are assumed to be in steady-state, which means that the diffusively driven transport of carrier/proton(H) complexes through the organic film equals their short-way diffusion through the aqueous film to the reaction plane (which is assumed to be located right next to the aqueous/organic interface) and also equals the counter diffusion of L-Phe cations coming from the bulk-side of the aqueous film.

---

[28] Recently, the idea of considering a 'reaction plane' was also followed by Lazarova *et al.* [LSS02] introducing a 'reaction zone' in their hollow fiber mass transfer model for the removal of penicillin G with the aid of the secondary amine Amberlite LA-2.

The consideration of the reaction plane in the aqueous film is motivated by the existing (low) solubility of the carriers in the aqueous solution (together with the non-solubility of L-Phe cations in the organic phase) and allows the identification of potential mass transfer limitations caused by the low carrier solubility. Proton-exchange rates are known to be very fast (reaction rate constant: $1.4 \cdot 10^{11} L \cdot (Mol \cdot s)^{-1}$ [Atk94]), which consequently leads to thin reaction planes, from which newly produced carrier/L-Phe complexes diffuse back to the aqueous/organic interface. Rates and reactant concentrations (L-Phe in the donor phase ($c_{Phe,D}$); carrier (D$_2$EHPA) c_{CHO} and carrier/L-Phe complexes c_{CPheO} in the organic phase) are assumed to vary only slightly along the module (see modeling assumptions), which makes them dependent on the variable z. Corresponding mass transfer coefficients inside the films k_{PheD}, k_{CHD} and k_{CHO} are defined with respect to the total module length (see Figure 4.49) and the total film thickness δ. At the aqueous/organic interface an equilibrium of carrier/proton(H) complexes in the organic phase with their counterparts in the aqueous phase is presumed. A detailed list of all variables and parameters used for modeling is given in the tables B.5 and B.6, Appendix B.

Focusing the L-Phe mass transfer near by the aqueous/organic interface, the steady-state assumption for all educts leads to the formulation of the area-specific L-Phe transfer rate $\dot{r}''(z)$

$$\dot{r}''_{PheD}(z) = k_{PheD} \left(c_{PheD}(z) - 0\right) \frac{\delta_D}{\delta_D - x} = k_{CHD} \left(c_{CHD}(z) - 0\right) \frac{\delta_D}{x} =$$

$$= k_{CHO} \left(c_{CHO}(z) - c_{CHO,I}(z)\right) \qquad (4.4)$$

Note that the educts are supposed to react completely at the reaction plane. The variable x is introduced to achieve a length-proportional reduction of the mass transfer coefficients and to allow a study of the presumed carrier-complex diffusion into the aqueous donor and into the acceptor phase. Because both reaction planes are assumed to be located right next to the organic/aqueous interface, $x \ll \delta_D$. Further re-arrangement of equations 4.4 leads to

$$\dot{r}''_{PheD}(z) = \frac{c_{CHOEx} \cdot k_{CHD} + c_{PheD} \cdot k_{PheD} \cdot K_C}{\frac{k_{CHD}}{k_{CHO}} + K_C} \qquad (4.5)$$

where K_C describes an equilibrium constant taking into account the interface concentrations of the carrier/proton(H) complex in organic and aqueous phase, which was experimentally estimated at 99.6 with the help of NMR measurements. It is noteworthy that equation 4.5 is only valid for $c_{CHOEx} \succ 0 \cap c_{PheD} \succ 0$.

By analogy, the modeling of the organic/aqueous mass transfer in the back-extraction module is realized

$$\dot{r}''_{PheA}(z) = \frac{c_{CPheOBex} \cdot k_{CPheA} + c_{HA} \cdot k_{HA} \cdot K_C}{\frac{k_{CPheA}}{k_{CPheO}} + K_C} \qquad (4.6)$$

considering the coefficients for mass transfer of the carrier/L-Phe complex in the aqueous acceptor k_{CPheA} and organic phase k_{CPheO} as well as proton(H) transport inside the aqueous acceptor phase k_{HA}. To model the complete experimental setup of figures 4.48 and 4.49, the following differential equation system is used:

Extraction module

$$\frac{dc_{PheD}(z)}{dt} = -v_D \cdot \frac{\partial c_{PheD}(z)}{\partial z} - \frac{4}{D_{cap}} \cdot \dot{r}''_{PheD}(z) \qquad (4.7)$$

$$\frac{dc_{CPheOEx}(z)}{dt} = -v_O \cdot \frac{\partial c_{CPheOEx}(z)}{\partial z} - \frac{4}{D_{cap}} \cdot \dot{r}''_{PheD}(z) \qquad (4.8)$$

$$c_{CHOEx}(z) = c_{Cconst} - c_{CPheOEx}(z) \qquad (4.9)$$

Back-extraction module

$$\frac{dc_{PheA}(z)}{dt} = -v_A \cdot \frac{\partial c_{PheA}(z)}{\partial z} - \frac{4}{D_{cap}} \cdot \dot{r}''_{PheA}(z) \qquad (4.10)$$

$$\frac{dc_{HA}(z)}{dt} = -v_A \cdot \frac{\partial c_{HA}(z)}{\partial z} - \frac{4}{D_{cap}} \cdot \dot{r}''_{PheA}(z) \qquad (4.11)$$

$$\frac{dc_{CPheOBex}(z)}{dt} = -v_O \cdot \frac{\partial c_{CPheOBex}(z)}{\partial z} - \frac{4}{D_{cap}} \cdot \dot{r}''_{PheA}(z) \qquad (4.12)$$

$$c_{CHOBex}(z) = c_{Cconst} - c_{CPheOBex}(z) \qquad (4.13)$$

Additionally, four tanks must be considered (see Figure 4.48) leading to four additional ordinary differential balance equations

$$\text{acceptor tank: } \frac{dc_{PheA}(0)}{dt} = \frac{\dot{V}_A}{V_A} \left(c_{PheA}(L) - c_{PheA}(0) \right) \qquad (4.14)$$

$$\text{buffer tank B: } \frac{dc_{CPheOBex}(0)}{dt} = \frac{\dot{V}_O}{V_B} \left(c_{CPheOEx}(L) - c_{CPheOBex}(0) \right) \qquad (4.15)$$

$$\text{buffer tank C: } \frac{dc_{CPheOEx}(0)}{dt} = \frac{\dot{V}_O}{V_C} \left(c_{CPheOBex}(L) - c_{CPheOEx}(0) \right) \qquad (4.16)$$

$$\text{donor tank: } \frac{dc_{PheD}(0)}{dt} = \frac{\dot{V}_D}{V_D} \left(c_{PheD}(L) - c_{PheD}(0) \right) \qquad (4.17)$$

Please notice that index 0 and L refer to the entrance and to the exit of the hollow fiber modules, respectively. For the sake of brevity only L-Phe balances are given.

Modeling Results

Using this differential equation system, model identification was performed. It turned out that of the six mass transfer coefficients initially considered, only two are necessary to model the experiments. While k_{CHD}, k_{CHO}, k_{CPheO} and k_{HA} showed only poor statistical significance leading to typical over-parameterization problems (poor parameter accuracy - error $\gg$ 100%, singular parameter covariance matrix etc.), the step-by-step model reduction finally lead to a reduced model that only consists of k_{PheD} and k_{CPheA} as model parameters. Table 4.6 shows high accuracies by giving small relative standard deviations $<< 1\%$ of the respected parameters.

Figures 4.50 and 4.51 represent an overview of the resulting model predictions compared to the experimental observations. It can be stated that the predicted concentration courses in the donor and acceptor tank are well mirrored by the model, which is indicated by high regression coefficients of L-Phe courses in the donor 0.983 ± 0.019 and acceptor tank 0.994 ± 0.005. This result might be surprising with respect to the significant simplifying assumptions which were the basis for model formulation. However it indicates that their obviously exists a small number mass transfer limitations dominating the overall L-Phe transfer.

Motivated by the result that only k_{PheD} and k_{CPheA} revealed to be significant under different experimental conditions, the conclusion can be drawn that in the extraction module neither the transport of carrier/proton(H) complexes in the organic phase nor their short-way diffusion in the aqueous phase is limiting – but, obviously, the L-Phe diffusion in the aqueous film is the most significant transfer step k_{PheD} is estimated at 128 E-7 $cm \cdot s^{-1}$. By analogy it is assumed that in the back-extraction module, no significant limitation of the carrier/Phe-complex transport as well as of the proton(H) exists. However, the transfer of L-Phe-loaded carriers into the aqueous acceptor phase seems to be limiting. Here a mass transfer coefficient k_{CPheA} of 178 E-5 $cm \cdot s^{-1}$ was estimated. The mass transfer coefficients differ in two orders of magnitude. This is most presumably a consequence of the significantly different L-Phe concentrations in the corresponding phases which is compensated by different mass transfer coefficients under the constraint of steady-state flux.

TABLE 4.6. Final parameters of the L-Phe mass transfer model identified from the ten pilot scale experiments

parameter	unit	value	standard deviation
k_{PheD}	$cm \cdot s^{-1}$	128 E-7	$\ll 1\%$
k_{CPheA}	$cm \cdot s^{-1}$	178 E-5	$\ll 1\%$
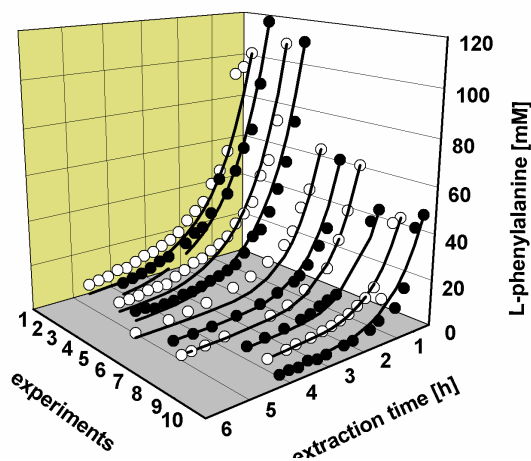
FIGURE 4.50. Experimental (circles) and simulated (lines) courses of the L-Phe extraction from the donor tank in a series of ten experiments using the pilot-scale reactive extraction setup.
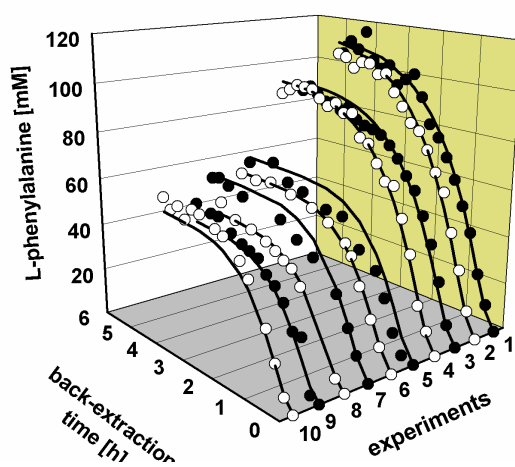
FIGURE 4.51. Experimental (circles) and simulated (lines) courses of the L-Phe back-extraction into the acceptor tank in a series of ten experiments using the pilot-scale reactive extraction setup.

The fact that no mass transfer limitation is identified in the organic phase might be surprising, especially if lower diffusivity for the carrier/L-Phe complex and extensive laminar films in the organic phase are expected. However, one should also consider the very low solubility of the carrier/L-Phe complex in the aqueous phase which is two orders of magnitude smaller than in the organic phase and which consequently limits the mass transfer. The model identification results based on the different experimental conditions (see tables 4.4 and 4.5) and the accuracy of model predictions support this simple mass transfer model. Additional mass transfer studies focusing on the aqueous/organic interface would be desirable, however they could not be performed within this project.

Macrokinetic Model of the L-Phe-Producing Strain

To study whether and how the reactive extraction model can be used for total *ISPR* modeling, a complete model including the fed-batch fermentation process has to be formulated. In order to enable a comparison of pure simulation and large-scale experiments, the fermentation model was identified using a different database – namely a small-scale (20-*L*) fed-batch process. It was the general aim to keep the macrokinetic approach as simple as possible, which resulted in the following non-segregated, non-structured approach:

$$\mu = \mu_{\max}\frac{c_{Tyr}}{c_{Tyr} + K_{STyr}} \tag{4.18}$$

$$\sigma_{Tyr} = m_{Tyr} + \frac{\mu}{Y_{xTyr}} \tag{4.19}$$

$$\pi_{Phe} = \pi_{Phe\,\max}\frac{K_{IPhe}}{K_{IPhe} + c_{Phe}} \tag{4.20}$$

It is thus assumed that the growth of L-Phe-producing *E. coli* cells is only dependent on the (limiting) supply of the auxotrophic amino acid tyrosine, because glucose concentrations were controlled at a saturating level of 5 $g \cdot L^{-1}$ during the whole fermentation (see preceding sections). A tyrosine maintenance consumption is considered (see equation 4.19). L-Phe production is supposed to be completely growth-decoupled but inhibited by high product concentrations as observed with respect to AroF activity. This macrokinetic model was used together with ordinary differential balancing equations (not shown) taking the concentrations of cell-dry weight (c_{CDW}), L-Phe (c_{Phe}), tyrosine (c_{Tyr}) and the liquid volume (V_R) as dependent variables and considering the common feed of glucose and tyrosine as an independent input variable.

Figure 4.52 presents a comparison of modeled and measured values. The model parameters are given in Table 4.7. Only a poor estimation of Y_{XTyr} and m_{Tyr} was achieved thus leading to temporary inaccurate model predictions of tyrosine consumption. The inaccuracies are the consequence of
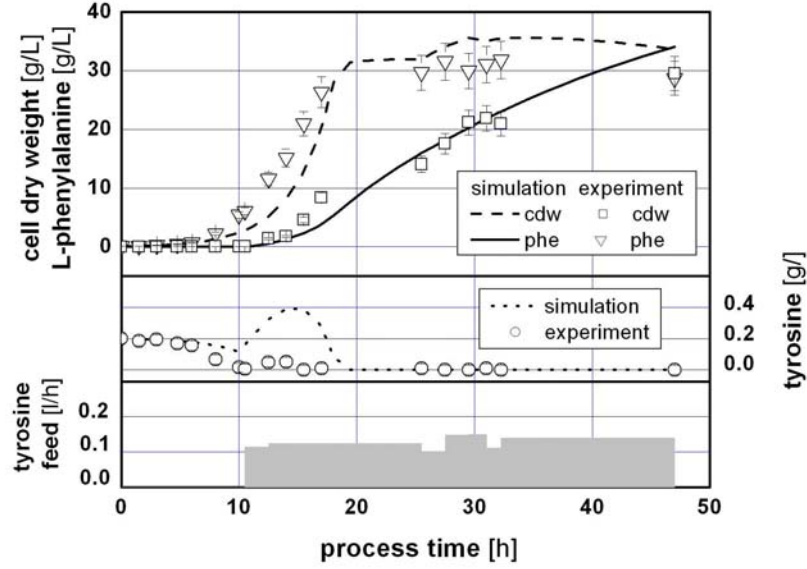
FIGURE 4.52. Comparison of modeled and measured values of cell dry weight (cdw), L-phenylalanine (Phe), tyrosine (tyr) and the tyrosine feeding rate in a lab-scale fermentation process using an L-Phe-producing *E. coli* strain.

experimental difficulties caused by partial tyrosine precipitation that occurred inside the feed tubing owing to the very low tyrosine solubility of $0.38\ g \cdot L^{-1}$.[29] However, the modeling of the L-Phe course is not hampered, which is qualified as most important for the purpose of this study. Note,

---

[29] The problem of low tyrosine solublity has already been adressed in the foregoing sections and it was solved by titrating the tyrosine feed to $pH \sim 10$ to increase tyrosine solubility. However, the data used for this analysis based on the 'old' protocol without pH adaption.

TABLE 4.7. Final parameters of the unstructured, kinetic model of an L-Phe producing *E. coli* strain based labscale fed-batch experiments.

parameter	unit	value	standard deviation
$\mu_{\max}$	h^{-1}	0.321	± 0.01127
$K_{S,Tyr}$	$g_{Tyr} \cdot L^{-1}$	0.00152	$\pm 2.53E-6$
Y_{XTyr}	$g_{CDW} \cdot g_{Tyr}^{-1}$	35.29	$\succ 100\%$
m_{Tyr}	$g_{Tyr} \cdot (g_{CDW}h)^{-1}$	0.00245	$\succ 100\%$
$\pi_{Phe\,\max}$	$g_{Phe} \cdot (g_{CDW}h)^{-1}$	0.0756	± 0.049
K_{IPhe}	$g_{Phe} \cdot L^{-1}$	20	± 1.35

that a significant L-Phe inhibition constant of 20 ± 1.35 $g \cdot L^{-1}$ is identified confirming previous AroF inhibition results.

Modeling the Total Process

Combining the fermentation model with the reactive-extraction modeling approach, a total process model is constructed aiming at the <u>simulation</u> of the 300-L $ISPR$ approach, which was presented in the preceding subsection. Figure 4.53 compares simulated and measured values of L-Phe concentration in the bioreactor and in the acceptor tank together with the bioreactor tyrosine course. Additionally the glucose/tyrosine feeding profile is given. As indicated in Figure 4.48, the reactive extraction was combined with the fed-batch process via an ultrafiltration unit, of which the permeate rates were taken as independent (measured) input variables for the simulations varying between 22 and 8 $L \cdot h^{-1}$ (caused by biofouling which occurred during filtration).

Figure 4.53 illustrates a good conformity between measured and simulated courses. In particular the L-Phe accumulation in the acceptor tank is well reflected by the model predictions. Thus, the conclusion is drawn that the simple $ISPR$ model is applicable to model the overall process. This offers the possibility to study the non-measurable carrier/L-Phe complex in the organic phase taking into account the modeled values.

As an example, the 3-dimensional plot of the carrier/L-Phe-complex in the extraction module is given in Figure 4.54. It can be seen that reactive-extraction started after 13.6 hours and lasted until the end of the process at 48 h process time. Surprisingly, the simulation reveals that still loaded carrier re-enter the extraction module causing a significant accumulation of the carrier/L-Phe complex in the organic phase up to 45 mM at the outlet after 48 hours. This result is especially remarkable as there was no alternative analytical approach to measure the loaded carrier/L-Phe fraction in the organic phase. Furthermore, the accumulation of the loaded carrier/L-Phe complex can be regarded as a potential candidate of existing mass transfer limitations which need to be studied in detail.

Optimization of the $ISPR$ Process

As a consequence, one might think of increasing the back-extraction membrane area to reduce the amount of still-loaded carriers re-entering the extraction unit. Thus, corresponding simulations were carried out by increasing the number of back-extraction modules – installed in series – from one to three. As indicated in Figure 4.55, the concentration of still-loaded carriers re-entering the extraction module decreased significantly, as it was previously assumed. However, the rate of L-Phe transfer, which is monitored at the entrance of the back-extraction module, did not increase as
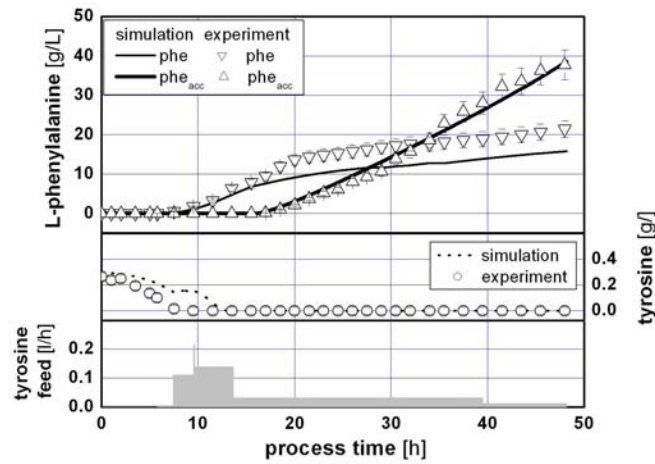
FIGURE 4.53. Simulation of the total *ISPR* L-Phe production process based on the model parameters which were identified separately. Shown are the concentration courses of measured and simulated L-phenylalanine in the bioreactor (phe) and in the acceptor tank of reactive extraction (phe$_{acc}$), together with the corresponding values of tyrosine (tyr) in the fermentation suspension during the fed-batch process. Additionally, the tyrosine feed is given.
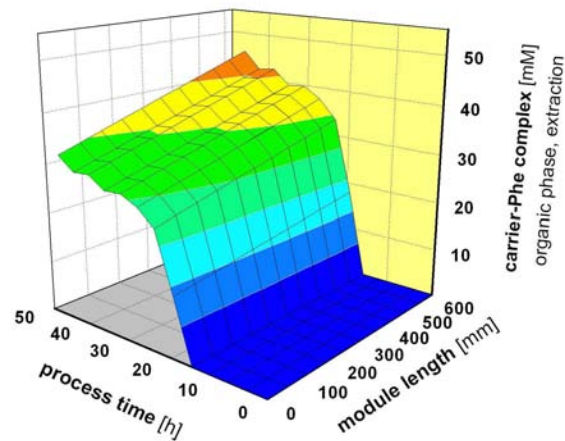
FIGURE 4.54. Simulated course of the carrier/L-Phe complex in the organic phase in the extraction module as a function of process time and module length during the on-line reactive extraction of L-Phe from the fed-batch process on the 300-*L* scale.
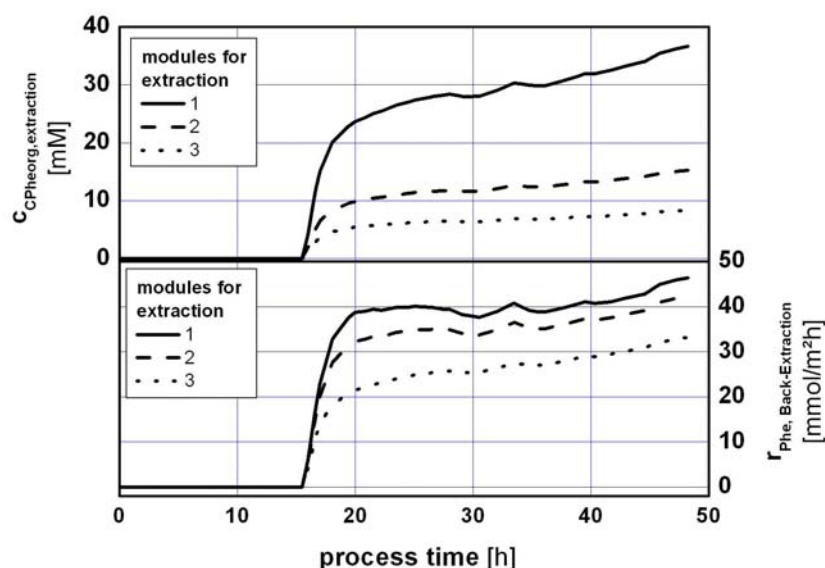
FIGURE 4.55. Comparison of the carrier/L-Phe complex concentration at the entrance of the extraction module with the resulting L-Phe mass transfer rates mirrored at the entrance of the back-extraction module. Both variables are presented as functions of process time. Three simulation runs are shown for each variable considering up to three similar back-extraction modules installed in series

expected. In contrast, a decrease of L-Phe transfer is found by increasing the number of extraction modules used.

This result might be surprising at first sight, however, taking into account the identified main transfer limitations – namely k_{PheD} and k_{CPheA} - a phenomenological explanation can be given. The identification of k_{PheD} indicates that L-Phe mass transfer inside the extraction module is only dependent on the mass transfer of L-Phe cations through the aqueous film to the reaction plane and not on the carrier/L-Phe complex in the organic phase inside the module. Hence, extraction rates are independent of the back-extraction membrane area (data not shown). On the contrary, back-extraction rates are significantly reduced because of reduced carrier/L-Phe concentrations in the organic phase (because of the extended extraction membrane area). Decreasing carrier/L-Phe concentrations in the organic phase also cause decreasing carrier/L-Phe concentrations in the aqueous acceptor phase which are most dominant for total back-extraction (indicated by k_{CPheA}). As a consequence, the back-extraction rates decline with increasing extraction membrane area, which maybe contrasts primary pre-simulation assumptions.

The preceding analysis reveals the complexity of the total L-Phe mass transfer and consequently stresses the need to perform corresponding simulation studies. Most strikingly, this fact was also outlined by the independent studies of Lazarova *et al.* [LSS02], who investigated the penicillin G removal with anion-selective carriers in hollow fiber modules. In accordance with the independent findings presented in the preceding paragraphs, these authors outlined that '... *the extraction of penicillin G is dominated by the diffusional resistance in the aqueous layer...*' and   '...*the stripping of penicillin G from the loaded organic solution to the regenerating aqueous buffer ... is controlled by the rate of the reverse chemical reaction, or the membrane resistance, or the combination of them.*' which correspond to the identification of k_{CPheA} in this study. In addition these authors stress the importance of 'carefully' optimizing the whole reactive extraction system by '...*taking into account not only the effective removal of penicillin G from the feed ... but also its successful stripping and solvent regeneration ...*'. The authors also localized the main process resistance in the back-extraction module, in analogy to the findings of this study. Hence it can be concluded that the simple modeling approach applied in this study succeeded to identify the key limitations of L-Phe transport in the pilot-scale setup thus offering the chance for simulative *ISPR* optimization.

As shown, there are two major limitation steps which are localized inside the aqueous films regarding the L-Phe cations in the donor and the carrier/L-Phe complex in the acceptor phase. As a consequence, the following strategies for total process optimization can be discussed:

- If k_{PheD} is addressed, high L-Phe concentrations in the permeate (and also in the fermentation suspension) are advantageous. With respect to the identified product inhibition at $20\ g \cdot L^{-1}$, there obviously exists an upper limit for process optimization. However, one can think of a later start of the reactive-extraction unit during the process run, provided that the product accumulation does not exceed critical L-Phe titers. Furthermore, the use of optimized L-Phe producers (with higher production rates) can also be considered. Here, the consideration of on-line L-Phe separation would be most advantageous to prevent a fast accumulation of the inhibiting product.

- By analogy, the mass transfer described by k_{CPheA} can be discussed leading to simulation studies with extended extraction membrane area or considering alternative carriers, which possess higher aqueous solubility and which are still tolerated by the cells.

- Finally, one should consider the striking fact that all identified candidates for mass transfer limitations are located in the films of the aqueous phase. These films originate from the strict laminar conditions inside the hollow fiber modules. Hence, the optimization of the

integrated reactive extraction should also focus on the improvement of hydrodynamics at the organic/aqueous interface in order to minimize aqueous film extension and to eliminate corresponding transfer limitations subsequently.

It is especially the last item, namely the alleviation of mass transfer limitations by improved hydrodynamic conditions, which was the basic motivation to perform the reactive extraction studies with a different reactive extraction technology finally leading to an improved *ISPR* process as it will be presented in the next subsection.

4.5.5   Reactive Extraction with Centrifugal Extractors

Significant parts of the following subsection are submitted for publication in Rüffer *et al.* [RHK$^+$03] and applied for patent [RWT02]. Results are acquired during the Ph.D. thesis of N. Rüffer [Rüf03] and during the master thesis of U. Heidersdorf [Hei02] and I. Kretzers [Kre02] who have been co-supervised by the author.

Motivated by the beneficial effects of the *ISPR* approach (e.g. increase of L-Phe/glucose yield, concentration of L-Phe in acceptor, simplified downstream processing and product purification by final precipitation) and being aware of the obviously existing mass transfer limitation because of the strictly laminar conditions inside the hollow fibre modules, the aim was formulated to develop a novel *ISPR* process which should lead to even improved overall process performance. This decision was also supported by the finding that the interface stability between the aqueous and the organic phase inside the pores of the hollow fiber modules is strongly dependent on the trans-membrane pressure difference. Thus, pressure peaks occurring during the filling or the operation of the modules could cause phase instabilities and breakthroughs, which finally could terminate the process. Obviously, this technical drawback can hamper the scale-up of the technology.

Accordingly, future *ISPR* process developments should alleviate the (so far existing) L-Phe transport limitations concomitantly offering a facilitated handling of the total reactive extraction unit in combination with low investment costs. Hence, liquid-liquid centrifuges have been considered as an alternative solution for *ISPR* process development.

Liquid-liquid centrifuges are well-known for phase separation and have even been applied for the off-line recovery of penicillin from fermentation supernatant ([Van84], [LS87], [Sch94], [Sch00]). Compared to the previously used hollow fiber membrane contactors, liquid-liquid centrifuges offer the advantage of being more robust in case of pressure changes, which could easily occur during a fermentation. This facilitates their handling and also their scale-up quality [MMF$^+$02]. Because of the turbulent conditions inside the centrifuges, increased mass transfer rates could be assumed, too. However, this advantage could easily be reversed if large amounts of solvent or carrier permeate into the aqueous solution to be recycled into the bioreactor. Because of their toxicity, a severe process inhibition of microbial metabolism could be the result.

Considering both the chances and the risks of integrating centrifugal extractors in a microbial production process, studies were performed to develop a novel *ISPR* approach using centrifugal reactive-extraction for on-line L-Phe separation. Emphasis laid on

- the identification of some basic characteristics of the L-Phe transfer in the liquid-liquid centrifuges

- the integration of the technology in the fed-batch process for L-Phe production

- the qualification of the total *ISPR* process.

Experimental Setup

For fermentation experiments, the tyrosine-auxotrophic L-Phe producer *E. coli* 4pF81 was used. As indicated in section A.1.1 (Appendix), this strain represents a further development of *E. coli* 4pF20, which was considered during the first period of the *ISPR* studies. Compared to *E. coli* 4pF20, *E. coli* 4pF81 additionally possesses the plasmid-encoded genes *aroB* and *aroL* coding for 3-dehydroquinate synthase and shikimate kinase II, respectively, both representing 'well-known' *metabolic engineering* targets of the aromatic amino acid pathway (see section 2.6.1). Because previous studies of Gerigk *et al.* [GBGN$^+$02] uncovered that *aroF^{wt}* was superior to *aroF^{fbr}* (provided that appropriate tyrosine control is applied) *aroF^{wt}* was used instead.

Fed-batch fermentations were performed in a 20-*L* bioreactor (ISF 200; Infors, Switzerland) using the same medium, cultivation conditions, technical devices and analytical approaches as in previous experiments (see sections A.2.1, A.4.2, A.3.3, Appendix). Depending on the experimental purpose 7.5 to 10 *L* initial volume were used. Glucose was controlled at 5 $g \cdot L^{-1}$ applying the Process Trace System (Trace AG, Braunschweig,

see section A.4.3, Appendix). During the L-Phe production period (which started after OD_{620} $\sim$80 was reached) the tyrosine supply was reduced to a minimum of 125 $mg \cdot h^{-1}$ sufficient for maintenance. pH 6.5 was adjusted by 25% ammonia titration. Temperature was controlled at 37 °C during the aerobic cultivation at dissolved oxygen set at 40 %. L-Phe production was induced with 100 μM IPTG at OD_{620} $\sim$8-12. The drain off of cell-free (and protein-free) permeate via the bypass started during the production phase after growth was stopped.

Two liquid-liquid centrifuges (Model V2; CINC, Brakel, Germany) were used for reactive extraction of L-Phe. The rotation speed of the centrifuges was adjusted by the system's control units and the volumetric flow by peristaltic pumps (Watson & Marlow, Germany). The volume of this model is $\sim$140 mL, rotor speed is 2,000 – 5,900 rpm and maximum flow rate is 2 $L \cdot \min^{-1}$. One centrifuge was used for L-Phe extraction with the carrier D_2EHPA (cation exchanger) in kerosene. The second centrifuge was used for back-extraction with the acceptor H_2SO_4 in water.

A scheme of the liquid-liquid centrifuge used is given in Figure 4.56. Heavy (aqueous) and light (organic) phases enter the centrifuge tangentially and flow down to the bottom through a fissure between the rotating cylinder and the inner wall of the centrifuge. Mixing of both phases and extraction of L-Phe takes place in the space between the rotor and support container. By a continuous addition of new liquid the fluid inside the centrifuge is transported into the inner part of the rotor where phase separation takes place on the basis of the different liquid densities. The heavy phase leaves the centrifuge at the outer, the light phase at the inner outlet.

Experiments for the characterization of the centrifuges for reactive extraction were performed with aqueous model solutions of L-Phe in 0.9 % NaCl as well as with cell- and/or protein-free fermentation supernatant. Heavy (aqueous) and light (organic) phases were circulated through the running centrifuges for 4-6 hours with peristaltic pumps (Watson and Marlow, Germany). Samples were taken at the inlet and outlet of the heavy phase of each centrifuge.

In analogy to the previously used *ISPR* setup, a bioreactor bypass was installed to prepare cell- and also protein-free permeate. Cells were retained with the aid of a cross-flow hollow fibre ultrafiltration (UF) module (3600 cm^2, 500 kDa cut off; Schleicher & Schuell, Germany). To avoid oxygen limitation by-pass residence time of about 3.6 s were realized by pumping. was necessary. The primary UF drain off was 4.8 $L \cdot h^{-1}$ and reduced to 2 $L \cdot h^{-1}$ because of biofouling. For the production of protein-free permeate, cell-free permeate was pumped through the second ultrafiltration unit consisting of 5 cassettes (Ultran-Lab, 10 kDa cut off; Schleicher & Schuell)
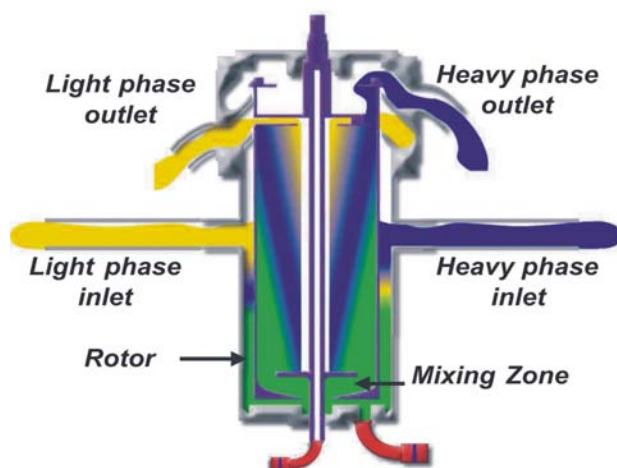
FIGURE 4.56. Scheme of the liquid-liquid centrifuge used (CINC, Brakel, Germany) showing the inlets and outlets of light (organic) and heavy (aqueous) phases.
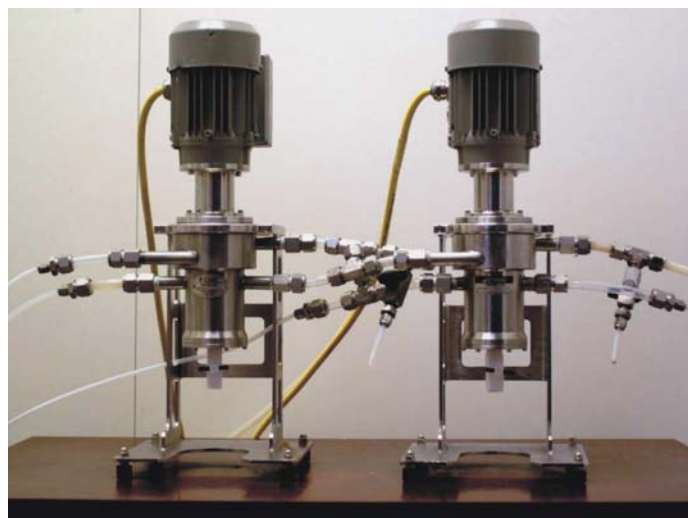
FIGURE 4.57. Experimental setup for reactive extraction using the two liquid-liquid centrifuges for extraction and back-extraction. It is noteworthy that this system completely replaced the membrane based approach shown in Figure 4.42.
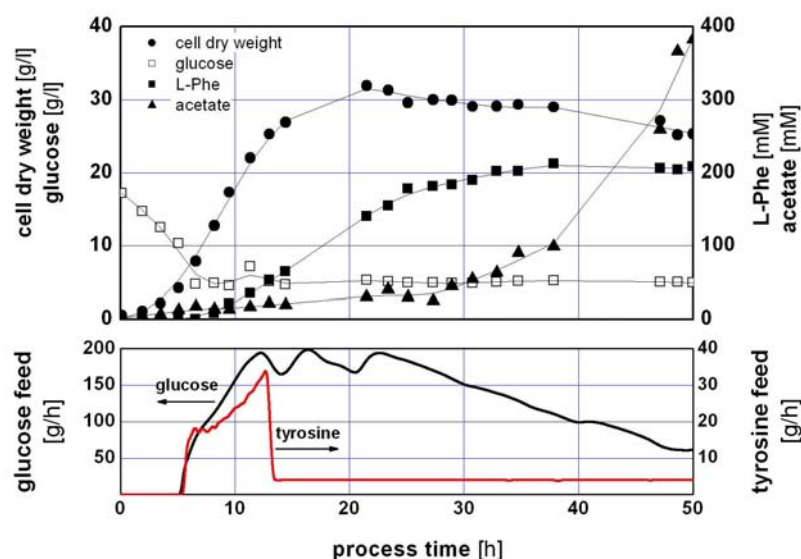
FIGURE 4.58. Curves of cell dry weight, glucose, L-Phe and acetate concentrations during the fed-batch reference fermentation for the L-Phe production using *E. coli* 4pF81 in a 20-*L* lab-scale bioreactor are shown. Additionally the controlled feed-profiles for glucose (700 $g \cdot L^{-1}$) and tyrosine (25 $g \cdot L^{-1}$) are given.

at a flow rate of up to 4 $L \cdot h^{-1}$. Protein- and cell-free permeate was continuously recycled into the reactive extraction unit with a volumetric flow rate of $1.5 - 3.5$ $L \cdot h^{-1}$. The L-Phe reduced permeate originating from the reactive extraction unit was recycled as well.

Typical Fed-Batch Fermentations

Fed-batch fermentations for L-Phe production using the strain *E. coli* 4pF81 were performed with glucose control at 5 $g \cdot L^{-1}$ to prevent acetate formation caused by overflow metabolism at high glucose concentrations, as well as to avoid carbon limitations resulting in reduced L-Phe formation rates [GBGN$^+$02]. Based on the previous studies, the L-tyrosine-limited feeding was successfully applied to avoid an unwanted feedback inhibition DAHP synthase encoded by *aroF*^{wt}.

A typical fermentation with *E. coli* 4pF81 is depicted in Figure 4.58. As indicated, the glucose concentration was controlled at a setpoint of 5 ± 0.5 $g \cdot L^{-1}$ after the initial batch phase was completed. The biomass increased exponentially to 30 $g_{CDW} \cdot L^{-1}$ until the growth rate dropped to maintenance metabolism because the significantly reduced tyrosine supply was installed after 14 hours. L-Phe production was induced with IPTG after 6

hours process time, which was subsequently followed by the feeding of the substrates glucose and tyrosine as indicated. L-tyrosine was only detectable in the initial feeding phase (data not shown). A biomass-coupled rise of L-Phe titers was observed during the exponential phase which slowed down when 180 $mmol \cdot L^{-1}$ was reached (in accordance with the macrokinetic model which was presented in the preceding subsection)[30]. Final L-Phe titers of 206 $mmol \cdot L^{-1}$ (34 $g \cdot L^{-1}$) were measured after 50 hours process time[31]. Because of the glucose control, acetate production was very low. However, significant acetate formation started after L-Phe production decreased, which led to a final concentration of 380 $mmol \cdot L^{-1}$. It is noteworthy that the availability for glucose and oxygen kept constant during the whole production period thus indicating that acetate formation was obviously not a consequence of 'classical' overflow metabolism.

Basic Characteristics of the L-Phe Separation Using Liquid-Liquid Centrifuges

To characterize the reactive extraction in the centrifuges, off-line experiments with aqueous model solution were performed. According to the previous findings 10 $g \cdot L^{-1}$ L-Phe solution, 10 % D_2EHPA in kerosene and 1 M H_2SO_4 were used to study the effects of different volumetric flow rates and rotor speeds on the L-Phe extraction. For the sake of brevity, only basic findings are listed in the following:

- **Rotor Speed**: Within the typical range from 2,400 to 3,600 rpm, the rotor speed had almost no influence on the extraction performance.

- **Volumetric Flow Rates**: Extraction and back-extraction mass transfer was improved by increasing volumetric flow rates of the aqueous donor and of the organic phase. Technical, upper limits were found at 8 $L \cdot h^{-1}$ aqueous flow rate.

- **System Stability**: The system was less stable when unequal flow rates of light and heavy phase were used. Flow rates below 4 $L \cdot h^{-1}$ showed the best system stability. As expected, the system was more stable when L-Phe was separated from salt solution (9 $g \cdot L^{-1}$ NaCl) or from fermentation supernatant instead from pure water. In the latter case, emulsions tended to occur readily. The fermentation supernatant had to be filtered to remove cell debris and proteins, otherwise unwanted protein precipitation occurred at the aqueous/organic interface in the centrifuge. As a consequence the centrifuges were operated such that the organic/aqueous interface was radially driven

---

[30] The molar weight of L-Phe is about 165 $g \cdot mol^{-1}$.

[31] Please notify that this value is only slightly higher than the maximum concentrations found using *E. coli* 4pF20.
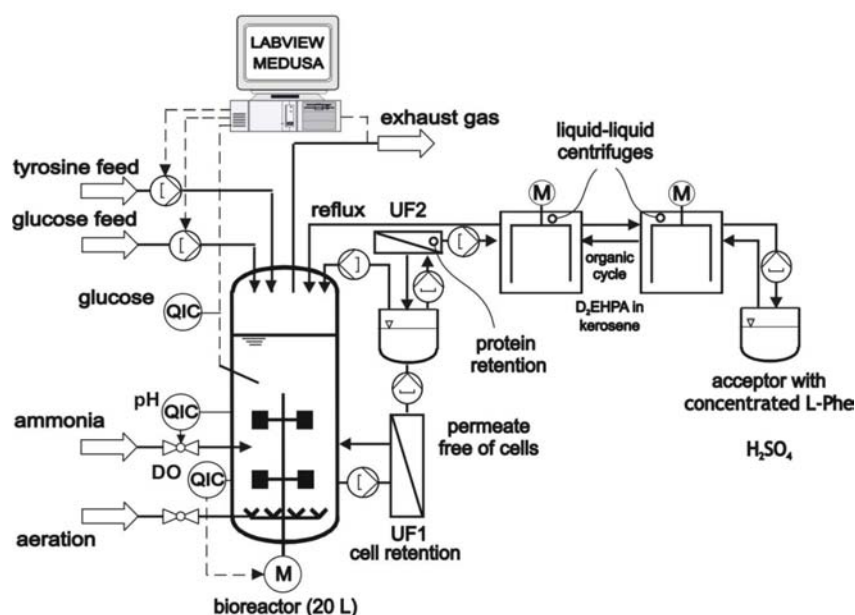
FIGURE 4.59. Experimental setup of the total *ISPR* process using two liquid-liquid centrifuges for reactive L-Phe extraction out of cell- and protein-free permeate drained off from the ultrafiltration module 1 (UF1, 500 kD) which is installed in the bypass of the 20-L bioreactor. As indicated, glucose and tyrosine are controlled, as well as pH, dissolved oxygen (DO), temperature (not indicated) and pressure (not indicated). Via the reflux, the reactive extraction unit is fully integrated in the production process. Reference fermentations are carried out solely using the fermentation equipment as shown.

> into the centre of the centrifuge thus enabling a small fraction of the heavy phase to leave the device via the light phase outlet.

- **Extraction components**: Different concentrations of L-Phe (from 60 to 120 mM), carrier (from 10 to 20 %) and sulfuric acid (from 1 to 2 M) were investigated. The carrier concentration was identified as the most dominating component. A six fold L-Phe concentration of (initially) 15 $g \cdot L^{-1}$ in the aqueous phase to 90 $g \cdot L^{-1}$ in the acceptor (leaving 4 $g \cdot L^{-1}$ L-Phe back in the donor phase) was achieved with 1 M H_2SO_4.

Integrated Experiments

The total *ISPR* experimental setup is illustrated in Figure 4.59. While running the fermentation process, cell-containing biosuspension was recycled through the bypass which retained the cells with an ultrafiltration module. Cell-free permeate flowed into a buffer tank and from there into an addi-
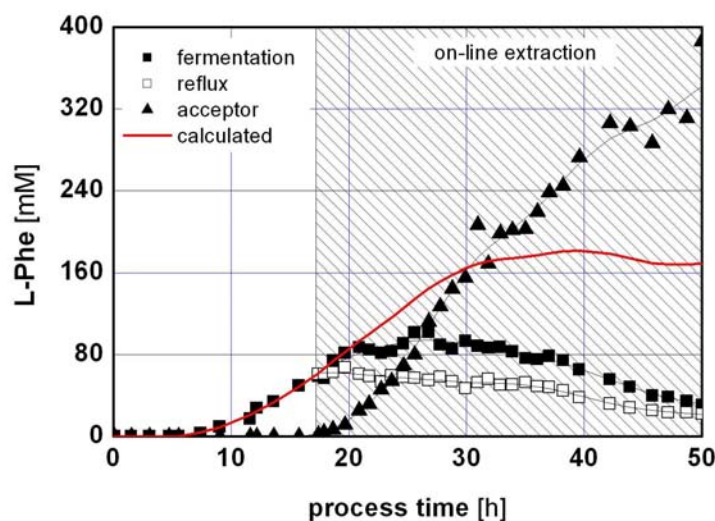
FIGURE 4.60. L-Phe concentration courses are shown regarding the acceptor phase, the fermentation suspension and the reflux during a 32-*h ISPR* experiment (marked area) with integrated reactive extraction. Additionally, the calculated L-Phe course (line) is given with respect to the total amount of separated and accumulated L-Phe relative to the working volume of the bioreactor.

tional ultrafiltration unit for protein retention[32]. The setup of two subsequent filtration units was chosen to minimize the cell-containing by-pass volume thus avoiding unwanted oxygen or *pH* gradients. Nevertheless the ultrafiltration area had to be large enough to allow 1.5 - 3.5 $L \cdot h^{-1}$ to permeate to the extraction devices. The L-Phe-reduced aqueous donor phase leaving the centrifuge was recycled into the bioreactor. Back-extraction of L-Phe took place in the second centrifuge.

All fed-batch fermentations were started without running the bypass. L-Phe production was induced after 7 hours process time (see Figure 4.60) and cell growth was stopped by limited tyrosine supply after 14-15 hours. After 18 hours process time a product concentration of about 65 $mmol \cdot L^{-1}$

---

[32] The additional protein retention step was found to be essential to prevent unwanted precipitation of proteins and/or cell debris in the liquid-liquid centrifuges. Compared to the previously presented *ISPR* process, this additional separation step complicated the setup at first sight. However, the handling of the centrifuge-based reactive extraction unit turned out to be (still) significantly easier than the operation of the hollow fiber modules.

was achieved, and bypass recycling together with reactive extraction was started simultaneously.

Based on the preliminary experiments the reactive-extraction conditions with respect to the best phase stability were installed: rotor speed: 2,400 rpm, organic flow rate: 2 $L \cdot h^{-1}$, acceptor flow rate: 2 $L \cdot h^{-1}$, permeate flow rate: $1.5 - 3.5$ $L \cdot h^{-1}$. In the case of the permeate stream, the flow depended on the time-variant filtration permeability, basically caused by biofouling.

As indicated in Figure 4.60, production and extraction worked at the same time. While the L-Phe concentration in the bioreactor remained constant for 20 hours and even decreased during the last 12 hours of the process time, the L-Phe level in the reflux of the centrifuge was about half of the bioreactor concentration, thus indicating the extraction capacity. In the 5 L acceptor tank, L-Phe titers steadily increased to 360 $mmol \cdot L^{-1}$ (60 $g \cdot L^{-1}$), which is more than 10-fold higher than the concentration in the bioreactor. Relative to the bioreactor working volume, a maximum L-Phe concentration of about 180 $mmol \cdot L^{-1}$ (30 $g \cdot L^{-1}$) would have been achieved. Although this value is slightly lower than the maximum titer of the reference fermentation (see Figure 4.58), the benefits of the on-line reactive extraction should be considered leading to highly concentrated L-Phe in the acceptor that can easily be further processed by precipitation.

Most strikingly, the fully integrated centrifugal reactive-extraction showed its general applicability by allowing stable operation conditions for more than 32 hours. Obviously, the primary assumed inhibiting effects of the solvent and/or of the carrier were not dominant. During the first 20 hours, the L-Phe separation rate kept pace with its microbial formation rate, indicating that cellular metabolism was not hampered. However, after 38 hours indications were observed that the metabolism activity declined thus reducing the L-Phe formation rates (data not shown).

From this the conclusion was drawn that reactive extraction based on liquid-liquid centrifuges is promising and that the duration of on-line extraction should be a parameter for total process optimization.

Hence a shorter on-line extraction period was studied. Additionally, the flow rates of the organic and the acceptor phase were set to 3.5 and ~ 2 $L \cdot h^{-1}$ to increase L-Phe separation rates and to stabilize the extraction system. The resulting L-Phe concentration curves are shown in Figure 4.61. indicating that L-Phe production started after 7 hours. Compared to the preceding experiment, reactive extraction was actuated later (after 22 h process time) because the pre-chosen threshold value of 90 $mmol \cdot L^{-1}$ was also achieved later owing to a slightly lower biomass concentration.
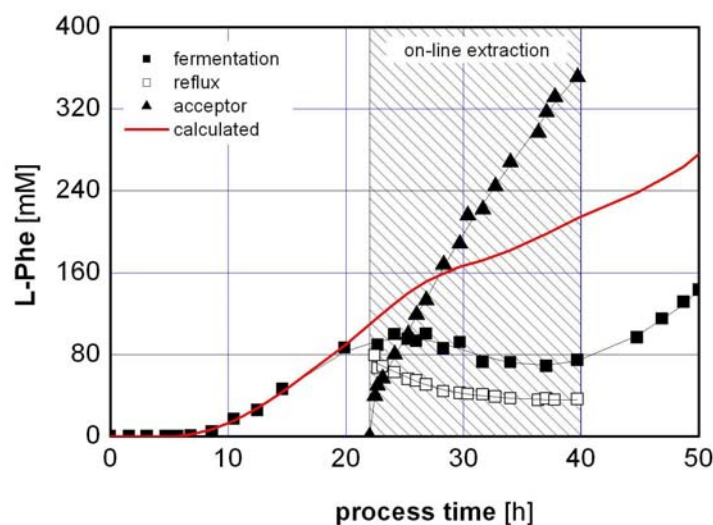
FIGURE 4.61. L-Phe concentration courses are shown regarding the acceptor phase, the fermentation suspension and the reflux during a 18-*h ISPR* experiment (marked area) with integrated reactive extraction. Additionally, the calculated L-Phe course (line) is given with respect to the total amount of separated and accumulated L-Phe relative to the working volume of the bioreactor.

As shown, the on-line L-Phe separation was running for 18 hours. During this period, the L-Phe level in the bioreactor slightly decreased and the reflux contained about half of the amount of L-Phe in the reactor. 350 $mmol \cdot L^{-1}$ (58 $g \cdot L^{-1}$) L-Phe was concentrated in the acceptor, which is almost nine times higher than the level in the fermentation suspension. After 40 hours the extraction was stopped whereas the fermentation continued until 50 hours. This procedure was performed to test the metabolic activity of the cells after reactive extraction. As shown in Figure 4.61, product formation still took place increasing the L-Phe titers in the fermentation supernatant to 143 $mmol \cdot L^{-1}$ (23.5 $g \cdot L^{-1}$). Thus we concluded that the cells were still active and they were not inhibited by, for example, too high kerosene or carrier concentrations. Relative to the final working volume in the bioreactor, a maximum titer of 275 $mmol \cdot L^{-1}$ (45.5 $g \cdot L^{-1}$) was achieved.

To qualify the *ISPR* process, the space-time yield (STY) based on the calculated L-Phe concentrations (see Figure 4.61) is given in Figure 4.62. As shown, STY values from 0.8 to 2.0 $g \cdot (Lh)^{-1}$ (5 to 11.5 $mmol \cdot (Lh)^{-1}$) were achieved during the production phase. The initial drop of the production STY (immediately after the reactive-extraction start) is similar to
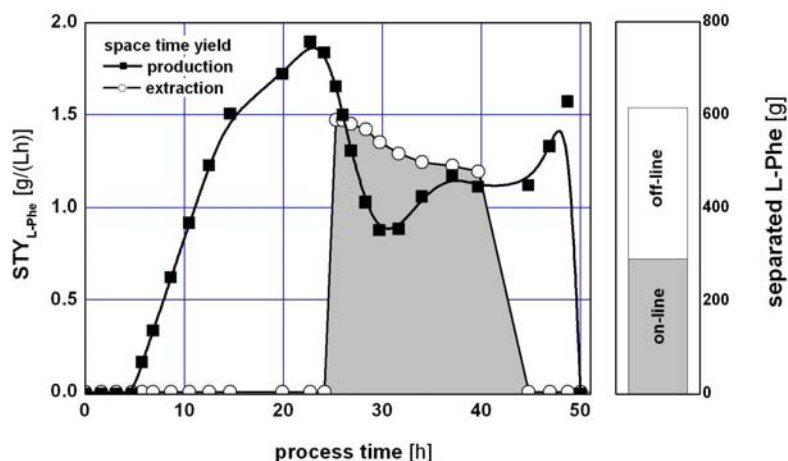
FIGURE 4.62. Space time yield (STY [g/(Lh)]) during the 18-*h ISPR* process considering L-Phe formation and on-line L-Phe extraction. The total amount of L-Phe produced [g] and separated during the experiment is shown at the right-hand side

previous findings described by Gerigk *et al.* [GMK$^+$02] and – strictly speaking - not yet fully understood. Because any gradients of dissolved oxygen, concentration or pH inside the bypass circulation can be ruled out due to low bypass residence times of 3 to 4 seconds, the working hypothesis is formulated that product formation declined owing to the increased shear stress which is imposed on the cells during their bypass circulation. This negative effect is more or less compensated during the course of separation. In general, L-Phe extraction rates from 1.2 to 1.5 $g \cdot (Lh)^{-1}$ (7 to 9 $mmol \cdot (Lh)^{-1}$) were maintained during the whole separation period thus keeping the L-Phe level in the suspension almost constant. In total, 616 g (3.73 mol) L-Phe was produced and approximately half (290 g which represents 1.76 mol) could be extracted on-line. The rest was left in the biosuspension for off-line separation after fed-batch production.

Besides L-Phe separation analysis, differences between the experiments with and without integrated reactive extraction can also be seen regarding the acetate formation (data not shown). In the reference fermentation, acetate production started already after 30 hours when L-Phe formation decreased. Similar results were obtained in the fermentation using long-lasting (32 hours) reactive extraction, when acetate formation began after 38 hours process time, again correlated to the decline of L-Phe formation.
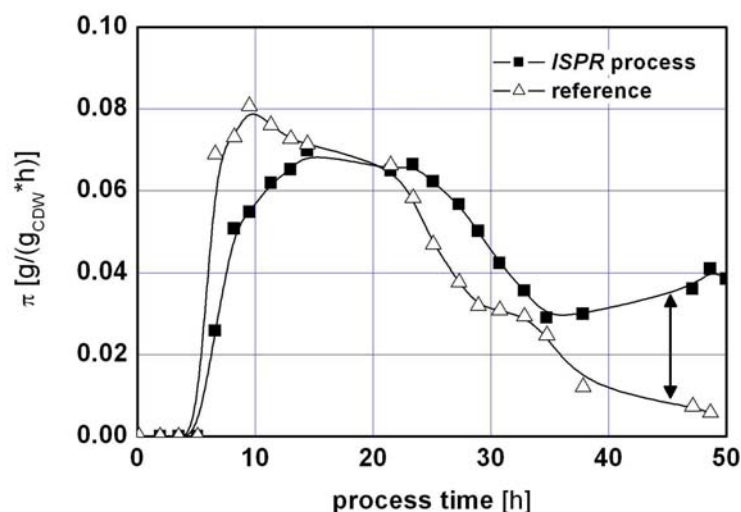
FIGURE 4.63. Comparison of biomass-specific product formation rates in the reference fed-batch fermentation without integrated reactive extraction and in the *ISPR* process considering the 18 hours lasting reactive extraction.

Therefore and because glucose and oxygen supply remained constant during the whole production period, we regard acetate formation as a cellular response to the diminishing ability to convert glucose into L-Phe which, for instance, can be caused by decreasing DAHP synthase activity. The latter was observed experimentally [GBGN⁺02] and can also be a consequence of L-Phe feedback inhibition, shown in the preceding subsection. Interestingly, almost no acetate production was found during the 18-hours-lasting reactive extraction experiment. As already emphasized, no cessation of L-Phe formation was observed which consequently resulted in low acetate titers, thus outlining an additional benefit of the integrated reactive extraction approach.

Clear differences can be seen in comparing the production rates of a reference fermentation without integrated L-Phe separation with those of the *ISPR* approach using integrated reactive extraction for 18 hours (Figure 4.63). During the *ISPR* period, the production rate was maintained at a constant level of about 0.03-0.04 $g \cdot (gh)^{-1}$ until the end of the experiment whereas it decreased to zero after 35 h in the reference fermentation. As a consequence, the integral, molar L-Phe/glucose yield enhanced from 14.5 % in the reference fermentation to 18.6 % in the *ISPR* approach, which represents a 28 % <u>relative</u> yield rise. This relative yield improve-

ment is comparable to the results of the membrane based *ISPR* approach using *E. coli* 4pF20 for L-Phe production. From this we concluded that the on-line L-Phe separation obviously avoids the inhibitory product accumulation (with respect to the DAHP synthase activity). However, this phenomenological finding cannot be substantiated by e.g. *in vivo* enzyme activity measurements or by quantitative analysis of the potentially beneficial effect of D_2EHPA addition, as previously proposed [Maa00]. The relevant studies have not yet been completed.

Concluding Remarks

The novel *ISPR* process based on reactive extraction with liquid-liquid centrifuges proved its applicability for on-line L-Phe separation and concentration using the strain *E. coli* 4pF81. This system represents the first approach known so far for fully integrated reactive extraction based on liquid-liquid centrifuges to separate bioproducts from a microbial production process.

It was shown that the *ISPR* approach (using reactive extraction for 18 hours) is superior to the reference fermentation without product separation because of

- the significantly extended high-level product formation period of 0.03 to 0.04 $g \cdot (gh)^{-1}$ (about 0.25 $mmol \cdot (gh)^{-1}$) to the end of the process,

- the prevention of unwanted by-product accumulation (acetate), and

- the consequently increased integral L-Phe/glucose yield from. 14.5 % (without) to 18.6 % (with) fully integrated reactive extraction.

Compared to the membrane based reactive extraction approach the centrifuge technique offers the advantage of simplified handling and higher L-Phe permeability, which consequently leads to a facilitated system scale-up. While both approaches enable an on-line concentration of L-Phe, the liquid-liquid centrifuges support higher L-Phe concentrations in the acceptor (up to 360 mM, 60 $g \cdot L^{-1}$), which significantly reduces the amount of liquid to be handled during further product purification, for instance during precipitation.

This approach allows the online separation of almost half of the total L-Phe produced during the fed-batch process, which is higher than the previously described value of 26.7 %. If volumetric extraction rates are compared, the *ISPR* approach using liquid-liquid centrifuges also offers some advantages. Here 1.19 – 1.47 $g_{L-Phe} \cdot (Lh)^{-1}$ is extracted, while the membrane-based extraction only achieved approximately 1/3 of this, i.e.

$0.3 - 0.5 \ g_{L-Phe} \cdot (Lh)^{-1}$. Hence, the primary formulated aims of developing a novel *ISPR* process to reach higher L-Phe permeability, improved L-Phe/glucose yields and simplified operation procedures are fulfilled by applying liquid-liquid centrifuges for reactive extraction thus qualifying this tool as interesting for the on-line (cation) separation of inhibitory products.

4.6 L-Phenylalanine Process Development: Conclusions and Outlook

- **Preliminary Studies**: An experimental bioreactor setup was installed allowing 6-fold, parallel fed-batch fermentations of novel strains under realistic process conditions. The application of exhaust gas analysis enabled the analysis of carbon balances already in this small-scale as one of the first steps of strain qualification. Principal component analysis (PCA) was successfully applied for fermentation data identifying tyrosine and acetate as fermentation key variables which were thus focused in subsequent experiments.

- **Fed-Batch Process Development:** A tyrosine and glucose - controlled fed-batch strategy was developed that even allowed to use the tyrosine feedback-sensitive (wild-type) enzyme AroF instead of the usually applied feedback resistant AroF^{fbr}. This strategy is even superior to the alternatives (using AroF^{fbr}) because higher L-Phe titers (up to 32.2 $g \cdot L^{-1}$) and maximum L-Phe/glucose yields of about 18% $mol \cdot mol^{-1}$ were reached. The glucose and tyrosine control approach was shown to be upscalable to the 300-L bioreactor. Experiments with *E. coli* 20pMK12 (possessing a non-PTS based glucose uptake based on the glucose facilitator from *Zymomonas mobilis*) revealed that the glucose uptake and the L-Phe formation rate strongly depend on the extracellular glucose levels. Because PTS^{+} strains reached higher L-Phe titers and better L-Phe/glucose yields than the PTS^{-} construct, future strain development focused on PTS^{+} strains.

- **Identification of the Reactive Extraction System:** Motivated by the obviously existing L-Phe feedback inhibition on product formation, studies were performed to identify an appropriate reactive extraction technique which was intended to be used as a fully integrated L-Phe removal approach. After detailed preliminary studies, the cation-selective carrier D$_2$EHPA, dissolved in kerosene using H$_2$SO$_4$ as counter ion donor was identified as a suitable system for on-line L-Phe separation using hollow fiber modules for extraction and back-extraction on pilot scale. High product purity up to 99% was achieved by subsequent (simple) precipitation of the concentrated L-Phe in the acceptor (stripping) phase. Reactive extraction worked at pH 6.5 thus allowing its application at typical fermentation pH (and temperature). In lab-scale fermentation experiments the addition of D$_2$EHPA resulted in enhanced L-Phe/glucose yields. Simple mass transfer studies gave rise to the assumption that the carrier regeneration might be incomplete during back-extraction.

- **Membrane Based *ISPR* Process:** Combining a 300-L bioreactor with the reactive extraction unit, pilot-scale experiments studying

the total *ISPR* process were performed. It was found that total L-Phe/glucose yield was improved from about 13 $mol\%$ (without) to 17.5 ($mol\%$) with reactive extraction. L-Phe was extracted on-line with maximum rates of 110 $g \cdot h^{-1}$ leading to final titers of 37 $g \cdot L^{-1}$ (after 48 h) in the aqueous acceptor. Hence reactive extraction proved its applicability as a fully integrated technique at the same time purifying and concentrating the product in the acceptor phase.

- **Total Process Modeling**: The total, pilot-scale *ISPR* process was modeled using a coupled, differential equation system considering the reactive extraction unit as well as the 300-L fed-batch bioreactor. The model was applied for total process optimization revealing the complex interactions of the reactive extraction unit thus underlining the necessity for detailed simulation studies. The analysis of L-Phe mass transfer experiments uncovered that the dominating mass transfer limitation is located in the back-extraction module, expressed by k_{CPheA}, which denotes the transport resistance of the low-soluble carrier/L-Phe complex entering the aqueous acceptor phase. Furthermore, L-Phe extraction is limited by the diffusive transport of L-Phe cations to the aqueous/organic interface, encoded by k_{PheD}. Because both transport resistances are located in the aqueous phases in strictly laminar hydrodynamic conditions the conclusion is drawn that total mass transfer enhancement can be achieved by installing turbulent hydrodynamics instead.

- **Reactive Extraction with Centrifugal Extractors:** Motivated by the modeling results, liquid-liquid centrifugal extractors were applied for the first time to separate a bioproduct such as L-Phe from a fed-batch process in a fully integrated *ISPR* approach. As a result, the overall L-Phe/glucose yield of the reference fermentation with *E. coli* 4pF81 of 14.5 mol % was increased to 18.6 % in the *ISPR* approach. L-Phe was concentrated to 60 $g \cdot L^{-1}$ in the aqueous acceptor phase thus significantly reducing the amount of liquid to be handled for further product purification, such as precipitation (see preceding results). Because of the improved mass transfer conditions inside the turbulent mixing chamber of the liquid-liquid extractors, about 3-times higher L-Phe permeability was observed (about 1.2 to 1.5 $g \cdot (Lh)^{-1}$) compared to the membrane based *ISPR* process. The online separation of L-Phe using liquid-liquid centrifuges fully compensated the product formation rate thus leading to constant L-Phe levels during the *ISPR* period. Furthermore the handling of the liquid-liquid centrifugal extractors turned out to be much more robust than the use of the hollow fiber modules which were sensitive with respect to transmembrane pressure changes. An optimum duration of the online liquid-liquid centrifugal extraction should be considered to prevent too high permeation of the organic compounds used.

TABLE 4.8. Comparison of some characteristic process values such as the final product titer, the integral L-Phe/glucose yield and the space-time yield regarding the 'best' L-Phe production processes published so far

approach	$c_{Phe,final}$	$Y_{L-Phe,glucose}$	STY_{int}
-	$[g \cdot L^{-1}]$	[mol%]	$[g \cdot (Lh)^{-1}]$
Konstantinov *et al.* [KYNS91]	46	17	0.85
Backman *et al.* [BOM^{+}90]	50	25	1.39_{36h}
Rüffer *et al* [RHK^{+}03].	$45.5/60^{a}$	18.6	0.91_{50h}^{b}

^{a}45.5 $g \cdot L^{-1}$ represent the calculated titer with respect to the final working volume in the bioreactor and about 60 $g \cdot L^{-1}$ in the acceptor

^{b}50 h process time were considered, however the optimum process time can be reduced thus increasing the total STY

To sum up, Table 4.8 is given comparing only the best L-Phe process results published so far with those of our own studies regarding *E. coli* 4pF81 in the *ISPR* process using the liquid-liquid centrifugal extractors. As it is shown, the characteristic process values considering the *ISPR* approach are superior to those of Konstantinov *et al.* [KYNS91]. However they do not yet achieve the overall L-Phe/glucose yield and the space-time yield of Backman *et al.* [BOM^{+}90]. With respect to the precedingly mentioned L-Phe inhibition, Backman *et al.* [BOM^{+}90] obviously succeeded to select an appropriate L-Phe production strain which is not L-Phe inhibited anymore thus possessing an inherent advantage even compared to the *ISPR* process.

However, as pointed out in the introductory section, such a fully feedback resistant strain was not available for our process development. Hence the *ISPR* results obtained basically illustrate the quality of these techniques achieving significant process improvements to a competitive level even considering non-feedback resistant strains (see summarizing Figure 4.64). Additionally one should consider that L-Phe has to be separated and purified from the biosuspension anyway - also in the Backman *et al.* [BOM^{+}90] process. Therefore, the concentration of L-Phe in the acceptor phase subsequently allowing a simple product purification represents an additional advantage of the *ISPR* process which was not even considered in the competing process developments published so far. Presumably this is also why the cooperating partner DSM regards this process as such interesting to perform economical evaluations.

Additionally it should be mentioned that the 'L-Phe'-technology presented in the preceding section was one of the driving forces to start a new cooperation (CHORUS) with the same industrial partner in 2002 - now focusing on derivatives of chorismate, the branch point intermediate of the aromatic amino acid pathway. As shown in Figure 4.65, recent experiments of Bujnicki [Buj03] succeeded to produce the precursors for pharmaceutical drugs 2,3 cyclohexane diol (not shown) and 3,4 cyclohexane diol (3,4
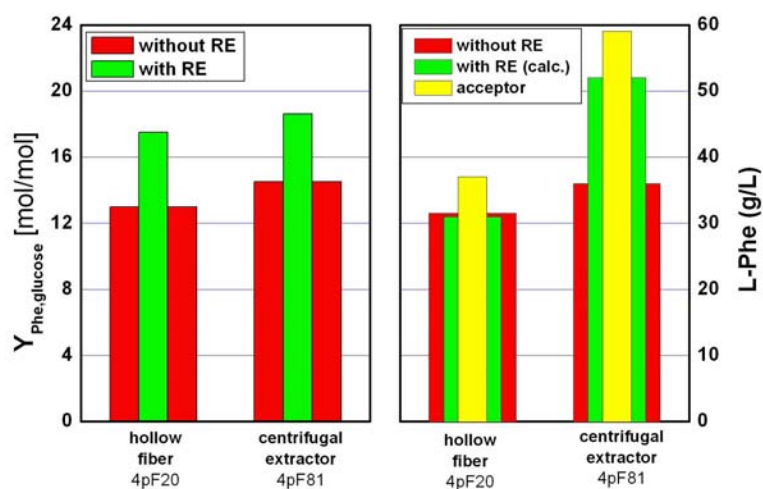
FIGURE 4.64. Comparison of the integral L-Phe/glucose yields $Y_{Phe,glucose}$ and the final L-Phe titers achieved using the reactive extraction $ISPR$ processes with hollow fiber modules or liquid-liquid centrifuges and the *E. coli* L-Phe producers *E. coli* 4pF20 or *E. coli* 4pF81, respectively.
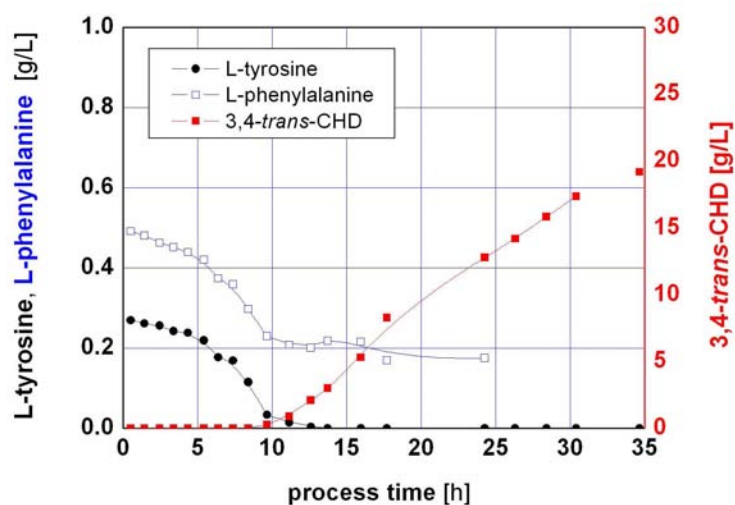
FIGURE 4.65. Example of a typical fermentation for the *E. coli* based production of 3,4 cyclohexane *trans* diol (3,4 *trans* CHD) using L-tyrosine and L-phenylalanine auxotrophic strains.

trans CHD) up to the 300-*L* bioreactor scale with *E. coli* constructs. For the sake of brevity and because of intellectual property reasons, strain as well as fermentation details are not presented. However, it can be outlined that reactive extraction is again considered for product separation together with some basic process and strain properties introduced in the preceding sections.

5

Pyruvate Bioprocess Development
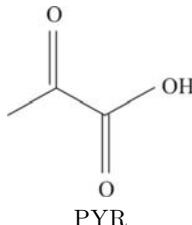
Significant parts of the following section were already published by
Zelić *et al.* [ZGB[+]03] or are currently in press [ZGV[+]03] and have
been applied for patents ([GBZT01], [BGZT02]). Results are ac-
quired during the Ph.D. thesis of B. Zelić [Zel03] who was co-supervised
by the author.

5.1   Introduction

While the preceding chapter regarded the production of a building block
(the aromatic amino acid L-Phe), this chapter focuses on the production
of a primary metabolite of the central metabolism - namely pyruvic acid
or its salt pyruvate (see Table 5.1)[1]. The carboxylic acid pyruvate rep-
resents without doubt one of the most important metabolites in central
metabolism, due, for instance, to its significance for the phosphotransferase
(PTS) dependent glucose uptake, its role as a precursor for amino acid syn-
thesis, overflow metabolism and so on. Fell and Wagner [FW00] outlined
the importance of pyruvic acid as a reactant in the *E. coli* network by
identifying it as one of the mostly used reactants (apart from common
coenzymes).

---

[1]It is noteworthy that pyruvic acid production and L-Phe formation are obviously
closely related because of the precursor PEP, needed for the latter, which also represents
a predecessor of intracellular pyruvate formation.

TABLE 5.1. Some selected characteristics of pyruvic acid

Structure	Properties.	
PYR		$C_3H_4O_3$
	M_r	88.063
	solubility	hydrophilic
	stability	decomposition observed in fermentation medium at room temperature
	pK_a	2.49, strong acid
	comment	smells like acetic acid
		melting point at $12°C$
		boiling point at $165°C$
		salts are called 'pyruvate'
		commercially sold as calcium pyruvate, etc.

Apart from its significance in metabolism, pyruvate might not be known as a commercially interesting building block for chemical synthesis. However, it serves as an effective starting material for the synthesis of many drugs, cosmetics and agrochemicals such as crop protecting agents [LCL01] and it even found application in the food industry as a fat burner ([Sta82], [Sta85], [SRG+90]). The latter is motivated by pyruvate's attributed quality to accelerate the catabolism of fatty acids in the human body. Furthermore, medical studies (using rats) indicated that pyruvate serves as a potent antioxidant [DBHS93] thus reducing anoxic injury and free radical formation [BS93] and it finally can prevent the neuronal degeneration associated with ischemia [IO95]. The carboxylic acid is also a valuable substrate for the enzymatic production of amino acids [YK78] such as L-tryptophane ([NEOY72], [TYT84], [KYT96]), L-tyrosine [YKK+72] and L-dihydroxyphenylalanine (L-DOPA, [LCL01]).

Own studies estimated a worldwide pyruvate market of about 800 to 1,200 tons per year with current market prices of 10 to 25 € kg^{-1} for ton-scale production. Even much higher pyruvate prices were found applying pyruvate salts as fat burner. While approximately 60% of the total pyruvate production are used as a moisturizer in the cosmetic industry, the remaining amount is mostly applied for L-ephedrine synthesis (asthma drug), L-DOPA synthesis (active agent for Parkinson disease treatment) and as food ingredients.

Regarding the classical chemical synthesis (see Figure 5.1), which is still in use today [Röm95], pyruvate is produced by the dehydration and decarboxylation of the raw source tartaric acid in the presence of potassium hydrogen sulfate at $220°C$ [HF32]. It is noteworthy that this classical process is energy intensive because of the first pyrolysis step preparing the raw pyruvate and because of the following vacuum distillation at $80°C$. Additionally it should be notified that pyruvate production thus depends on the
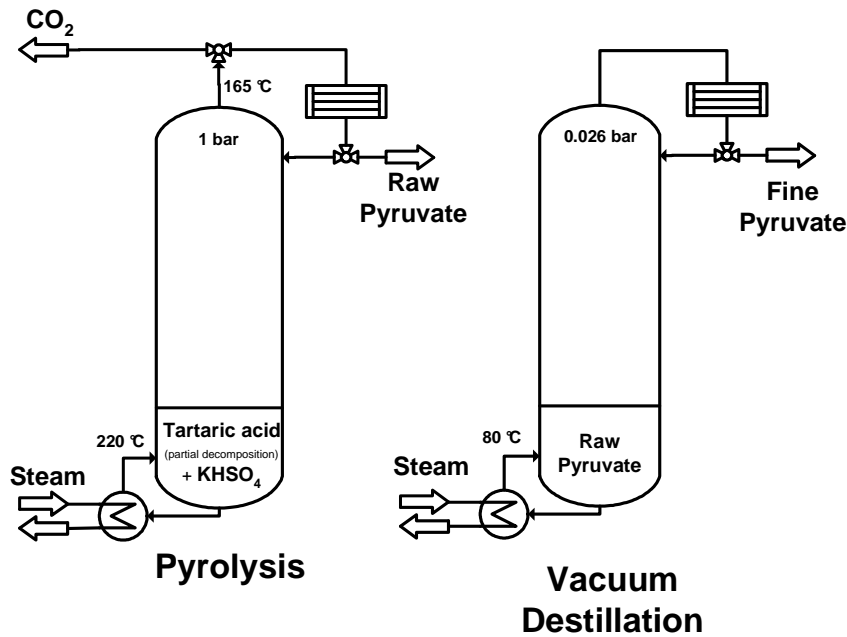
FIGURE 5.1. Classical production of pyruvate from tartaric acid in a two-step approach using pyrolysis for the production of raw pyruvate followed by vaccum distillation for product purification. Ample amounts of $KHSO_4$ were needed to decompose the raw material tartaric acid at $220°C$. The classical production process, dated from 1932, is still in use.

availability of tartaric acid, which as a raw product, is subject to seasonal chances.

Besides, the decarboxylation of diethyl tartrate [SFKH92], oxidation of propylene glycol ([TOS$^+$92], [IKI93]), dehydration of ethylene glycol [SFI$^+$91] and oxidative dehydrogenation of lactic acid [AO95], in the presence of heavy metals as catalysts and high temperatures, are common methods of pyruvate production. These "classical" processes have in common that they are energy-intensive and that they make use of heavy metals, which is controversial with respect to environmental protection and sustainable process development. Additionally, these processes turned out to be cost-intensive as well [LCL01]. As a consequence more sustainable "green" process alternatives have been developed in the last two decades.

Among these approaches, the following variants can be found:

- **enzymatic approaches** using either isolated enzymes [BS87] or permeabilized *Hansenula polymorpha* or *Pichia pastoris* cells ([ADW96], [ESG$^+$97]) to convert glycolate or lactate to pyruvate

- **resting cells** converting for instance 1,2 propanediol with *Acinetobacter sp.*.[IMTY82], or saccharified citrus peel extract with *Debaryomyces couderii* cells [MSH84], or using lipoic acid auxotroph *Enterobacter aerogenes* [YT89], or converting R-lactate with *Proteus sp.*.[SS93], or applying fumarate as substrate [OSIS01]

- **fermentation processes,** to be presented further down.

Although the above-mentioned approaches are promising, they have some inherent disadvantages as follows:

- The maximum theoretical yield of lactate-based pyruvate production is $1\ mol \cdot mol^{-1}$, whereas $2\ mol \cdot mol^{-1}$ can be produced theoretically using a C6-skeleton such as glucose.

- Current large-scale market prices of lactate, the alternative substrate of glucose (see above), are approximately five times higher (about 1.5 € kg^{-1}) than glucose prices (0.3 € kg^{-1}), not taking into account the advantages in atom-economy, as mentioned in the preceding item.

- Following the route of enzymatic synthesis, hydrogen peroxide may be produced, which leads to an unwanted pyruvate decomposition to acetate, carbon dioxide and water, and finally lowers the reachable production yield.

- Often, the above-mentioned methods only achieve low titers (about $30\ g \cdot L^{-1}$), which make the total process development unattractive for an industrial scale-up because of high downstream costs for pyruvate recovery.

- In the case of the resting cell approach, an expensive multiple step procedure including biomass concentration together with costly wastewater removal is proposed.

Hence, fermentation processes can be superior to the aforementioned approaches because fermentations offer the opportunity to produce pyruvate from the sustainable, low-cost substrate glucose with high product / substrate yield while at the same time avoiding the coproduction of unwanted by-products such as H_2O_2.

Therefore fermentation development was performed typically based on glucose as the main substrate. Several examples are given considering the multi-auxotrophic yeast *Torulopsis glabrata* ([MYYT90], [YM94], [MY96], [HYS99], [HS99], [MY99], [LCLL00], [HAKS01], [LCLR01] and [LHCL02]). Other approaches studied lipoic acid auxotrophic (F_1-ATPase deficient) *E. coli* strains ([YST$^+$94], [YTT$^+$94], [YHT$^+$97]). In general, both approaches followed the same idea, namely to control pyruvic acid production

by the supply of e.g. lipoic acid, which, in the case of *E. coli*, reached 30 $g \cdot L^{-1}$ in 24 hours with glucose as the sole carbon source. Additionally, other approaches were published using for instance *Schizophyllum commune* [TT82], *Photobacterium mandapamensis* [AVRS81] *Enterobacter* [YT89] and *Enterococcus* [YMM^{+}92] strains.

Among the pyruvate production processes published so far, the fermentation approach followed by Li *et al.* [LHCL02] using *Torulopsis glabrata* achieved the highest titer of 69 $g \cdot L^{-1}$ pyruvate together with the highest pyruvate/glucose yield of 0.636 $g \cdot g^{-1}$ thus offering the best possibilities for further downstream processing. However, the volumetric productivity of this process is relatively low (29.8 $g \cdot (Ld)^{-1}$), which obviously hampers its use for industrial purposes. Additionally, the production strain is multi-vitamin auxotrophic, thus demanding the maintenance of a concentration balance between thiamine, nicotinic acid, pyridoxine and biotin [LHCL02] during the large-scale production which can cause severe problems in industrial applications.

Hence, the aim was followed to develop a novel fermentation process that achieves as high titers and pyruvate/glucose yields as the best *Torulopsis glabrata* process (known so far) concomitantly offering significantly improved space-time yields to enable its industrial application.

In the following, the activities for process development will be presented which based on the *E. coli* strains resulting from a fruitful cooperation with biochemists and molecular biologists at the Institute of Biotechnology 1 (namely M. Bott and T. Gerharz [Ger03]) together with the industrial partners Rhein Biotech GmbH (Düsseldorf, Germany) and later on Amino GmbH (Frellstedt, Germany). Because indications were given that high pyruvate titers ($\succ 500\ mM$) might inhibit pyruvate production [LCLR01], the integration of downstream processing as an *ISPR* approach was considered as well as appropriate process alternatives to alleviate the pyruvate burden.
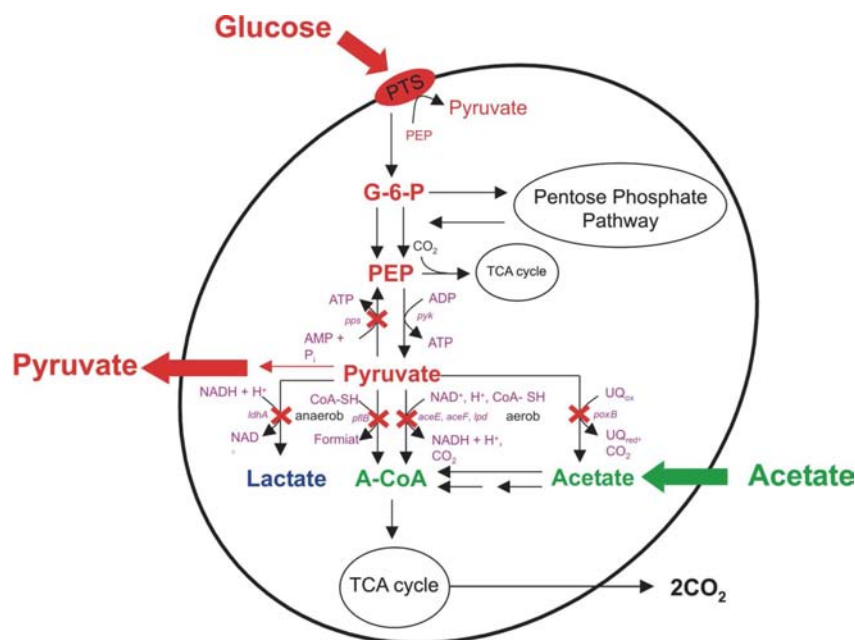
FIGURE 5.2. Scheme of the favored pyruvate producing strain *E. coli* YYC202 ldhA::Kan, which is blocked in its ability to convert pyruvate into formate, acetyl Co-A, acetate and lactate. Acetate must be supplemented for cell growth. Glucose is used as the main carbon source for pyruvate production.

5.2 Experimental Conditions

Primary fermentations were performed using the strain *E. coli* YYC202, which was subsequently replaced by the pyruvate producer *E. coli* YYC202 *ldhA*::*Kan*. Both strains were acetate auxotrophic as indicated in section A.1.2, Appendix. As shown in Figure 5.2 *E. coli* YYC202 *ldhA*::*Kan* is blocked in its ability to convert pyruvate into acetate, formate, acetyl-CoA or lactate[2]. Fed-batch experiments were carried out in a 7.5-L bioreactor (INFORS, Switzerland) containing 2.5 L starting medium (see section A.2.3, Appendix) which was equipped with standard control units for pH, pressure, temperature, aeration, stirrer speed etc. (see section A.4.2, Appendix). After sterilization of the bioreactor and peripheral equipment, fermentation medium was filled into the bioreactor through a sterile mi-

---

[2]It is noteworthy that a very similar *E. coli* strain was recently presented by Tomar *et al.* [TEA03]. However, the strains presented by this group only achieved space-time yields of 28.8 to 36 $g \cdot (Ld)^{-1}$, pyruvate/glucose yields of 0.72 to 0.78 $g \cdot g^{-1}$ and final pyruvate titers about 35 $g \cdot L^{-1}$ which is inferior to the results achieved with our *E. coli* producers, as it will be shown in the following.
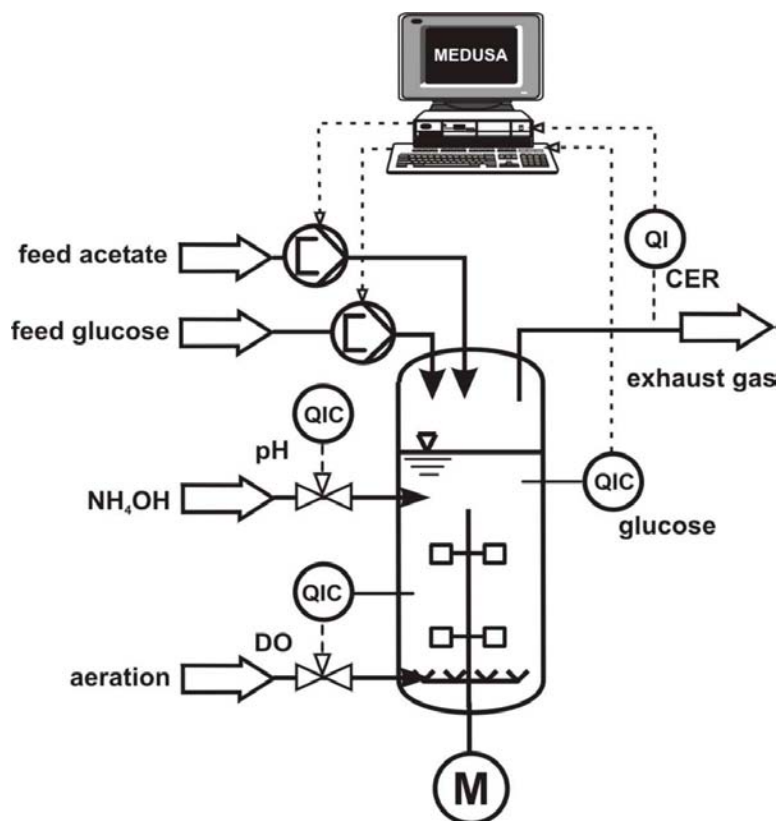
FIGURE 5.3. Scheme of the experimental setup used for lab-scale experiments with the acetate auxotrophic pyruvate producing *E. coli* strains. The glucose feed is directly controlled while acetate feeding followed a control strategy using the on-line estimated carbon dioxide production rate (CER) as described in the text.

crofiltration unit (0.2 μm cut-off, Sartobran, Satorius, Germany) and the pH was adjusted to 7.0 by 25 % ammonia titration, also during the later fermentation process. All experiments were carried out at a temperature of 37 °C. Sufficient aeration (dissolved oxygen DO $\succeq$ 40 %) was obtained by vigorous stirring (200 – 1800 rpm), airflow rate ($1 - 10\ L \cdot \min^{-1}$) and reactor overpressure (0.2 – 0.8 bar). The bioreactor was inoculated with 10 % of the working volume of a preculture. Standard analytical approaches (section A.3.3, Appendix) were used for fermentation analysis.

Glucose was used as the main carbon source together with acetate, which was only supplemented during cell growth (see section A.2.3, Appendix). Glucose feeding was started when the initial concentration was reduced to about 5 $g \cdot L^{-1}$. The glucose control followed the procedure describe in

section A.4.3, Appendix. An acetate feed, according to a specific feeding strategy (see following subsections), was started after the depletion of the initial batch amount, which was indicated on-line by decreasing carbon dioxide emission rates. The feed was stopped after the biomass concentration had remained constant for 3 hours. A schematic diagram of the fermentation set-up is shown in Figure 5.3.

5.3   Development of the Fermentation Process

5.3.1   Controlled Acetate Feeding

Pyruvate process development started by using the strain *Escherichia coli* YYC202, which is completely blocked in its ability to convert pyruvate into acetyl-CoA or acetate. Consequently, acetate is required for growth on glucose minimal medium. Under acetate-limited conditions (non-growing cells) in shake flask experiments at low glucose concentration, a maximum yield of 1.7 $mol_{pyruvate} \cdot mol_{glu\cos e}^{-1}$ was achieved ([GBZT01], [BGZT02]), which could be increased up to 1.9 $mol_{pyruvate} \cdot mol_{glu\cos e}^{-1}$ using resuspended cells in buffer. These high yields were not obtained during the growth phase, when glucose is used for biomass production to a significant extent.

Hence, process development had to find an optimum between highly selective pyruvate formation and necessary biomass production – both at high reaction rates to maximize the final space-time yield. It was assumed that acetate represents a key fermentation variable to control biomass growth and highly selective pyruvate production. Because methods for on-line acetate measurements were not accessible (and presumably not successful because very-low acetate levels had to be controlled to achieve acetate limitations), an indirect controlling approach was favored. Therefore, the correlation between acetate consumption rate (ACR) and CO_2 production rate (CTR) was a matter of detailed analysis to enable an optimal on-line process control via exhaust gas analysis. Additionally, glucose concentrations were controlled on-line to ensure ample supply of the carbon source for pyruvate production.

As indicated in Figure 5.4, the retrospective analysis of a series of batch (and fed-batch) lab-scale experiments using the acetate auxotrophic *E. coli* strain revealed a close relation between the optimum acetate consumption rate (ACR) and the CO_2 production rate (CTR). To our surprise, an equal molar ratio was identified (using an acetate feed containing 109 $g \cdot L^{-1}$ potassium acetate)

$$ACR = CTR \tag{5.1}$$
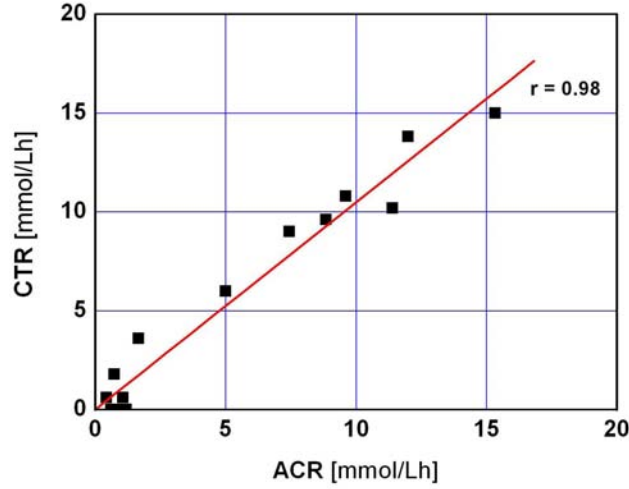
FIGURE 5.4. Relation between the CO_2 emission rate (CTR) and the acetate consumption rate (ACR) found in typical batch experiments studying pyruvate production with an acetate auxotrophic *E. coli* strain.

This heuristic finding motivated the formulation of the CTR related acetate feed $\dot{V}_{acetate}$ according to

$$\dot{V}_{acetate}[g \cdot h^{-1}] = \frac{927[g \cdot mol^{-1}] \cdot CTR[mmol \cdot (Lh)^{-1}] \cdot V_R}{f[-]} \qquad (5.2)$$

The idea of considering the parameter f was to perform process studies under acetate limitation ($f \succ 1$), saturation ($f \sim 1$) and accumulation ($f \prec 1$) just by changing parameter f.

To study the effect of different acetate feed rates (as a consequence of the open-loop control chosen) a series of experiments was performed using *E. coli* YYC202 with f set as 1.5 (limitation), 1 (saturation) and 0.8 (accumulation). To qualify the results the achieved values of molar pyruvate/glucose yield (Y_{PG}), space-time yield (STY) and final pyruvate titer c_P were considered. Superimposing impacts of potentially variant glucose levels were ruled out by controlling the glucose concentration at 5 ± 1 $g \cdot L^{-1}$ thus ensuring saturated glucose uptake conditions because of the active PTS in *E. coli* ([PLJ93], [Fer96], [Fer99]). Fermentations were realized as a two-stage fed-batch process. During the first phase (cell growth and early pyruvate production stage) glucose and acetate were fed according to the process control developed. After biomass concentration remained constant for 3 hours, the second phase (high-selective pyruvate production

stage) was started by stopping the acetate feed resulting in single glucose feeding.

As a result, reduced biomass (OD_{600} $\sim$20, compared to OD_{600} $\sim$30 at best conditions) and pyruvate titers were observed when limiting acetate supply (f set as 1.5) was installed (see Table 5.2). This finding can be explained by the strain's acetate auxotrophy demanding a sufficient external acetate supply for cell growth and maintenance, which obviously was not achieved using the acetate-limiting feeding procedure ($f = 1.5$).

TABLE 5.2. Comparison of some characteristic process values such as the final product titer, the integral pyruvate/glucose yield and the space-time yield regarding the different f-values set for acetate feeding. The strain *E. coli* YYC202 was used.

acetate supply	$c_{PYR,final}$	$Y_{PYR,glucose}$	STY_{int}
-	$[mmol \cdot L^{-1}]$	$[mol\%]$	$[g \cdot (Ld)^{-1}]$
f = 1.5[a]	209 (18.4)[d]	34	12.3
f = 1.0[b]	521 (45.8)[d]	86	46.5
f = 0.8[c].	500 (44.0)[d]	80	30.0

[a]acetate limitation

[b]acetate saturation

[c]acetate accumulation

[d]pyruvate concentration in $g \cdot L^{-1}$

On the other hand, no negative effect of acetate accumulation on pyruvate production and biomass growth was observed. This seems to be in contrast to previously published results focusing on other *E. coli* strains, where inhibiting acetate concentrations were identified at about 5 to 10 $g \cdot L^{-1}$ [LS90]. Acetate concentrations even higher than 20 $g \cdot L^{-1}$ were still tolerated by *E. coli* YYC202.

The maximal product titer $c_{PYR,final}$ was limited to concentrations of about 500 ± 20 $mmol \cdot L^{-1}$, irrespective whether saturating or accumulating acetate feeds were used (see Table 5.2). Even at optimized process conditions ($f \leq 1.0$) a significant coproduction of lactate (final lactate titer: $\succ$ 300 $mmol \cdot L^{-1}$ (26 $g \cdot L^{-1}$)) was observed in each experiment. Interestingly, the most significant increase of lactate formation occurred after the final pyruvate concentration reached its maximal value of about 500 ± 20 $mmol \cdot L^{-1}$.

From this the conclusion was drawn that the coproduction of lactate cannot be suppressed by process engineering means and that the construction of a new genotype is advantageous. As a consequence, the new production strain *E. coli* YYC202 *ldhA*::*Kan* was constructed by our cooperating
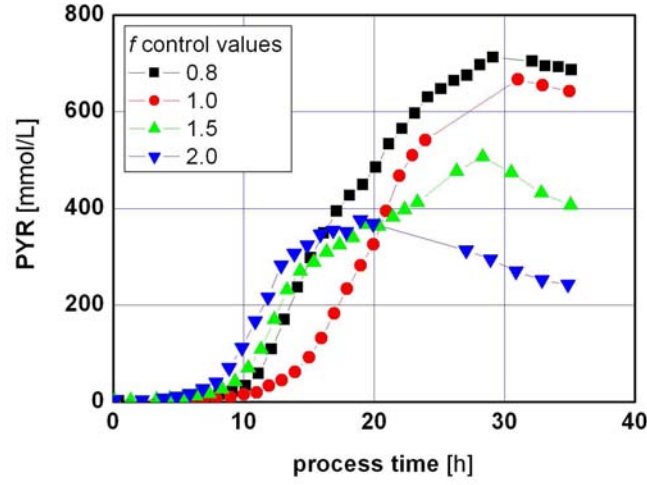
FIGURE 5.5. Resulting pyruvate (PYR) concentrations as a function of process time and the acetate feeding using *E. coli* YYC202 *ldhA::Kan* fed-batch fermentations. Acetate limiting supply ($f \succ 1.0$) as well as acetate saturated ($f = 1.0$) and acetate accumulating ($f \prec 1.0$) open-loop controls were studied.

partners, in which the gene *ldhA* encoding for lactate dehydrogenase was mutated such that the conversion of pyruvate to lactate was inactivated (see section A.1.2, Appendix).

A new series of fed-batch experiments was performed with the new strain using the same process control as described above. The effects of different acetate feeding strategies at constant glucose concentration of 5 $g \cdot L^{-1}$ were analyzed. As a result, the same acetate limiting effect on biomass growth and on pyruvate production was observed, but lactate was not produced at all. In analogy to the experimental results using *E. coli* YYC202, acetate limitation subsequently caused lower biomass growth and pyruvate production. There was no significant difference between the effect of saturated or accumulated acetate feeding on pyruvate production (Figure 5.5).

It is noteworthy that the long lag-phase during the acetate accumulating experiment ($f \prec 1.0$) was caused by technical pH control problems and is not characteristic for the typical process. From Figure 5.5 it was concluded that the proper selection of factor f of Equation 5.2 clearly influences the optimal fermentation performance (see also Table 5.3). As a result, a final titer $c_{PYR,final}$ higher than 700 $mmol \cdot L^{-1}$ (62 $g \cdot L^{-1}$), $Y_{PYR,glu\cos e}$ of 111 mol % and STY of 42 $g \cdot (Ld)^{-1}$ were achieved under the best conditions, which means with f set at 0.8.

TABLE 5.3. Comparison of some characteristic process values such as the final product titer, the integral pyruvate/glucose yield and the space-time yield regarding the different f-values set for acetate feeding. The strain E. coli YYC202 ldhA::Kan was used.

acetate supply	$c_{PYR,final}$	$Y_{PYR,glucose}$	STY_{int}
-	$[mmol \cdot L^{-1}]$	$[mol\%]$	$[g \cdot (Ld)^{-1}]$
f = 2.0[a]	242 (21.3)[d]	42	14.7
f = 1.5[a]	406 (35.7)[d]	68	24.4
f = 1.0[b]	633 (55.7)[d]	96	36.0
f = 0.8[c].	704 (62.0)[d]	111	42.0

[a]acetate limitation

[b]acetate saturation

[c]acetate accumulation

[d]pyruvate concentration in $g \cdot L^{-1}$

Comparing these results with those of *E. coli* YYC202, a 40 % increase of the final pyruvate titer can be stated together with a 39 % increase of integral pyruvate/glucose yield. The final titer and (to a certain extent) also the final yield are comparable to the best results of Li *et al.* [LHCL02] using *Torulopsis glabrata*. However, it should be noticed that the space-time yield of the *E. coli* process is much higher. Using *E. coli* 42 $g \cdot (Ld)^{-1}$ is produced, which is more than 40 % higher than the yeast process which needs 56 hours compared to only 30 hours with the *E. coli* strain.

However, when pyruvate curves, given in Figure 5.5, are studied the question arises why the maximum titer of about 700 mM cannot be further increased. To elucidate the problem Figure 5.6 is depicted indicating that pyruvate production rates strongly decline with increasing extracellular pyruvate concentrations. During the last 5 hours process time there was even no pyruvate production at all. Because similar observations were found in other fermentations, it was assumed that high extracellular pyruvate titers might have an inhibiting effect, as already indicated by Li *et al.* [LCLR01].

Further experiments were performed to test the hypothesis. For instance, cell samples were taken after the end of the fed-batch fermentation (at high pyruvate concentrations), washed several times in physiological solution (to avoid any inhibiting effect of pyruvate), resuspended in a buffer solution without any nutrient except for glucose and cultivated on the shaker. The treated biomass, which had previously stopped pyruvate production in the bioreactor, was then capable of converting glucose into pyruvate almost stoichiometrically (data not shown), which sustained our hypothesis.

Additionally, cell samples, taken during lab-scale fed-batch pyruvate production, were used to determine their intracellular pyruvate concentra-
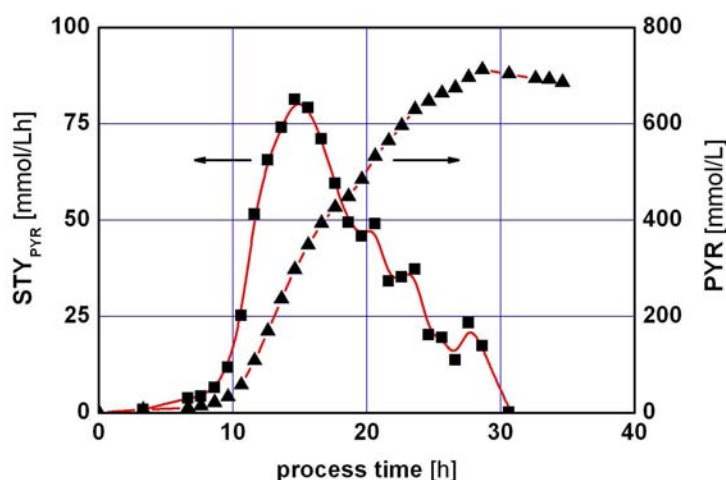
FIGURE 5.6. Space-time yield (STY) and pyruvate concentrations (PYR) as a function of process time using the strain *E. coli* YYC202 *ldhA*::*kan* in a lab-scale fed-batch fermentation with f set to the optimal value as 0.8.

tions according to the in-house developed protocol, described elsewhere [BTW01]. As a result, intracellular pyruvate concentrations of about 4 to 5 $mmol \cdot L^{-1}$ were measured while the extracellular levels were about 102-fold higher. This finding gave rise to the assumption that an active pyruvate transport is most likely to export pyruvate into the supernatant, which contrasted with our original assumption of pyruvate transport by diffusion.[3] Additionally, intracellular ATP levels were determined (again using the method of [BTW01]), which appeared to be very low (in the range of 0.5 $mmol \cdot L^{-1}$). Hence, the working hypothesis was formulated that pyruvate might be exported actively and re-enters the cell by diffusion thus causing a futile-cycling (ATP consumption) that finally can limit (and terminate) the total pyruvate production process.

However, it must be stressed that this working hypothesis was not further investigated (despite its attractiveness)[4]. Instead, the pyruvate production process development continued concentrating on bioprocess engineering means to overcome the assumed product inhibition. These are:

---

[3] No active pyruvate exporters in *E. coli* are known so far, although lactate specific acitve import systems are published that might also accept pyruvate as substrate.

[4] Although the postulated active pyruvate export was not further studied in the author's group, corresponding research was performed by the cooperating biochemists and molecular biologists (IBT1), which, for the sake of brevity, cannot be presented here.
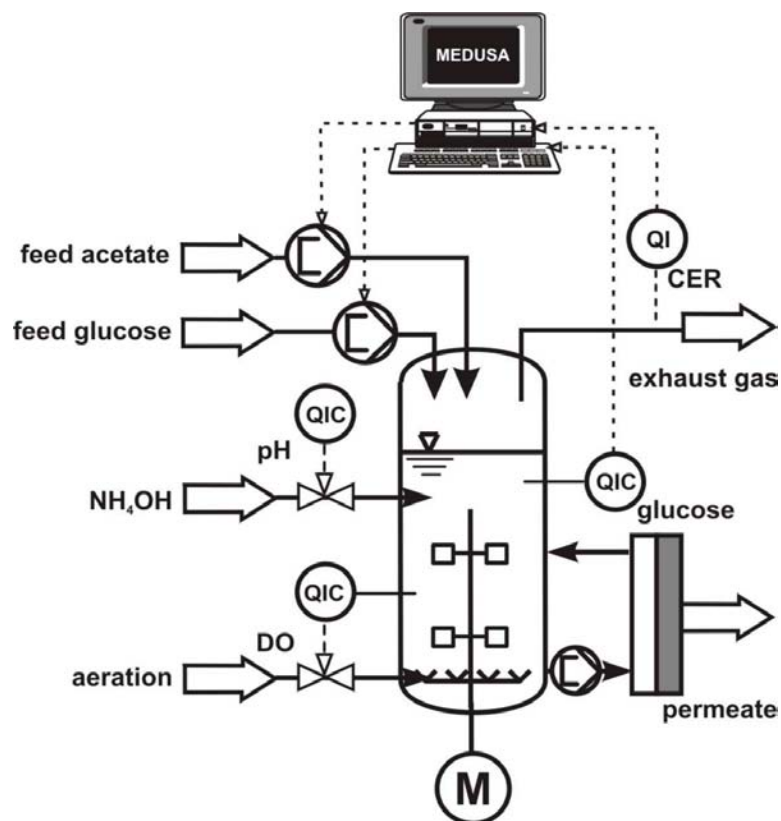
FIGURE 5.7. Experimental setup used for continuous experiments with cell-retention as well as for repetitive fed-batch experiments. Glucose and acetate control was applied as previously described. Cell-free permeate was drained off from an ultrafiltration unit, installed in the by-pass of the bioreactor.

- continuous pyruvate production with retained cells

- repetitive fed-batch production

- *ISPR* process with integrated pyruvate removal.

For all experiments presented in the following the strain *E. coli* YYC202 *ldhA*::Kan was applied.

5.3.2   Continuous Fermentation with Cell Retention.

Continuous fermentations with cell retention were conducted using the experimental setup with the 7.5-*L* bioreactor as depicted in Figure 5.7. The process was performed in analogy to the fed-batch process using a relatively

small by-pass (cross-flow hollow-fiber module: 0.15 m^2 filtration area, cut-off of 500 kDa, Schleicher & Schuell). When the maximal optical density in the fed-batch fermentation was achieved (OD$_{600}$ ∼30, after about 14 h process time), the acetate feed was stopped and the dia-filtration was started. During the following period, the glucose feed kept constant in the range of 60 to 80 $g \cdot h^{-1}$ depending on the acetate concentration in the feeding medium. An overall dilution rate of 0.1 h^{-1} was set.

The glucose-containing feed of the following period also contained 0, 20 and 40 $g \cdot L^{-1}$ acetate in a series of three subsequent experiments. To our surprise we observed that only the acetate-free feed enabled a continuous process lasting for more than 80 h process time. In addition, relatively high pyruvate concentrations of about 600 $mmol \cdot L^{-1}$ were achieved in all experiments, which caused a significant drop of the biomass specific pyruvate production rate from about 6 (at the end of the fed-batch phase) to 2.0 – 2.5 $mmol \cdot (g_{CDW}h)^{-1}$ in the presence of pyruvate titers ∼500 $mmol \cdot L^{-1}$. Thus, space-time yields of 104 to 117 $g_{PYR} \cdot (Ld)^{-1}$ were achieved together with low pyruvate/glucose yields of 1.10 to 1.24 $mol \cdot mol^{-1}$. From these results we concluded that an increase of the dilution rate would be advantageous to maintain pyruvate formation on a high level. However, we found the long-term stability of the strain and the achievable product/substrate yields to be insufficient. Hence other process alternatives were studied.

5.3.3   Repetitive Fed-Batch Approach

On account of the problems observed during the continuous experiments, the repetitive fed-batch alternative with cell retention was studied. The following (heuristic) guidelines were formulated in order to achieve an optimized process development:

- the process time should not exceed the "critical" value of approximately 40 h process time to prevent strain instability,

- product formation should preferably occur with non-growing cells to enable a highly selective glucose conversion to pyruvate,

- a series of multiple production cycles should be realized to increase volumetric productivity (space-time yield) and to minimize the production period with high extracellular pyruvate titers.

For repetitive fed-batch experiments the same setup was used as already presented in Figure 5.7 except for the cross-flow hollow-fiber ultra filtration module in the by-pass, which was larger than the one previously applied

TABLE 5.4. Comparison of some characteristic process values - namely the integral pyruvate/glucose yield and the space-time yield - regarding each period of the repetitive fed-batch experiment using E. coli YYC202 ldhA::Kan.

period	$Y_{PYR, glu\cos e}$	STY_{int}
-	$[mol\%]$	$[g \cdot (Ld)^{-1}]$
cycle I	146	68.0
cycle II	171	145.1
cycle III	172	81.9
cycle IV	178	80.1
cycle V	121	38.9

(area 0.98 m^2, cut-off 500 kDa, Schleicher & Schuell, Germany). The repetitive fed-batch process was started in analogy to the fed-batch process. After the biomass concentration remained constant for 3 hours, the acetate feed was stopped, the suspension was pumped through the by-pass and the cell-free permeate was drained off while the biomass was retained. When 60 % of fermentation medium has been pumped out of the system, an equal volume of fresh fermentation medium was added to the bioreactor through the same dia-filtration unit to prevent disposal of the biomass in the by-pass. A new cycle of biomass retention (medium dilution) was started after the calculated glucose feed rate (MEDUSA) decreased to the previously estimated threshold of 10 $g \cdot h^{-1}$.

As indicated in Figure 5.8, altogether four production cycles (II-V) were realized in repetitive fed-batch experiments with cell retention after the strain has been cultivated for biomass production in phase I. Figure 5.8 shows the changes in biomass concentration, pyruvate concentration and specific pyruvate production rate (π_{PYR}) during the experiment. Furthermore, the integral molar yield pyruvate/glucose ($Y_{PYR, glu\cos e}$) and the integral space-time yield (STY_{int}) were calculated for each cycle (Table 5.4).

In general the experiment can be divided into two parts. Part I (cycle I), characterized by cell growth, enabled pyruvate and biomass production at the same time and was glucose- and acetate-controlled. Part II (cycles II – V) enabled highly selective pyruvate production with non-growing cells. The highest STY of 145 $g \cdot (Ld)^{-1}$ was observed in the second cycle (pyruvate production with non-growing cells), which represents a more than 3-fold increase compared to our own, best E. coli fed-batch results (42 $g \cdot (Ld)^{-1}$). The pyruvate/glucose yields $Y_{PYR, glu\cos e}$ achieved in cycles II, III and IV were higher than 170 mol % (0.83 $g \cdot g^{-1}$), which is significantly better than the best fed-batch results of 111 mol % and is well comparable to the results using non-growing cells in shaking flasks with low external pyruvate titers ([GBZT01], [BGZT02]).
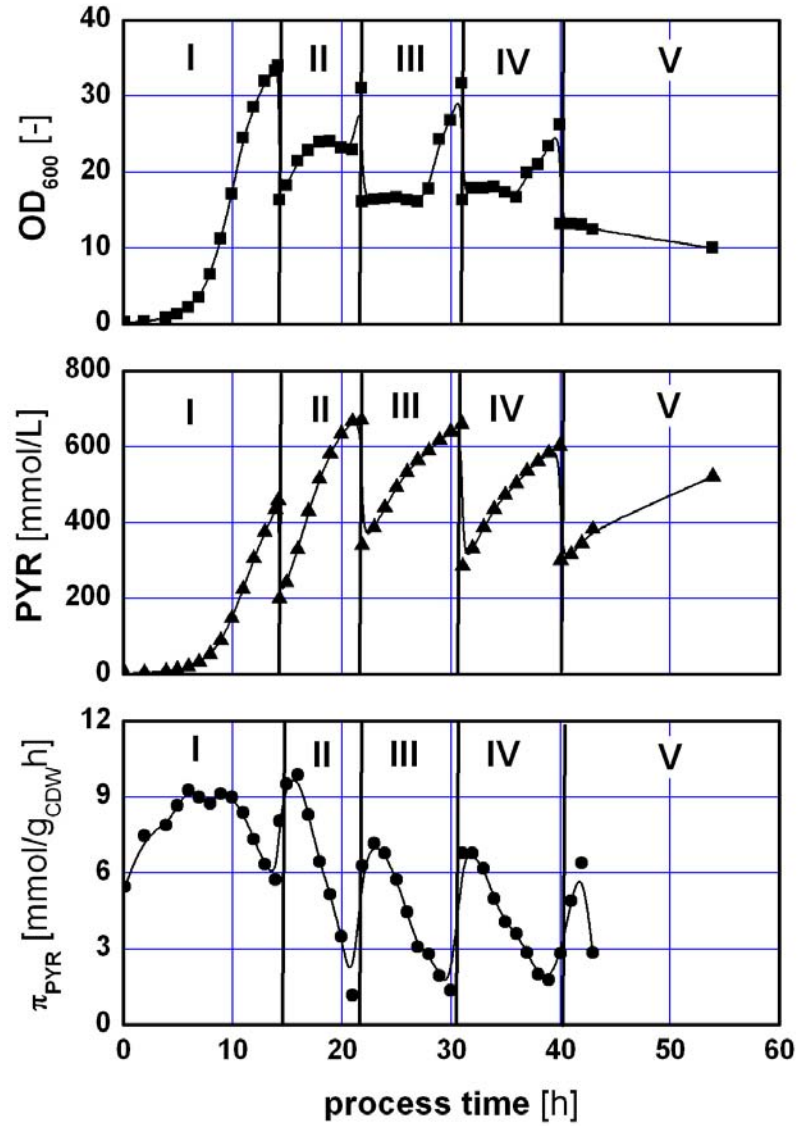
FIGURE 5.8. Optical density (OD_{600}), pyruvate concentration (PYR) and biomass specific pyruvate production rate (π_{PYR}) as a function of process time in a sequence of four repetitive fed-batch experiments (II-V) with an initial growth phase (I).

The final pyruvate titers in cycles II-IV are comparable to the best results of Li *et al.* [LHCL02] using *Torulopsis glabrata*. However, it should be noticed that the STY and $Y_{PYR,glu\cos e}$ of the *E. coli* process are significantly improved. Using *E. coli* the STY is more than 5-fold higher leading to 145 $g\cdot(Ld)^{-1}$, which coincides with even more efficient pyruvate/glucose yields $Y_{PYR,glu\cos e}$ of up to 1.78 $mol\cdot mol^{-1}$ (0.87 $g\cdot g^{-1}$) compared to the best value of 0.80 $g\cdot g^{-1}$ published so far (Li *et al.*, [LHCL02]).

Figure 5.8 also indicates a close correlation between decreasing specific pyruvate formation rates (π_{PYR}) and rising pyruvate concentrations during each cycle. From that we concluded that an inhibition of pyruvate production caused by high extracellular pyruvate concentrations obviously exists. If the cell concentration courses are analyzed, one might wonder about the increase of biomass concentration at the beginning of the second cycle. However, it is noteworthy that this was not growth-dependent but due to the apparently too slow cell recycling from the ultra-filtration unit into the bioreactor. By analogy, no cell growth occurred at the end of the cycles (II-IV). Increasing optical density values only mirror the concentration of biomass during the ultra filtration period. Because of biofouling effects in the ultra filtration unit the membrane permeability was reduced (as indicated by extended filtration periods) which might also cause the sequential decreases of $Y_{PYR,glu\cos e}$ and STY from one cycle to the next.

5.4   *ISPR* Approach Using Electrodialysis

As an alternative to the process approaches of the preceding subsection, the on-line separation of pyruvate in an *ISPR* process was studied to remove the (most presumably) inhibitory product from the fermentation supernatant. Reviewing the *ISPR* approaches of the last twenty years, Stark and von Stockar [SS03] outlined that reactive extraction, (immobilized) ion-exchange or electrodialysis should be preferred if hydrophobic products - such as pyruvic acid - need to be separated from the fermentation supernatant. Because it was known from our own studies (see preceding chapter) that anion-selective carriers are toxic for the cells, (immobilized) anion-exchange and/or electrodialysis had to be favored for this purpose. Preliminary studies of Zelić and the cooperating industrial partner (data not shown) revealed significant problems while using anion-adsorbers for pyruvic acid separation. Most striking, the relatively low capacity of resins and the need to use concentrated acids as eluents made this technology not attractive in terms of sustainable process development and in a commercial respect [LCL01]. Hence, electrodialysis was favored for the subsequent studies.

Applying electrodialysis in *ISPR* approaches is not new. According to Stark and von Stockar [SS03], about 12 examples were published within the last 20 years focusing on the separation of acetic acid, lactic acid and/or propionic acid from biosuspensions [SS03]. Additional applications were also found for the separation of amino acids ([TVRW90], [WBdG96]). However, it may be noteworthy that electrodialysis has not yet been applied to remove pyruvic acid from the fermentation supernatant. In general, the charge-dependent ion separation in the electric field of electrodialysis is regarded as a promising approach for the downstream processing of organic acids from fermentation broth [BB02].

5.4.1   Preliminary Separation Experiments

For electrodialysis a three-compartment water splitting electrodialysis unit (WSED) was used, as presented in subsection A.4.4, Appendix. The apparatus, which is shown in the pictures 5.9 and 5.10 was rent from the Fraunhofer Institute IGVT (Institut für Grenzflächen und Bioverfahrenstechnik), Stuttgart, Germany.

Preliminary experiments using a synthetic solution ($48.0 \; g \cdot L^{-1}$ pyruvate in water) and pre-treated fermentation suspension were performed in order to study the effect of medium components on the performance of the electrodialysis process. Experimental results are summarized in Table 5.5 and Figure 5.11.
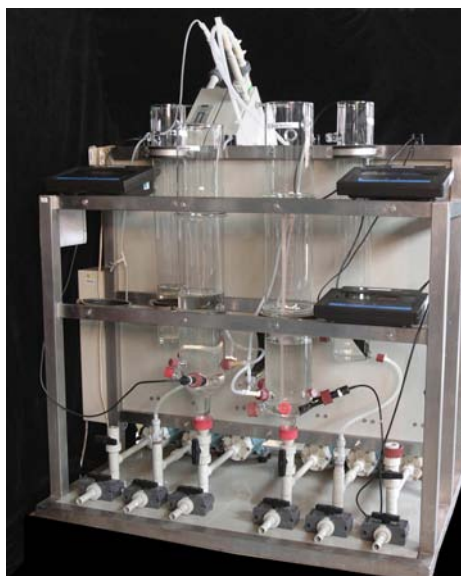
FIGURE 5.9. Electrodialysis unit used for the separation of pyruvic acid.

FIGURE 5.10. Electrodialysis cell (four stacks) used for the separation of pyruvic acid.

TABLE 5.5. Results of the pyruvic acid separation from different donors considering aqueous model solution, cell-free (CF) and cell- and protein-free (CPF) fermentation supernatant. Pyruvate (PYR) titers are given for the aqueous start solution as well as for the final concentration in the acid medium. For process validation, the PYR recovery and the current efficiency (CE) are shown.

	start PYR_{aq}	final PYR_{acid}	PYR recovery	CE
	$[g \cdot L^{-1}]$	$[g \cdot L^{-1}]$	$[\%]$	$[\%]$
model solution	48.0	43.8	91.2	99.4
CFB	41.3	24.9	60.2	99.8
CPFB	41.3	34.8	84.3	95.6

Each experiment was stopped when the stack voltage increased to a maximum value of 40 V to prevent a possible membrane rupture. Current efficiencies (CE) higher than 99 % and 91 % pyruvate recovery were achieved in the experiment with the model solution. Compared to this best result, a 30 % recovery decrease was observed by the use of cell-free fermentation supernatant (CF) with a similar current efficiency. However, when fermentation supernatant was used, higher voltage levels and an accelerated voltage increase were measured, indicating membrane fouling by high-molecular medium components like proteins, cell debris etc. Hence, an ultrafiltration step (cut-off 10 kDa) was installed for protein separation, which resulted in an 84 % pyruvate recovery achieving 90 % current efficiency. From this it was concluded that cell- and protein-free biosuspension (CPF) should be used for electrodialysis. However, a slightly reduced pyruvate recovery and current efficiency compared to the model solution (presumably due to salts in the fermentation medium) must be taken into account.

Additionally, it was observed that 95 % of the glucose in the cell- and protein –free fermentation medium was rejected by passing the electrodialysis unit. The final pH of the recycled feed solution in each experiment was higher than 3, which ensured sufficient amounts of pyruvic acid ions ($pK_{a,pyruvate} \sim 2.5$) in the feed.

5.4.2   Integration of Electrodialysis into the Fed-Batch Process

Motivated by the promising findings of the preliminary experiments, the total *ISPR* setup was build up, as shown in Figure 5.12. The process consists of four main steps:

- fermentation with cell retention by ultrafiltration and recycling

- protein separation by ultrafiltration

- product removal by electrodialysis
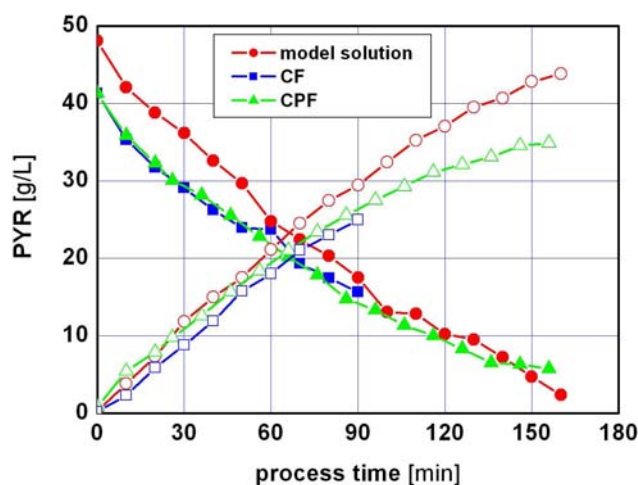
FIGURE 5.11. Pyruvate (PYR) concentratrion courses using the electrodialysis approach with PYR containing model solution, cell-free (CF) and cell- and protein-free (CPF) fermentation supernatant. Full symbols indicate the donor while hollow symbols denote the acceptor (acid) solution.

- sterilization by microfiltration and recycling of pyruvate-reduced fermentation supernatant

The protein separation was conducted using planar modules (ULTRAN, Schleicher & Schuell, Germany), which consisted of four cassettes with pore size of 10 kDa. Pyruvate-reduced fermentation permeate was pumped back into the bioreactor through a sterile microfiltration unit (0.2 μm cut-off, Sartobran, Satorius, Germany).

As depicted in Figure 5.12, three streams leave the electrodialysis unit: the pyruvic-acid reduced fermentation supernatant, the pyruvate-enriched acid stream and the NH_4OH-enriched base stream. The pyruvic-acid reduced fermentation permeate contained glucose with some nutrients and could be reused in a continuous recycling process. Consequently, a reduction of raw material costs was expected. NH_4OH produced in the three-compartment electrodialysis could also be recycled to decrease the amount of fresh base needed for pH titration. Based on the preliminary experiments, it was expected that pyruvate could be concentrated in the acid stream thus allowing a simplified purification later on.

As indicated, fermentation suspension was first ultra filtrated (cut-off: 500 kD) to produce a cell-free permeate which was pumped through a
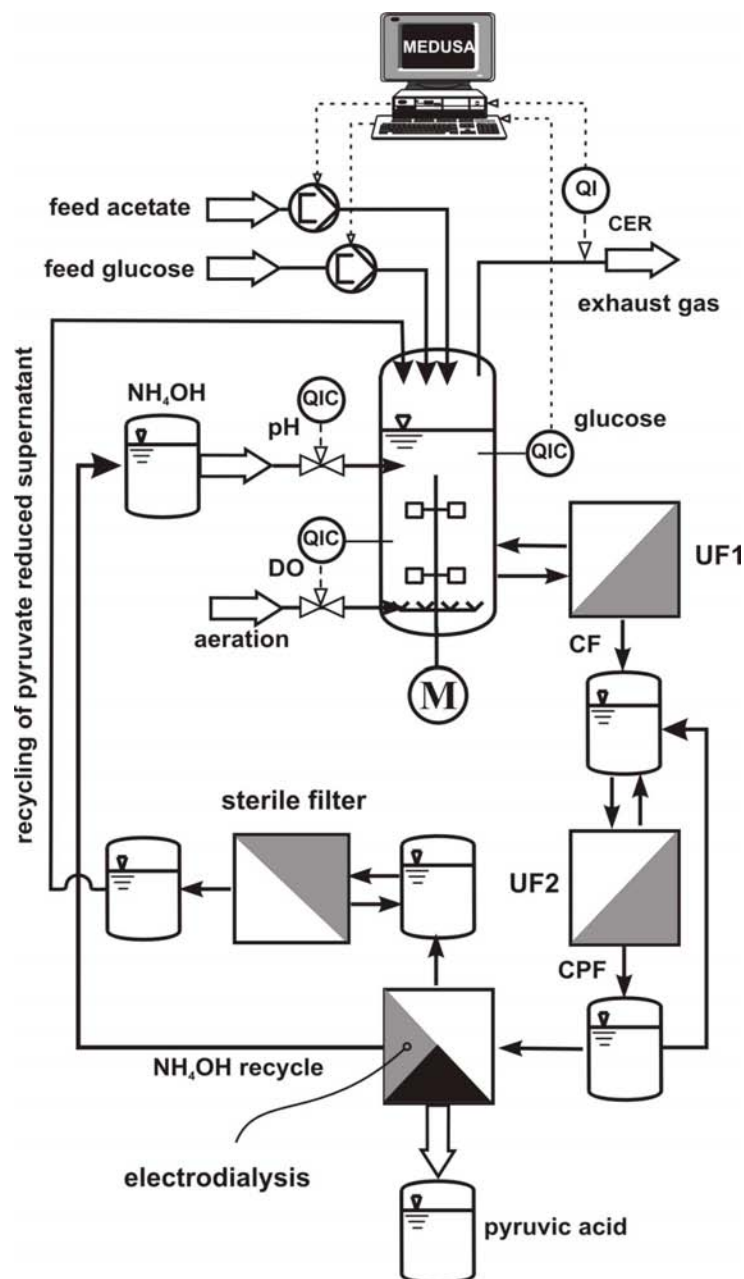
FIGURE 5.12. Scheme of the experimental setup used for the *in situ* product recovery (*ISPR*) with fully integrated three-compartment electrodialysis. Abbreviations: UF - ultrafiltration unit; CF - cell-free permeate; CPF - cell- and protein-free permeate; CER - CO_2 emission/transfer rate. For details see text.

second ultrafiltration unit (cut-off: 10 kD) to separate the proteins and cell debris. Then, cell- and protein-free fermentation solution entered the electrodialysis. The pyruvic-acid-reduced fermentation permeate was recycled into the bioreactor through a sterile micro filtration unit to prevent a possible contamination by the non-sterile pyruvate separation process.

As shown by the pyruvate concentration and formation courses (see Figure 5.13), the process can be divided into three parts: a fed-batch phase (I), a continuous phase (II) and an $ISPR$ phase (III). During the first phase, an increase of the pyruvate level was observed in analogy to preliminary experiments. In the following the pyruvate concentration remained constant which indicates an equilibrium between pyruvate production (by retained cells) and wash-out. The relatively high level of 600 mM pyruvate was chosen to make high pyruvate levels available to the electrodialysis unit and to observe increasing (recovering) product formation rates owing to the on-line separation of the inhibiting product.

Then, pyruvate separation via electrodialysis started after 29 hours process time and lasted for approximately 14 hours. During this phase (III) the pyruvate concentration in the bioreactor decreased by more than 20%. At the same time, the microbial pyruvate production was still active – though on a reduced level. Whereas the volumetric pyruvate formation rate STY was about 60 $mmol \cdot (Lh)^{-1}$ during phase (II), it dropped down to approximately half of its original value during the $ISPR$ phase. This finding was in contrast to the assumption that a pyruvate separation might prevent a potential product inhibition and would consequently lead to higher (or longer lasting) pyruvate formation rates. However, we concluded that the (unwanted) co-separation of medium components via electrodialysis – which for instance was not prevented by additional nutrient supplement - caused this unexpected result. As a consequence, low STY (68 $g \cdot (Lh)^{-1}$) and low $Y_{PYR,glu\cos e}$ (1.19 $mol \cdot mol^{-1}$) were observed, which do not represent a process improvement in comparison to the repetitive fed-batch process.

However, it can be stated that the fully integrated separation of pyruvic acid via electrodialysis was successfully realized. Indications are given in Figure 5.13 (mid-diagram) by showing the courses of pyruvate concentration in the feed (representing the pyruvate level in the permeate stream originating from the bioreactor) and in the acid compartment of the electrodialysis unit. When both courses are compared, a 2.5-fold higher pyruvate concentration is observed. However, the current efficiency (56 %) and the pyruvate recovery (72 %) were not as high as measured by previous experiments (see Table 5.5). This was presumably a consequence of membrane fouling caused by the precipitation of medium components like hardness material, which was more intensive during the 14 h of the $ISPR$ approach than during the 2.5 h of the preliminary batch experiments. Finally, pyruvate was concentrated in ED up to 550 mM with purity higher than 95
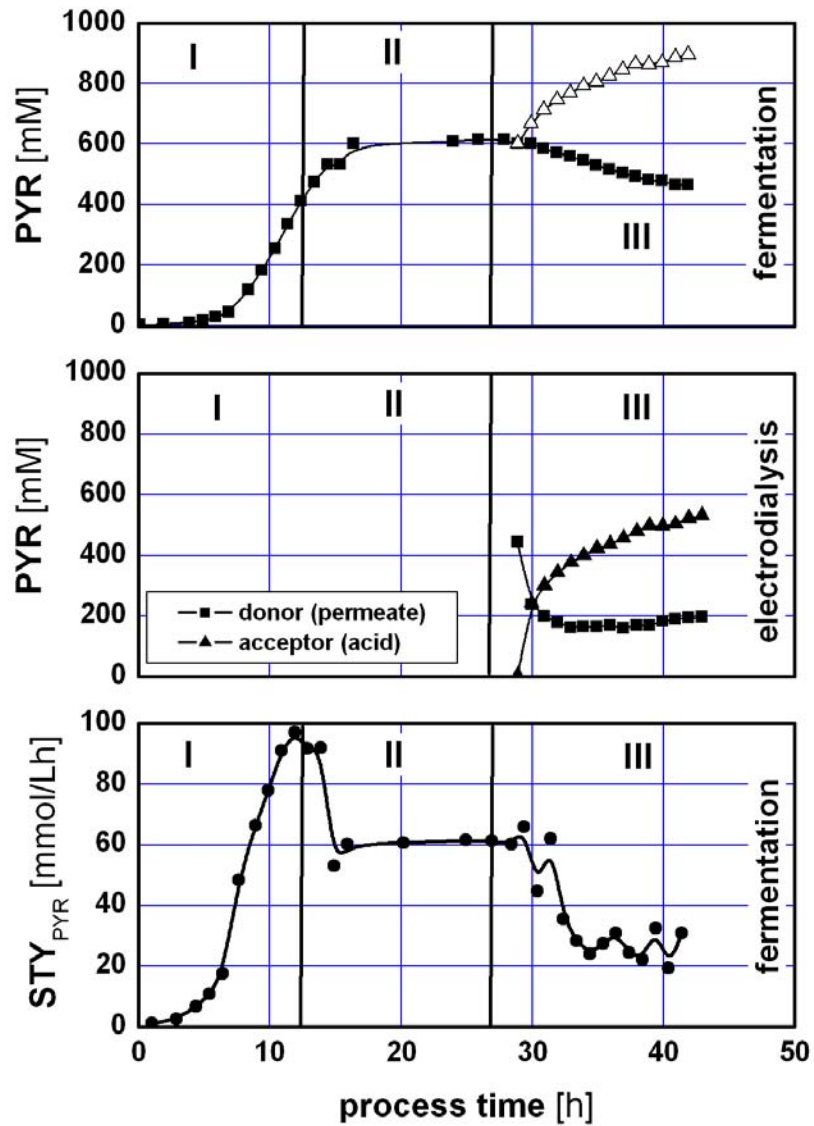
FIGURE 5.13. Overview of the results obtained during the *ISPR* process using electrodialysis for pyruvate removal. Pyruvate (PYR) courses in the fementation supernatant together with the calculated concentrations (top diagram), PYR curves measured in the cell- and protein-free permeate and in the acid acceptor solution (middle) and the resulting space-time yield (STY) qualifying the celluar productivity (diagram at the bottom) are given.

%. Only 7% of glucose was also co-separated, which is comparable to the results of the preliminary experiments. If the total amount of pyruvate produced is related to the real working volume of the bioreactor, a final concentration of about 900 mM (79 $g \cdot L^{-1}$) would have been achieved.

5.5   Pyruvate Process Development: Conclusions and Outlook

Based on the pyruvate producing strain *E. coli* YYC202 *ldhA::Kan,* which was constructed by our cooperating partners (M. Bott and T. Gerharz), an acetate and glucose controlled fed-batch process was developed achieving pyruvate titers $c_{PYR,final}$ higher than 700 $mmol \cdot L^{-1}$ (62 $g \cdot L^{-1}$), $Y_{PYR,glu\cos e}$ of 111 mol % and STY of 42 $g \cdot (Ld)^{-1}$, provided that the appropriate acetate feeding is applied. Because indications were found that high pyruvate titers have an inhibiting effect on pyruvate production, several process alternatives such as continuous production with cell retention, repetitive fed-batch and on-line pyruvate removal conducting electrodialysis in an *ISPR* approach have been studied. While the continuous process revealed significant cell stability problems, the repetitive fed-batch approach uncovered to be best suited for pyruvate production. In four subsequent production cycles titers up to 650 mM were repeatedly reached, concomitantly showing PYR/glucose yields $Y_{PYR,glu\cos e}$ of up to 178 mol % (0.87 $g \cdot g^{-1}$) and maximum STY of 145 $g \cdot (Ld)^{-1}$. Especially the STY is more than 5-fold higher than the competing *Torulopsis glabrata*-process, at the same time offering improved PYR/glucose yields and similar pyruvate titers.

Although the *ISPR* process showed to be inferior to the repetitive fed-batch approach, the application of electrodialysis for pyruvate removal should not be neglected. Considering the pyruvate levels in the cell- and protein-free permeate together with those of the acid solution, a 2.5-fold concentration was observed which qualifies this approach for further (off-line) studies to remove the product from the fermentation supernatant.

The *E. coli* based pyruvate production process has been evaluated economically by several industrial partners, which cannot be named here. However, typical production costs of about 1 to 3 $\in \cdot kg^{-1}$ were estimated thus making the process interesting for industrial applications.

Currently, additional studies were performed focusing on the immobilization of the pyruvate-producing *E. coli* cells on carriers such as Lentikats^{TM}. Furthermore, modeling studies were carried out of which the results were already submitted for publication by Zelić *et al.* [ZVRWT03]. For the sake of brevity, no details are given here. However it can be stated that of the ten unstructured models considered for modeling substrate consumption, cell growth and pyruvate formation, one appropriate model was identified. The model not only succeeded to fit well to one set of experimental data (used for parameter identification), it was also applied to simulate product formation and cell growth of two additional fed-batch experiments. As a basic property, a maximum tolerated pyruvate titer (for product formation) of

63.6 $g \cdot L^{-1}$ was considered as well as a pyruvate inhibition of growth with $K_P = 3.93 \pm 1.32$ $g \cdot L^{-1}$. Hence, these findings support the precedingly formulated hypothesis that high pyruvate titers inhibit product formation.

6
Summary

Regarding the *biochemical engineering* definitions given by Bailey [Bai99a], Leib *et al.* [LPV01], von Stockar [SVM$^+$03] and Stephanopoulos [Ste03], this 'Habilitationsschrift' may be characterized as a typical *biochemical engineering* report. Methods and apparatus are presented that aim at providing a quantitative understanding of cellular metabolism considering intracellular pools and fluxes. Furthermore results of 'classical' bioprocess developments are given focussing on the production of L-phenylalanine and pyruvate with recombinant strains. The following list comprises the essentials of these works:

- **Analysis of *In Vivo* Metabolic Dynamics:** Using the previously developed and optimized rapid sampling device together with optimized analytical protocols, stimulus-response experiments (e.g. with glucose) were conducted ([SBTWB99], [BHWT02]) based on different *E. coli* strains, among those also recombinant L-phenylalanine producers [OKDT03]. Intracellular metabolite dynamics in central metabolism as well as in the aromatic amino pathway were measured with the aid of novel LC-MS/MS approaches ([BTW01], [OT03]). Preliminary experiments revealed a close relation between glucose pulse intensity and the length of maximum reaction sequence in the anabolic pathway to allow the resulting signal detection (signal dilution, [SHBT02]). The novel analysis of corresponding dynamics in the anabolic pathway requested the access to non-commercial standards, which was successfully achieved. Based on the experimental results AroB, AroL and AroA were identified as *metabolic engineer-*

ing targets to enhance L-phenylalanine production. In parallel, the software Metabolic Modeling Tool (MMT [HBA$^+$02]) for the analysis of stimulus-response data sets was developed, a statistical approach for complex metabolic model reduction was presented [DFDT03] and the problem of model discrimination was critically addressed [WT03].

- **Sensor Reactor:** The 1-L Sensor reactor was developed to monitor temporary changing intracellular carbon flux distributions in industry-like production processes by serial ^{13}C based metabolic flux analysis ([MSD$^+$03], [MFdGT01]). Using the Sensor reactor, the L-lysine producing strain *C. glutamicum* MH20-22B was studied during the growth phase [DMM$^+$03] as well as during the L-leucine limited production phase [DMW$^+$03] with non-growing cells. As a result five flux maps were obtained indicating the correlation between decreasing decarboxylating (PEP carboxykinase) fluxes and increasing lysine production rates. Hence the need to fortify PEP carboxylase and/or pyruvate carboxylase activity was unravelled. Further ^{13}C labeling studies [WMS$^+$03] analyzing the L-phenylalanine producing *E. coli* 4pF81 during the L-tyrosine limited production phase revealed the need to overexpress *pps* (coding for PEP synthase). Three subsequent flux maps were calculated giving rise to the working hypothesis that intracellular pool accumulations of oxaloacetate (OAA) and 2-oxoglutarate (AKG) are presumably the reasons for the deteriorating L-Phe formation rates.

- **L-Phenylalanine Bioprocess Development:** Preliminary statistical studies using principal component analysis revealed the importance of tyrosine and acetate as fermentation key variables [TGPW01] in tyrosine auxotrophic L-phenylalanine producing *E. coli* strains. With the aid of an appropriate tyrosine and glucose control reproducible fermentation results were obtained (up to 300-L scale) even allowing the use of the tyrosine sensitive wildtype-gene *aroF^{wt}* which turned out to be superior to the (tyrosine) feedback resistant *aroF^{fbr}* ([GRST01], [GBGN$^+$02]). Motivated by experimental observations indicating an L-Phe inhibition of AroF, a reactive extraction approach was developed using hollow fibers to separate the organic phase kerosene with the cation selective carrier D$_2$EHPA from the aqueous donor phase and the aqueous H$_2$SO$_4$ containing acceptor (stripping) phase ([MTP$^+$00], [MGK$^+$02]). Motivated by the promising L-Phe/glucose yield improvement found in pilot-scale *ISPR* experiments (300-L bioreactor, [GMK$^+$02]), the question was studied why only 26 % L-Phe was separated on-line. With the aid of modeling, mass transfer resistances in the aqueous phases were identified that suggested turbulent hydrodynamic conditions for reactive extraction optimization [Tak03]. As a consequence centrifugal extractors were considered in a novel approach ([RWT02], [RHK$^+$03]). The overall

L-Phe/glucose yield of the reference fermentation with *E. coli* 4pF81 of 14.5 *mol* % was thus increased to 18.6 % in the *ISPR* approach and L-Phe was concentrated to 60 $g \cdot L^{-1}$ in the aqueous acceptor phase which significantly reduced the amount of liquid to be handled for further product purification (to 99%) via precipitation. About 3-times higher L-Phe permeability was observed (about 1.2 to 1.5 $g \cdot (Lh)^{-1}$) compared to the membrane based *ISPR* process which coincided with a more robust handling of the *ISPR* unit. The process is considered for economical evaluation at the industrial partner DSM.

- **Pyruvate Bioprocess Development:** Using the pyruvate producer *E. coli* YYC202 *ldhA*::*Kan* an acetate and glucose controlled fed-batch process was developed achieving pyruvate titers $c_{PYR,final}$ higher than 700 $mmol \cdot L^{-1}$ (62 $g \cdot L^{-1}$), $Y_{PYR,glucose}$ of 111 *mol* % and *STY* of 42 $g \cdot (Ld)^{-1}$, provided that the appropriate acetate feeding was applied ([ZGB$^+$03], [GBZT01], [BGZT02]). Because indications were found that high pyruvate titers possess inhibitory effects on pyruvate production, several process alternatives (continuous production with cell retention, repetitive fed-batch and on-line pyruvate removal conducting electrodialysis in an *ISPR* approach) were studied [ZGV$^+$03]. The repetitive fed-batch approach revealed to be best suited for pyruvate production achieving titers up to 650 mM in four subsequent production cycles with PYR/glucose yields $Y_{PYR,glucose}$ of up to 178 *mol* % (0.87 $g \cdot g^{-1}$) and maximum *STY* of 145 $g \cdot (Ld)^{-1}$. The *STY* is more than 5-fold higher than the competing *Torulopsis glabrata*-process, at the same time offering improved PYR/glucose yields and similar pyruvate titers. Electrodialysis could be applied in an *ISPR* approach thus recommending this technique for pyruvate removal.

Figure 6.1 depicts an overview of the major topics which are addressed in this 'Habilitationsschrift'. As shown the Sensor reactor as well as the *metabolic profiling* approach were applied to study the L-phenylalanine production in *E. coli* strains. While the Sensor reactor based metabolic flux analysis revealed an insufficient precursor supply (PEP), the *metabolic profiling* analysis focussed on the aromatic pathway intermediates reconfirming AroB, AroL and AroA as promising *metabolic engineering* targets each exerting considerable flux control. Hence both approaches showed their applicability for *metabolic engineering* purposes and are currently applied for additional *biochemical engineering* studies, apart from L-phenylalanine and pyruvate production, which have been presented in this thesis. The application of these tools is intended to build up a bridge between the classical *biochemical engineering* and the biological sciences to allow an efficient bioprocess development based on *metabolic engineering*.
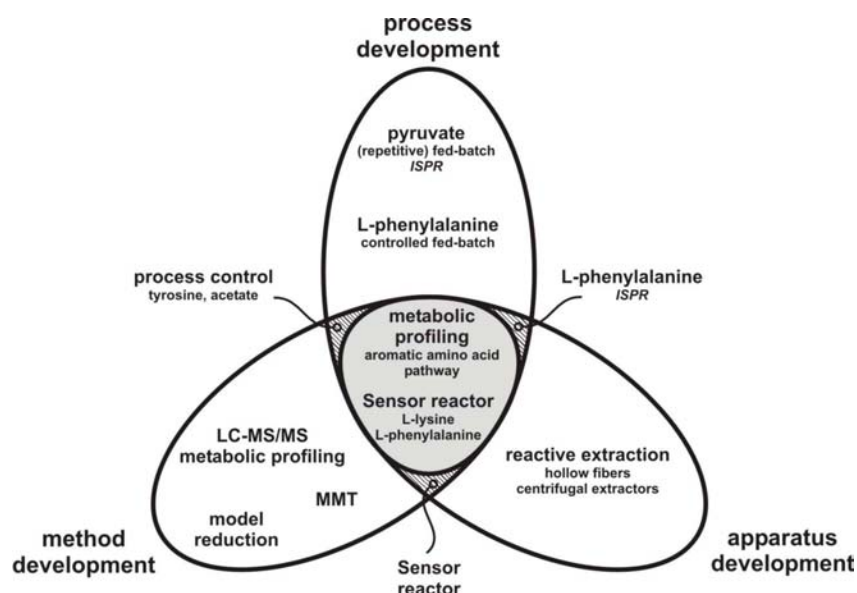
FIGURE 6.1. *Biochemical engineering* items treated in this 'Habilitationsschrift' (only a selection is given). Examples for method development are the software Metabolic Modeling Tool (MMT), the model reduction approach using principal component analysis (PCA) and the LC-MS/MS based quantification of intracellular metabolites of the central metabolism as well as of the aromatic amino acid pathway. The reactive extraction approach, based on hollow fibers or centrifugal extractors is given as an example of apparatus development. A combination of method and apparatus development was followed studying the Sensor reactor technology. Process development examples are given for pyruvate and L-phenylalanine. Both were tested (and modelled) as *ISPR* processes. The latter was studied in pilot-scale using reactive extraction, as indicated. As a combination of method and process development, process control approaches for the auxotrophic substrates tyrosine and acetate were studied as well. The *metabolic profiling* methodology and the Sensor reactor were applied to analyze the L-phenylalanine production with respect to the intracellular pools and the corresponding fluxes under industry-like process conditions. This is why both applications are finally considered in the center of the figure.

Acknowledgment

References

[AB97]   J.P. Akowski and R. Bauerle. Steady state kinetics and inhibitor binding of 3-deoxy-d-arabino-heptulosonate 7-phosphate synthase (tryptophan sensitive) from escherichia coli. *Biochemistry* **36**, 15817 – 15822 (1997).

[AB01]   T. Anderlei and J. Büchs. Device for sterile online measurement of the oxygen transfer rate in shaking flasks. *Biochem. Eng. Journal* **7**, 157 – 162 (2001).

[ADB⁺03] J. Allen, H.M. Davey, D. Broadhurst, J.K. Heald, J.J. Rowland, S.G. Oliver, and D.B. Kell. High-throughput classification of yeast mutants for functional genomics using metabolic footprinting. *Nature Biotechnol.* **6(21)**, 692 – 696 (2003).

[ADS89]   K. Abbasian, W. Degener, and K. Schügerl. Reactive extraction of primary and secondary metabolites. *Ber. Bunsenges. Phys. Chem.* **93**, 967 – 980 (1989).

[ADW96]   D.L. Anton, R. DiCosimo, and V.G. Witterholt. Process for the preparation of pyruvic acid using permeabilized transformants of h. polymorpha and p. pastoris which express glycolate oxidase and catalase. Technical Report, US Patent 5,538,875 (1996).

[AN87]   Y. Asano and A. Nakazawa. High yield synthesis of l-amino acids by phenylalanine dehydrogenase from sporosarcina ureae. *Agric. Biol. Chem.* **51**, 2305 – 2306 (1987).

[AO95]   M. Ai and K. Ohdan. Formation of pyruvic acid by oxidative dehydrogenation of lactic acid. *Chem. Lett.* **5**, 405 (1995).

[AS97]   L. Agius and H.S.A. Sherratt. "Channelling in Intermediary Metabolism". ISBN 1 85578 075 5, Portland Press Ltd., London (1997).

[ASH79]   K. Akashi, H. Shibai, and Y. Hirose. Effect of oxygen supply on l-phenylalanine, l-proline, l-glutamine and l-arginine fermentations. *J. Ferment. Technol.* **57**, 321 – 327 (1979).

[ASJP97]   J.A. Adarkar, S.B. Sawant, J.B. Joshi, and V.G. Pangarkar. Extraction of amino acids using immobilized liquid membranes. *Biotechnol. Prog.* **13**, 493 – 495 (1997).

296   References

[ASR97]   A. ARKIN, P. SHEN, AND J. ROSS. A test case of correlation metric construction of a reaction pathway from measurements. *Science* **277**, 1275 – 1279 (1997).

[Atk94]   P.W. ATKINS. "Physical Chemistry, 5th Edition". Oxford University Press (1994).

[AVRS81]   R.I. ANDREEVA, E.S. VYSOTSKII, E.K. RODICHEVA, AND G.Y. SHERBARKOVA. Production of pyruvic acid by the luminescent bacterium. *Mikrobiologiya* **50**, 776 – 780 (1981).

[BA94]   L. BOYADZHIEV AND I. ATANASSOVA. Extraction of phenylalanine from dilute solutions by rotatin film pertraction. *Proc. Biochem.* **29**, 237 – 243 (1994).

[Bad80]   M. BADER. A systematic approach to standard addition methods in instrumental analysis. *J Chem. Education* **57**, 703 – 706 (1980).

[Bai91]   J. E. BAILEY. Towards a science of metabolic engineering. *Science* **252**, 1688–1674 (1991).

[Bai98]   J.E. BAILEY. Mathematical modeling and analysis in biochemical engineering: Past accomplishments and future opportunities. *Biotechnol. Prog.* **14**, 8 – 20 (1998).

[Bai99a]   J.E. BAILEY. Biochemical engineering: Molecular, cellular, and process frontiers. *Curr. Opinion Biotechnol.* **10**, 115 – 116 (1999).

[Bai99b]   J.E. BAILEY. Lessons from metabolic engineering for functional genomics and drug discovery. *Nature Biotechnol.* **17**, 616 – 618 (1999).

[Bai00]   A. BAIROCH. The enzyme database in 2000. *Nucleic Acid Res., Swiss-Prot Enzyme nomenclature database, http://www.expasy.ch/enzyme* **28**, 304 – 305 (2000).

[Bai01a]   J.E. BAILEY. Complex biology with no parameters. *Nature Biotechnol.* **19**, 503 – 504 (2001).

[Bai01b]   J.E. BAILEY. Reflections on the scope and the future of metabolic engineering and its connections to functional genomics and drug discovery. *Metab. Eng.* **3**, 111 – 114 (2001).

[BB02]   M. BAILLY AND D. BAR. Hybrid separation schemes for producing organic acids: The potential, promise and production. *Chem. Eng.* **109**, 51 – 53 (2002).

[BBB$^+$02]   S. BUZIOL, I. BASHIR, A. BAUMEISTER, W. CLAASSEN, N. NOISOMMIT-RIZZI, W. MAILINGER, AND M. REUSS. New bioreactor-coupled rapid stopped-flow sampling technique for measurements of metabolite dynamics on subsecond time scale. *Biotechnol. Bioeng.* **80**, 632 – 636 (2002).

[BBG01]   J.L. BAEZ, F. BOLIVAR, AND G. GOSSET. Determination of 3-deoxy-d-arabino-heptulosonate 7-phospahte productivity and yield from glucose in escherichia coli devoid of the glucose phosphotransferase transport system. *Biotechnol. Bioeng.* **73(6)**, 530 – 535 (2001).

[BC85]   E. BULOT AND C.L. COONEY. Selective production of phenylalanine from phenylpyruvate using growing cells of corynebacterium glutamicum. *Biotechnol. Lett.* **7**, 93 – 98 (1985).

[BCKF93]   J. BABUL, D. CLIFTON, M. KRETSCHMER, AND D. FRAENKEL. Glucose-metabolism in escherichia coli and the effect of increased amount of aldolase. *Biochemistry* **32**, 4685 – 4692 (1993).

[BD90a]   G. BASTIN AND D. DOCHAIN. "On-Line Estimation and Adaptive Control of Bioreactors". Elsevier, Amsterdam (1990).

[BD90b]   L.D. BOER AND L. DIJKHUIZEN. Microbial and enzymatic processes for l-phenylalaine production. *Adv. Biochem Eng./Biotechnol.* **41**, 1 – 27 (1990).

[BEK93]   S. Bröer, L. Eggeling, and R. Krämer. Strains of corynebacterium glutam-
            icum with differernt lysine productivities may have different excretion sys-
            tems. *Appl. Environ. Microbiol.* **59**, 316–321 (1993).

[Ber85]   H. Bergmeyer. "Methods of Enzymatic Analysis, 3rd Edition, Vol. 6 and 7".
            Verlag Chemie, Weinheim, Germany (1985).

[Ber96]   A. Berry. Improving production of aromatic compounds in escherichia coli
            by metabolic engineering. *TIBTECH* **14**, 250 – 256 (1996).

[BF72]   A.S. Bagnara and L.R. Finch. Quantitative extraction and estimation of
            intracellular nucleoside triphosphates of escherichia coli. *Anal. Biochem.* **45**,
            24 (1972).

[BFI95]   M. Bhattacharya, M. Fuhrman, and A. Ingram. Single-run separation and
            detection of multiple metabolic intermediates by anion-exhange high perfor-
            mance liquid chromatography and application to cell pool extracts prepared
            from escherichia coli. *Anal. Biochem.* **232**, 98 – 106 (1995).

[BGZT02]   M. Bott, T. Gerharz, B. Zelic, and R. Takors. Verfahren sowie mikroor-
            ganismus zur mikrobiellen herstellung von pyruvat aus kohlenhydraten sowie
            alkoholen. Technical Report, German Patent Application DE 102 20 234.6
            (2002).

[BHWT02]   A. Buchholz, J. Hurlebaus, C. Wandrey, and R. Takors. Metabolomics:
            Quantification of intracellular metabolite dynamics. *Biomolecular Engineer-
            ing* **19(1)**, 5 – 15 (2002).

[BKM+01]   J. Bongaerts, M. Krämer, U. Müller, L-Raeven, and M. Wubbolts.
            Metabolic engineering for microbial production of aromatic amino acids and
            derived compounds. *Metabolic Engineering* **3**, 289 – 300 (2001).

[BLM01]   J. Büchs, S. Lotter, and C. Milbradt. Out-of-phase operating conditions, a
            hitherto unknown phenomenon in shaking bioreactors. *Biochem. Eng. Jour-
            nal* **7**, 135 – 141 (2001).

[BM01]   A.P. Burgard and C. D. Maranas. Probing the performance limits of the
            escherichia coli metabolic network subject to gene additions or deletions.
            Biotechnol. Bioeng. **74**, 364 – 375 (2001).

[BMJLC97]   P.K. Bunch, F. Mat-Jan, N. Lee, and D.P. Clark. The ldha gene encoding
            the fermentative lactate dehydrogenase of escherichia coli. *Microbiology* **143**,
            187 – 195 (1997).

[BOM+90]   K. Backman, M.J. O'Connor, A. Mayuya, E. Rudd, D. McKay, R. Balakrish-
            nan, M. Radjai, V. DiPasquantonio, D. Shoda, R. Hatch, and K. Venkatasub-
            ramian. Genetic engineering of metabolic pathways applied to the production
            of phenylalanine. *Ann. New York Ac. Sci.* pages 16 – 24 (1990).

[Bra76]   M.M. Bradford. A rapid and sensitive method for the quantification of mi-
            crogram quantities of protein utilising the principle of protein-dye binding.
            Anal. Biochem. **72**, 248 – 254 (1976).

[Bre]   Brenda, the comprehensive enzyme information system.
            http://www.brenda.uni-koeln.de.

[BS87]   B.A. Burdick and J.R. Schaeffer. Co-immobilized coupled enzyme systems
            on nylon mesh capable of gluconic and pyruvic acid production. *Biotechnol.
            Lett.* **9**, 253 – 258 (1987).

[BS93]   A. Borle and R.T. Stanko. Pyruvate reduces anoxic injury and free radical
            formation in perfused rat hepytocytes. *J. Appl. Physiol.* pages 535 – 540
            (1993).

[BST97]   H.P. Bonarius, G. Schmid, and J. Tramper. Flux analysis of underdetermined
            metabolic networks: The quest for the missing constraint. *TibTech* **15**, 308–
            314 (1997).

298   References

[BTW01]   A. BUCHHOLZ, R. TAKORS, AND C. WANDREY. Quantification of intracellular metabolites in escherichia coli k12 using liquid chromatographic-electrospray ionization tandem mass spectrometric techniques. *Anal. Biochem.* **295**, 129 – 137 (2001).

[Buc01a]   A. BUCHHOLZ. "Quantifizierung Intrazellulärer Metabolitdynamiken Zur Untersuchung Mikrobieller Stoffwechselnetzwerke". PhD thesis, University of Bonn (2001).

[Büc01b]   J. BÜCHS. Intoduction to advantages and problems of shaken cultures. *Biochem. Eng. Journal* **7**, 91 – 98 (2001).

[Bud01]   A. BUDZINSKI. Aminosäuren, peptide und die chemie dazu. *Chemische Rundschau* **54**(6), 10 (2001).

[Buj01]   R. BUJNICKI. Untersuchung reaktionstechnischer parameter zur produktion von l-phenylalanin mit escherichia coli im fed-batch verfahren. Master's thesis, Technical University of Berlin (2001).

[Buj03]   R. BUJNICKI. "Prozessentwicklung Zur Produktion Von Cyclitolen und Anderen Chorismat-Derivaten mit Rekombinanten Escherichia Coli Stämmen im Fed-Btach Verfahren (Current Ph.D. Study, Preliminary Titel)". PhD thesis, Technical University of Berlin (2003).

[BWG+03]   H.H.J. BLOEMEN, L. WU, W.M. VAN GULIK, J.J. HEIJNEN, AND M.H.G. VERHAEGEN. Reconstruction of the o2 uptake and CO2 evolution rate on a time scale of seconds. *AICHE Journal* **49(7)**, 1895 – 1908 (2003).

[BWT01]   A. BUCHHOLZ, C. WANDREY, AND R. TAKORS. Verfahren zur dosierung exakter volumina von flüssigkeiten in eine vorlage sowie dafür geeignete vorrichtung. Technical Report, German Patent Application DE 100 03 416.0-52 (2001).

[CA73]   M. CHULAVATNATOL AND D.E. ATKINSON. Phosphoenolpyruvate synthetase from escherichia coli. *The Journal of Biological Chemistry* **248(8)**, 2712 – 2715 (1973).

[Car97]   J.P. CARDOSO. Purification of penicillin g amidase using quaternary ammonium salts and effect on the activity of the immobilized enzyme. *Bioproc. Eng.* **16**, 209 – 218 (1997).

[CB95]   A. CORNISH-BOWDEN. "Fundamentals of Enzyme Kinetics". Portland Press Ltd., ISBN 1 85578 072 0, London (1995).

[CBC+87]   J.R. COGGINS, M.R. BOOCOCK, S. CHAUDHURI, J.M. LAMBERT, J. LUMSDEN, G.A. NIMMO, AND D.D.S. SMITH. "Metabolism of the Aromatic Amino Acids, 142", chapter The Arom Multifunctional Enzyme from Neurospora Crassa, page 325. (1987).

[CBC00]   A. CORNISH-BOWDEN AND M. L. CARDENAS. From genome to cellular phenotype - a role for metabolic flux analysis. *Nature Biotechnol.* **18**, 267 – 268 (2000).

[CBC02]   A. CORNISH-BOWDEN AND M.L. CARDENAS. Metabolic balance sheets. *Nature* **420**, 129 – 130 (2002).

[CBH91]   A. CORNISH-BOWDEN AND J.H. HOFMEYER. METAMODEL: A program for modeling and control of metabolic pathways on the IBM PC and compatibles. *Comput. Appl. Biosci.* **7(1)**, 89 – 93 (1991).

[CCG+01]   B. CHRISTENSEN, T. CHRISTIANSEN, A.K. GOMBERT, J. THYAKER, AND J. NIELSEN. Simple and robust method for estimation of the split between the oxidative pentose phosphate pathway and the embden-meyerhoff-parnas pathway in microorganisms. *Biotechnol. Bioeng.* **74(6)**, 517 – 523 (2001).

[CDC87]   S. CHAUDHURI, K. DUNCAN, AND J.R. COGGINS. 3-dehydroquinate dehydratase from escherichia coli. *Methods in Enzymology* **142**, 320 – 324 (1987).

[CES91]   J. Cremer, L. Eggeling, and H. Sahm. Cloning the dapA dapB cluster of
            the lysine-secreting bacterium coryneacterium glutamicum. *Appl. Environ.
            Microbiol.* **Appl. Environ. Microbiol.**, 1746–1752 (1991).

[CGN02]   B. Christensen, A.K. Gombert, and J. Nielsen. Analysis of flux estimates
            based on 13c labelling experiments. *Eur. J. Biochem.* **269**, 2795–2800 (2002).

[Cha97]   J.B. Chaudhuri. Biochemical engineering - past, present and future.
            TIBTECH **15**, 383 – 384 (1997).

[Chm91]   H. Chmiel. "Bioprozesstechnik 1/2". ISBN 3-437-20480-7 (1991).

[CHY+97]   R. Chen, V. Hatzimanikatis, W.M.G.J. Yap, P.W. Postma, and J.E. Bai-
            ley. Metabolic consequences of phosphotranferase (PTS) mutation in a
            phenylalanine-producing recombinant escherichia coli. *Biotechol. Prog.* **13**,
            768 – 775 (1997).

[CK74]   R.A. Cooper and H.L. Kornberg. The enzymes. *3rd edition, Ed. P.D. Boyer*
            16, 631 – 649 (1974).

[CLaJC99]   Y.P. Chao, Z.J. Lai, and P.Chen an J.T. Chern. Enhanced conversion rate
            of l-phenylalanine by coupling reactions of aminotransferases and phospho-
            enolpyruvate carboxykinase in escherichia coli k-12. *Biotechnol. Prog.* **15**,
            453 – 458 (1999).

[CLL00]   Y.-P. Chao, T.-E. Lo, and N.-S. Luo. Selective production of l-aspartic acid
            and l-phenylalanine by coupling reactions of aspartase and aminotransferase
            in escherichia coli. *Enzyme and Microbial Tech.* **27**, 19 – 25 (2000).

[CLMC86]   S. Chaudhuri, J.M. Lambet, L.A. McColl, and J.R. Coggins. Purification
            and chracterization of 3-dehydroquinase from escherichia coli. *Biochem. J.*
            239, 699 – 704 (1986).

[CN99]   B. Christensen and J. Nielsen. Isotopomer analysis using GC-MS. *Metabolic
            Engineering* **1**, 282–290 (1999).

[CN00]   B. Christensen and J. Nielsen. Metabolic network analysis of penicillium
            chryseogenum using 13c-labeled glucose. *Biotechnol. Bioeng.* **68(6)**, 652 –
            659 (2000).

[CN02]   B. Christensen and J. Nielsen. Reciprocal labelling: A method for investi-
            gating the catabolism of cosubstrates. *Biotechnology Progress* **18**, 163–166
            (2002).

[CNRS+02]   C. Chassagnole, N. Noisommit-Rozzi, J.W. Schmid, K. Mauch, and M. Reuss.
            Dynamic modeling of the central carbon metabolism of escherichia coli.
            Biotechnol Bioeng **79(1)**, 53 – 73 (2002).

[COG01]   D. Cascaval, C. Oniscu, and A.-I. Galaction. Selective separation of amino
            acids by reactive extraction. *Biochem. Eng. J.* **7**, 171 – 176 (2001).

[Cos99]   C.E. Costello. Bioanalytic applications of mass spectrometry. *Curr. Opin-
            ion Biotechnol.* **10**, 22 – 28 (1999).

[Cou02]   Calorie Control Council. Low-calorie sweeteners: Aspartame (2002).
            http://www.caloriecontrol.org/aspartame.html.

[CP97]   A.J. Cosgriff and A.J. Pittard. A topological model for the general aromatic
            amino acid permease, aroP. *J. Bacteriol.* **179**, 3317 – 3323 (1997).

[CPH78]   R.J. Mc Candliss, M.D. Poling, and K.M. Herrmann. 3-deoxy-d-arabino-
            heptulosonate 7-phosphate synthase - purification and molecular characteri-
            zation of phenylalanine - sensitive isoenzyme from escherichia coli. *J. Biol.
            Chem.* **253(12)**, 4259 – 4265 (1978).

[CR86]   J.M. Coulson and J.M. Richardson. "Chemical Engineering Vol. II". Perga-
            mon Press, Oxford (1986).

[CSF⁺01] M.W. COVERT, C.H. SCHILLING, I. FAMILI, J.S. EDWARDS, I.I. GORYANI, E. SELKOV, AND B.O. PALSSON. Metabolic modeling of microbial strains in silico. *TIBS* **26(3)**, 179 (2001).

[CT82] Y.J. CHOI AND D.E. TRIBE. Continuous production of phenylalanine using escherichia coli regulatory mutant. *Biotechnol. Lett.* **4**, 223 – 228 (1982).

[CT93] D.C. CAMERON AND I.-T. TONG. Cellular and metabolic engineering. *Appl. Biochem. Biotechnol.* **38**, 105–140 (1993).

[CTN00] B. CHRISTENSEN, J. THYKAER, AND J. NIELSEN. Metabolic characterization of high- and low-yielding strains of penicillium chrysogenum. *Appl. Microbiol. Biotechnol.* **54**, 212 – 217 (2000).

[CWO⁺86] G.J. CALTON, L.L. WOOD, M.H. OPDIKE, I.I. LANTZ, AND J.P. HAMMAN. The production of l-phenylalanine by polyazetidine immobilized microbes. *Biotechnol.* **4**, 317 – 320 (1986).

[CYD⁺03] S.S. CHANDRAM, J. YI, K.M. DRATHS, R. VON DAENIKEN, W. WEBER, AND J.W. FROST. Phosphoenolpyruvate availability and the biosynthesis of shikimic acid. *Biotechnology Progress* **in press** (2003).

[CYPB97] R. CHEN, W.M.G.J. YAP, P.W. POSTMA, AND J.E. BAILEY. Comparative studies of escherichia coli strains using different glucose uptake systems: Metabolism and energetic. *Biotechnology and Bioengineering* **56(5)**, 583 – 590 (1997).

[DAM91] A.J. DAUGULIS, D.B. AXFORD, AND P.J. MCLELLAN. The economics of ethanol production by extractive fermentation. *Cand. J. Chem. Eng.* **69**, 488 – 497 (1991).

[DBHS93] L.W.V. DEBOER, P.A. BEKX, L. HAN, AND L. STEINKE. Pyruvate enhances recovery of rat hearts after ischemia and and reperfusion by preventing free radicals generation. *J. Appl. Physiol.* **265**, 1571 – 1576 (1993).

[DDS73] A.B. DELEO, J. DAYAN, AND D.B. SPRINSON. Purification and kinetics of tyrosine-sensititve 3-deoxy-d-arabino-heptulosonoc acid 7-phosphate synthetase. *J. Biol. Chem.* **248**, 2344 – 2353 (1973).

[DEF⁺02] J.C. VAN DAM, M.R. EMAN, J. FRANK, H.C. LANGE, G.W.K. VAN DEDEM, AND J.J. HEIJNEN. Analysis of glycolytic intermediates in saccharomyces cerevisiae using anion exchange chromatography and electrospray ionization with tandem mass spectrometric detection. *Analytica Chimica Acta* **460**, 209 – 218 (2002).

[Deg03] D. DEGENRING. "Erstellung und Validierung Metabolischer Modelle Zur Auswertung Von Substrat-Puls Experimenten (Preliminary Title)". PhD thesis, University of Rostock, (intended) (2003).

[DF90] K.M. DRATHS AND J.W. FROST. Synthesis using plasmid-based biocatalysis: Plasmid assembly and 3-deoxy-d-arabino-heptulosonate production. *J. Am. Chem. Soc.* **112**, 1657 – 1659 (1990).

[DF93] K.A. DELL AND J.W. FROST. Identification and removal of impedients to biocatalytic synthesis of aromatics from d-glucose: Rate-limiting enzymes in the common pathway of aromatic amino acid biosynthesis. *J. Am. Chem. Soc.* **115**, 11581 – 11589 (1993).

[DF97] Q. DANG AND C. FRIEDEN. New PC versions of the kinetic simulation and fitting programs KINSIM and FITSIM. *Trends Biochem. Sci.* **22(8)**, 317 (1997).

[DFDT03] D. DEGENRING, C. FROEMEL, G. DIKTA, AND R. TAKORS. Sensitivity analysis for the reduction of complex metabolism models. *J Process Control* **in press** (2003).

[dG00a] A.A. DE GRAAF. "Bioreaction Engineering - Modeling and Control (Eds. K. Schügel and K.H. Bellgardt)", chapter Metabolic Flux Analysis of Corynebacterium glutamicum, pages 506 – 555. Springer-Verlag Berlin (2000).

[dG00b] A.A DE GRAAF. "Bioreaction Engineering - Modeling and Control (Eds.: K. Schügerl and K.H.Bellgardt)", chapter Metabolic Analysis of Zymomonas mobilis, pages 478 – 505. Springer-Verlag, Berlin (2000).

[dGES01] A.A. DE GRAAF, L. EGGELING, AND H. SAHM. "Advances in Biochemical Engineering/Biotechnology, Vol. 73, Ed. T. Scheper", chapter Metabolic Engineering for L-Lysine Production by Corynebacterium glutamicum, pages 9–29. Springer-Verlag, Berlin, Heidelberg (2001).

[dGSW+99] A.A DE GRAAF, K. STRIEGEL, R.M. WITTIG, B. LAUFER, G. SCHMITZ, W. WIECHERT, G.A. SPRENGER, AND H. SAHM. Metabolic state of zymomonas mobilis in glucose-, fructose- and xylose-fed continuous cultures as analysed by 13c and p31-NMR spectroscopy. *Archives of Microbiol.* **171**, 371 – 385 (1999).

[DHK+02] KH DRAUZ, B. HOPPE, A. KLEEMANN, H.P. KRIMMER, W.LEUCHTENBERGER, AND C. WECKBECKER. "Ullmann's Encyclopedia of Industrial Chemistry, 6th Edition, Electronic Release", chapter Amino Acids, pages –. Wiley-VCH, Weinheim, Germany (2002).

[dJ02] H. DE JONG. Modeling and simulation of genetic regulatory systems: A literature review. *J. Comp. Biol.* **9(1)**, 67 – 103 (2002).

[dKD92] W. DE KONING AND K. VAN DAM. A method for determination of changes of glycolytic metabolites in yeast on a subsecond time scale using extraction at neutral pH. *Anal. Biochem.* **204**, 118 (1992).

[DL97] J. DELGADO AND J.C. LIAO. Inverse flux analysis for reduction of acetate excretion in escherichia coli. *Biotechnol. Prog.* **13**, 361 – 367 (1997).

[DLC+84a] M.M. DOMACH, S.K. LEUNG, R.E. CAHN, G.G. COOKS, AND M.L. SHULER. Computer model for glucose-limited growth of a single copy of escerichia coli b/r-a. *Biotechnol. Bioeng.* **26**, 203 – 216 (1984).

[DLC84b] K. DUNCAN, A. LEWENDON, AND J.R. COGGINS. The purification of 5-enolpyruvoylshikimate 3-phosphate synthase from an overproducing strain of escherichia coli. *FEBS Lett.* **165**, 121 – 127 (1984).

[DMM+03] A. DRYSCH, M. EL MASSAOUDI, C. MACK, R. TAKORS, A.A. DE GRAAF, AND H. SAHM. Production process monitoring by serial mapping of microbial carbon flux distributions using a novel sensor reactor approach: II-13c-labelling -based metabolic flux analysis and l-lysine production. *Metabolic Engineering* pages 96–107 (2003).

[DMR90] P. DEBLAY, M. MINIER, AND H. RENON. Separation of l-valine from fermentation broths using supported liquid membrane. *Biotechnol. Bioeng.* **35**, 123 – 131 (1990).

[DMW+03] A. DRYSCH, M. EL MASSAOUDI, W. WIECHERT, A.A. DE GRAAF, AND R. TAKORS. Serial flux mapping of corynebacterium glutamicum during fed-batch production using the sensor reactor approach. *Biotechnology and Bioengineering* page accepted (2003). accepted.

[DPC+92] K.M. DRATHS, D.L. POMPLIANO, D.L. CONLEY, J.W. FROST, A. BERRY, G.L. DISBROW, R.J. STAVERSKY, AND J.C. LIEVENSE. Biocatalytic synthesis of aromatics from d-glucose: The role of transketolase. *J. Am. Chem. Soc.* **114**, 3956 – 3962 (1992).

[DS84a] M.M. DOMACH AND M.L. SHULER. A finite representation model for an asynchronous culture of e. coli. *Biotechnol. Bioeng.* **26** (1984).

[DS84b] M.M. DOMACH AND M.L. SHULER. Testing a potential mechnism for e. coli temporal cycle imprecision with a structural model. *J. Theor. Biol.* **106**, 577 – 585 (1984).

302   References

[DS00]   M. DAUNER AND U. SAUER. GS-MS analysis of amino acids rapidly provides rich information for isotopomer balancing. *Biotechnology Progress* **16**, 642–649 (2000).

[DT02]   D. DEGENRING AND R. TAKORS. In vivo investigation of metabolic dynamics in escherichia coli k12 by evaluation of rapid sampling experiments. In J. KIM, editor, "Proceedings of the 5th German Workshop of Artificial Life" (2002).

[DWJ$^+$99]   P. DZYGIEL, P. WIECZOREK, J.A. JONSSON, M. MILEWSKA, AND P. KAFARSKI. Separation of amino acid enantiomers using supported liquid membrane extraction with chiral phosphates and phosphonates. *Tetrahedron* **55**, 9923 – 9932 (1999).

[EAOI98]   H. ESCALANTE, A.I. ALONSO, I. ORTIZ, AND A. IRABIEN. Separation of l-phenylalanine by nondispersive extraction and backextraction. equilibrium and kinetic parameters. *Sep. Sci. and Technol.* **1**, 119 – 139 (1998).

[EBG$^+$87]   C.T. EVANS, W. BELLAMY, M. GLEESON, H. AOKI, K. HANNA, W. PETERSON, D. CONRAD, AND M. MISAWA. A novel, efficient biotransformation for the production of l-phenylalanine. *Biotechnol.* **5**, 818 – 823 (1987).

[ECPM87]   C.T. EVANS, C. COMA, W. PETERSON, AND M. MISAWA. Bioconversion of trans-cinnamic acid to l-phenylalanine in an immobilized whole cell reactor. *Biotechnol. Bioeng.* **30**, 1067 – 1072 (1987).

[EDP$^+$02]   M. EMMERLING, M. DAUNER, A. PONTI, J. FIAUX, M. HOCHHULI, T. SZYPERSKI, K. WÜTHRICH, J.E. BAILEY, AND U. SAUER. Metabolic flux responses to pyruvate kinase knockout in escherichia coli. *Journal of Bacteriology* **184**, 152–164 (2002).

[EES93]   B.J. EIKMANNS, L. EGGELING, AND H. SAHM. Molecular aspects of lysine, threonine and isoleucine biosynthesis in corynebacterium glutamicum. *Antonie v. Leeuwenhoek* **64**, 145–163 (1993).

[EFD91]   L. EHNSTROM, J. FRISENFELT, AND M. DANIELSSON. The biostil process. *Extractive Bioconversions* pages 303 – 321 (1991).

[EFGS89]   B.J. EIKMANNS, M.T. FOLLETTIE, M.U. GRIOT, AND A.J. SINSKEY. The phosphoenolpyruvate carboxylase gene of corynebactrium glutamicum: Molecular cloning, nucleotide sequence and expression. *Mol. Gen. Genet.* **218**, 330–339 (1989).

[EMP]   Enzyme and metabolic pathways (EMP). http://www.empproject.com.

[EOI96]   H. ESCALANTE, M.I. ORTIZ, AND J.A. IRABIEN. Concentration of l-phenylalanine by non-dispersive extraction extraction in hollow fibre modules. In "ISEC 96", pages 1493 – 1498, Melbourne, Australia (1996).

[EOS98]   L. EGGELING, S. OBERLE, AND H. SAHM. Improved l-lysine yield with corynebacterium glutamicum: Use dapA resulting in increased flux combined with growth limitation. *Appl. Microbiol. Biotechnol.* **49**, 24–30 (1998).

[EP98]   J.E. EDWARDS AND B.O. PALSSON. How will bioinformatics influence metabolic engineering. *Biotechnol. Bioeng.* **58(2)**, 162 – 169 (1998).

[ERP02]   J.S. EDWARDS, R. RAMAKRISHNA, AND B.O. PALSSON. Characterizing the metabolic phenotype: A phenotype phase plane analysis. *Biotechnol. Bioeng.* **77(1)**, 27 – 36 (2002).

[ES99]   L. EGGELING AND H. SAHM. L-glutamate and l-lysine: Traditional products with impetuous developments. *Appl. Microbiol. Biotechnol.* **52**, 146 – 153 (1999).

[ESG$^+$97]   A. EISENBERG, J.E. SEIP, J.E. GOVAGAN, M.S. PAYNE, D.L. ANTON, AND R. DICOSIMO. Pyruvic acid production using methylotrophic yeast transformants as catalysts. *J. Mol. Catal. B.: Enzymatic* **2**, 223 – 232 (1997).

[EY02]   ERNST AND YOUNG. "Neue Chancen - Deutscher Biotechnologie-Report 2002".
            Ernst and Young Deutsche Allgemeine Treuhand AG, Nürnberg - München -
            Stuttgart (2002).

[EZ95]   M. EHLDE AND G. ZACCHI. MIST: A user-friendly metabolic simulator. *Comput. Appl. Biosci.* **11(2)**, 201 – 207 (1995).

[FD95]   J.W. FROST AND K.M. DRATHS. Biocatalytic syntehsis of aromatics from d-glucose: Renewable microbial sources of aromatic compounds. *Annu. Rev. Microbiol.* **49**, 557 – 559 (1995).

[FEH88]   C. FÖRBERG, T. ELIASON, AND L. HÄGGSTRÖM. Correlation of theoretical and experimental yields of phenylalanine from non-growing cells of a rec escherichia coli strain. *J. Biotechnol.* **7**, 319 – 332 (1988).

[Fel92]   D. A. FELL. Metabolic control analysis: A survey of its theoretical and experimental development. *Biochem. J.* **286**, 313–330 (1992).

[Fer96]   T. FERENCI. Adaption to life at micromolecular nutrient levels: The regulation of escherichia coli glucose transport by endoinduction and cAMP. *FEMS Microbiology Reviews* **18**, 301 – 317 (1996).

[Fer99]   T. FERENCI. Growth of bacterial cultures 50 years on: Towards an uncertainty principle instead of constants on bacterial growth kinetics. *Res. Microbiol.* **150**, 431–438 (1999).

[Fey87]   R. DE FEYTER. Shikimate kinases from escherichia coli k12. *Methods Enzymol.* **142**, 355 – 361 (1987).

[FGF⁺02]   S. FLORES, G. GOSSET, N. FLORES, A.A. DE GRAF, AND F. BOLIVAR. Analysis of carbon metabolism in escherichia coli strains with an inactive phosphotransferase system by 13c labeling and NMR spectroscopy. *Metab. Eng.* **4(2)**, 124 – 137 (2002).

[FGN02]   J. FÖRSTER, A.K. GOMBERT, AND J. NIELSEN. A functional genomics approach using metabolomics and in silico pathway analysis. *Biotechnol. Bioeng.* **79 (7)**, 703 – 712 (2002).

[FH87]   C. FÖRBERG AND L. HÄGGSTRÖM. Effects of cultural conditions on the production of phenylalanine from a plasmid-harboring e. coli strain. *Microbiol. Biotechnol.* **26**, 136 – 140 (1987).

[FH88]   C. FÖRBERG AND L. HÄGGSTRÖM. Phenylalanine production from rec escherichia coli-strain in fed-batch culture. *J. Biotechnol.* **8**, 291 – 300 (1988).

[Fie01]   O. FIEHN. Combining genomics, metabolome analysis and biochemical modeling to understand metabolic networks. *Comp. Funct. Genom.* **2**, 155 – 168 (2001).

[Fie02]   O. FIEHN. Metabolomics - the link between genotypes and phenotypes. *Plant. Mol. Biol.* **48**, 155 – 171 (2002).

[FKD⁺00]   O. FIEHN, J. KOPKA, P. DÖRMANN, T. ALTMANN, R.N. TRETHEWEY, AND L. WILLMITZER. Metabolite profiling for plant functional genomics. *Nature Biotechnol.* **18**, 1157 – 1161 (2000).

[FL93]   J.W. FROST AND J. LIEVENSE. Prospects for biocatalytic synthesis of aromatics in the 21st century. *New J. Chem.* **18**, 341 – 348 (1993).

[FL94]   J.W. FROST AND J. LIEVENSE. Prospects for biocatalytic synthesis of aromatics in the 21st century. *New J . Chem.* **18**, 341 – 348 (1994).

[FLE⁺03]   D. FRANKE, V. LORBACH, S. ESSER, C. DOSE, G.A. SPRENGER, M. HALFAR, J. THÖMMES, R. MÜLLER, R. TAKORS, AND M. MÜLLER. (s,s)-2,3-dihydroxy-2,3-dihyxyobenzoic acid: Microbial access with engineered cells of escherichia coli and applicability as starting material in natural-product synthesis. *Chem. Eur. J.* **9**, 2 – 10 (2003).

[Fot98]   I.G. FOTHERINGHAM. Improved transaminase biotransformation process. Technical Report, PCT/US 98/10169, WO 98/53088 (1998).

[FP86]   R.C. DE FEYTER AND J. PITTARD. Purification and properties of shikimate kinase II from escherichia coli k-12. *J. Bacteriol.* **165**, 331 – 333 (1986).

[FPF$^+$86]   J.P. FÜRSTE, W. PANSEGRAU, R. FRANK, H. BLÖCKER, P. SCHOLZ, M. BAGDASARIAN, AND E. LANKA. Molecular cloning of the plasmid RP4 primase region in a multi-host-range tacP expression vector. *Gene* **48**, 119 – 131 (1986).

[Fro92]   J.W. FROST. Enhanced production of common aromatic pathway compounds. Technical Report, US patent 5,168,056 (1992).

[Fro03]   C. FROEMEL. Parameterreduktion in stoffwechselmodellen mit methoden der statistik. Master's thesis, Fachhochschule (University of Applied Sciences) Aachen/Jülich (2003).

[FS99]   P. VON FRIELING AND K. SCHÜGERL. Recovery of lactic acid from aqueous model solutions and fermentation broths. *Proc. Biochem.* **34**, 685 – 696 (1999).

[FSM03]   D. FRANKE, G.A. SPRENGER, AND M. MÜLLER. Easy access to (r,r)-3,4-dihydroxy-3,4-dihydrobenzoic acid with engineered strains of escherichia coli. *Chem Bio Chem* **4**, 775 – 777 (2003).

[FTH94]   I.G. FOTHERINGHAM, J.L. TON, AND C. HIGGINS. Materials and methods for hypersecretion of amino acids. Technical Report, US patent 5354672 (1994).

[FW00]   D. FELL AND A. WAGNER. The small world of metabolism. *Nature Biotechnol.* **18**, 1121 – 1122 (2000).

[FWL93]   A. FREEMAN, J.: WOODLEY, AND M.D. LILLY. In situ product removal as a tool for bioprocessing. *Bio/Technology* **11**, 1007 – 1012 (1993).

[FXB$^+$96]   N. FLORES, J. XIAO, A. BERRY, F. BOLIVAR, AND F. VALLE. Pathway engineering for the production of aroamtic compounds in escherichia coli. *Nature Biotechnology* **14**, 620 – 623 (1996).

[GBB$^+$96]   A. GOFFEAU, B.G. BARRELL, H. BUSSEY, R.W. DAVIS, B. DUJON, H. FELDMANN, F. GALIBERT, J.D. HOHEISEL, C. JACQ, M. JOHNSTON, E.J. LOUIS, H.W. MEWES, Y. MURAKAMI, P. PHILIPPSEN, H. TETTELIN, AND S.G. OLIVER. Life with 6000 genes. *Science* **274**, 546 – 567 (1996).

[GBGN$^+$02]   M. GERIGK, R. BUJNICKI, E. GANPO-NKWENKWA, J. BONGAERTS, G. SPRENGER, AND R. TAKORS. Process control for enhanced l-phenylalanine production using different recombinant e. coli strains. *Biotechnol. Bioeng.* **80(7)**, 746 – 754 (2002).

[GBK95]   E.D. GILLES, G. BREUEL, AND A. KREMLING. "ISBN 3-00-000360-6", chapter A Modular Concept for the Modeling of the Dynamics of Bacterial Metabolism, pages 156 – 158. (1995).

[GBZT01]   T. GERHARZ, M. BOTT, B. ZELIC, AND R. TAKORS. Verfahren zur fermentativen herstellung von pyruvat. Technical Report, German Patent Application DE 101 29 711.4 (2001).

[GdLL92]   W.J. GROOT, R.G.J.M. VAN DER LANS, AND K.CH.A.M. LUYBEN. Technologies for butanol recovery integrated with fermentations. *Process Biochem.* **27**, 61 – 75 (1992).

[GdLVH00]   W.M. VAN GULIK, W.T.A.M. DE LAAT, J.L. VINKE, AND J.J. HEIJNEN. Application of metabolic flux analysis for the identification of metabolic bottlenecks in the biosynthesis of penicillin-g. *Biotechnology and Bioengineering* **68**, 602–618 (2000).

[GEA00]   R.R. GOKARN, M.A. EITEMAN, AND E. ALTMAN. Metabolic analysis of escherichia coli in the presence and absence of the carboxylating enzymes phosphoenolpyruvate carboxylase and pyruvate carboxylase. *Appl. Environ. Microbiol.* **66(5)**, 1844 – 1850 (2000).

[Ger01]   M. Gerigk. "Integrierte Prozessentwicklung Zur Herstellung Von L-Phenylalanin mit Escherichia Coli". PhD thesis, Technical University of Berlin (2001).

[Ger03]   T. Gerharz. "Pyruvat-Produktoion Durch Acetatauxotrophe Escherichia Coli-Stämme". PhD thesis, University of Düsseldorf, Berichte des Forschungszentrum Jülich GmbH, ISSN 0944-2952, Jül-4097 (2003).

[GFR97]   B. Gonzalez, J. Francois, and M. Renaud. A rapid and reliable method for metabolite extraction in yeast using boiling buffered ethanol. *Yeast* **13**, 1347 – 1355 (1997).

[GHS99]   I. Goryanin, T.C. Hodgman, and E. Selkov. Mathematical simulation and analysis of cellular metabolism and regulation. *Bioinformatics* **9**, 749 – 758 (1999).

[GIS+81]   A. Goto, M. Ishihara, M. Sakurai, H. Enei, and K. Takinami. Method for producing l-phenylalanine fy fermentation. Technical Report, Jap. Patent 56-64793 (1981).

[GJ56]   R. Grewe and J.P. Jeschke. Die synthese der 5-dehydro-chinasäure. *Ber.* **89**, 2080 – 2088 (1956).

[GKBL85]   G.H. Gil, S.R. Kim, J.C. Bae, and J.H. Lee. Pilo-scale production of l-phenylalanine from d-glucose. *Enzyme Microb. Technol.* **7**, 370 – 372 (1985).

[GMK+02]   M.R. Gerigk, D. Maass, A. Kreutzer, G. Sprenger, J. Bongaerts, M. Wubbolts, and R. Takors. Enhancd pilot-scale fed-batch l-phenylalanine production with recombinant escherichia coli by fully integrated reactive extraction. *Bioproc. Biosyst. Eng.* **25**, 43 – 52 (2002).

[GN00]   A.K. Gombert and J. Nielsen. Mathematical modelling of metabolism. *Curr. Opinion Biotechnol.* **11**, 180 – 186 (2000).

[GN01]   E. Ganpo-Nkewnkwa. Influence of the tyrosine-availability on growth and l-phenylalanine production in the fed-batch fermentation using e. coli strains. Master's thesis, University for Applied Sciences, Mannheim (2001).

[GRGG99]   Z. Gu, D.A. Rickert, B.A. Glatz, and C.E. Glatz. Feasibility of propionic acid production by extractive fermentation. *Lait* **79**, 137 – 148 (1999).

[Gri98]   N.J. Grinter. Developing an l-phenylalanine process. *ChemTech.* **July**, 33 – 37 (1998).

[GRST01]   M. Gerigk, L. Raeven, G. Sprenger, and R. Takors. Process for the production of aromatic amino acid metabolites and derivatives thereof. Technical Report, European patent application EP 02078876.6 (2001).

[GSCN01]   A.K. Gombert, M. M. Dos Santos, B. Christensen, and J. Nielsen. Network identification and flux quantification in the central metabolism of saccharomyces cerevisiae under different conditions of glucose repression. *Journal of Bacteriology* **183**, 1441–1451 (2001).

[GWS92]   K.J. Gruys, M.C. Walker, and J. Sikorski. Substrate synergism and the steady-state kinetic reaction mechanism for EPSP synthase from escherichia coli. *Biochemistry* **31**, 5534 – 5544 (1992).

[GWS+03]   R. Gerstmeier, V.F. Wendisch, S. Schnicke, H. Ruan, M. Farwick, D. Reinscheid, and B.J. Eikmanns. Acetate metabolism and its regulation in corynebacterium glutamicum. *J. Biotechnol.* **104**, 99 – 122 (2003).

[GYXB96]   G. Gosset, J. Yong-Xiao, and A. Berry. A direct comparison of approaches for increasing carbon flow to aromatic biosynthesis in escherichia coli. *J. Ind. Microbiol.* **17**, 47 – 52 (1996).

[GZS67]   E.G. Gollub, H. Zalkin, and D.B. Sprinson. Correlation of genes and enzymes and studies on regulation of the aromatic pathway in salmonella. *J. Biol. Chem.* **242**, 389 – 395 (1967).

[HAKS01]   Q. Hua, M. Araki, Y. Koide, and K. Shimizu. Effects of glucose, vitamins and DO concentrations on pyruvate fermentation using torulopsis glabrata IFO 0005 with metabolic flux analysis. *Biotechnol. Prog.* **17**, 62 – 68 (2001).

[Hat99]   V. Hatzimanikatis. Nonlinear metabolic control analysis. *Metabolic Engineering* **1**, 75–87 (1999).

[Hay74]   J.G. Hayes. Numerical methods for curve and surface fitting. *Bulletin of the Insitute of Mathematics and its Application* **10**, 144 – 152 (1974).

[HB96]   V. Hatzimanikatis and J.E. Bailey. MCA has more to say. *J. theor. Biol.* **182**, 233–242 (1996).

[HBA+02]   J. Hurlebaus, A. Buchholz, W. Alt, W. Wiechert, and R. Takors. MMT - a pathway modeling tool for data from rapid sampling experiments. *In Silico Biology* **2**, 467 – 484 (2002).

[HBC+00]   B. Hitzmann, O. Broxtermann, Y.L. Cha, O. Sobiah, E. Stärk, and T. Scheper. The control of glucose concentration during yeast fed-batch cultivation using fast measurement complemented by an extended kalman filter. *Bioproc. Eng.* **23**, 337 – 341 (2000).

[HBGF98]   H. Hajjaj, P.J. Blanc, G. Goma, and J. Francois. Sampling techniques and comparative extraction procedures for quantitative determination of intra- and extracellular metabolites in filamentous fungi. *FEMS Microbiol. Lett.* **164**, 195 – 200 (1998).

[Hei02]   U. Heidersdorf. Untersuchung zur integrierten extraktion von l-phenylalanin aus fermentationen mit rekombinanten escherichia coli. Master's thesis, Fachhochschule (University for Applied Sciences) Flensburg (2002).

[Her03]   T. Hermann. Industrial production of amino acids by coryneform bacteria. *J. Biotechnol.* **104**, 155 – 172 (2003).

[HF32]   J.W. Howard and W.A. Fraser. Pyruvic acid. *Org. Synth. Coll.* **1**, 475 – 476 (1932).

[HFWT02]   M.D. Haunschild, B. Freisleben, W. Wiechert, and R. Takors. Distributed simulation of metabolic networks. In "Modelling and Simulation 2002, SCS Europe, ISBN: 90-77039-07-4, 16th European Simulation Multiconferences ESM'2002, Darmstadt, 03.-05.06.", pages 436 – 440. SCS Europe (2002).

[HG03]   G.G. Harrigan and R. Goodacre. "Metabolic Profiling: Its Role in Biomarker Discovery and Gene Function Analysis". Kluwer Academic Publisher, Norwell, Massachusetts 02061 USA (2003).

[HGC+85]   S.O. Hwang, G.H. Gil, Y.J. Cho, K.R. Kang, J.H. Lee, and J.C. Bae. The fermentation process for l-phenylalanine production using an auxotrophic regulatory mutant of escherichia coli. *Appl. Microbiol. Biotechnol.* **2**, 108 – 113 (1985).

[HH73]   D.J. Harvey and M.G. Horning. Characterization of trimethylsilyl derivatives of sugar phosphates and related compounds by gas chromatography and gas chromatography mass spectrometry. *J. Chromatrography* **76**, 51 – 62 (1973).

[HHW01]   M.A. Hans, E. Heinzle, and C. Wittmann. Quantification of intracellular amino acids in batch cultures of saccharomyces cerevisiae. *Appl. Microbiol. Biotechnol.* **56**, 776 – 779 (2001).

[HHW03]   M.A. Hans, E. Heinzle, and C. Wittmann. Free intracellular amino acid pools during autonomous oscillations in saccharomyces cerevisiae. *Biotechnol. Bioeng.* **82**, 143 – 151 (2003).

[Hir01]   E. HIRSCH. Reaktionstechnische untersuchungen zur auswirkung von glucose-pulsen auf den aromatenbiosynthese-weg bei glucoselimitierten e. coli stäm-men. Master's thesis, Fachhochschule (University for Applied Sciences) Flens-burg (2001).

[HK79]   I.S. HUNTER AND H.L. KORNBERG. Glucose transport of escherichia coli growing in glucose-limited continuous culture. *Biochem. J.* **178**, 97 – 101 (1979).

[Hof91]   J.S. HOFMEYER. Metabolite channelling and metabolic regulation. *J. Theor. Biol.* **52**, 101 (1991).

[Hol86]   W. HOLMS. "Current Topics in Cellular Regulation, Eds: B.L. Horecker and E.R. Stadtman", chapter The central metabolic pathways of Escherichia coli: relationships between flux and control at a branch point; efficiency of conver-sion to biomass, and excretion of acetate, pages 69 – 105. Academic Press, NY (1986).

[HS98]   R. HEINRICH AND S. SCHUSTER. The modelling of metabolic systems. structure, control and optimality. *BioSystems* **47**, 61 – 77 (1998).

[HS99]   Q. HUA AND K. SHIMIZU. Effect of dissolved oxygen concentration on the intra-cellular flux distribution for pyruvate fermentation. *J. Biotechnol.* **68**, 135 – 147 (1999).

[HSS$^+$87]   W. HUMMEL, H. SCHUTTE, E. SCHMIDT, C. WANDREY, AND M.R. KULA. Isolation of l-phenylalanine dehydrogenase fromRhodococcus sp. m4 and its application for the production of l-phenylalanine. *Appl. Microbiol. Biotechnol.* **26**, 409 – 416 (1987).

[HSWK86]   W. HUMMEL, E. SCHMIDT, C. WANDREY, AND M.R. KULA. L-phenylalanine de-hydrogenase from brevibacerium sp. for production of l-phenylalanine by re-ductive amination of phenylpyruvate. *Appl. Microbiol. Biotechnol.* **25**, 175 – 185 (1986).

[HTT$^+$95]   H. HONDA, Y. TOYAMA, H. TAKAHASHI, T. NAKAZEKO, AND T. KOBAYASHI. Ef-fective lactic acid production by two-stage extractive fermentation. *J. Ferm. Bioeng.* **79(6)**, 589 – 593 (1995).

[Hur01]   J. HURLEBAUS. "A Pathway Modeling Tool for Metabolic Engineering". PhD thesis, Rheinische Friedrich-Wilhelms-Universität, University of Bonn (2001).

[HYS99]   Q. HUA, C. YANG, AND K. SHIMIZU. Metabolic flux analysis for efficient pyruvate fermentation using vitamin-auxotrophic yeast torulopsis glabrata. *J. Biosci. Bioeng.* **87**, 206 – 213 (1999).

[IEP02]   R.U. IBARRA, J.S. EDWARDS, AND B.O. PALSSON. Escheichia coli k-12 undergoes adaptive evolution to achieve in silico predicted optimal growth. *Nature* **420**, 186–189 (2002).

[IFKN97]   Y. ISONO, K. FUKUSHIMA, T. KAWAKATSU, AND M. NAKAJIMA. Integration of charged membrane into perstraction system for separation of amino acid derivatives. *Biotechnol. Bioeng.* **56(2)**, 162 – 167 (1997).

[IK92]   M. IKEDA AND R. KATSUMATA. Metabolic engineering to produce tyrosine or phenylalanine in a tryptophane-producing corynebacterium glutamicum strain. *Appl. Environ. Microbiol.* **58**, 781 – 785 (1992).

[IKI93]   M. IMANARI, K. KUJIRA, AND H. IWANE. Process for preparing pyruvate. Tech-nical Report, US patent 5,225,593 (1993).

[IMTY82]   Y. IZUMI, Y. MATSUMURA, Y. TANI, AND H. YAMADA. Pyruvic acid produc-tion from 1,2-propanediol by thiamin-requiring acinetobacter sp. 80-m. *Biol. Chem.* **46**, 2673 – 2679 (1982).

[Inc]   THE MATHWORKS INC. "MATLAB / SIMULINK". http://www.mathworks.com.

[IO95]   Y. Izumi and J.W. Olney. Use of pyruvate to prevent neuronal degeneration associated with ischemia. Technical Report, US Patent 5,395,822 (1995).

[IOK93]   M. Ikeda, A. Ozaki, and R. Katsumata. Phenylalanine production my metabolically engineered corynabacterium glutamicum with the pheA gene of escherichia coli. *Appl. Microbiol. Biotechnol.* **39**, 318 – 323 (1993).

[JBS01]   R. Jossek, J. Bongaerts, and G.A. Sprenger. Characterization of a new feedback-resistant 3-deoxy-d-arabino-heptulosonate 7-phosphate synthase AroF of escherichia coli. *FEMS Microbiol. Lett.* **202**, 145 (2001).

[JCN01]   E. Jonsbu, B. Christensen, and J. Nielsen. Changes of in vivo fluxes through central metabolic pathways during the production of nystatin by streptomyces noursei in batch culture. *Appl. Microbiol Biotechnol* **56**, 93–100 (2001).

[JJV99]   N.B.S. Jensen, K.V. Jokumsen, and J. Villadsen. Determination of the phosphorylated sugars of the emden-meyerhoff-parnas pathway in lactococcus lactis using a fast sampling technique and solid phase extraction. *Biotechnol. Bioeng.* **63**, 356 – 362 (1999).

[JK96]   Jacobi and R. Krämer. unpublished results (1996).

[JLLL97]   J.-L-Lu and J.C. Liao. Metabolic engineering and control analysis for production of aromatics: Role of transaldolase. *Biotechnology and Bioengineering* **53(2)**, 132 – 138 (1997).

[JNVM95]   H.S. Jorgensen, J. Nielsen, J. Villadsen, and H. Mollgaard. Metabolic flux distributions in penicillium chrysogenum during fed.batch cultivations. *Biotechnology and Bioengineering* **46**, 117–131 (1995).

[Jol72]   I.T. Jolliffe. Discarding variables in a principal component analysis. i: Artificial data. *J Royal Stat. Soc.* **21**, 160 – 172 (1972).

[Jol86]   I.T Jolliffe. "Principal Component Analysis". Springer-Verlag, New York (1986).

[JQMS99]   A. Jaquet, L. Quan, I.W. Marison, and U. Von Stockar. Factors influencing the potential use of aliquat 336 for the in situ extraction of carboxylic acids from cultures of pseudomonas putida. *J. Biotechnol.* **68**, 185 – 196 (1999).

[JS93]   M.S.M. Jetten and A.J. Sinskey. Characterization of phosphoenolpyruvate carboxykinase from corynebacterium glutamicum. *FEMS Microbiol. Lett.* **111**, 183–188 (1993).

[JS95]   M.S.M. Jetten and A.J. Sinskey. Purification and properties of oxaloacetate decarboxylase from corynebacterium glutamicum. *Antonie v. Leeuwenhoek* **67**, 221–227 (1995).

[KA93]   H. Kacser and L. Acerenza. A universal method for achieving increases in metabolite production. *Eur. J. Biochem* **216**, 361–367 (1993).

[Kab69]   H.R. Kaback. The regulation of sugar transport in isolated bacterial membrane preparations from escherichia coli. In "Proceedings of the National Academic of Science 63, USA", pages 724 – 731 (1969).

[Kaf99]   N. Kaftzik. Reaktionstechnische untersuchungen zur membrangestützten reaktiv-extraktion aromatischer aminosäuren. Master's thesis, Mathematisch-Naturwissenschaftliche Fakultät der Rheinischen Friedrich-Wilhelms-Universität, University of Bonn (1999).

[Kar80]   D.M. Karl. Cellular nucleotide measurements and applications in microbial ecology. *Microbiological Reviews* **44(4)**, 739 – 796 (1980).

[KAS03a]   M.I. Klapa, J.C. Aon, and G. Stephanopoulos. Ion-trap mass spectrometry used in combination with gas chromatography for high-resolution metabolic flux determination. *BioTechniques* **34(4)**, 832 – 849 (2003).

[KAS03b]   M.I. KLAPA, J.C. AON, AND G. STEPHANOPOULOS. Systematic quantification of complex metabolic flux networks using stable isotopes and mass spectrometry. *Eur. J. Biochem.* **270**, 3525 – 3542 (2003).

[KBL⁺01]   A. KREMLING, K. BETTENBROCK, B. LAUBE, K. JAHREIS, J.W. LENGELER, AND E.D. GILLES. The organization of metabolic reaction networks. *Metab. Eng.* **3**, 362 – 379 (2001).

[KBR⁺03]   M. KRÄMER, J. BONGAERTS, R.BOVENBERG, S. KREMER, U. MÜLLER, S. ORF, M. WUBBOLTS, AND L. RAEVEN. Metabolic engineering for microbial production of shikimic acid. *Metab. Eng.* **5**, 277 – 283 (2003).

[KBW93]   Y. F. KO, W. E. BENTLEY, AND W. A. WEIGAND. An integrated metabolic modeling approach to describe the energy efficiency of escherichia coli fermentations under oxygen limited conditions: Cellular energetics, carbon flux and acetate production. *Biotechnol. Bioeng.* **42**, 843 – 853 (1993).

[KBW94]   Y.-F. KO, W.E. BENTLEY, AND W.A. WEIGAND. A metabolic model of cellular energetics and carbon flux during aerobic escherichia coli fermentation. *Biotechnol. Bioeng.* **43**, 847 – 855 (1994).

[KCH⁺98]   B.N. KHOLODENKO, M. CASCANTE, J.B. HOEK, H.V. WESTERHOFF, AND J. SCHWABER. Metabolic design: How to engineer a living cell to desired metabolite concentrations and fluxes. *Biotechnology and Bioengineering* **59**(2), 239–247 (1998).

[KCLS91a]   G.L. KLEMAN, J.J. CHALMERS, G.W. LULI, AND W. STROHL. Glucose-stat, a glucose-controlled continuous culture. *Appl. Env. Microbiol.* **57**, 918 – 923 (1991).

[KCLS91b]   G.L. KLEMAN, J.J. CHALMERS, G.W. LULI, AND W.R. STROHL. A predictive and feedback control algorithm maintains a constant glucose concentration in fed-batch fermentations. *Appl. Env. Microbiol.* **57**, 910 – 917 (1991).

[KDK⁺92]   C. KLEANTHOUS, R. DEKA, K. DAVIS ANDS.M. KELLY, A. COOPER, S.E. S.E. HARDING, N.C. PRICE, A.R. HAWKINS, AND J.R. COGGINS. A comparison of the enzymological and biophysical properties of two distinct classes of dehydroquinase enzymes. *Biochem. J.* **282**, 687 – 695 (1992).

[KG01]   A. KREMLING AND E.D. GILLES. The organization of metabolic reaction networks: II. signal processing in hierachical structured functional units. *Metab. Eng.* **3**, 138 – 150 (2001).

[Kit02]   H. KITANO. Computational systems biology. *Nature* **420**, 206 – 210 (2002).

[KJAS02]   M.A.G. KOFFAS, G.Y. JUNG, J.C. AON, AND G. STEPHANOPOULOS. Effect of pyruvate carboxylase overexpression on the physiology of corynebacterium glutamicum. *Appl. Environ. Microbiol.* **68**(11), 5422 – 5428 (2002).

[KJLG00]   A. KREMLING, K. JAHREIS, J.W. LENGELER, AND E.D. GILLES. The organization of metabolic reaction networks: A signal-oriented approach to cellular models. *Metab. Eng.* **2**, 190 – 200 (2000).

[KKSS99]   M. KRÄMER, M. KARUTZ, G. SPRENGER, AND H. SAHM. Microbial preparation of substances from aromatic metabolism, part III. Technical Report, PCT/NL99/00232, WO 99/55877 (1999).

[KKSY90]   K.B. KONSTANTINOV, M. KISHIMOTO, T. SEKI, AND T. YOSHIDA. A balanced DO-stat and its application to the control of acetic acid secretion by recombinant escherichia coli. *Biotechnol. Bioeng.* **36**, 750 – 758 (1990).

[KLB⁺96]   R. KELLE, B. LAUFER, C. BRUNZEMA, D. WEUSTER-BOTZ, R. KRÄMER, AND C. WANDREY. Reaction engineering analysis of l-lysine transport by corynebacterium glutamicum. *Biotechnol. Bioeng.* **51**, 40 – 50 (1996).

310   References

[KNY90]   K.B. KONSTANTINOV, N. NICHIO, AND T. YOSHIDA. Glucose feeding strategy accounting for the decreasing oxidative capacity of recombinant escherichia coli in fed-batch cultivation for phenylalanine production. *J. Ferment. Bioeng.* **70**, 253 – 260 (1990).

[Kos98]   D.E. KOSHLAND. The era of pathway quantification. *Science* **280**, 852 – 853 (1998).

[Krä96]   R. KRÄMER. Genetic an physiological approaches for the production of amino acids. *J. Biotechnol.* **45**, 1–21 (1996).

[Krä00]   M. KRÄMER. "Investigations on the Influence of Increased Availability of Erythrose 4-Phosphate and Phosphenolpyruvate on the Carbon Flux Into the Aromatic Amino Acid Pathway of Escherichia Coli". PhD thesis, University of Düsseldorf/Fortschrittsberichte des Forschungszentrum Jülich GmbH, ISSN 0944-2952 (2000).

[Kre02]   I. KRETZERS.   Reaction engineering studies for reactive extraction of l-phenylalanine with liquid-liquid centrifuges.   Master's thesis, Noordedijke Hogenschool Leuwarden, The Netherlands (2002).

[KRL+94]   H.Y. KIM, H. RHYM, D.J. LEE, C.H. WON, B.L. LIM, AND H.G. CHOI. Method for production of l-phenylalanine by recombinant escherichia coli. Technical Report, US patent 5304475 (1994).

[KRL+95]   H.Y. KIM, H. RHYM, D.J. LEE, C.H. WON, B.L. LIM, AND H.G. CHOI. Method for production of l-phenylalanine by escherichia coli mutant that is resistant to osmotic pressure. Technical Report, US patent 5409830 (1995).

[KRS+00]   P.D. KARP, M. RILEY, M. SAIER, I.T. PAULSEN, S.M. PALEY, AND A. PELLEGRINI-TOOLE. The EcoCyc and MetaCyc databases. *Nucleic Acids Res.* **28**, 56 – 59 (2000).

[KS89]   J.-I. KIM AND P. STROEVE. Uphill transport in mass separation devices with reactive membranes: Counter-transport. *Cehm. Eng. Sci.* **44(5)**, 1101 – 1111 (1989).

[KS03]   S. KLAMT AND J. STELLING. Two approaches for metabolic pathway analysis? *Trends in Biotechnol.* **21(2)**, 64 – 69 (2003).

[KSG94]   S.E. KELLER, D.S. STEWART, AND S.M. GENDEL. Application of pattern recognition to monitoring fermentations of bacillus amyloliquefaciens. *J. Ind. Microbiol.* **13(6)**, 382 – 388 (1994).

[KSMP99]   Z.F. KATONA, P. SASS, AND I. MOLNAR-PERL. Simultaneous determination of sugars, sugar alcohols, acids and amino acids in apricots by gas chromatography - mass spectrometry. *J. Chromatography A* **847(1-2)**, 91 – 162 (1999).

[KT72]   S. KINOSHITA AND K. TANAKA. "The Microbial Production of Amino Acids, Ed. K. Yamada,", chapter Glutamic acid, pages 263–324. Wiley, New York (1972).

[KTHN+00]   KIM, TAE-HYUN, S. NAMGOONG, J.H. KWAK, S.-Y. LEE, AND H.-S. LEE. Effects of tktA, aroFfbr and aroL expression in the tryptophane-producing escherichia coli. *J. Microbiol. Biotechnol.* **10(6)**, 789 – 796 (2000).

[Kun03]   M. KUNZE. Entwicklung und anwendung von pulsexperimenten in fed-batch fermentationen zur untersuchung des stoffwechsels in e. coli l-phenylalanin produzenten. Master's thesis, Technical University of Dresden (2003).

[KUS57]   S. KINOSHITA, S. UDAKA, AND M. SHIMONO. Studies of the amino acid fermentation i. production of l-glutamic acid by various microorganisms. *J. Gen. Appl. Microbiol.* **3**, 193–205 (1957).

[Kuz96]   P. KUZMIC. Program DYNAFIT for the analysis of enzyme kinetic data: Application to HIV proteinase. *Anal. Biochem.* pages 260 – 273 (1996).

[KW01]   B.H. TER KUILE AND H.V. WESTERHOFF. Transcriptome meets metabolome: Hierachical and metabolic regulation of the glycolytic pathway. *FEBS letters* **500**, 169 – 171 (2001).

[KY90]   K.B. KONSTANTINOV AND T. YOSHIDA. On-line monitoring of representative structural variables in fed-batch cultivation of recombinant escherichia coli for phenylalanine production. *J. Ferment. Bioeng.* **70**, 420 – 426 (1990).

[KYNS91]   K.B. KONSTANTINOV, T. YOSHIDA, N. NICHIO, AND T. SEKI. Physiologically motivated strategies for control of the fed-batch cultivation of recombinant escherichia coli for phenylalanine production. *J. Ferment. Bioeng.* **71(5)**, 350 – 355 (1991).

[KYT96]   K. KAWASAKI, A. YOKOTA, AND F. TOMITA. L-traptophane production by a pyruvic acid producing escherichia coli strain carrying the enterobacter aerogenes tryptophanase gene. *J. Ferment. Bioeng.* **82**, 604 – 606 (1996).

[LC87]   A. LEWENDON AND J.R. COGGINS. 3-phosphoshikimate 1-carboxyvinyltransferase from escherichia coli. *Methods in Enzymology* **142**, 342 – 348 (1987).

[LCL01]   Y. LI, J. CHEN, AND S.Y. LUN. Biotechnological production of pyruvic acid. *Appl. Microbial Biotechnol.* **57**, 451 – 459 (2001).

[LCLL00]   Y. LI, J. CHEN, D.-F. LIANG, AND S.-Y. LUN. Effect of nitrogen concentration on the production of pyruvate by torulopsis glabrata. *J. Biotechnol.* **81**, 27 – 34 (2000).

[LCLR01]   Y. LI, J. CHEN, S.-Y. LUN, AND X.-S. RUI. Efficient pyruvate production by a multi-vitamin auxotroph of torulopsis glabarata: Key role and optimization of vitamin levels. *Appl. Microbiol. Biotechnol.* **55**, 680 – 685 (2001).

[LD98]   J. C. LIAO AND J. DELGADO. Flux calculation using metabolic control constraints. *Biotechnol. Prog.* **14(4)**, 554 – 560 (1998).

[LD03]   Y.-S. LIU AND Y.-Y. DAI. Distribution behavior of alpha-amino acids and aminobenzoic acid by extraction with trioctylamine. *Sep. Sci. and Technol.* **38(5)**, 1217 – 1228 (2003).

[Len00]   J.W. LENGELER. Metabolic networks: A signal-oriented approach to cellular models. *Biol. Chem.* **381**, 911 – 920 (2000).

[Leu96]   W. LEUCHTENBERGER. "Biotechnology, Vol 6, Products of Primary Metabolism, Eds: H.-J. Rehm, G. Reed, A. Pühler, A. Stadler", chapter Amino acids - technical production and use, pages 465–502. Verlag Chemie, Weinheim (1996).

[LEZ+01]   H.C. LANGE, M. EMAN, G. VAN ZUIJLEN, D. VISSER, J.C. VAN DAM, J. FRANK, M.J.T. DE MATTOS, AND J.J. HEIJNEN. Improved rapid sampling for in vivo kinetics of intracellular metabolites in saccharomyces cerevisiae. *Biotechnol. Bioeng.* **75**, 406 – 415 (2001).

[LF95]   T.O. LARSEN AND J.C. FRISVAD. Chemosystematics of penicillium based on profiles of volatile metabolites. *Mycol. Res.* **99**, 1167 – 1174 (1995).

[LF99]   K. LI AND J.W. FROST. Utilizing succinic acid as a glucose adjunct in fed-batch fermentation: Is butane a feedstock option in microbe-catalyzed synthesis? *J. Am. Chem. Soc.* **121**, 9461 – 9462 (1999).

[LHC96]   J.C. LIAO, S.-Y. HOU, AND Y.-P. CHAO. Pathway analysis, engineering, and physiological consideration for redirecting central metabolism. *Biotechnol. Bioeng.* **52**, 129 – 140 (1996).

[LHCL02]   Y. LI, J. HUGENHOLTZ, J. CHEN, AND S.Y. LUN. Enhancement of pyruvate production by torulopsis glabrata using a two-stage oxygen supply control strategy. *Appl. Microbiol. Biotechnol.* **60**, 101 – 107 (2002).

312   References

[Lia89]   J.C. Liao. Fermentation data analysis and state estimation in presence of incomplete mass balance. *Biotechnol. Bioeng.* **33**, 613 – 622 (1989).

[Lig]   Ligand, database of chemical compounds and reactions in biological pathways. http://www.genome.ad.jp/ligand.

[LKR$^+$96] M. Lukhezo, N.A. Kelly, B.G. Reuben, L.J. Dunne, and M.S. Verall. Reactive solvent extraction of amino acids. In "Proc. ISEC 96", pages 87 – 92 (1996).

[LMD$^+$99] K. Li, M.R. Mikola, K.M. Draths, R.M. Worden, and J.W. Frost. Fed-batch fermentor synthesis of 3-dehydroshikimic acid using recombinant escherichia coli. *Biotechnology and Bioengineering* **64(1)**, 61 – 73 (1999).

[LMG$^+$98] H. Liden, C.F. Mandenius, I. Gorton, N.Q. Meiander, I. Lundstroem, and F. Winquist. Online monitoring of a cultivation using electronic nose. *Anal. Chim. Acta.* **361(3)**, 223 – 231 (1998).

[LPV01]   L. M. Leib, C.J. Pereira, and J. Villadsen. Bioreactors: A chemical engineering perspective. *Chem. Eng. Sci.* **56**, 5485 – 5497 (2001).

[LS87]   Z. Likidis and K. Schügerl. Recovery of penicillin by reactive extraction in centrifugal extractors. *Biotechnol. Bioeng.* **30**, 1032 – 1040 (1987).

[LS90]   G.W. Luli and W.R. Strohl. Comparison of growth, acetate production and acetate inhibition of escherichia coli strains in batch and fed-btach fermentations. *Appl. Environ. Microbiol.* **56**, 1004 – 1011 (1990).

[LS94]   L. Laffend and M.L. Shuler. Structured model of genetic control via the lac promotor in escherichia coli. *Biotechnol. Bioeng.* **43**, 399 – 410 (1994).

[LS99]   J.W. Lengeler and G. Drews Ans H.G. Schlegel. Biology of the procaryotes. *Thieme Stuttgart, New York* **ISBN 3-13-108411-1** (1999).

[LSS02]   Z. Lazarova, B. Syska, and K. Schügerl. Application of large-scale hollow fiber membrane contactors for simultaneous extractive removal and stripping of penicillin. *J. Membrane Sci.* **202**, 151 – 164 (2002).

[LSW00]   A. Liese, K. Seelbach, and C. Wandrey. "Industrial Biotransformations". WILEY-VCH Verlag, ISBN 3-527-30094-5, Weinheim, Germany (2000).

[Ltd]   Process Systems Enterprise Ltd. "gPROMS". London, UK.

[LW99]   G.J. Lye and J.M. Woodley. Application of in situ product-removal techniques to biocatalytic processes. *TIBTECH* **17**, 395 – 402 (1999).

[LWPL91]   S.B. Lee, C.H. Won, C. Park, and B.S. Lim. Method for production of l-phenylalanine by recombinant e. coli. Technical Report, US patent 5008190 (1991).

[Maa00]   D. Maass. "Prozessentwicklung Zur Simultanen Produktabtrennung Von L-Phenylalanin (Jül-Report: 3888, ISSN 0944-2952)". PhD thesis, Technical University of Berlin (2000).

[Map]   Waterloo Maple. "MAPLE". http//www.maplesoft.com.

[MAR97]   K. Mauch, S. Arnold, and M. Reuss. Dynamic sensitivity analysis for metabolic systems. *Chem. Eng. Sci.* **52 (15)**, 2589 – 2598 (1997).

[Mat93]   C.K. Mathews. The cell - bag of enzymes or network of channels. *J. Bacteriol.* **175**, 6377 – 6381 (1993).

[MB01a]   U. Maier and J. Büchs. Characterisation of the gas-liquid mass transfer in shaking bioreactors. *Biochem. Eng. Journal* **7**, 99 – 106 (2001).

[MB01b]   C.D. Maranas and A.P. Burgard. Review of EcoCyc and MetaCyc databases. *Metab. Eng.* **3**, 98 – 99 (2001).

[MBOH87] J.E. MILLER, K.C. BACKMAN, M.J. O'CONNOR, AND R.T. HATCH. Production of phenylalanine and organic acids by phosphoenolpyruvate carboxylase-deficient mutants of escherichia coli. *J. Ind. Microbiol.* **2**, 143 – 149 (1987).

[MBSR01] K. MAUCH, S. BUZIOL, J. SCHMID, AND M. REUSS. Computer aided design of metabolic networks. *AIChE Symp Series* (2001).

[MC85] D.M. MOUSDALE AND J.R. COGGINS. High-perfomrance liquid chromatography of shikimate pathway intermediates. *J. Chromatogr.* **329**, 268 – 272 (1985).

[McG86] J.C. MCGUIRE. Phenylalanine ammonia lyase producing microbial cells, US patent 4598047. Technical Report, Genex (1986).

[MD90] R.A. MAJEWSKI AND M.M. DOMACH. Simple constrained-optimization view of acetate overflow in e. coli. *Biotechnol. Bioeng.* **35**, 732 – 738 (1990).

[MdGW$^+$96] A. MARX, A. DE GRAAF, W. WIECHERT, L. EGGELING, AND H. SAHM. Determination of the fluxes in central metabolism of corynebacterium glutamicum by NMR spectroscopy combined with metabolite balancing. *Biotechnology and Bioengineering* **49**, 111–129 (1996).

[ME97] C.F. MANDENIUS AND T. EKLOV. Sensor fusion with on-line as emission multi-sensor arrays and standard process measuring devices in baker's yeast manu-facturing process. *Biotechnol. Bioeng.* **55(2)**, 427 – 438 (1997).

[Men93] P. MENDES. GEPASI: A software package for modeling the dynamics, steady-states and control of biochemical and other systems. *Comp. Appl. Biosci.* **9(5)**, 563 – 571 (1993).

[Men97] P. MENDES. Biochemistry by numbers: Simulation of biochemical pathways with gepasi. *TIBS* **22**, 361 – 363 (1997).

[MES$^+$99] A. MARX, B.J. EIKMANNS, H. SAHM, A.A. DE GRAAF, AND L. EGGELING. Response of the central metabolism in corynebacterium glutamicum to the use of an NADH- dependent glutamate dehydrogenase. *Metabolic Engineering* **1**, 35–48 (1999).

[MF03] R. P. MAHARJAN AND T. FERENCI. Global metabolite analysis: The influence of extraction methodology on metabolome profiles of escherichia coli. *Anal. Biochem.* **313**, 145 – 154 (2003).

[MFdGT01] M. EL MASSAOUDI, A. FRANZ, A.A. DE GRAAF, AND R. TAKORS. Verfahren und vorrichtung zur untersuchung von fermentationsprozessen. *Patent Application* **DE 10120839.1-41** (2001).

[MFK87] S. MEHDI, J.W. FROST, AND J. KNOWLES. Dehydroquinate synthase from escherichia coli and its substrate 3-deoxy-d-arabino-heptulosonic acid 7-phosphate. *Methods in Enzymology* **142**, 306 – 314 (1987).

[MFLA80] P. LE MARCHAL, C. FRANCOIS, M. LEVEL, AND R. AZERAD. The interaction of phosphonate and homophosphonate analogues of DAHP with 3-DHQ synthase in e. coli. *Biochem. Biophys. Res. Comm.* **92**, 1104 – 1109 (1980).

[MG03] T. NUTSCH R. REHNER E.D. GILLES M. GINKEL, A. KREMLING. Modular modeling of cellular systems with ProMoT/Diva. *Bioinformatics* **19(9)**, 1169 – 1176 (2003).

[MGK$^+$02] D. MAASS, M. GERIGK, A. KREUTZER, D. WEUSTER-BOTZ, M. WUBBOLTS, AND R. TAKORS. Integrated l-phenylalanine separation in e. coli fed-batch process: From laboratory to pilot scale. *Bioproc. Biosys. Eng.* **25**, 85 – 96 (2002).

[MGVH03] M.R. MASHEGO, W.M. VAN GULIK, J.L. VINKE, AND J.J. HEIJNEN. Critical eval-ualtion of sampling techniques for residual glucose determination in carbon-limited chemostat culture of saccharomyces cerevisiae. *Biotechnol. Bioeng.* **83**, 395 – 399 (2003).

314   References

[MHBG87]   W. Marquardt, P. Holl, D. Butz, and E.D. Gilles. DIVA - a flow-sheet oriented dynamic process simulator. *Chem. Eng. Technol.* **10**, 164 – 173 (1987).

[MHD⁺98]   C.F. Mandnius, A. Hagman, F. Dunas, H. Sundgren, and I. Lundstrom. A multisensor array for visualising continuous state transitions in biopharmaceutical processes using principal component analysis. *Biosens. Bioelectron.* **13(2)**, 193 – 199 (1998).

[MHM⁺03]   A. Marx, S. Hans, B. Möckel, B. Bathe, and A.A. de Graaf. Metabolic phenotype of phosphoglucose isomerase mutants of corynebacterium glutamicum. *J. Biotechnol.* **104**, 185 – 197 (2003).

[Miy96a]   H. Miyoshi. Donnan dialysis with ion-exchange membranes. i theroretical equation. *Sep. Sci. Technol.* **31(15)**, 2117 – 2129 (1996).

[Miy96b]   H. Miyoshi. Donnan dialysis with ion-exchange membranes. II diffusion coefficients using same valence ions. *Sep. Sci. Technol.* **31(16)**, 2183 – 2194 (1996).

[MJ74]   J.J. McEvoy and A. Joyce. Production of l-phenylalanine by d,l-hydroxamate-resistant tyr mutants of bacillus subtilis. *Mol. Cell. Biochem.* **4**, 191 – 195 (1974).

[MJC⁺01]   C.R. Melchiorsen, N.B.S. Jensen, B. Christensen, K.V. Jokumsen, and J. Villadsen. Dynamics of pyruvate metabolism in lactococcus lactis. *Biotechnol. Bioeng.* **74(4)**, 271 – 279 (2001).

[MK96]   P. Mendes and D.B. Kell. On the analysis of the inverse problem of metabolic pathways using artificial neural networks. *BioSystems* **38**, 15 – 28 (1996).

[MK98]   P. Mendes and D.B. Kell. Non-linear optimization of biochemical pathways: Applications to metabolic engineering and parameter estimation. *Bioinformatics* **14 (10)**, 869 – 883 (1998).

[MMF⁺02]   D.H. Meikrantz, L.L. Macaluso, W.D. Flim, C.J. Heald, G. Mendoza, and S.B. Meikrantz. A new annular centrifugal contactor for pharmaceutical processes. *Chem. Eng. Comm.* **189**, 1629 – 1639 (2002).

[MNRRN99]   S. Meyer, N. Noisommit-Rizzi, M. Reuss, and P. Neubauer. Optimized analysis of intracellular adenosine and guanosine phosphates in escherichia coli. *Anal. Biochem.* **271(1)**, 43 – 52 (1999).

[MS85]   M. Mori and I. Shiio. Synergistic inhibition of phosphoenolpyruvate carboxylase by aspartate and 2-oxoglutarate in brevibacterium flavum. *J. Biochem.* **98**, 1621 – 1630 (1985).

[MS87]   U.S. Maitra and D.B. Sprinson. 5-dehydro-3-deoxy-d-arabino-heptulosonic acid 7-phosphate. *J. Biol. Chem.* **253(15)**, 5426 – 5430 (1987).

[MSD⁺03]   M. El Massaoudi, J. Spelthahn, A. Drysch, A. de Graaf, and R. Takors. Production process monitoring by serial mapping of microbial carbon flux distributions using a novel sensor reactor approach: I - sensor reactor system. *Metabolic Engineering* **5**, 86–95 (2003).

[MSdG⁺97]   A. Marx, K. Striegel, A.A. de Graaf, H. Sahm, and L. Eggeling. Response of the central metabolism of corynebacterium glutamicum to different flux burdens. *Biotechnol. Bioeng.* **56**, 168–180 (1997).

[MSH84]   M. Moriguchi, K. Shuto, and T. Hashimoto. Production of pyruvic acid from saccharified citrus peel extract by dried cells of debaryomyces coudertii. *J. Ferment. Technol.* **62**, 243 – 248 (1984).

[MTES89]   E. Menkel, G. Thierbach, L. Eggeling, and H. Sahm. Influence of increased aspartate availability on lysine formation by a recombinant strain of corynebacterium glutamicum and utilization of fumarate. *Appl. Environ, Microbiol.* **55**, 684–688 (1989).

[MTP⁺00]   D. MAASS, R. TAKORS, H. PASCHOLD, D. WEUSTER-BOTZ, AND C. WANDREY. "Verfahren Zur Abtrennung Organischer Substanzen Aus Einem Wäßrigen Gemisch, DE 199 19 490.4-44, EP 00/03705, WO 00/66253". German Patent Application DE 199 19 490.4-44, EP00/03705, WO 00/66253 (2000).

[Mül01]   A. MÜLLER. Hartes gerangel um den futtertrog. *Chemische Rundschau* **54**(6), 1 (2001).

[MV93]   M. MOLNAR AND M. VAS. Mg2+ affects the binding of ADP but not ATP to 3-phosphoglycerate kinase. correlation between equilibrium dialysis binding and enzyme kinetic data. *Biochem. Journal* **293**, 595 – 599 (1993).

[MVR00]   K. MAUCH, S. VASEGHI, AND M. REUSS. "Bioreaction Engineering - Modeling and Control (Eds. K. Schügerl and K.H. Bellgardt)", chapter Quantitative Analysis of Metabolic and Signalling Pathways in Saccharomyces cerevisiae, pages 435 – 477. Springer-Verlag, Heidelberg ISBN 3-540-66906-X (2000).

[MWKdG99]   M. MÖLLNEY, W. WIECHERT, D. KOWANTZKI, AND A.A. DE GRAAF. Bidirectional reaction steps in metabolic networks. IV. optimal design of isotopomer labeling experiments. *Biotechnol. Bioeng.* **66**, 86–103 (1999).

[MY96]   R. MIYATA AND T. YONEHARA. Improvement of fermentative production of pyruvate from glucose by torulopsis glabrata IFO 0005. *J. Ferment. Bioeng.* **82**, 475 – 479 (1996).

[MY99]   R. MIYATA AND T. YONEHARA. Breeding of high-pyruvate-producing torulopsis glabrata with acquired reduced pyruvate decarboxylase. *J. Biosci. Bioeng.* **88**, 173 – 177 (1999).

[MYYT90]   R. MIYATA, T. YONEHARA, K. YOTSUMOTO, AND H. TSUTSUI. Method for producing pyruvic acid by fermentation. Technical Report, US Patent 4,971,907 (1990).

[NCB]   National center for biotechnology information. http://www.ncbi.nlm.nih.gov.

[NEOY72]   H. NAKAZAWA, H. ENEI, S. OKUMURA, AND H. YAMADA. Synthesis of l-tryptophane from pyruvate, ammonia and indole. *Agr. Biol. Chem.* **36**, 2523 – 2528 (1972).

[Nie97]   J. NIELSEN. Metabolic control analysis of biochemical pathways based on a thermokinetic description of reaction rates. *Biochem. J.* **321**, 133 – 138 (1997).

[Nie98]   J. NIELSEN. Metabolic engineering: Techniques for analysis of targets for genetic manipulations. *Biotechnology and Bioengineering* **58**(2), 125–132 (1998).

[Nie01]   J. NIELSEN. Metabolic engineering. *Appl. Microbiol. Biotechnol.* **55**, 263 – 283 (2001).

[NM65]   J.A. NELDER AND R. MEAD. The downhill simplex method. *Comp. J.* **7**, 308 (1965).

[NMDF97]   L. NOTLEY-MCROBB, A. DEATH, AND T. FERENCI. The relationship between external concentration and cAMP levels inside escherichia coli: Implications for models of phosphotransferase-mediated regulation of adenylate cyclase. *Microbiology* **143**, 1909 – 1918 (1997).

[NNNT89]   K. NAKAMICHI, K. NABE, Y. NISHIDA, AND T. TOSA. Production of l-phenylalanine from phenylpyruvate by paracoccus denitrificans containing aminotransferase activity. *Appl. Microbiol. Biotechnol.* **30**, 243 – 246 (1989).

[NO02]   J. NIELSEN AND L. OLSSON. An expanded role for microbial physiology in metabolic engineering and functional genomics: Moving towards system biology. *FEMS Yeast Research* **2**, 175 – 181 (2002).

[NSNV97] T. L. NISSEN, U. SCHULZE, J. NIELSEN, AND J. VILLADSEN. Flux distributions in anaerobic, glucose-limited continuous cultures of saccharomyces cerevisiae. *Microbiology* **143**, 203–218 (1997).

[OF92] G. OGDEN AND P. FÖLDI. Amino acid analysis: An overview of current methods. *LC-GC Int.* **5**, 28–39 (1992).

[OGMH82] T. OGINO, C. GARNER, J.L. MARKLEY, AND K.M. HERRMANN. Biosynthesis of aromatic compounds: 13c NMR spectroscopy of whole escherichia coli cells. *Proc. Natl. Acad. Sci. USA* **79**, 5828 – 5832 (1982).

[OKDT03] M. OLDIGES, M. KUNZE, D. DEGENRING, AND R. TAKORS. Stimulation, monitoring and analysis of pathway dynamics by metabolic profiling - example: Aromatic amino acid pathway. **submitted** (2003).

[OKOF85] A. OZAKI, R. KATSUMATA, T. OKA, AND A. FURUYA. Cloning of the genes concerned in phenylalanine biosynthesis in corynebacterium glutamicum and its application to breeding of a phenylalanine producing strain. *Agric. Biol. Chem.* **49**, 2925 – 2930 (1985).

[Old03] M. OLDIGES. "Metabolomanalyse Zur Untersuchung der Dynamik imAromatenbiosynthese-Weg in E. Coli L-Phenylalanin-Produzenten (Preliminary Titel)". PhD thesis, Rheinische Friedrich-Wilhelms-Universität, University of Bonn (2003).

[OON01] S. OSTERGAARD, L. OLSSON, AND J. NIELSEN. In vivio dynamics of galactose metabolism in saccharomyces cerevisiae: Metabolic fluxes and metabolite levels. *Biotechnol. Bioeng.* **73(5)**, 412 – 425 (2001).

[ORCAB97] A.C. OLIVEIRA, M.F. ROSA, J.M.S. CABRAL, AND M.R. AIRES-BARROS. Immobilization of saccharomyces cerevisiae cells and rhizomucor mihei lipase for the production and extractive biocatalysis of ethanol. *Bioproc. Eng.* **16**, 349 – 353 (1997).

[OS69] H. OZAKI AND I. SHIIO. Regulation of the TCA and glyoxylate cycles in brevibacterium flavum. II regulation of phosphoenolpyruvate carboxylase and pyruvae kinase. *J. Biochem.* **66**, 297 – 311 (1969).

[OSIS01] J. OGAWA, C.-L. SOONG, M. ITO, AND S. SHIMIZU. Enzymatic production of pyruvate from fumarate - an application of microbial cyclic-imide-transforming pathway. *J. Mol. Catal. B: Enzymatic* **11**, 355 – 359 (2001).

[OT03] M. OLDIGES AND R. TAKORS. Applying metabolic profiling techniques for stimulus-response experiments: Chances and pitfalls. *Adv. Biochem. Eng. Biotechnol.* **submitted** (2003).

[Ott97] M. OTTER. "Simulationstechnik (Eds.: A. Kuhn, S. Wenzel), 11. Symposium Dortmund, Fortschritte in der Simulationstechnik", chapter MODELICA - die Modellierungssprache der nächsten Generation für den Modellaustausch, pages 212 – 217. Vieweg Verlag (1997).

[Pal00] B. PALSSON. The challenges of in silico biology. *Nature Biotechnol.* **18**, 1147 – 1150 (2000).

[Pal02] B. PALSSON. In silico biology through 'omics'. *Nature Biotechnol.* **20**, 649 – 650 (2002).

[Pat97] P.R. PATNAIK. Principal component anaylsis of the effect of in-flow disturbances on recombinant beta-galactosidase fermentation. *Hung. J. Ind. Chem.* **15(4)**, 261 – 264 (1997).

[PCED00] K. PETRITIS, P. CHAIMBAULT, C. ELFAKIR, AND M. DREUX. Parameter optimization for the analysis of underderivatized protein amino acids by liquid chromatography and ionspray tandem mass spectrometry. *J. Chromatography* **896**, 253 – 263 (2000).

[PdGE+00]   S. Petersen, A.A. de Graaf, L. Eggeling, M. Möllney, W. Wiechert, and H. Sahm. In vivo quantification of parallel and bidirectional fluxes in the anaplerosis of corynebacterium glutamicum. *J. Biol. Chem.* **275**, 35932–35941 (2000).

[PG70]   J. Pittard and F. Gibson. The regulation of aromatic amino acids and vitamins. *Curr. Cell. Reg.* **2**, 29 – 63 (1970).

[PGW+03]   W. Prathumpai, J.B. Gabelgaard, P. Wanchanthuek, P.J.I. Van de Vondervoort, M.J.L. de Groot, M. McIntire, and J. Nielsen. Metabolic control analysis of xylose catabolism in aspergillus. *Biotechnol. Prog.* **19**, 1136 – 1141 (2003).

[PH]   L.R. Petzold and A.C. Hindmarsh. "Livermore Solver for Ordinary Differential Equations". http//www.netlib.org.

[Pit96]   A.J. Pittard. "Escherichia Coli and Salmonella Typhimurium - Cellular and Molecular Biology, Edt. F.C. Neidhardt", chapter Biosynthesis of the Aromatic Amino Acids, pages 458 – 484. ASM press (1996).

[PL94]   R. Patnaik and J.C. Liao. Engineering of escherichia coli central metabolism for aromatic metabolite production with near theoretical yield. *Applied and Environmental Microbiology* **60(10)**, 3903 – 3908 (1994).

[PLJ93]   P.W. Postma, J.W. Lengeler, and G.R. Jacobson. Phosphoenolpyruvate:carbohydrate phosphotransferase systems of bacteria. *Microbiol. Rev.* **57(2)**, 543 – 594 (1993).

[PMBM03]   W. Pfefferle, B. Möckel, B. Bathe, and A. Marx. "Adv. Biochem. Eng/Biotechnol. Microbial Production of L-Amino Acids (58)", chapter Biotechnological manufacture of lysine, pages 59 – 112. Springer, Berlin (2003).

[PMdG+01]   S. Petersen, C. Mack, A.A. de Graaf, C. Riedel, B.J. Eikmanns, and H. Sahm. Metabolic consequences of altered phosphoenolpyruvate carboxykinase activity in corynebacterium glutamicum reveal anaplerotic regulation mechanisms in vivo. *Metab. Eng.* **3**, 344–361 (2001).

[PMTS03]   M.R. Pursell, M.A. Mendes-Tatsis, and D.C. Stuckey. Coextraction during reactive extraction of phenylalanine using aliquat 336: Modeling extraction equilibrium. *Biotechnol. Bioeng.* **82(5)**, 533 – 542 (2003).

[PP96]   J. Pi and A.J. Pittard. Topology of the phenylalanine-specific permease of escherichia coli. *J. Bacteriol.* **178**, 2650 – 2655 (1996).

[PR]   N.H. Park and P.L. Rogers. "Horizons of Biochemical Engineering", chapter Batch and Fed-Batch Culture Studies on a Hyperproducing Mutant of E. Coli for L-Phenylalanine Production, pages 171 – 185. S. Aiba (Ed.).

[PR86]   N.H. Park and P.L. Rogers. L-phenylalanine production in continuous culture using hyperproducing mutant of escherichia coli k12. *Chem. Eng. Commun.* **45**, 185 – 196 (1986).

[PR89]   N.H. Park and P.L. Rogers. Kinetic equations for l-phenylalanine production by a hyperproducing mutant of escherichia coli. *Biocatalysis* **2**, 79 – 87 (1989).

[PR03]   L. Paegle and M. Ruklisha. Lysine synthesis control in corynebacterium glutamicum RC 115 in mixed substrate (glucose-acetate) medium. *J. Biotechnol.* **104**, 123 – 128 (2003).

[PSL95]   R. Patnaik, R.G. Spitzer, and J.C. Liao. Pathway engineering for production of aromatics in escherichia coli: Confirmation of stoichiometric analysis by independent modulation of AroG, TktA and pps activities. *Biotechnology and Bioengineering* **46**, 361 – 370 (1995).

[PSVN+99]   T. Pfeiffer, I. Sánches-Valedenbro, J.C. Nuno, F. Montero, and S. Schuster. METATOOL: For studying metabolic networks. *Bioinformatics* **15(3)**, 251 – 257 (1999).

[PWBSB98]   H. Paschold, D. Weuster-Botz, U. Schäfer, and W. Boos.   Verfahren
zur schnellen probennahme biologischer proben. Technical Report, German
Patent DE 19705289 C (1998).

[PWWdG+96] P.G. Peters-Wendisch, V.F. Wendisch, A.A. de Graaf, B.J. Eikmanns, and
H. Sahm. C3-carboxylation as an anaplerotic reaction in phosphoenolpyruvate
carboxylase-deficient corynebacterium glutamicum.   *Arch. Mircobiol.* **165**,
387–396 (1996).

[PWWP+97]   P.G. Peters-Wendisch, V.F. Wendisch, S. Paul, B.J. Eikmanns, and H. Sahm.
Pyruvate carboxylase as an anaplerotic enzyme in corynebacteium glutam-
icum. *Microbiology* **143**, 1095–1103 (1997).

[RBTR97]   M. Rizzi, M. Baltes, U. Theobald, and M. Reuss. In vivo analysis of metabolic
dynamics in saccharomyces cerevisiae: II. mathematical model. *Biotechnol.
Bioeng.* **55(4)**, 592 – 608 (1997).

[RBW87]   S. Roffler, H.W. Blanch, and C.R. Wilke. Extractive fermentation of ace-
tone and butanol: Provess design and economic evaluation. *Biotechnol. Prog.*
3, 131 – 140 (1987).

[RC95]   J. Russel and G. Cook.   Energetics of bacterial growth-balance of anabolic
and catabolic reactions. *Microbiol. Rev.* **59(1)**, 48 – 62 (1995).

[RE97]   C.A. Ramilo and J.N.S. Evans. Overexpression, purification and characteri-
zation of tyrosine-sensitive 3-deoxy-d-arabino-heptulosonic acid 7-phosphate
synthase from escherichia coli. *Protein Expre. Purif.* **9**, 253 – 261 (1997).

[Ree97]   A. Reeve. Saving money with process diagnostics. *Control. Instrum.* **29(10)**,
59 – 60 (1997).

[RHK+03]   N. Rüffer, U. Heidersdorf, I. Kretzers, G.A. Sprenger, L. Raeven, and
R. Takors. Fed-batch l-phenylalanine production with recombinant e. coli
using liquid-liquid centrifuges for integrated product separation and concen-
tration. *Bioproc. Biosyst. Eng.* **submitted** (2003).

[RMR+00]   J.M. Rohwer, N.D. Meadow, S. Roseman, H.V. Westerhoff, and P.W.
Postma. Understanding glucose transport by the bacterial phosphoenolpyru-
vate: Glycose phosphotransferase system on the basis of kinetic measurements
in vitro. *J. Biol. Chem.* **45**, 34909 – 34921 (2000).

[Roe83]   J.A. Roels. "Energetics and Kinetics in Biotechnology". Elesevier Biomedical
Press, Amsterdam, New York, Oxford (1983).

[Roe03]   Roempp. "Aminoacylase". Georg Thieme Verlag (2003).

[ROL01]   L. Rohlin, M.-K. Oh, and J.C. Liao. Microbial pathway engineering for in-
dustrial purposes: Evolution, combinatorial biosynthesis and rational design.
Curr. Opinion in Microbiol. **4**, 330 – 335 (2001).

[Röm95]   Römpp. "Chemie Lexikon". Georg Thieme Verlag (1995).

[Ros03]   J. Ross. New approaches to the deduction of complex reaction mechanisms.
Acc. Chem. Res. **36**, 839 – 847 (2003).

[Row90]   T. Rowan. "Functional Stability of Numerical Algorithms". PhD thesis, Uni-
versity of Texas (1990).

[Roz85]   J.D. Rozzell. Production of l-amino acids by transamination. Technical Re-
port, US patent 4518692 (1985).

[Roz89]   J.D. Rozzell. Production of amino acids using coupled amino transferases.
Technical Report, US patent 4826766 (1989).

[RRD⁺01]   C. RIEDEL, D. RITTMANN, P. DANGEL, B. MÖCKEL, S. PETERSEN, H. SAHM, AND
            B. EIKMANNS. Characterization of the phosphoenolpyruvate carboxykinase
            gene from corynebacterium glutamicum and significance of the enzyme for
            growth and amino acid production. *J. Mol. Microbiol. Biotechnol.* **3**, 573 –
            583 (2001).

[RTB⁺01]   L.M. RAAMSDONK, B. TEUSINK, D. BROADHURST, N. ZHANG, A. HAYES, M.C.
            WALSH, A.A. BERDEN, K.M. BRINDLE, D.B. KELL, J.J. ROWLAND, H.V. WEST-
            ERHOFF, K. VAN DAM, AND S.G. OLIVER. A functional genomics strategy that
            uses metabolome data to reveal the phenotype of silent mutations. *Nature
            Biotechnol.* **19**, 45 – 50 (2001).

[Rüf03]   N. RÜFFER. "L-Phenylalanin Produktion mit Escherichia Coli und Zentrifugal-
            Extraktion Zur Produktabtrennung".   PhD thesis, Technical University
            Carolo-Wilhelmina, Braunschweig (2003).

[RV99]   G.J.G. RUIJTER AND J. VISSER. Characterization of aspergillus niger phos-
            phoglucose isomerase. use for quantitative determination of erythrose 4-
            phosphate. *Biochimie* **81(3)**, 267 – 272 (1999).

[RWT02]   N. RÜFFER, C. WANDREY, AND R. TAKORS. Integrierte abtrennung organischer
            substanzen aus einem wässrigen bioprozessgemisch. Technical Report, Ger-
            man Patent Application DE 10220235.4-43 (2002).

[Sau]   H.M. SAURO. "JARNAC-SCAMP II". http//www.members.tripo.co.uk/sauro/
            biotech.html.

[SAY⁺94]   J.L. SNOEP, N. ARFMAN, L.P. YOMANO, R.K. FLIEGE, T. CONWAY, AND L.O. IN-
            GRAM. Reconstruction of glucose uptake and phosphoryation in a glucose-
            negative mutant of escherichia coli by using zymomonas mobilis genes encod-
            ing the glucose fascilitator protein and glucokinase. *J. Bacteriol.* **176**, 2133
            – 2135 (1994).

[SB99]   U. SAUER AND J.E. BAILEY. Estimation of p-to-o ration in bacillus subtilis and
            its influence on maximum riboflavin yield. *Biotechnology and Bioengineering*
            64, 750–754 (1999).

[SBE84]   J. SILHAVY, M. BERMAN, AND L. ENQUIST. Experiments with gene fusions. *Cold
            Spring Harbor Laboratory* (1984).

[SBTWB99]   U. SCHÄFER, W. BOOS, R. TAKORS, AND D. WEUSTER-BOTZ. Automated sampling
            device for monitoring intracellular metabolite dynamics. *Anal. Biochem.* **270**,
            88 – 96 (1999).

[SCB⁺98]   H.P. SMITS, A. COHEN, T. BUTTLER, J. NIELSEN, AND L. OLSSON. Cleanup and
            analysis of sugar phosphates in biological extracts by using solid phase ex-
            traction and anion-exchange chromatography with pulsed amperometric de-
            tection. *Anal. Biochem.* **261**, 36 – 42 (1998).

[Sch94]   K. SCHÜGERL. "Solvent Extraction in Biotechnology, ISBN 3-540-57694-0".
            Springer-Verlag, Berlin, Heidelberg, New York (1994).

[Sch99a]   U. SCHÄFER.   "Automatisierte Probennahme Zur Messung Intrazel-
            lulärer Metabolitdynamiken". PhD thesis, Rheinische Friedrich-Wilhelms-
            Universität, University of Bonn (1999).

[Sch99b]   K. SCHMIDT. Personal communication. (1999).

[Sch00]   K. SCHÜGERL. Integrated processing of biotechnology products. *Biotechnology
            Advances* **18**, 581 – 599 (2000).

[SCNV97]   K. SCHMIDT, M. CARLSEN, J. NIELSEN, AND J. VILLADSEN. Modelling isotopomer
            distribution in biochemical networks using isotopomer mapping matrices.
            Biotechnology and Bioengineering **55**, 831–840 (1997).

[SCS00]   A. SALTELLI, K. CHAN, AND E.M. SCOTT. "Sensitivity Analysis". John Wiley
            and Sons, New York (2000).

[SD76]   R.J. SIMPSON AND B.E. DAVIDSON. Studies on 3-deoxy-d-arabinoheptulosonate-7-phosphate synthetase (phe) from escherichia coli k12. 2. kinetic properties. *Eur. J. Biochem.* **70**, 509 – 516 (1976).

[SDF96]   K.D. SNELL, K.M. DRATHS, AND J.W. FROST. Synthetic modification of escherichia coli chromosome: Enhancing the biocatalytic convesion of glucose into aromatic chamicals. *J. Am. Chem. Soc.* **118**, 5605 – 5614 (1996).

[SDH$^+$01]   A. SCHMID, J.S. DORDICK, B. HAUER, A. KIENER, M. WUBBOLTS, AND B. WITHOLT. Industrial biocatalysis today and tomorrow. *Nature* **409**, 258 – 268 (2001).

[SEdGS93]   K. SONNTAG, L. EGGELING, A.A. DE GRAAF, AND H. SAHM. Flux partitioning in the split pathway of lysine synthesis in corynebacterium glutamicum. *Eur. J. Biochem.* **213**, 1325 – 1331 (1993).

[Seg75]   I. SEGEL. "Enzyme Kinetics Behavior and Analysis of Rapid Equilibrium and Steady State Enzyme Systems". John Wiley and Sons, New York (1975).

[SES92]   B. SCHRUMPF, L. EGGELING, AND H. SAHM. Isolation and prominent characteristics of an l-lysine hyperproducing strain of corynebacterium glutamicum. *Appl. Microbiol. Biotechnol.* **37**, 566–571 (1992).

[SFD00]   S. SCHUSTER, D.A. FELL, AND T. DANDEKAR. A general definition of metabolic pathways useful for systematic organization and analysis of complex metabolic networks. *Nature Biotechnol.* **18**, 326 – 332 (2000).

[SFI$^+$91]   S. SUGIYAMA, S. FUKUNAGA, K. ITO, S. OHIGASHI, AND H. HAYASHI. Catalysts for vaporphase dehydration of ethylene glycol and their application to pyruvic acid synthesis. *J. Catal.* **129**, 12 – 18 (1991).

[SFKH92]   S. SUGIYAMA, S. FUKUNAGA, K. KAWASHIRO, AND H. HAYASHI. Catalytic conversion of diethy tartrate into pyruvate over silica-supported potassium disulfate. *Bull. Chem. Soc. Jpn.* **65**, 2083 – 2085 (1992).

[SH76]   R. SCHONER AND K.M. HERRMANN. 3-deoxy-d-arabino-heptulosonate 7-phosphate synthase. purification, properties and kinetics of the tyrosine-sensitive isoenzyme from escherichia coli. *J. Biol. Chem.* **251**, 5440 – 5447 (1976).

[SHB$^+$97]   U. SAUER, V. HATZIMANIKATIS, J.E. BAILEY, M. HOCHULI, T. SZYPERSKI, AND K. WÜTHRICH. Metabolic fluxes in ribovlafin-producing bacillus subtilis. *Nat. Biotchnol.* **15**, 448–452 (1997).

[SHBT02]   M. SCHMITZ, E. HIRSCH, J. BONGAERTS, AND R. TAKORS. Pulse experiments as a prerequisite for the quantification of in vio enzyme kinetics in the aromatic amino acid pathway in escherichia coli. *Biotechnol. Prog.* **18**, 935 – 941 (2002).

[SHHM91]   S. SEEVARATNAM, O. HOLST, S. HJÖRLEIFSDOTTIR, AND M. MATTHIASSON. Extractive bioconversion for lactic acid production using solid sorbent and organic solvent. *Bioproc. Eng.* **6**, 35 – 41 (1991).

[SHR81]   M. SCHAUER, R. HEINRICH, AND S.M. RAPOPORT. Mathematische modellierung der glykolyse und des adeninnukleotidstoffwechsels menschlicher erythrocyten. *Acta Biol. Med. Germ.* **40**, 1659 – 1682 (1981).

[Sil99]   K. SILBERBACH. Reaktionstechnische untersuchungen zur verweilzeitentkopplung bei fermentationen mit escherichia coli. Master's thesis, Rheinisch-Westfälische Technische Hochschule (RWTH) Aachen (1999).

[Sim50]   S. SIMMONDS. The metabolism of phenylalanine and tyrosine in mutant strains of escherichia coli. *J. Biol. Chem.* **185**, 755 – 762 (1950).

[SKB$^+$02a]   T. SAUTER, A. KREMLING, K. BETTENBROCK, S. FISCHER, AND E.D. GILLES. Analysis of the dynamics of the escherichia coli glucose PTS in different time windows. In "Proceedings of the 5th German Workshop on Artificial Life, Eds.: D. Polani, J. Kim, T. Martinetz, ISBN 3-89838-030", pages 33 – 42. IOS Press (2002).

[SKB⁺02b]   J. STELLING, S. KLAMT, K. BETTENBROCK, S. SCHUSTER, AND E.D. GILLES. Metabolic network structure determines key aspects of functionality and regulation. *Nature* **420**, 190 – 193 (2002).

[SKD03]   A. SCHMIDT, M. KARAS, AND T. DÜLCKS. Effect of different solution flow rates on analyte ion signals in nano-ESI MS, or: When does ESI turn into nano-ESI? *J Am Soc Mass Spectrom* **14**, 492 – 500 (2003).

[SKH⁺85]   P.K. SMITH, R.I. KROHN, G.T. HERMANSON, A.K. MALLIA, F.H. GARTNER, M.D. PROVENZANO, E.K. FUJIMOTO, N.M. GOEKE, B.J. OLSEN, AND D.C. KLENK. Measurement of protein using bicinchoninic acid. *Anal. Biochem.* **150**, 76–85 (1985).

[SKK⁺90]   S. SUGIMOTO, N. KATO, N. KITAOKA, T. SEKI, T. YOSHIDA, AND H. TAGUCHI. Phenylalanine production by periodic induction of gene expression using a temperature-distributed dual fermenter system. *J. Ferment. Bioeng.* **70**, 376 – 380 (1990).

[SKM⁺03]   D. STARK, H. KORNMANN, T. MÜNCH, B. SONNLEITNER, I.W. MARISON, AND U. VON STOCKAR. Novel type of in situ extraction: Use of solvent containing microcapsules for the bioconversion of 2-phenylethanol from l-phenylalanine by saccharomyces cerevisiae. *Biotechnol. Bioeng.* **83(4)**, 376 – 385 (2003).

[SKW⁺02]   S. SCHUSTER, S. KLAMT, W. WECKWERTH, F. MOLDENHAUER, AND T. PFEIFFER. Use of network analysis of metabolic systems in bioengineering. *Bioproc. Biosyst. Eng.* **24**, 363 – 372 (2002).

[SL76]   M.J. SAEZ AND R. LAGUNAS. Determination of intermediary metabolites in yeast - critical examination of effect of sampling conditions and recommendations for obtaining true levels. *Molecular and Cellular Biochemistry* **13(2)**, 73 – 78 (1976).

[SL02]   C.H. SHU AND C.C. LIAO. Optimization of l-phenylalanine production of corynebacterium glutamicum under product feedback inhibition by elevated oxygen transfer rate. *Biotechnol. Bioeng.* **77(2)**, 131 – 141 (2002).

[SLD79]   M.L. SHULER, S. LEUNG, AND C.C. DICK. A methematical model for the growth of a single bacterial cell. *Ann. N.Y. Acad. Sci.* **326**, 35 – 55 (1979).

[SLEEK95]   H. SAHM, L-EGGELING, B.J. EIKMANNS, AND R. KRÄMER. Metabolic design in amino acid producing bacterium corynebactrium glutamicum. *FEMS Microbiol. Rev.* **16**, 243–252 (1995).

[SNV99]   K. SCHMIDT, J. NIELSEN, AND J. VILLADSEN. Quantitative analysis of metabolic fluxes in e. coli, using 2-dimensional NMR spectroscopy and complete isotopomer models. *J. Biotechnology* **71**, 175–190 (1999).

[SOT62]   I. SHIO, S.I. OTSUKA, AND M. TAKAHASHI. Effect of biotin on the bacterial formation of glutamic acid. *J. Biochem.* **52**, 108–116 (1962).

[SOU⁺03]   T. SOGA, Y. OHASHI, Y UENO, H. NARAOKA, M. TOMITA, AND T. NISHIOKA. Quantitative metabolome analysis using capillary electrophoresis mass spectrometry. *J. Proteome Research* **2**, 488 – 494 (2003).

[Spe02]   J. SPELTHAHN. Entwicklung und einsatz einer pulsaufgabe-einheit zur durchführung von 13c markierungsexperimenten. Master's thesis, Fachhochschule (University for Applied Sciences) Aachen/Jülich (2002).

[SPND98]   P. SCHÖNER, P. PLUCINSKI, W. NITSCH, AND U. DAIMINGER. Mass transfer in the shell side of cross flow fiber modules. *Chem. Eng. Sci.* **53(3)**, 2319 – 2326 (1998).

[SRB86]   J.C. SHRYOCK, R. RUBIO, AND R.M. BERNE. Extraction of adenine-nucleotides from cultured endothelial-cells. *Anal. Biochem.* **159**, 73 – 81 (1986).

322   References

[SRG$^+$90]   R.T. Stanko, R.J. Robertson, R.W. Galbreath, J.I. Reilly, K.D.Jr. Greenawalt, and F.L. Goss. Enhanced leg exercise endurance with a high-carbohydrate diet and dihydroxyacetone and pyruvate. *J. Appl. Physiol.* **69**, 1651 – 1656 (1990).

[SS92]   U. Sauer and G. Stephanopoulos. Application of pattern recognition techniques to fermentation data analysis. In M.N. Karim and G. Stephanopoulos, editors, "IFAC Mod. and Control of Biotechnol. Proc., 10", pages 123 – 128, Colorado, USA (1992).

[SS93]   C. Schinsschel and H. Simon. Preparation of pyruvate from r-lactate with proteus species. *J. Biotechnol.* **31**, 191 – 203 (1993).

[SS00]   J.T. Scarpello and D.C. Stuckey. The reactive extraction of phenylalanine with aliquat 336: Buffer co-extraction equilibrium and mass transfer kinetics. *Biotechnol. Bioeng.* **69(5)**, 469 – 477 (2000).

[SS01]   D.E. Stafford and G. Stephanopoulos. Metabolic engineering as an integrating platform for strain development. *Curr. Opinion Microbiol.* **4**, 336 – 340 (2001).

[SS02]   G. Stephanopoulos and D.E. Stafford. Metabolic engineering: A new frontier of chemical reaction engineering. *Chem. Eng. Sci.* **57**, 2595 – 2602 (2002).

[SS03]   D. Stark and U. Von Stockar. "Adv. Biochem. Eng./Biotechnol., Vol. 80", chapter In Situ Product Removal (ISPR) in Whole Cell Biotechnology During the Last Twenty Years, pages 149 – 175. Springer-Verlag, Berlin Heidelberg (2003).

[SSB$^+$92]   H.J. Stoffers, E.L. Sonnhammer, G.J. Blommestijn, N.J. Raat, and H.V. Westerhoff. METASIM: Object-oriented modeling of cell regulation. *Comput. Appl. Biosci.* **8(5)**, 443 – 449 (1992).

[SSC82]   C. Seigneur, G. Stephanopoulos, and R.W. Carr. Dynamic sensitivity analysis of chemical-reaction systems - a variational method. *Chem. Eng. Scie.* **37(6)**, 845 – 853 (1982).

[SSdG$^+$95]   K. Sonntag, J. Schwinde, A.A. de Graaf, A. Marx, B.J. Eikmanns, W. Wiechert, and H. Sahm. 13c NMR studies of the fluxes in the central metabolism of corynebacterium glutamicum during growth and overproduction of amino acids in batch cultures. *Appl. Microbiol Biotechnol.* **44**, 489–495 (1995).

[SSK88]   I. Shiio, S. Sugimoto, and K. Kawamura. Breeding of phenylalanine-producing brevibacterium flavum strains by removing feedback regulation of both two key enzymes in its biosynthesis. *Agric. Biol. Chem.* **52**, 2247 – 2253 (1988).

[SSPH99]   C.H. Schilling, S. Schuster, B.O. Palsson, and R. Heinrich. Metabolic pathway analysis: Basic concepts and scientific applications in the post-genomic era. *Biotechnol. Prog.* **15**, 296 – 303 (1999).

[SSS89]   U. Schmid, K.L. Schimz, and H. Sahm. Determination of intracellular puridine nucleotide levels by bioluminescence using anaerobic bacteria. *Anal. Biochem.* **180**, 17 – 23 (1989).

[SSS$^+$98a]   G. Sprenger, R. Siewe, H. Sahm, M. Karutz, and T. Sonke. Microbial preparation of substances from aromatic metabolism, part. Technical Report, WO98/18936. Patent granted in the USA (6316232), ZA (9568/97) and pending for EP, CN, JP, KR and DE. (1998).

[SSS$^+$98b]   G. Sprenger, R. Siewe, H. Sahm, M. Karutz, and T. Sonke. Microbial preparation of substances from aromatic metabolism, part II. Technical Report, WO 98/18937 (1998).

[Sta82]   R.T. Stanko. Method for preventing body fat deposition in mammals. Technical Report, US Patent 4,351,835 (1982).

[Sta85]   R. T. STANKO. Method for preventing body fat deposition in mammals. Technical Report, US Patent 4,548,937 (1985).

[STB95]   P.P. SCHMIDT, F. TRAVERS, AND T. BARMAN. Transient and equilibrium kinetic studies on yeast 3-phosphoglycerate kinase. evidence that intermediate containing 1,3-bisphophoglycerate accumulates in the steady-state. *Biochem.* **34**, 824 – 832 (1995).

[Ste99]   G. STEPHANOPOULOS. Metabolic fluxes and metabolic engineering. *Metabolic Engineering* **1**, 1–11 (1999).

[Ste00]   G. STEPHANOPOULOS. Bioinformatics and metabolic engineering. *Metab. Eng.* **2**, 157 – 158 (2000).

[Ste02]   G. STEPHANOPOULOS. Metabolic engineering: Perspective of a chemical engineer. *AIChE Journal* **48(5)**, 920 – 926 (2002).

[Ste03]   G. STEPHANOPOULOS. Invited comment: Chemical and biological engineering. *Chem. Eng. Sci.* **58**, 4931 – 4933 (2003).

[Str93]   B. STRIEGEL. "Entwurf und Implementierung Von Regelungskonzepten Für Biotechnologische Prozesse". PhD thesis, Rheinisch-Westfälische Technische Universität Aachen, RWTH (1993).

[Str99]   M.A. STREGE. High-performance liquid chromatographic-electrospray ionization mas spectrometric analyses for the integration of natural products with modern high-throughput screening. *J. Chromatography B* **725**, 67 – 78 (1999).

[SUN$^+$02]   T. SOGA, Y. UENO, H. NARAOKA, Y. OHASHI, M. TOMITA, AND T. NISHIOKA. Simultaneous determination of anionic intermediates for bacillus subtilis metabolic pathways by capillary electrophoresis electrospray ionization mass spectrometry. *Anal. Chem.* **74**, 2233 – 2239 (2002).

[SVC02]   D. SEGRÈ, D. VITKUP, AND G.M. CHURCH. Analysis of optimality in natural and perturbed metabolic networks. *PNAS* **99(23)**, 15112 – 15117 (2002).

[SVM$^+$03]   U. VON STOCKAR, S. VALENTINOTTI, I. MARISON, C. CANNIZZARO, AND C. HERWIG. Know-how and know-why in biochemocal engineering. *Biotechnol. Advances* **21**, 417 – 430 (2003).

[SW71]   T.G. SPRING AND F. WOLD. The purification and characterization of escherichia coli enolase. *J Biol. Chem.* **52**, 6797 – 6802 (1971).

[SWG$^+$91]   J.P. SARSEO, P.J. WOOKEY, P. GOLLNICK, C. YANOFSKY, AND A.J. PITTARD. A new family of integral membrane proteins involved in transport of aromatic amino acids in escherichia coli. *J. Bacteriol.* **173**, 3231 – 3224 (1991).

[SYK$^+$87]   S. SUGIMOTO, M. YABUTA, N. KATO, S. TATSUJI, T. YOSHIDA, AND H. TAGUCHI. Hyperproduction of phenylalanine by escherichia coli: Application of a temperature-controllable expression vector carrying the repressor-promotor system of bacteriophage lambda. *J. Biotechnol.* **5**, 237 – 253 (1987).

[Sys]   RELATIONAL DATABASE SYSTEM. "MySQL". http//www.mysql.com.

[SYUS97]   H. SHIMIZU, K. YASUOKA, K. UCHIYAMA, AND S. SHIOYA. On-line fault diagnosis for optimal rice alpha-amylase production process of a temperature-sensitive mutant of saccharomyces cerevisiae by autoassociatice neural network. *J. Ferment. Bioeng.* **83(5)**, 435 – 442 (1997).

[Szy95]   T. SZYPERSKY. Biosynthetically directed fractional 13c-labeling of proteinogenic amino acids. an efficient analytical tool to investigate intermediary metabolism. *Eur. J. Biochem.* **232**, 433 – 448 (1995).

[Szy98]   T. SZYPERSKI. 13c-NMR, MS and metabolic flux balancing in biotechnology research. *Quaterly Reviews of Biophysics* **31**(1), 41–106 (1998).

[Tak03]   R. Takors. Model-based analysis and optimization of an ISPR approach using reactive extraction for pilot-scale l-phenylalanine production. *Biotechnol. Prog.* **in press** (2003).

[TBM01]   N. Tik, E. Bayraktar, and Ü. Mehmetoglu. In situ reactive extraction of lactic acid from fermentation media. *J. Chem. Technol. and Biotechnol.* **76**, 764 – 768 (2001).

[TBWO98]   B. Teusink, F. Baganz, H.V. Westerhoff, and S.G. Oliver. In A.J.P. Brown and M. Tuite, editors, "Method Microbiology", pages 297 – 336. Academic press, San Diego (1998).

[TCN02]   J. Thykaer, B. Christensen, and J. Nielsen. Metabolic network analysis of an adipoyl-7-ADCA-producing strain of penicillium chrysogenum: Elucidation of adipate degradation. *Metab. Eng.* **4**, 151 – 158 (2002).

[TCP76]   D.E. Tribe, H. Camakaris, and J. Pittard. Constitutive and repressible enzymes of the common pathway of aromatic biosynthesis in escherichia coli k-12: Regulation of enzyme synthesis at different growth rates. *J. Bacteriol.* **127**, 1085 – 1097 (1976).

[TdGS99]   M. Tesch, A.A. de Graaf, and H. Sahm. In vivo fluxes in the ammonium-assimilatory pathways in corynebacterium glutamicum studied by 15n nuclear magnetic resonance. *Appl. Environ. Microbiol.* **65**, 1099 – 1109 (1999).

[TDN+87]   J. Then, A. Doherty, H. Netherway, H. Marquardt, H.-M. Deger, H. Voelskow, G. Wöhner, and P. Präve. Production of l-phenylalanine from phenylpyruvate using resting cells of escherichic coli. *Biotechnol. Lett.* **9**, 680 – 684 (1987).

[TEA03]   A. Tomar, M.A. Eiteman, and E. Altman. The effect of acetate pathway mutations on the production of pyruvate in escherichia coli. *Appl. Microbiol. Biotechnol.* **62**, 76 – 82 (2003).

[TGB97]   J. Torres, V. Guixe, and J. Babul. A mutant phosphofructokinase produces a futile cycle during gluconeogenesis in escherichia coli. *J. Biochem.* **327**, 675 – 684 (1997).

[TGPW01]   R. Takors, M. Gerigk, H. Paschold, and C. Wandrey. Principal component analysis for microbial l-phenylalanine production. *Bioproc. Biosys. Eng.* **24**, 93 – 99 (2001).

[TGZG97]   F. Tränkle, A. Gerstlauer, M. Zeitz, and E.D. Gilles. PROMOT / DIVA: A prototype of a process modeling and simulation environment. In I. Troch and F. Breitenecker, editors, "IMACS Symposium on Mathematical Modelling, 2nd MATHMOD", pages 341 – 346, Vienna, Austria (1997). ARGESIM Report.

[THT+99]   M. Tomita, K. Hashimotot, K. Takahashi, T.S. Shimizu, Y. Matsuzaki, F. Miyoshi, K. Saito, S. Tanida, K. Yugi, J.C. Venter, and C.A. Hutchison III. E-cell: A software environment for whole cell simulation. *Bioinformatics* **15(1)**, 72 – 84 (1999).

[THW86]   M.P. Thien, T.A. Hatton, and D.I.C. Wang. Separation of amino aids from fermentation broth using liquid emulsion membranes. In "Reprints Vol.3, Int. Solvent Extraction Conf." DECHEMA (1986).

[TKM+87]   T. Tsuchida, K. Kubota, Y. Morinaga, H. Matsui, H. Enei, and F. Yoshinaga. Production of l-phenylalanine by mutant of brevibacterium lactofermentum 2256. *Agric. Biol. Chem.* **51**, 2095 – 2101 (1987).

[TMB+97]   U. Theobald, W. Mailinger, M. Baltes, M. Rizzi, and M. Reuss. In vivo analysis of metabolic dynamics in sccharomyces cerevisiae: I. experimental observations. *Biotechnol. Bioeng.* **55(2)**, 305 – 316 (1997).

[TMRR93]   U. Theobald, W. Mailinger, M. Reuss, and M. Rizzi. In vivo analysis of glucose-induced fast changes in yeast adenine nucleotide pool applying a rapid sampling technique. *Anal. Biochem.* **214**, 31 – 37 (1993).

[TNMF98]   H. Tweeddale, L. Notley-McRobb, and T. Ferenci. Effect of slow growth on metabolism of escherichia coli, as revealed by global metabolite pool ('metabolome') analysis. *J. Bacteriol.* **180**, 5109 – 5116 (1998).

[TNOY96]   M. Takagi, Y. Nishio, G. Oh, and T. Yoshida. Control of l-phenylalanine production by dual feeding of glucose and l-tyrosine. *Biotechnol. Bioeng.* **52**, 653 – 660 (1996).

[TOS+92]   T. Tsujino, S. Ohigashi, S. Sugiyama, K. Kawashiro, and H. Hayashi. Oxidation of propylene glycol and lactic acid to pyruvic acid in aqueous phase catalyzed by lead-modified palladium-on-carbon and related systems. *J. Mol. Catal.* **71**, 25 – 35 (1992).

[TR01]   M. Tatarko and T. Romeo. Disruption of a global regulator gene to enhance central carbon flux into phenylalanine biosynthesis in escherichia coli. *Current Microbiology* **17**, 458 – 462 (2001).

[TRTP99]   A. Teleman, P. Richard, M. Toivari, and M. Pentilla. Identification and quantitation by phosphorus metabolites in yeast neutral pH extracts by nuclear magnetic resonance spectroscopy. *Anal. Biochem.* **272**, 71 – 79 (1999).

[TT82]   S. Takao and M. Tanida. Pyruvic acid production by schizophyllum commune. *J. Ferment. Technol.* **60**, 277 – 280 (1982).

[Tur90]   T. Turányi. Sensitivity analysis of complex kinetic systems. tools and applications. *J Math. Chem.* **5**, 203 – 248 (1990).

[TVRW90]   S. Tichy, D. Vasic-Racki, and C. Wandrey. Electrodialysis as an integrated downstream process in amino acid production. *Chem. Biochem. Eng.* **Q4**, 127 – 135 (1990).

[TWK+02]   A. Tholey, C. Wittmann, M.-J. Kang, D. Bungert, K. Hollemeyer, and E. Heinzle. Derivatization of small biomolecules for optimized matrix-assisted laser desorption/ionization mass spectrometry. *J. Mass Spectrometry* **37**, 963 – 973 (2002).

[TYI+91]   M. Teramoto, T. Yamashiro, A. Inoue, H. Matsuyama, and Y. Miyake. Extraction of amino acids by liquid membranes containing di(2-ethyl)phosphoric acid as a carrier. *J. Mem. Sci.* **58**, 11 – 32 (1991).

[TYT84]   S. Takao, A. Yokota, and M. Tanida. Enzymatic production of tryptophane coupled to pyruvic acid fermentation. *J. Ferment. Technol.* **62**, 329 – 334 (1984).

[UHLC92]   M. S. Uddin, K. Hidajat, B.-G. Lim, and C.B. Ching. Interfacial mass transfer in stripping of phenylalanine in a liquid-liquid extraction process. *J. Chem. Tech. Biotechnol.* **53**, 353 – 357 (1992).

[Van84]   E.J. Vandamme. "Biotechnology of Industrial Antibiotics". Marcel Dekker, Inc., New York (1984).

[Var00]   J.D. Varner. Large-scale prediction of phenotype: Concept. *Biotechnol. Bioeng.* **69 (6)**, 664 – 678 (2000).

[VBDAN03]   S. G. Villas-Boas, D. G. Delicado, M. Akesson, and J. Nielsen. Simultaneous analysis of amino and nonamino organic acids as methyl chloroformate derivatives using gas chromatography-mass spectrometry. *Anal. Biochem.* **322**, 134 – 138 (2003).

[VBRR99]   S. Vaseghi, A. Baumeister, M. Rizzi, and M. Reuss. In vivo dynamics of the pentose phosphate pathway in saccharomyces cerevisiae. *Metab. Eng.* **1**, 128 – 140 (1999).

[VdHM+00]   D. Visser, R. Van der Heiden, K. Mauch, M. Reuss, and S. Heijnen. Tendency modeling: A new approach to obtain simplified kinetic models of metabolism applied to saccharomyces cerevisiae. *Metab. Eng.* **2**, 252 – 275 (2000).

[VH02]   D. VISSER AND J.J. HEIJNEN. The mathematics of metabolic control analysis revisited. *Metabolic Engineering* **4**, 114–123 (2002).

[VH03]   D. VISSER AND J.J. HEIJNEN. Dynamic simulation and metabolic re-desgin of a branched pathway using linlog kinetics. *Metab. Eng.* **5**, 164 – 176 (2003).

[Vis02]   D. VISSER.   "Measuring and Modeling in Vivo Kinetics of Primary Metabolism". Isbn 90-9015559-7, Technical University of Delft (2002).

[VJGG⁺96]   P.A. VANROLLEGHEM, P.DE JONG-GUBBELS, W.M. VAN GULIK, J.T. PRONK, J.P. VAN DIJKEN, AND J.J. HEIJNEN. Validation of a metabolic network of saccharomyces cerevisiae using mixed substrate studies. *Biotechnology Progress* **12**, 434–448 (1996).

[VMP⁺96]   F. VALLE, E. MUNOZ, E. PONCE, N. FLORES, AND F. BOLIVAR. Basic and applied aspects of metabolic diversity: The phosphoenolpyruvate node. *J. Ind. Microbiol.* **17**, 458 – 462 (1996).

[VMZR01]   S. VASEGHI, F. MACHERHAMMER, S. ZIBEK, AND M. REUSS. Signal transduction dynamics of the protein kinase-A/Phosphofructokinase-2 system in saccharomaces cerevisiae. *Metab. Eng.* **3**, 163 – 172 (2001).

[VP94a]   A. VARMA AND B. O. PALSSON. Stoichiometric flux balance models quantitatively predict growth and metabolic by-product secretion in wild-type escherichia coli w3110. *Applied and Environmental Microbiology* **60**, 3724–3731 (1994).

[VP94b]   A. VARMA AND B.O. PALSSON. Metabolic flux balancing: Basic concepts, scientific and practical use. *Bio/Technology* **12**, 994–998 (1994).

[VR99a]   J. VARNER AND D. RAMKRISHNA. Metabolic engineering from a cybernetic perspective. 1. theroretical perliminaries. *Biotechnol. Prog.* **15**, 407 – 425 (1999).

[VR99b]   J. VARNER AND D. RAMKRISHNA. Metabolic engineering from a cybernetic perspective. 2. qualitative investigation of nodal architechtures and their response to genetic perturbation. *Biotechnol. Prog.* **15**, 426 – 438 (1999).

[VS93]   J.J. VALLINO AND G. STEPHANOPOULOS.   Metabolic flux distributions in corynebacterium glutamicum during growth and lysine overproduction. *Biotechnology and Bioengineering* **41**(6), 633–646 (1993).

[VS94]   J.J. VALLINO AND G. STEPHANOPOULOS. Carbon flux distributions at the glucose 6-phosphate branch point in corynebacterium glutamicum during lysine overproduction. *Biotechnol. Prog.* **10**, 327–334 (1994).

[VSE96]   M. VRLJIC, H. SAHM, AND L. EGGELING. A new type of transporter with a new type of cellular function: L-lysine export from corynebacterium glutamicum. *Mol. Microbiol.* **22**, 815–826 (1996).

[VVT85]   S. VAJDA, P. VALKÓ, AND T. TURÁNYI. Principal component analysis of kinetic models. *Int. J. Chem. Kinetics* **17**, 55 – 81 (1985).

[VZD⁺02]   D. VISSER, G.A. VAN ZUYLEN, J.C. VAN DAM, A. OUDSHOORN, M.R. EMAN, C. RAS, W.M. VAN GULIK, J. FRANK, G.W.K. VAN DEDEM, AND J.J. HEIJNEN. Rapid sampling for analysis of in vivo kinetics using the BioScope: A system for continuous-pulse experiments. *Biotechnol. Bioeng.* **79**, 674 – 681 (2002).

[Wan01]   C. WANDREY. Bio- ohne technik? *Chem.Ing. Technol.* **73(7)**, 787 (2001).

[WB97]   D. WEUSTER-BOTZ. Sampling tube device for monitoring intracellular metabolite dynamics. *Anal. Biochem.* **246**, 225 – 233 (1997).

[WB98a]   S. WIECZOREK AND H. BRAUER. Continuous production of citric acid with recirculation of the fermentation broth after product recovery. part 1: Continuous production of citric acid. *Bioproc. Eng.* **18**, 1 – 5 (1998).

[WB98b]   S. WIECZOREK AND H. BRAUER. Continuous production of citric acid with re-circulation of the fermentation broth after product recovery. part 2: Product recovery and recirculation of the broth. *Bioproc. Eng.* **18**, 75 – 77 (1998).

[WB99]   D. WEUSTER-BOTZ. "Die Rolle der Reaktionstechnik in der Mikrobiellen Verfahrensentwicklung, ISBN 3-89336-245-2". Forschungszentrum Jülich GmbH, Jülich, Germany (1999).

[WB03]   D. WEUSTER-BOTZ. Bioverfahrenstechnik - ingenieure auf dem weg ins jahrhundert der biologie. *Chem. Ing. Tech.* **75(10)**, 1515 – 1518 (2003).

[WBARA01]   D. WEUSTER-BOTZ, J. ALTENBACH-REHM, AND M. ARNOLD. Parallel substrate feeding and pH-control in shaking-flask. *Biochem. Eng. Journal* **7**, 163 – 170 (2001).

[WBdG96]   D. WEUSTER-BOTZ AND A.A. DE GRAF. "Advances in Biochemical Engineering and Biotechnology, Vol. 54", chapter Reaction engineering methods to study intracellular metabolite concentrations, pages 76 – 108. Springer Verlag, Berlin, Heidelberg, New York (1996).

[WBDM80]   J.F. WILLIAMS, P.F. BLACKMORE, C.C. DUKE, AND J.K. MACLEOD. Fact, uncertainty and speculation concerning biochemistry of d-erythrose-4-phosphate and its metabolic roles. *Int. J. Biochem.* **12**, 339 – 344 (1980).

[WBK89]   T. WIDLANSKI, S.L. BENDER, AND P.F. KNOWLES. Dehydroquinate synthase - a sheep in wolfs clothing. *Am Chem. Soc.* **111**, 2299 – 2300 (1989).

[WBW96]   D. WEUSTER-BOTZ AND C. WANDREY. Verfahren und vorrichtung zur serien-probenahme biologischer proben. Technical Report, German Patent DE 4407439 C2 (1996).

[WC88]   L.L. WOOD AND G.J. CALTON. Production of phenylalanine with immobilized cells, US patent 4728611. Technical Report, (1988).

[WdG97]   W. WIECHERT AND A.A. DE GRAAF. Bidirectional reaction steps in metabolic networks: I. modeling and simulation of carbon isotope labeling experiments. *Biotechnology and Bioengineering* **55**, 101–117 (1997).

[WdGSE00]   V.F. WENDISCH, A.A. DE GRAAF, H. SAHM, AND B.J. EIKMANNS. Quantitative determination of metabolic fluxes during co-utilization of two carbon sources: Comparative analyses with corynebacterium glutamicum during growth on acetate and/or glucose. *J. Bacteriol.* **182**, 3088 – 3096 (2000).

[Wes98]   S. WESTALL. Characterisation of yeast species by their production of volatile metabolites. *J. Food Mycol.* **1**, 187 – 201 (1998).

[Wes01]   H. V. WESTERHOFF. The silicon cell, not dead but live! *Metabolic Engineering* **3**, 207–210 (2001).

[WGS⁺03]   W.A. VAN WINDEN, W.M. VAN GULIK, D. SCHIPPER, P.J.T. VERHEIJEN, P. KRABBEN, J.L. VINKE, AND J.J. HEIJNEN. Metabolic flux and metabolic network analysis of penicillium chrysogenum using 2d [13c, 1h] COSY NMR measurements and cumulative bondomer simulation. *Biotechnol. Bioeng.* **83**, 75 – 92 (2003).

[WH00]   C. WITTMANN AND E. HEINZLE. MALDI-TOF MS for quantification of substrates and products in cultivation of corynebacterium glutamicum. *Biotechnology and Bioengineering* **72**, 642–647 (2000).

[WH01a]   C. WITTMANN AND E. HEINZLE. Application of MALDI-TOF MS to lysine-producing corynebacterium glutamicum. *Eur. J. Biochem.* **268**, 2441–2455 (2001).

[WH01b]   C. WITTMANN AND E. HEINZLE. Modeling and experimental design for metabolic flux analysis of lysine-producing corynebacteriy by mass spectrometry. *Metabolic Engineering* **3**, 173–191 (2001).

328   References

[WH02]   C. Wittmann and E. Heinzle. Genealogy profiling through strain improve-
            ment by using metabolic network analysis: Metabolic flux genealogy of several
            generations of lysine-producing corynebacteria. *Appl. Environ. Microbiol.*
            68, 5843 – 5846 (2002).

[WHH02]   C. Wittmann, M. Hans, and E. Heinzle. In vivo analysis of intracellular amino
            acid labelings by GC/MS. *Anal. Biochem.* **307**, 379 – 382 (2002).

[WHVP02]   K.L. Wasewar, A.B.M. Heesink, G.F. Versteeg, and V.G. Pangarkar. Re-
            active extraction of lactic acid using alamine 336 in MIBK: Equilibria and
            kinetics. *J. Biotechnol.* **97**, 59 – 68 (2002).

[Wie91]   W. Wiechert. "Interaktive Datenanalyse Bei Biotechnischen Prozessdaten".
            PhD thesis, University of Bonn (1991).

[Wie01]   W. Wiechert. 13c metabolic flux analysis. *Metabolic Engineering* **3**, 195 –
            206 (2001).

[Wie02a]   W. Wiechert. "Genetic Engineering: Principles and Methods", chapter An
            Introduction to 13C Metabolic Flux Analysis, pages 215 – 238. Kluwer Aca-
            demic (2002).

[Wie02b]   W. Wiechert. Modeling and simulation: Tools for metabolic engineering.
            Journal of Biotechnology **94**, 37–63 (2002).

[Win02]   W. Van Winden. "13C-Labeling Techniques for Metabolic Network and
            Flux Analysis". Delft University of Technology, The Netherlands, ISBN 90-
            9016251-8 (2002).

[Wit02]   C. Wittmann. "Advances in Biochemical Engineering/Biotechnology, Vol
            74", volume 74, chapter Metabolic Flux Analysis Using Mass Spectrome-
            try, pages 39–64. Springer-Verlag Berlin, advances in biochemical engineer-
            ing/biotechnology edition (2002).

[WJM97]   P. Wieczorek, J.A. Jönsson, and L. Mathiasson. Concentration of amino
            acids using supported liquid membranes with di-2-ethyhexyl phosphoric acid
            as carrier. *Anal. Chim. Acta* **346**, 191 – 197 (1997).

[WK96]   H.V. Westerhoff and D.B. Kell. What biotechnologists knew all along...?
            J. Theor. Biol. **182**, 411 – 420 (1996).

[WKss]   H.V. Westerhoff and B.N. Kholodenko. "Metabolic Engineering in a Post
            Genomic Era". Elsevier (2003 (in press)).

[WKS96]   P. Weisser, R. Krämer, and G.A. Sprenger. Expression of the escherichia coli
            pmi gene, encoding phosphomannose-isomerase in zymomonas mobilis, leads
            to utilization of mannose as a novel growth substrate, which can be used as a
            selective marker. *Appl. Environ. Microbiol.* **11**, 4155 – 4161 (1996).

[WKSS95]   P. Weisser, R. Krämer, H. Sahm, and G.A. Sprenger. Functional expression
            of the glucose transporter of zymomonas mobilis leads to restoration of glucose
            and fructose uptake in escherichia coli mutants and provides evidence for its
            fascilitator action. *J. Bacteriol.* **177**, 3351 – 3354 (1995).

[WLGH03]   L. Wu, H.C. Lange, W.M. Van Gulik, and J.J. Heijnen. Determination of
            the in vivo oxygen uptake and carbon dioxide evolution rates from off-gas
            measurements undr highly dynamic conditions. *Biotechnol. Bioeng.* **81 (4)**,
            448 – 458 (2003).

[WMI⁺99]   W. Wiechert, M. Möllney, N. Isermann, M. Wurzel, and A.A. de Graaf.
            Bidirectional reaction steps in metabolic networks. part III: Explicit solution
            and analysis of isotopomer labeling systems. *Biotechnology and Bioengineer-
            ing* **66**, 69–85 (1999).

[WMS⁺03]   A. Wahl, M. El Massaoudi, D. Schipper, W. Wiechert, and R. Takors. Serial
            13c flux analysis of an l-phenylalanine producing e. coli strain under industry-
            like production conditions. *Biotechnology Progress* **submitted** (2003). sub-
            mitted.

[WN03]   W. Wiechert and K. Nöh. "Adv. Biochem. Eng. Biotechnol.", chapter From Stationary to Instationary Metabolic Flux Analysis, page submitted. *** (2003).

[WSB98]   C. Weikert, U. Sauer, and J.E. Bailey. Increased phenylalanine production by growing and nongrowing escherichia coli strain CWML2. *Biotechnol. Prog.* **14(3)**, 420 – 424 (1998).

[WSdGM97]   W. Wiechert, C. Siefke, A.A. de Graaf, and A. Marx. Bidirectional reaction steps in metabolic networks. part II: Flux estimation and statistical analysis. *Biotechnology and Bioengineering* pages 118–135 (1997).

[WT03]   W. Wiechert and R. Takors. "Metabolic Engineering in a Post Genomic Era", chapter Validation of Metabolic Models: Concepts, Tools and Problems, page in press. Eds.: H.V. Westerhoff and B.N. Kholodenko (2003).

[WVH01]   W. Van Winden, P. Verheijen, and S. Heijnen. Possible pitfalls of flux calculations based on 13c-labeling. *Metabolic Engineering* **3**, 151–162 (2001).

[WWS+01]   B. Wilms, A. Wiese, C. Syldatk, R. Mattes, and J. Altenbucher. Development of an escherichia coli whole cell biocatalyst for the production of l-amino acids. *J. Biotechnol.* **86**, 19 – 30 (2001).

[WYSL94]   P.M. Wang, C.Y. Yeh, C.H. Shu, and C.C. Liao. A substrate feedig strategy using an oxystat for l-phenylalanine fermentation by corynebacterium glutamicum. *Biotechnol. Techniques* **8**, 843 – 846 (1994).

[XJE99]   B. Xu, M. Jahic, and S.-O. Enfors. Modeling of overflow metabolism in batch and fed-btach cultures of escherichia coli. *Biotechnol. Prog.* **15**, 81 – 90 (1999).

[XWZ+03]   H. Xu, P. Wei, H. Zhou, W. Fan, and P. Ouyang. Efficient production of l-phenylalanine by a coupled enzymatic system of transaminase and aspartase. *Enzyme and Microbial Tech.* **33**, 537 – 543 (2003).

[YC00]   C. Yang and E.L. Cussler. Reactive extraction of penicillin g in hollow-fiber and hollow-fiber fabric modules. *Biotechnol. Bioeng.* **69(1)**, 66 – 73 (2000).

[YDLF03]   J. Yi, K.M. Draths, K. Li, and J.W. Frost. Altered glucose transport and shikimate pathway product yields in e. coli. *Biotechnol. Prog.* **19**, 1450 – 1459 (2003).

[YHT+97]   A. Yokota, M. Henmi, N. Takaoka, C. Hayashi, C. Takezawa, Y. Fukumori, and F. Tomita. Enhancement of glucose metabolism in a pyruvic acid-hyperproducing escherichia coli mutant defective in f1-ATPase activity. *J. Ferment. Bioeng.* **83**, 132 – 138 (1997).

[YJS96]   K. Ye, S. Jin, and K. Shimizu. Performance of lactic acid fermentation by multistage extractive fermentation. *J. Ferm. Bioeng.* **81(3)**, 240 – 246 (1996).

[YK78]   H. Yamada and H. Kumagai. Microbial and enzymatic processes for amino acid production. *Pure Appl. Chem.* **50**, 1117 – 1127 (1978).

[YKK+72]   H. Yamada, H. Kumagai, N. Kashima, H. Torii, H. Enei, and S. Okumura. Synthesis of l-tyrosine from pyruvate , ammonia and phenol by crystalline tyrosine phenol lyase. *Biochem. Biophys. Res. Commun.* **46**, 370 – 374 (1972).

[YLDF02]   J. Yi, K. Li, K.M. Draths, and J.W. Frost. Modulation of phosphoenolpyruvate synthase expression increases shikimate pathway product yields in e. coli. *Biotechnol. Prog.* **18**, 1141 – 1148 (2002).

[YM94]   T. Yonehara and R. Miyata. Fermentative production of pyruvate from glucose by torulopsis glabrata. *J. Ferment. Bioeng.* **78**, 155 – 159 (1994).

[YMM+92]   H. Yanase, N. Mori, M. Masuda, K. Kita, M. Shimao, and N. Kato. Pyruvate production by enterococcua casseliflavus a-12 from gluconate in an alkaline medium. *J. Ferment. Bioeng.* **73**, 287 – 291 (1992).

330   References

[YST+94]   A. Yokota, H. Shimizu, Y. Terasawa, N. Takaoka, and F. Tomita. Pyruvic acid production by a lipoic acid auxotroph of escherichia coli w 1485. *Appl. Microbiol. Biotechnol.* **41**, 638 – 643 (1994).

[YT89]   A. Yokota and S. Takao. Pyruvic acid production by lipoic acid auxotrophs of enterobacter aerogenes. *Agric. Biol. Chem.* **53**, 705 – 711 (1989).

[YTT+94]   A. Yokota, Y. Terasawa, N. Takaoka, H. Shimizu, and F. Tomita. Pyruvic acid production by a f1-ATPase-defective mutant of escherichia coli w1485lip2. *Biosci. Biotech. Biochem.* **58**, 2164 – 2167 (1994).

[YW91]   V.M. Yabannavar and D.I.C. Wang. Extractive fermentation for lactic acid production. *Biotechnol. Bioeng.* **37**, 1095 – 110 (1991).

[YYG86]   G.A. Yagoding, E.V. Yurtov, and A.S. Golubkov. Liquid membrane extraction of amino acids. *Intern. Solvent. Extraction Conf., DECHEMA* **3** (1986).

[Zel03]   B. Zelic. "Study of the Process Development for Escherichia Coli Based Pyruvate Production". PhD thesis, University of Zagreb (2003).

[ZGB+03]   B. Zelic, T. Gerharz, M. Bott, D. Vasic-Racki, C. Wandrey, and R. Takors. Fed-batch process for pyruvate production by recombinant escherichia coli. *Chem. Eng. Sci/Eng.Life Sci.* **7**, 299 – 305 (2003).

[ZGV+03]   B. Zelic, S. Gostovic, K. Vuorilehto, D. Vasic-Racki, and R. Takors. Process strategies to enhance pyruvate production with recombinant escherichia coli: From repetitive fed-batch to ISPR with fully integrated electrodialysis. *Biotechnol. Bioeng.* **in press** (2003).

[Zim03]   D. Zimmer. Introduction to quantitative liquid chromatography - tandem mass spectrometry (LC - MS - MS). *Chromatographia* **57**, 325 – 332 (2003).

[ZKS+87]   H. Ziehr, M.R. Kula, E. Schmidt, C. Wandrey, and J. Klein. Continuous production of l-phenylalanine by transaminoation. *Bioechnol. Bioeng.* **26**, 409 – 416 (1987).

[ZLLJ00]   T. Zeppenfeld, C. Larisch, J.W. Lengeler, and K. Jahreis. Glucose transporter mutants of escherichia coli k-12 with changes in substrate recognition of IICB(Glc) and induction behaviour of the ptsG gene. *Journal of Bacteriology* **182**, 4443 – 4452 (2000).

[ZS94]   C. Zupke and G. Stephanopoulos. Intracellular flux analysis in hybridomas using mass balance and in vitro 13c NMR. *Biotechnology and Bioengineering* **45**, 292–303 (1994).

[ZVRWT03]   B. Zelic, D. Vasic-Racki, C. Wandrey, and R. Takors. Modeling of the pyruvate production with escherichia coli in a fed-batch bioreactor. **submitted** (2003).

Appendix A
Material and Methods

A.1   Strains and Feedstocks

A.1.1   E. coli Strains of the 'L-Phe Project'

As indicated in the table, most of the recombinant strains were derived from *E. coli* K12 LJ110 [ZLLJ00]. The plasmids were based on the expression vector pJF119EH [FPF$^+$86] which contains an ampicillin resistance gene amp^R and an IPTG (isopropyl beta-D-thiogalactoside) inducible tac-promotor. All strains were thankfully constructed and supplied by members of cooperating groups as indicated in the table.

The following phenomenological strain characterization can be given:

- ***E. coli* DAHP, *E. coli* DHS. *E. coli* S3P**: As indicated in Table A.1, the strains are knock-out mutants because the enzymes AroB, AroE or AroA were inactivated, making the strains auxotrophic for L-tyrosine, L-phenylalanine and L-tryptophane. Additionally 4-amino-benzoic acid, 2,3-dihydroxybenzoic acid and 4-hydroxybenzoic acid were supplemented to the medium to ensure that growth was not limited by other aromatic compounds except for the aromatic amino acids. To enable high carbon fluxes for DAH(P), DHS and S3P synthesis, some upstream enzyme activities were fortified by plasmid-encoded gene expression as indicated.

- ***E. coli* 4pF20:** The L-Phe producing strain is tyrosine auxotrophic, thus enabling a selective glucose conversion into L-Phe with non-growing cells. To avoid feedback inhibition by L-Phe or tyrosine, the

feedback resistant chorismate mutase/prephenate dehydratase (encoded by $pheA^{fbr}$) and the tyrosine-feedback resistant DAHP isoenzyme, encoded by $aroF^{fbr}$ [JBS01], were used.

- **E. coli 4pF26 (aroF-fbr):** The L-Phe producing strain is similar to *E. coli* 4pF20. However, *aroL* coding for shikimate kinase II was inserted on the plasmid pF26 to compensate transcriptional repression of *aroL* by *tyrR* - regulon which is activated by 'high' tyrosine levels.

- **E. coli 4pF69 (aroF-wt):** This L-Phe producer contained the wild-type, tyrosine sensitive *aroF* gene (plasmid-encoded) which necessitated the on-line tyrosine control during L-Phe production as indicated in the text. Apart from $pheA^{fbr}$, *aroL* was overexpressed on pF69 to ensure sufficient shikimate kinase II activity.

- **E. coli 4pF78:** The L-Phe producing strain is similar to *E. coli* 4pF20, except for the additional use of plasmid-encoded *aroB* (coding for 3-DHQ synthase) to ensure a sufficient carbon flux into the AAA pathway after DAHP synthesis.

- **E. coli 4pF79**: The L-Phe producer is similar to E. coli 4pF78 except for the wild-type *aroF* which replaced $aroF^{fbr}$ contained on plasmid pF78.

- **E. coli 4pF81:** The strain is tyrosine auxotrophic to prevent unwanted carbon flux into tyrosine biosynthesis during L-Phe production. Limited tyrosine supply thus limits cell growth allowing a highly selective L-Phe production with non-growing cells. To avoid a feedback inhibition of PheA by L-Phe accumulation, the feedback resistant PheA^{fbr} was used. It is noteworthy that this strains contains the native AroF making its activity sensitive to tyrosine accumulation, which consequently must be prevented by appropriate process control.

- **E. coli 20pMK12**: The L-Phe producing strain represents the only strain of this list with an inactivated PTS for glucose uptake. As indicated, the PTS-coding genes *ptsH*, *ptsI* and *crr* were deleted and replaced by kanamycin resistant gene *kan*. Instead, *glf* (coding for the glucose facilitator from *Zymomonas mobilis*) was inserted on the plasmid pMK12 together with the feedback resistant genes $aroF^{fbr}$ and $pheA^{fbr}$. Additionally, these feedback resistant genes ($aroF^{fbr}$ and $pheA^{fbr}$) were inserted in the chromosome under the control of the P$_{tac}$ promoter.

- **E. coli DSM:** Because of intellectual property reasons, the genotype of this strain, which was provided by the cooperating partner DSM,

cannot be presented in detail. Only the following explanations can be given: A feedback resistant gene $aroF^{fbr}$ together with $pheA^{fbr}$ was inserted and tyrosine auxotrophy was caused by the inactivation of $tyrA$.

TABLE A.1. Genotype of *E. coli* strains used according to F- nomenclature

E. coli synonym	synonym	Host *E. coli* characteristic	synonym	Plasmid derivatives of pJF119EH characteristic	Constructed by
DAHP	F5	LJ110 aroB351	pF15	$aroF^{fbr}$	Krä, Jos
DHS	AB2834	λ^- glnV42(AS) tsr-352 malT352(λ^R) aroE353	pF42	$aroF^{fbr}$ aroB	GSC, Bon, Deg
S3P	AB2829	λ^- glnV42(AS) aroA354	pF84	$aroF^{fbr}$ aroB aroL	GSC, Bon, Deg, Krä
4pF20	F4	Δ (pheA tyrA aroF)	pF20	$aroF^{fbr}$ $pheA^{fbr}$	Jos, Bon, Deg, Spre
4pF26, aroF-fbr	F4	Δ (pheA tyrA aroF)	pF26	$aroF^{fbr}$ $pheA^{fbr}$ aroL	Bon, Spr
4pF69, aroF-wt	F4	Δ (pheA tyrA aroF)	pF69	aroF $pheA^{fbr}$ aroL	Bon, Spr
4pF78	F4	Δ (pheA tyrA aroF)	pF78	$aroF^{fbr}$ $pheA^{fbr}$ aroB	Jos, Deg, Spr
4pF79	F4	Δ (pheA tyrA aroF)	pF79	aroF $pheA^{fbr}$ aroB	Spr, Deg
4pF81	F4	Δ (pheA tyrA aroF)	pF81	aroF $pheA^{fbr}$ aroB aroL	Spr, Deg
20pMK12	F20	Δ (pheA tyrA aroF)::P_{tac} ($aroF^{fbr}$ $pheA^{fbr}$) Δ (ptsH ptsI crr)::kan	pMK12	$aroF^{fbr}$ glf $pheA^{fbr}$	Spr, Deg
DSM	n.d.	Δ (pheA tyrA aroF)	n.d.	n.d.	DSM*

gene	coding for:		Abbreviations	
aroB	3-dehydroquinate synthase		Bon	J. Bongaerts
aroF	tyrosine sensitive DAHP synthase		Deg	U. Degner
$aroF^{fbr}$	tyrosine feedback resistant DAHP synthase		DSM*	industrial partner DSM
aroL	shikimate kinase II		GSC	*E. coli* Genetic Stock Center, Yale University
glf	glucose fascilitator from Zymomonas mobilis		Jos	R. Jossek [JBS01]
pheA	chorismate mutase / prephenate dehydratase		Krä	M. Krämer [Krä00]
$pheA^{fbr}$	L-Phe feedback resistant mutant of pheA		Spr	G.A. Sprenger
tyrA	chorismate mutase / prephenate dehydrogenase			

A.1.2   Pyruvate Producing E. coli Strains

The pyruvic acid producing strains were *Escherichia coli* YYC202 and *Escherichia coli* YYC202 *ldhA*::*Kan* constructed at the Institute of Biotechnology 1 (Forschungszentrum Jülich GmbH, Germany) by M. Bott and T. Gerharz ([GBZT01], [BGZT02]). Both strains are completely blocked in their ability to convert pyruvate into acetyl-CoA, phosphoenolpyruvate (PEP) or acetate, which was realized by the complete chromosomal deletion of genes coding for pyruvate dehydrogenase (*aceEF*), pyruvate formate lyase (*pflB*), pyruvate oxidase (*poxB*) and PEP synthetase (*pps*). Thus, the strains were acetate auxotrophic. In the strain *Escherichia coli* YYC202 *ldhA*::*Kan*, the lactate dehydrogenase (*ldhA*), responsible for the conversion of pyruvate into lactate, is additionally inactivated. The *ldhA* mutation was performed by P1vir transduction [SBE84] using *E. coli* NZN117 [BMJLC97] as a donor. Culture samples were stored in cryogenic vials at –80 °C in Luria-Bertani (LB) medium containing 50 % glycerol.

Precultures was performed by inoculating 750 μL of cryoculture 1-L flasks containing 200 mL medium. Flasks were incubated in the rotation shaker (3033, GFL GmbH, Germany) at 37 °C and 160 rpm for 15 hours.

A.1.3   C. glutamicum

The L-leucine auxotrophic strain *Corynebacterium glutamicum* MH-20-22B, derived from *C. glutamicum* ATCC 13032 (wild-type) by undirected mutagenesis [SES92] with feedback-resistant aspartate kinase and altered L-lysine export carrier was maintained at −80 °C as a 1.8 mL glycerol stock solution (30 %v/v).

A.2   Medium and Cultivation Conditions

A.2.1   E. coli Strains of the 'L-Phe Project'

.

Cryocultures were stored in Luria-Bertani (LB) medium containing 50% glycerol at –80°C. Of precultivation medium SK (see Table A.2) 250 mL was usually filled into 1000-mL shake flasks, 1 mL from feedstocks was inoculated and cultivated for 16 h at 37°C on a shaking flask incubator (145 rpm). *E. coli* fermentations were usually performed at *pH* 6.5 (titrated by addition of 10 % NH$_4$OH) and 37°C under aerobic conditions (for instance 30% dissolved oxygen concentration at 0.5 bar overpressure and aeration of 1 vvm) unless otherwise indicated in the text. Usually, the antifoaming agent S289 (Sigma) was used.

TABLE A.2. Medium compositions used for *E. coli* fermentations

Component	Unit	SK[a]	BR[b]	FBR[c]	Feed[d]	GPM[f]	DSM[g]
glucose H$_2$O	$\frac{g}{L}$	5.0	5.0	15.0	600	15	15
NaCl	$\frac{g}{L}$	0.1	0.1	0.1		1.0	1.0
MgSO$_4$.7H$_2$O	$\frac{g}{L}$	0.3	0.3	0.3		3.0	3.0
(NH$_4$)$_2$SO$_4$	$\frac{g}{L}$	5.0	5.0	5.0		5.0	5.0
ampicillin	$\frac{g}{L}$	0.1	0.1	0.1		0.1	0.1
L-tyrosine	$\frac{g}{L}$	0.08	0.08	0.08	25/2.5[e]		0.3
K$_2$HPO$_4$	$\frac{g}{L}$	12.0	12.0	12.0			
KH$_2$PO$_4$	$\frac{g}{L}$	3.0	3.0	3.0		3.0	3.0
thiamine HCl	$\frac{mg}{L}$	7.5	7.5	7.5		7.5	7.5
FeSO$_4$.7H$_2$O	$\frac{g}{L}$	0.075	0.075	0.1125		0.1125	0.1125
Ca$_2$Cl 2H$_2$O	$\frac{g}{L}$	0.015	0.015	0.015		0.015	0.015
spore el. sol.	$\frac{mL}{L}$	1.5	1.5	1.5		1.5	1.5
Na citrate	$\frac{g}{L}$	1.0	1.0	1.5		1.5	
L-TYR	$\frac{g}{L}$					0.7	
L-Phe	$\frac{g}{L}$					0.7	
L-TRP	$\frac{g}{L}$					0.35	
aba.	$\frac{g}{L}$					0.01	
dhba.	$\frac{g}{L}$					0.01	
hdba.	$\frac{g}{L}$					0.01	

[a]shaking flask medium for precultures; [b]medium of 30-L bioreactor (preculture for 300-L bioreactor); [c]start medium for the 300-L fed-batch; [d]feed medium for 300-L fed-batch; [e]25 $g \cdot L^{-1}$tyrosine were dissolved in 5 % NH$_3$ for the 300-L bioreactor feed, 2.5 $g \cdot L^{-1}$were used for the Sensor reactor; [f]medium used for glucose pulse experiments with knock-out mutants; [g]DSM medium; aba - 4-aminobenzoic acic; dhba - 2,3 dihydroxybenzoic acid; hdba - 4-hydroxybenzoic acid;

TABLE A.3. Spore element solution used for *E. coli* fermentations

Component	Unit	Content
$Al_2(SO_4)_3$ 18 H_2O	$\frac{g}{L}$	2.0
$CoSO_4$ 7H_2O	$\frac{g}{L}$	0.75
$CuSO_4.5H_2O$	$\frac{g}{L}$	2.5
H_3BO_3	$\frac{g}{L}$	0.5
$MnSO_4$	$\frac{g}{L}$	24.0
$Na_2MO_4.2H_2O$	$\frac{g}{L}$	3.0
$NiSO_4$ 6H_2O	$\frac{g}{L}$	2.5
$ZnSO_4.7H_2O$	$\frac{g}{L}$	15

A.2.2   *C. glutamicum MH20-22B*

The organisms were cultured in 100 mL complex medium (1 L shaking flask, 12 h, 150 rpm, 30°C). The cultures were then cultivated in 9 1-L shaking flasks containing 200 mL synthetic medium and 10 mL of the complex medium culture (12 h, 150 rpm, 30 °C). A 30-L stirred bioreactor (filled with 15.1 L synthetic medium) was inoculated with the contents of 9 shaking flasks and cultured for 15 h. The fermentation broth was transferred to a 300-L stirred bioreactor (filled with 160 L synthetic medium) and cultivated in batch mode. Please notice the presence of the auxotrophic substance L-leucine in the feed medium which is thus co-fed considering the glucose feeding profile of Figure 3.18. The medium is given in Table A.4.

A.2.3   *Pyruvate Producing E. coli*

The fermentation medium contained per liter: 1.50 g $NaH_2PO_4 \cdot H_2O$, 3.25 g KH_2PO_4, 2.50 g K_2HPO_4, 0.20 g NH_4Cl, 2.00 g $(NH_4)_2SO_4$, 0.50 g $MgSO_4$, 1 mL trace element solution, 11 g glucose monohydrate and 0.79 g potassium acetate.

The trace element solution contained per liter: 10.00 g $CaCl_2 \cdot 2H_2O$, 0.50 g ZnSO4·7H2O, 0.25 g CuCl2·2H2O, 2.50 g $MnSO_4 \cdot H_2O$, 1.75 g $CoCl_2 \cdot 6H_2O$, 0.12 g H_3BO_3, 2.50 g $AlCl_3 \cdot 6H_2O$, 0.50 g $Na_2MoO_4 \cdot 2H_2O$, 10.00 g $FeSO_4$.

The shake flask growth medium contained per liter: 3.00 g Na_2HPO_4, 1.50 g KH_2PO_4, 0.25 g NaCl, 0.50 g NH_4Cl, 0.05 g $MgSO_4$, 0.01 g $CaCl_2$, 2.00 g glucose monohydrate, 0.10 g potassium acetate. The fed-batch fermentation feed medium consisted of 700 $g \cdot L^{-1}$ glucose monohydrate and 109 $g \cdot L^{-1}$ potassium acetate.

Continuous fermentation feed medium was the same as fermentation medium with the following changes (per liter): no glucose monohydrate,

0, 10 and 20 g potassium acetate and 0.5 mL antifoam S 289 (for details see text). Pyruvate model solution used in the electrodialysis experiment was 48 $g \cdot L^{-1}$ sodium pyruvate in water.

TABLE A.4. Medium compositions used for *C. glutamicum* fermentations

Component	Unit	CM[a]	SK[b]	BR[c]	FBR[f]	Feed[h]
yeast extract	$\frac{g}{L}$	10	-	-	-	-
peptone	$\frac{g}{L}$	10	-	-	-	-
glucose H_2O	$\frac{g}{L}$	20	110	110/100[d]	40/10[g]	600
NaCl	$\frac{g}{L}$	2.5	-	-	-	-
$MgSO_4.7H_2O$	$\frac{g}{L}$	0.25	0.285	0.285	0.285	0.285
$(NH_4)_2SO_4$	$\frac{g}{L}$	-	46	60	30	-
urea	$\frac{g}{L}$	-	5	6	6	-
L-leucine	$\frac{g}{L}$	-	0.315	1.3	0.8	0.5
K_2HPO_4	$\frac{g}{L}$	-	0.5	0.5	0.5	0.2
KH_2PO_4	$\frac{g}{L}$	-	0.5	0.5	0.5	0.2
$CaCO_3$	$\frac{g}{L}$	-	5	-	-	-
biotine	$\frac{mg}{L}$	-	0.85	0.85	0.85	0.85
$FeSO_4.7H_2O$	$\frac{mg}{L}$	-	2.85	2.85	2.85	2.85
$MnSO_4.H_2O$	$\frac{mg}{L}$	-	1.165	1.165	1.165	1.165
$CuSO_4.5H_2O$	$\frac{mg}{L}$	-	0.0763	0.0763	0.0763	0.0763
$ZnSO_4.7H_2O$	$\frac{mg}{L}$	-	0.63	0.63	0.63	0.63
CoCl	$\frac{mg}{L}$	-	0.013	0.013	0.013	0.013
$NiCl.6H_2O$	$\frac{\mu g}{L}$	-	4.25	4.25	4.25	4.25
$Na_2MO_4.2H_2O$	$\frac{\mu g}{L}$	-	6.5	6.5	6.5	6.5
$KAlSO_4.12H_2O$	$\frac{mg}{L}$	-	0.019	0.019	0.019	0.019
$Na_2SeO_3.5H_2O$	$\frac{\mu g}{L}$	-	1.93	1.93	1.93	1.93
H_3BO_3	$\frac{\mu g}{L}$	-	5.0	5.0	5.0	5.0
$SrCl_2.6H_2O$	$\frac{\mu g}{L}$	-	5.0	5.0	5.0	5.0
$BaCl_2.2H_2O$	$\frac{\mu g}{L}$	-	5.0	5.0	5.0	5.0
Ca_2Cl	$\frac{g}{L}$	-	-	0.05	0.05	0.05
EDTA[e]	$\frac{g}{L}$	-	-	0.1	0.1	0.1
citric acid	$\frac{g}{L}$	-	-	0.1	0.1	0.1

[a]complex medium ; [b]synthetic shaking flaks medium used for preculters; [c]synthetic medium for the batch reactor with glucose as sole carbon source; [d]110 $g \cdot L^{-1}$ were used for the 30-L bioreactor and 100 $g \cdot L^{-1}$ for the 300-L bioreactor; [e]ethylenedinitrilotetraacetic acid; [f]synthetic (start) medium used for fed-batch fermentations; [g]40 $g \cdot L^{-1}$ for the 30-L bioreactor and 10 $g \cdot L^{-1}$ for the 300-L bioreactor;[h]feed medium for fed-batch process

A.3 Analytical Methods

A.3.1 Sampling During Sensor reactor Fed-batch Experiments with C. glutamicum

During the labeling period, $4\ mL$ samples were taken at 20 minute intervals from both reactors in order to quantify process similarities. At the end of the labeling period, approximately $5\ g$ cell-dry weight ($200\ mL$ cell suspension) were pumped out of the Sensor reactor into a $1000\ mL$ flask pre-filled with $800\ mL$ of 60 % (v/v) methanol ($-58°C$). As a result, cell metabolism was inactivated by methanol quenching. After this, aliquots of $50\ mL$ were prepared, and washed with 45 % (v/v) methanol at $–20°C$. In each case, two aliquots were filled into $30\ mL$ of 35 % (v/v) perchloric acid solution and the suspension was treated by ultrasound in an ice batch for 10 minutes (Bransonis 2200, Branson Ultrasonics, Danbury, USA). Using centrifugation for $30\ min$ at 41,000 g ($0\ °C$), the cell debris was separated and the supernatant subsequently neutralized with 5M K_2CO_3. Afterwards, the resulting precipitate of potassium chlorate was separated by $10\ min$ centrifugation at 4,500 g ($4°C$). The supernatant was freeze-dried.

A.3.2 Standard Analysis of C. glutamicum Fermentations

Biomass dry weight was determined gravimetrically and showed a good linear relationship with photometric turbidity measurements at $600\ nm$ ($CDW[g{\cdot}L^{-1}] = 0.25\ [g \cdot L^{-1}]{\cdot}OD_{600}$). Glucose was measured by using an enzymatic analysis kit (Boehringer, Mannheim, Germany) with hexokinase (EC 2.7.1.1.) and glucose-6-phosphate-dehydrogenase (EC 1.1.1.49). Amino acids were analyzed by HPLC after derivatization with ortho-phthaldi-aldehyde (OPA), separation on a reverse phase column and detection of the fluorescence of the OPA derivative [OF92]. Organic acids were measured by using an Aminex HPX-87H column (Biorad, Munich, Germany) eluted at 40 $°C$ with 0.2 N NaH$_2$SO$_4$. The UV absorption was detected at $254\ nm$.

A.3.3 Standard Analysis of E. coli Fermentations

The same standard analysis protocols for glucose, amino acids and organic acids were used for *E. coli* samples as for *C. glutamicum* samples, already described in the foregoing subsection. Turbidity measurements were performed at $620\ nm$ allowing the identification of a linear optical density/cell-dry weight correlation according to $CDW[g \cdot L^{-1}] = 0.25\ [g \cdot L^{-1}]{\cdot}OD_{620}$. Cell dry weight (CDW) was measured by filtration of 2.5 to 10.0 mL fermentation broth through a preweighted microfilter (0.2 μm cut off, Schleicher&Schuell; Germany). After drying the filter for 24 h at $80°C$ and postweighting, the cell dry mass was calculated. Immediately after

sampling, glucose was measured by an enzyme-based biosensor appliance Accutrend® (Hoffmann LaRoche Diagnostics; Switzerland) after appropriate dilution.

A.3.4   AAA Pathway Intermediates in the Fermentation Supernatant

2 mL of cell suspension was centrifuged at 13,000 g for 10 min and the supernatant was stored at –25°C prior to use. For ^{1}H-NMR 400 μL of culture supernatant was concentrated to dryness in a vacuum centrifuge and was redissolved in deuterium oxide (D_2O) containing 4 mM of the sodium salt of 3-(trimethylsilyl)propionic-2,2,3,3-d4 acid, TSP (Lancaster). The concentration of DAHP and its dephosphorylated derivative DAH in the NMR sample was calculated by a comparison of metabolite integrals with the integral of the TSP standard signal ($\delta = 0$ ppm). All ^{1}H-NMR spectra were recorded on a Bruker AMX300 FT-NMR spectrometer (300 MHz). DHS and shikimate (Sigma) were measured using HPLC with an Aminex HPX-87X column (Biorad) at 40 °C with 0.5 $mL \cdot min^{-1}$ 0.1 N H_2SO_4 and detection at 215 nm [MC85]. DHS was purified of the culture supernatant of *E. coli* DHS as described previously [DF93]. S3P was measured indirectly by converting it into shikimate with the aid of the enzyme alkaline phosphatase (Roche Diagnostics) and then correct it for the *in vivo* produced shikimate.

A.3.5 ^{1}H-NMR of C. glutamicum Fermentation Supernatants

Concentrations of glucose, lysine, leucine and by-products (such as trehalose, lactate, isopropylmalate) in culture supernatants were determined by using standard $1D$ ^{1}H-NMR. For each measurement, 0.35 mL of culture supernatant was mixed with 0.35 mL D_2O containing 2 mM sodium trimethylsilyl-(2,2,3,3-2H4) propionate (TSP; Aldrich) as the concentration standard. The spectral parameters used were as follows: 90° pulses, 8 kHz spectral width, 16 K data points, 15 s repetition time, 7 s presaturation time of the water signal and 8 accumulations. The samples obtained from the Sensor reactor were measured with broadband ^{13}C-decoupling using the GARP-1 composite pulse decoupling scheme.

A.3.6   Measurement of L-Phe Enrichments in the Supernatant

^{13}C NMR spectra (with proton decoupling) were recorded at 90.56 MHz in 5 mm tubes on a Bruker AMX 360. Prior to measurements, samples were lyophilized and redissolved in D_2O at twice the original concentration. A small amount of EDTA was added (5 $mg \cdot mL^{-1}$) to chelate the metal ions. To eliminate Noe (Nuclear Overhauser enhancement) and to ensure

quantitative results, the decoupler was switched off during the 45 s recycling delay (5 times the longest T1). Acquisition parameters: spectral width 240 ppm; pulse width 6 μs (90° flip angle); data size 80K; acquisition time 1.88 s; number of scans 4800. A line broadening of 1 Hz was applied and 128K data were used for the processed spectra. The enrichments were calculated from the integrals of the individual carbon atoms, where positions 2, 4 and 6+8 gave identical integral values and were assumed to not be enriched. For nomenclature details of the carbon position numbering see A.7.10.

A.3.7 Preparation of Proteinogenic Amino Acids

Proteinogenic amino acids were analyzed at the end of the labeling experiments using the Sensor reactor. The (almost) complete Sensor reactor content of several 100 mL was pumped in an ice-cold 1-L flask within 70 seconds and a culture equivalent of 4 g dry weight of cells was immediately centrifuged (4,500 x g, 10 min, 4 $°C$), washed in ice-cold demineralized water and stored at -70 $°C$. After lyophilization, 250 mg of freeze-dried cells was resuspended in 12 mL of 6.0 N HCl, hydrolyzed at 105 $°C$ in a sealed flask for 12 hours and 12 mL of demineralized water was added. The hydrolysate was filtrated to remove insoluble impurities, lyophilized and resuspended in 2 mL deuterium oxide (D$_2$O; Deutero, Kastellaun, Germany) containing 10 % trichloroacetic acid and 2 mM sodium trimethylsilyl-(2,2,3,3-2H4) propionate (TSP; Aldrich) as a chemical shift and concentration standard.

A.3.8 Isotopomer Analysis in the Proteinogenic Amino Acids of C. glutamicum

For the determination of isotopomer distributions in various amino acids, 0.7 mL of prepared hydrolysate was filled into a 5 mm NMR sample tube and analyzed by using two-dimensional $\left[^1H, ^{13}C \right]$ HSQC NMR spectroscopy [Szy95]. All NMR measurements were carried out on a Bruker AMX400-WB spectrometer system (Bruker, Karlsruhe, Germany) equipped with a 5 mm inverse probe head for ^{1}H at 400.13 MHz using the 2D-NMR parameters described previously [PdGE[+]00]. NMR data processing was performed using the Bruker XWINNMR software. Multiplets were extracted as 1D traces from the 2D spectrum by summing those traces along the ^{13}C-axis that contained the multiplet signals at a good signal-to-noise ratio. After a baseline correction, interactive integration was performed to obtain the relative intensities of singlet, doublet, triplet and quartet multiplet components needed for flux calculation.

A.3.9   Fine Structure of NMR Signals Used for C. glutamicum Growth Analysis

Total multiplet intensities for each specified carbon atom position are normalized as 100%. Abbreviations used: *s*, singlet peak (no neighboring labeled carbons); d_{-1} and d_{+1}, doublet peaks split by scalar coupling with different coupling constants to preceding or next carbon in a sequence, respectively; *dd*, doublet of doublet signals resulting from simultaneous identical scalar couplings to two neighboring labeled carbons; *ddd*, doublets of doublets of doublets signal resulting from simultaneous coupling to three neighboring carbons with all identical scalar coupling constants. Symbols in brackets are taken from [Szy95]. [a]Sum of d_{-1} and d_{+1}: peaks overlap because of equal or nearly equal coupling constants. [b]Coupling to carbon atom 3. [c]Two carbon atoms of tyrosine give rise to only one ^{13}C fine structure.

TABLE A.5. 13C labeling data of biomass compounds isolated from phase (1). Abbreviations used: Amino acid of the biomass (AA), Histidine (His), Glycine (Gly), Phenylalanine (Phe), Tyrosine (Tyr), Alanine (Ala), Glutamate (Glu), Asparatate (Asp), Threonine (Thr), Isoleucine (Iso), Valine (Val), Lysine (Lys)

AA	C-pos.	Fine structure of ^{13}C multiplet signal [%]				
		s	d_{-1}	d_{+1}	dd	ddd
His	2	27.1±1.0	6.6±2.0	6.3±3.0	59.9±3.0	
	3	31.7±1.0	31.5±2.0	5.3±3.0	31.4±2.0	
	5	41.8±1.0	58.2±3.0			
Gly	2	39.9±1.0	60.1±1.0			
Phe	2	31.3±1.0	3.0±3.0	10.4±2.0	55.4±1.0	
	3	28.8±2.0	61.7±4.0^a		9.6±3.0	
Tyr	5+9(δ^x)^c	29.3±2.5	60.5±2.0^a		10.2±4.0	
	6+8(ϵ^x)^c	42.9±1.0	24.3±1.5^a		32.8±3.0	
Ala	2	30.9±1.0	3.4±2.5	8.4±2.0	57.3±1.0	
	3	35.5±1.0	64.5±1.0			
Glu	2	42.9±2.5	27.1±2.0	22.0±3.0	7.9±4.0	
	3	66.5±1.0	30.5±2.0^a		3.1±2.0	
	4	32.3±1.0	2.5±1.5	61.2±1.0	4.0±2.5	
Asp	2	43.2±1.0	27.1±2.0	6.3±1.0	23.4±2.0	
	3	43.8±1.0	23.0±1.0	26.8±1.0	6.4±1.5	
Thr	2	45.2±2.0	26.8±1.0	7.1±2.0	21.0±1.5	
	3	43.0±1.0	48.4±1.0^a		8.5±2.6	
	4	63.1±1.0	36.9±1.0			
Iso	3	35.8±1.0	51.0±3.0^a		9.2±5.0	4.0±4.0
	4	58.7 ±1.0	31.4±2.0^a		9.9±6.0	
	5	72.0±1.0	28.0±2.5			
	6	45.3±1.0	54.7±3.0			
Val	3	36.1±2.0	52.4±3.0^a		7.5±3.0	4.0±4.0
	4 (γ^1)	45.1±1.0	54.9±3.0			
	5 (γ^2)	90.9±1.0	9.1±2.0^b			
Lys	3	43.0±2.0	52.0±3.0^a		5.0±3.0	
	4	56.4±1.0	31.2±4.0^a		12.4±5.0	
	5	36.0±2.0	56.8±3.0^a		7.2±3.0	
	6	46.3±1.0	53.7±3.0			

TABLE A.6. 13C labeling data of biomass compounds isolated from phase (2). Abbreviations used: Amino acid of the biomass (AA), Histidine (His), Glycine (Gly), Phenylalanine (Phe), Tyrosine (Tyr), Alanine (Ala), Glutamate (Glu), Asparatate (Asp), Threonine (Thr), Isoleucine (Iso), Valine (Val), Lysine (Lys)

AA	C-pos.	Fine structure of ^{13}C multiplet signal [%]				
		s	d_{-1}	d_{+1}	dd	ddd
His	2	27.1±1.0	4.9±2.0	2.2±3.0	59.9±3.0	
	3	29.4±1.0	33.4±2.0	6.4±3.0	30.9±2.0	
	5	44.8±1.0	55.2±3.0			
Gly	2	38.1±1.0	61.9±1.0			
Phe	2	29.9±1.0	3.3±3.0	8.1±2.0	58.7±1.0	
	3	27.5±2.0	64.6±4.0^a		7.9±3.0	
Tyr	5+9(δ^x)^c	28.5±2.5	63.0±2.0^a		8.5±4.0	
	6+8(ϵ^x)^c	42.8±1.0	24.1±1.5^a		33.2±3.0	
Ala	2	29.1±1.0	2.6±2.5	8.3±2.0	59.9±1.0	
	3	33.6±1.0	66.4±1.0			
Glu	2	41.0±2.5	29.2±2.0	23.8±3.0	6.0±4.0	
	3	67.2±1.0	30.3±2.0^a		2.5±2.0	
	4	30.4±1.0	2.5±1.5	63.0±1.0	4.1±2.5	
Asp	2	41.8±1.0	29.3±2.0	6.5±1.0	22.3±2.0	
	3	43.1±1.0	22.6±1.0	28.5±1.0	5.8±1.5	
Thr	2	41.9±2.0	29.0±1.0	6.1±2.0	23.0±1.5	
	3	41.9±1.0	50.5±1.0^a		7.6±2.6	
	4	63.2±1.0	36.8±1.0			
Iso	3	33.8±1.0	56.8±3.0^a		6.1±5.0	4.0±4.0
	4	65.4 ±1.0	30.9±2.0^a		3.7±2.5	
	5	72.0±1.0	28.0±2.5			
	6	42.5±1.0	57.5±3.0			
Val	3	35.8±2.0	52.5±3.0^a		7.8±3.0	4.0±4.0
	4 (γ^1)	47.1±1.0	52.9±3.0			
	5 (γ^2)	91.1±1.0	8.9±2.0^b			
Lys	3	40.8±2.0	53.5±3.0^a		5.8±3.0	
	4	54.3±1.0	30.7±4.0^a		15.0±5.0	
	5	33.6±2.0	57.8±3.0^a		8.5±3.0	
	6	44.2±1.0	55.8±3.0			

TABLE A.7. 13C labeling data of biomass compounds isolated from phase (3). Abbreviations used: Amino acid of the biomass (AA), Histidine (His), Glycine (Gly), Phenylalanine (Phe), Tyrosine (Tyr), Alanine (Ala), Glutamate (Glu), Asparatate (Asp), Threonine (Thr), Isoleucine (Iso), Valine (Val), Lysine (Lys)

AA	C-pos.	Fine structure of ^{13}C multiplet signal [%]				
		s	d_{-1}	d_{+1}	dd	ddd
His	2	31.9±1.0	5.2±2.0	3.0±3.0	60.0±3.0	
	3	32.4±1.0	36.3±2.0	4.8±3.0	26.5±2.0	
	5	51.9±1.0	48.1±3.0			
Gly	2	42.51±1.0	57.5±1.0			
Phe	2	31.5±1.0	3.8±3.0	7.7±2.0	57.0±1.0	
	3	31.0±2.0	57.5±4.0^a		11.5±3.0	
Tyr	5+9(δ^x)^c	31.6±2.5	58.3±2.0^a		10.1±4.0	
	6+8(ϵ^x)^c	44.5±1.0	23.3±1.5^a		32.3±3.0	
Ala	2	32.6±1.0	3.1±2.5	6.8±2.0	57.5±1.0	
	3	36.6±1.0	63.4±1.0			
Glu	2	39.2±2.5	30.1±2.0	18.9±3.0	11.8±4.0	
	3	65.1±1.0	31.1±2.0^a		3.9±2.0	
	4	27.3±1.0	2.1±1.5	62.7±1.0	7.9±2.5	
Asp	2	45.3±1.0	27.8±2.0	6.0±1.0	20.9±2.0	
	3	46.7±1.0	19.6±1.0	27.3±1.0	6.4±1.5	
Thr	2	49.7±2.0	25.5±1.0	6.2±2.0	18.6±1.5	
	3	50.6±1.0	43.7±1.0^a		5.7±2.6	
	4	65.7±1.0	34.3±1.0			
Iso	3	38.38±1.0	49.2±3.0^a		9.5±6.0	3.0±3.0
	4	64.9 ±1.0	27.3±2.0^a		7.8±6.0	
	5	70.6±1.0	29.4±2.5			
	6	46.4±1.0	53.6±3.0			
Val	3	53.2±3.0	33.2±3.0^a		5.9±3.0	7.7±6.0
	4 (γ^1)	59.1±1.0	40.9±3.0			
	5 (γ^2)	90.8±1.0	9.2±2.0^b			
Lys	3	43.3±2.0	50.8±3.0^a		5.9±3.0	
	4	51.8±1.0	35.9±4.0^a		12.4±5.0	
	5	32.8±2.0	55.6±3.0^a		11.5±3.0	
	6	42.3±1.0	57.7±3.0			

A.3.10 Fine Structure of NMR Signals Used for Analysis of L-lysine Production in C. glutamicum

Total multiplet intensities for each specified carbon atom position are normalized as 100%. Abbreviations used: s, singlet peak (no neighboring labeled carbons); d_{-1} and d_{+1}, doublet peaks split by scalar coupling with different coupling constants to preceding or next carbon in a sequence, respectively; dd, doublet of doublet signals resulting from simultaneous identical scalar couplings to two neighboring labeled carbons;Symbols in brackets are taken from [Szy95]. [a]Sum of $d_{-1}$and d_{+1}: peaks overlap because of equal or nearly equal coupling constants.

TABLE A.8. 2D-NMR isotopomer 13C labeling data focussing on the C-atome of different metabolites and amino acids during L-lysine production phase 1 using *C. glutamicum* MH20-22B

cytoplasmic compound	C-pos.	Fine structure of ^{13}C multiplet signal [%]			
		s	d_{-1}	d_{+1}	dd
trehalose	1	26.2±2	73.8±3.0		
	2	22.4±2.5	15.9±4^a		61.7±8
	3	36.2±5	13.3±5^a		50.6±10
	4	30.4±8	20.6±5^a		49.0±11
	5	19.6±5	6.0±2.5^a		74.4±8
aspartate	2	24.5±2	37.5±2	8.1±3	29.9±4
	3	24.1±1	25.5±1	35.4±1	14.9±2
alanine	2	6.5±2.5	3.7±3	3.8±3	86.1±7
	3	16.2±2	83.8±2.5		
citrate	2	20.5±3	51.5±3	15.5±3.5	12.5±3.5
	4	20.5±3	15.5±3.5	51.5±3	12.5±3.5
valine	4	29.2±3	70.8±4		
	5	90.4±2	9.6±4		
glutamate	2	24.5±1.5	34.2±2	32.3±2	9.1±2.5
	3	48.9±2	45.3±2^a		5.9±1.5
	4	13.5±1.5	1.4±0.7	74.1±1.5	11.0±2
isoleucine	4	63.7±3	33.9±5^a		2.4±2
	5	69.2±1.5	30.8±3		
	6	30.3±1.5	69.7±1.5		
lysine	3	40.1 ±30	54.2±2.5^a		5.7±1.5
	4	57.7±40	37.4±3^a		5.0±2
	5	34.9±20	56.3±3.5^a		8.9±3
	6	42.5±30	57.5±4		
threonine	2	27.7±2	32.5±1.5	10.3±2.5	29.5±2.5
	3	19.9±3	61.1±2^a		18.9±3
	4	56.3±1.5	43.7±1.5		

TABLE A.9. 2D-NMR isotopomer 13C labeling data focussing on the C-atome of different metabolites and amino acids during L-lysine production phase 2 using *C. glutamicum* MH20-22B

cytoplasmic compound	C-pos.	Fine structure of ^{13}C multiplet signal [%]			
		s	d_{-1}	d_{+1}	dd
trehalose	1	26.3±2	73.8±3.0		
	2	25.5±2.5	16.4±4^a		61.7±8
	3	42.7±5	10.7±5^a		50.6±10
	4	37.2±8	15.4±4.5^a		49.0±11
	5	22.9±5	2.4±2.5^a		74.4±8
aspartate	2	21.4±2	33.7±2	12.4±3.5	29.9±4
	3	24.2±1	33.8±1	28.1±1	14.9±2
alanine	2	9.1±2.5	1.8±2	4.0±3	86.1±7
	3	15.7±2	84.3±2.5		
citrate	2	16.2±3	53.1±2.5	18.2±3.5	12.5±3.5
	4	20.5±3	18.2±3.5	53.1±2.5	12.5±3.5
valine	4	25.0±3	75.0±4		
	5	89.2±2	10.8±4.5		
glutamate	2	23.8±1.5	35.0±2	31.2±2	9.1±2.5
	3	49.9±2	44.8±2^a		5.9±1.5
	4	12.7±1.5	2.0±0.8	75.4±1.5	11.0±2
isoleucine	4	60.6±3	33.2±5^a		2.4±2
	5	71.5±1.5	28.5±3		
	6	31.6±1.5	68.4±1.5		
lysine	3	44.7 ±30	50.5±2.5^a		5.7±1.5
	4	60.7±3.5	35.3±3^a		5.0±2
	5	39.2±20	52.4±3.5^a		8.9±3
	6	48.1±30	51.9±4		
threonine	2	28.4±2	31.5±1.5	9.5±2.5	29.5±2.5
	3	25.9±3	59.0±2^a		18.9±3
	4	56.8±1.5	43.2±1.5		

A.3.11 PEP Carboxykinase Assay

Studying the anaplerotic reactions of *C. glutamicum*, the intracellular activity of PEP carboxykinase was measured to qualify the *MFA* findings. To determine PEP carboxykinase activity in cell-free extracts, *C. glutamicum cells* (0.3 - 0.5 *g*) were harvested by centrifugation after each Sensor reactor fermentation (4,500 x *g*, 10 *min*, 4°*C*), washed in disruption buffer [PMdG$^+$01] and resuspended in 1 *mL* of the same buffer. The cells were disrupted on ice for 7 *min* by sonication using a UP 200S ultrasonic disintegrator (Dr. Hielscher, Teltow, Germany, settings: amplitude 55 %, cycle 0.5) and cell debris were removed by centrifugation for 30 minutes at 15,000 x *g* at 4°*C*. The resulting crude extracts were used for the determination of specific PEP carboxykinase activity in the direction of oxaloacetate formation as described previously [PMdG$^+$01] monitored by following the decrease in absorbance of NADH at 340 *nm*. The protein concentrations in the crude extracts were determined with bicinchoninic acid according to a protocol adapted from the work of Smith *et al.* [SKH$^+$85] using bovine serum albumin as standard.

A.3.12 DAHP Activity Measurements

DAHP-synthase activity depends on different regulation mechanisms [Pit96] and was measured in *E. coli* strains using the method of Schoner and Herrmann [SH76] as follows: 2 *mL* fermentation broth was centrifuged, and washed three times by ice cold 0.9 % NaCl solution. Cell pellets were dissolved in 1.0 *mL* buffer containing 10 *mM* BTP (1,3-bis(tris(hydroxymethly)-methyl-amino)propane) and 0.2 *mM* PEP (phosphoenolpyruvate). Cells were disrupted by ultrasonic treatment in an ice bath. The homogenized cells were centrifuged at 4°*C* lasting for 1 *h* at 15,300 *rpm* (21,460 *g*) and the supernatant was used as cell-free extract for the determination of protein content ('Bradford'-assay [Bra76]) and DAHP-synthase activity. For activity measurement 50 *μL* cell extract (after an appropriate dilution that depends on the protein concentration), 500 *μL* BTP solution (100 *mM* BTP in distilled water), 50 *μL* PEP solution (10 *mM* PEP in distilled water), 10 *μL* FeSO$_4$ solution (1 *mM* FeSO$_4$*7 H$_2$O in distilled water) and 360 *μL* distilled water were merged and changes in absorption were measured in a photospectrometer (DU 640, Beckmann; Germany) at 232 *nm*. At halftime measurement the addition of 30 *μL* E4P solution (50 *mM* erythrose-4-phosphate in distilled water) started the enzyme reaction leading to a decrease of absorption. Equation A.1 was used to calculate the DAHP-synthase activity:

$$Activity[U] = \frac{\Delta A \diagup \min \cdot V}{\epsilon \cdot v \cdot d} \tag{A.1}$$

With: $\Delta A \diagup \min$ - change of absorption per minute main run, corrected by the pre-run; V - starting volume [μL]; ϵ - extinction coefficient (28,800

$M^{-1} \cdot cm^{-1}$); v - sample volume [μL]; d - layer thickness of the cuvette [cm]. The activity divided by the protein concentration resulted in the biomass-specific enzyme activity ($U_{spec.}$).

A.3.13   2D-NMR Measurements for Supernatant Analysis

For two-dimensional (2D) $\left[^1H,^{13}C\right]$ HSQC-NMR spectroscopy ([PdGE$^+$00], [PMdG$^+$01]), the total amount of dried supernatant – containing the cytoplasmic components of approximately 5 g biomass (cell-dry weight) - was dissolved in 2 mL D$_2$O containing 10 % (v/v) trichloroacetic acid and 2 mM of the chemical shift standard sodiumtrimethylsilylproprionate-2,2,3,3-d4 (TSP) (Aldrich) at pH 1.0. 700 μL were used for NMR measurements in 5 mm NMR tubes (Norell, Mays Landing, USA) in a Bruker AMX400-WB spectrometer system (Bruker, Karlsruhe, Germany). The measurement device was equipped with a 5 mm inverse probe head for ^{1}H analysis at 400.13 Mhz. NMR data processing was performed using the Bruker XWINNMR software.

A.3.14   Isotopomer Labeling Used for MFA with E. coli

Please note that data correction followed the procedure described in subsection A.5.5.

TABLE A.10. Lable measurements at certain C-positions focusing on L-Phe in the culture supernatant. Corrections owing to signal dilution (13C memory effect) are included. p denotes the fraction of L-Phe produced during the labeling experiment compared to the total amount found in the supernatant.

	raw data			corrected data	
	C3 [%]	C5+C9 [%]	p [%]	C3 [%]	C5+C9 [%]
phase 1	4.50	3.90	39.26	9.76	8.23
phase 2	3.80	3.10	23.66	12.51	9.55
phase 3	3.20	2.60	11.83	18.86	13.78

A.3.15   Reactive Extraction with Separation Funnels

Before experiments, separation funnels were filled with equal volumes of aqueous and organic phase (organic phase consisted of a mixture of solvent with 10 % v/v carrier). Then funnels were shaken intensively for 2 minutes to ensure a good mixture of aqueous and organic phase. After this, at least 10 minutes were taken for phase settling. When phase separation had been completed, the aqueous phase was analyzed and the organic phase was used for back extraction. Back extraction was performed by mixing

the preloaded organic phase with an equal volume of stripping phase in separation funnels. In the stripping phase counter ions were added to enable the L-Phe unloading of the carrier. As a result L-Phe was extracted into the stripping phase and the carrier was loaded with corresponding ions from the stripping phase. L-Phe titers in the aqueous phase were measured via HPLC analysis in order to estimate the amount of extracted L-Phe and to calculate the degree of extraction E according to

$$E = \frac{c_{Phe,aq}^{eq}}{c_{Phe,org}^{eq}} \cdot 100 \qquad (A.2)$$

$c_{Phe,aq}^{eq}$ and $c_{Phe,org}^{eq}$ are the equilibrium concentrations of L-Phe in the aqueous and organic phase after extraction, respectively. While $c_{Phe,aq}^{eq}$ is accessible via HPLC measurement, $c_{Phe,org}^{eq}$ can be estimated using L-Phe mass balance with the aid of the aqueous L-Phe concentration $c_{Phe,aq,0}$ which was measured before extraction was started.

A.4 Technical Set-up

A.4.1 Sensor Reactor

Bioreactors

The 300-L stirred tank reactor (Chemap, Volketswil, Switzerland) was inoculated with a preculture from a 30-L bioreactor (same manufacturer) and contained 160 L of synthetic medium. The temperature setpoint was 30 $°C$ and the pH was automatically maintained at 7.0 by adding 25 % NH$_4$OH. Pressure and air flow were set manually. The stirrer speed was controlled automatically to maintain the dissolved oxygen level DO at 30 % CO$_2$ and O$_2$ in the exhaust gas were analyzed by an off-gas analyzer with NIR and paramagnetic sensors (Fischer-Rosemount, Haan, Germany).

Sensor Reactor

The Sensor reactor (Infors, Basel, Switzerland) is a specially designed stainless steel stirred tank reactor with a total volume of 2 L and a maximum working volume of 1.2 L. The stirrer is driven by a magnetic coupling which allowed stirrer speeds of up to 1500 rpm (during fermentations usually 400-800 rpm). The Sensor reactor is equipped with a pH and DO electrode (Mettler Toledo,Giessen, Germany). Additionally a pressure sensor (piezoelectric device, Infors, Basel, Switzerland) is coupled to the off-gas cooler of the Sensor reactor. A device consisting of a welded steel tube, a flexible tube and a quick disconnect coupling (type 6-DB,Gather Industrie, Mettmann, Germany) connected the Sensor reactor to a rapid inoculation unit. Samples were taken manually by a special sampling unit.

Automated control of the Sensor reactor was performed by a LABFORS ® control unit (Infors, Basel, Switzerland). Air flow was adjusted manually. The DO was regulated by automated control of the rpm and pH was controlled by automatically adding a 10 % NH$_4$OH solution. The temperature was controlled by a combination of heating with an electric blanket and cooling with water.

Mixing Time Measurements

Mixing time measurements were performed in the Sensor reactor using a pulsing device controlled by the central process control unit. The pulsing device consisted of a storage tank with a maximum volume of 60 mL, which was connected via a quick disconnect coupling (Swagelok, B.E.S.T, Cologne, Germany) to a solenoid valve (type 330, Bürkert, Menden, Germany) and the Sensor reactor. Mixing time experiments were performed by using glucose solutions (250 $g \cdot L^{-1}$ or 500 $g \cdot L^{-1}$) with KCl as a tracer substance. The conductivity was measured with a microelectrode (Microelectrodes Inc., Bedford, USA) and a conductivity meter (LF300, WTW, Weil-

heim, Germany). Data acquisition was performed with a measurement device (AT-MIO-16XE-50, National Instruments Corporation, Austin, USA) installed in the central process unit (Pentium II $^{\circledR}$, Windows $^{\circledR}$). The electrode was installed near the outlet valve of the Sensor reactor.

Process Control

The fermentation parameters of pH, pressure, DO and temperature measured in the Sensor reactor were controlled automatically by a LABFORS $^{\circledR}$ control unit. The actual process data of pH, DO, pressure and temperature were collected from the control unit of the 300-L reactor (update time 1 s), sent to a central process unit (Pentium II $^{\circledR}$, Windows $^{\circledR}$) and processed by special control software (LABVIEW, National Instruments Corporation, Austin, USA). A moving average of 5 measuring points was calculated and routed to the LABFORS $^{\circledR}$ control unit (30 to 60 seconds update) to serve as new setpoints for the automated regulation of the Sensor reactor.

A.4.2   E. coli Fermentations

Typically, exhaust gas analysis was applied for oxygen and carbon dioxide measurements using a BINOS 100 2M System (Rosemount, Germany). Dissolved oxygen (DO) was determined with an amperometric electrode (Mettler-Toledo, Germany). Data acquisition was performed via MEDUSA, an in-house software development. This software tool is currently replaced by LABVIEW (National Instruments Corporation, Austin, USA).

A.4.3   On-line Glucose Control

The application of on-line glucose concentration measurement and its control during (fed-) batch fermentations is not a new approach. Several studies are already published. Examples are given by Kleman *et al.* ([KCLS91b], [KCLS91a]), Kelle *et al.* [KLB^{+}96] and Hitzmann *et al.* [HBC^{+}00].

Three peristaltic pumps (U 501 and U 101, Watson&Marlow; Germany) were used to ensure continuous sampling. With a flow rate of 800 $mL \cdot min^{-1}$ the biosuspension was pumped through the by-pass (total volume: $\sim$20 mL, mean residence time: $\sim$2s) containing a cross-flow hollow fiber ultrafiltration unit (500 kDa cut-off, 23 cm^2 filtration area, Schleicher&Schuell, Germany). 1.0 - 2.0 $mL \cdot min^{-1}$ cell-free permeate was drained off and pumped to the manifold of the sequential on-line glucose measurement system (OLGA, IBA GmbH; Germany) where 10 μL samples were drained off for analysis every 120 s. Unused permeate was recycled into the bioreactor. Hence, not more then 100 mL permeate was used for on-line glucose measurement during fermentation. The whole sampling system was sterilized

with 1 M NaOH at 50°C for 30 min. Measured values of glucose concentrations were subsequently used to estimate glucose consumption rates as well as derivatives of the glucose consumption rates by application of a semi-continuous, extended Kalman-Filter [Wie91] which was combined with a minimal variance controller [Str93] to calculate necessary glucose pump rates (see Bastin and Dochain [BD90a]).

As a technical alternative to the OLGA system, the Process Trace System was used (Trace AG, Braunschweig) which simplified the experimental set up by using a probe instead of an ultrafiltration by-pass to prepare cell-free permeate which has to be further pumped to the analyzer. This system was used in the experiments as indicated in the text.

A.4.4 Electrodialysis

The experimental equipment for electrodialysis used a three-compartment water splitting electrodialysis (WSED) unit (Goema, Germany, Figure A.1) with a membrane stack having four cells pairs.

The three-compartment WSED stack consisted of anion-exchange, cation-exchange and bipolar membranes (Tokuyama Co., Japan) with a total effective membrane area of 0.56 m^2. An electric power unit (Rohde & Schwarz, Germany) supplied power to the WSED stack such that a constant current in the range of 5 A was realized. The WSED consisted of four solution tanks providing the acid, the base, the feed and the electrode rinse solution. Initially the acid and the base compartments were filled with demineralized water. All streams were recycled using centrifugal pumps (Iwaki Co., Japan) at a flow rate of 1 $L \cdot h^{-1}$. pH (Methrom, Germany) and conductivity (WTW, Germany) of the acid, the base and the feed solutions were measured continuously. 0.5 $mol \cdot L^{-1}$ Na$_2$SO$_4$ was used as the electrolyte solution.
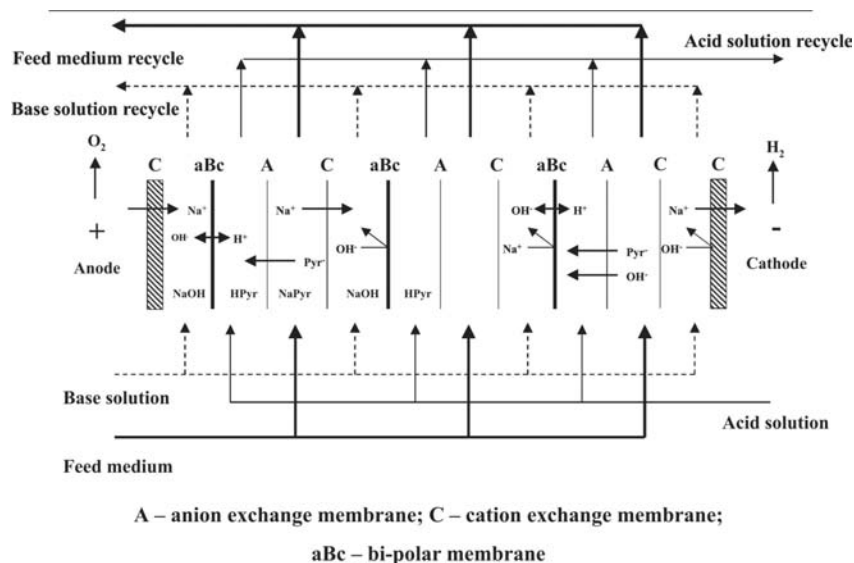
FIGURE A.1. Basic principle of three-compartment electrodialysis. Pyruvate ions and sodium ions in the feed compartment simultaneously moved into the acid and the base compartment through anion- and cation-exchange membranes, respectively, during ED operation. Free pyruvic acid was formed by combination of pyruvate ions and hydrogen ions generated on the cation-exchange layer of the bipolar membrane. Sodium hydroxide was simultaneously generated by the combination of sodium ions and hydroxyl ions formed on the anion-exchange side of the bipolar membrane. The electrolyte solution was circulated continuously to transfer the electric current and to remove gases (O_2 and H_2) produced by the electrode reaction during the operation of the ED. A - anion exchange membrane; C - cation exchange membrane; aBc - bipolar membrane; HPyr - pyruvic acid; Na^+ - sodium ions; Pyr^- - pyruvate ions

A.5   Sensor Reactor Labeling

A.5.1   C. glutamicum in Batch Process

The fermentation was started in the production reactor with a working volume of 160 L with an initial OD_{600} of 3.8 and an initial glucose concentration of 130 $g \cdot L^{-1}$. Labeling experiments were performed during the exponential growth phase after 8.5, 11 and 14 hours of cultivation. Each labeling experiment started when an inoculum of about 1 L was drained off the production reactor into the Sensor reactor and $\left[U - ^{13}C\right]$ glucose (Cambridge Isotope Laboratories, Andover, MA) was added immediately to the culture in the Sensor reactor (phase 1: 4 g, phase 2: 3 g and phase 3: 2 g, respectively). The final concentrations of $\left[U - ^{13}C\right]$ glucose in all three Sensor reactor phases were determined by NMR spectroscopy to be

7.7 % (phase 1), 7.2 % (phase 2) and 10.5 % (phase 3) of the total glucose, respectively. After the addition of the $\left[U-^{13}C\right]$ glucose, both reactors were run for approximately 2 hours in parallel while 2-mL samples were taken at 30-minute intervals from both reactors in order to quantify process similarities.

A.5.2   Correction for Incomplete Labeling of Biomass

When the growth phase of *C. glutamicum* was studied using ^{13}C based metabolic flux analysis, it was considered that the 2 - 3 hours of labeling were (most presumably) not sufficient to achieve stationary labeling patterns in the proteinogenic amino acids. Therefore the measured NMR signals of the labeled samples were subsequently corrected such that only a fraction of labeled glucose was used as input value for metabolic flux analysis. The basic motivation of this simplifying procedure was given by Drysch *et al.* [DMM+03] as follows:

In an experiment employing a fraction L of $\left[U-^{13}C\right]$ glucose together with a fraction $(1-L)$ of unlabeled glucose as the sole carbon sources, the ^{13}C labeling p at true steady state of any metabolite carbon in the system under investigation (including biomass) equals:

$$p = (1-L) \cdot 0.011 + L \cdot 1.0 \tag{A.3}$$

where 0.011 is the natural abundance ^{13}C labeling and the $\left[U-^{13}C\right]$ glucose is assumed to be 100% pure.

If $L \ll 1$ the carbons originating from naturally labeled glucose backbone fragments will rarely give rise to any other than singlet signals in ^{13}C NMR, and it follows from A.3 that in this case the ^{13}C NMR multiplet signal m extracted from a 2D HSQC spectrum can be represented as

$$m = (1-L) \cdot 0.011 \cdot S + L \cdot 1.0 \cdot M \tag{A.4}$$

where S symbolizes a unity area singlet peak and M a unity area multiplet pattern (composed of singlet, doublets, triplet and/or doublet-of-doublet peaks).

The investigations of *C. glutamicum* growth phase were performed as batch experiments with excess glucose in the Sensor reactor. The reactor was inoculated to a cell density of X_1 of unlabeled cells at the start of the experiment. Simultaneously, a pulse of $\left[U-^{13}C\right]$ labeled glucose was added to the residual unlabeled medium typically resulting in a final fraction $L < 0.08$ of labeled glucose. Thereafter, cells grew on the mixture of labeled and unlabeled glucose to a density of X_2 and were then harvested, hydrolyzed and subjected to NMR analysis. Therefore, the measured NMR signal from

the cells cultivated in the Sensor reactor contains a fraction $\frac{X_1}{X_2}$ of singlet signal exclusively contributed by unlabeled cells and a fraction $\frac{X_2 - X_1}{X_2}$ of combined singlet and multiplet pattern signals as defined by Eq. A.4 from the labeled biomass. In analogy to Eq. A.4 it follows that the measured NMR signal n can be written as

$$n = (1 - L^*) \cdot 0.011 \cdot S + L^* \cdot 1.0 \cdot M \qquad (A.5)$$

where

$$L^* = \frac{X_2 - X_1}{X_2} \qquad (A.6)$$

The fact that Eqs. A.4 and A.5 take identical forms shows that to first order, the incomplete labeling of the biomass as encountered in our experiments can simply be accounted for by using a fraction of labeled glucose L^* as given by Eq. A.6 as input to the flux estimation algorithm instead of the true L. Given the fact that typically $L < 0.08$ and in view of the fact that during 2 - 3 hours of batch cultivation a true metabolic steady state cannot be expected, this approximation is thought to be adequate for these first Sensor reactor experiments. It is noteworthy that alternative approaches are already under investigation to allow ^{13}C based MFA of growing cells within 'short' labeling experiments using the Sensor reactor (see 3.6).

A more fundamental concern regarding isotopic stationarity focussing proteinogenic amino acids is that after application of the pulse of labeled glucose, the free metabolites in the cell go through a transient phase during which their isotopic labeling gradually approaches steady state. Since protein synthesis also takes place during this phase, these transient isotopic labeling patterns are also stored in the proteinogenic amino acids and potentially interfere with the analysis which is based on full isotopic stationarity during the complete incubation (this also applies to Eqs. A.3 to A.5). The mathematical treatment of these phenomena requires complex instationary approaches and is still under investigation (see 3.6).

However, a first approximation of the relevance of such transient effects can be made by considering the carbon throughput in the system. During the growth phase, *C. glutamicum* exhibited specific glucose uptake rates of 3.2 $mmol \cdot g_{CDW}^{-1} \cdot h^{-1}$, i.e. 19.2 $mmol_{carbon} \cdot g_{CDW}^{-1} \cdot h^{-1}$. As a more or less realistic figure for *C. glutamicum* MH20-22B one might assume ,for example, that the major intracellular free metabolite components are 100 mM glutamate, 50 mM glutamine, 25 mM aspartate, 20 mM lysine and 30 mM trehalose and C6 branched chain amino acids, i.e. a total carbon content of 1150 mM carbon, or 2.3 $mmol_{carbon} \cdot g_{CDW}^{-1}$. Therefore, one would expect a turnover time of this total free metabolite pool of 0.12 hours, or 7 minutes. While this value is necessarily somewhat arbitrary,

the order of magnitude nevertheless should be representative of the true *in vivo* situation and it seems sufficiently short in comparison to the total incubation times of 2 - 3 hours employed in the Sensor reactor study to exclude a significant distortion of the analyses. Please notice that additional measurement for turnover times are given in section 3.4.2.

A.5.3   Labeling Non-Growing C. glutamicum in a Fed-Batch Process

For labeling, $[U-^{13}C]$ glucose (99 % atom enrichment, Cambridge Isotope Laboratories, Andover, MA) was used. To ensure a 15 % content of labeled glucose in the Sensor reactor immediately upon the start of the labeling period, samples were taken out of the 300-L reactor before the inoculation of the Sensor reactor, and the glucose concentration was measured. From this, the liquid volume of the glucose pulse containing 140 $g \cdot L^{-1}$ $[U-^{13}C]$ glucose was calculated and injected immediately after inoculation such that the resulting glucose ^{13}C enrichment was 15 %. Then, the glucose feed (600 $g \cdot L^{-1}$) was started, containing 15 % labeled glucose. Following this procedure, the glucose ^{13}C enrichment was kept constant at 15 % at all times during the whole labeling period of 3 h in the Sensor reactor.

A.5.4   Labeling Non-Growing E. coli in a Fed-Batch process

In general, the ^{13}C labeling of non-growing *E. coli* under fed-batch conditions followed the same procedure as already described in the preceding subsection, however $[1-^{13}C]$ glucose was used instead of $[U-^{13}C]$ glucose in the case of *C. glutamicum*. $[1-^{13}C]$ glucose was chosen considering the results of Möllney *et al.* [MWKdG99] and own studies [Sch99b].

   Immediately before each labeling experiment, the current glucose concentration of the production process was measured and the liquid volume containing 140 $g \cdot L^{-1}$ $[1-^{13}C]$ glucose (99% atom enrichment, Cambridge Isotope Laboratories, Andover, MA) was calculated and subsequently pulsed into the Sensor reactor to ensure a 25% content of labeled glucose. Then, the scaled-down glucose feed of the Sensor reactor was started, containing the same fraction (25%) of labeled glucose. Following this procedure, the ^{13}C enrichment was kept constant at 25% throughout the whole labeling period. Samples were taken in 20 min intervals from the Sensor reactor and from the production process. They were centrifuged and the supernatant was stored at -20°C for subsequent HPLC and NMR analysis.

A.5.5 Correction for ^{13}C Memory Effects in the Culture Supernatant

As outlined in section 3.5, the ^{13}C labeling analysis using L-Phe producing *E. coli* was focused on the culture supernatant, namely the accumulated (by-) products, which originated from the microbial production during the labeling period. Because a (significant) amount of already produced and natively (1.1%) labeled (by-) products were found in the samples of the labeling experiments, the NMR signals obtained had to be corrected such that only the ^{13}C labeling information which originated from the labeling period was calculated and could thus be used for subsequent metabolic flux analysis.

As a basic assumption it was assumed that the Sensor reactor was in pseudo-steady state, i.e. the intra- and extracellular fluxes were constant over the timespan of the labeling experiment leading to equilibrated labeling patterns in the metabolite pools. Then, the measured ^{13}C enrichments of the supernatant pools had to be corrected due to the dilution by non-labeled metabolites which were produced before the labeling experiment.

Therefore, the enrichment (x) [%] achieved during the labeling period was calculated from the ^{1}H - NMR measurements (y) [%] with the molar fraction (p) [mol/mol %] of produced L-Phe following the equation

$$y = p \cdot x + (1 - p) \cdot 0.011 \tag{A.7}$$

leading to

$$x = \frac{y - (1 - p) \cdot 0.011}{p} \tag{A.8}$$

Raw and corrected data are given in Table A.10.

A.6 Mathematics

A.6.1 Total Differential Operator

The following illustrative example is taken from Hurlebaus [Hur01].

To illustrate the difference between the total differential operator $\mathbf{D_x}$ and the partial derivative $\frac{\partial}{\partial x}$ the following equation is considered:

$$f(x, y, t) = x^2 + y^2 + t \tag{A.9}$$

with

$$x(t) = \sin t \tag{A.10}$$

$$y(t) = \cos t \tag{A.11}$$

Obviously, the partial derivatives result in the following equations

$$\frac{\partial f}{\partial x} = 2x \tag{A.12}$$

$$\frac{\partial f}{\partial y} = 2y \tag{A.13}$$

$$\frac{\partial f}{\partial t} = 1 \tag{A.14}$$

Please notice that only one variable is considered in each derivative while the others were regarded as constant. Instead, the total differential operator considers each variable to be a function of t leading to the equation system

$$\mathbf{D_x} = \begin{pmatrix} D_x \\ D_y \\ D_t \end{pmatrix} = \begin{pmatrix} \frac{\partial f}{\partial x} \cdot \frac{\partial x}{\partial x} + \frac{\partial f}{\partial y} \cdot \frac{\partial y}{\partial x} + \frac{\partial f}{\partial t} \cdot \frac{\partial t}{\partial x} \\ \frac{\partial f}{\partial x} \cdot \frac{\partial x}{\partial y} + \frac{\partial f}{\partial y} \cdot \frac{\partial y}{\partial y} + \frac{\partial f}{\partial t} \cdot \frac{\partial t}{\partial y} \\ \frac{\partial f}{\partial x} \cdot \frac{\partial x}{\partial t} + \frac{\partial f}{\partial y} \cdot \frac{\partial y}{\partial t} + \frac{\partial f}{\partial t} \cdot \frac{\partial t}{\partial t} \end{pmatrix}$$

$$= \begin{pmatrix} 2x \\ 2y \\ 2\cos t - 2\sin t + 1 \end{pmatrix} \tag{A.15}$$

A.6.2 Local sensitivity functions

Basically, local sensitivities represent the slope of the calculated model output at a given set of parameter values, in this case the optimal parameter estimates. The effect of a (small) parameter variation on the solution of Equation 2.7 can be expressed by the well-known Taylor expansion [SCS00]:

$$c^i(t, p_g + \Delta p_g, p_{k=1...p, k \neq g}) = c^i(t, \mathbf{p}) + \sum_{k=1}^{p} \frac{\partial c^i(t, \mathbf{p})}{\partial p_g} \Delta p_g + \quad (A.16)$$

$$\frac{1}{2} \sum_{l=1}^{p} \sum_{k=1}^{p} \frac{\partial^2 c^i(t, \mathbf{p})}{\partial p_h \partial p_g} \Delta p_h \Delta p_g + \dots$$

Often, only the first order partial derivatives $\partial c^i(t, \mathbf{p})/\partial p_g$ are used for a linear approximation. These partial derivatives can be estimated numerically by a finite difference approximation ([SCS00], [Tur90]) changing the gth parameter initially at time t_0 by Δp_g, while the other parameters are held constant. Consequently the sensitivity functions are derived as follows:

$$\frac{\partial c^i(t, \mathbf{p})}{\partial p_g} \approx \frac{c^i(t, p_g + \Delta p_g, p_{k=1...p,k\neq g}) - c^i(t, p_g - \Delta p_g, p_{k=1...p,k\neq g})}{2\Delta p_g}$$

(A.17)

This method of the sensitivity calculation can readily be implemented. However, the accuracy of the resulting slope strictly depends on the parameter change Δp_g. Therefore, preliminary calculation were conducted using the sensitivity functions of model 11 to identify an optimal parameter change Δp_g which is small enough to fulfill the assumption of the local linearity of the nonlinear models and which is large enough to avoid numerical round-off errors during simulation. For comparison, the direct computation method based on the explicit solution making use of the total differential operator (see section A.6.1) was applied. Equation 2.7 was formulated in matrix notation as follows:

$$\frac{d\mathbf{c}}{dt} = \mathbf{N} \cdot \mathbf{v}(\mathbf{c}, \mathbf{p}) \qquad \mathbf{c}(0) = \mathbf{c}^0 \qquad (A.18)$$

where t is the time, $\mathbf{v}$ is the vector of the rate equations, $\mathbf{N}$ is the stoichiometric matrix, $\mathbf{p}$ denotes the vector of the kinetic parameters, $\mathbf{c}$ is the vector of the metabolite concentrations and $\mathbf{c}^0$ is the vector of the steady-state concentrations. The parameter variation equation system of ODEs, obtained by differentiating Equation A.18 with respect to the parameter vector, is then integrated simultaneously with Equation A.18:

$$\frac{d}{dt}\frac{\partial \mathbf{c}(t, \mathbf{p})}{\partial \mathbf{p}} = D_{\mathbf{p}}\left[\frac{d}{dt}\mathbf{c}(t, \mathbf{p})\right] \qquad (A.19)$$

$$= D_{\mathbf{p}}[\mathbf{N} \cdot \mathbf{v}(\mathbf{c}, \mathbf{p})] = \mathbf{N} \cdot \left(\frac{\partial \mathbf{v}}{\partial \mathbf{c}}\frac{\partial \mathbf{c}}{\partial \mathbf{p}} + \frac{\partial \mathbf{v}}{\partial \mathbf{p}}\right) = \mathbf{N} \cdot (\mathbf{J} \cdot \mathbf{S} + \mathbf{F})$$

where $\mathbf{J}$ is called the Jacobian matrix and $\mathbf{F}$ is called the parametric Jacobian matrix (see also section A.6.1). In contrast to Mauch *et al.* [MAR97], $\frac{\partial \mathbf{c}}{\partial \mathbf{p}}(0) = 0$ was chosen as the initial condition for the integration of the ODE system, because the sensitivity functions were employed for the model reduction and not for the calculation of the elasticity coefficients. The sensitivity calculations via the direct method were realized with the updated MMT version MMT2 [HFWT02].

In a subsequent calculation step, the sensitivity coefficients were made dimensionless to allow a comparison of different sensitivity courses:

$$s_k^i(t) = \frac{p_k}{c^i} \cdot \frac{\partial c^i(t, \mathbf{p})}{\partial p_k} = \frac{\partial \ln c^i(t, \mathbf{p})}{\partial \ln p_k} \qquad (A.20)$$

The resulting matrixes, $\mathbf{S}^i$, composed of the normalized local sensitivity coefficients $s^i_{j,k}$ at $j = 1 \ldots n$ time intervals:

$$\mathbf{S}^i = \begin{pmatrix} s^i_{1,1} & \cdots & s^i_{1,p} \\ \vdots & \ddots & \vdots \\ s^i_{n,1} & \cdots & s^i_{n,p} \end{pmatrix}, \tag{A.21}$$

were the basis for the model reduction methods.

A.6.3   PCA for Model Reduction

To decide which parameters can be discarded, we used three methods which are published in [Jol72]. For all three methods the eigenvalues and eigenvectors of $\mathbf{R}^i = \mathbf{S}^{i^T} \cdot \mathbf{S}^i$ are computed. Here, $\mathbf{S}^{i^T}$ denotes the transposed normalized sensitivity matrix $\mathbf{S}^i$. The eigenvalues, λ_k, are ordered according to their absolute value

$$|\lambda_1| < |\lambda_2| < \ldots < |\lambda_p| \tag{A.22}$$

and their corresponding eigenvectors are given by:

$$\mathbf{\Gamma}^i = (\boldsymbol{\gamma}_1, \boldsymbol{\gamma}_2, \ldots, \boldsymbol{\gamma}_p) = \begin{pmatrix} \gamma_{1,1} & \cdots & \gamma_{1,p} \\ \vdots & \ddots & \vdots \\ \gamma_{p,1} & \cdots & \gamma_{p,p} \end{pmatrix}, \tag{A.23}$$

where $\boldsymbol{\gamma}_j = (\gamma_{1,j}, \ldots, \gamma_{p,j})^T, \quad 1 \le j \le p.$

Method 1:
Given p^* as the number of parameters to reject, the first p^* eigenvectors, starting with the eigenvector corresponding to the smallest eigenvalue, were considered in turn. The variable, which had the largest component (absolute value) in the considered vector and which has not already been marked, was now selected according to:

$$x_1 = \arg\left(\max_{1 \le k \le p} |\gamma_{k,1}|\right) \tag{A.24}$$

$$l > 1: \quad x_l = \arg\left(\max_{\substack{1 \le k \le p \\ k \ne x_1 \ldots x_{l-1}}} |\gamma_{k,l}|\right)$$

The p^* columns $\mathbf{x}_l$, $l = 1, \ldots, p^*$, of $\mathbf{S}^i$ were marked to reject.

Method 2:
Only the eigenvectors corresponding to the p^* smallest eigenvalues were

considered. For each of the p parameters the sum of squares of their components in the considered p^* eigenvectors was evaluated and the p^* parameters with the largest amounts were selected.

$$x_1 = \arg\left(\max_{1\leq k \leq p} \sum_{h=1}^{p^*} \gamma_{k,h}^2\right) \tag{A.25}$$

$$l > 1: \qquad x_l = \arg\left(\max_{\substack{1\leq k \leq p \\ k\neq x_1\ldots x_{l-1}}} \sum_{h=1}^{p^*} \gamma_{k,h}^2\right)$$

The p^* columns x_l, $l = 1\ldots p^*$, of $\mathbf{S}^i$ were marked to reject.

Method 3:
For this method only $q = p - p^*$ eigenvectors were considered in turn, now starting with the eigenvector corresponding to the largest eigenvalue. The parameter, which had the largest component (absolute value) in the considered vector and which has not already been chosen, was now selected.

$$x_0 = \arg\left(\max_{1\leq k \leq p} |\gamma_{k,p}|\right) \tag{A.26}$$

$$l > 0: \qquad x_l = \arg\left(\max_{\substack{1\leq k \leq p \\ k\neq x_0\ldots x_{l-1}}} |\gamma_{k,p-l}|\right)$$

The q columns x_l, $l = 0\ldots q - 1$, of $\mathbf{S}^i$ were the one to retain.

Hence, methods 1 and 2 focus on the eigenvectors with the lowest eigenvalue, identifying the most important variables and eliminating them. Beyond it, method 3 follows another strategy by focusing on the most important eigenvector which is then 'liberated' from variables with low input. The three PCA methods were applied to all m matrices $\mathbf{R}^i$ and only these parameters, which were identified as unimportant in all matrices and by all methods were rejected. Only this intersection of irrelevant parameters was discarded because it was found that the identified parameter importance could differ with respect to the metabolite knot investigated and the PCA approach used.

A.6.4 *Parameter Tuning Importance for Model Reduction*

The 'classical' study of the normalized sensitivity matrix $\mathbf{S}^i$ allows the identification of a parameter ranking with respect to the effects of initial small parameter changes on the resulting courses of c^i. If several species, $c^i, i = 1\ldots m$, are considered, objective functions, $e(\Delta p_g)$, can be introduced ([Tur90], [SSC82]) which represent an integral value of the time-averaged deviations in the trajectories of all species due to small changes

of a parameter Δp_g at the initial time t_0. In the present work the sensitivity of the following objective function:

$$e(\Delta p_g) = \sum_{j=1}^{n} \sum_{i=1}^{m} \left[\frac{c_j^i(p_{k=1...p, k \neq g}, p_g + \Delta p_g) - c_j^i(\mathbf{p})}{c_j^i(\mathbf{p})} \right]^2, \qquad (A.27)$$

was calculated by the use of the local concentration coefficients:

$$os(p_g) = \frac{\partial e}{\partial \ln p_g} = \sum_{j=1}^{n} \sum_{i=1}^{m} \left[\frac{\partial \ln c_j^i(\mathbf{p})}{\partial \ln p_g} \right]^2. \qquad (A.28)$$

The sum of squares of the normalized sensitivities is termed overall sensitivity, $os(p_g)$, and closely related to the least-square sum, see Equation A.32. The overall sensitivities provide information on the tuning importance of the model parameters, which reflects the effectiveness of parameter changes around their nominal values for the investigated measure, i.e. the objective function.

A.6.5 PCA for Fermentation Data Analysis

For fermentation data analysis a linear multivariate PCA was used. Fermentation data sets were collected in a data matrix $\mathbf{X} = [\mathbf{x}_1, \mathbf{x}_2, ... \mathbf{x}_n]$ possessing the dimensionality $[n \times p]$ with n measurement vectors $\mathbf{x}_i$ $[p \times 1]$ $(1 \leq i \leq n)$ and p observations. Altogether $n = 123$ measurement vectors each consisting of $p = 7$ observations formed the data basis. Observations were defined by measurements of optical density (od), concentrations of glucose (c_{glu}), tyrosine (c_{tyr}), L-phenylalanine (c_{phe}), acetate (c_{ace}), dissolved oxygen (DO) and the respiration quotient (rq). To enable data comparability all measurements were standardized according to $x_{ki}^* = \frac{x_{ki} - \bar{x}_k}{\bar{x}_k}$ where $\bar{x}_k$ represents the average value of observation k $(1 \leq k \leq p)$ considering every n measurements of this observation. Thus a transformed data matrix $\mathbf{X}^*$ with $\mathbf{x}_i^* = \begin{bmatrix} od^* & c_{glu}^* & c_{tyr}^* & c_{phe}^* & c_{ace}^* & DO & rq \end{bmatrix}$ was used for calculations.

Based on $\mathbf{X}^*$ the system matrix $\mathbf{M} = \mathbf{X}^{*T}\mathbf{X}^* \frac{1}{n-1}$ was calculated and a set of orthogonal eigenvectors was estimated such that a maximum system variance was achieved. In terms of PCA an eigenvector should be called loading vector $\boldsymbol{\alpha}_k$ possessing the dimension $[1 \times p]$. A certain hierarchy of loading vectors could be established based on the corresponding eigenvalues λ_k that indicate the part of total variance that is described by loading vector $\boldsymbol{\alpha}_k$. Thus the first loading vector $\boldsymbol{\alpha}_1$ describes most of the fermentation data variance followed by the second loading vector $\boldsymbol{\alpha}_2$ and so on. Hence it is the aim of PCA to identify a small set of loading vectors that represents

the vast majority of fermentation data variance. This set of loading vectors could then be used for the identification of fermentation key parameters.

Loading and measurement vectors could be used to calculate scores. According to equation A.29 the scores

$$pc_{ki} = \boldsymbol{\alpha}_k \mathbf{x}_i \tag{A.29}$$

pc_{1i}, pc_{2i}, ..., pc_{ki} could be determined for each loading vector k and every measurement vector i. Scores could be used to describe fermentation courses alternatively in phase diagrams (see A.2).
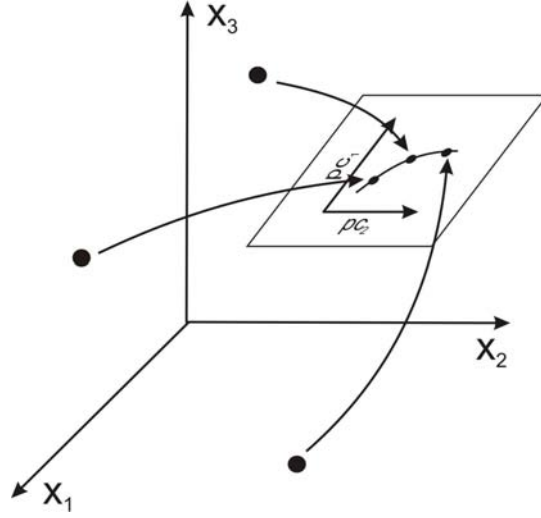
FIGURE A.2. Principle of PCA dimensionality reduction. For instance, fermentation variables x_1, x_2, x_3 of a 3-dimensional space are transformed via PCA to a 2 dimensional principal component phase diagram.

A.6.6   PCA Error Estimation

Equation A.29 indicates that scores are dependent on measurement vectors as well as on loading vectors. If observations contain measurement errors, inaccuracies of the corresponding eigenvectors (loading vectors) and eigenvalues must be considered as well. By applying the first order Taylor approach (used for score error estimation), the error Δpc_{ki} could be estimated as:

$$\Delta pc_{ki} = \frac{dpc_{ki}}{d\mathbf{x}_i^*} \cdot \Delta \mathbf{x}_i^* = \nabla \left(\boldsymbol{\alpha}_k \mathbf{x}_i^* \right) \cdot \Delta \mathbf{x}_i^* \tag{A.30}$$

with a measurement error $\Delta \mathbf{x}_i^*$ $[p \times 1]$ for the ith measurement of $\mathbf{x}^*$. Equation A.30 indicates that principal component errors are dependent on

measurement errors $\mathbf{x}_i^*$ as well as on loading vectors $\boldsymbol{\alpha}_k$. To consider this relationship, Monte-Carlo simulations were used for score error estimation. Entries of the data matrix $\mathbf{X}$ were superimposed by a randomly chosen, normally distributed ± 10 % measurement noise. Based on this noisy data principal component analysis was carried out to identify loading vectors and eigenvalues. Totally, the results of 5000 calculations were used to estimate corresponding errors. All calculations were carried out using MatLab 5.1, The MathWorks, Inc.

A.7   Modeling

A.7.1   Stimulus-Response Model Simplifications

Pentose phosphate pathway

Since it is known, that the interconversions between R5P, Ri5P and X5P are fast enzymatic transformations ([Kab69], [NMDF97]), a lumped pool of these compounds (C5P) is formulated, that represents the experimentally determined sum of the concentrations. Following the stoichiometric constraints of the pentose phosphate pathway, this pathway is further simplified as follows:

$$
\begin{aligned}
2\,\text{C5P} &\rightleftharpoons GAP + S7P \\
GAP + S7P &\rightleftharpoons E4P + F6P \\
P5P + E4P &\rightleftharpoons F6P + GAP \\
\hline
3\,P5P &\rightleftharpoons 2\,F6P + GAP
\end{aligned}
$$
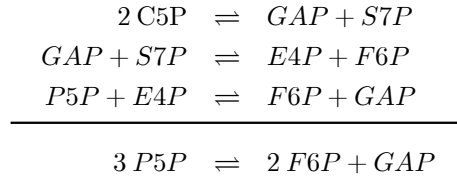
The formulation of a differential equation (DE) for the non-measurable component E4P is circumvented by re-defining the reaction into the aromatic amino acid synthesis

$$4 : \text{P5P} + 5 : \text{PEP} \rightleftharpoons 5 : \text{DAHP} \qquad \text{instead of} \qquad \text{P5P} + \text{E4P} \rightleftharpoons \text{DAHP}$$
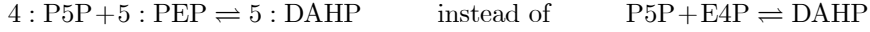
since one P5P molecule is equivalent to 4/5 E4P molecules regarding the number of carbon atoms.

Simplifications within the glycolysis

The linear reaction sequence, $\text{GAP} \rightleftharpoons \text{BPG} \rightleftharpoons \text{3PG} \rightleftharpoons \text{2PG} \rightleftharpoons \text{PEP}$, is substituted by one combined reaction, $\text{GAP} \rightarrow \text{PEP}$, because the conversions are known to be fast and not significantly affected by regulatory effectors ([SW71], [MV93], [STB95]).

Rate equations

Often, kinetic rate equations are too complex to be fully identifiable using the data set of the substrate pulse experiment. Hence simplified kinetic equations are used instead. One frequently used example is the multiplicative Michaelis-Menten equation:

$$\frac{dc^{(3)}}{dt} = \frac{V_{max} \cdot c^{(1)} \cdot c^{(2)}}{(K_{m,c^{(1)}} + c^{(1)}) \cdot (K_{m,c^{(2)}} + c^{(2)})} \tag{A.31}$$

where $c^{(1)}, c^{(2)}, c^{(3)}$ are the chemical reactants, V_{max} is the maximal reaction rate and $K_{m,c^{(i)}}$ is the half saturation constant for the respective

substrate. This approach is, for instance, well suited to replace complex terms like the irreversibly ordered or ping-pong bi-bi kinetic [CB95]. Effects of known effectors can be considered by multiplicative terms which are added to the basic form of the kinetic equations.

A.7.2   Stimulus-Response Model Identification

As most of the published parameter values are obtained from *in vitro* experiments with purified enzymes and not from experiments performed under physiological *in vivo* conditions, their validity for describing *in vivo* cell experiments is questionable. This finding has been outlined by the studies of Mauch *et al.* [MVR00] focusing on the well-known enzyme phosphofructokinase I in *S. cerevisiae*. Therefore, enzyme kinetic parameters were estimated numerically using initial guess values for saturation constants between 1 to 10 mM and for maximal reaction velocities between 1 to 10 $mM \cdot s^{-1}$ according to Segel [Seg75].

TABLE A.11. Steady-state concentrations of the metabolites used for the ODE solution.

Metabolite	Concentration [mM]
G6P	0.16
F6P	0.16
FBP	2.70
GAP	5.57
DHAP	5.01
G3P	0.39
PEP	0.95
PYR	1.25
6PG	3.66
P5P	1.36

The initial conditions for the integration of the dynamic model, i.e. the experimentally determined steady-state concentrations, are shown in Table A.11. The concentrations of the co-metabolites were not simulated but read in from the data owing to the wide range of feasible reactions, in which these co-metabolites can participate. This simplifying assumption is valid because only the carbon atoms are balanced by the models. The experimentally determined trajectories were approximated by smoothing splines before use because of the underlying measurement noise (see subsection A.7.6, Appendix). Simulation and model optimization was performed using the MMT software [HBA$^+$02]. For model identification, the error functional ζ

was used with

$$\zeta = \frac{1}{n} \sum_{j=1}^{n} \sum_{i=1}^{m} \left(b_j^i - c_j^i \right)^2 \tag{A.32}$$

where n is the number of the j time intervals, m is the number of the i variables, i.e. metabolites, c_j^i denotes the simulated and b_j^i the experimentally determined metabolite trajectories. As an example, 2318 'measurements' derived from the smoothed data with a time grid of 0.01 s and an observation window from -5 to 18.18 seconds were used as a data basis to identify model 11 consisting of 122 parameters.

A.7.3   Model 11

TABLE A.12. Mass balances used for model 11.

$$\frac{dG6P}{dt} = v_{pts} - v_{pgi} - v_{glp} - v_{g6pdh}$$

$$\frac{dF6P}{dt} = v_{pgi} - v_{pfk} - v_{mur} + v_{FBPase} + 2 \cdot v_{tkata}$$

$$\frac{dFBP}{dt} = v_{pfk} - v_{aldo} - v_{FBP-BM} - v_{FBPase}$$

$$\frac{dGAP}{dt} = v_{aldo} - v_{GAP-PEP} - v_{Ser} + v_{tim} + v_{tkata}$$

$$\frac{dDHAP}{dt} = v_{aldo} - v_{g3pdh} - v_{tim}$$

$$\frac{dG3P}{dt} = v_{g3pdh} - v_{gly}$$

$$\frac{dPEP}{dt} = v_{GAP-PEP} - v_{pk} - v_{pts} - v_{dahps} - v_{PEP-BM} - 5 \cdot v_{dahps}$$

$$\frac{dPyr}{dt} = v_{pk} - v_{pdh} + v_{pts}$$

$$\frac{d6PG}{dt} = v_{g6pdh} - v_{pgdh} - v_{pghl}$$

$$\frac{dP5P}{dt} = v_{pgdh} - 3 \cdot v_{tkata} - v_{rppk} - 4 \cdot v_{dahps}$$

Abbreviations:

v_{pts}	phosphotransferase system
v_{pgi}	phosphogluco isomerase
v_{glp}	polysaccharide synthesis
v_{g6pdh}	glucose 6-phosphate dehydrogenase
v_{pfk}	phosphofructokinase
v_{mur}	murein synthesis
v_{FBPase}	fructose 1,6-bisphosphatase
v_{tkata}	lumped transaldolase/transketolase
v_{aldo}	aldolase
v_{FBP-BM}	'biomass' synthesis from FBP
$v_{GAP-PEP}$	lumped GAP to PEP reaction
v_{Ser}	serine synthesis
v_{tim}	triosephosphate isomerase
v_{g3pdh}	glycerol 3-phosphate dehydrogenase
v_{gly}	glycerol synthesis
v_{pk}	pyruvate kinase
v_{dahps}	DAHP synthase
v_{PEP-BM}	'biomass' synthesis from PEP
v_{pdh}	pyruvate dehydrogenase
v_{pgdh}	6-phosphogluconate dehydrogenase
v_{rppk}	nucleotide biosynthesis

TABLE A.13. Kinetic rate equations used for model 11. Bold typing indicates terms that are discarded after model reduction. Part I

Phosphotransferase system (v_{pts})

$$k_{f,pts}\,Gluc^{n_{pts,1}}PEP^{n_{\,pts,2}} - k_{b,pts}\,G6P^{n_{pts,3}}\mathbf{Pyr^{n_{pts,4}}}$$

Phosphoglucosisomerase (v_{pgi})

$$k_{f,pgi}\,G6P^{n_{pgi,1}} - k_{b,pgi}\;F6P^{n_{pgi,2}}$$

Polysaccharide synthesis (v_{glp})

$$\frac{V_{f,glp}\,G6P\,ATP}{(K_{m,G6P,glp}+G6P)(K_{m,ATP,glp}+ATP)(G6P+K_{i,G6P,glp})^{n_{glp,1}}}$$

Phosphofructokinase (v_{pfk})

$$\frac{2\,b\cdot D\cdot e\cdot F6P\left(\mathbf{1+FBP}\right)^{\mathbf{2}}\left(1+\frac{\mathbf{F6P}}{\mathbf{e+1}}\right)}{(\mathbf{e+1})\left(\mathbf{L(1+F6P\,c)^2}+(\mathbf{1+FBP})^{\mathbf{2}}\left(\mathbf{1+\frac{F6P}{e+1}}\right)^{\mathbf{2}}\right)}\cdot\frac{ATP}{K_{m,ATP,pfk}+ATP}\cdot$$

$$\frac{\mathbf{ADP^{n_{pfk,1}}F6P^{n_{pfk,2}}}}{\left(\mathbf{ADP^{n_{pfk,1}}+K_{i,ADP,pfk}{}^{n_{pfk,1}}}\right)\left(\mathbf{F6P^{n_{pfk,2}}+K_{i,F6P,pfk}{}^{n_{pfk,2}}}\right)\cdot A}$$
$$A=\left(K_{i,PEP,pfk}{}^{n_{pfk,3}}+PEP^{n_{pfk,3}}\right)$$

Mureine synthesis (v_{mur})

$$\frac{\mathbf{V_{f,mur}F6P\cdot ATP}}{(\mathbf{K_{m,F6P,mur}+F6P})(K_{m,ATP,mur}+\mathbf{ATP})}$$

Fructose 1,6-Bisphosphatase (v_{FBPase})

$$\frac{\mathbf{V_{f,FBPase}FBP^{n_{FBPase}}}}{K_{m,FBPase}{}^{\mathbf{n_{FBPase}}}+\mathbf{FBP^{n_{FBPase}}}}$$

Aldolase (v_{aldo})

$$\frac{V_{\max,aldo}FBP^{n_{aldo,1}}\left(\frac{G3P}{K_{G3P,aldo}}\right)^{n_{aldo,2}}}{K_{m,aldo}{}^{n_{aldo,1}}+FBP^{n_{aldo,1}}}$$

Flux of FBP into biomass (v_{FBP-BM})

$$\frac{\mathbf{V_{f,FBP-BM}FBP^{n_{FBP-BM}}}}{\mathbf{K_{m,FBP-BM}{}^{n_{FBP-BM}}+FBP^{n_{FBP-BM}}}}$$

Triosephosphate Isomerase (v_{tim})

$$\frac{\left(\frac{V_{f,tim}DHAP}{K_{m,DHAP,tim}}\right)-\left(\frac{V_{b,tim}GAP}{K_{m,GAP,tim}}\right)}{1+\frac{DHAP}{K_{m,DHAP,tim}}:+:\frac{GAP}{K_{m,GAP,tim}}}$$

TABLE A.14. Kinetic rate equations used for model 11. Bold typing indicates terms that are discarded after model recuction. Part II

Glycerol 3-Phosphate dehydrogenase (v_{g3pdh})

$$\frac{V_{f,g3pdh}DHAP^{\mathbf{n_{g3pdh,1}}}\left(\frac{Citrate}{K_{a,Cit,g3pdh}}\right)^{n_{g3pdh,2}}}{K_{m,DHAP,g3pdh}{}^{\mathbf{n_{g3pdh,1}}}+DHAP^{\mathbf{n_{g3pdh,1}}}}$$ *Glycerol synthesis (v_{gly})*

$$\frac{V_{f,gly}G3P^{n_{gly,1}}\left(\frac{F6P}{K_{a,F6P,gly}}\right)^{n_{gly,2}}}{K_{m,G3P,gly}{}^{n_{gly,1}}+G3P^{n_{gly,1}}}$$

Combined reactions: $v_{GAP-PEP} = v_{GAPDH}$

$$\cdot v_{PGM} \cdot v_{PK} \cdot v_{eno}$$

$$\frac{V_{f,GAP-PEP}\,GAP\,NAD\,ADP}{(K_{m,GAP,GAP-PEP}+GAP)(K_{m,NAD,GAP-PEP}+NAD)(K_{m,ADP,GAP-PEP}+ADP)}$$

Serine synthesis (v_{Ser})

$$\frac{\mathbf{V_{f,Ser}GAP^{n_{Ser}}}}{\mathbf{K_{m,Ser}{}^{n_{Ser}}+GAP^{n_{Ser}}}}$$

Pyruvate kinase (v_{pk})

$$\frac{V_{f,pk}\left(PEP\,ADP-\frac{Pyr\,ATP}{K_{eq,pk}}\right)\left(\frac{K_{i,G6P,pk}}{G6P}\right)^{n_{pk,1}}\left(\frac{\mathbf{K_{i,C5P,pk}}}{\mathbf{C5P}}\right)^{\mathbf{n_{pk,2}}}}{A+B}$$

$$A=PEP\,ADP\left(1+\frac{Pyr}{K_{i,Pyr,pk}}\right)+K_{m,ADP,pk}(PEP+K_{i,PEP,pk})+K_{m,PEP,pk}ADP$$

$$B=\frac{V_f}{V_r K_{eq}}\left(K_{m,ATP,pk}Pyr\left(1+\frac{PEP}{K_{i,PEP,pk}}\right)+ATP\cdot C\right)$$

$$C=\left[K_{\mathbf{m,Pyr,pk}}\left(1+\frac{\mathbf{K_{m,PEP,pk}ADP}}{\mathbf{K_{i,PEP,pk}K_{m,ADP,pk}}}\right)+Pyr\left(1+\frac{ADP}{K_{i,ADP,pk}}\right)\right]$$

from PEP into 'biomass' (v_{PEP-BM})

$$\frac{\mathbf{V_{f,PEP-BM}PEP\,ATP}}{\mathbf{A+K_{m,ATP,PEP-BM}PEP+K_{m,PEP,PEP-BM}ATP+PEP\,ATP}}$$
$$A = \mathbf{K_{i,PEP,PEP-BM}K_{m,ATP,PEP-BM}}$$

Pyruvate dehydrogenase (v_{pdh})

$$\frac{V_{f,pdh}Pyr\,NAD}{(K_{m,Pyr,pdh}+Pyr)(K_{m,NAD,pdh}+NAD)}\frac{1}{(K_{i,AcCoA,pdh}+AcCoA)^{n_{pdh}}}$$

Glucose-6-phosphate dehydrogenase (v_{g6pdh})

$$\frac{\mathbf{V_{f,g6pdh}G6P\,NADP}}{A\cdot B+\mathbf{NADP\,G6P}+\mathbf{K_{m,G6P,g6pdh}NADP}}$$

$$A = \left(\mathbf{K_{m,NADP,g6pdh}G6P + K_{m,NADP,g6pdh}K_{i,G6P,g6pdh}}\right)$$

$$B = \left(1+\frac{\mathbf{K_{eq,g6pdh}-NADP}}{\mathbf{K_{i,NADP,g6pdh}}}\right)$$

TABLE A.15. Kinetic rate equations used for model 11. Bold typing indicates terms that are discarded after model recuction. Part III

6-Phosphogluconate dehydrogenase (v_{pgdh})

$$\frac{V_{f,pgdh}\left(6PG\ NADP - \frac{C5P}{K_{eq,pgdh}}\right)\left(\frac{K_{i,G6P,pgdh}}{G6P}\right)^{n_{pgdh,1}}}{A+B}$$

$$A = 6PG\ NADP + \mathbf{K_{m,6PG,pgdh}NADP} + \mathbf{K_{m,NADP,pgdh}6PG}$$

$$B = \frac{V_{f,pgdh}}{V_{r,pgdh}K_{eq,pgdh}}\left(K_{m,P5P,pgdh} + P5P\left(1 + \frac{6PG}{K_{i,6PG,pgdh}}\right)\right) + \left(\frac{\mathbf{K_{i,F6P,pgdh}}}{\mathbf{F6P}}\right)^{\mathbf{n_{pgdh,2}}}$$

Entner Doudoroff pathway (v_{pghl})

$$\frac{V_{f,pghl}6PG^{n_{pghl,1}}\left(\frac{F6P}{K_{a,F6P,pghl}}\right)^{n_{pghl,2}}}{K_{m,pghl}^{n_{pghl,1}} + 6PG^{n_{pghl,1}}}$$

Lumped transketolase and transaldolase reactions (v_{tkata})

$$\frac{\mathbf{V}_{f,\mathbf{tkta}}\left(\mathbf{P5P} - \frac{\mathbf{GAP\ F6P}}{\mathbf{K_{eq,tkta}}}\right)}{\left(\mathbf{K_{m,P5P,tkta}} + \mathbf{P5P}\left(1 + \frac{\mathbf{GAP}}{\mathbf{K_{i,GAP,tkta}}}\right) + A\right)}$$

$$A = \frac{\mathbf{V_{f,tkta}(K_{m,F6P,tkta}\ GAP + K_{m,\ GAP,tkta}F6P + GAP\ F6P)}}{\mathbf{V_{r,tkta}K_{eq,tkta}}}$$

Nucleotide biosynthesis (v_{rppk})

$$\frac{\mathbf{V_{f,rppk}P5P^{n_{rppk,1}}}\left(\frac{\mathbf{ADP}}{\mathbf{K_{a,ADP,rppk}}}\right)^{\mathbf{n_{rppk,2}}}}{\mathbf{K_{m,P5P,rppk}^{n_{rppk,1}} + P5P^{n_{rppk,1}}}}$$

DAHP synthase (v_{dahps})

$$\frac{V_{f,dahps}P5P\ PEP}{(K_{m,P5P,dahps} + P5P)(K_{m,PEP,dahps} + PEP)}$$

A.7.4   Parameters of Model 11 - Before and After Reduction

TABLE A.16. Parameters of model 11 before and after the model reduction process. Part I

rate equ.	parameter	before reduct.	after reduct.	unit
v_{pts}	$k_{f,pts}$	4.358	3.269	$\mathrm{mM}^{-(n_{pts,1}+n_{pts,2}-1)}\mathrm{s}^{-1}$
	$n_{pts,1}$	0.996	0.747	1
	$n_{pts,2}$	1.053	1.566	1
	$k_{b,pts}$	0.814	1.218	$\mathrm{mM}^{-(n_{pts,3}+n_{pts,4}-1)}\mathrm{s}^{-1}$
	$n_{pts,3}$	1.183	1.591	1
	$n_{pts,4}$	0.141		1
v_{pgi}	$k_{f,pgi}$	0.999	0.994	$\mathrm{mM}^{-(n_{pgi,1}-1)}\mathrm{s}^{-1}$
	$n_{pgi,1}$	0.952	1.405	1
	$k_{b,pgi}$	0.997	0.993	$\mathrm{mM}^{-(n_{pgi,2}-1)}\mathrm{s}^{-1}$
	$n_{pgi,2}$	0.996	1.000	1
v_{glp}	$V_{f,glp}$	1.976	1.886	$\mathrm{mM}^{(n_{glp,1}+1)}\mathrm{s}^{-1}$
	$K_{m,G6P,glp}$	0.991	0.976	mM
	$K_{m,ATP,glp}$	1.133	1.161	mM
	$K_{i,G6P,glp}$	0.626	0.629	mM
	$n_{glp,1}$	0.769	1.262	1
v_{pfk}	b	1.003	1.037	1
	D	0.999	1.065	1
	e	0.999	1.046	1
	L	0.959		1
	c	0.998		1
	$K_{m,ATP,pfk}$	0.838	0.811	mM
	$n_{pfk,1}$	0.999		1
	$K_{i,ADP,pfk}$	0.999		mM
	$n_{pfk,2}$	0.981		1
	$K_{i,F6P,pfk}$	0.999		mM
	$n_{pfk,3}$	14.811	20.104	1
	$K_{i,PEP,pfk}$	0.988	0.984	mM
v_{pdh}	$V_{f,pdh}$	0.996	1.026	$\mathrm{mM}^{n_{pdh}+1}s^{-1}$
	$K_{m,Pyr,pdh}$	0.996	0.992	mM
	$K_{m,NAD,pdh}$	0.996	0.985	mM
	$K_{i,AcCoA,pdh}$	0.998	0.973	mM
	n_{pdh}	1.696	1.700	1

TABLE A.17. Parameters of model 11 before and after the model reduction process. Part II

rate equation	parameter	before reduction	after reduction	unit
v_{pghl}	$K_{a,F6P,pghl}$	1.135	1.143	mM
	$n_{pghl,2}$	7.404	11.977	1
v_{mur}	$V_{f,mur}$	0.399	-	mM s^{-1}
	$K_{m,F6P,mur}$	1.786	-	mM
	$K_{m,ATP,mur}$	10.740	-	mM
v_{FBPase}	$V_{f,FBPase}$	0.124	-	mM s^{-1}
	$K_{m,FBPase}$	68.429	-	mM
	n_{FBPase}	1.960	-	1
v_{aldo}	$V_{max,aldo}$	0.897	0.991	mM s^{-1}
	$n_{aldo,1}$	3.091	3.203	1
	$K_{m,F6P,aldo}$	4.991	4.601	mM
	$K_{G3P,aldo}$	0.811	0.789	mM
	$n_{aldo,2}$	2.671	2.872	1
v_{FBP-BM}	$V_{f,FBP-BM}$	0.044	-	mM s^{-1}
	n_{FBP-BM}	5.040	-	1
	$K_{m,FBP-BM}$	8.505	-	mM
v_{tim}	$V_{f,tim}$	1.557	1.513	mM s^{-1}
	$K_{m,DHAP,tim}$	1.034	1.032	mM
	$V_{b,tim}$	1.114	1.166	mM s^{1}
	$K_{m,GAP,tim}$	0.834	0.830	mM
v_{g3pdh}	$V_{f,g3pdh}$	1.559	1.783	mM s^{-1}
	$n_{g3pdh,1}$	1.092	-	1
	$K_{m,DHAP,g3pdh}$	3.812	4.066	mM
	$K_{a,Cit,g3pdh}$	2.072	2.064	mM
	$n_{g3pdh,2}$	5.692	5.900	1
v_{gly}	$V_{f,gly}$	2.947	4.674	mM s^{-1}
	$n_{gly,1}$	1.592	2.242	1
	$K_{m,G3P,gly}$	1.662	1.609	mM
	$K_{a,F6P,gly}$	1.818	1.782	mM
	$n_{gly,2}$	6.135	5.696	1
$v_{GAP-PEP}$	$V_{f,GAP-PEP}$	1.929	1.936	mM s^{-1}
	$K_{m,GAP,GAP-PEP}$	3.672	3.250	mM
	$K_{m,NAD,GAP-PEP}$	4.290	4.069	mM
	$K_{m,ADP,GAP-PEP}$	6.783	6.399	mM
v_{Ser}	$V_{f,Ser}$	0.285	-	mM s^{-1}
	n_{Ser}	10.551	-	1
	$K_{m,GAP,Ser}$	15.114	-	mM
v_{PEP-BM}	$V_{f,PEP-BM}$	1.321	-	mM s^{-1}
	$K_{i,PEP,PEP-BM}$	1.246	-	mM
	$K_{m,ATP,PEP-BM}$	41.119	-	mM
	$K_{m,PEP,PEP-BM}$	14.726	-	mM

TABLE A.18. Parameters of model 11 before and after the model reduction process. Part III

rate equation	parameter	before reduction	after reduction	unit
v_{pk}	$V_{f,pk}$	1.113	1.390	mM s^{-1}
	$K_{eq,pk}$	0.801	0.778	1
	$K_{i,pyr,pk}$	1.259	1.884	mM
	$K_{m,ADP,pk}$	1.010	0.760	mM
	$K_{i,PEP,pk}$	0.391	0.341	mM
	$K_{m,PEP,pk}$	1.094	0.827	mM
	$V_{r,pk}$	2.444	3.662	mM s^{-1}
	$K_{m,ATP,pk}$	0.799	0.609	mM
	$K_{m,Pyr,pk}$	0.107	-	mM
	$K_{i,ADP,pk}$	2.232	3.322	mM
	$K_{i,G6P,pk}$	1.030	1.064	mM
	$n_{pk,1}$	2.074	2.483	1
	$K_{i,P5P,pk}$	1.949	-	mM
	$n_{pk,2}$	0.089	-	1
v_{pgdh}	$V_{f,pgdh}$	0.283	0.222	mM s^{-1}
	$K_{eq,pgdh}$	1.712	1.811	mM^{-1}
	$K_{m,6PG,pgdh}$	26.696	-	mM
	$K_{m,NADP,pgdh}$	5.813	-	mM
	$V_{b,pgdh}$	1.130	0.883	mM s^{-1}
	$K_{m,P5P,pgdh}$	3.353	5.018	mM
	$K_{i,6PG,pgdh}$	1.388	1.045	mM
	$K_{i,G6P,pgdh}$	11.543	8.676	mM
	$n_{pgdh,1}$	3.268	2.454	1
	$K_{i,F6P,pgdh}$	24.530	-	mM
	$n_{pgdh,2}$	54.790	-	mM
v_{tkata}	$V_{f,tkata}$	1.134	-	mM s^{-1}
	$K_{eq,tkata}$	1.043	-	mM
	$K_{m,P5P,tkata}$	2.265	-	mM
	$K_{i,GAP,tkata}$	0.810	-	mM
	$V_{r,tkata}$	0.218	-	mM s^{-1}
	$K_{m,F6P,tkata}$	13.410	-	mM
	$K_{m,GAP,tkata}$	0.868	-	mM
v_{rppk}	$V_{f,rppk}$	0.308	-	mM s^{-1}
	$n_{rppk,1}$	1.477	-	1
	$K_{m,P5P}$	2.346	-	mM
	$K_{a,ADP}$	14.891	-	mM
	$n_{rppk,2}$	2.263	-	1
v_{dahps}	$V_{f,dahps}$	0.400	0.043	mM s^{-1}
	$K_{P5P,dahps}$	5.591	16.996	mM
	$K_{PEP,dahps}$	6.238	17.827	mM

TABLE A.19. Parameters of model 11 before and after the model reduction process. Part IV

rate equ.	parameter	before reduct.	after reduct.	unit
v_{g6pdh}	$V_{f,g6pdh}$	8.384	1.700	mMs^{-1}
	$K_{m,NADP,g6pdh}$	3.533	-	mM
	$K_{i,G6P,g6pdh}$	0.727	-	mM
	$K_{eq,g6pdh}$	2.131	-	mM
	$K_{i,NADP,g6pdh}$	0.145	-	mM
	$K_{m,G6P,g6pdh}$	4.058	-	mM
v_{pghl}	$V_{f,pghl}$	1.551	1.514	mMs^{-1}
	$n_{pghl,1}$	4.293	7.381	1
	$K_{m,6PG,pghl}$	2.979	3.032	mM

A.7.5   Model 13

TABLE A.20. Mass balances used for model 13.

$$\frac{dG6P}{dt} = v_{pts} - v_{pgi} - v_{g6pdh}$$

$$\frac{dF6P}{dt} = v_{pgi} - v_{pfk} + v_{FBPase} + v_{tkb} + v_{tkata}$$

$$\frac{dFBP}{dt} = v_{pfk} - v_{aldo} - v_{FBPase}$$

$$\frac{dGAP}{dt} = v_{aldo} - v_{GAP-PEP} - v_{Ser} - v_{tim} + v_{tkb}$$

$$\frac{dDHAP}{dt} = v_{aldo} + v_{tim}$$

$$\frac{dPEP}{dt} = v_{GAP-PEP} - v_{pk} - v_{pts} - v_{dahps} - v_{PEP-BM}$$
$$- v_{dahps}$$

$$\frac{dPyr}{dt} = v_{pk} - v_{pdh} + v_{pts}$$

$$\frac{d6PG}{dt} = v_{g6pdh} - v_{pgdh}$$

$$\frac{dP5P}{dt} = v_{pgdh} - v_{tkb} - 2 \cdot v_{tkata} - v_{dahps}$$

$$\frac{dE4P}{dt} = 2 \cdot v_{tkata} - v_{tkb} - v_{dahps}$$

Abbreviations:

v_{pts}	phosphotransferase system
v_{pgi}	phosphoglucoisomerase
v_{g6pdh}	glucose 6-phosphate dehydrogenase
v_{pfk}	phosphofructokinase
v_{FBPase}	fructose 1,6-bisphosphatase
v_{tkata}	lumped transaldolase/transketolase A
v_{aldo}	aldolase
$v_{GAP-PEP}$	lumped GAP to PEP reaction
v_{tim}	triosephosphate isomerase
v_{gly}	glycerol synthesis
v_{pk}	pyruvate kinase
v_{dahps}	DAHP synthase
v_{PEP-BM}	'biomass' synthesis from PEP
v_{pdh}	pyruvate dehydrogenase
v_{pgdh}	6-phosphogluconate dehydrogenase
v_{tkb}	transketolase B
v_{Ser}	serine synthesis

TABLE A.21. Kinetic rate equations used for model 13. Bold typing indicates terms that are discarded after model reduction. Part I

Phosphotransferase system (v_{pts})

$$\frac{V_{\max,pts}\, Gluc\, PEP}{(K_{m,Gluc,pts}+Gluc)(K_{m,PEP,pts}+PEP)(K_{i,G6P,pts}+G6P)^{n_{pts}}}$$

Phosphoglucosisomerase (v_{pgi})

$$\frac{\left(\frac{V_{f,pgi}\, G6P}{K_{m,G6P,pgi}}\right)-\left(\frac{V_{b,pgi}\, F6P}{K_{m,F6P,pgi}}\right)}{1+\frac{G6P}{Km,G6P,pgi}:+:\frac{F6P}{Km,F6P,pgi}}$$

Phosphofructokinase (v_{pfk})

$$\frac{2\, D{\cdot}e{\cdot}F6P\,(1+FBP)^2\left(1+\frac{F6P}{e+1}\right)}{(e+1)\left(L(1+F6P\, c)^2+(1+FBP)^2\left(1+\frac{F6P}{e+1}\right)^2\right)}\cdot\frac{ATP}{K_{m,ATP,pfk}+ATP}$$

Aldolase (v_{aldo})

$$\frac{V_{f,aldo}\left(FBP-\frac{DHAP\, GAP}{K_{eq,aldo}}\right)}{K_{m,FBP,aldo}+FBP\left(1+\frac{DHAP}{K_{i,DHAP,aldo}}\right)+A}\cdot$$

$$\left(\frac{K_{i,GAP,aldo}}{GAP}\right)^{n_{GAP,aldo}}\left(\frac{K_{i,DHAP,aldo}}{DHAP}\right)^{n_{DHAP,aldo}}\cdot$$

$$\left(\frac{K_{i,E4P,aldo}}{E4P}\right)^{n_{E4P,aldo}}\left(\frac{K_{i,ATP,aldo}}{ATP}\right)^{n_{ATP,aldo}}\cdot$$

$$\left(\frac{\mathbf{PEP}}{\mathbf{K_{a,PEP,aldo}}}\right)^{\mathbf{n_{PEP,aldo}}}\left(\frac{Citrate}{K_{a,Cit,aldo}}\right)^{n_{Cit,aldo}}$$

$$A=\frac{V_{f,aldo}}{V_{r,aldo}K_{eq,aldo}}$$
$$\cdot\left(K_{m,GAP,aldo}DHAP+K_{m,DHAP,aldo}GAP+DHAP\, GAP\right)$$

Triosephosphate Isomerase (v_{tim})

$$\frac{\left(\frac{V_{f,tim}\, GAP}{K_{m,GAP,tim}}\right)-\left(\frac{V_{b,tim}\, DHAP}{K_{m,DHAP,tim}}\right)}{1+\frac{GAP}{K_{m,GAP,tim}}:+:\frac{DHAP}{K_{m,DHAP,tim}}}$$

combined reactions: $v_{GAP-PEP}=v_{GAPDH}\cdot v_{PGM}\cdot v_{PK}\cdot v_{eno}$

$$\frac{V_{\max,GAP-PEP}\, GAP\, NAD}{A+K_{m,NAD,GAP-PEP}\, GAP+K_{m,GAP,GAP-PEP}\, NAD+GAP\, NAD}$$
$$A=K_{m,GAP,GAP-PEP}K_{m,NAD,GAP-PEP}$$

Serine synthesis (v_{Ser})

$$\frac{V_{max,Ser}\mathbf{GAP^{nSer}}}{\mathbf{K_{m,Ser}}^{\mathbf{nSer}}+\mathbf{GAP^{nSer}}}$$

Pyruvate Kinase (v_{pk})

$$\frac{\left(\frac{V_{f,pk}\, PEP}{K_{m,PEP,pk}}\right)-\left(\frac{V_{b,pk}\, Pyr\, ATP}{K_{m,Pyr,pk}}\right)}{1+\frac{PEP}{K_{m,PEP,pk}}:+:\frac{Pyr\, ATP}{K_{m,Pyr,pk}}}$$

TABLE A.22. Kinetic rate equations used for model 13. Bold typing indicates terms that are discarded after model reduction. Part II

Pyruvate dehydrogenase (v_{pdh})

$$\frac{V_{f,pdh}\left(Pyr\,NAD-\frac{AcCoA}{K_{eq,pdh}}\right)}{Pyr\,NAD+K_{m,pyr,pdh}NAD+K_{m,NAD,pdh}Pyr+A+\left(\mathbf{\frac{AcCoA}{K_{i,pdh}}}\right)^{\mathbf{n_{pdh}}}}$$

$$A=\frac{V_{f,pdh}}{V_{b,pdh}K_{eq,pdh}}\left(K_{m,AcCoA,pdh}+AcCoA\left(1+\frac{Pyr}{K_{i,Pyr,pdh}}\right)\right)$$

Fructose 1,6-Bisphosphatase (v_{FBPase})

$$\frac{V_{\max,FBPase}FBP^{n_{FBPase}}}{K_{m,FBPase}{}^{n_{FBPase}}+FBP^{n_{FBPase}}}$$

Glucose 6-phosphate dehydrogenase (v_{g6pdh})

$$\frac{V_{max,g6pdh}G6P\,NADP}{(K_{m,G6P,g6pdh}+G6P)(K_{m,NADP,g6p}+NADP)(K_{i,G6P,g6pdh}+G6P)^{n_{g6pdh}}}$$

6-Phosphogluconate dehydrogenase (v_{pgdh})

$$\frac{V_{f,pgdh}6PG\,NADP}{K_{ia,pgdh}K_{m,NADP,pdgh}+K_{m,NADP,pgdh}6PG+K_{m,6PG,pgdh}NADP+6PG\,NADP}$$

Transketolase B (v_{tkb})

$$\frac{V_{f,tkb}E4P\,C5P}{(K_{m,E4P,tkb}+E4P)(K_{m,C5P,tkb}+C5P)\left(K_{F6P,tkb}+\frac{F6P}{K_{i,F6P,tkb}}\right)^{n_{tkb,1}}}\cdot$$

$$\frac{1}{\left(K_{GAP,tkb}+\frac{GAP}{K_{i,GAP,tkb}}\right)^{n_{tkb,2}}\left(K_{AMP,tkb}+\frac{AMP}{K_{i,AMP,tkb}}\right)^{n_{tkb,3}}}$$

Lumped transketolase A / transaldolase reaction (v_{tkata})

$$\frac{V_{f,tkata}C5P^{n_{tkata,1}}}{\left(K_{m,C5P,tkata}+C5P^{n_{tkata,1}}\right)\left(K_{AMP,tkata}+\frac{AMP}{K_{i,tkata}}\right)^{n_{tkata,2}}}$$

DAHP synthase(v_{dahps})

$$\mathbf{\frac{V_{\max,dahps}PEP\cdot NADPH\cdot E4P}{A+B}}$$

$$\mathbf{A=K_{m,PEP,dahps}(Aa+K_{i,E4P,dahps}PEP+PEP\,E4P)}$$
$$Aa=K_{i,E4P,dahps}K_{i,NADPH,dahps}+K_{i,NADPH,dahps}E4P$$

$$\mathbf{B=NADPH(Bb+K_{m,E4P,dahps}E4P+PEP+NADPH)}$$
$$Bb=K_{i,E4P,dahps}K_{m,PEP,dahps}+K_{m,NADPH,dahps}E4P$$

A.7.6   Spline function

Smoothing splines were used for data processing by implementing the routine, e02bac of the NAG C library (http://www.nag.com/numeric/cl/ CLdescription.asp). This method supports to assign weights to the data, which turned out to be important if different data accuracies are considered as well as varying numbers and positions of interior knots. For splining, the analytical function of the weighted cubic B-splines [Hay74] was found to be well suited and superior to alternative approaches.

A.7.7   Metabolic Flux Analysis (MFA)

The mathematical modeling of ^{13}C labeled isotopomer information for the determination of metabolic fluxes in *C. glutamicum* and *E. coli* was performed using the ^{13}C-flux software package ([WMI$^+$99], [MWKdG99], [PdGE$^+$00]). A flux balance analysis was integrated into the flux analysis, and the inputs and outputs of the metabolic network, as determined from measurements of substrate uptake and excretion rates, were input into the analysis. Using this mathematical framework, fluxes in the central metabolism were identified by the best fit of simulated labeling data to the NMR measurements, minimizing the sum of squared deviations between simulation and NMR data.

A.7.8   C. glutamicum Model for MFA with Growing Cells

The precursor fluxes for biomass synthesis and the reaction network describing the central metabolism of *Corynebacterium glutamicum* were taken from [MdGW$^+$96]. This included the reactions of glycolysis, the pentose-phosphate pathway (*PPP*), the tricarboxylic acid cycle (*TCA*) cycle and the glyoxylate pathway. The various pentose-5-phosphates and the triose phosphate pools were each lumped together. In the model, PEP and pyruvate as well as oxaloacetate and malate were merged into single PEP/ pyruvate and oxaloacetate/malate pools, respectively. The total set of anaplerotic C3-carboxylating and C4-decarboxylating reactions was handled mathematically as a single bidirectional reaction step between PEP/pyruvate and oxaloacetate/malate. The following enzyme reactions were also programmed as being reversible: transketolase, transaldolase, succinate dehydrogenase and fumarase. The substrate uptake and all precursor effluxes into biomass polymers were set as unidirectional. In the present study, the model also included the biosynthesis of trehalose from glucose-6-phoshate.

A.7.9   C. glutamicum Model for MFA with Non-Growing Cells

The approach of Marx *et al.* [MdGW$^+$96] was used to model the intracellular fluxes of the glycolysis, the pentose-phosphate pathway (PPP),

the tricarboxylic acid (TCA) cycle and the glyoxylate pathway during L-lysine production with non-growing, L-leucine limited *C. glutamicum* MH20-22B cells. The various pentose-5-phosphates and the triose phosphate pools were each lumped together. In the model, PEP and pyruvate as well as oxaloacetate and malate were merged into single PEP/pyruvate and oxaloacetate/malate pools, respectively. The total set of anaplerotic C3-carboxylating and C4-decarboxylating reactions was handled mathematically as a single bidirectional reaction step between PEP/pyruvate and oxaloacetate/malate. The following enzyme reactions were also programmed as being reversible: glucose 6-phosphate isomerase, (glycerin aldehyde) GAP – 3 phospho glycerate (PGA) conversion (lumped reaction), PGA-PEP/PYR conversion (lumped reaction), transketolase, transaldolase, succinate dehydrogenase and fumarase. The substrate uptake and all precursor effluxes into biomass polymers (as far as considered due to numerical reasons) were set as unidirectional. In the present study, the model also included the biosynthesis of trehalose from glucose-6-phoshate.

A.7.10   E. coli Model for MFA with Non-Growing Cells

The metabolic model included reactions from glycolysis, pentose phosphate pathway and the tricarboxylic acid cycle (see following Table A.23). The glyoxylate shunt was assumed to be inactive under the aerobic experimental conditions. This also held also true for the Etner-Doudoroff (ED) pathway. The pools phosphoenolpyruvate (PEP) and pyruvate (PYR) as well as oxaloacetate (OAA) and malate (MAL) were lumped leading to a PTS decoupling from the PEP/PYR conversion. The reactions of the L-Phe production pathway and the respective C-atom transitions were implemented as shown (see also Figure A.3). Fluxes were estimated by using an evolutionary optimization which was followed by a local optimization (optimizers are CooolEvoAlpha and CooolBFGSAlpha from the Coool library http://coool.mines.edu/).

TABLE A.23. Model reactions for metabolite flux analysis studying non-growing *E. coli* 4pF81 during L-Phe production. upt1 and upt2 denote the non-labeled and the [1-13C] labled glucose uptake, respectively. The initial labeling position is given by *. It is noteworthy that bsPHEa and psPheb code for the same PHEaux synthesis leading to two isotopomers which are equally found by NMR. C-atom transitions are indicated by letter sequences and represent the basis for the set-up of the isotopomer mapping matrix.

Name	Reaction	C-atom transition
upt1	Glu13C>G6P	*ABCDEF > *ABCDEF
upt2	GlucNat>G6P	ABCDEF > ABCDEF
emp1	G6P>F6P	ABCDEF > ABCDEF
emp2	F6P>FBP	ABCDEF > ABCDEF
emp3	FBP>GAP+GAP	ABCDEF > CBA+DEF
emp4	GAP>PEP/PYR	ABC > ABC
ppp1	G6P>CO2+Ru5P	ABCDEF > A+BCDEF
ppp2	Ru5P>X5P	ABCDE > ABCDE
ppp3	Ru5P>Ri5P	ABCDE > ABCDE
ppp4	X5P+E4P>	ABCDE+abcd >
	GAP+F6P	CDE+ABabcd
ppp5	X5P+Ri5P>	ABCDE+abcde >
	S7P+GAP	ABabcde+CDE
ppp6	GAP+S7P>	ABC+abcdefg >
	E4P+F6P	defg+abcABC
tcc1	PEP/PYR >AcCoA+CO2	ABC > BC+A
tcc2	AcCoA+MAL/OAA>ICIT	AB+abcd > dcbaBA
tcc3	ICIT>AKG+CO2	ABCDEF > ABCEF+D
tcc4	AKG>SUC+CO2	ABCDE > BCDE+A
tcc5a	SUC>MAL/OAA	ABCD > ABCD
tcc5b	SUC>MAL/OAA	ABCD > DCBA
ana1	PEP/PYR+CO2>	ABC+a >
	MAL/OAA	ABCa
bsUracil	MAL/OAA+CO2>	ABCD+a >
	Uracil+CO2	CBAa+D
Uracilaux	Uracil>UracilAux	abcd > abcd
bsDAHP	PEP/PYR+E4P>DAHP	ABC+abcd > ABCabcd
bsSHI	DAHP>SHI	ABCDEFG > BCDEFGA
bsPheA	PEP/PYR+SHI>	ABC+abcdefg >
	L-Phe+CO2	ABCabcdef+g
bsPheB	PEP/PYR+SHI>	ABC+abcdefg >
	L-Phe+CO2	ABCafedcb+g
Pheaux	PHE>PHEAux	ABCEFGHIJ > ABCDEFGHIJ
CO2aux	CO2>CO2Aux	A > A
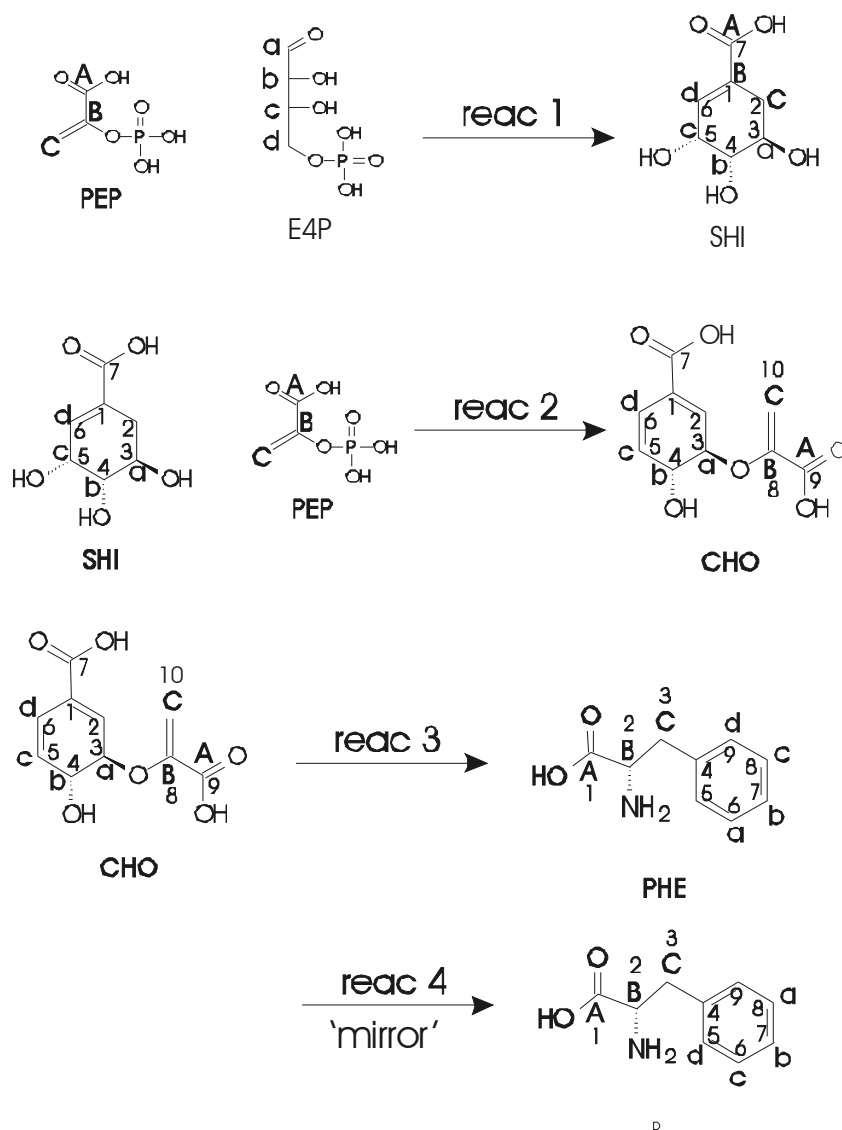
FIGURE A.3. Overview of the simplified aromatic amino acid pathway model used for ^{13}C based metabolic flux analysis. Please note that all carbon atoms that originate from PEP are indicated with large letters while E4P origins are considered with small letters. 'reac 1' describes the lumped reaction from PEP and E4P via DAHP synthase, 3-DHQ synthase, 3-DHQ dehydratase and SHI dehydrogenase to SHI. 'reac 2' sums up the following conversion from SHI to S3P including PEP via EPSP synthase to EPSP and later on to chorismate (CHO). The reactions 'reac 3' and 'reac 4' both symbolize the last conversions from CHO to L-Phe.

A.7.11   E. coli Model Used for Linear Programming

The linear programming approach used to study the optimum L-Phe formation with non-growing *E. coli* used the stoichiometric matrix as presented in Table A.24. The underdetermined reaction system (two degrees of freedom) was solved by considering the following constraints:

- The P/O ratio was assumed to be constant at 1.8, a heuristic value already used by previous studies [Sch99b] which (more or less) corresponds to typical assumptions published elsewhere [Wie02b].

- Reactions of the tricarboxylic acid cycle were lumped to one tca flux, because no efflux into biomass synthesis had to be considered (non-growing cells).

- Balances for NADH, NADPH, ATP were not closed but open.

- Flux limit constraints were used: respiration (resp), tricarboxylic acid cycle (tca) and futile cycling (fut) had to be positive.

- For optimization the following constraints were used: maximization of L-Phe flux and minimization of futile cycling activity (fut).

TABLE A.24. Stoichiometry and flux constraints used for linear programming considering L-Phe production in non-growing *E. coli*

Met.	pts	emp1	emp2	emp3	emp4	emp5	ppp1	ppp2	ppp3	ppp4	ppp5	ppp6	tca	dahp	shi	phe	resp	fut	thy
G6P	1	-1					-1												
F6P		1	-1							1		1							
FBP			1	-1															
GAP				2	-1					1		-1							
PEP	-1				1	-1								-1		-1			
PYR	1					1							-1						
Ru5P							1	-1	-1										
X5P								1		-1	-1								
Ri5P									1	-1	-1								
E4P										-1		1		-1					
S7P											1	-1							
DAHP														1	-1				
SHI															1	-1			
NADH					1								3				-1		-1
NADPH							2								-1				1
ATP		-1			1											-1	1.8	-1	
Upt=1	1																		

A.7.12   Estimation of Equilibrium Constants for Reactive Extraction

Because of the relatively low solubility of the carriers in the aqueous phase, L-Phe transfer is assumed to take place at the aqueous/organic interface. If the cation-specific reactive extraction process is focused (such as D_2EHPA), the extraction procedure can be described as follows ([TYI$^+$91], [Sch94], [WJM97])

$$A_{aq}^+ + 2\,(CH)_{2,org} \rightleftarrows AC(CH)_{3,org} + H_{aq}^+ \tag{A.33}$$

Here, A$^+$ denotes the cation amino acid species, C codes for the carrier and H represents the proton (counter ion). It is assumed that cation-specific carriers occur as dimers $(CH)_2$. Thus, altogether four carrier molecules CH are used to extract one A$^+$. Using reaction equation A.33 an equilibrium constant K was estimated according to

$$K = \frac{c_{AC(CH)_{3,org}} \cdot c_{H_{aq}^+}}{c_{A_{aq}^+} \cdot c_{(CH)_2}^2} \tag{A.34}$$

with c as the molar concentration of the respected species introduced in reaction A.33. For further analysis the equilibrium constant K was derived from experimental data, estimating the amount of carrier/L-Phe complex in the organic phase by simple mass balancing

$$c_{AC(CH)_{3,org}} = \left(c_{A,aq}^0 - c_{A,aq}^1\right) \cdot \frac{V_{aq}}{V_{org}} \tag{A.35}$$

Here $c_{A,aq}^0$ and $c_{A,aq}^1$ represent the start and equilibrium concentrations of the amino acid (here: L-Phe) before (0) and after (1) extraction from the aqueous phase V_{aq} into the organic phase V_{org}.

A.7.13   Estimation of Mass Tranfer Coefficients by Simple Modeling

Coefficients for the description of mass transfer from the aqueous donor phase into the organic phase (β_D) and from the organic phase into the aqueous stripping phase (β_A) were estimated by a simple modeling approach. Mass balances were formulated for the donor tank and module 1 as well as for the stripping tank and module 2. For simplification, it was assumed that concentration gradients inside the modules could be neglected as previously described [EOI96]. Thus L-Phe mass transfer $\dot{m}_{PheD}$ from aqueous donor to organic phase can be formulated as

$$\dot{m}_{PheD} = \beta_D \cdot A_M \left(c_{Phe,D} - c_{Phe,D}^{eq}\right) \tag{A.36}$$

with A_M as the effective membrane area, $c_{Phe,D}$ as the L-Phe concentration in aqueous phase and $c_{Phe,D}^{eq}$ as the equilibrium concentration in

aqueous phase. Hence the donor tank can be balanced as follows:

$$V_D \frac{dc_{Phe,D}}{dt} = \beta_D \cdot A_M \left(c_{Phe,D} - c_{Phe,D}^{eq} \right) \tag{A.37}$$

taking into account the tank volume V_D, which was constant with $V_D \gg V_{\mathrm{mod}\,ule}$. By analogy, a corresponding equation was derived for mass transfer form organic to stripping phase.

Using MicroMath^{TM} Scientist^{TM} (Salt Lake City, USA) parameters β_D, β_A, $c_{Phe,D}^{eq}$ and $c_{Phe,A}^{eq}$ were estimated using experimental results. It is noteworthy that for model simplification $c_{Phe,D}^{eq}$ and $c_{Phe,A}^{eq}$ were considered as constant and not as time-variant equilibrium concentrations, which contradicts usual assumptions. However, this modeling approach only intended to allow only a rough parameter identification (in analogy to previously published results of Escalante *et al.* [EOI96].

Appendix B
Legends

TABLE B.1. List of abbreviations used for metabolites. Part I

Abbreviation	Full name
6PG	6-phospho-d-gluconate
AcCoA	acetyl-CoA
AKG	α−ketoglutarate
ALA	alanine
Asp	aspartate
CHO(R)	chorismate
DAHP	3-desoxy-arabino-heptulosonate-7-phosphate
DHAP	dihydroxy acetone-phosphate
DHS	3-dehydroshikimate
E4P	D-erythrose-4-phosphate
EPSP	5-enolpyruvoylshikimate-3-phosphate
F6P	fructose-6-phosphate
FUM	fumarate
G3P	glycerol-3-phosphate
G6P	glucose-6-phosphate
GAP	glyceraldehyde-3-phosphate
Glu13C	^{13}C labeled glucose
GluNat	natively labeled glucose
GLN	glutamine
GLU	glutamate
HPPY	4-hydroxy phenylpyruvate
ICIT	isocitrate
ILE	isoleucine
Isopmal	isopropylmalate
KIVAL	α-ketoisovalerate
LEU	leucine
Lys	lysine
MAL	malate
OAA	oxaloacetate
Oxival	oxoisovalerate
P5P	lumped pool of pentose phosphates
PEP	phosphoenolpyruvate
PGA	3-phosphoglycerate
PP	phenylpyruvate
PPA	prephenate
PPY	phenylpyruvate
PYR	pyruvate
Ri5P	ribose-5-phosphate
Ru5P	ribulose-5-phosphate

TABLE B.2. List of abbreviations used for metabolites Part II

Abbreviation	Full name
S7P	sedoheptulose-7-phosphate
SHI	shikimate
SUC(C)	succinate
URA	uracil
X5P	xylose-5-phosphate

TABLE B.3. List of abbreviations of miscellaneous purpose

Abbreviation	Full name
A^+	amino acid cation
AAA	aromatic amino acid (pathway)
CTR	carbon dioxide transfer rate
$(CH)_2$	dimer of the carrier (C) proton (H) complex
E. coli	Escherichia coli
ED	electrodialysis
FCC	flux control coefficient
ISPR	in situ product recovery
MFA	metabolic flux analysis
MS	mass spectrometry
OD	optical density
TCA	tricarboxylic acid cycle
PPP	pentose-phosphate pathway
OD	optical density
(O)DE	(ordinary) differential equation
OUR	oxygen uptake rate
PCA	principal component analysis
Pps	phosphoenolpyruvate synthase
PPP	pentose-phosphate pathway
PTS	phosphoenolpyruvate:carbohydrate transferase system
PykA/PykF	pyruvate kinase (isoenzymes)
S. cerevisiae	Saccharomyces cerevisiae
Tal	transaldolase
TCA	tricarboxylic acid cycle
Tkt	transketolase
Z. mobilis	Zymomonas mobilis

TABLE B.4. List of abbreviations used for mathematical terms and variables

Abbreviation	Full name
A_M	effective membrane area
b	metabolite concentration, measured
c	metabolite concentration, simulated
$\mathbf{c}$	vector of all metabolite concentrations, simulated
$\mathbf{c}^0$	vector of all steady-state metabolite concentrations, simulated
$e(\Delta p)$	objective function with respect to a small parameter change
$\mathbf{F}$	parametric Jacobian matrix
g	index, parameter
$\boldsymbol{\Gamma}$	matrix of eigenvectors
$\boldsymbol{\gamma}$	eigenvector, represents a column of Γ
h	index, parameter
i	index, metabolite/variable
j	index, time interval
$\mathbf{J}$	Jacobian matrix
k	index, parameter (and row in Γ)
λ	eigenvalue
m	total number of independent metabolites/variables
n	total number of time intervals
$\mathbf{N}$	stoichiometry matrix
ν	stoichiometric coefficient
$os(p)$	overall sensitivity with respect to parameter p
p	total number of parameter
$\mathbf{p}$	vector of parameters
Δp	small parameter change
$\mathbf{R}$	Covariance matrix
s	standardized, local sensitivity coefficient
$\mathbf{S}$	sensitivity matrix
t	time
v	reaction rate
v^*	standardized pool velocity
$\mathbf{v}$	vector of rate equations
V	volume
x	discarded entry of an eigenvector
ζ	error functional

TABLE B.5. List of parameters and variables used in the total *ISPR* process model, Part I

Symbol	Unit	Meaning
c_{Cconst}	$mmol \cdot L^{-1}$	total amount of carrier in the organic phase, constant
c_{HA}	$mmol \cdot L^{-1}$	proton conc. in the aqueous acceptor phase
carrier/proton complex concentrations at		
c_{CHD}	$mmol \cdot L^{-1}$	at the organic/aqueous interface
c_{CHO}	$mmol \cdot L^{-1}$	in the organic bulk
c_{CHOBex}	$mmol \cdot L^{-1}$	in the organic bulk in the back-extraction module
c_{CHOEx}	$mmol \cdot L^{-1}$	in the organic bulk in the extraction module
$c_{CHO,I}$	$mmol \cdot L^{-1}$	at the organic/aqueous interface
L-Phe concentration		
c_{Phe}	$mmol \cdot L^{-1}$	in the fermentation suspension
c_{PheA}	$mmol \cdot L^{-1}$	in the bulk of the acceptor phase
c_{PheD}	$mmol \cdot L^{-1}$	in the bulk of the aqueous phase
carrier/L-Phe concentration		
$c_{CPheOBex}$	$mmol \cdot L^{-1}$	in the organic bulk in the back-extraction module
$c_{CPheOEx}$	$mmol \cdot L^{-1}$	in the organic bulk in the extraction module
miscellaneous		
D_{cap}	m	outer diameter of the hollow fibers
δ_D	m	thickness of the aqueous film in the donor phase
K_C	-	equilibrium constant between the interface conc. of the carrier complex in organic and aqueous phase, estimated experimentally
x	m	small distance between reac. plane and interface
mass transfer coefficient of carrier/proton complex from the		
k_{CHD}	$m \cdot s^{-1}$	aqueous organic interface to the reaction plane inside the aqueous film of the donor phase
k_{CHO}	$m \cdot s^{-1}$	organic bulk to the organic/aqueous interface inside the organic film
mass transfer coefficient of carrier/L-Phe complex from the		
k_{CPheA}	$m \cdot s^{-1}$	aqueous/organic interface to the reaction plane inside the aqueous film of the acceptor phase
k_{CPheO}	$m \cdot s^{-1}$	bulk of the organic phase to the organic/aqueous interface inside the organic film
mass transfer coefficient of		
k_{HA}	$m \cdot s^{-1}$	protons from the bulk to the reaction plane inside the aqueous film of the acceptor phase
k_{PheD}	$m \cdot s^{-1}$	L-Phe from the bulk to the reaction plane inside the aqueous film of the donor phase
area specific L-Phe flux		
$\dot{r}''_{PheA}$	$mmol \cdot (m^2 s)^{-1}$	at the aqueous acceptor and organic interface
$\dot{r}''_{PheD}$	$mmol \cdot (m^2 s)^{-1}$	at the aqueous donor and organic interface

TABLE B.6. List of parameters and variables used in the total *ISPR* process model, Part II

Symbol	Unit	Meaning
average velocity of the aqueous		
v_A	$m \cdot s^{-1}$	acceptor phase inside the hollow fibers
		of the back-extraction modules
v_D	$m \cdot s^{-1}$	donor phase inside the hollow fibers
		of the extraction modules
liquid streams of		
$\dot{V}_A$	$L \cdot h^{-1}$	acceptor
$\dot{V}_D$	$L \cdot h^{-1}$	donor
$\dot{V}_O$	$L \cdot h^{-1}$	organic phase
(buffer) tank volumes of		
V_A	L	acceptor
V_B	L	organic cycle (upper tank)
V_C	L	organic cycle (lower tank)
V_D	L	donor
macrokinetic parameters		
μ	h^{-1}	specific growth rate
$\mu_{\max}$	h^{-1}	max. specific growth rate
K_{IPhe}	$mmol \cdot L^{-1}$	inhibition constant with respect to L-Phe
K_{STyr}	$g \cdot L^{-1}$	Monod-constant for tyrosine affinity
m_{Tyr}	$mmol \cdot (g_{CDW}h)^{-1}$	maintenace for TYR
π_{Phe}	$mmol \cdot (g_{CDW}h)^{-1}$	biomass specific L-Phe formation rate
$\pi_{Phe\,\max}$	$mmol \cdot (g_{CDW}h)^{-1}$	max. biomass specific L-Phe formation rate
σ_{Tyr}	$mmol \cdot (g_{CDW}h)^{-1}$	biomass specific TYR consumption rate
Y_{XTyr}	$g_{CDW} \cdot mmol^{-1}$	biomass/tyrosine yield.

TABLE B.7. List of Indices

Index	Full name
A	acceptor, stripping phase
aq	aqueous phase
C	carrier
CDW	cell-dry weight
D	donor
eq	(at) equilibrium
H	proton, counter ion
org, O	organic phase

Schriften des Forschungszentrums Jülich
Reihe Lebenswissenschaften / Life Sciences

Schriften des Forschungszentrums Jülich
Reihe Lebenswissenschaften / Life Sciences

10. **Regulation der *clp*-Genexpression durch ClgR und Definition des ClgR-Regulons aus *Corynebacterium glutamicum***
by S. Engels (2004), V, 125 pages
ISBN: 3-89336-379-3

11. **Metabolomanalyse zur Untersuchung der Dynamik im Aromatenbiosyntheseweg in L–Phenylalanin Produzenten von *Escherichia coli***
by M. Oldiges (2005), XVI, 181 pages
ISBN: 3-89336-380-7

12. **Identifizierung und Charakterisierung eines Transkriptionsregulators der Aconitase von *Corynebacterium glutamicum***
by A. Krug (2005), VI, 122 pages
ISBN: 3-89336-382-3

13. **Prozessentwicklung der elektroenzymatischen Sulfoxidation mit Chloroperoxidase**
by S. Lütz (2005), XIV, 178 pages
ISBN: 3-89336-387-4

14. **Export von Proteinen mit Zwillingsarginin-Signalsequenzen über den Tat-Weg in *Escherichia coli***
by P. J. Kreutzenbeck (2005), 118 pages
ISBN: 3-89336-388-2

15. **Untersuchungen zur Fettsäure- und Zellwandsynthese sowie zur Glutamatbildung mit *Corynebacterium glutamicum***
by E. Radmacher (2005), 130 pages
ISBN: 3-89336-389-0

16. **Monomodale und multimodale Registrierung von autoradiographischen und histologischen Bilddaten**
by A. Vieten (2005), 116 pages
ISBN: 3-89336-390-4

17. **Biosynthese von Phosphonaten: Charakterisierung des rekombinanten Enzyms Phosphonopyruvat-Decarboxylase aus *Streptomyces viridochromogenes* Tü494**
von S. Johnen (2005), 128 Seiten
ISBN: 3-89336-400-5

18. **Ex-vivo Generierung von neutrophilen Zellen zur Prävention und Therapie der Sepsis**
von R. Herbold (2005), 202 Seiten
ISBN: 3-89336-407-2

Schriften des Forschungszentrums Jülich
Reihe Lebenswissenschaften / Life Sciences

19. **Entwicklung eines Donor/Akzeptor-Konzeptes für die asymmetrische Synthese unsymmetrischer Benzoine mit Hilfe ThDP-abhängiger Enzyme**
von P. Dünkelmann (2005), 222 Seiten
ISBN: 3-89336-408-0

20. **Analyse der Bindungsspezifität der humanen Lck-SH3-Domäne anhand artifizieller und physiologischer Peptid-Liganden und strukturelle Charakterisierung dieser Peptide im Komplex mit SH3-Domänen**
von T. T. Tran (2005), 155 Seiten
ISBN: 3-89336-412-9

21. **Modeling Based Process Development of Fed-Batch Bioprocesses: L-Valine Production by *Corynebacterium glutamicum***
by M. Brik Ternbach (2005), 202 Seiten
ISBN: 3-89336-413-7

22. **Charakterisierung der Ausscheidung von L-Glutamat bei *Corynebacterium glutamicum***
von K. C. Stansen (2005), 151 Seiten
ISBN: 3-89336-416-1

23. **Metabolic and Bioprocess Engineering – a Fruitful Symbiosis**
by R.Takors (2005), 399 Seiten
ISBN: 3-89336-420-X

Forschungszentrum Jülich
in der Helmholtz-Gemeinschaft